

Phase 1 study of CPX-1, a fixed ratio formulation of irinotecan (IRI) and floxuridine (FLOX), in patients with advanced solid tumors

G. Batist, K. Chi, W. Miller, S. Chia, F. Hasanbasic, A. Fistic...

[Show More](#)

Abstract

2014

Background: *In vitro* studies have shown that varying the ratio of individual agents in drug combinations can result in synergistic, additive or antagonistic activity against tumor cells. CPX-1 is a liposomal formulation of IRI and FLOX in a fixed 1:1 molar ratio which was selected as optimal *in vitro* and confirmed to be synergistic *in vivo* in preclinical tumor models. CPX-1 overcomes the dissimilar pharmacokinetics (PK) of the individual drugs, enables sustained maintenance of this ratio after IV administration, and was evaluated in a Phase I open-label, dose-escalation study. **Methods:** Starting dose was 30 U/m² (1 Unit of CPX-1 contains 1 mg IRI + 0.36 mg FLOX) given on day 1 and 15 of each 28-day cycle. Dose escalation was by modified Fibonacci with 4 subjects/cohort. Eligibility included: ≥ 18 yo; advanced solid tumor; ECOG PS ≤ 2; adequate bone marrow/liver/renal function. PK analysis was done on day 1 and 15 of the first cycle. **Results:** 26 subjects (16M:10F), median age 54.5 y (21–72), all with prior therapy, enrolled in 6 cohorts with the 5th cohort expanded to 6 subjects. Diagnoses: 8 colorectal, 3 pancreatic, 3 ovarian, 2 breast, 2 gastric, 2 esophageal, 2 sarcomas, 1 renal cell, 1 prostate, 1 NSCLC and 1 sphenoid sinus. Response: 20 subjects evaluable: 2 confirmed PRs (NSCLC 8+ wks; Colon 13+ wks, in a patient with prior IRI

exposure) and 13 with SD (8--24+wks). Safety: DLTs were observed at the 6th dose level: 4 subjects with DLTs: 3 diarrhea (one resulting in death due to dehydration/ARF) and one neutropenia. Other possibly related grade 3 and 4 events included one each of: grade 3 diarrhea, grade 3 vomiting, grade 3 neutropenia, grade 3 fatigue, grade 3 compression fracture and arthralgia and pulmonary embolism grade 4. PK: In all 14 subjects analyzed to date the 1:1 molar ratio of IRI to FLOX was maintained for 24 hours and metabolites 5-FU and SN-38 were present in the plasma. **Conclusions:** CPX-1 represents a new approach to developing drug combinations in which drug ratios are pre-selected *in vitro* based on optimal antitumor activity and maintained systemically through pharmacokinetic control. Phase 2 studies are planned with a recommended dose of 210U/m² of CPX-1.

AD

ADVERTISEMENT

Journal of Clinical Oncology®

An American Society of Clinical Oncology Journal

Log In Submit E-Alerts Subscribe

[Open Access/Subscription »](#)

MENU

[Journal of Clinical Oncology](#) > [List of Issues](#) >
[Volume 25, Issue 18, suppl.](#) >

Article Tools

DEVELOPMENTAL THERAPEUTICS: CYTOTOXIC
 CHEMOTHERAPY

Ratiometric dosing of irinotecan (IRI) and floxuridine (FLOX) in a phase I trial: A new approach for enhancing the activity of combination chemotherapy

 Check for updates

G. Batist, W. Miller, L. Mayer, A. Janoff, C. Swenson, A. Louis...

[Show More](#)

Abstract

2549

Background: Like many pairs of chemotherapy agents, the combination of IRI and FLOX displays ratio-dependent activity *in vitro*. CPX-1, a

OPTIONS & TOOLS

ADVERTISEMENT

[Export Citation](#)

[Track Citation](#)

[Add To Favorites](#)

[Rights & Permissions](#)

COMPANION ARTICLES

No companion articles

ARTICLE CITATION

DOI:
 10.1200/jco.2007.25.18_suppl.2549
*Journal of Clinical
 Oncology* 25, no. 18_suppl
 (June 20, 2007) 2549-2549.

Published online June 20,
 2007.

ADVERTISEMENT

CSPC Exhibit 1109
 Page 3 of 339

liposome formulation of IRI:FLOX, was developed to maintain a synergistic 1:1 molar ratio *in vivo*, was highly active in preclinical models, and was evaluated in a phase 1 trial (CLTR0104-101).

Methods: Doses were escalated from 30U/m² (1U= 1 mg IRI + 0.36 mg FLOX) to 270 U/m² given on day 1 and 15 of each 28 day cycle. Adult patients (pts) with advanced solid tumors, ECOG PS≤2, adequate bone marrow, liver, and renal function were eligible; 4 pts per cohort. After defining the MTD, additional pts with CRC were enrolled (extension phase). IRI completed greater than 12 months prior to this trial was allowed in the absence of resistance to IRI. PK was done on day 1 and 15 of the 1st cycle. **Results:** Safety: The dose escalation phase enrolled 24 pts in 6 cohorts and added 2 pts in the 5th cohort (210U/m²; the MTD) after noting dose limiting diarrhea (3 pts) and neutropenia (1 pt) including one death from dehydration and renal failure due to prolonged diarrhea (gr3) & vomiting (gr2) at 270U/m². An additional 7 pts with CRC received 210U/m² in the extension phase. Grade 3/4 adverse events included diarrhea, nausea, vomiting, neutropenia and thrombocytopenia with most occurring at 270U/m². No new toxicities were observed for this combination. Response: 30/33 pts were evaluable with 2 confirmed PRs (NSCLC and CRC), 21 SD and 7 PD. Median PFS was 5.4 mos. (0.3-11.8 mos.) in 15 pts w/CRC. PK: All pts maintained synergistic plasma IRI:FLOX ratios for 24h. IRI and FLOX AUCs (0-inf) were greater for CPX-1 than expected for conventional drugs. AUCs for SN-38 and 5FU at 210U/m² were 0.8 ± 0.1 and 10 ± 8.7 µg-hr/mL, respectively, indicating bioavailability for both drugs. **Conclusion:** CPX-1 was well tolerated in the outpatient setting and evidence of anti-tumor activity was obtained. This is the first clinical evaluation of ratiometric dosing in which a synergistic drug ratio, pre-selected *in vitro* based on optimal anti-tumor activity, was maintained systemically to enhance therapeutic benefit.

Author Disclosure

Employment or Leadership	Consultant or Advisory	Stock Ownership	Other Remuneration

WE RECOMMEND

ADVERTISEMENT

A phase 1b dose-escalation trial of erlotinib, capecitabine and oxaliplatin in metastatic colorectal cancer (MCRC) patients
J. P. Delord, J Clin Oncol, 2016

Phase I dose-escalation trial investigating the safety and tolerability of EPO906 plus estramustine in patients with advanced cancer
M. Wojtowicz, J Clin Oncol, 2016

Phase I and pharmacokinetic (PK) study of IHL-305 (pegylated liposomal irinotecan) in patients with advanced solid tumors
S. F. Jones, J Clin Oncol, 2016

Results of a phase I trial of BAY 43-9006 in combination with oxaliplatin in patients with refractory solid tumors
P. Kupsch, J Clin Oncol, 2016

Phase I evaluation of SF1126, a vascular targeted PI3K inhibitor, administered twice weekly IV in patients with refractory solid tumors
E. G. Chiorean, J Clin Oncol, 2016

A phase I study of oral UFT/leucovorin and irinotecan, plus radiation for locally recurrent rectal cancer
Masataka Ikeda et al., Journal of the Anus, Rectum and Colon, 2017

P01.01 A Phase 1a/1b dose-escalation study of intravenously administered SB 11285 alone and in combination with nivolumab in patients with advanced solid tumors
A ABBAS et al., Jtcc, 2020

Phase I/II intra-patient dose escalation study of vorinostat in children with relapsed solid tumor, lymphoma, or leukemia

ert
ony
Other
Remuneration

CSPC Exhibit 1109
Page 4 of 339

Employment or Leadership	Consultant or Advisory	Stock Ownership
Celator Pharmaceuticals	Celator Pharmaceuticals	Celator Pharmaceuticals
American Society of Clinical Oncology		

Cornelis M. van Tilburg et al. Clin Epigenetics, 2019

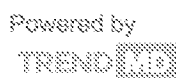
Other Remuneration

A phase 1 dose escalation study of the oncolytic adenovirus enadenotucirev, administered intravenously to patients with epithelial solid tumors (EVOLVE)

Jean-Pascal Machiels et al., Jitc, 2019

What's Your Therapy Selection & Phenotyping Strategy for Severe Asthma with Type 2 Inflammation?

ReachMD



WHAT'S POPULAR

Most Read

Most Cited

Vencou
Thromboembolism
Prophylaxis and
Treatment in Patients
With Cancer: ASCO
Clinical Practice
Guideline Update
Key et al.

Prognostic Index for
Acute- and Lymphoma-
Type Adult T-Cell
Leukemia/Lymphoma
Katsuya et al.

Management of
Immune-Related Adverse
Events in Patients
Treated With Immune
Checkpoint Inhibitor
Therapy: American
Society of Clinical
Oncology Clinical Practice
Guideline
Brahmer et al.

Updated Analysis From
KEYNOTE-189:
Pembrolizumab or
Placebo Plus Pemetrexed

[and Platinum for Previously Untreated Metastatic Nonsquamous Non-Small-Cell Lung Cancer](#)
Gadgeel et al.

[Abernethi Combined With Endocrine Therapy for the Adjuvant Treatment of HR+, HER2-, Node-Positive, High-Risk Early Breast Cancer \(monarch\)](#)
Johnston et al.



QUICK LINKS

Content

[Newest Articles](#)
[Archive](#)
[Meeting Abstracts](#)

Journal Information

[About](#)
[Editorial Roster](#)
[Contact Us](#)
[Permissions](#)

Resources

[Authors](#)
[Reviewers](#)
[Subscribers](#)
[Institutions](#)
[Advertisers](#)

Submit Your Manuscript

[Subscribe to this journal](#)



ASCO FAMILY OF SITES

Journals

[Journal of Clinical Oncology](#)
[JCO Oncology Practice](#)
[JCO Global Oncology](#)
[JCO Clinical Cancer Informatics](#)
[JCO Precision Oncology](#)

Publications

[ASCO Educational Book](#)
[ASCO Daily News](#)
[ASCO Connection](#)
[The ASCO Post](#)
[JCO OP DAIS](#)

Education

[ASCO eLearning](#)
[ASCO Meetings](#)
[Cancer.Net](#)

Other Sites

[ASCO.org](#)
[ASCO Author Services](#)
[ASCO Career Center](#)
[CancerLinQ](#)
[Conquer Cancer Foundation](#)
[TAPUR Study](#)



Treatment Patterns and Clinical Outcomes in Patients With Metastatic Colorectal Cancer Initially Treated with FOLFOX–Bevacizumab or FOLFIRI–Bevacizumab: Results From ARIES, a Bevacizumab Observational Cohort Study

JOHANNA C. BENDELL,^a TANIOS S. BEKAI-SAAB,^b ALLEN L. COHN,^c HERBERT I. HURWITZ,^d
MARK KOZLOFF,^e HALUK TEZCAN,^f NANCY ROACH,^g YONG MUN,^h SUSAN FISH,^h E. DAWN FLICK,^h
DARSHAN DALAL,^h AXEL GROTHEYⁱ

^aSarah Cannon Research Institute, Nashville, Tennessee, USA; ^bThe Ohio State University Medical Center, Columbus, Ohio, USA; ^cRocky Mountain Cancer Center, Denver, Colorado, USA; ^dDuke University Medical Center, Durham, North Carolina, USA; ^eIngalls Hospital and University of Chicago, Harvey, Illinois, USA; ^fKootenai Cancer Center, Coeur d'Alene, Idaho, USA; ^gFightColorectalCancer.org, Patient Advocacy, Alexandria, Virginia, USA; ^hGenentech, Inc., South San Francisco, California, USA; ⁱMayo Clinic College of Medicine, Rochester, Minnesota, USA

Key Words. Bevacizumab • FOLFOX protocol • FOLFIRI protocol • Safety • Treatment outcome

Disclosures: **Tanios S. Bekai-Saab:** Bristol-Myers Squibb, Genentech, Amgen (C/A, H); **Allen L. Cohn:** Novartis, Amgen (H); **Herbert I. Hurwitz:** Genentech, Roche (C/A, RF); GlaxoSmithKline, Amgen (RF); **Mark Kozloff:** Roche, Genentech (H); **Haluk Tezcan:** Roche, Genentech (RF); **Nancy Roach:** Chair of Fight Colorectal Cancer's Board of Directors; **Yong Mun:** Genentech, Roche (E, OI); **Susan Fish:** Genentech, Roche (E, OI); **E. Dawn Flick:** Genentech, Roche (E, OI); **Darshan Dalal:** Genentech, Roche (E, OI); Roche (OI); **Axel Grothey:** Bayer, Genentech (C/A); Genentech (RF). The other author indicated no financial relationships.

(C/A) Consulting/advisory relationship; (RF) Research funding; (E) Employment; (H) Honoraria received; (OI) Ownership interests; (IP) Intellectual property rights/inventor/patent holder; (SAB) Scientific advisory board

ABSTRACT

Background. The Avastin® Registry: Investigation of Effectiveness and Safety (ARIES) study is a prospective, community-based observational cohort study that evaluated the effectiveness and safety of first-line treatment patterns, assessing the impact of chemotherapy choice and treatment duration.

Methods. The ARIES study enrolled patients with metastatic colorectal cancer (mCRC) receiving first-line chemotherapy with bevacizumab and followed them longitudinally. The protocol did not specify treatment regimens or assessments. Analyses included all patients who initiated bevacizumab in combination with either first-line oxaliplatin with infusional 5-fluorouracil and leucovorin (FOLFOX) or irinotecan with infusional 5-fluorouracil

and leucovorin (FOLFIRI). Progression-free survival (PFS) and overall survival (OS) times were estimated using Kaplan–Meier methods. Hazard ratios (HRs) were estimated with multivariate Cox regression analysis, adjusting for potential confounding factors.

Results. In total, 1,550 patients with first-line mCRC were enrolled (median follow-up, 21 months) and most received FOLFOX–bevacizumab ($n = 968$) or FOLFIRI–bevacizumab ($n = 243$) as first-line therapy. The baseline characteristics and median treatment duration were generally similar between subgroups. There were no significant differences in the median PFS (10.3 months vs. 10.2 months) or OS (23.7 months vs. 25.5 months) time between the FOLFOX–bevacizumab and FOLFIRI–

Correspondence: Johanna C. Bendell, M.D., GI Oncology Research and Drug Development Unit, Sarah Cannon Research Institute, 250 25th Avenue N, Suite 100, Nashville, Tennessee 37203, USA. Telephone: 615-329-7423; Fax: 615-329-7523; e-mail: jcbendell@tnonc.com Received May 2, 2012; accepted for publication September 4, 2012; first published online in *The Oncologist Express* on September 26, 2012. ©AlphaMed Press 1083-7159/2012/\$20.00/0 <http://dx.doi.org/10.1634/theoncologist.2012.0190>

CSPC Exhibit 1109

bevacizumab subgroups, respectively, by unadjusted analyses. Multivariate analyses showed FOLFIRI–bevacizumab resulted in a similar PFS (HR, 1.03; 95% confidence interval [CI], 0.88–1.21) and OS (HR, 0.95; 95% CI, 0.78–1.16) outcome as with FOLFOX–bevacizumab. The incidence proportions of bevacizumab-associated

adverse events were similar for FOLFOX- and FOLFIRI-based therapies.

Conclusions. In first-line mCRC patients, the FOLFOX–bevacizumab and FOLFIRI–bevacizumab regimens were associated with similar treatment patterns and clinical outcomes. *The Oncologist* 2012;17:1486–1495

INTRODUCTION

Oxaliplatin with infusional 5-fluorouracil (5-FU) and leucovorin (LV) (FOLFOX) and irinotecan with infusional 5-FU and LV (FOLFIRI) are standard chemotherapy regimens for the treatment of patients with advanced or metastatic colorectal cancer (mCRC) who are appropriate for intensive therapy [1]. Data from comparative, randomized trials indicate that, in the absence of a biologic agent, these regimens appear to be noninferior, and exposure to oxaliplatin, irinotecan, and 5-FU throughout the course of treatment is more important than the sequence of administration [2–4].

Bevacizumab (Avastin®; Genentech, Inc., South San Francisco, CA), a recombinant, humanized monoclonal antibody against vascular endothelial growth factor A, has been shown to result in superior progression-free survival (PFS) and overall survival (OS) outcomes when added to 5-FU–based chemotherapy in patients with previously treated and untreated mCRC [5–7]. The pivotal trial of bevacizumab in mCRC patients demonstrated the benefit of adding the agent to irinotecan with bolus 5-FU and LV (IFL) in first-line treatment [5]. Subsequently, however, the clinical use of IFL diminished with the emergence of the FOLFOX and FOLFIRI regimens [8–10]. Given the similar efficacy profiles of these latter two regimens, along with evidence for the superiority of FOLFIRI–bevacizumab over modified IFL–bevacizumab [2, 9–12], it was assumed that FOLFOX and FOLFIRI could be used interchangeably with bevacizumab as first-line treatment.

Initial data from randomized trials further supported the efficacy of bevacizumab with oxaliplatin-containing regimens [7, 13]. However, the phase III NO16966 trial of oxaliplatin-containing chemotherapy regimens with or without bevacizumab for previously untreated mCRC showed only a modestly better PFS outcome in the bevacizumab-containing arms, without any significant difference in the OS outcome [14, 15]. Importantly though, it was noted that a high percentage of patients did not receive bevacizumab until progressive disease (PD), as was specified in the study protocol, potentially because bevacizumab and chemotherapy were discontinued simultaneously upon the development of unacceptable chemotherapy-related toxicity. A subsequent phase II randomized trial reported that 50% of patients discontinued therapy with FOLFOX–bevacizumab for reasons other than PD [16]. Given the possibility that a significant number of patients treated with oxaliplatin-based regimens stop therapy prematurely because of chemotherapy-related toxicity, some clinicians believe that oxaliplatin-based chemotherapy regimens may not be optimal partners for bevacizumab in practice or clinical trials.

Based on the potential effect of both the chemotherapy partner and the related treatment pattern on outcomes, this

analysis describes the safety and effectiveness of bevacizumab when used in combination with FOLFOX or FOLFIRI in patients with first-line mCRC enrolled in the Avastin® Registry: Investigation of Effectiveness and Safety (ARIES) observational cohort study (OCS) (ClinicalTrials.gov identifier, NCT00388206). The objectives of this analysis of a large community-based cohort were to understand how baseline characteristics influence treatment patterns with first-line FOLFOX–bevacizumab and FOLFIRI–bevacizumab, as well as to describe chemotherapy and bevacizumab treatment patterns and the associated outcomes in these patient subgroups.

MATERIALS AND METHODS

Study Design, Patients, and Treatment

The ARIES study is a prospective OCS that longitudinally follows patients with previously untreated mCRC who are initially treated with chemotherapy plus bevacizumab. The study planned to enroll ~1,500 patients in the first-line mCRC cohort. There were four protocol-specified inclusion criteria: (a) signed informed consent, (b) locally recurrent CRC or mCRC, (c) eligibility for bevacizumab as a component of intended therapy (in the judgment of the treating physician), and (d) first-line chemotherapy plus bevacizumab initiated within 4 months prior to study enrollment. There were no treatments, assessments, or exclusions specified by the protocol, including the dose and frequency of bevacizumab or regimens of chemotherapy (including biologic agents) and the method or frequency of clinical assessments. Notably, no exclusions were made on the basis of the sites of metastasis, the use of concurrent anticoagulation, or the Eastern Cooperative Oncology Group (ECOG) performance status score—criteria used in previous randomized controlled trials for patient exclusion [5, 15]. All treatments, including bevacizumab, and all supportive care were via commercial supplies or local access-to-care mechanisms. The study was approved by a central institutional review board (IRB), the New England IRB, as well as by local IRBs where they existed. All enrolled patients provided informed consent.

Data Collection

Patient data were collected prospectively from study sites via electronic data capture at baseline and subsequently every 3 months until death, withdrawal of consent, loss to follow-up, or study closure. Dates of actual bevacizumab administration, as well as chemotherapy plus biologic treatment start and stop dates, were captured.

Sites were asked to report, within 48 hours of their knowledge, the following adverse events (AEs) termed protocol-

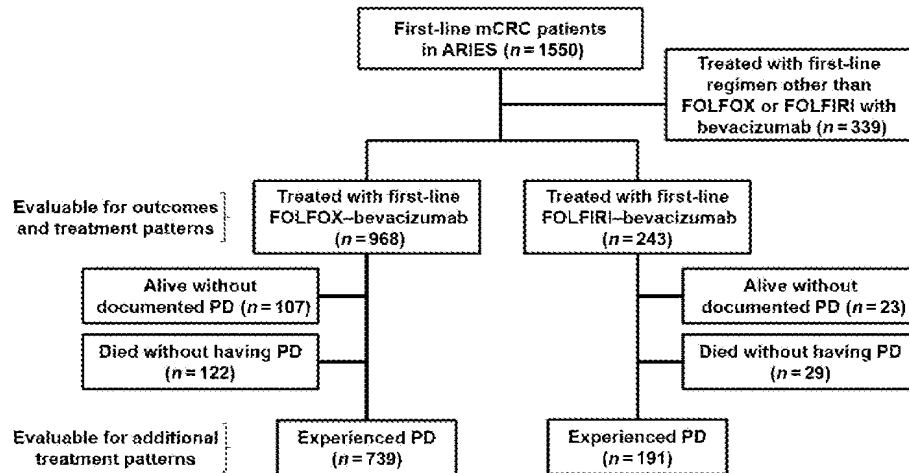


Figure 1. Disposition of analysis population.

Abbreviations: ARIES, Avastin® Registry: Investigation of Effectiveness and Safety; FOLFIRI, irinotecan, infusional 5-fluorouracil, and leucovorin; FOLFOX, oxaliplatin, infusional 5-fluorouracil, and leucovorin; mCRC, metastatic colorectal cancer; PD, progressive disease.

specified AEs, that occurred up to 90 days after the last bevacizumab dose: (a) bevacizumab-select AEs, regardless of severity; (b) any AE that resulted in the discontinuation of bevacizumab; and (c) any serious AE (SAE) suspected to be associated with bevacizumab. Bevacizumab-select AEs included gastrointestinal perforation, new or worsening hypertension requiring medication, severe bleeding events, venous thromboembolic events (VTEs), postoperative wound-bleeding or wound-healing complications, symptomatic congestive heart failure, arterial thromboembolic events, and reversible posterior leukoencephalopathy syndrome, regardless of its association with bevacizumab and whether or not the event was considered serious. AEs were graded according to the National Cancer Institute Common Toxicity Criteria for Adverse Events, version 3.0. An AE was to be classified as serious if the patient outcome was death, was considered life-threatening, resulted in hospitalization, was a disability or congenital anomaly, or required intervention to prevent permanent impairment or damage. Per standard practice, sites were instructed to report any SAE not suspected to be associated with bevacizumab through the MedWatch program.

Statistical Methods and Considerations

This analysis evaluated outcomes in the subgroup of patients who received first-line FOLFOX-bevacizumab or FOLFIRI-bevacizumab at baseline (Fig. 1). Additional data on treatment patterns were obtained for patients who experienced and survived PD, because it was possible to evaluate the use of chemotherapy and bevacizumab from initiation in the metastatic setting until and beyond first PD. PD was determined by the investigator via clinical and/or radiographic assessment.

Baseline characteristics were described using summary statistics. PFS and OS outcomes were measured from the date of initiation of therapy, which was defined as the earlier of chemotherapy or bevacizumab dosing. The PFS time was defined as the time from the start of therapy to investigator-assessed

PD or death from any cause on study. The OS time was defined as the time from the start of therapy to death from any cause. Kaplan-Meier methods, along with 95% confidence intervals (CIs), were used to characterize the distribution of the PFS and OS probabilities. Patients without an event (PD or death) were censored at the study termination or data cutoff date, whichever occurred first.

A Cox proportional hazards model was used to assess the effect of first-line chemotherapy (FOLFOX or FOLFIRI) with bevacizumab on PFS and OS outcomes, adjusting for the following baseline covariates: age, sex, race, ECOG performance status score, serum albumin and alkaline phosphatase levels, site of primary tumor, adjuvant therapy, disease-free interval, and history of cardiovascular disease, diabetes, hypertension, or hypercholesterolemia.

Safety analyses were conducted on all bevacizumab-treated patients, who were defined as those who received at least one dose of bevacizumab on study. Incidence proportions of AEs were estimated for the entire follow-up period, starting from the date of the actual first bevacizumab dose. If a patient had multiple occurrences of the same event, it was only counted once. For patients who started bevacizumab prior to study enrollment, sites were asked to record any AE that occurred prior to study enrollment while on bevacizumab therapy. Protocol-specified AEs with an onset date >90 days after the patient's last bevacizumab dose were excluded.

RESULTS

Enrollment and Follow-Up

In total, 1,550 patients who received first-line bevacizumab-containing therapy for mCRC were enrolled in the ARIES study between November 2006 and January 2008 from 248 study sites in 43 U.S. states. The sites are geographically diverse and include community-based practices (~75%), academic centers (~9%), and other institutions, mainly hospitals

(~16%). As of September 20, 2010, the median follow-up time was 21 months (range, 0.3–48.2 months). Of the 1,550 first-line mCRC patients, 968 (62.5%) received FOLFOX–bevacizumab and 243 (15.7%) received FOLFIRI–bevacizumab as first-line therapy (Fig. 1). Approximately 76.8% (930 of 1,211) of patients treated with FOLFOX–bevacizumab or FOLFIRI–bevacizumab had experienced PD at the time of this analysis. More than 90% of the PD events were determined using a scan (e.g., computed tomography, positron emission tomography, or magnetic resonance imaging).

Patient Baseline Characteristics

Baseline characteristics for all first-line mCRC patients enrolled in the ARIES study ($n = 1,550$) and patients who received FOLFOX or FOLFIRI with bevacizumab ($n = 1,211$) are summarized in Table 1. Patient and disease characteristics were generally similar to those of the overall first-line CRC population and across first-line chemotherapy subgroups, with a few notable exceptions: a higher percentage of patients in the FOLFIRI–bevacizumab subgroup were treated for recurrent disease (60.9% vs. 27.3%), had received prior adjuvant therapy (53.5% vs. 16.0%), and had surgical resection of their initial disease (90.9% vs. 77.2%) than in the FOLFOX–bevacizumab subgroup, respectively. There did not appear to be substantial differences in the use of concomitant medications between the chemotherapy subgroups.

Treatment Patterns

Among patients treated with first-line FOLFOX–bevacizumab and FOLFIRI–bevacizumab, the median duration of first-line bevacizumab and chemotherapy treatment as well as the median total duration of both bevacizumab and chemotherapy were similar, irrespective of the first-line chemotherapy used (Table 2). In the study, bevacizumab was stopped (e.g., temporarily held, permanently discontinued) before PD in >59% of patients who survived first PD, with a slightly higher percentage of patients in the FOLFIRI–bevacizumab subgroup halting bevacizumab before PD (66.0% vs. 59.9%). Among patients who survived first PD, the most common reasons for bevacizumab being temporarily held for >28 days in both the FOLFOX–bevacizumab and FOLFIRI–bevacizumab subgroups were chemotherapy holiday, AE or SAE, and planned surgery (Table 3). The most common reasons for bevacizumab being permanently discontinued >28 days prior to PD were AEs or SAEs, achievement of maximum benefit, and physician decision to discontinue. Of the patients who permanently discontinued bevacizumab prior to PD, approximately two thirds (FOLFOX–bevacizumab, 67.5%; FOLFIRI–bevacizumab, 65.2%) had no further treatment with bevacizumab, whereas subsequent use of bevacizumab within 2 months after PD was seen in 17.3% of FOLFOX–bevacizumab and 18.2% of FOLFIRI–bevacizumab patients. In cases in which bevacizumab was held temporarily, 47.4% of patients in the FOLFIRI group and 55.3% of those in the FOLFOX group restarted bevacizumab therapy within 2 months after PD. In 46 cases, disease progression was cited as a reason for discontinuing bevacizumab prior to PD, which

may reflect a diagnosis of clinical progression rather than a confirmation of radiographic progression.

Although similar percentages of patients in both subgroups continued chemotherapy until PD (53.9%–56.0%), a greater percentage of patients treated with FOLFOX–bevacizumab had a change in their first-line chemotherapy regimen than those treated with FOLFIRI–bevacizumab (23.7% vs. 16.2%, respectively) (Table 2). Any change in the regimen, including discontinuing oxaliplatin or irinotecan, was recorded as a change.

Overall, a higher percentage of patients in the FOLFOX–bevacizumab subgroup than in the FOLFIRI–bevacizumab subgroup were exposed to all three active chemotherapies (i.e., 5-FU, oxaliplatin, and irinotecan) in the metastatic setting (59.1% vs. 34.6%, respectively). Approximately 85%–90% of patients who survived first PD across the chemotherapy subgroups received second-line therapy, with 63.5% of patients in the FOLFOX–bevacizumab subgroup receiving second-line irinotecan-containing therapy and 21.0% of patients in the FOLFIRI–bevacizumab subgroup receiving second-line oxaliplatin-containing therapy (Table 2). In addition, 29.4% and 37.0% of patients in the FOLFOX–bevacizumab and FOLFIRI–bevacizumab subgroups, respectively, received an epidermal growth factor receptor inhibitor as part of second-line treatment.

Effectiveness Outcomes

The median PFS estimates were similar for first-line mCRC patients who were treated with FOLFOX–bevacizumab (10.3 months; 95% CI, 9.9–11.0) and for those treated with FOLFIRI–bevacizumab (10.2 months; 95% CI, 9.0–11.4) (Table 4, Fig. 2A). Patients treated with FOLFIRI–bevacizumab (25.5 months; 95% CI, 20.9–28.4) had a numerically higher median OS time than those treated with FOLFOX–bevacizumab (23.7 months; 95% CI, 22.1–25.6), although the 95% CIs did overlap (Fig. 2B). Outcomes in these chemotherapy subgroups are consistent with those reported in the overall first-line CRC population. A multivariate Cox proportional hazards model was used to assess the effect of first-line chemotherapy with bevacizumab on PFS and OS outcomes, adjusting for potential confounding factors. In the multivariate analysis, the use of FOLFIRI–bevacizumab resulted in PFS (hazard ratio [HR], 1.03; 95% CI, 0.88–1.21; $p = .688$) and OS (HR, 0.95; 95% CI, 0.78–1.16; $p = .625$) probability profiles similar to those seen with FOLFOX–bevacizumab.

Protocol-Specified AEs

Observed incidence proportions of bevacizumab-associated AEs in first-line mCRC patients treated with either FOLFOX–bevacizumab or FOLFIRI–bevacizumab were largely similar (Table 5). A higher proportion of patients treated with FOLFIRI–bevacizumab experienced a VTE than those treated with FOLFOX–bevacizumab (13.2% vs. 6.4%, respectively). Patients in the FOLFOX–bevacizumab subgroup had a slightly higher incidence of grade 3–5 bleeding events, postoperative wound-healing or wound-bleeding complications,

Table 1. Selected baseline patient and disease characteristics by first-line chemotherapy regimen

Characteristic	All first-line CRC patients (n = 1,550)	First-line regimen	
		FOLFOX-BV (n = 968)	FOLFIRI-BV (n = 243)
Median (range) age, yrs	62 (18–92)	61 (18–88)	62 (29–88)
≥75 years, n (%)	234 (15.1)	116 (12.0)	26 (10.7)
Female sex, n (%)	669 (43.2)	413 (42.7)	108 (44.4)
Race, n (%)			
White	1,251 (80.7)	784 (81.0)	193 (79.4)
Black	199 (12.8)	116 (12.0)	41 (16.9)
Other	100 (6.5)	68 (7.0)	9 (3.7)
ECOG PS score, n (%)			
0	761 (49.1)	472 (48.8)	123 (50.6)
1	659 (42.5)	415 (42.9)	99 (40.7)
≥2	109 (7.0)	70 (7.2)	18 (7.4)
Unknown	21 (1.4)	11 (1.1)	3 (1.2)
Disease categorization, n (%)			
Metastatic	1,488 (96.0)	935 (96.6)	234 (96.3)
Locally advanced and unresectable	62 (4.0)	33 (3.4)	9 (3.7)
Site of primary tumor, n (%)			
Colon	1,179 (76.1)	719 (74.3)	183 (75.3)
Rectum	366 (23.6)	245 (25.3)	60 (24.7)
Unknown	5 (0.3)	4 (0.4)	0 (0)
Disease-free interval, ^a n (%)			
De novo (no interval)	992 (64.0)	704 (72.7)	95 (39.1)
Recurrent			
<12 months	156 (10.1)	68 (7.0)	42 (17.3)
12 to <24 months	160 (10.3)	54 (5.6)	64 (26.3)
≥24 months	242 (15.6)	142 (14.7)	42 (17.3)
Surgical resection of initial disease, n (%)	1,253 (80.8)	747 (77.2)	221 (90.9)
Prior adjuvant therapy, n (%)	385 (24.8)	155 (16.0)	130 (53.5)
History of cardiovascular disease, ^b n (%)	351 (22.6)	199 (20.6)	58 (23.9)
History of diabetes mellitus, ^b n (%)	245 (15.8)	140 (14.5)	53 (21.8)
Use of selected concomitant medications, ^c n (%)			
Prophylactic anticoagulation	101 (6.5)	67 (6.9)	16 (6.6)
Therapeutic anticoagulation	72 (4.6)	43 (4.4)	11 (4.5)
Antiplatelet	238 (15.4)	141 (14.6)	38 (15.6)
Cholesterol lowering	347 (22.4)	208 (21.5)	57 (23.5)
Antihypertensive or cardiovascular	739 (47.7)	451 (46.6)	120 (49.4)
First-line chemotherapy, n (%)			
FOLFOX	968 (62.5)	968 (100)	0 (0)
FOLFIRI	243 (15.7)	0 (0)	243 (100)
CAPEOX	133 (8.6)	0 (0)	0 (0)
XELIRI	22 (1.4)	0 (0)	0 (0)
Bolus 5-fluorouracil and leucovorin	51 (3.3)	0 (0)	0 (0)
Capecitabine	44 (2.8)	0 (0)	0 (0)
Other ^d	89 (5.7)	0 (0)	0 (0)

^aInterval between resection of the primary tumor and metastasis.

^bThis condition required drug therapy.

^cA patient could receive more than one therapy or class of medication.

^dIncludes IFL, infusional 5-fluorouracil, investigational drug regimen, and other.

Abbreviations: BV, bevacizumab; CAPEOX, capecitabine and oxaliplatin; CRC, colorectal cancer; ECOG PS, Eastern Cooperative Oncology Group performance status; FOLFIRI, irinotecan and infusional 5-fluorouracil and leucovorin; FOLFOX, oxaliplatin and infusional 5-fluorouracil and leucovorin; IFL, irinotecan and bolus 5-fluorouracil and leucovorin; PD, progressive disease; XELIRI, capecitabine and irinotecan.

Table 2. BV and chemotherapy treatment patterns and duration by first-line chemotherapy regimen

Treatment pattern	First-line regimen	
	FOLFOX–BV (<i>n</i> = 968)	FOLFIRI–BV (<i>n</i> = 243)
BV duration		
Median (range) first-line BV duration, mos	4.9 (0.03–36.8)	4.4 (0.03–35.2)
Median (range) total BV duration, mos	6.7 (0.03–43.5)	5.9 (0.03–35.2)
BV treatment pattern		
	(<i>n</i> = 739) ^a	(<i>n</i> = 191) ^a
Continued BV to PD, <i>n</i> (%)	296 (40.1)	65 (34.0)
Stopped BV before PD, <i>n</i> (%)	443 (59.9)	126 (66.0)
No BV within 28 days, <i>n</i> (%)	13 (1.8)	3 (1.6)
BV temporarily held, <i>n</i> (%)	199 (26.9)	57 (29.8)
BV permanently discontinued, <i>n</i> (%)	231 (31.3)	66 (34.6)
Median (range) time from last BV dose to PD, mos	5.3 (0.03–31.5)	6.0 (0.03–31.3)
CT duration		
Median (range) first-line CT duration, mos	6.1 (0.03–36.4)	6.0 (0.03–31.3)
Median (range) total CT duration, mos	11.5 (0.1–45.3)	10.5 (0.03–41.6)
CT treatment patterns		
	(<i>n</i> = 739) ^a	(<i>n</i> = 191) ^a
Continued the same CT to PD, <i>n</i> (%)	223 (30.2)	76 (39.8)
Changed CT before PD, <i>n</i> (%)	175 (23.7)	31 (16.2)
Stopped CT before PD, <i>n</i> (%)	341 (46.1)	84 (44.0)
Exposure to all 3 active chemotherapies^b in the metastatic setting, <i>n</i> (%)		
	572 (59.1)	84 (34.6)
Second-line treatment, <i>n</i> (%)		
	(<i>n</i> = 663)	(<i>n</i> = 162)
Oxaliplatin-containing regimen ^c	92 (13.9)	34 (21.0)
Irinotecan-containing regimen ^d	421 (63.5)	83 (51.2)
Treatment with an EGFR inhibitor ^e	195 (29.4)	60 (37.0)

^aPatients who survived first PD.

^b5-FU, oxaliplatin, and irinotecan.

^cFOLFOX or CAPEOX.

^dFOLFIRI, XELIRI, IFL, or irinotecan monotherapy.

^eOverlapping with other second-line treatments.

Abbreviations: 5-FU, 5-fluorouracil; BV, bevacizumab; CAPEOX, capecitabine and oxaliplatin; CRC, colorectal cancer; CT, chemotherapy; EGFR, epidermal growth factor receptor; FOLFIRI, irinotecan and infusional 5-FU and LV; FOLFOX, oxaliplatin and infusional 5-FU and LV; IFL, irinotecan with bolus 5-FU and LV; LV, leucovorin; PD, progressive disease; XELIRI, capecitabine and irinotecan.

and arterial thromboembolic events than patients in the FOLFIRI–bevacizumab subgroup.

DISCUSSION

One of the advantages of an OCS is that it allows for outcome analyses in less-selected, real-world patient populations. This analysis from the ARIES OCS sought to evaluate treatment patterns and clinical outcomes in patients with mCRC who were treated in the first-line setting with FOLFOX–bevacizumab or FOLFIRI–bevacizumab. Given recent evidence suggesting that a high percentage of patients enrolled in clinical trials discontinue bevacizumab prior to PD [14–16], the ARIES study affords an opportunity to directly compare the two chemotherapy backbones to determine if the choice of regimen affects the

duration of treatment and the effectiveness of bevacizumab in clinical practice.

The majority of first-line mCRC patients enrolled in the ARIES study were treated with FOLFOX–bevacizumab, as has been reported in previous studies [17, 18]. This is reflective of practice patterns in the U.S. and is likely a result, in part, of perceived differences in the toxicity profiles of FOLFOX [19] and FOLFIRI [20]. There were a small number of notable discrepancies in the baseline characteristics of patients receiving FOLFOX–bevacizumab compared with those receiving FOLFIRI–bevacizumab in the ARIES study, which may have influenced treatment choice. More patients receiving FOLFIRI–bevacizumab had recurrent disease at enrollment and had received prior adjuvant therapy, both characteristics that

Table 3. Reasons for temporarily holding or permanently discontinuing BV treatment for >28 days prior to PD in patients who survived first PD

Reason, <i>n</i> (%)	Reported temporary hold of BV		Reported permanent discontinuation of BV	
	FOLFOX-BV (<i>n</i> = 199)	FOLFIRI-BV (<i>n</i> = 57)	FOLFOX-BV (<i>n</i> = 231)	FOLFIRI-BV (<i>n</i> = 66)
AE or SAE	63 (31.7)	17 (29.8)	60 (26.0)	25 (37.9)
Chemotherapy holiday	60 (30.2)	20 (35.1)	3 (1.3)	3 (4.5)
Completed planned course	2 (1.0)	1 (1.8)	7 (3.0)	1 (1.5)
Disease progression ^a	5 (2.5)	1 (1.8)	32 (13.9)	8 (12.1)
Lost to follow-up	NA	NA	1 (0.4)	0 (0.0)
Maximum benefit achieved	14 (7.0)	6 (10.5)	54 (23.4)	14 (21.2)
Other	2 (1.0)	2 (3.5)	NA	NA
Patient discontinues	5 (2.5)	2 (3.5)	17 (7.4)	3 (4.5)
Physician discontinues	12 (6.0)	1 (1.8)	44 (19.0)	10 (15.2)
Planned surgery	36 (18.1)	7 (12.3)	13 (5.6)	2 (3.0)

^aDisease progression was cited as the reason for holding or discontinuing BV, although the actual date of progressive disease was reported more than 28 days after the stoppage of treatment.

Abbreviations: AE, adverse event; BV, bevacizumab; FOLFIRI, irinotecan and infusional 5-fluorouracil and leucovorin; FOLFOX, oxaliplatin and infusional 5-fluorouracil and leucovorin; NA, not applicable; PD, progressive disease; SAE, serious AE.

Table 4. Effectiveness by first-line chemotherapy regimen as of September 20, 2010

Effectiveness outcome	All first-line CRC patients (<i>n</i> = 1,550)	First-line regimen	
		FOLFOX-BV (<i>n</i> = 968)	FOLFIRI-BV (<i>n</i> = 243)
Patients with PD, <i>n</i> (%)	1174 (75.7)	739 (76.3)	191 (78.6)
Deaths, <i>n</i> (%)	1002 (64.6)	627 (64.8)	152 (62.6)
Best first-line response, %			
Complete response	19.6	21.3	20.6
Partial response	33.8	35.1	31.7
Stable disease	31.1	30.2	33.7
Median (95% CI) PFS, mos	10.2 (9.8–10.5)	10.3 (9.9–11.0)	10.2 (9.0–11.4)
Median (95% CI) OS, mos	23.3 (21.6–25.0)	23.7 (22.1–25.6)	25.5 (20.9–28.4)
1-year survival rate (95% CI)	76.3% (74.2%–78.5%)	78.0% (75.3%–80.6%)	77.4% (72.0%–82.7%)

Abbreviations: BV, bevacizumab; CI, confidence interval; CRC, colorectal cancer; FOLFIRI, irinotecan and infusional 5-fluorouracil and leucovorin; FOLFOX, oxaliplatin and infusional 5-fluorouracil and leucovorin; OS, overall survival; PD, progressive disease; PFS, progression-free survival.

are associated with a poorer prognosis. The choice of FOLFIRI in these patients was logical given the likelihood of exposure to oxaliplatin during treatment for early-stage colon cancer [21, 22]. Taken together, these data suggest that physicians in the U.S. prefer to use FOLFOX with bevacizumab and that the substitution of an alternate chemotherapy regimen is a tailored response to certain patient and disease characteristics.

Of the patients receiving first-line FOLFOX-bevacizumab who survived first PD, 13.9% went on to receive an oxaliplatin-containing regimen as second-line chemotherapy.

We speculate that this population largely comprised of patients who were switched to an alternate first-line chemotherapy prior to PD and later resumed oxaliplatin as part of what the treating investigator defined as second-line therapy.

We did not observe any significant differences in treatment patterns between FOLFOX-bevacizumab and FOLFIRI-bevacizumab. The first-line duration and total duration of both bevacizumab and chemotherapy treatment were roughly equivalent with each regimen. Collectively, the data show that, in the nontrial management of patients who experience PD fol-

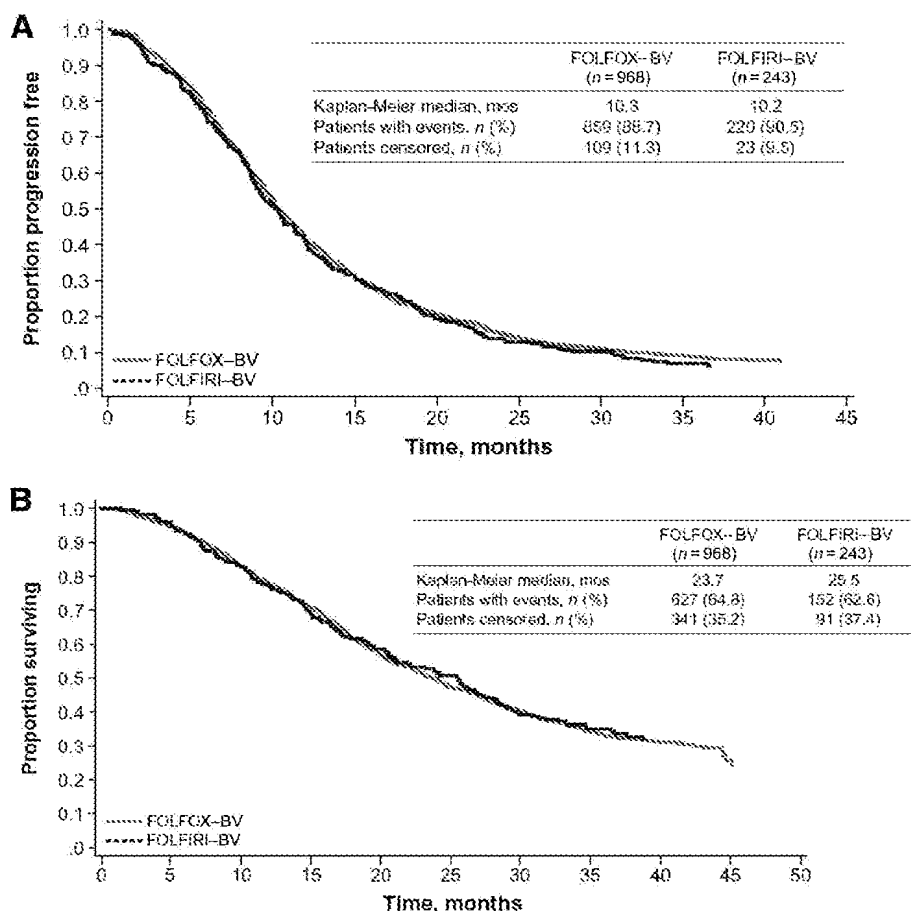


Figure 2. Kaplan-Meier estimates of survival outcomes by first-line chemotherapy regimen. **(A):** Progression-free survival probability. **(B):** Overall survival probability.

Abbreviations: BV, bevacizumab; FOLFIRI, irinotecan, infusional 5-fluorouracil, and leucovorin; FOLFOX, oxaliplatin, infusional 5-fluorouracil, and leucovorin.

lowing therapy for first-line mCRC, bevacizumab is stopped in ~60% of patients before PD. Notably, nearly half of these patients have bevacizumab treatment temporarily discontinued. All chemotherapy was stopped in ~45% of patients before PD, irrespective of the chemotherapy backbone used. AEs, irrespective of their association with bevacizumab, were cited as the reason for stopping bevacizumab prior to PD in ~30% of patients who had a temporary hold or permanent discontinuation. Additionally, chemotherapy holiday, achievement of maximum benefit, and physician decision were key reasons for stopping bevacizumab. Thus, it appears that the decision to switch or stop chemotherapy increases the probability of discontinuing bevacizumab at the time of treatment change. This apparent treatment practice has broad-reaching implications both for clinical trial design and outcomes. In particular, survival benefits with bevacizumab have been reported from clinical trials in which bevacizumab was largely continued until PD [5–7, 9]. Furthermore, several analyses have suggested an association between bevacizumab duration and efficacy [15, 23, 24], which supports data from a phase III study that recently reported a significantly better OS outcome with the continuation of bevacizumab beyond first progression for mCRC [25].

The safety profiles of FOLFOX–bevacizumab and FOLFIRI–bevacizumab appeared to be similar with regard to the overall incidence of bevacizumab-associated SAEs and nonserious AEs. No new or unexpected AEs with a suspected relation to bevacizumab were reported. An observed imbalance in VTEs between the two subgroups was noted, but the overall incidence proportion of VTEs in the first-line mCRC population (7.2%) was within the range reported previously [26]. It is also important to note that the ARIES OCS only collected information on protocol-specified AEs; thus, the incidence proportions of all SAEs and nonserious AEs with a possible or probable relation to chemotherapy treatment are not evaluable.

With regard to study limitations, this analysis is dependent on the accurate and timely reporting of events by investigators and study sites. Also, because patients could be enrolled up to 4 months after the initiation of treatment, the timing of enrollment may have affected the inclusion of patients with early progression or death events, as well as the collection of data on AEs occurring prior to study participation. It should also be noted that the ARIES study primarily collected data on bevacizumab-associated AEs, and differences in chemotherapy-related toxicities between the FOLFOX–bevacizumab and FOLFIRI–bevacizumab regimens were not evaluated.

Table 5. Bevacizumab-associated adverse events by first-line chemotherapy regimen

AE, n (%)	All first-line CRC patients (n = 1,550)	First-line regimen	
		FOLFOX–BV (n = 968)	FOLFIRI–BV (n = 243)
Patients with any protocol-specified AE ^{a,b}	345 (22.3)	217 (22.4)	66 (27.2)
Patients with a BV-associated SAE	154 (9.9)	98 (10.1)	31 (12.8)
Protocol-specified AE by type			
GI perforation (any grade)	14 (0.9)	11 (1.1)	1 (0.4)
Bleeding event (grade 3–5)	47 (3.0)	34 (3.5)	3 (1.2)
Postoperative wound-healing or wound-bleeding complication ^c (any grade)	12/339 (3.5)	11/223 (4.9)	1/62 (1.6)
ATE ^d (any grade)	35 (2.3)	29 (3.0)	1 (0.4)
VTE ^e (any grade)	111 (7.2)	62 (6.4)	32 (13.2)
New or worsening hypertension requiring medication	127 (8.2)	89 (9.2)	21 (8.6)

^aInclude select BV AEs regardless of severity, any AEs that result in the discontinuation of BV, and any SAEs suspected to be associated with BV. BV-select AEs include GI perforation; new or worsening hypertension that requires medication, severe bleeding events, VTEs, postoperative wound-bleeding or -healing complications, symptomatic congestive heart failure, ATEs, and reversible posterior leukoencephalopathy syndrome.

^bPatients may have had more than 1 type of event.

^cDenominator is equal to the number of patients with postbaseline surgery.

^dATEs include myocardial infarction, cerebral vascular accident, transient ischemic attack, and sudden cardiac death.

^eVTEs include deep vein thrombosis and pulmonary emboli.

Abbreviations: AE, adverse event; ATE, arterial thromboembolic event; BV, bevacizumab; CRC, colorectal cancer; FOLFIRI, irinotecan and infusional 5-fluorouracil and leucovorin; FOLFOX, oxaliplatin and infusional 5-fluorouracil and leucovorin; GI, gastrointestinal; SAE, serious AE; VTE, venous thromboembolic event.

In the ARIES study, there did not appear to be significant differences in PFS or OS outcomes when either FOLFOX or FOLFIRI was combined with bevacizumab as first-line treatment for mCRC, despite some differences in the baseline characteristics that suggest a poorer prognosis for patients receiving first-line FOLFIRI–bevacizumab. Importantly, imbalances in baseline characteristics did not result in disparities in the total duration of chemotherapy or bevacizumab administered in each chemotherapy subgroup. Multivariate analyses, which adjusted for differences in exposure to adjuvant therapy and the disease-free interval, showed the estimated PFS and OS probability profiles of the two regimens to be equivalent, further supporting the interchangeability of first-line FOLFOX and FOLFIRI when used in combination with bevacizumab. As a result of the largely unrestricted enrollment of patients in the ARIES study, this analysis represents the comparative effectiveness of these chemotherapy backbones in the overall mCRC population for whom the regimen and management were not dictated by trial protocol. However, there may be certain subgroups of patients who benefit preferentially from one of the chemotherapy backbones; for example, excision repair crosscomplementing 1 may act as a resistance marker for platinum-based therapy [27, 28]. For that reason, a prospective, randomized study is actively evaluating potential differences in efficacy between the FOLFOX–bevacizumab and FOLFIRI–bevacizumab regimens according to biomarker stratification [29].

CONCLUSIONS

Results from the ARIES study suggest that both first-line FOLFOX and first-line FOLFIRI are equally compatible chemotherapy partners for bevacizumab. Similarities between the two regimens were observed with respect to both treatment patterns and effectiveness outcomes. These results refute the notion that FOLFOX–bevacizumab is associated with inferior clinical efficacy or a higher incidence of treatment discontinuation than with FOLFIRI–bevacizumab. The observed frequency of stopping chemotherapy and bevacizumab before PD has broader implications on how clinical trial endpoints are designed, and it further underscores the need for a more explicit understanding that the discontinuation of chemotherapy prior to PD need not necessitate bevacizumab stoppage, particularly if the reason for discontinuation is cumulative toxicity resulting from individual components of the chemotherapy regimen. Further research is warranted and ongoing to identify specific subgroups of the mCRC population that may benefit more from one chemotherapy backbone than the other.

ACKNOWLEDGMENTS

The authors take full responsibility for the content of the manuscript. Support for third-party writing assistance for this manuscript, furnished by Glen M. Miller, Ph.D., was provided by Genentech, Inc.

Data from this analysis were previously presented at the 2011 Gastrointestinal Cancers Symposium, Bendell JC, CSPE Exhibit 1109

Bekaii-Saab TS, Cohn AL et al. Similarities in treatment patterns and clinical outcomes in patients with metastatic colorectal cancer initially treated with FOLFOX/BV or FOLFIRI/BV:

Results from ARIES, a bevacizumab observational study. *J Clin Oncol* 2011;29.

The ARIES study was funded by Genentech, Inc.

REFERENCES

- National Comprehensive Cancer Network. NCCN Clinical Practice Guidelines in Oncology: Colon Cancer, version 1.2012. Available at http://www.nccn.org/professionals/physician_gls/f_guidelines.asp, accessed September 22, 2011.
- Tournigand C, André T, Achille E et al. FOLFIRI followed by FOLFOX6 or the reverse sequence in advanced colorectal cancer: A randomized GERCOR study. *J Clin Oncol* 2004;22:229–237.
- Colucci G, Gebbia V, Paoletti G et al. Phase III randomized trial of FOLFIRI versus FOLFOX4 in the treatment of advanced colorectal cancer: A multicenter study of the Gruppo Oncologico Dell'Italia Meridionale. *J Clin Oncol* 2005;23:4866–4875.
- Grothey A, Sargent D, Goldberg RM et al. Survival of patients with advanced colorectal cancer improves with the availability of fluorouracil-leucovorin, irinotecan, and oxaliplatin in the course of treatment. *J Clin Oncol* 2004;22:1209–1214.
- Hurwitz H, Fehrenbacher L, Novotny W et al. Bevacizumab plus irinotecan, fluorouracil, and leucovorin for metastatic colorectal cancer. *N Engl J Med* 2004;350:2335–2342.
- Kabbinavar FF, Hambleton J, Mass RD et al. Combined analysis of efficacy: The addition of bevacizumab to fluorouracil/leucovorin improves survival for patients with metastatic colorectal cancer. *J Clin Oncol* 2005;23:3706–3712.
- Giantonio BJ, Catalano PJ, Meropol NJ et al. Bevacizumab in combination with oxaliplatin, fluorouracil, and leucovorin (FOLFOX4) for previously treated metastatic colorectal cancer: Results from the Eastern Cooperative Oncology Group Study E3200. *J Clin Oncol* 2007;25:1539–1544.
- Goldberg RM, Sargent DJ, Morton RF et al. Randomized controlled trial of reduced-dose bolus fluorouracil plus leucovorin and irinotecan or infused fluorouracil plus leucovorin and oxaliplatin in patients with previously untreated metastatic colorectal cancer: A North American Intergroup trial. *J Clin Oncol* 2006;24:3347–3353.
- Fuchs CS, Marshall J, Mitchell B et al. Randomized, controlled trial of irinotecan plus infusional, bolus, or oral fluoropyrimidines in first-line treatment of metastatic colorectal cancer: Results from the BICC-C study. *J Clin Oncol* 2007;25:4779–4786.
- Fuchs CS, Marshall J, Barneco J. Randomized, controlled trial of irinotecan plus infusional, bolus, or oral fluoropyrimidines in first-line treatment of metastatic colorectal cancer: Updated results from the BICC-C study. *J Clin Oncol* 2008;26:689–690.
- Sobrero A, Ackland S, Clarke S et al. Phase IV study of bevacizumab in combination with infusional fluorouracil, leucovorin and irinotecan (FOLFIRI) in first-line metastatic colorectal cancer. *Oncology* 2009;77:113–119.
- Kopetz S, Hoff PM, Morris JS et al. Phase II trial of infusional fluorouracil, irinotecan, and bevacizumab for metastatic colorectal cancer: Efficacy and circulating angiogenic biomarkers associated with therapeutic resistance. *J Clin Oncol* 2010;28:453–459.
- Hochster HS, Hart LL, Ramanathan RK et al. Safety and efficacy of oxaliplatin and fluoropyrimidine regimens with or without bevacizumab as first-line treatment of metastatic colorectal cancer: Results of the TREE study. *J Clin Oncol* 2008;26:3523–3529. Erratum in: *J Clin Oncol* 2008;26:4697.
- Saltz LB, Clarke S, Díaz-Rubio E et al. Bevacizumab (Bev) in combination with XELOX or FOLFOX4: Updated efficacy results from XELOX-1/NO16966, a randomized phase III trial in first-line metastatic colorectal cancer. *J Clin Oncol* 2007;25(18 suppl):170s.
- Saltz LB, Clarke S, Díaz-Rubio E et al. Bevacizumab in combination with oxaliplatin-based chemotherapy as first-line therapy in metastatic colorectal cancer: A randomized phase III study. *J Clin Oncol* 2008;26:2013–2019.
- Berlin J, Bendell J, Hart LL et al. A phase 2, randomized, double-blind, placebo-controlled study of hedgehog pathway inhibitor (HPI) GDC-0449 in patients with previously untreated metastatic colorectal cancer (mCRC). *Ann Oncol* 2010;21(suppl 8):viii10.
- Kozloff M, Yood MU, Berlin J et al. Clinical outcomes associated with bevacizumab-containing treatment of metastatic colorectal cancer: The BRiTE observational cohort study. *The Oncologist* 2009;14:862–870.
- van Cutsem E, Rivera F, Berry S et al. Safety and efficacy of first-line bevacizumab with FOLFOX, XELOX, FOLFIRI and fluoropyrimidines in metastatic colorectal cancer: The BEAT study *Ann Oncol* 2009;20:1842–1847.
- Eloxatin [package insert]. Bridgewater, NJ: Sanofi-Aventis, 2009.
- Camptosar [package insert]. New York: Pharmacia & Upjohn Co, 2010.
- André T, Boni C, Mounedji-Boudiaf L et al. Oxaliplatin, fluorouracil, and leucovorin as adjuvant treatment for colon cancer. *N Engl J Med* 2004;350:2343–2351.
- Kuebler JP, Wieand HS, O'Connell MJ et al. Oxaliplatin combined with weekly bolus fluorouracil and leucovorin as surgical adjuvant chemotherapy for stage II and III colon cancer: Results from NSABP C-07. *J Clin Oncol* 2007;25:2198–2204.
- Grothey A, Sugrue MM, Purdie DM et al. Bevacizumab beyond first progression is associated with prolonged overall survival in metastatic colorectal cancer: Results from a large observational cohort study (BRiTE). *J Clin Oncol* 2008;26:5326–5334.
- Grothey A, Bekaii-Saab TS, Hurwitz H et al. Cumulative exposure to bevacizumab (BV) after progression correlates with increased survival in patients (pts) with metastatic colorectal cancer (mCRC): A time-dependent analysis of the ARIES observational cohort study. *Eur J Cancer* 2011;47(suppl 1):395.
- F. Hoffman-La Roche. Investor Update: Avastin-Based Regimen Extends Survival When Continued Beyond Initial Treatment in Patients with Metastatic Colorectal Cancer. Available at http://www.roche.com/investors/ir_update/inv-update-2012-01-26.htm, accessed March 26, 2012.
- Hurwitz H, Saltz LB, Van Cutsem E et al. Venous thromboembolic events with chemotherapy plus bevacizumab: A pooled analysis of patients in randomized phase II and III studies. *J Clin Oncol* 2011;29:1757–1764.
- Metzger R, Leichman CG, Danenberg KD et al. ERCC1 mRNA levels complement thymidylate synthase mRNA levels in predicting response and survival for gastric cancer patients receiving combination cisplatin and fluorouracil chemotherapy. *J Clin Oncol* 1998;16:309–316.
- Griminger PP, Shi M, Barrett C et al. TS and ERCC-1 mRNA expressions and clinical outcome in patients with metastatic colon cancer in CONFIRM-1 and -2 clinical trials. *Pharmacogenomics J* 2011 July 26 [Epub ahead of print]. doi:10.1038/tpj.2011.29.
- ClinicalTrials.gov. Study of Bevacizumab/mFOLFOX6 Versus Bevacizumab/FOLFIRI with Biomarker Stratification in Patients with Previously Untreated Metastatic Colorectal Cancer (NCT01374425). Available at <http://clinicaltrials.gov/ct2/show/NCT01374425>, accessed March 26, 2012.

Liposomal Irinotecan Achieves Significant Survival and Tumor Burden Control in a Triple Negative Breast Cancer Model of Spontaneous Metastasis

Nicholas Bernards,^{†,‡} Manuela Ventura,^{†,‡} Inga B. Fricke,^{†,§} Bart S. Hendriks,[‡] Jonathan Fitzgerald,[‡] Helen Lee,[†] and Jinzi Zheng^{*,†,§}

[†]TECHNA Institute for the Advancement of Technology for Health, University Health Network, Toronto, Ontario M5G 1L7, Canada

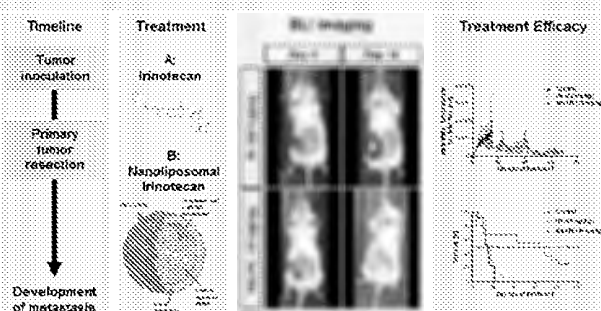
[‡]Merrimack Pharmaceuticals, Inc., Cambridge, Massachusetts 02139, United States

[§]Institute of Biomaterial and Biomedical Engineering, University of Toronto, Toronto, Ontario M5S 3G9, Canada

Supporting Information

ABSTRACT: Triple negative breast cancer (TNBC) represents a significant therapeutic challenge due to its highly aggressive nature and lack of effective treatment options. Liposomal irinotecan (nal-IRI, ONIVYDE) was approved in 2015 (by the Food and Drug Administration, European Medicines Agency, and Therapeutic Goods Administration) and is a topoisomerase inhibitor indicated, in combination with fluorouracil and leucovorin, for the treatment of patients with metastatic adenocarcinoma of the pancreas after disease progression following gemcitabine-based therapy. This study investigates the potential therapeutic benefit of nal-IRI for the treatment of advanced TNBC in a clinically relevant mouse model of spontaneous metastasis (LM2–4). Female SCID mice were orthotopically inoculated with TNBC LM2–4-luc cells in the lower mammary fat pad. Following primary tumor resection, bioluminescence imaging (BLI) was used to monitor both metastasis formation and spread as well as response to treatment with nal-IRI. Weekly treatment with 10 mg/kg of nal-IRI provided a 4.9-times longer median survival compared to both 50 mg/kg irinotecan treated and untreated animals. The survival benefit was supported by a significant delay in the regrowth of the primary tumor, effective control, and eventual regression of metastases assessed using longitudinal BLI, which was confirmed at the study end point with magnetic resonance (MR) imaging and post-mortem observation. This preclinical investigation demonstrates that, at a five-times lower dose compared to the free drug, liposomal irinotecan provides significant survival benefit and effective management of metastatic disease burden in a clinically relevant model of spontaneous TNBC metastases. These findings support the evaluation of nal-IRI in patients with advanced and metastatic TNBC.

KEYWORDS: triple negative breast cancer (TNBC), chemotherapy, liposomal irinotecan, metastasis, bioluminescence imaging



INTRODUCTION

Despite ongoing marked improvements in medical research and healthcare delivery, breast cancer remains the third leading cause of cancer related deaths in women worldwide.¹ In part, this is due to the complexity, heterogeneity, and variability in the presentation of this disease as it consists of up to 21 different histologically distinguishable subtypes.^{2–5} These are then categorized into four main molecular subtypes with significant differences in therapeutic options and prognosis. For example, roughly 15–20% of breast cancer patients fall under the triple negative subtype meaning that their cancer is negative for estrogen and progesterone receptors and does not overexpress human epidermal growth factor receptor 2 (HER2).^{3,4,6,7} More importantly, the triple negative breast cancer (TNBC) group has the poorest prognosis both due to the aggressive nature of the

disease and due to the lack of effectiveness of hormonal therapies.^{8,9} For these patients, their treatment options typically include a combination of surgery, radiation therapy, and chemotherapy. Irinotecan (IRI), a topoisomerase I inhibitor, is an established chemotherapy drug with demonstrated benefit in patients with colorectal cancer.¹⁰ Its efficacy has also been evaluated in preclinical and clinical studies in cervical, esophageal, gastric, glioma, lung, mesothelioma, pancreatic, and advanced metastatic breast cancer.^{11–19} However, in preclinical breast cancer models, IRI showed limited therapeutic

Received: May 22, 2018

Revised: July 26, 2018

Accepted: July 30, 2018

Published: July 30, 2018

activity and dose-limiting toxicity side effects.^{18,19} Additional clinical trials have yielded inconclusive results regarding the optimal administration schedule and have questioned the effectiveness of IRI in treating patients with advanced metastatic breast cancers altogether.^{20–22} A viable solution to increase the efficacy and decrease toxicity of a small molecule drug is nanoencapsulation. In fact, the liposomal formulation of irinotecan (nal-IRI, ONIVYDE) has demonstrated improved activity with decreased toxicity in a number of animal models of human cancer compared to nonliposomal IRI.²³

The therapeutic benefits of nal-IRI over conventional IRI are associated with the ability of liposomal encapsulation to increase tumor exposure relative to systemic exposure to the cytotoxic drug IRI, enabling a higher dose to be administered safely in a preclinical setting. In preclinical models, the exploitation of passive tumor targeting through the enhanced permeability and retention (EPR) effect enables nal-IRI to achieve significantly larger area-under-the-curve for the active drug exposure at tumor site, which ultimately leads to improved therapeutic outcome.²⁴ For example, 10 mg/kg of nal-IRI and 50 mg/kg of IRI have a similar exposure in plasma and tumor of SN-38, the active metabolite of IRI.²⁴ In 2015, nal-IRI, in combination with 5-fluorouracil and leucovorin, demonstrated an overall survival advantage with a manageable safety profile in a randomized Phase III trial in patients with advanced pancreatic cancer who were previously treated with gemcitabine-based therapy.²⁵ This led to the Food and Drug Administration (FDA), European Medicines Agency (EMA), and the Therapeutic Goods Administration (TGA) approval of ONIVYDE in that patient population.

This study aims to investigate the therapeutic advantage of nal-IRI when used as a monotherapy compared to conventional IRI for treatment of advanced metastatic TNBC in a mouse xenograft model of spontaneous metastatic disease previously reported by Guerin et al.,²⁶ which was shown to effectively recapitulate the clinical presentation of TNBC, and further characterized by our group.²⁷ Specifically, we use noninvasive *in vivo* bioluminescence imaging (BLI) to longitudinally track and evaluate disease burden progression and metastatic spread as well as response to treatment over the course of three months.

EXPERIMENTAL SECTION

Animal Experiments. All animal experiments were approved by the University Health Network (UHN) Animal Care Committee and adhered to the ethical guidelines of the Canadian Council on Animal Care. Experiments were performed and reported in compliance with the ARRIVE guidelines. Female SCID mice (Ontario Cancer Institute, UHN, Toronto, Ontario, Canada) were housed at constant temperature (20 °C) and relative humidity (40%) under a 12 h light/12 h dark cycle and were given *ad libitum* access to food and water. Study end point criteria were extensive body weight loss ($\geq 20\%$), tumor ulceration ($\geq 20\%$), and tumor size (volume $\geq 1800 \text{ mm}^3$).

Metastatic Breast Cancer Model. LM2–4-Luc cells were kindly provided by Dr. Robert Kerbel's laboratory (Sunnybrook Research Institute, Toronto, Ontario, Canada; obtained at passage 6 in 2012)²⁸ and grown as monolayer cultures in RPMI medium with 10% FBS. Upon receipt, the cell line was confirmed negative for Mycoplasma contamination using a PCR-based test method (Department of Paediatric Laboratory Medicine, The Hospital for Sick Children, Toronto, ON, Canada). Further genetic authentication was not carried out.

Forty-two female SCID mice (8 weeks of age) were inoculated with 4×10^6 cells (\leq passage 25) in 50 μL of medium without supplements into the right lower inguinal mammary fat pad (MFP). Cell viability and localization were confirmed using BLI. Primary tumors were surgically resected 2–3 weeks post inoculation as previously described²⁸ once they reached a volume of $220 \pm 60 \text{ mm}^3$. The volume of the primary tumor was determined prior to surgical removal using caliper measurement. The following equation was used to calculate tumor volume: $(\text{length} \times \text{width}^2)/2$.

Treatment Efficacy Study. Mice were randomized into three groups consisting of (1) no treatment control group ($n = 13$), (2) IRI (50 mg/kg intravenous (IV)) treatment once per week ($n = 13$), and (3) nal-IRI (10 mg/kg IV) treatment once per week ($n = 16$). Randomization occurred between day 5 and day 9 post primary tumor resection, when animals presented with at least one metastasis detected via BLI in addition to any tumor regrowth at the site of the primary tumor removal. The metastatic BLI photon flux measured prior to treatment initiation showed no statistical differences among the three groups ($p = 0.9973$, one-way ANOVA) (Supplementary Figure S1). Both IRI and nal-IRI were provided by Merrimack Pharmaceuticals (Cambridge, MA, USA). Nal-IRI, the liposomal form of IRI, was described previously.^{23,24} Briefly, its lipid composition was DSPC, cholesterol, and PEG-DSPE in a 3:2:0.015 molar ratio. The initial drug-to-lipid ratio was 500 g μmol phospholipid and liposomes were extruded through a 0.1 μm polycarbonate filter.

Bioluminescence Imaging. Primary and metastatic tumor development was monitored longitudinally by *in vivo* BLI using an IVIS Spectrum Imaging System (PerkinElmer, Waltham, MA, USA) and Living image 4.0 software. Mice were injected subcutaneously with 150 mg/kg D-Luciferin (Caliper Life Sciences, Hopkinton, MA, USA) 10 min before BLI acquisition (exposure time, 0.5–60 s; field of view, D; subject height, 1.5 cm; binning, 8; f-stop, 1). Analysis was carried out using Living Image (version 4.3.1 Advanced Acquisition and Analysis Tools for IVIS, Hopkinton, MA, USA). The metastatic burden was determined by subtracting the signal of the primary tumor regrowth (using a 25% of maximum signal threshold) from the total whole body signal measured in the mouse (using a 2% of maximum signal threshold) in supine position.

Magnetic Resonance Imaging (MRI). Anatomical MRI was acquired using a T2W FSE 2D sequence (repetition time/echo time = 5000 ms/54 ms, slice thickness = 1 mm, interslice gap = 0 mm, FOV = 30 mm \times 60 mm, matrix = 192 \times 192, 90° flip angle, 180° refocusing flip angle, number of excitations = 7, echo train length = 16) at the study end point using a 1T MRI (Aspect imaging, Shoham, Israel). Images were analyzed using Inveon Research Workplace v.4.0 (Siemens Medical Solutions, USA).

Statistical Analysis. Statistical analysis was performed using GraphPad Prism 7 (GraphPad Software, La Jolla, CA, USA). A p -value < 0.05 was considered as statistically significant. One-way ANOVA test and unpaired t -tests were used where applicable. Linear correlations were quantified with a Pearson correlation coefficient.

RESULTS

Following removal of the primary tumor, all animals developed metastatic disease between day 9 and day 15 post resection. Treatment for each animal was initiated once BLI signal was observed in any distal area from the primary tumor site (Figure

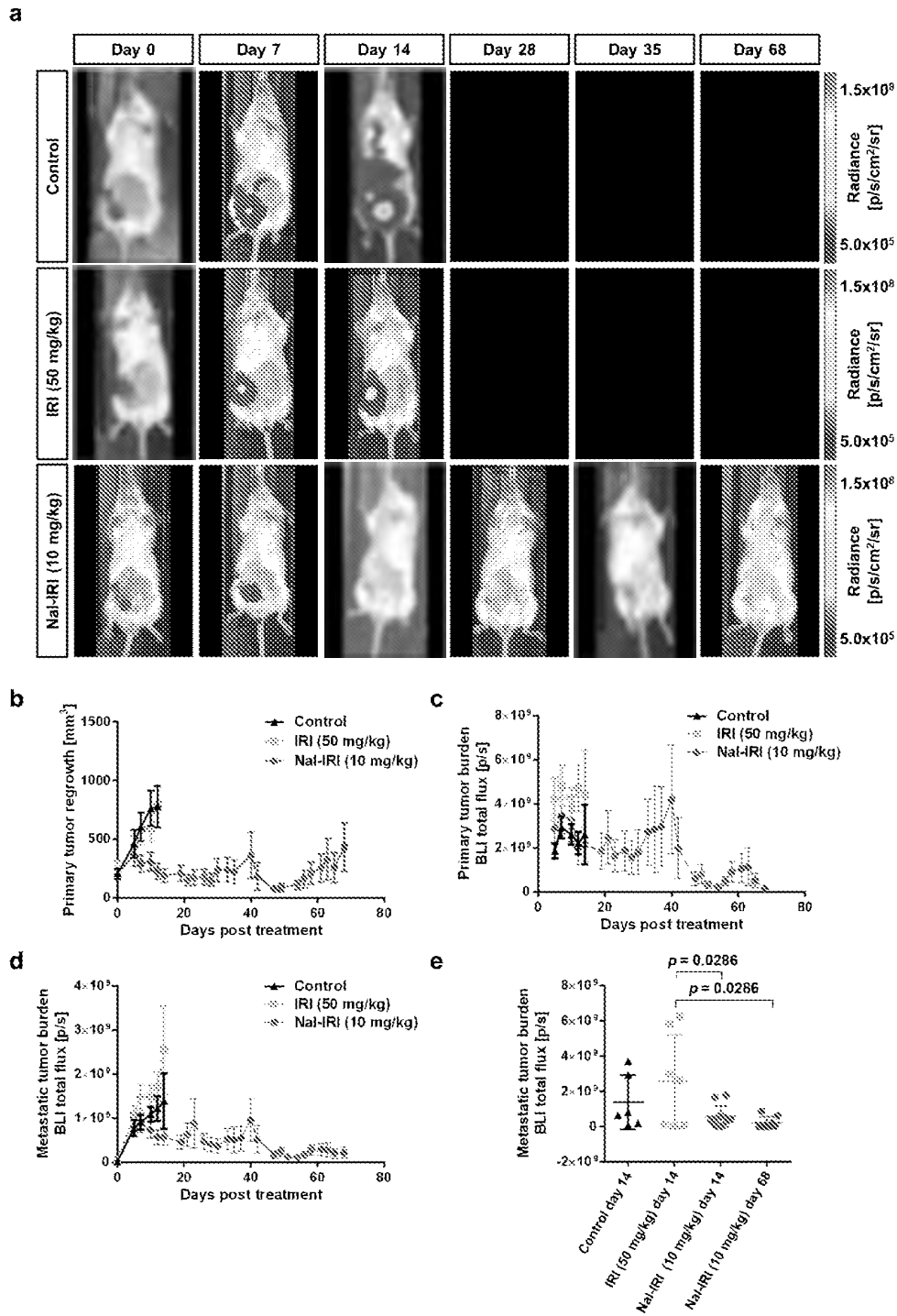


Figure 1. Metastatic disease response to treatment. (a) Representative BLI images showing metastatic disease burden over the course of treatment for the three groups. (b) Primary tumor regrowth volume measured by caliper expressed in mm³ up to the time point of 50% survival for each group. (c, d) BLI-based assessment of (c) primary tumor regrowth and (d) metastatic tumor burden up to the time point of 50% survival, excluding signal from the primary tumor regrowth region. (e) Metastatic tumor burden evaluated using BLI of each group at day 14 (50% survival for control and IRI groups) and day 66 for nal-IRI (50% survival).

1a). We differentiated the regrowth of tumor at the site of the initial tumor implantation (i.e., primary tumor regrowth) and the metastatic spread of disease to distal sites (i.e., metastatic burden). Because of the superficial and confined nature of the primary regrowth nodules, caliper-based and BLI based measurements were possible to quantify their growth and

treatment response (Figure 1b,c), while the distal metastatic disease burden (excluding the primary tumor regrowth) was assessed only using BLI (Figure 1d).

Treatment with nal-IRI administered once a week for up to 13 weeks was able to control the regrowth of the primary tumor as well as the distal metastatic disease burden compared to both the

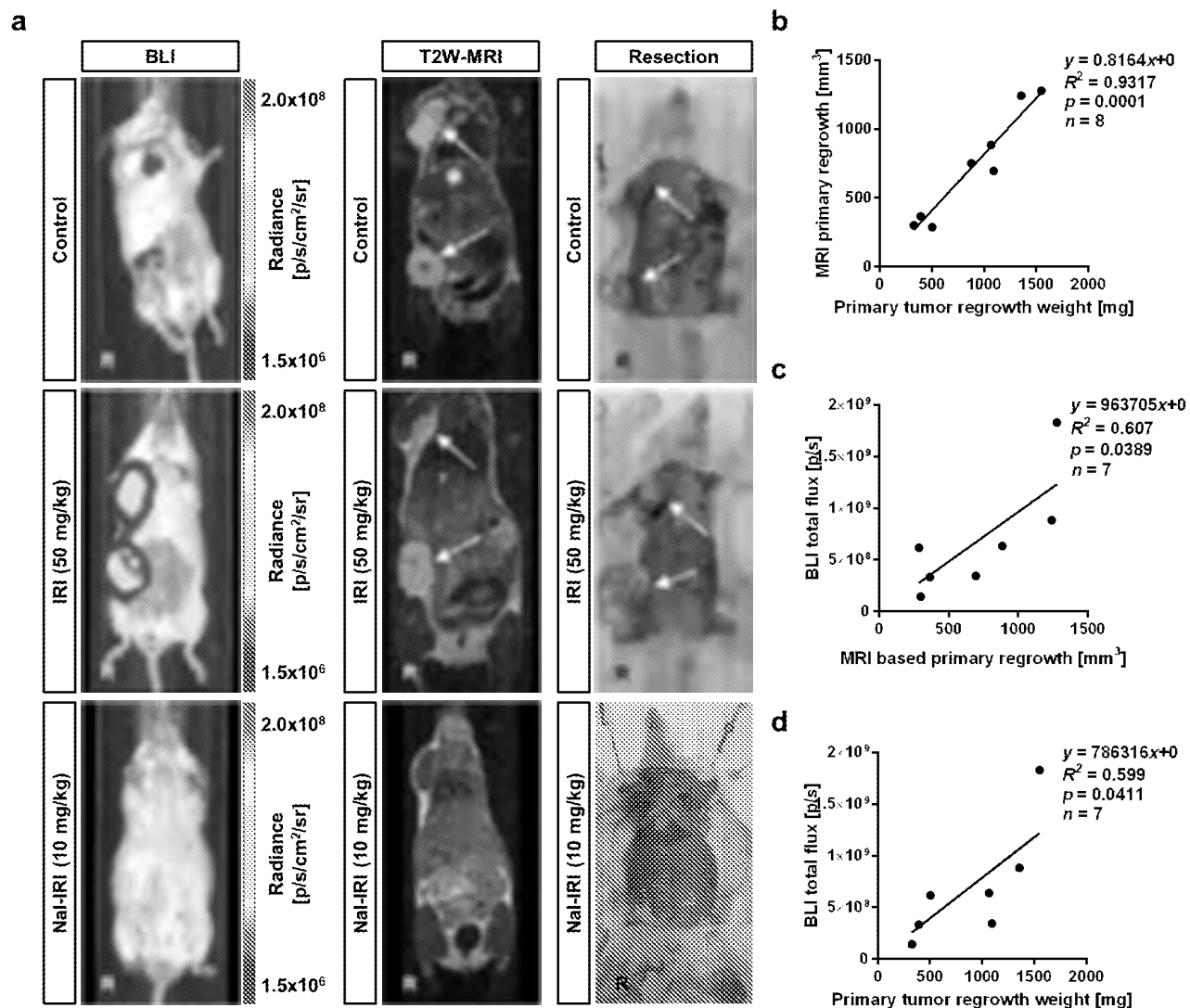


Figure 2. Total tumor burden at study end point. (a) *In vivo* BLI and T2W-MRI images showing tumor burden for a representative mouse from each group acquired at study end point prior to sacrificing the animals as well as photograph images acquired for the same animals during tumor resection. Arrows indicate locations of tumor nodules. R: right. (b) Correlation of the primary tumor regrowth volume measured using MRI and caliper at the study end point for all mice. (c) Correlation of BLI signal of primary tumor regrowth and MRI-based tumor measurement after removal of one outlier. (d) Correlation of BLI signal of primary tumor regrowth and the excised weight of the primary tumor regrowth nodules after removal of one outlier.

IRI treated and the untreated control animals (Figure 1a–e). The mean metastatic burden photon flux expressed as photons per second at the 50% survival time point for the nal-IRI treated animals (measured on day 68) was an order of magnitude lower ($2.2 \times 10^8 \pm 3.4 \times 10^8$ p/s) than for both the IRI treated group ($2.6 \times 10^9 \pm 2.7 \times 10^9$ p/s) ($p = 0.0286$, *t*-test, day 14) and the untreated control group ($1.4 \times 10^9 \pm 1.5 \times 10^9$ p/s) ($p = 0.0286$, *t*-test, day 14), which indicated effective control of the metastatic burden by nal-IRI. This lower signal was already present on day 14 between nal-IRI treated group ($2.6 \times 10^9 \pm 1.01 \times 10^9$ p/s) and IRI on the same day ($p = 0.0286$, *t*-test, day 14). Between the IRI treated and the untreated control animals, no difference in primary regrowth ($p = 0.5425$, *t*-test) or in the distal metastatic disease burden ($p = 0.3672$, *t*-test) was observed on day 14 post treatment initiation when 50% of the animals in each of these two groups still survived. It is interesting to note the lack of effectiveness of IRI for the treatment of metastatic disease (and the primary regrowth) of LM2–4, as previous reports have

observed therapeutic effect in animal models bearing MDA-MB 231,¹³ the parental TNBC cell line to LM2–4, as a primary tumor.

When animals reached one or more ethical end points previously established and reported in the Experimental section, *in vivo* BLI, *in vivo* anatomical MR imaging, and post-mortem resection-based evaluation of the tumor burden and location were performed (Figure 2a). These measurements served to validate the accuracy of the two imaging techniques for the assessment of metastatic disease burden both in terms of anatomical location and nodule size. MRI-based tumor volumes and the weight of the excised primary tumor regrowth mass showed a strong positive correlation (slope = 0.8164, $R^2 = 0.9317$, $p = 0.0001$, $n = 8$, Pearson) (Figure 2b). The BLI signal provided a good indication of the possible anatomical location of the metastatic nodules and enabled relative comparison of disease burden among treatment groups. However, it showed no correlation with both the MR-based tumor volumes (slope =

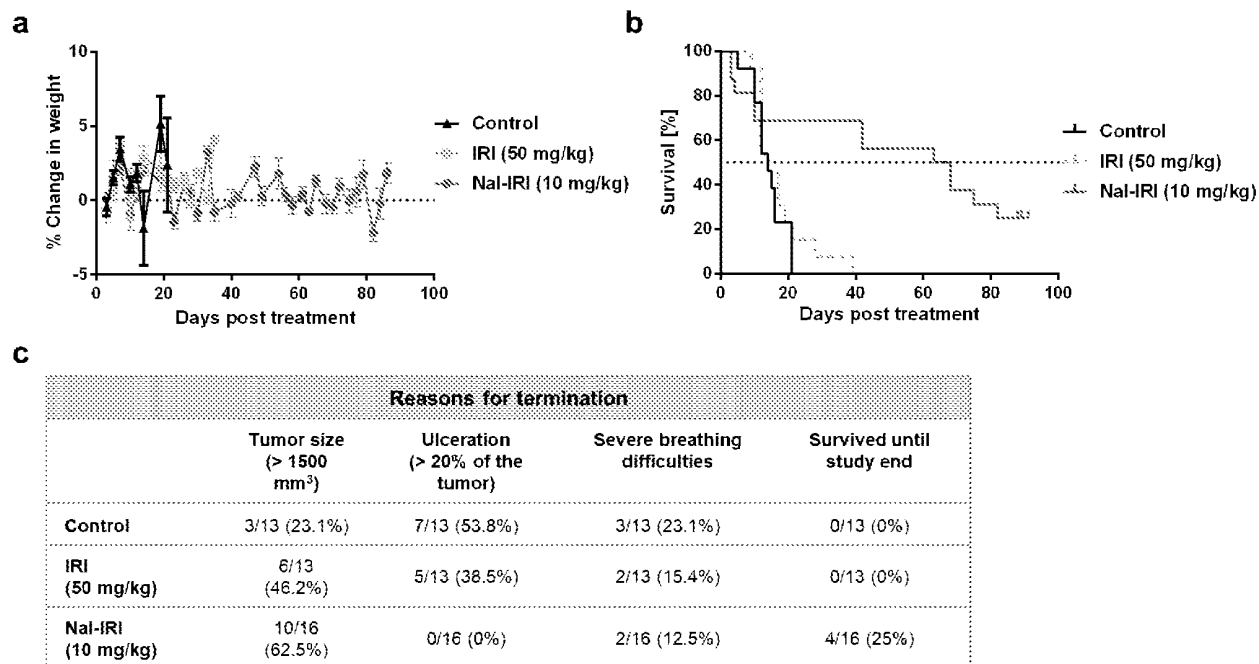


Figure 3. Treatment effect on survival and treatment tolerability. (a) Percent change in animal body weight of each group over the course of the study. (b) Survival post treatment initiation. The dotted horizontal line indicates 50% survival. (c) Table indicating reasons that led to the ethical end points per treatment group.

1 213 902, $R^2 = 0.2612$, $p = 0.1956$, $n = 8$) and the weight of the resected tumors (slope = 987 730, $R^2 = 0.2254$, $p = 0.2345$, $n = 8$). After removal of one outlier (ROUT method, $Q = 5\%$), we observed a strong correlation of primary tumor BLI signal and both MR-based tumor volumes (slope = 963 705, $R^2 = 0.607$, $p = 0.0389$, $n = 7$) and resected tumor weight (slope = 786 316, $R^2 = 0.599$, $p = 0.0411$, $n = 7$) (Figure 2c, d) at the study end point. On day 86 post treatment initiation, our end point evaluation further confirmed the treatment efficacy of nal-IRI. In fact, we could not locate any visible nodules post-mortem in three out of four surviving animals from the nal-IRI treated group.

Overall, treatment with weekly IRI or nal-IRI was well tolerated as no animal in these groups dropped more than 10.6% in body weight over the course of the study (Figure 3a). However, upon visual inspection of the mice, the IRI treated animals were generally less groomed and less active compared to both the nal-IRI treated group and the untreated control group while the overall disease burden was similar to that of the untreated control group. This suggested a higher level of discomfort as a result of treatment-associated toxicity. The therapeutic efficacy of nal-IRI was further demonstrated by the fact that the nal-IRI treated animals reached a median survival time that was 4.9-times longer compared to both the untreated control and the IRI treated groups (68 days for nal-IRI vs 14 days for IRI and control, Figure 3b,c). A smaller subset of the nal-IRI treated animals (25%, 4/16) further survived with minimal to no disease burden until day 86 post treatment initiation with continued weekly administration of 10 mg/kg of nal-IRI.

DISCUSSION

There is a high unmet need for the identification of an effective treatment for patients with metastatic TNBC. Nanoencapsulation is a viable solution to increase the efficacy and decrease toxicity of nonencapsulated therapeutics. Nal-IRI has previously

demonstrated improved activity and decreased toxicity compared to the nonencapsulated irinotecan in animal models of human cancer. Therefore, we explored the benefits of nal-IRI in treating advanced metastatic breast cancer in a mouse model of a highly aggressive metastatic variant (LM2-4) of the parental TNBC MDA-MB-231 model. The unique feature of this model is that it generates spontaneous metastasis, closely recapitulating the clinical presentation of metastatic breast cancer.²⁶ In our studies, we evaluated nal-IRI in animals with established metastases by resecting the primary tumor and waiting until at least one metastatic lesion had developed before starting treatment. However, in future studies, it would be valuable to investigate the treatment outcome following earlier administration of nal-IRI (i.e., post primary tumor establishment and prior to metastasis formation) to assess the effectiveness of treatment with nal-IRI in preventing the development of metastases.

We leveraged noninvasive small animal imaging, using BLI, to enable objective randomization of metastatic treatment groups and longitudinal disease burden tracking as well as relative comparison of treatment response among the different groups. This is in contrast to many of the studies found in literature that do not exploit imaging to provide a time-course evaluation of treatment progression or response and solely base their findings on end point information. However, it is important to note that due to the attenuation and scattering of light photons inside the body, and its high dependence on local ATP and O₂ levels, BLI is only a semiquantitative imaging method.²⁹

An important outcome from this study is that we caution the use of primary tumor models for testing of therapies designed for use in metastatic disease, as primary tumors were shown to respond differently to IRI chemotherapy than our metastatic tumor model.³⁰ Specifically, other groups have previously observed some limited activity of IRI on primary MDA-MB-231 tumors,¹⁸ while our results indicate that IRI has no

therapeutic advantage compared to no treatment in the LM2–4 metastatic tumor model. This is in contrast to the metastatic LM2–4 tumors that received treatment with nal-IRI. These tumors benefited from effective control and, in some cases, complete suppression of any metastatic disease burden achieving a 4.9-times or 54 days longer median survival compared to the other two groups. To generate the highly metastatic LM2–4 cell line from MDA-MB-231, two rounds of *in vivo* selection composed of orthotopic inoculation of tumor cells, primary tumor removal, and isolation of cells from lung metastases were performed.²⁸ As several studies reported changes in genetic signature in MDA-MB-231-derived cell lines with increased metastatic potential,^{31,32} genetic differences might be the cause for the observed difference in therapeutic response to IRI treatment.

The good tolerability of the nal-IRI treatment was also reflected in the animals' wellbeing. Achieving this level of therapeutic efficacy in this highly aggressive mouse model when the conventional chemotherapy drug itself shows no effect strongly supports the evaluation of nal-IRI for treatment of advanced breast cancer into the clinical setting. This study supports an ongoing clinical study (NCT01770353).

While nal-IRI demonstrated significantly greater antitumor activity than conventional IRI, we did observe the development of a single instance of brain metastasis in the nal-IRI treated group toward the end of the study (day 65) when the overall disease burden for this mouse had been controlled for a prolonged time. This observation is in line with previous reports of increased incidence of brain metastases following successful control of primary disease. It is hypothesized that the prolonged survival achieved gives micrometastases sufficient time to develop in the brain, in an anatomically privileged location.^{33,34} This is further justified by the fact that many therapies only have limited efficacy in the brain due to challenges associated with crossing the blood–brain barrier; as such, the brain can become a sanctuary site for micrometastatic spread of tumor cells.³⁵ In line with this, we did not observe brain metastasis in the untreated control or IRI treated groups, both of which had a significantly shorter survival time.

In conclusion, this preclinical investigation of nal-IRI in a highly aggressive TNBC tumor model of spontaneous metastasis demonstrated that nal-IRI was well-tolerated and provided significant survival benefit compared to conventional IRI. BLI was successfully used as a noninvasive and high-throughput technique to monitor metastatic disease progression, metastatic spread, and response to therapy in mice longitudinally. These results indicate that nal-IRI has potential for the treatment of patients with TNBC and warrants clinical evaluation.

■ ASSOCIATED CONTENT

Supporting Information

The Supporting Information is available free of charge on the ACS Publications website at DOI: 10.1021/acs.molpharmaceut.8b00540.

Whole body BLI signal at day of randomization (PDF)

■ AUTHOR INFORMATION

Corresponding Author

*E-mail: jinzi.zheng@rmp.uhn.on.ca. Phone: +1 (416) 581 7790. Fax: +1 (416) 506 1828.

ORCID

Inga B. Fricke: 0000-0002-8136-3375

Jinzi Zheng: 0000-0002-7650-3910

Author Contributions

[†]Equal contribution.

Notes

The authors declare the following competing financial interest(s): Authors affiliated with Merrimack Pharmaceuticals as indicated were employees of Merrimack Pharmaceuticals (at the time of study) and received salaries and stock options from Merrimack Pharmaceuticals. University Health Network has received research funding as part of a sponsored research agreement from Merrimack Pharmaceuticals with Jinzi Zheng as the lead Principal Investigator.

■ ACKNOWLEDGMENTS

The authors would like to thank Dr. Robert Kerbel and lab for kindly providing us with the LM2-4-luc cell line. We would also like to thank Maria Bisa and the Animal Resource Centre (ARC) for their technical support throughout the animal handling and monitoring procedures. The authors would like to acknowledge the Spatio-Temporal Targeting and Amplification of Radiation Response (STTARR) program and its affiliated funding agencies. This study was funded in part by Merrimack Pharmaceuticals and a start-up research fund from the Princess Margaret Cancer Foundation. Additional writing and editorial support was provided by Ipsen Biopharmaceuticals. The postdoctoral salaries were supported in part by the MITACS Elevate and Accelerate Programs (Industry Sponsored Postdoctoral Fellowship).

■ ABBREVIATIONS

ARC, Animal Resource Centre; BLI, bioluminescence imaging; EMA, European Medicines Agency; EPR, enhanced permeability and retention; FDA, Food and Drug Administration; HER2, human epidermal growth factor receptor 2; IRI, irinotecan; MFP, mammary fat pad; MRI, magnetic resonance imaging; Nal-IRI, nanoliposomal irinotecan; TGA, Therapeutic Goods Administration; TNBC, triple negative breast cancer

■ REFERENCES

- (1) Siegel, R. L.; Miller, K. D.; Jemal, A. Cancer Statistics, 2016. *Ca-Cancer J. Clin.* **2016**, *66* (1), 7–30.
- (2) Barnard, M. E.; Boeke, C. E.; Tamimi, R. M. Established Breast Cancer Risk Factors and Risk of Intrinsic Tumor Subtypes. *Biochim. Biophys. Acta, Rev. Cancer* **2015**, *1856* (1), 73–85.
- (3) Gilcrease, M. Z. How Many Etiological Subtypes of Breast Cancer: Two, Three, Four, or More? *Breast Dis.* **2015**, *26* (4), 296–297.
- (4) Blows, F. M.; Driver, K. E.; Schmidt, M. K.; Broeks, A.; van Leeuwen, F. E.; Wesseling, J.; Cheang, M. C.; Gelmon, K.; Nielsen, T. O.; Blomqvist, C.; Heikkilä, P.; Heikkinen, T.; Nevanlinna, H.; Akslen, L. A.; Bégin, L. R.; Foulkes, W. D.; Couch, F. J.; Wang, X.; Cafourek, V.; Olson, J. E.; Baglietto, L.; Giles, G. G.; Severi, G.; McLean, C. A.; Southey, M. C.; Rakha, E.; Green, A. R.; Ellis, I. O.; Sherman, M. E.; Lissowska, J.; Anderson, W. F.; Cox, A.; Cross, S. S.; Reed, M. W. R.; Provenzano, E.; Dawson, S. J.; Dunning, A. M.; Humphreys, M.; Easton, D. F.; García-Closas, M.; Caldas, C.; Pharoah, P. D.; Huntsman, D. Subtyping of Breast Cancer by Immunohistochemistry to Investigate a Relationship between Subtype and Short and Long Term Survival: A Collaborative Analysis of Data for 10,159 Cases from 12 Studies. *PLoS Med.* **2010**, *7* (5), e1000279.
- (5) Cheang, M. C.; Martin, M.; Nielsen, T. O.; Prat, A.; Voduc, D.; Rodriguez-Lescure, A.; Ruiz, A.; Chia, S.; Shepherd, L.; Ruiz-Borrego, M.; Calvo, L.; Alba, E.; Carrasco, E.; Caballero, R.; Tu, D.; Pritchard, K. I.; Levine, M. N.; Bramwell, V. H.; Parker, J.; Bernard, P. S.; Ellis, M. J.; Perou, C. M.; Di Leo, A.; Carey, L. A. Defining Breast Cancer Intrinsic

Subtypes by Quantitative Receptor Expression. *Oncologist* 2015, 20 (5), 474–482.

(6) Adrada, B. E.; Miranda, R. N.; Rauch, G. M.; Arribas, E.; Kanagal-Shamanna, R.; Clemens, M. W.; Fanale, M.; Haideri, N.; Mustafa, E.; Larrinaga, J.; Reisman, N. R.; Jaso, J.; You, M. J.; Young, K. H.; Medeiros, L. J.; Yang, W. Breast Implant-Associated Anaplastic Large Cell Lymphoma: Sensitivity, Specificity, and Findings of Imaging Studies in 44 Patients. *Breast Cancer Res. Treat.* 2014, 147 (1), 1–14.

(7) Parise, C. A.; Caggiano, V. Breast Cancer Survival Defined by the er/pr/her2 Subtypes and a Surrogate Classification according to Tumor Grade and Immunohistochemical Biomarkers. *J. Cancer Epidemiol.* 2014, 2014, 469251.

(8) Brenton, J. D.; Carey, L. A.; Ahmed, A.; Caldas, C. Molecular Classification and Molecular Forecasting of Breast Cancer: Ready for Clinical Application? *J. Clin. Oncol.* 2005, 23 (29), 7350–7360.

(9) Kathryn, J. C.; Sireesha, V. G.; Stanley, L. Triple Negative Breast Cancer Cell Lines: One Tool in the Search for Better Treatment of Triple Negative Breast Cancer. *Breast Dis* 2012, 32, 35–48.

(10) Fuchs, C.; Mitchell, E. P.; Hoff, P. M. Irinotecan in the Treatment of Colorectal Cancer. *Cancer Treat. Rev.* 2006, 32 (7), 491–503.

(11) Lhomme, C.; Fumoleau, P.; Fargeot, P.; Krakowski, Y.; Dieras, V.; Chauvergne, J.; Vennin, P.; Rebattu, P.; Roche, H.; Misset, J. L.; Lentz, M. A.; Van Glabbeke, M.; Matthieu-Boue, A.; Mignard, D.; Chevallier, B. Results of a European Organization for Research and Treatment of Cancer/Early Clinical Studies Group Phase II Trial of First-Line Irinotecan in Patients with Advanced or Recurrent Squamous Cell Carcinoma of the Cervix. *J. Clin. Oncol.* 1999, 17 (10), 3136–3142.

(12) Ilson, D. H.; Saltz, L.; E, P.; et al. Phase II Trial of Weekly Irinotecan plus Cisplatin in Advanced Esophageal Cancer. *J. Clin. Oncol.* 1999, 17 (10), 3270–3275.

(13) Boku, N.; Ohtsu, A.; Shimada, Y.; Shirao, K.; Seki, S.; Saito, H.; Sakata, Y.; Hyodo, I. Phase II Study of a Combination of Irinotecan and Cisplatin against Metastatic Gastric Cancer. *J. Clin. Oncol.* 1999, 17 (1), 319–323.

(14) Friedman, H. S.; Petros, W. P.; Friedman, A. H.; Schaaf, L. J.; Kerby, T.; Lawyer, J.; Parry, M.; Houghton, P. J.; Lovell, S.; Rasheed, K.; Cloughsey, T.; Stewart, E. S.; Colvin, O. M.; Provenzale, J. M.; McLendon, R. E.; Bigner, D. D.; Cokgor, I.; Haglund, M.; Rich, J.; Ashley, D.; Malczyn, J.; Elfring, G. L.; Miller, L. L. Irinotecan Therapy in Adults with Recurrent or Progressive Malignant Glioma. *J. Clin. Oncol.* 1999, 17 (5), 1516–1525.

(15) DeVore, R. F.; Johnson, D. H.; Crawford, J.; Garst, J.; Dimery, I. W.; Eckardt, J.; Eckhardt, S. G.; Elfring, G. L.; Schaaf, L. J.; Hanover, C. K.; Miller, L. L. Phase II Study of Irinotecan plus Cisplatin in Patients with Advanced Non-Small-Cell Lung Cancer. *J. Clin. Oncol.* 1999, 17 (9), 2710–2720.

(16) Negoro, S.; Noda, K.; Nishiwaki, Y.; Kawahara, M.; Tamura, T.; Sugiura, T.; Yokayama, A.; Mori, K.; Fukuoka, M.; Yoshimura, K.; Saijo, N. A Randomized Phase III Study of Irinotecan and Cisplatin versus Etoposide and Cisplatin in Extensive-Disease Small-Cell Lung Cancer: Japan Clinical Oncology Group Study (JCOG 9511). In *World Conference on Lung Cancer*; JCOG, 2000; Vol. 29, pp 1–30.

(17) Rocha Lima, C.; Svarese, D.; Bruckner, H.; et al. Multicenter Phase II Trial of First-Line Irinotecan and Gemcitabine (Irinogem) in Patients with Locally Advanced or Metastatic Pancreatic Cancer. *Gastrointest. Cancer* 2000, 263a.

(18) Schluep, T.; Hwang, J.; Cheng, J.; Heidel, J. D.; Bartlett, D. W.; Hollister, B.; Davis, M. E. Preclinical Efficacy of the Camptothecin-Polymer Conjugate IT-101 in Multiple Cancer Models. *Clin. Cancer Res.* 2006, 12 (5), 1606–1614.

(19) Okuno, S.; Harada, M.; Yano, T.; Yano, S.; Kiuchi, S.; Tsuda, N.; Sakamura, Y.; Imai, J.; Kawaguchi, T.; Tsujihara, K. Complete Regression of Xenografted Human Carcinomas by Camptothecin Analogue-Carboxymethyl Dextran Conjugate (T-0128). *Cancer Res.* 2000, 60 (11), 2988–2998.

(20) Perez, E. A.; Hillman, D. W.; Mailliard, J. A.; Ingle, J. N.; Ryan, J. M.; Fitch, T. R.; Rowland, K. M.; Kardinal, C. G.; Krook, J. E.; Kugler, J. W.; Dakhil, S. R. Randomized Phase II Study of Two Irinotecan

Schedules for Patients with Metastatic Breast Cancer Refractory to an Anthracycline, a Taxane, or Both. *J. Clin. Oncol.* 2004, 22 (14), 2849–2855.

(21) Shigeoka, Y.; Itoh, K.; Igarashi, T.; Ishizawa, K.; Saeki, T.; Fujii, H.; Minami, H.; Imoto, S.; Sasaki, Y. Clinical Effect of Irinotecan in Advanced and Metastatic Breast Cancer Patients Previously Treated with Doxorubicin- and Docetaxel-Containing Regimens. *Jpn. J. Clin. Oncol.* 2001, 31 (8), 370–374.

(22) Kümler, I.; Brünner, N.; Stenvang, J.; Balslev, E.; Nielsen, D. L. A Systematic Review on Topoisomerase I Inhibition in the Treatment of Metastatic Breast Cancer. *Breast Cancer Res. Treat.* 2013, 138 (2), 347–358.

(23) Drummond, D. C.; Noble, C. O.; Guo, Z.; Hong, K.; Park, J. W.; Kirpotin, D. B. Development of a Highly Active Nanoliposomal Irinotecan Using a Novel Intraliposomal Stabilization Strategy. *Cancer Res.* 2006, 66 (6), 3271–3277.

(24) Kalra, A. V.; Kim, J.; Klinz, S. G.; Paz, N.; Cain, J.; Drummond, D. C.; Nielsen, U. B.; Fitzgerald, J. B. Preclinical Activity of Nanoliposomal Irinotecan Is Governed by Tumor Deposition and Intratumor Prodrug Conversion. *Cancer Res.* 2014, 74 (23), 7003–7013.

(25) Wang-Gillam, A.; Li, C. P.; Bodoky, G.; Dean, A.; Shan, Y. S.; Jameson, G.; MacArulla, T.; Lee, K. H.; Cunningham, D.; Blanc, J. F.; Hubner, R. A.; Chiu, C. F.; Schwartzmann, G.; Siveke, J. T.; Braiteh, F.; Moyo, V.; Belanger, B.; Dhindsa, N.; Bayever, E.; Von Hoff, D. D.; Chen, L. T. Nanoliposomal Irinotecan with Fluorouracil and Folinic Acid in Metastatic Pancreatic Cancer after Previous Gemcitabine-Based Therapy (NAPOLI-1): A Global, Randomised, Open-Label, Phase 3 Trial. *Lancet* 2016, 387 (10018), 545–557.

(26) Guerin, E.; Man, S.; Xu, P.; Kerbel, R. S. A Model of Postsurgical Advanced Metastatic Breast Cancer More Accurately Replicates the Clinical Efficacy of Antiangiogenic Drugs. *Cancer Res.* 2013, 73 (9), 2743–2748.

(27) Fricke, I. B.; De Souza, R.; Costa Ayub, L.; Francia, G.; Kerbel, R. S.; Jaffray, D. A.; Zheng, J. Spatiotemporal Assessment of Spontaneous Metastasis Formation Using Multimodal in Vivo Imaging in HER2+ and Triple Negative Metastatic Breast Cancer Xenograft Models in Mice. *PLoS One* 2018, 13 (5), e0196892.

(28) Munoz, R.; Man, S.; Shaked, Y.; Lee, C. R.; Wong, J.; Francia, G.; Kerbel, R. S. Highly Efficacious Nontoxic Preclinical Treatment for Advanced Metastatic Breast Cancer Using Combination Oral UFT-Cyclophosphamide Metronomic Chemotherapy. *Cancer Res.* 2006, 66 (7), 3386–3391.

(29) Jones, L.; Richmond, J.; Evans, K.; Carol, H.; Jing, D.; Kurmasheva, R. T.; Billups, C. A.; Houghton, P. J.; Smith, M. A.; Lock, R. B. Bioluminescence Imaging Enhances Analysis of Drug Responses in a Patient-Derived Xenograft Model of Pediatric ALL. *Clin. Cancer Res.* 2017, 23 (14), 3744–3755.

(30) Steeg, P. S.; Theodorescu, D. Metastasis: A Therapeutic Target for Cancer. *Nat. Clin. Pract. Oncol.* 2008, 5, 206–219.

(31) Minn, A. J.; Gupta, G. P.; Siegel, P. M.; Bos, P. D.; Shu, W.; Giri, D. D.; Viale, A.; Olshen, A. B.; Gerald, W. L.; Massagué, J. Genes That Mediate Breast Cancer Metastasis to Lung. *Nature* 2005, 436 (7050), 518–524.

(32) Minn, A. J.; Gupta, G. P.; Padua, D.; Bos, P.; Nguyen, D. X.; Nuyten, D.; Kreike, B.; Zhang, Y.; Wang, Y.; Ishwaran, H.; Foekens, J. A.; van de Vijver, M.; Massague, J. Lung Metastasis Genes Couple Breast Tumor Size and Metastatic Spread. *Proc. Natl. Acad. Sci. U. S. A.* 2007, 104 (16), 6740–6745.

(33) Leone, J. P.; Leone, B. A. Breast Cancer Brain Metastases: The Last Frontier. *Exp. Hematol. Oncol.* 2015, 4 (1), 33.

(34) Lin, N. U.; Winer, E. P. Brain Metastases: The HER2 Paradigm. *Clin. Cancer Res.* 2007, 13 (6), 1648–1655.

(35) Puhalla, S.; Elmquist, W.; Freyer, D.; Kleinberg, L.; Adkins, C.; Lockman, P.; McGregor, J.; Muldoon, L.; Nesbit, G.; Peereboom, D.; Smith, Q.; Walker, S.; Neuwelt, E. Unsanctifying the Sanctuary: Challenges and Opportunities with Brain Metastases. *Neuro. Oncol.* 2015, 17 (5), 639–651.

Liposomal Irinotecan Injection (nal-IRI) Achieves Significant Survival and Tumor Burden Control in a Triple Negative Breast Cancer Model of Spontaneous Metastasis

Nicholas Bernards^{1,*}, Manuela Ventura^{1,*}, Inga B. Fricke¹, Bart S. Hendriks^{2,†}, Jonathan Fitzgerald^{2,†}, Helen Lee^{2,†}, Jinzi Zheng^{1,3}

¹TECHNA Institute for the Advancement of Technology for Health, University Health Network, Toronto, Ontario, Canada; ²Merrimack Pharmaceuticals Inc., Cambridge, Massachusetts, USA; ³Institute of Biomaterials and Biomedical Engineering, University of Toronto, Ontario, Canada; *Equal contribution; †At time of study



Introduction

Triple negative breast cancer (TNBC) represents a significant treatment challenge due to its highly aggressive and metastatic nature.

Non-liposomal irinotecan (IRI) has been used in combination with other chemotherapeutics to treat metastatic breast cancer and TNBC, but showed toxicity and limited activity in patients [1]. Liposomal chemotherapeutics address these shortcomings allowing for decreased toxicity and increased drug exposure at the target site.

Liposomal irinotecan (nal-IRI, ONIVYDE®) was approved, in combination with fluorouracil and leucovorin, for the treatment of patients with metastatic adenocarcinoma of the pancreas after disease progression following gemcitabine-based therapy.

Aim

This study aims to investigate the potential therapeutic benefit of nal-IRI for the treatment of advanced TNBC in a clinically relevant mouse model of spontaneous metastasis.

Methods

- Female SCID mice inoculated with TNBC LM2-4-luc cells in the lower right mammary fat pad
- Primary tumors resected at 2-3 weeks post inoculation (mean tumor volume $230 \pm 60 \text{ mm}^3$)
- Metastasis formation followed using bioluminescence imaging (BLI) 2-3 times per week
- Randomization into 3 groups between day 5 and 9 post primary tumor resection, when animals presented with at least one BLI-detectable distant metastasis:
 - 1) No treatment control ($n = 13$)
 - 2) IRI (50 mg/kg, i.v.) once per week ($n = 13$)
 - 3) Nal-IRI (10 mg/kg, hydrochloride salt, i.v.) once per week ($n = 16$)

Bioluminescence Imaging of Tumor Burden

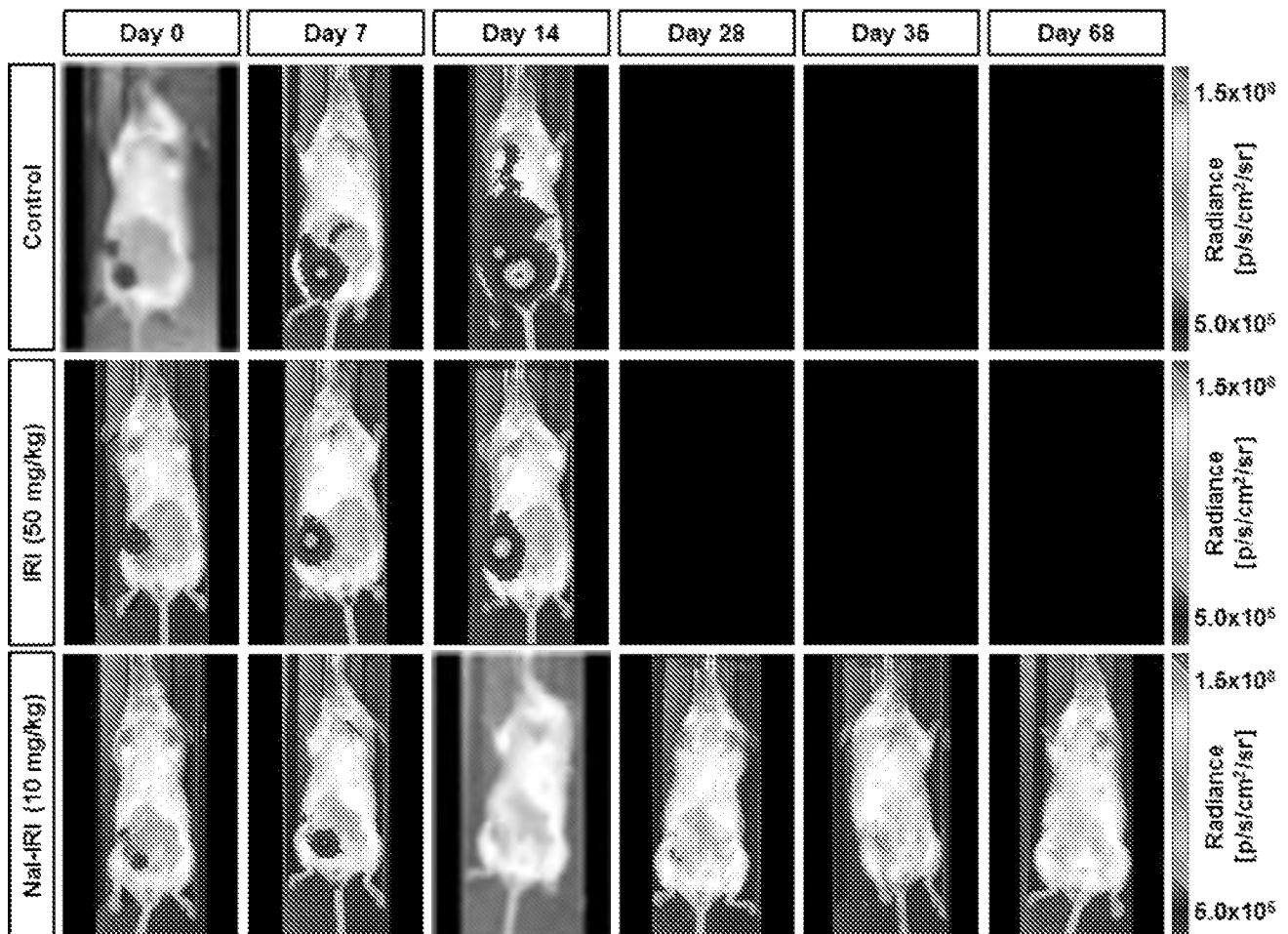
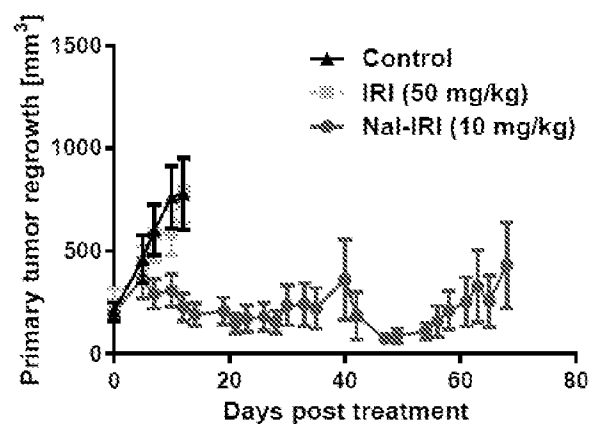
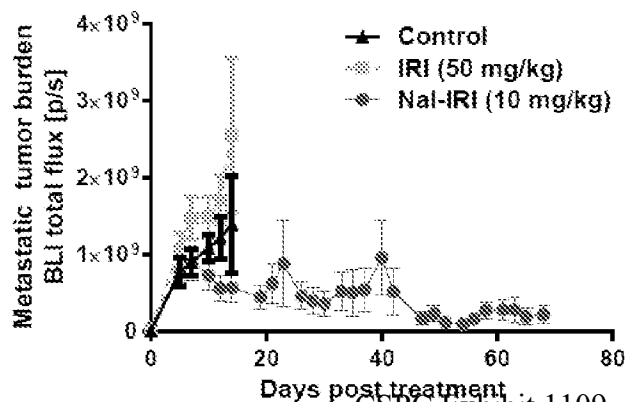


Figure 1: Representative BLI images showing primary tumor regrowth and metastatic disease burden up to the 50% survival time point for the three treatment groups: A delay in tumor regrowth at the site of the excised primary tumor and a reduced overall metastatic burden was observed for the nal-IRI treated animals compared to IRI treated and untreated controls.

A



B



CSPC Exhibit 1109

Page 26 of 339

Figure 2: Quantification of primary tumor regrowth (A) and metastatic tumor burden (B) in the three treatment groups up to the time point of 50% survival: (A) Primary tumor regrowth volume measured by caliper expressed in mm³ for each group. Treatment with nal-IRI was able to control the regrowth of the primary tumor compared to both the IRI treated and the untreated control animals. (B) BLI-based assessment of metastatic tumor burden, excluding signal from the primary tumor regrowth region. BLI measured mean photon flux at the 50% survival time point for the nal-IRI treated animals (day 68) was an order of magnitude lower ($2.2 \times 10^8 \pm 3.4 \times 10^8$ p/s) than for the IRI treated group ($2.6 \times 10^9 \pm 2.7 \times 10^9$ p/s) ($p = 0.0286$, t -test, day 14). This lower signal was already present on day 14 between nal-IRI treated group ($2.6 \times 10^9 \pm 1.01 \times 10^9$ p/s) and IRI ($p = 0.0286$, t -test, day 14), indicating effective control of the metastatic burden by nal-IRI.

Treatment Tolerability & Survival

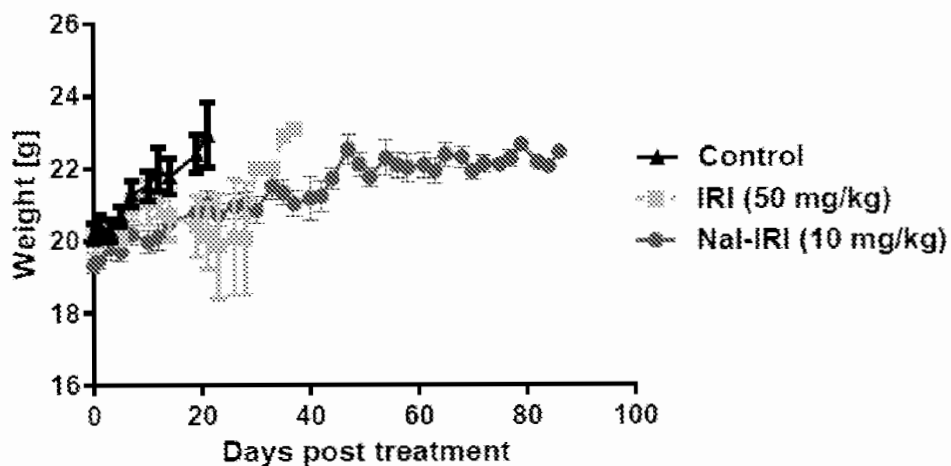


Figure 3: Animal body weight following treatment initiation: No significant changes in body weight were observed during the course of the study, indicating no adverse effects from the treatment.

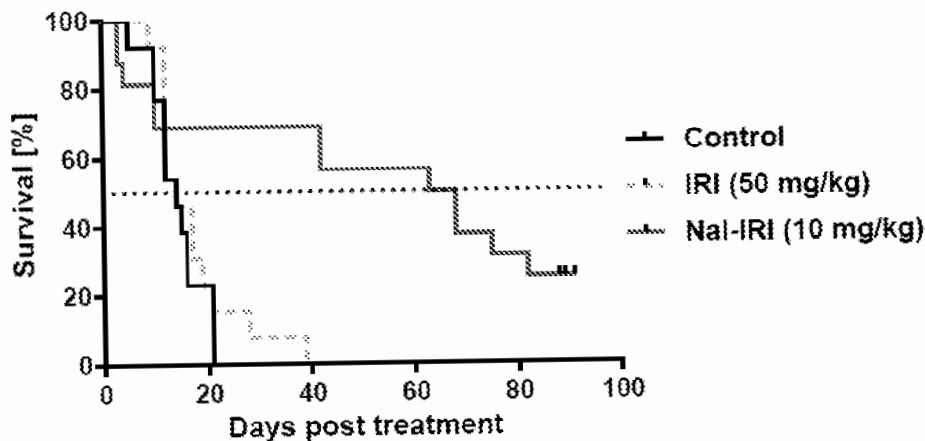


Figure 4: Survival post treatment initiation: Nal-IRI provided significant survival benefit (4.9 times longer than control or IRI treated groups) with 50% of the animals surviving until day 68 post treatment initiation, while 50% of the control and IRI-treated animals only survived until day 14. The dotted horizontal line indicates 50% survival.

Conclusion

In a highly aggressive TNBC model of spontaneous metastasis, **nal-IRI** demonstrated **superior anti-tumor activity** and provided **significant survival benefit** compared to IRI-treated and untreated groups, while being **well-tolerated**. **BLI** was successfully used as a **non-invasive and high-throughput technique to monitor** whole body **disease progression, metastatic spread** and **response to therapy** in mice longitudinally. These results indicate that nal-IRI has potential for the treatment of patients with TNBC and warrants clinical evaluation.

References

- [1] Kümler I, Brünner N, Stenvang J, Balslev E, Nielsen DL. A systematic review on topoisomerase 1 inhibition in the treatment of metastatic breast cancer. *Breast Cancer Res. Treat.* 2013. page 347–58.

Acknowledgements

The authors would like to thank Dr. Robert Kerbel and his lab for kindly providing us with the LM2-4-luc cell line and Ms. Maria Bisa and the Animal Resource Centre (ARC) for their technical support throughout the animal handling and monitoring procedures.

Liposomal Irinotecan Injection (nal-IRI) Achieves Significant Survival and Tumor Burden Control in a Triple Negative Breast Cancer Model of Spontaneous Metastasis

Nicholas Bernarda^{1,2*}, Manuela Ventura^{1,2*}, Inga B. Fricke¹, Bart S. Hendriks^{3,4*}, Jonathan Fitzgerald^{2,5*}, Helen Lee^{2,6*}, Jinzi Zheng^{1,3}

¹TECHNA Institute for the Advancement of Technology for Health, University Health Network, Toronto, Ontario, Canada; ²Merrimack Pharmaceuticals Inc., Cambridge, Massachusetts, USA; ³Institute of Biomaterials and Biomedical Engineering, University of Toronto, Ontario, Canada; *Equal contribution; †At time of study

Introduction

Triple negative breast cancer (TNBC) represents a significant treatment challenge due to its highly aggressive and metastatic nature. Non-liposomal irinotecan (IRI) has been used in combination with other chemotherapeutics to treat metastatic breast cancer and TNBC, but showed toxicity and limited activity in patients [1]. Liposomal chemotherapeutics address these shortcomings allowing for decreased toxicity and increased drug exposure at the target site. Liposomal irinotecan (nal-IRI; ONI-015) was approved, in combination with fluorouracil and leucovorin, for the treatment of patients with metastatic adenocarcinoma of the pancreas after disease progression following gemtuzabine-based therapy.

Aims

This study aims to investigate the potential therapeutic benefit of nal-IRI for the treatment of advanced TNBC in a clinically relevant mouse model of spontaneous metastasis.

Methods

- Female SCID mice inoculated with TNBC LM2-4-loc cells in the lower right mammary fat pad
- Primary tumors resected at 2-3 weeks post inoculation (mean tumor volume $230 \pm 60 \text{ mm}^3$)
- Metastasis formation followed using bioluminescence imaging (BLI) 2-3 times per week
- Randomization into 3 groups between day 5 and 9 post primary tumor resection, when animals presented with at least one BLI-detectable distant metastasis:
 - No treatment control (n = 12)
 - IRI (50 mg/kg, i.v.) once per week (n = 12)
 - Nal-IRI (10 mg/kg, hydrochloride salt, i.v.) once per week (n = 12)

Bioluminescence imaging of Tumor Burden

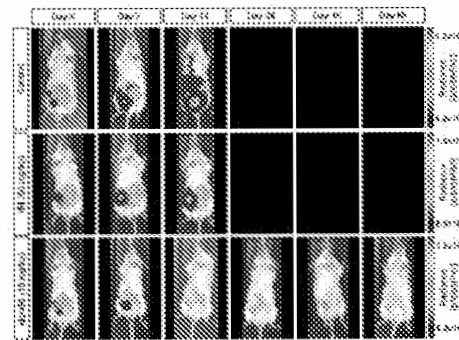


Figure 1: Representative BLI images showing primary tumor regrowth and metastatic disease burden up to the 50% survival time point for the three treatment groups. A delay in tumor regrowth at the site of the excised primary tumor and a reduced overall metastatic burden was observed for the nal-IRI treated animals compared to IRI treated and untreated controls.

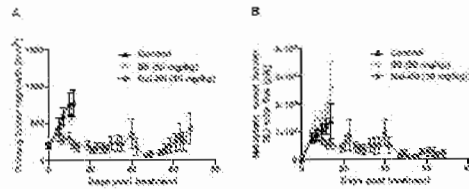


Figure 2: Quantification of primary tumor regrowth (A) and metastatic tumor burden (B) in the three treatment groups up to the time point of 50% survival: (A) Primary tumor regrowth: volume measured by caliper expressed in mm^3 for each group. Treatment with nal-IRI was able to control the regrowth of the primary tumor compared to both the IRI treated and the untreated control animals. (B) BLI-based assessment of metastatic tumor burden, excluding signal from the primary tumor regrowth region. BLI measured mean photon flux at the 50% survival time point for the nal-IRI treated animals (day 65) was an order of magnitude lower ($2.2 \times 10^3 \pm 3.4 \times 10^3 \text{ p/s}$) than for the IRI treated group ($2.6 \times 10^4 \pm 2.7 \times 10^4 \text{ p/s}$) ($p = 0.0205$, t-test, day 14). This lower signal was already present on day 14 between nal-IRI treated group ($2.8 \times 10^3 \pm 1.6 \times 10^3 \text{ p/s}$) and IRI ($p = 0.0205$, t-test, day 14), indicating effective control of the metastatic burden by nal-IRI.

Treatment Tolerability & Survival

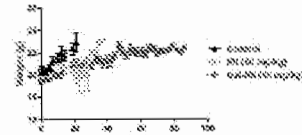


Figure 3: Animal body weight following treatment initiation: no significant changes in body weight were observed during the course of the study, indicating no adverse effects from the treatment.

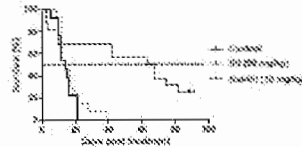


Figure 4: Survival post treatment initiation: Nal-IRI provided significant survival benefit (2.9 times longer than control or IRI treated groups) with 50% of the animals surviving until day 65 post treatment initiation, while 50% of the control and IRI-treated animals only survived until day 14. The dashed horizontal line indicates 50% survival.

Conclusion

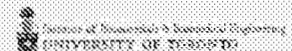
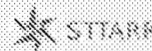
In a highly aggressive TNBC model of spontaneous metastasis, nal-IRI demonstrated superior anti-tumor activity and provided significant survival benefits compared to IRI-treated and untreated groups, while being well-tolerated. BLI was successfully used as a non-invasive and high-throughput technique to monitor whole body disease progression, metastatic spread and response to therapy in mice longitudinally. These results indicate that nal-IRI has potential for the treatment of patients with TNBC and warrants clinical evaluation.

References

- [1] Kübler I, Brünner H, Stehling J, Baizer F, Nielsen DL. A systematic review on topoisomerase 1 inhibition in the treatment of metastatic breast cancer. *Breast Cancer Res Treat*. 2013; page 347–58.

Acknowledgements

The authors would like to thank Dr. Robert Karbel and his lab for kindly providing us with the LM2-4-loc cell line and Ms. Maria Eisa and the Animal Resource Centre (ARC) for their technical support throughout the animal handling and monitoring procedures.



BBAMEM 76110

Optimization of the retention properties of vincristine in liposomal systems

Nancy L. Boman^{a,*}, Lawrence D. Mayer^b and Pieter R. Cullis^a

^a The University of British Columbia, Biochemistry Department, 2146 Health Sciences Mall Vancouver, British Columbia V6T 1Z3 (Canada) and ^b British Columbia Cancer Agency, 600 West 10th Avenue, Vancouver, British Columbia V5Z 4E6 (Canada)

(Received 23 February 1993)

(Revised manuscript received 4 June 1993)

Key words: Liposome; Vincristine; Drug retention; Lipid composition; pH, internal; Internal buffering capacity

The influence of lipid composition, internal pH and internal buffering capacity on the retention properties of vincristine loaded into large unilamellar vesicle (LUV) systems in response to transmembrane pH gradients has been assessed. It is shown that increasing the (saturated) acyl chain length of the phosphatidylcholine molecule, increasing the internal buffering capacity, and decreasing the internal pH all result in increased drug retention. Further, a study of the pH dependence on the rates of accumulation indicate that uptake proceeds via the neutral form of the vincristine molecule. This uptake is associated with an activation energy of 37 kcal/mol for DSPC/Chol LUVs. It is shown that the major improvement in drug retention in vitro is achieved by employing low initial internal pH values, where 90% retention is obtained over 24 h for an initial internal pH of 2. Improved retention in vivo was also observed where a drug-to-lipid ratio approx. 4-fold greater at 24 h was maintained.

Introduction

Encapsulation of various antineoplastic agents within lipid vesicles has been shown to decrease toxic side effects while increasing or maintaining therapeutic activity [1–12]. This includes the vinca alkaloid vincristine [13]. Since the vinca alkaloids are cell-cycle-specific cytotoxic drugs, it may be conjectured that an ability to maintain high serum levels of drug for extended periods would be advantageous. A liposome system which allows extended payout in the circulation is therefore desirable. Previous work employing doxorubicin has shown that increased drug retention leads to an increase in drug circulation time [14] and increased anti-tumor activity [15]. However, currently available retention properties for vincristine are not optimal, as the best available formulation of liposomal vincristine releases drug in vivo with a half-life of less than 8 h, leading to more than 90% release by 24 h.

In this work we explore three parameters which may be expected to result in improved retention characteristics of liposomal formulations of vincristine and other lipophilic, amino-containing drugs. These include the use of phospholipids with increased acyl chain length, reduction of the interior pH and increased interior

buffering capacity. The latter two parameters are important factors in the loading of lipophilic amines, such as vincristine, into vesicles exhibiting a transmembrane pH gradient (ΔpH ; inside acidic) [13,16]. It is shown that the major factor resulting in improved retention is the interior pH, where initial interior pH values of 2 result in nearly 50% retention at 24 h in vivo.

Materials and Methods

Dimyristoyl PC (DMPC), dipalmitoyl PC (DPPC), distearoyl PC (DSPC), diarachidoyl PC (DAPC) and dibehenoyl PC (DBPC) were purchased from Avanti Polar Lipids, and were > 99% pure. Cholesterol and all salts were obtained from Sigma (St. Louis, MO, USA). Vincristine sulfate was purchased from the British Columbia Cancer Agency (Vancouver, British Columbia, Canada). [¹⁴C]cholesteryl hexadecyl ether was purchased from New England Nuclear (Ontario, Canada) and was > 95% pure. It was chosen as a lipid marker due to its stability in vivo [17]. Tritiated vincristine was obtained from Amersham (Oakville, Ontario, Canada). Normal mouse serum was purchased from Cedar Lane Laboratories and female BDF1 mice (6–8 weeks old) were purchased from Charles River Laboratories.

PC/Chol (55:45 molar ratio) liposomes were prepared by first dissolving the lipid mixture in 95% CSPC Exhibit 1109

* Corresponding author. Fax: +1 (604) 822 4843.

ethanol at a lipid concentration of 100 mg/ml. Multilamellar vesicles (MLVs) were formed by adding citrate buffer to the ethanol solution to achieve a final concentration of 25 mg total lipid/ml. The samples were then maintained above the transition temperature for an additional 30 min to allow equilibration of buffer across the lipid bilayers (65°C for DMPC, DPPC and DSPC; 85°C for DAPC; and 100°C for DBPC). These MLVs were then extruded 10 times through an extrusion device obtained from Lipex Biomembranes (Vancouver, British Columbia, Canada) equilibrated at the same temperature [18]. The extruder was fitted with two Nucleopore polycarbonate filters with a pore size of 100 nm. Ethanol was then removed from the resulting LUVs by dialysis against two changes of 100 volumes of citric acid buffer over a 24-h period employing Spectra/Por 2 dialysis tubing (cutoff 12–14 kDa). This procedure has shown to remove > 99.9% of the ethanol from the liposomes (employing [¹⁴C]EtOH).

For the vincristine uptake experiments, drug was added to the various liposome preparations to achieve a maximum drug-to-lipid ratio of 0.1:1. The exterior pH of the vesicles was then raised to pH 7.0–7.2 with 0.5 M Na₂HPO₄ and incubated at 37°C over a 4-h period. Aliquots were removed at various time points for determination of vincristine uptake. External untrapped vincristine was removed by running the samples over G-50 Sephadex columns prior to dual label scintillation counting of the liposomal fractions contained in the void volume.

Vincristine release experiments were performed as follows. Vincristine was entrapped in the liposomes using the same procedure as for the drug uptake experiments, except that the samples were immediately heated to their lipid transition temperatures for 10 min. This ensured > 95% trapping efficiencies at a drug-to-lipid ratio of 0.1:1 for all lipid compositions studied [13].

The liposomally entrapped drug was then diluted in either HBS (pH 7.4) or normal mouse serum by a factor of 10. These samples were dialyzed using Spectra/Por 2 dialysis tubing against 200 vols. of HBS (pH 7.4) at 37°C. Aliquots were removed at various time points, run down G-50 Sephadex columns, and retained vincristine analyzed by dual label scintillation counting.

In vivo experiments were performed by injecting liposomal vincristine into BDF-1 mice via a lateral tail vein (2 mg/kg vincristine, 20 mg/kg lipid). At varying time points, mice were anaesthetized with i.p. ketamine (160 mg/kg) and xylazine (20 mg/kg). Blood was removed via cardiac puncture and placed into EDTA-coated microtainer tubes (Becton Dickenson). Samples were then centrifuged and plasma was analyzed for lipid and vincristine content by dual label liquid scintillation counting.

Kinetic analysis of vincristine uptake and release

An initial-rates treatment of the uptake of lipophilic amino containing drugs into vesicles with an acidic interior has been previously developed for doxorubicin [23]. We consider first weak bases with a single ionizable group with a dissociation constant (K_d) where $K_d \ll [H^+]_o$ where $[H^+]_o$ is the exterior proton concentration. Assuming that V_o , the aqueous volume, is much larger than V_m , where V_m is the volume of the membrane, it can be shown that

$$[D(t)]_i = [D(eq)]_i(1 - e^{-kt}) \quad (1)$$

where $[D(t)]_i$ is the interior concentration of drug at time t , $[D(eq)]_i$ is the interior drug concentration at equilibrium and k is the rate constant associated with uptake. The rate constant k can be written as [23]

$$k = \frac{PA_m K}{V_o [H^+]_o} K_d \quad (2)$$

where P is the membrane permeability coefficient for the neutral form of the weak base, A_m is the area of the membrane, and K is the lipid-water partition coefficient of the drug. It is straightforward to perform a similar analysis for a drug such as vincristine, which contains two basic functions. Under the assumption that $[H^+]_o \gg K_{d1}, K_{d2}$ (where K_{d1}, K_{d2} are the dissociation constants associated with the two basic groups) it can be shown that

$$k = \frac{PA_m K}{V_o [H^+]_o^2} K_{d1} K_{d2} \quad (3)$$

As noted in Results, the condition $[H^+]_o \gg K_{d1}, K_{d2}$ is difficult to observe for vincristine as the ionizable groups exhibit relatively low pK values of $pK_1 = 5.0$ and $pK_2 = 7.4$. Thus, at external pH values below 5 the rate constant associated with uptake would be expected to increase as the pH is raised in proportion to $[H^+]_o^{-2}$, whereas in the interval $5 < pH_o < 7.4$ it would be expected that $k \propto [H^+]_o^{-1}$.

Results

Influence of acyl chain length on vincristine retention

Previous studies on doxorubicin [19] and vincristine [13] have shown that drug retention after loading in response to a ΔpH (inside acidic) is enhanced in DSPC-cholesterol LUVs in comparison to EPC-cholesterol LUVs. It may be expected that the presence of longer chain saturated PCs will further improve the retention properties. The uptake and release properties of LUVs composed of diarachidoyl PC (DAPC) and dibehenoyl PC (DBPC), in combination with cholesterol, were therefore investigated.

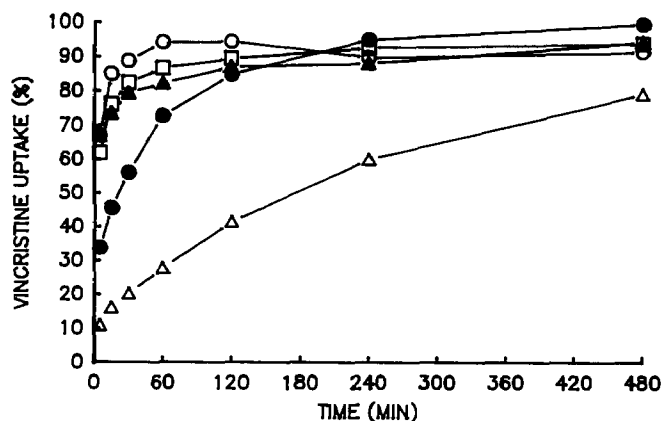


Fig. 1. Vincristine uptake across a pH gradient at 37°C for DMPC/Chol (○), DPPC/Chol (●), DSPC/Chol (△), DAPC/Chol (▲) and DBPC/Chol (□). Vincristine was added to vesicle preparations at a potential drug-to-lipid ratio of 0.1:1. Internal pH was 4.0 and external pH was 7.5. All vesicles were sized through 100-nm filters.

As a first step in this process, the production of LUVs containing the C_{20} compound DAPC and the C_{22} compound DBPC was required. Extrusion of DAPC dispersions, even in mixtures with cholesterol, is difficult at temperatures below the gel-liquid crystalline transition temperature of the DAPC (approx. 80°C). It was found that extrusion of DBPC/cholesterol (55:45) dispersions required an extrusion temperature in excess of 95°C, which proved experimentally inconvenient. The procedure detailed in Materials and Methods was therefore employed which involved extrusion in the presence of 25% ethanol, which markedly facilitated the ease of extrusion through 100 nm pore size. As indicated in Materials and Methods, the ethanol was subsequently removed by dialysis. For comparative purposes, LUVs for drug loading were prepared from mixtures of cholesterol with DMPC (C_{14}), DPPC (C_{16}), DSPC (C_{18}), DAPC (C_{20}) and DBPC (C_{22}). Standard procedures were employed, which involved hydration at pH 4.0 in the presence of 300 mM citrate, extrusion and ethanol removal as indicated in Materials and Methods and subsequently raising the exterior pH to 7.5 with 0.5 M Na_2HPO_4 . The uptake of vincristine into these LUVs at 37°C is shown in Fig. 1. As expected, the rate of uptake was fastest for the DMPC-cholesterol system, and decreased progressively for DPPC-cholesterol and DSPC-cholesterol systems. Surprisingly, this progression was reversed for DAPC- and DBPC-cholesterol systems, which exhibited rates of vincristine uptake which increased as the acyl chain length increased.

The release characteristics of vincristine from the liposomes on prolonged incubation (24 h) at 37°C in the presence of buffer and serum were also investigated (results not shown). The DMPC-cholesterol system exhibits the most rapid leakage, whereas the DAPC-cholesterol and DBPC-cholesterol exhibit the

best retention, with approx. 40% of the drug remaining at 24 h in the presence of mouse serum.

Influence of interior buffering capacity on vincristine retention

As has been well described elsewhere for doxorubicin [23], the ability to accumulate high levels of weak base drugs in response to ΔpH is a sensitive function of the interior buffering capacity. This is because the molecules permeate across the bilayer in the neutral form and are protonated on reaching the interior, thus consuming a proton and raising the interior pH. This will, in turn, limit the equilibrium uptake of drug. In the case of vincristine, for example, which contains two basic functions it is straightforward to show that, in the absence of membrane partitioning effects, and assuming that $[\text{H}^+]_o, [\text{H}^+]_i \gg K_{d1}, K_{d2}$ that

$$\frac{[\text{Drug}]_i}{[\text{Drug}]_o} \leq \frac{[\text{H}^+]_i^2}{[\text{H}^+]_o^2} \quad (4)$$

and thus the amount of drug entrapped will decrease as the square of the internal proton concentration as the internal pH rises.

The influence of interior buffering capacity on the retention properties of DBPC-cholesterol LUVs at 37°C was also investigated for both buffer and serum media (results not shown). As expected, higher initial internal citrate levels resulted in improved retention, however, these improvements were not significant for internal citrate concentrations in excess of 400 mM. At internal citrate concentrations of both 400 and 500 mM, >50% drug retention was achieved at 24 h when incubated in mouse serum.

Influence of internal pH on drug retention

As indicated in Materials and Methods, a model based on the assumption that only the neutral form of the vincristine is membrane permeable predicts that the rate constant for transbilayer movement of vincristine should be proportional to the inverse square of the proton concentration. Thus, if the interior pH is lowered, the efflux of entrapped vincristine should be significantly slower. The first set of experiments was designed to examine the dependence of the rate constant k on the pH. As indicated in Materials and Methods, when $[\text{H}^+]_o \gg K_{d1}, K_{d2}$ it is expected that $k \propto [\text{H}^+]_o^{-2}$ and, thus, $\log k \propto 2\text{pH}_o$. Thus, a plot of $\log k$ vs. pH_o should result in a straight line with a slope of 2. Uptake behaviour was therefore monitored over the external pH range 4–5 for DSPC-cholesterol LUVs. As shown in Fig. 2A, the uptake rates vary dramatically over this range. The rate constants k can be calculated from the slopes of the semilogarithmic plots shown in Fig. 2B, leading to a plot of $\log k$ vs. pH_o (Fig. 2C) which exhibits a slope of 1.6. The devia-

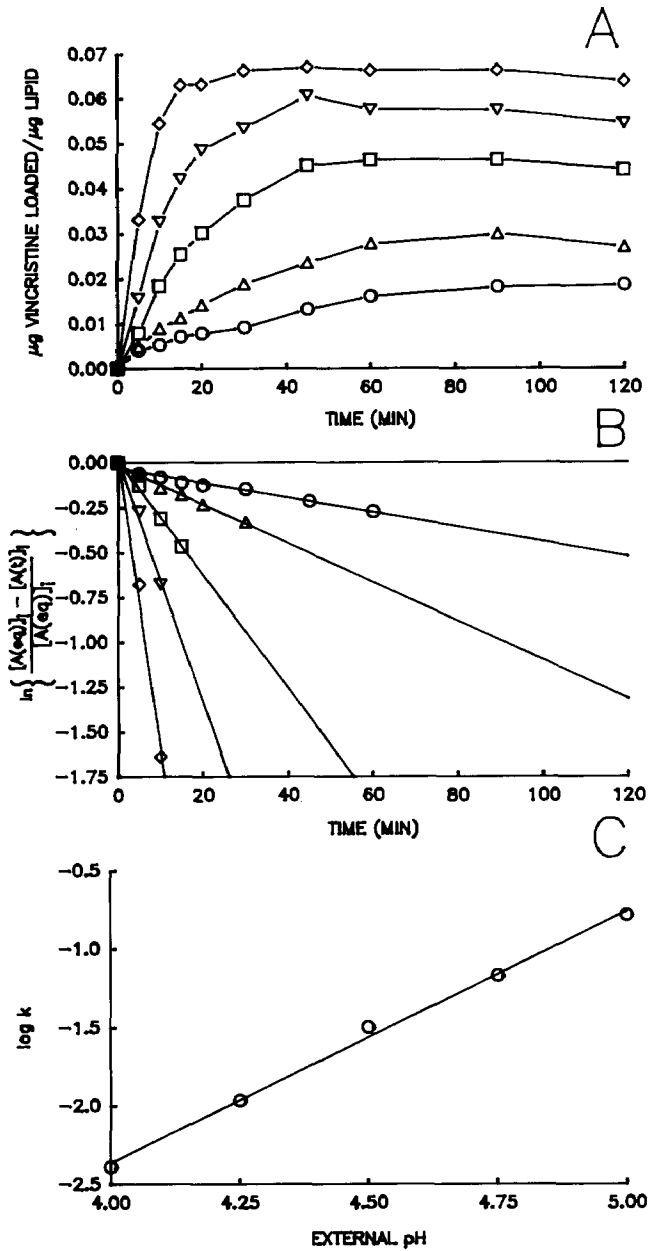


Fig. 2. (A) Time-course for vincristine uptake into 100-nm DSPC/Chol vesicles for different external pH values. The internal pH for all systems was 3.0. The external pH values were 4.00 (○), 4.25 (△), 4.50 (□), 4.75 (▽), and 5.00 (◇). All samples were loaded at 60°C with a potential drug-to-lipid ratio of 0.1:1. (B) Plot of $\ln\{([A(eq)]_i - [A(t)]_i) / [A(eq)]_i\}$ vs. time, where $[A(t)]_i$ is the internal concentration of the accumulated drug at time t and $[A(eq)]_i$ is the internal concentration at equilibrium. The slopes of these lines give the rate constant (k) for the transport of vincristine across the liposome membrane. (C) Plot of $\log k$ vs. external pH. The slope of this line is 1.60.

tion from the slope of 2 expected is likely due to the low value of the first pK_1 of vincristine ($pK_1 = 5.0$), and thus the condition $[H^+]_o \gg K_1$ is not well observed.

The results of Fig. 2 indicate that efflux rates will be extremely sensitive to the interior pH after loading vincristine, and that lower internal pH values should

markedly increase retention. DSPC/cholesterol (55:45) LUVs were therefore prepared with initial interior pH values of 2.0, 3.0, 4.0 and 5.0, employing the 300 mM citrate buffer. As shown in Fig. 3, these variations had a profound effect on vincristine retention, with (initial) pH_i values of 3 or less, giving rise to essentially complete retention of contents for 24-h incubations in the presence of both buffer and serum. Lowering the internal pH appears to exhibit its greatest effect on improving drug retention initially. The slopes of the curves in Fig. 3 are not as markedly different after the 1 h time point.

Influence of temperature on vincristine uptake

A final variable which would be expected to influence vincristine uptake (and, by extension, release) is temperature. It has been shown elsewhere that weak bases such as doxorubicin (unpublished data), as well as amino acid and peptide derivatives [20] can exhibit high activation energies for uptake rates in the range of 30 kcal/mol. An activation energy of 30 kcal/mol corresponds to an uptake rate which increases by ap-

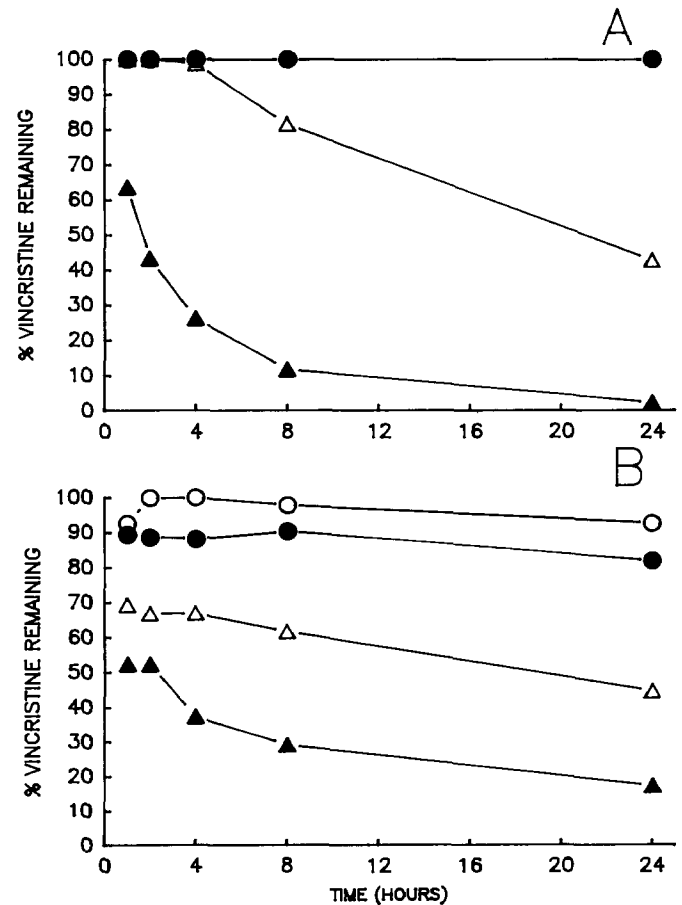


Fig. 3. Vincristine release from 100-nm DSPC/Chol vesicles incubated in buffer (A) and mouse serum (B) at 37°C for internal pH of 2.0 (○), 3.0 (●), 4.0 (△) and 5.0 (▲). Internal buffering capacity was 300 mM citrate for all systems. Initial drug-to-lipid ratios were 0.1:1.

prox. a factor of 5 for every 10°C increase in temperature. Vincristine uptake into DSPC-cholesterol LUVs was therefore monitored over the temperature range 30–60°C which resulted in remarkable differences in uptake rates as shown in Fig. 4A. An Arrhenius plot (Fig. 4C) of the rate constants derived from these data resulted in an activation energy of 37 kcal/mol.

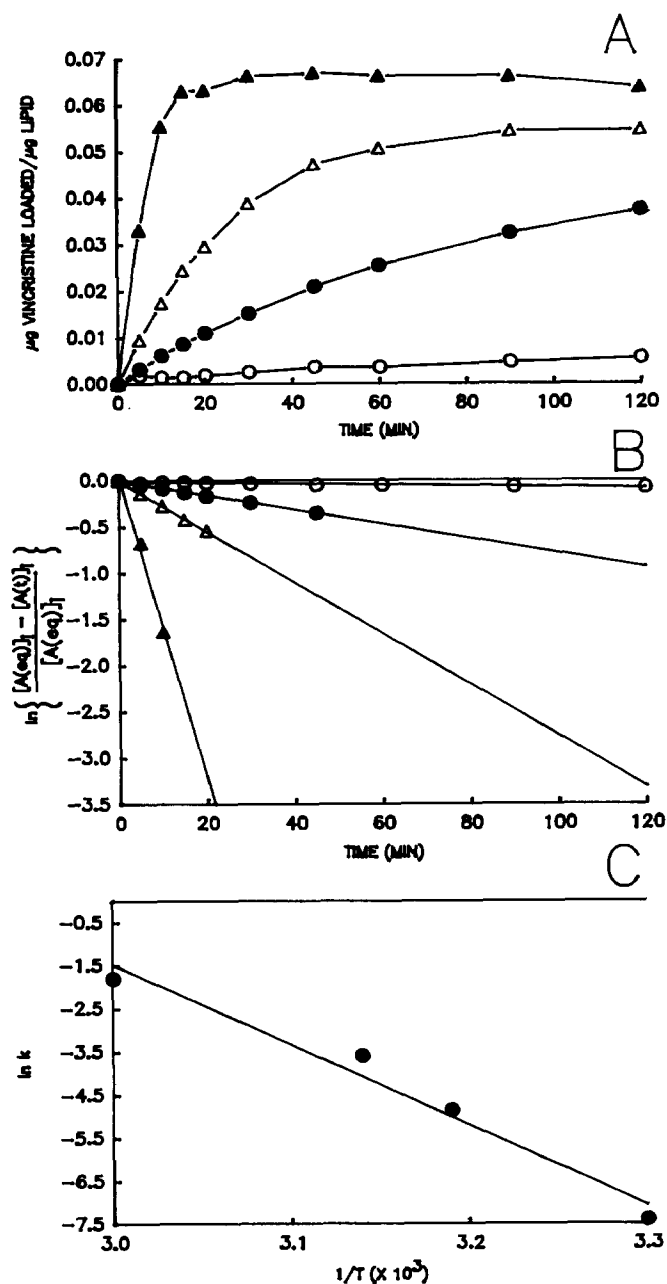


Fig. 4. (A) Time-course of vincristine uptake into 100-nm DSPC/Chol vesicles exhibiting a Δ pH ($pH_i = 3.0$; $pH_o = 5.0$). Uptake was conducted at 30 (○), 40 (●), 45 (△), and 60°C (▲). (B) Plot of $\ln \left\{ \frac{[A(eq)]_i - [A(t)]_i}{[A(eq)]_i} \right\}$ vs. t , where $[A(t)]_i$ and $[A(eq)]_i$ are the same as for Fig. 2. (C) Arrhenius plot of the rate constants (k) for vincristine uptake. The activation energy calculated from the slope of this plot is 37 kcal/mol.

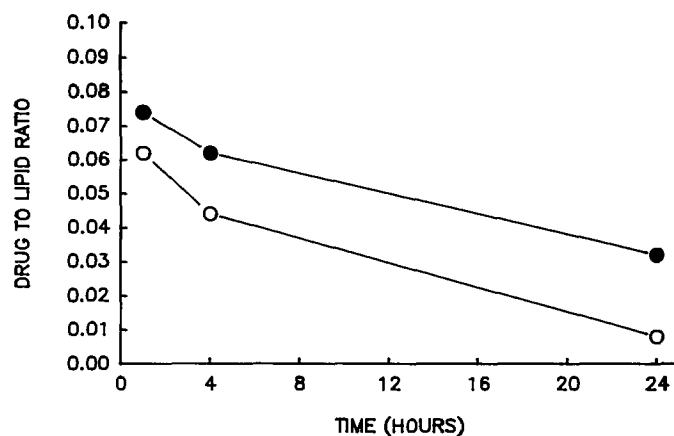


Fig. 5. Drug-to-lipid ratios for DSPC/Chol vesicles in vivo with internal pH of 2.0 (●) and 4.0 (○). Both systems were loaded with an initial drug-to-lipid ratio of 0.1:1. Each point represents the average value obtained from four BDF1 mice.

Vincristine retention in DSPC / cholesterol LUVs in vivo

A basic aim of these studies was to identify parameters which would lead to a formulation of liposomal vincristine which is able to better retain the drug in vivo to allow for extended circulation lifetime and payout characteristics. It is clear from the studies presented above that the internal pH is the most important variable for retention, and that DSPC/cholesterol LUVs prepared with an (initial) pH_i of 3 or less exhibit retention of 90% or more over 24 h in the presence of buffer or serum. However, it is also known that liposome leakage in vivo is usually more extensive than in vitro [21]. The release properties in vivo, of DSPC-cholesterol LUVs with (initial) interior pH values of 2 and 4 and loaded with vincristine were assessed by monitoring the drug-to-lipid ratio in plasma (Fig. 5). It may be observed that whereas the 90% retention over 24 h obtained in vitro was not achieved for the $pH_i = 2$ formulation, a value of 40% was achievable. This is approx. a factor of 5 higher than obtained with the $pH_i = 4.0$ formulation. It is once again apparent, as in vitro, that the most marked difference in vincristine release rates is seen before 1 h post-injection. It is of interest that DBPC/cholesterol (55:45) preparations with 0.5 M internal citrate at $pH_i = 2.0$ did not result in improved retention in vivo over the DSPC-cholesterol systems (results not shown). It should be noted that > 99% of injected free vincristine (no liposomal carrier) is cleared from the circulation within 5 min post injection (Mayer et al., unpublished data).

Discussion

This report presents a detailed study of factors leading to improved retention of vincristine in liposomal systems. These results may also be expected to extend to other members of the large class of drugs

which are lipophilic weak bases. Here we discuss the influence of the experimental parameters investigated on vincristine uptake and release and the implications for design of liposomal formulations of lipophilic amino containing drugs.

Increases in acyl chain length are shown to exhibit the type of retention improvements expected. Thus, the half-times for vincristine release at 37°C in buffer increase from approx. 1 h for DMPC/Chol LUVs to approx. 12 h for DAPC- and DBPC-containing systems. The uptake of vincristine into these systems exhibits anomalous behavior in that the rates of uptake first decrease, as expected, as acyl chain length is increased to 18 carbons (DSPC), and then increase markedly for the DAPC and DBPC systems. It is possible that this reflects an increased lipid-water partition coefficient for vincristine for the outer monolayer of the DAPC and DBPC systems. An increased hydrophobicity of this interface would be consistent with packing effects expected for longer chain lipids in small vesicular systems, and this is reflected by the increased tendency of the longer chain DAPC and DBPC LUV systems to aggregate after extrusion. Conversely, for the inner monolayer, it would be expected that these effects would result in tighter packing in the headgroup region, and correspondingly reduced leakage, as shown experimentally.

With regard to interior buffer capacity, the results presented here show that increasing the interior citrate concentration above 400 mM does not result in significant improvements in vincristine retention. This is consistent with the osmotic properties of extruded LUV systems. As shown for 100 nm egg PC/cholesterol systems [23], extruded LUVs exhibit tubular 'sausage' shapes and respond to osmotic gradients (high interior osmolarity) first by 'rounding up' to increase the interior volume and subsequently undergo osmotically induced lysis. For EPC/Chol LUVs the 'effective' osmotic difference that can be sustained is approx. 650 mosmol/kg. The osmolarity of 400 mM citrate, pH 4.0, is 700 mosmol/kg, resulting in an effective osmotic imbalance of 400 mosmol/kg when the liposomes are in normal saline solution (osmolarity 300 mosmol/kg). This initial effective osmotic imbalance will increase on drug loading. Vincristine, after crossing the liposomal bilayer in its neutral form, becomes protonated in the vesicle interior due to the low internal pH, consequently raising the internal osmolarity.

Lower internal pH values are clearly critical for improving vincristine retention in liposomal systems. There are two factors which lead to this effect. The first involves the improved internal buffering capacity resulting from initial interior pH values which are below the lowest pK ($pK_1 = 3.13$) of the citrate carboxyl functions. However, the dominant effect is likely due to the dependence of the rate constant for vin-

cristine movement on the inverse square of the proton concentration (Eqn. 3). This predicts a 100-fold reduction in leakage rates for every unit the interior pH is lowered.

In conclusion, the internal pH is the most important parameter in enhancing liposomal vincristine retention both in vitro and in vivo. These effects can likely be extended to enhance retention of other basic drugs in liposomes in vitro and in vivo.

Acknowledgements

This research was supported by the National Cancer Institute of Canada. N.L.B. is a recipient of a Fellowship from the Medical Research Council of Canada.

References

- Herman, E.H., Rahman, A., Ferrans, V.J., Vicks, J.A. and Schein, P.S. (1983) *Cancer Res.* 43, 5427–5432.
- Forsen, E.A. and Tokes, A.A. (1981) *Proc. Natl. Acad. Sci. USA* 78, 1873–1877.
- Gregoriadis, G. and Neerunjun, E.D. (1975) *Res. Commun. Chem. Pathol. Pharmacol.* 10, 351–362.
- Woo, S.Y., Dilliplane, P., Rahman, A. and Sinks, L.F. (1983) *Cancer Drug Deliv.* 1, 59–62.
- Mayhew, E. and Rustum, Y.M. (1985) *Prog. Clin. Biol. Res.* 172B, 301–310.
- Gabizon, A., Goren, D., Fuks, Z., Barenholz, Y., Dagan, A. and Meshorer, A. (1982) *Cancer Res.* 43, 4730–4735.
- Kobayashi, T., Kataoka, T., Tsukagoshi, S. and Sakurai, Y. (1977) *Int. J. Cancer* 20, 581–587.
- Hunt, C.A., Rustum, Y.M., Mayhew, E. and Papahadjopoulos D. (1979) *Drug Metab. Dispos.* 7, 124–128.
- Rahman, A., More, N. and Schein, P.S. (1982) *Cancer Res.* 42, 1817–1825.
- Gregoriadis, G. (ed.) (1988) *Liposomes as Drug Carriers*, Wiley, New York.
- Fichtner, I., Reszka, R., Elbe, B. and Arndt, D. (1981) *Neoplasma* 28, 141–149.
- Gabizon, A., Dagan, A., Goren, D., Barenholz, Y. and Fuks, Z. (1982) *Cancer Res.* 42, 4734–4739.
- Mayer, L.D., Bally, M.B., Loughrey, H., Masin, D. and Cullis, P.R. (1990) *Cancer Res.* 50, 575–579.
- Bally, M.B., Nayar, R., Masin, D., Hope, M.J., Cullis, P.R. and Mayer, L.D. (1990) *Biochim. Biophys. Acta* 1023, 133–139.
- Mayer, L.D., Bally, M.B., Cullis, P.R., Wilson, S.L. and Emerman, J.T. (1990) *Cancer Lett.* 53, 183–190.
- Mayer, L.D., Tai, L.C.L., Bally, M.B., Mitilenes, G.N., Ginsberg, R.S. and Cullis, P.R. (1990) *Biochim. Biophys. Acta* 1025, 143–151.
- Derksen, J.T.P., Morselt, H.W.M. and Scherphof, G.L. (1987) *Biochim. Biophys. Acta* 931, 33–40.
- Olson, F., Hunt, C.A., Szoka, F.C., Vail, W.J. and Papahadjopoulos, D. (1979) *Biochim. Biophys. Acta* 557, 9–23.
- Mayer, L.D., Bally, M.B. and Cullis, P.R. (1990) *J. Liposome Res.* 1, 463–480.
- Chakrabarti, A.C., Clark-Lewis, I., Harrigan, P.R. and Cullis, P.R. (1992) *Biophys. J.* 61, 228–234.
- Mayer, L.D., Tai, L.C.L., Ko, D.S.C., Masin, D., Ginsberg, R.S., Cullis, P.R. and Bally, M.B. (1989) *Cancer Res.* 49, 5922–5930.
- Mui, B.L.S., Cullis, P.R., Evans, E.A. and Madden, T.D. (1993) *Biophys. J.* 64, 443–453.
- Harrigan, P.R., Wong, K.F., Redelmeier, T.E., Wheeler, J.J. and Cullis, P.R. (1993) *Biochim. Biophys. Acta* 1149, 329–338.

A randomized phase II trial of capecitabine and two different schedules of irinotecan in first-line treatment of metastatic colorectal cancer: efficacy, quality-of-life and toxicity

M. M. Borner*, J. Bernhard, D. Dietrich, R. Popescu, M. Wernli, P. Saletti, D. Rauch, R. Herrmann, D. Koeberle, H. Honegger, P. Brauchli, D. Lanz & A. D. Roth
On behalf of the Swiss Group for Clinical Cancer Research (SAKK), Berne, Switzerland

Received 29 July 2004; revised 6 September and 14 September 2004; accepted 15 September 2004

Background: To determine the efficacy, impact on quality-of-life (QoL) and tolerability of two different irinotecan administration schedules in combination with capecitabine as first-line treatment of metastatic colorectal cancer.

Patients and methods: We carried out a randomized phase II trial to select one of the following treatment regimens for further investigation: weekly irinotecan at a dose of 70 mg/m² days 1, 8, 15, 22, 29 (arm A) or 3-weekly irinotecan at a dose of 300/240 mg/m² day 1 and days 22 (arm B) in combination with capecitabine 1000 mg/m² twice daily days 1–14 and days 22–35 every 6 weeks.

Results: Seventy-five patients with good performance status entered the trial. The two arms were well balanced for relevant patient and disease characteristics. The most frequent toxic effects were grade 3/4 diarrhea (arm A: 34%, B: 19%), grade 3/4 neutropenia (A: 5%, B: 19%) and grade 2/3 alopecia (A: 26%, B: 65%). Other grade 3/4 toxic effects were rare (<5%). Response rates were 34% [95% confidence interval (CI) 20% to 51%] in arm A and 35% (95% CI: 20% to 53%) in arm B. Median time to progression was 6.9 (4.6–10.1) and 9.2 (7.9–11.5) months and median overall survival was 17.4 (12.6–23.0+) and 24.7 (16.3–26.4+) months. Patients with an objective tumor response reported better physical well-being ($P < 0.01$), mood ($P < 0.05$), functional performance ($P < 0.05$) and less effort to cope ($P < 0.05$) compared with the non-responders and stable disease patients.

Conclusions: The primary end point of this study was the objective response rate and based on the statistical design of the trial, the 3-weekly irinotecan schedule was selected over weekly irinotecan administration. The 3-weekly irinotecan schedule also seemed advantageous in terms of grade 3/4 diarrhea, time to progression, overall survival and patient convenience, but the study was not designed to detect differences in these parameters. In addition, tumor response was shown to have a beneficial effect on QoL indicators.

Key words: irinotecan, metastatic colorectal cancer, randomized phase II, schedule

Introduction

Irinotecan was the first drug to add survival to standard fluorouracil and leucovorin in first-line treatment of colorectal cancer [1, 2]. Different fluorouracil schedules were used in the two trials. The comparison of the toxicity data of both studies seemed to suggest a better tolerability in terms of gastrointestinal and hematological toxicity with the infusional schedule. However, an important drawback of continuous intravenous infusion is the need for implantable access devices and porta-

ble infusion pumps. The availability of oral fluoropyrimidines has very much improved the feasibility of prolonged fluoropyrimidine administration. Most patients clearly prefer oral fluoropyrimidine therapy over intravenous bolus fluorouracil [3]. Oral capecitabine is active in colorectal cancer and two large randomized studies have shown a higher tumor response rates and at least equivalent time to disease progression and overall survival compared with intravenous bolus fluorouracil/leucovorin [4–6]. In addition, capecitabine was better tolerated with a significantly lower incidence of stomatitis, diarrhea, nausea and alopecia.

Several schedules of irinotecan administration are in clinical use. Rothenberg et al. have established the 'weekly' schedule, administering irinotecan at a dose of 125 mg/m² weekly for

*Correspondence to: Dr M. M. Borner, Institute of Medical Oncology, Inselspital, 3010 Berne, Switzerland. Tel: +41-31-6328442; Fax: +41-31-6324119; E-mail: markus.borner@insel.ch

4 consecutive weeks, followed by a 2-week rest period [7]. Another frequently used schedule is 350 mg/m² every 3 weeks, also given as a 30–90-min intravenous infusion [8]. The dose-limiting toxic effects of both administration schedules are neutropenia and diarrhea. Recently, a randomized phase III study comparing the two schedules in second-line therapy of metastatic colorectal cancer has shown comparable 1-year survival, median survival and median time to progression [9]. The main difference was a significantly higher incidence of severe diarrhea with the weekly schedule.

Combining irinotecan with oral capecitabine instead of intravenous fluorouracil is an interesting alternative in view of the practicability of the treatment. Tewes et al. have carried out an extended phase I study of capecitabine in combination with weekly irinotecan administered day 1, 8, 15, 22, 29 and 36, repeated day 50 [10]. The recommended dose from this study was capecitabine 1000 mg/m² twice daily day 1–14 and day 22–36 in combination with irinotecan 70 mg/m² weekly. Still, 19% of the patients experienced grade 4 diarrhea at this dose level. Bajetta et al. have presented their pilot experience of capecitabine in combination with two schedules of irinotecan [11]. Capecitabine 1250 mg/m² twice daily day 2–15 was combined with irinotecan 150/120 mg/m² day 1 and 8 or irinotecan 300/240 mg/m² day 1 every 21 days. Grade 3/4 diarrhea occurred in 17% and 23% of the patients, respectively.

We carried out an exploratory analysis of the weekly and the 3-weekly irinotecan schedule in combination with capecitabine in a formal randomized phase II setting. The weekly irinotecan regimen described by Tewes et al. [10] was slightly modified to allow an identical capecitabine regimen in both treatment arms. Thus, the irinotecan administration schedule was the only variable between the two treatment arms. The goal of this trial was to select the combination regimen of capecitabine and irinotecan, which should be used in further studies of this group.

Materials and methods

Eligibility and patient evaluation

Eligible patients had histologically or cytologically confirmed advanced or metastatic adenocarcinoma of the colon or the rectum, which was no longer amenable to surgical treatment. Other eligibility criteria were measurability of tumor lesions, not pretreated with chemotherapy for metastatic cancer, age 18–75 years, WHO performance status of 0 or 1, adequate organ function and a life expectancy of at least 3 months. Stratification factors for randomization were performance status (0 versus 1), the presence of disease symptoms, weight loss >5% during the last 6 months or a tumor-free interval of >6 months (all yes versus no) [12]. The protocol was approved by local ethics review boards of all participating institutions, and all patients gave written informed consent before enrollment.

Pretreatment evaluation included a complete medical history and physical examination, a complete blood count, chemistry profile and CEA measurement, a chest X-ray and a radiological tumor parameter assessment. For patients in arm A ('weekly' irinotecan schedule), a complete blood count was obtained weekly throughout the treatment phase. For patients in arm B (3-weekly irinotecan schedule), a complete blood count was obtained weekly in the first two 3-week treatment cycles and

thereafter before the start of each 3-week treatment cycle. A serum chemistry profile, CEA measurement, physical examination and toxicity assessment was done before the start of each 3-week cycle. Patients had radiological tumor parameter assessment every 9 weeks. Tumor response classification was based on standard World Health Organization criteria.

Response assessment

Computed tomography scans or magnetic resonance imaging of those patients with a CR, PR or minor response (at least a 25% decrease in tumor size) were reviewed by an independent radiology panel, which consisted of two experienced medical oncologists.

In arm A, scans of 21 patients were ordered according to the above criteria. Scans of three responding patients were not reviewed because of missing scan images, and a further two patients could not be assessed as their baseline target lesions were too small for evaluation (below 20 mm). In arm B, scans of 24 patients were ordered. Scans of one responding patient were not reviewed because of missing scan images.

Assessment of toxicity

Toxic effects were assessed according to the NCIC CTG expanded common toxicity grading. Hand-foot syndrome (palmar-plantar erythrodysesthesia) was classified as grade 1 (numbness, dysesthesia, painless swelling, erythema not disrupting normal activities), grade 2 (painful swelling, disrupting daily activities), or grade 3 (moist desquamation, ulceration, blistering, severe pain, inability to work or carry out daily living activities).

Treatment

This trial was conducted at eight centers. Patients were randomized centrally before starting treatment. In arm A, patients received irinotecan at a dose of 70 mg/m²/day given as a 1-h infusion on day 1, 8, 15, 22 and 29 repeated every 6 weeks. In arm B, patients received irinotecan at a dose of 300 mg/m²/day given as a 1-h infusion on day 1 repeated every 3 weeks. After December 20, 2001 (date of the amendment to the study protocol), the irinotecan dose in arm B was reduced to 240 mg/m²/day because of the report by Bajetta et al. [11]. Eighteen patients in arm B were randomized before December 20, 2001, eight of them finished treatment before irinotecan reduction. Treatment was continued until disease progression, unacceptable adverse effects, or withdrawal of consent by the patient.

Dose modifications

Capecitabine and irinotecan administration were interrupted in case of grade ≥ 2 non-hematological toxicity and were not resumed until the adverse effect improved to grade ≤ 1 . The doses were reduced by 25% in the subsequent treatment cycles in case of grade 3 non-hematological toxicity or by 50% in case of grade 4 hematological toxicity.

Quality-of-life assessment

The objective of the quality-of-life (QoL) study was to evaluate patients' QoL by tumor response and to describe QoL within and between the treatment groups. All randomized patients were asked to complete the QoL form at baseline, at day 1 of any subsequent 6-week cycle and at the first visit following treatment failure. To eliminate any differential anticipatory effects on baseline scores, the baseline QoL form had to be completed before randomization. The subsequent QoL forms were to be completed before diagnostic procedures and treatment administration.

Key components of QoL were assessed with linear analog self-assessment (LASA) indicators. This comprised global indicators for physical

well-being, mood, coping effort (PACIS) and functional performance [13–15]. We selected physical well-being as primary end point for evaluating the impact of tumor response. In addition, we asked the patient, "Overall, how much are you bothered by any treatment related difficulties?" [14] as primary end point for evaluating side-effects. This global indicator was designed to be responsive to the whole spectrum of toxicity and thus to be a comparative measure of overall burden. Finally, LASA indicators specific to symptoms of nausea and vomiting, diarrhea and hair loss were included. All LASA indicators range from 0 to 100, with higher values indicating better QoL (e.g. less side-effects).

Statistical analysis

The randomized two-arm phase II design was used to select the more promising schedule of the two in terms of response [16]. In this design, the schedule with the higher response rate is to be selected, irrespective of the difference. To have at least 90% probability of selecting the truly better schedule when the absolute difference in true response proportions (complete response+partial response) is 15% or greater, 37 patients are needed for each arm. Additionally, a stopping rule was included: A trial arm would have been stopped if there was no response in the first 14 patients. Since a selection design was chosen, no formal statistical comparisons between the arms were planned. Time to treatment failure was measured from randomization to treatment stop from any cause, time to progression from randomization to progression, and overall survival from randomization to death. Time to event data were analyzed by the Kaplan–Meier method. Confidence intervals for response rates and selected toxicity rates were calculated by the Clopper–Pearson method [17].

QoL indicators were descriptively evaluated as changes from baseline. The effects of tumor response, treatment, time and treatment–time interactions were longitudinally analyzed by a non-parametric mixed effects model using all available data within the observation period. As a general measure for a clinically meaningful effect between groups, we defined a difference in median changes from baseline of $\geq 8\%$ of full scale range for at least two succeeding time points, based on the difference in nausea/vomiting between observation only and 5-FU 600 mg/m² 2 months after the beginning of adjuvant therapy in patients with early colon cancer within a randomized trial [13]. Based on the decline in patients with 5-FU 600 mg/m² over this period, we estimated a median change of $\geq 5\%$ for at least two succeeding time points as a minimal clinically relevant change.

All tests were two-sided. All treated patients were included in the evaluation of the primary end point response rate. No adjustment was made for multiple testing. The *P* values have descriptive value only in this phase II trial. Statistical analyses were carried out using SAS 8.1 (SAS Institute Inc., Cary, NC, USA), S-PLUS 6.1 (Insightful Corporation, Seattle, WA, USA) and StatXact 5.0 (Cytel Software Corporation, MA, USA).

Results

Patients and treatment

From February 2001 until May 2002, a total of 75 patients were randomized to one of the two treatment arms. All patients were eligible. Table 1 lists the demographic data and baseline disease and pretreatment characteristics for all patients. Patients were well balanced for these characteristics with the exception of the number of metastatic sites per patient. Twenty-nine per cent of patients in arm A had more than one metastatic lesion compared with 46% in arm B. Fifty-

Table 1. Patient and disease characteristics

	Weekly irinotecan (n = 38)		3-weekly irinotecan (n = 37)	
	No.	%	No.	%
Age (years)				
Median (range)	58 (36–74)		61 (47–74)	
>65	11	29	9	24
Sex				
Female	13	34	14	38
Male	25	66	23	62
WHO performance status				
0	25	66	24	65
1	13	34	13	35
Tumor localization (multiple^a)				
Local	6	16	4	11
Liver	30	79	34	92
Lung	10	26	9	24
Peritoneum	1	3	4	11
Bone	2	5	0	–
Other	4	11	4	11
No. of metastatic locations				
1	27	71	20	54
2	7	18	16	43
3	4	11	1	3
Site of primary				
C. ascendens	11	29	6	16
C. transversum	3	8	3	8
C. descendens/sigmoideum	13	34	13	35
Rectum	11	29	14	38
No information	0	–	1	3
Metastatic at diagnosis				
Adjuvant radiotherapy	4	11	4	11
Adjuvant chemotherapy	6	16	5	14

^aEach patient may have more than one localization.

eight per cent of the patients had liver metastases only in arm A compared with 49% in arm B.

The median number of 3-week cycles received was six (range 1–15) for arm A and eight (range 1–23) for arm B. The median dose intensity for capecitabine and irinotecan in the first eight treatment cycles is summarized in Table 2. Since the irinotecan dose was reduced from 300 to 240 mg/m² after the toxicity report from the Bajetta study [11], the data for both dose levels are shown separately for arm B. Ninety-three of the total 301 treatment cycles in arm B were administered at the original higher dose level. Table 2 demonstrates that in arm B, considerable dose reductions had to be done for both capecitabine and irinotecan before the protocol dose adaptation for irinotecan. After the irinotecan dose adaptation from 300 to 240 mg/m², the planned dose for both drugs could

Table 2. Cycle number and median dose intensity

Cycle	Weekly irinotecan (n = 38)		3-weekly irinotecan (n = 37)		
	Capecitabine 2000 ^a	Irinotecan 70	Capecitabine 2000	Irinotecan 300	Irinotecan 240
1+2	1953 ^b	69	1923	295	234
3+4	1946	68	1915	227	234
5+6	1946	68	1914	222	233
7+8	1953	69	1878	216	233

^aPlanned dose.^bEffectively administered dose.Capecitabine: mg/m²/day; irinotecan: mg/m²/infusion.

be given with only slight dose modifications. The median cycle duration remained stable at 21 days from the first to the sixth treatment cycle for arm A and arm B. Seven per cent of the cycles in arm A and 13% of the cycles in arm B were delayed (duration >25 days). Besides other reasons, the most frequent reasons for treatment delays were hematological toxicity (arm B) and diarrhea (both arms, mainly arm A). Sixty-

three per cent of patients in arm A and 57% of patients in arm B received oxaliplatin containing second-line treatment.

Toxicity

The incidence of grade 3/4 toxicity is summarized in Table 3. The main toxicity was grade 3/4 diarrhea, which occurred in 34% of patients in arm A and 19% of patients in arm B. Severe (grade 3/4) neutropenia occurred in 5% and 19% of patients in arm A and B, respectively, during the first two treatment cycles. The information on the hematological toxicity in later cycles is limited since weekly blood counts were not mandatory. Severe hand-foot syndrome occurred in 5% and 8% of the patients. Grade 3 alopecia was observed in 11% of patients in arm A and in 38% of patients in arm B. Another important toxicity was grade 3 lethargy, which occurred in 5% and 8% of the patients. Severe stomatitis, neuropathy, anemia and thrombopenia were not observed with this treatment combination. Generally, patients >65 years experienced more severe toxicity compared with younger patients. One sudden death occurred in arm A during the third treatment cycle due to a rupture of an aortic aneurysm. This event was considered treatment unrelated by the investigator. Other severe toxic effects in arm A were a myocardial infarction (cycle 2, possible related to study treatment), an arterial thromboembolism (cycle 2, probably related to study treatment), a deep vein thrombosis (cycle 1, unlikely related to study treatment), and unexplained renal failure (cycle 2). In arm B, a deep vein thrombosis (cycle 2, unlikely related to study treatment), three events of bowel obstruction (cycle 1 and 2), and one patient with acute cholecystitis were observed. Unacceptable toxicity was given as the reason for treatment failure in 26% of patients in arm A and 19% of patients in arm B. Among the seven patients in arm B with unacceptable toxicity as the reason for treatment failure, two stopped treatment before December 20, 2001 (date of the amendment).

Table 3. Toxicity

	Weekly irinotecan (n = 38, courses = 251)		3-weekly irinotecan (n = 37, courses = 301)	
	% Patients	% Courses	% Patients	% Courses
NCIC CTG grade 3 toxicity				
Nausea/vomiting	3	<1	5	1
Diarrhea	29	6	14	3
By age 65/>65 years	26/36	5/7	14/11	3/2
By irinotecan 300/240 mg/m ²	n.a. ^a	n.a. ^a	n.a. ^b	4/2
Alopecia	11	11	38	21
Hand-foot syndrome	5	1	8	1
Lethargy	5	2	8	2
Neutropenia in cycle 1	5	n.a. ^c	14	n.a. ^c
By age 65/>65 years	0/18	n.a. ^c	7/33	n.a. ^c
NCIC CTG grade 4 toxicity				
Nausea/vomiting	0	0	0	0
Diarrhea	5	1	5	1
By age 65/>65 years	4/9	<1/2	4/11	<1/1
By irinotecan 300/240 mg/m ²	n.a. ^a	n.a. ^a	n.a. ^b	1/<1
Alopecia	—	—	—	—
Hand-foot syndrome	0	0	0	0
Lethargy	0	0	0	0
Neutropenia in cycle 1	0	n.a. ^c	5	n.a. ^c
By age 65/>65 years	0/0	n.a. ^c	4/11	n.a. ^c
Cardiovascular toxicity	5	<1	0	0

^aNot applicable because irinotecan reduction only in the 3-weekly arm.^bNot applicable because several patients reduced from 300 to 240 mg/m².^cNot applicable because measurements only for cycle 1.

Efficacy end points

Response rates as indicated by the investigators were 34% [95% confidence interval (CI) 20% to 51%] in arm A and 35% (95% CI: 20–53%) in arm B. The confirmed response rate by independent radiology review was 18% (95% CI 8%

to 34%) in arm A and 35% (95% CI 20% to 53%) in arm B. The reasons for this discrepancy, which mainly affected arm A, were technicalities such as missing scans, including missing response confirmation. There were no response reclassifications by the reviewers due to measurement discrepancies with the investigators. Study treatment allowed resection of liver metastases for two patients in each arm. Seven patients were not assessable for response in arm A due to early treatment stop because of toxicity (six) and one patient undergoing elective reanastomosis surgery. In arm B, four patients had early treatment stop due to toxicity and one patient suffered from bowel obstruction deemed independent of the study treatment by the investigator. All patients were included in the response calculation. Stabilization of disease was observed in 26% of patients in arm A and 34% in arm B.

The median follow-up time for alive patients was 16.1 months (range 11.2–26.4). The Kaplan–Meier curve for overall survival is depicted in Figure 1. The median overall survival was 17.4 months (95% CI 12.6–23.0+) for arm A and 24.7 months (95% CI: 16.3–26.4+) for arm B. The median time to treatment failure (defined as stop of treatment due to any reason, progression or death) was 4.6 months (95% CI 3.6–6.6) for arm A and 5.8 months (95% CI 4.4–7.0) for arm B (Figure 2). The median time to progression was 6.9 months (95% CI 4.6–10.1) for arm A and 9.2 months (95% CI 7.9–11.5) for arm B (Figure 3).

Quality of life

Pre-failure QoL data were evaluated up to and including week 24 (i.e. day 1 of cycle 5); thereafter, too few patients were left on trial. Of all expected QoL forms in this period, 246 (95%) were received, 74 (99%) at baseline and 172 (94%) under treatment. Timing deviations between QoL assessment and day 1 of cycle were balanced between the arms; the median difference across all assessments and both treatment arms was 0 days (25–75% range = 3 days). After treatment failure, 51 QoL forms (70%) were available. Almost all missing data were due to local administrative failure; one patient refused

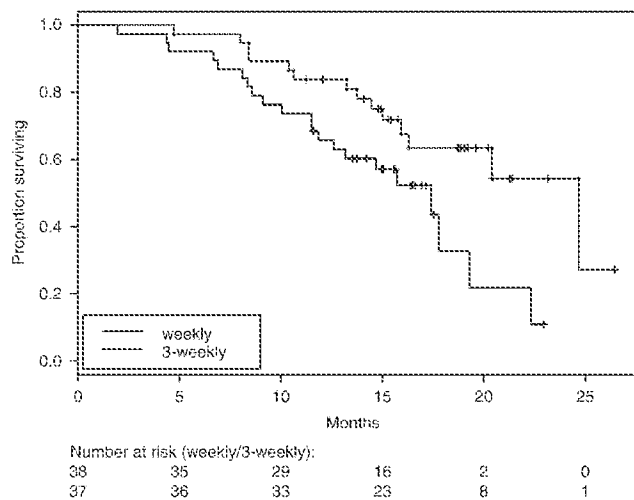


Figure 1. Overall survival.

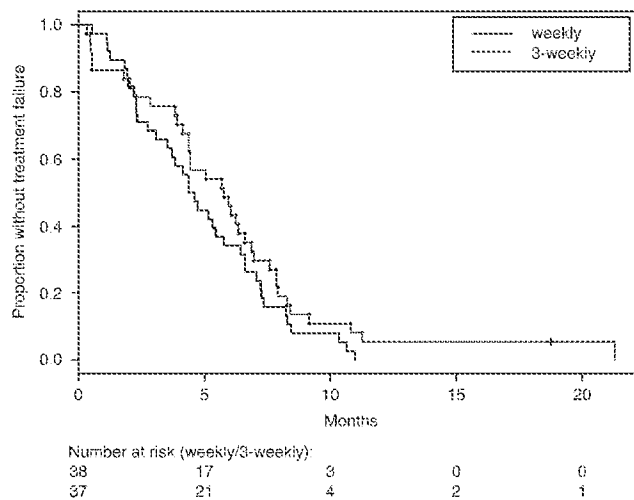


Figure 2. Time to treatment failure.

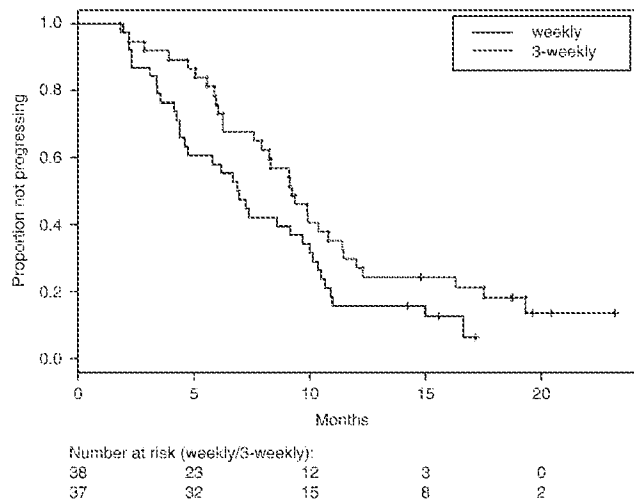


Figure 3. Time to progression.

the QoL assessment, and two assessments were not done due to medical complications.

At baseline, patients reported moderately to substantially impaired physical well-being ($n=74$, median = 84), mood ($n=74$, median = 69) and functional performance ($n=72$, median = 82), a low treatment burden ($n=58$, median = 89) and considerable coping effort ($n=73$, median = 55). Overall, there was an indication for less coping effort ($P<0.05$) and more treatment burden ($P<0.01$) over the first 6 months on study treatment. The only substantial treatment difference was in hair loss, with more hair loss ($P<0.01$) in Arm B over cycles 2–5.

Over this period, across both treatments, patients with tumor response reported better physical well-being ($P<0.01$), mood ($P<0.05$), functional performance ($P<0.05$) and coping ($P<0.05$) compared with the non-responders and stable disease patients. Figure 4 shows the changes in physical well-being. It has to be noted that there is considerable overlap of the two groups due to the small sample sizes. All of these indicators fulfilled our criterion of a clinically meaningful

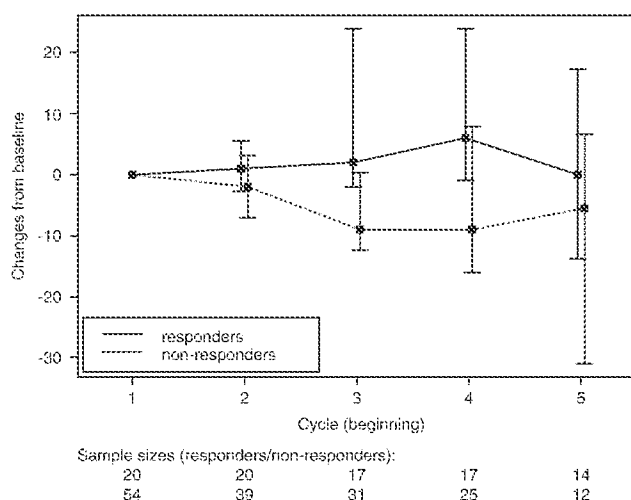


Figure 4. Median changes in physical well-being from baseline by tumor response with 95% CIs. Higher scores indicate better well-being.

effect between (response) groups. There was no baseline difference by tumor response in any of the QoL indicators.

The median time interval between treatment failure and the corresponding QoL assessment was 27 days (25–75% range = 70 days). Compared with baseline, patients reported worse physical well-being ($n=51$, median change = -10 , $P<0.01$) and treatment burden ($n=39$, median change = -14 , $P<0.01$), specifically hair loss ($n=45$, median change = -9 , $P<0.01$), diarrhea ($n=46$, median change = -4 , $P<0.05$) and vomiting ($n=49$, median change = -2 , $P<0.01$).

Discussion

The results of this trial demonstrate that two different regimens of irinotecan in combination with oral capecitabine can be safely and effectively combined in first-line treatment of metastatic colorectal cancer. Treatment with 3-weekly irinotecan led to a slightly higher tumor response rate, and the chosen selection design therefore leads to the recommendation to prefer this schedule. In support of this decision, the 3-weekly irinotecan arm yielded less severe diarrhea. Time to tumor progression, time to treatment failure and overall survival were also longer in the 3-weekly irinotecan arm. However, the observed differences should not be over-interpreted due to the selected study design.

Since a selection design was chosen, no formal statistical comparisons between the arms were planned. The small sample size of the study could have led to an imbalance of major prognostic factors affecting outcome independently of the assigned treatment. Looking at the patient and disease characteristics of the study population, an obvious source of bias could not be identified. The only clear imbalance was the higher percentage of patients with more than one metastatic site in arm B. The number of metastatic sites is an important prognostic factor for survival in advanced colorectal cancer [18], which would have favored longer survival in the weekly irinotecan arm. Liver metastases, another negative prognostic

factor in the study by Kohne et al. [18], were also more prevalent in arm B (92%) than in arm A (79%). Thus, the imbalance of these prognostic factors between the treatment arms cannot explain the better outcome with 3-weekly irinotecan in this study.

Other investigators have found comparable response rates of 31–44% with weekly irinotecan [10, 11, 19, 20] and 47–50% with 3-weekly irinotecan [11, 21, 22] in combination with capecitabine. Although we planned to validate our results by carrying out an independent response review, the relevance of this review was severely hampered by the few missing scans in arm A. In addition, the measurements of the investigators were confirmed by the reviewers, suggesting good investigator assessment quality and no additional benefit by carrying out this review.

A recent meta-analysis supports the view that the tumor response rate is a clinically meaningful end point. These analyses confirmed that an increase in tumor response rate translates into an increase in overall survival for patients with first-line chemotherapy for advanced colorectal cancer [23]. Objective tumor response proved to be a meaningful end point also from patients' subjective point of view in our trial. Over the first 6 months on treatment, patients with objective tumor response indicated better QoL performance compared with non-responding patients. A similar association between tumor response and QoL as perceived by the patient has recently been presented in another colorectal cancer trial [24]. Based on patients' responses, the detrimental impact of more severe hair loss of the 3-weekly schedule was outweighed by the beneficial impact of better antitumor activity. In individual decision making, the differential impact on hair loss needs to be addressed.

Toxicity was manageable in both treatment arms. Potentially life-threatening toxicity consisted mainly of diarrhea and was more frequent in the weekly irinotecan arm as assessed by the investigators. This is consistent with the results of a recently published randomized phase III study on two different irinotecan second-line dosing regimens in metastatic colorectal cancer. In this trial, Fuchs et al. [9] found that 3-weekly irinotecan was associated with a significantly lower incidence of severe diarrhea compared with weekly irinotecan. Others, exploring comparable schedules of the irinotecan plus capecitabine combination, described similar experiences in terms of toxicity. The recommended dose from the phase I study by Tewes et al. was 1000mg/m^2 twice daily capecitabine and 70mg/m^2 irinotecan weekly [10]. Still, 19% of the patients experienced dose-limiting grade 4 diarrhea at this dose level. Bajetta et al. recently reported the results of a randomized phase II study comparing weekly 2 out of 3 weeks irinotecan and 3-weekly irinotecan in combination with capecitabine [11]. An interim analysis of this study was the basis of our dose reduction amendment since severe diarrhea occurred in 17% and 36% of the patients, respectively. Despite the fact that dose reductions were made for capecitabine and irinotecan in both treatment arms in that study, decreased occurrence of diarrhea was only observed in the 3-weekly irinotecan arm.

We have also found a reduction of toxicity after dose modification in the 3-weekly irinotecan arm. This translated into a higher dose intensity of both drugs as shown in Table 2. As compared with the 2 out of 3 weeks schedule of Bajetta et al. [11], our weekly irinotecan schedule seemed less toxic.

It will be important to prove that capecitabine can replace the established infusional fluorouracil plus leucovorin combinations without negatively affecting efficacy and toxicity. In terms of patient convenience, the oral fluoropyrimidine is clearly advantageous [3]. In this respect the results of EORTC 40015 are eagerly awaited, which compares capecitabine plus irinotecan with infusional fluorouracil/leucovorin plus irinotecan. As a consequence of the results presented here, the 3-weekly irinotecan schedule in addition to capecitabine will be used for further comparative trials of our group.

Acknowledgements

We would like to thank Dr Tanja Čufer, Ljubljana, and Dr Luigina Rota, Brescia, for their valuable commitment and work in carrying out the review. This trial was supported by Roche Pharma (Schweiz) AG and Aventis Pharma (Schweiz) AG.

References

- Douillard JY, Cunningham D, Roth AD et al. Irinotecan combined with fluorouracil compared with fluorouracil alone as first-line treatment for metastatic colorectal cancer: a multicentre randomised trial. *Lancet* 2000; 355: 1041–1047.
- Saltz LB, Cox JV, Blanke C et al. Irinotecan plus fluorouracil and leucovorin for metastatic colorectal cancer. Irinotecan Study Group. *N Engl J Med* 2000; 343: 905–914.
- Borner MM, Schoeffski P, de Wit R et al. Patient preference and pharmacokinetics of oral modulated UFT versus intravenous fluorouracil and leucovorin. A randomised crossover trial in advanced colorectal cancer. *Eur J Cancer* 2002; 38: 349–358.
- Van Cutsem E, Twelves C, Cassidy J et al. Oral capecitabine compared with intravenous fluorouracil plus leucovorin in patients with metastatic colorectal cancer: results of a large phase III study. *J Clin Oncol* 2001; 19: 4097–4106.
- Twelves C. Capecitabine as first-line treatment in colorectal cancer. Pooled data from two large, phase III trials. *Eur J Cancer* 2002; 38 (Suppl 2): 15–20.
- Hoff PM, Ansari R, Batist G et al. Comparison of oral capecitabine versus intravenous fluorouracil plus leucovorin as first-line treatment in 605 patients with metastatic colorectal cancer: results of a randomized phase III study. *J Clin Oncol* 2001; 19: 2282–2292.
- Rothenberg ML, Eckardt JR, Kuhn JG et al. Phase II trial of irinotecan in patients with progressive or rapidly recurrent colorectal cancer. *J Clin Oncol* 1996; 14: 1128–1135.
- Armand JP, Exra YM, Catimel G et al. Rationale for the dosage and schedule of CPT-11 (irinotecan) selected for phase II studies, as determined by European phase I studies. *Ann Oncol* 1996; 7: 837–842.
- Fuchs CS, Moore MR, Harker G et al. Phase III comparison of two irinotecan dosing regimens in second-line therapy of metastatic colorectal cancer. *J Clin Oncol* 2003; 21: 807–814.
- Tewes M, Schileucher N, Achterath W et al. Capecitabine and irinotecan as first-line chemotherapy in patients with metastatic colorectal cancer: results of an extended phase I study dagger. *Ann Oncol* 2003; 14: 1442–1448.
- Bajetta E, Di Bartolomeo M, Mariani L et al. Randomized multicenter Phase II trial of two different schedules of irinotecan combined with capecitabine as first-line treatment in metastatic colorectal carcinoma. *Cancer* 2004; 100: 279–287.
- Borner MM, Castiglione M, Bacchi M et al. The impact of adding low-dose leucovorin to monthly 5-fluorouracil in advanced colorectal carcinoma: results of a phase III trial. Swiss Group for Clinical Cancer Research (SAKK). *Ann Oncol* 1998; 9: 535–541.
- Bernhard J, Hurry C, Maibach R et al. Quality of life as subjective experience: reframing of perception in patients with colon cancer undergoing radical resection with or without adjuvant chemotherapy. Swiss Group for Clinical Cancer Research (SAKK). *Ann Oncol* 1999; 10: 775–782.
- Bernhard J, Maibach R, Thurlimann B et al. Patients' estimation of overall treatment burden: why not ask the obvious? *J Clin Oncol* 2002; 20: 65–72.
- Bernhard J, Sullivan M, Hurry C et al. Clinical relevance of single item quality of life indicators in cancer clinical trials. *Br J Cancer* 2001; 84: 1156–1165.
- Simon R. Optimal two-stage designs for phase II clinical trials. *Control Clin Trials* 1989; 10: 1–10.
- Clopper CJ, Pearson E. The use of confidence or fiducial limits illustrated in the case of binomial. *Biometrika* 1934; 26: 404–413.
- Köhne CH, Cunningham D, Di CF et al. Clinical determinants of survival in patients with 5-fluorouracil-based treatment for metastatic colorectal cancer: results of a multivariate analysis of 3825 patients. *Ann Oncol* 2002; 13: 308–317.
- Burriss HA, Kalman L, Bertoli L et al. Continuous flat-dose capecitabine plus weekly irinotecan: an alternative first-line treatment for metastatic colorectal cancer. Proceedings of ASCO Gastrointestinal Cancers Symposium 2004; 1: (Abstr 229).
- Gold PJ, Godfrey T, Dhami M et al. Capecitabine and irinotecan as 1st line therapy for patients with metastatic colorectal cancer: Phase II study preliminary results. *Proc Am Soc Clin Oncol* 2003; 22: (Abstr 1158).
- Kerr DJ, Ten Bokkel Huinink WW, Ferry DR et al. A phase I/II study of CPT-11 in combination with capecitabine as first line chemotherapy for metastatic colorectal cancer (MCR). *Proc Am Soc Clin Oncol* 2002; 21: (Abstr 643).
- Pati YZ, Lin E, Leibmann J et al. Capecitabine plus irinotecan for chemotherapy-naïve patients with metastatic colorectal cancer. Proceedings of ASCO 2003; 22: (Abstr 1130).
- Buyse M, Thirion P, Carlson RW et al. Relation between tumour response to first-line chemotherapy and survival in advanced colorectal cancer: a meta-analysis. Meta-Analysis Group in Cancer. *Lancet* 2000; 356: 373–378.
- Hobday TJ, Kugler JW, Mahoney MR et al. Efficacy and quality-of-life data are related in a phase II trial of oral chemotherapy in previously untreated patients with metastatic colorectal carcinoma. *J Clin Oncol* 2002; 20: 4574–4580.

Expert Opinion

1. Introduction
2. Cisplatin and platinum drugs in chemotherapy
3. Extravasation of Lipoplatin nanoparticles into tumors and differentiating features
4. Molecular mechanisms of cisplatin and Lipoplatin
5. Preclinical studies on Lipoplatin
6. Lipoplatin as an antiangiogenesis factor
7. Phase I studies
8. Phase II studies
9. Tumor targeting in human studies
10. Phase III studies
11. Discussion
12. Conclusions and prospects
13. Expert opinion

informa
healthcare

Clinical overview on Lipoplatin™: a successful liposomal formulation of cisplatin

Teri Boulikas

Regulon, Inc. 715 N. Shoreline Blvd. Mountain View, CA 94043 and Regulon AE, Grigoriou Afentiou 7, Alimos, Athens 17455, Hellas, Greece

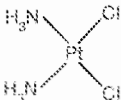
Nanoparticle formulations for packaging existing drugs have been used to treat cancer. Lipoplatin™ is a liposomal cisplatin encapsulated into liposome nanoparticles of an average diameter of 110 nm. Lipoplatin has substantially reduced the renal toxicity, peripheral neuropathy, ototoxicity, myelotoxicity as well as nausea/vomiting and asthenia of cisplatin in Phase I, II and III clinical studies with enhanced or similar efficacy to cisplatin. During clinical development, 10- to 200-fold higher accumulation of Lipoplatin in solid tumors compared to adjacent normal tissue was found in patients. Targeting of tumor vasculature by Lipoplatin in animals suggested its antiangiogenesis potential and Lipoplatin was proposed to act like a double-sword: as chemotherapy and an antiangiogenesis drug. Lipoplatin has finished successfully one Phase III non-inferiority clinical study as first-line against NSCLC in its combination with paclitaxel showing statistically significant reduction in nephrotoxicity; two more Phase III studies are in progress, one in NSCLC with gemcitabine also showing noninferiority with reduced toxicity and another in squamous cell carcinoma of the head and neck with 5-fluorouracil. A registrational Phase II/III study against pancreatic cancer is in progress under the orphan drug status granted to Lipoplatin by the European Medicines Agency. Phase II studies are continuing in advanced breast cancer with vinorelbine and gastrointestinal cancers with radiotherapy and 5-fluorouracil. The highlights of the clinical development of Lipoplatin are reviewed.

Keywords: angiogenesis, cisplatin, Lipoplatin™, liposomes, nanoparticle, NSCLC, platinum transporters, tumor targeting

Expert Opin. Investig. Drugs (2009) 18(8):1-22

1. Introduction

Cancer remains a devastating disease in spite of intense research for over 4 decades. Chemotherapy, surgery, radiation and patient management had major improvements. Maturation of the chemistry of chemotherapy from the 1960s to 1980s led to > 700 FDA-approved drugs. The six classes of chemotherapy drugs according to the FDA include: i) platinum compounds (cisplatin, carboplatin, oxaliplatin) (reviewed in [1]) (Box 1); ii) the two classes of antimicrotubule agents: vinca alkaloids (vinblastine, vinorelbine) and taxanes (paclitaxel, docetaxel) (reviewed in [2]); iii) antimetabolites (methotrexate, 5-fluorouracil (5-FU), gemcitabine); iv) antitumor antibiotics (actinomycin D, mitomycin C, bleomycin, the anthracyclines doxorubicin, daunorubicin, the podofylotoxines etoposide, teniposide, and the camptothecines irinotecan, topotecan); v) alkylating agents such as cyclophosphamide and vi) others. This last class includes natural products, monoclonal antibodies, antiangiogenesis drugs such as anti-VEGF agents [3], drugs that target signaling molecules including mTOR inhibitors [4], Bcl-2 inhibitors [5], MEK/ERK, Src, PI3K/Akt, Hedgehog and NF-κB inhibitors, anti-EGFR and

Box 1. Drug summary.	
Drug name	Cisplatin, Lipoplatin™, Regulon
Phase	Phase III
Indication	Cancer
Pharmacology description	DNA crosslinker, signaling modulator
Route of administration	Intravenous
Chemical structure	
Pivotal trial(s)	<p>Phase II with Lipoplatin + gemcitabine as first-line every 7 days in pancreatic cancer (EMEA)</p> <p>Phase III studies: Lipoplatin plus gemcitabine versus cisplatin plus gemcitabine as first line treatment in patients with NSCLC</p> <p>Phase III studies: Lipoplatin plus paclitaxel versus cisplatin plus paclitaxel as first-line treatment in NSCLC</p>

Pharmaprojects – copyright to Citeline Drug Intelligence (an Informa business). Readers are referred to Pipeline (<http://informa-pipeline.citeline.com>) and Citeline (<http://informa.citeline.com>).

55 several tyrosine kinase inhibitors. These agents are targeted against mitogenic pathways essential to cancer cells. This list also includes heat shock protein 90 inhibitors, CDK inhibitors and proteasome inhibitors.

60 Emerging anticancer technologies also include those targeting epigenetic mechanisms such as histone deacetylase inhibitors [6,7], poly(ADP-ribose) polymerase inhibitors [8,9] and inhibitors of DNA methyltransferase [10,11]. Important are exotic anticancer vaccines such as the GV1001 antitelomerase vaccine, as well as immunomodulatory agents aiming at
65 invigorating the immune system of the patient. Parallel efforts are exploiting the booming of gene discovery using genes as therapeutic molecules to induce biosynthesis of a protein by the patient's cells that could arrest tumor cell proliferation or kill tumor cells preferentially; this approach gave genesis to
70 the field of gene therapy (reviewed in [12,13]).

75 Attempts to target cancer cells in the human body without damaging normal cells have also been vigorous. Effective drug delivery and tumor targeting is of paramount importance in clinical oncology, which is expected to improve the quality of life of the cancer patients. A major effort has been directed to drug delivery in parallel with discovery of new anticancer molecules. Our group has been involved in nanoparticle formulations by liposomal encapsulation of pre-existing
79 chemotherapy drugs to achieve passive targeting of tumors;

emphasis has been in reducing the side effects and enhancing 80 targeting to both tumors and metastases. A breakthrough took place by the liposomal encapsulation of cisplatin leading to a nanoparticle liposomal formulation, Lipoplatin™ (Regulon, Inc., Mountain View, CA, USA) [14]. These nanoparticles integrate the reverse micelle technology followed by 85 conversion into true liposomes for efficient encapsulation yields but also integrate fusogenic lipids on the surface of the nanoparticles to unlock the cell membrane barrier by promoting a direct fusion with the cell membrane.

90

2. Cisplatin and platinum drugs in chemotherapy

Cisplatin, since its serendipitous discovery in 1965, identification in 1969 and clinical application in the early 1970s 95 continues to represent a cornerstone in modern chemotherapy playing an important role among cytotoxic agents in the treatment of epithelial malignancies. The drug of choice for the treatment of NSCLC is cisplatin [15]. The introduction of cisplatin has been a milestone achievement in clinical 100 oncology and has saved the lives of testicular cancer patients [16,17]; cisplatin is recommended by the FDA for metastatic testicular, metastatic ovarian, transitional cell bladder cancer, NSCLC (in combinations with gemcitabine) and cervical cancer (in combination with radiation) whereas 105 its off-label use has been extended to head and neck, esophageal, gastric, colorectal, hepatocellular, metastatic melanoma, and as second-line to metastatic breast, prostate and many other malignancies. However, its clinical use has been impeded by its severe toxicities, including nephrotoxicity [18], 110 gastrointestinal toxicity, peripheral neuropathy [19], ototoxicity [20], asthenia and hematological toxicity. The significant risk of cisplatin-induced nephrotoxicity frequently hinders the use of higher doses to maximize its antineoplastic effects and hydration of the patients is used to minimize its effects. 115

The clinical success of cisplatin has triggered an enormous effort to discover new platinum drugs of improved efficacy and lower side effects. Out of > 3000 platinum compounds synthesized, only about 35 have exhibited adequate pharmacological advantages relative to cisplatin to justify clinical testing (reviewed in [1]). Of these, carboplatin and oxaliplatin have been registered worldwide and entered clinical practice with big success. Nedaplatin has been registered in Japan for the treatment of head and neck, testicular, lung, ovarian, cervical and NSCLC. Although the activity of heptaplatin 125 (SKI2053R) was clearly lower than that of cisplatin in gastric cancer, its lower toxicity profile gave it registration in South Korea. Lobaplatin has been approved in China for the treatment of chronic myelogenous leukemia, inoperable, metastatic breast and small cell lung cancer after successful Phase II 130 testing (structures are shown in Figure 1; reviewed in [1]).

The three drugs (cisplatin, carboplatin, oxaliplatin) differ with respect to DNA adducts, import mechanisms across the cell membrane and toxicity profiles. The cytotoxicity of 134

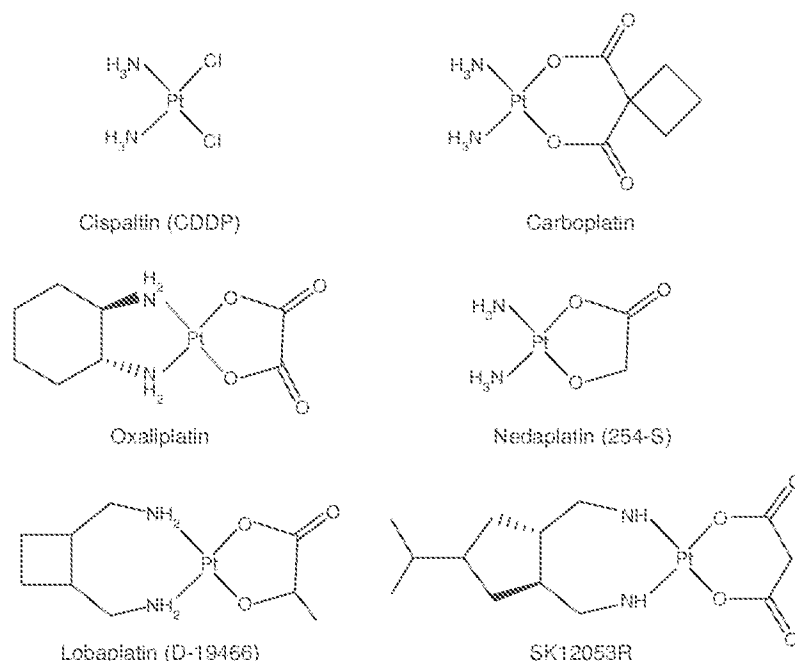


Figure 1. The structure of cisplatin, of the universally approved carboplatin and oxaliplatin and of nedaplatin, lobaplatin and hexaplatin (SKI2053R) approved in restricted Asian territories.

135 platinum derivatives ranked in the order: oxaliplatin > cisplatin
 136 > carboplatin in human colorectal tumor cell lines. Cellular
 137 accumulation and DNA-binding of platinum varied among
 138 the types of cells, but levels were similar on treatment
 139 with cisplatin and oxaliplatin, and lower in response to
 140 carboplatin [21].

The main objectives for the development of novel platinum
 141 drugs is the reduction in the side effects of cisplatin,
 142 the enhancement of their therapeutic index and their effective-
 143 ness against cisplatin-resistant tumors with a potential
 144 application in patients who relapse after first-line platinum-
 145 based treatment. In this respect, the clinical develop-
 146 ment of novel platinum compounds has been disappointing
 147 in spite of findings of low cross-resistance to cisplatin and
 148 superior therapeutic index in cell lines or in preclinical
 149 studies (reviewed in [1]).

3. Extravasation of Lipoplatin nanoparticles into tumors and differentiating features

3.1 Description and manufacturing of cisplatin nanoparticles

Lipoplatin is a formulation of the FDA-approved cisplatin
 150 wrapped up into tumor targeted 110 nm in diameter liposome
 151 nanoparticles using patented platform technologies.

Lipoplatin's liposomes are composed of soy phosphatidyl
 152 choline (SPC-3), cholesterol, dipalmitoyl phosphatidyl gly-
 153 cerol (DPPG) and methoxy-polyethylene glycol-distearoyl
 154 phosphatidylethanolamine (mPEG₂₀₀₀-DSPE). Lipoplatin is

155 composed of 8.9% cisplatin and 91.1% lipids (w/w) (ratio ~
 156 1:10). Lipoplatin has an opaque appearance reflecting its
 157 liposomal nature and is being provided in 50 ml glass vials
 158 of 3 mg/ml (concentration refers to cisplatin). The concen-
 159 tration of 3 mg/ml of cisplatin in Lipoplatin exceeds the
 160 solubility of the free drug, cisplatin, with solubility in water
 161 or saline of 1 mg/ml. Lipoplatin is stored at 4°C and has
 162 an expiration date of 3 years. Freeze thawing results in the
 163 formation of aggregates and should be avoided.

The Lipoplatin formulation is based on the formation of
 164 reverse micelles between cisplatin and DPPG under special
 165 conditions of pH, ethanol, ionic strength and other param-
 166 eters. During its manufacturing process, cisplatin-DPPG
 167 reverse micelles are subsequently converted into liposomes
 168 by interaction with neutral lipids. This process involving
 169 various steps sensitive to parameters including temperature,
 170 ethanol concentration, pH, ionic strength, type of salt, type
 171 and concentration of lipid and other sensitive variables leads
 172 to very high encapsulation efficiencies. About 15 repeated
 173 extrusions are performed using a Thermobarrel Extruder
 174 through membranes of 0.2, 0.1, 0.08 and 0.05 μm pore
 175 sizes under pressure in ultra pure nitrogen atmosphere to an
 176 average size of 110 nm.

Whereas non-PEGylated liposomes are taken up by liver
 177 macrophages and destroyed with a half-life in body fluids of
 178 20 min, the PEGylated liposomes of Lipoplatin display a
 179 half-life of 5 days in body fluids [22]. The longevity of the
 180 nanodrug in body fluids is a prerequisite for its extravasation
 181 into tumors.

193 3.2 Mechanism of extravasation of nanoparticles 195 into tumors

200 Tumor targeting by nanoparticles can be achieved at two levels: i) through nanoparticle formulations of drugs that extravasate and infiltrate tumors using imperfections in their vascular endothelium (passive targeting) and ii) by adding true targeting molecules on the outer surface of the nanoparticles with high affinity for proteins overexpressed in tumors.

205 Stealth (pegylated) liposomal doxorubicin (Doxil) has been extensively studied [23]. The vast majority of Stealth liposomes sterically inhibit both electrostatic and hydrophobic interactions of a variety of blood components at the liposome surface [24] and enter the tumor interstitium through gaps (fenestrae) in the endothelial cell walls of newly-formed vessels that feed the tumors [25]; a smaller proportion of liposomes may actually pass directly through the thin walls of the defective endothelial cells lining the neo-vessel, through a process called transcytosis [26].
210 Following their extravasation in the interstitial fluid surrounding the tumor, physico-chemical destabilization and subsequent breakdown of the liposomal envelope by the low pH and the presence of lipases released from dying neoplastic cells releases the drug at the extracellular space [27]. Microvascular permeability to fluorescently labeled macromolecules in human colon adenocarcinoma cells transplanted in dorsal skin chambers showed that tumor vessels were permeable to liposomes at sizes up to
220 400 nm in diameter [28].

Lipoplatin nanoparticles were proposed to extravasate into tumors in animal studies (Figure 2A) whereas human studies showed a higher concentration of total platinum in tumors and metastases of patients compared to platinum concentration in the adjacent normal tissue at about 20 h after intravenous (i.v.) administration [29]. The PEG polymer coating used on Lipoplatin was speculated to: i) give to the drug particles the ability to pass undetected by the macrophages and immune cells, ii) remain in circulation in body fluids
225 for long periods (half-life of 116 h for total blood platinum from Phase I pharmacokinetics, see below) and iii) extravasate preferentially and infiltrate solid tumors and metastases through the altered and often compromised tumor vasculature (Figure 2B). Although the mechanism of entry of Lipoplatin nanoparticles into cells has not been deciphered, tumor cells were proposed to uptake more avidly Lipoplatin particles because of: i) their tendency to uptake nutrients from the environment; ii) the higher concentration of the drug into tumors; and iii) the proposed fusion of liposomes with the tumor cell membrane; the anionic lipid DPPG was proposed to give to Lipoplatin its fusogenic properties (Figure 2C) [29,30].

235 3.3 Lipoplatin administration to patients

245 For patient treatment, the nanoparticle suspension is diluted into 1 l 5% dextrose; the i.v. infusion is slow to reduce side effects (~ 25 mg/(m² h)). It is an ~ 5 h infusion for protocols
247

using 120 mg/m² weekly or an 8 h infusion for protocols using 200 mg/m² every 14 days. Rapid infusion (1 – 2 h) results in higher nephrotoxicity and accentuates the other side effects of the nanodrug. 248 250

3.4 The differentiating features of Lipoplatin

The Lipoplatin formulation differs from another known formulation of cisplatin that was clinically tested, SPI-77, in several basic principles including loading method, type of lipids and ratio of cisplatin:lipids. Whereas the loading of cisplatin in Lipoplatin was based on reverse micelles, the mechanism of cisplatin loading in SPI-77 was passive. The Lipoplatin formulation used anionic and neutral lipids compared to SPI-77 that used only neutral lipids. The total lipid to cisplatin ratio was low (~ 10:1 mg lipid/mg cisplatin) in Lipoplatin, thus, limiting the total lipids injected to patients. For comparison, the ratio of lipids to cisplatin in the liposomal formulation SPI-77 was ~ 70:1 [31]. 255 260 265

Finally, the two formulations differ significantly in efficacy in human clinical trials. A significant response rate of Lipoplatin plus gemcitabine in NSCLC was obtained and most importantly, its comparison with the cisplatin arm in at least one randomized Phase II and two randomized Phase III trials, all in NSCLC, have shown its non-inferiority to cisplatin (see below). 270

On the contrary, the promising activity of SPI-77 in animal xenograft studies was not replicated in clinical trials; for example, in a Phase II study in patients with advanced NSCLC a modest response rate of 4.5% was obtained [32]. Similarly, no objective tumor responses occurred among 24 patients in a Phase I monotherapy study [33] and 3 of 17 patients showed responses in a combination of SPI-77 and vinorelbine in a Phase I study [34]. In another Phase II study in a NSCLC population of 12 patients, 2 (17%) had stable disease and 10 (83%) had progressive disease [35]. Finally, in patients with head and neck tumors, SPI-77 was administered safely with radiation and 10 (59%) of 17 patients finishing treatment achieved initial complete response [36]; however, SPI-77 as a single agent showed disappointing results with only 2 (11%) of 18 patients showing partial response [37]. 275 280 285

4. Molecular mechanisms of cisplatin and Lipoplatin 290

4.1 Import/export mechanisms of platinum drugs across the cell membrane

After infusion, cisplatin is rapidly excreted in the urine causing renal tubular damage. When it reaches normal and malignant cells, it uses the copper transporter Ctr1 for entry across the cell membrane barrier (Figure 2C). Two copper efflux transporters, ATP7A and ATP7B, regulate the efflux of cisplatin. Acquisition of cisplatin resistance was associated with a greatly reduced level of ATP7A [38]. hCtr1 could transport cisplatin, carboplatin and oxaliplatin [39]. 295 300 302

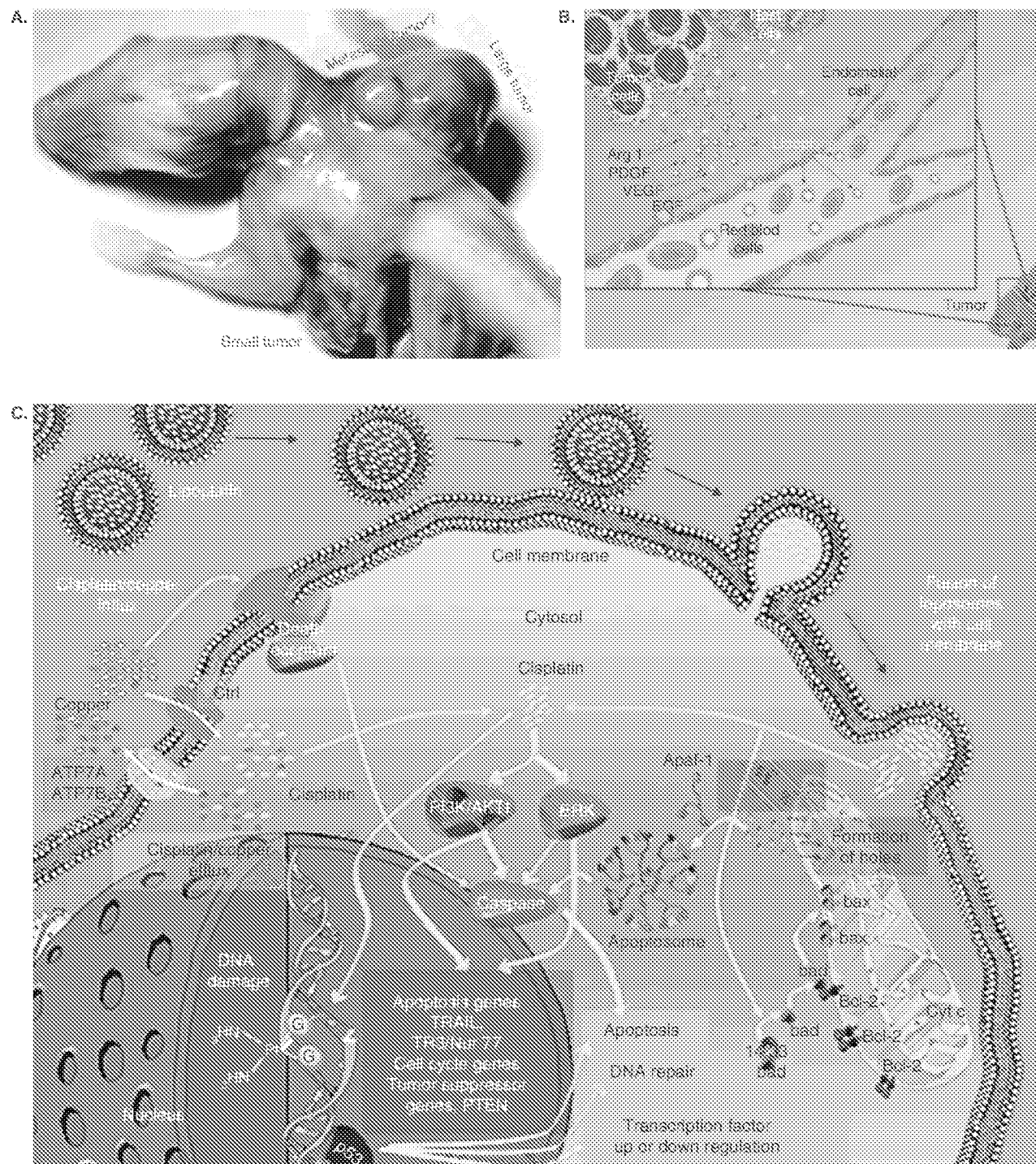


Figure 2. A. Targeting of the vasculature in SCID mice inoculated with MCF-7 cells and grown into subcutaneous solid tumors after systemic administration of liposomes containing the β -galactosidase gene (see [30] for details). B. Following i.v. injection, the nanoparticles extravasate through the leaky endothelium of the vasculature of the tumor which becomes compromised during the process of neovascularization and concentrates preferentially into solid tumors. C. Fusion of the Lipoplatin nanoparticle and the cell membrane of a tumor cell (or endothelial cell of tumor vasculature) is a proposed feature, thus, bypassing cisplatin resistance at the membrane barrier. Intracellular cisplatin is activating the mitochondrial as well as other signaling pathways and inflicting DNA damage leading to apoptosis.

From [1] reproduced with permission.

i.v.: Intravenous; SCID: Severe combined immunodeficient.

303 The body is equipped with broad-specificity transporters
 305 for the excretion and distribution of endogenous organic
 cations such the organic cation transporters (OCTs). Trans-
 porters also include the proton/cation antiporters MATE1,
 MATE2-K and MATE2-B [40]. These transporters could
 play predominant roles in the tissue distribution and anti-
 cancer effects and/or adverse effects of platinum agent-based
 310 chemotherapy [41].

ATP7A, XPD and SRPK1 gene expression was increased
 in oxaliplatin-resistant colon cancer cells; resistance was
 accompanied by defects in drug uptake (downregulation of
 the hCTR1 transporter) and enhanced DNA repair (upregu-
 315 lation of the XPD gene); in addition, superoxide
 dismutase 1 was found to play a role in oxaliplatin detoxi-
 fication [42]. Human ovarian carcinoma cells exported cis-
 platin through lysosomes [43]. The cellular accumulation of
 cisplatin was dependent on levels of ATP7A mRNA whereas
 320 the cytotoxicity of oxaliplatin was affected by the levels of
 ATP7A and hOCT1 mRNAs in human colorectal tumor
 cell lines [21].

Overexpression of ATP7A and ATP7B in Me32a fibro-
 blasts resulted in increased resistance to cisplatin, but not to
 325 carboplatin or oxaliplatin [44]. In other cell types, as for
 example in cisplatin-sensitive and -resistant tumor cell line
 pairs (ovarian A2780/A2780cis and cervical HeLa/HeLaCK
 cells), resistant cells expressed 1.5- to 1.8-fold lower levels of
 CTR1 compared to sensitive cells with a clear relationship
 330 between lower CTR1 expression, intracellular concentration,
 DNA platination and cytotoxicity of cisplatin [45].

Transfection of cells in culture with constructs expressing
 the ATP7A gene enhanced resistance not only to cisplatin
 but also to vincristine, paclitaxel, SN-38, etoposide, doxorubi-
 335 cin and CPT-11 [46]. Impaired activity in the cisplatin
 transporter transmembrane proteins contributed to cisplatin
 resistance through reduction of drug accumulation in the
 cell [47]. The transporters ATP7A, ATP7B, hCTR1, hOCT1
 and hOCT2 were upregulated in an established cisplatin-
 340 resistant oral carcinoma cell line [48]. Oxaliplatin, but not
 cisplatin, was transported by human and rat OCT3/
 SLC22A3; expression of this molecule was important for the
 cytotoxic effect of oxaliplatin in colorectal cancer [49]. OCT1
 and OCT2 were found to be the major determinants of the
 345 anticancer activity of oxaliplatin contributing to its anti-
 tumor specificity and the development of drugs, specifically
 targeted to OCTs, was proposed as a novel strategy for tar-
 geted drug therapy [50]. Thus, the import/export of platinum
 drugs is a complex process with many players.

350 4.2 Cisplatin detoxification

The S-containing tripeptide glutathione is present in cells at
 mM concentrations, and the formation of complexes plays
 an important role in the detoxification and biological activi-
 355 ty of platinum compounds. Depletion of glutathione levels
 has been shown to increase the toxicity of kidney cells to
 357 cisplatin and a clinical trial demonstrated that pretreatment

with glutathione reduced renal toxicity without affecting anti-
 tumor activity. Cancer cells that are resistant to cisplatin often
 have elevated glutathione levels. Glutathione could quench
 360 DNA-Pt monofunctional adducts before they could rearrange to
 toxic bifunctional adducts. High-level cisplatin resistance, attri-
 buted to human glutathione S-transferase P1, may not be due
 to catalysis of cisplatin conjugation but rather must be explained
 by other mechanisms, which may include GSTP1-mediated
 365 modulation of signaling pathways [51].

4.3 Induction of mitochondrial apoptosis by cisplatin

Cisplatin and other apoptotic stimuli trigger the release of
 cytochrome c from the mitochondrial intermembrane space to
 370 the cytosol, which induces the formation of the apopto-
 some and the activation of procaspase-9. The apoptosome is
 an Apaf-1 cytochrome c complex that activates procaspase-9.
 The 3D structure of the apoptosome has been determined
 at 27 Å resolution to reveal a wheel-like particle with seven-
 375 fold symmetry (Figure 2C) [52]. Procaspase-9 molecules can
 bind to the inner 'hub' region of the apoptosome. This
 complex promotes the efficient activation of procaspase-3.
 Therefore, the cleavage of procaspase-9 is not required to
 form an active cell death complex. Cisplatin can activate the
 380 proapoptotic protein Bax resulting in cytochrome c release,
 caspase activation and apoptosis; Bax activation is implicated
 in the nephrotoxicity of cisplatin [53]. Bcl-2 plays an impor-
 tant role in the mitochondrial apoptotic pathway. Although
 the general role of Bcl-2 is antiapoptotic, Bcl-2 fragments
 385 resulting by caspase cleavage after cisplatin treatment of cells
 in culture could promote the apoptotic process [54].

4.4 Induction of signaling pathways by cisplatin

During signal transduction, a cell senses both the external
 390 and internal environment and converts a stimulus into an
 ordered sequence of phosphorylation-dephosphorylation,
 protease degradation, gene regulation or ion flux events
 across the cell membrane. There is a great number of signal-
 ing cascades including MAPK, GPCRs/MAPK, ERK/
 395 MAPK, PKC, PKA, growth factor/survival factor/mitogen,
 PI3K/AKT/PTEN, ceramide, proteasome, integrin, Wnt/ β -
 catenin, insulin, cholesterol, RB/E2F, ubiquitination and
 cyclins/p27 regulating the cell cycle, p53/DNA damage, oxi-
 dative signaling for phosphatidyserine externalization, survival/
 400 BAD, death receptor/Bcl-2 and several others.

Cisplatin induces a number of signaling pathways
 (Figure 2C). The extracellular signal-regulated kinase pathway
 is activated by cisplatin. Acquisition of cisplatin resistance by
 ovarian carcinoma cells was associated with the loss of extra-
 405 cellular signal-regulated kinase activation in response to cis-
 platin [55]. The c-Abl nonreceptor tyrosine kinase and the
 c-Jun NH2-terminal kinase (JNK/stress-activated protein
 kinase) are activated during the injury response to cisplatin
 [56]. The phosphatidylinositol 3-kinase/AKT1 pathway is
 410 frequently activated in cancer cells. Downregulation of AKT1
 by siRNA could significantly enhance the sensitivity of
 412

413 gastric cancer cells to vincristine, adriamycin, 5-fluorouracil
415 and cisplatin [57]. The PKC pathway may play an important
role in cisplatin resistance [58].

Cisplatin can damage both extracellular protein domains and
cytoplasmic signal transduction molecules. Lipoplatin is pro-
posed to exert a different signaling effect from the cell mem-
brane presumably taking place because of the interaction of its
420 liposomes with the cell membrane; this mechanism might be
giving access to cisplatin of functional groups in membrane
molecules otherwise inaccessible to this drug; this mechanism is
under investigation in MCF-7 human breast and other cells in
culture looking at the up or downregulation of important sig-
425 naling molecules after cisplatin versus Lipoplatin treatment
(Bellirnezi and Boulikas, in preparation).

5. Preclinical studies on Lipoplatin

430 Preclinical studies have shown the lower nephrotoxicity and
other adverse effects of Lipoplatin, compared with cisplatin,
in mice, rats and in severe combined immunodeficient
mice [14,59]. In subsequent studies, mice and rats injected
with cisplatin developed renal insufficiency with clear evi-
435 dence for tubular damage, but those injected with the same
dose of Lipoplatin were almost completely free of kidney
injury [59]. Treatment of dogs with Lipoplatin led to the
conclusion that the drug can be safely administered to clini-
cally normal dogs at dosages of up to 150 mg/m² without
440 the need for concurrent hydration protocols [60].

Independent studies have deciphered one plausible mecha-
nism for Lipoplatin sensitivity of certain tumor cell
lines [61,62]. DNA mismatch repair is a post-replicative DNA
repair mechanism implicated in cell cycle control and apop-
445 tosis. Human colorectal adenocarcinoma cells lacking MLH1,
one of five proteins crucial to mismatch repair function,
showed a twofold resistance to Lipoplatin. Furthermore, the
Lipoplatin-sensitive phenotype of MLH1-proficient cells cor-
related with increased apoptosis, which was found to occur
450 through caspase-independent pathways [61]. Other studies
suggested a cross-talk between Lipoplatin DNA damage sig-
naling mediated by DNA mismatch repair and the Akt sig-
naling pathway [62]. These studies have important implications
in the treatment of colorectal cancer with Lipoplatin and Akt
455 signaling inhibitors. Moreover, analysis of molecular markers
known to be related to cisplatin resistance showed a direct
correlation between cisplatin and Lipoplatin resistance and
ERCC1 and LRP expression and was proposed as valid
predictors of sensitivity or resistance to these drugs [63].

460 The preclinical studies set the foundation for the clinical
use of Lipoplatin as an exciting new drug with lower toxicity
than cisplatin, endowed with pro-apoptotic properties.

6. Lipoplatin as an antiangiogenesis factor

465 A major effort against cancer focuses on targeting tumor
467 vasculature. Inhibiting tumor cells of their ability to build

vasculature is known to dramatically impair the ability of the
468 tumor for further growth by depriving of nutrients. The abil-
470 ity of 'lipogenes', that is, genes wrapped up in liposomes with
the same shell structure as Lipoplatin, to preferentially infil-
trate tumors after systemic delivery is shown in Figure 2A. The
photograph shows a severe combined immunodeficient mouse
implanted with MCF-7 human breast tumor cells that were
475 allowed to develop into large measurable solid tumors at
about 30 days post-inoculation. Following systemic injection
with the reporter β -galactosidase gene, the carcass was stained
with X-Gal to reveal the sites of transgene expression after
relocalization of the gene vehicles from the injected peritoneal
cavity to the various tissues through the arteries, veins and
480 lymph system. Preferential staining of the tumors, especially
of the vascular system around the tumors, was shown [30].

This result suggests that lipogenes (and presumably Lip-
oplatin nanoparticles) possess the ability to extravasate through
485 imperfections of the leaky and often compromised endothe-
lium of tumor vasculature and to concentrate in solid tumors;
during the process, endothelial cells of tumor vasculature can
be also targeted as shown by the blue staining after expression
of the reporter β -galactosidase gene; in this study, biosynthesis
490 of the β -galactosidase protein indicated that the nanoparticle
had successfully crossed the cell membrane barrier and deliv-
ered the gene to the nuclei which was expressed and its RNA
product was successfully translated into a functional protein
detected in our assay. A similar targeting by Lipoplatin inducing
495 apoptotic death to both endothelial cells of tumor vasculature
and epithelial tumor cells was proposed [30].

7. Phase I studies

A Phase I study on 27 patients used a dose escalation from
500 25 to 125 mg/m². All patients were at stage IV (19 pancre-
atic carcinomas, 6 renal cell carcinomas, 1 gastric cancer and
1 squamous cell carcinoma of the head and neck (SCCHN)).
In all cases, Lipoplatin was a second- or third-line treatment
and was administered when the disease was refractory to
505 standard treatment. Lipoplatin was administered as an 8 h
infusion diluted in 1 l 5% dextrose, repeated every 2 weeks.
There was no need for pre- or post-hydration of the patient
with Lipoplatin. This is in contrast to cisplatin chemother-
apy that requires admittance of the patient the night before
510 infusion for hydration as well as extended stay in the hospi-
tal after infusion for post hydration to reduce the nephro-
toxicity of the drug. The maximum tolerated dose (MTD)
was not reached even when the dose was increased up to
350 mg/m² in one patient as a single infusion. Because the
515 dose of cisplatin in the Lipoplatin formulation used in the
Phase I study was as high as double the dose of cisplatin
(100 mg/m² every 21 days) and as the future plan was the
combination of Lipoplatin with other cytotoxic drugs, the
experimental trial ended at this point [23].
520

The highlights of this study were that Lipoplatin had mild
hematological and gastrointestinal toxicity, did not show any
522

523 nephro-, neuro- and oto-toxicity, did not cause hair loss and
 525 was void of most other side effects characteristic of cisplatin
 treatment. Grade 1 and 2 myelotoxicity (neutropenia) and
 grade 1 and 2 GI tract toxicity (vomiting) were observed only
 at the dose of 125 mg/m² (Table 1). No other toxicity was
 observed even with repeated doses. At the beginning of the
 530 infusion, 8 (29.6%) of 27 patients described acute severe epi-
 gastric and back pain that lasted for about 5 min and sub-
 sided spontaneously without analgesic administration. This
 pain is characteristic of other liposomal drugs as well. Patients
 with mild renal insufficiency and with plasma creatinine of
 1.5 – 2.2, treated with a dose of Lipoplatin 100 mg/m²,
 535 showed no increase in plasma creatinine [22].

A further finding was the long circulation of Lipoplatin, a
 property necessary for its preferential extravasation through
 the leaky vasculature of tumors. Indeed, the half-life of total
 platinum in human plasma was determined to be 60 – 117 h
 540 depending on the dose. At the dose of 100 mg/m², the half-
 life was 117 h (about 5 days) compared to ~ 6 h for cispla-
 tin [22]. Although measurement of the response rate was not
 a primary goal of the study, 3 (11.1%) of 27 patients were
 recorded to have achieved a partial response; of the remain-
 545 ing 24 patients, 14 (51.9%) achieved stable disease and clinical
 benefit in a follow-up of 2 – 5 months [22]. Provided that
 all patients had failed previous chemotherapy, that they all
 were at stage IV of their disease and had a rather poor
 performance status, this finding is very encouraging.

550 In a different Phase I study, Lipoplatin, dose-escalated at
 100 mg/m² by increments of 10% on days 1 and 8, was
 combined with gemcitabine 1000 mg/m² days 1 and 8,
 repeated every 21 days in patients with refractory or resistant
 NSCLC with PS ≤ 2. The dose of 120 mg/m² of Lipoplatin
 555 was defined as the MTD in its combination with gemcit-
 abine. A disease control rate of 3 (23%) of 13 was found;
 the median overall survival was 29 weeks (range 4 – 52) and
 the median time to progression 12 weeks (range 3 – 36) [64].
 The drug was also successfully used for mesothelioma by the
 560 same group [65].

8. Phase II studies

565 8.1 Pilot Phase II with Lipoplatin + gemcitabine as second-line every 14 days

A pilot Phase II study using Lipoplatin at dose levels of
 75, 100 and 125 mg/m² every 14 days in a combination
 with gemcitabine 1 g/m² every 14 days was tested on
 26 patients (19 patients with pancreatic cancer and 7 with
 570 NSCLC), of a PS 1 – 2. All patients were resistant to pre-
 vious first- or second-line chemotherapy and Lipoplatin +
 gemcitabine was given as a third-line treatment. No renal
 toxicity, neuropathy, ototoxicity, hepatotoxicity, cardiotox-
 icity or allergic reactions were observed. Nausea and vom-
 575 iting grade I – II was seen in 4 (15.3%) patients and
 myelotoxicity of grade III was seen in 1 patient and of
 577 grade I – II in 15 (57.6%) patients. Mild asthenia was

common. Lipoplatin at 125 mg/m² and 1 g/m² gemcit-
 578 abine induced grade III and IV neutropenia and grade III
 580 nausea and vomiting. Six (23%) patients showed partial
 response. Stable disease was seen in 65.3% and clinical
 benefit in 42.3% of the patients [66].

8.2 Phase II with Lipoplatin + gemcitabine as 585 second-line every 14 days in pancreatic cancer

The standard cytotoxic treatment of advanced or metastatic
 pancreatic cancer is single agent gemcitabine. The addition
 of cisplatin, irinotecan, oxaliplatin and taxanes, in combina-
 tion with gemcitabine, has shown higher response rates but
 overall survival has not significantly increased. The horizon
 590 has been broadened by erlotinib (EGFR inhibitor) when
 combined with gemcitabine [67].

A Phase I – II cohort, dose escalation trial of Lipoplatin
 and gemcitabine was conducted on advanced-stage pre-
 treated pancreatic cancer patients who were refractory to
 595 previous chemotherapy. Twenty-four patients (11 male,
 13 female; median age 66 years, range 47 – 80 years) with
 histologically or cytologically confirmed adenocarcinoma of
 the pancreas and bidimensionally measurable disease, had a
 life expectancy of at least 3 months. WHO performance
 600 status was 0 in 4.2% of the patients, 1 in 45.8% and 2 in
 50%. The vast majority of patients were at stage IV (79.2%).
 All patients had undergone previous chemotherapy:
 11 patients with gemcitabine as a single agent treatment and
 13 with gemcitabine combined with irinotecan. 605

The gemcitabine dose was kept standard at 1000 mg/m²
 given as a 60 min i.v. infusion and the Lipoplatin was escalated
 from 25 to 125 mg/m² administered as an 8 h i.v. infusion on
 days 1 and 15 and cycles were repeated every 4 weeks (28 days).
 Lipoplatin 125 mg/m² was defined as the dose limiting toxicity
 610 and 100 mg/m² as the MTD in this combination treatment.
 Standard ondansetron antiemetic treatment was administered to
 all patients whereas prophylactic administration of recombinant
 human G-CSF was not allowed.

Temporary abdominal pain which lasted for 2 – 4 min,
 615 and which righted itself, was observed in 10/24 patients at
 the beginning of the Lipoplatin infusion. Grade 3 myelo-
 toxicity was observed in two out of four patients at the fifth
 dosage level. No febrile neutropenia was seen. No neurotox-
 icity or renal toxicity was observed. The non-hematological
 620 toxicities are summarized in Table 2.

Partial response (PR) was defined as > 50% reduction in
 the sum of the products of the perpendicular diameters of
 all measurable lesions compared with pretreatment measure-
 ments, lasting for at least 4 weeks, during which time no
 625 new lesions appeared and no existing lesions enlarged. Stable
 disease (SD) was defined as 50% reduction to a 25% increase
 in the sum of the products of the two perpendicular dia-
 meters of all measurable lesions and the appearance of no
 new lesions for 8 weeks. 630

Preliminary objective response rate data showed a PR in 2
 (8.3%) of 24 patients, disease stability in 14 (58.3%) patients 632

Table 1. Adverse effects of Lipoplatin monotherapy at a dose escalation up to 125 mg/m² every 14 days.

Toxicity	Grade 1	Grade 2	Grade 3	Grade 4
Neutropenia	19	10	10	0
Thrombocytopenia	5	10	5	0
Anemia (hemoglobin)	19	10	0	0
Renal (creatinine)	0	0	0	0
Hepatic	0	0	0	0
Nausea/vomiting	5	5	10	0
Neuropathy	0	0	0	0
Allergy	0	0	0	0
Cardiotoxicity	0	0	0	0
Ototoxicity	0	0	0	0
Hair loss	0	0	0	0

Numbers indicate percentage of patients from a total of 27 patients included in this study.

Table 2. Non-hematological toxicities using 1 g/m² gemcitabine and Lipoplatin dose escalation from 25 to 125 mg/m² every 14 days.

	Grade 1 n (%)	Grade 2 n (%)	Grade 2 n (%)	Grade 4 n (%)
Nausea	5 (20.8)	0	0	0
Vomiting	2 (8.3)	0	0	0
Alopecia	14 (58.3)	0	0	0
Fatigue	8 (33.3)	0	0	0
Diarrhea	2 (8.3)	0	0	0
Cardiotoxicity	0	0	0	0
Neurotoxicity	3 (12.5)	0	0	0
Nephrotoxicity	0	0	0	0
Thrombotic episodes	4 (16.7)	0	0	0

Data are based on 24 patients and are taken from [68].

633 for a median duration of 3 months (range 2 – 7 months)
 635 and clinical benefit in 8 (33.3%) patients. At the end of the
 study, seven (29.2%) patients were still alive. Median sur-
 640 vival from the beginning of second-line treatment was 4
 months (range 2 – 8+ months). The 14-day administration
 schedule of the combination was very well tolerated up
 to the dose of 100 mg/m² of Lipoplatin when gemcitabine
 was maintained at 1000 mg/m². Taking into account that all
 of the patients were refractory or in disease progression
 while on a previous treatment including gemcitabine, the
 response rate produced were attributed to the addition of
 Lipoplatin [68].

645 In subsequent studies, the schedule of Lipoplatin was changed
 from biweekly to weekly or was increased to 200 mg/m² every
 14 days (see Phase III) to allow administration of a higher total
 648 dose of Lipoplatin and enhance its efficacy.

649 **8.3 Lipoplatin orphan drug registrational EMEA study** 649 650 **in pancreatic cancer**

650 Pancreatic adenocarcinoma, the malignant tumor of pancreatic
 gland, constitutes a major unresolved health problem, affecting
 > 230,000 people worldwide each year. The term 'pancreatic
 cancer' usually refers to adenocarcinomas of the pancreatic duct,
 that is, of the exocrine part of the pancreas, which constitutes
 655 > 90% of the diagnosed pancreatic cancer cases. Pancreatic can-
 cers are very hard to diagnose because they grow in the absence of
 alarming symptoms; about 85% of the patients are usually diag-
 nosed at an advanced stage and have bad prognosis. Indeed, being
 the tenth most common cancer, pancreatic adenocarcinoma is the
 660 sixth leading cause of cancer-related deaths.

Lipoplatin received the orphan drug status by the Euro-
 pean Medicines Agency (EMA) [69]. A multi-center
 Phase II/III registrational clinical study is in progress using
 664

- 665 Lipoplatin plus gemcitabine as first-line treatment in inoperable, locally advanced or metastatic pancreatic cancer with the involvement of 20 oncology centers of excellence in various EU countries. Inclusion criteria are: adult male or female, 18 – 70 years of age with histologically or cytologically confirmed diagnosis of locally advanced or metastatic pancreatic adenocarcinoma; patients should have at least one bidimensionally measurable lesion, no previous chemotherapy or radiotherapy, a performance status 0 – 1, a life expectancy > 3 months and adequate hematologic/hepatic/renal functions. During Phase II, 61 patients will receive i.v. Lipoplatin 120 mg/m² (days 1, 8, 15 in a 21-day cycle) plus gemcitabine 1000 mg/m² (days 1, 8 in a 21-day cycle) for three cycles. Patients with absence of disease progression at response evaluation will continue with maintenance therapy (Lipoplatin 120 mg/m² and gemcitabine 1000 mg/m² days 1, 15 in a 28-day cycle), until disease progression or unacceptable toxicity. During Phase III, 328 patients will be randomized (164 in each arm) to compare the same schedule of Lipoplatin plus gemcitabine as in Phase II with i.v. gemcitabine 1000 mg/m² weekly for 7 weeks, followed by a 1-week break. The sample size calculation is based on a target 1-year survival rate of 30% versus an 18% rate for the gemcitabine-only arm.
- 670
- 675
- 680
- 685 It is worth noting that Tarceva, a small molecule targeting EGFR (Genentech/Roche Holding AG) was approved in 2005 for pancreatic cancer in combination with gemcitabine based on a 24% 1 year survival compared to 18% of patients receiving gemcitabine plus placebo.
- 690
- 695 **8.4 Weekly Lipoplatin + gemcitabine as first-line in NSCLC**
- A recently completed Phase II study used up to six 21-day cycles of Lipoplatin 120 mg/m² (days 1, 8 and 15) and gemcitabine 1000 mg/m² (days 1 and 8) (Arm A or LipoGem) versus cisplatin 100 mg/m² (day 1) and gemcitabine 1000 mg/m² days 1 and 8 (Arm B or CisGem) on 88 patients. The LipoGem treatment was better tolerated, with myelotoxicity as the main side effect. There was a significant reduction in nephrotoxicity in the LipoGem versus the CisGem arm (0 versus 5% Grade III, respectively, *p* value < 0.001). The ORR across all histological subtypes of NSCLC was 31.7% in the LipoGem arm versus 25.6% in the CisGem arm but not statistically significant (*p* value = 0.411). However, a preliminary efficacy of Lipoplatin/Gem versus cisplatin/Gem in the adenocarcinoma histological subtype of NSCLC showed 83.3 versus 54.2% response/stabilization rates [70]. This was an exciting finding proposed to be investigated further in a Phase III on non-squamous NSCLC.
- 700
- 705
- 710
- 715 **8.5 Weekly Lipoplatin + vinorelbine as first-line in advanced breast cancer**
- The frequent use of anthracyclins and taxanes in the adjuvant setting, leading to the development of drug resistance and cardiac insufficiency, raised the need for development
- of new agents against advanced or metastatic breast cancer. The cisplatin–vinorelbine combination has been studied recently and an overall response rate of 64% was obtained. Nevertheless, the use of cisplatin was limited by the frequently induced nausea, vomiting and nephrotoxicity. The aim of a Phase II study was to evaluate the efficacy and safety of the Lipoplatin–vinorelbine combination as first-line treatment in advanced breast cancer patients. Twenty of thirty-four programmed patients with advanced or metastatic breast cancer with no previous treatment, PS 0 – 2, HER2/neu negative, and at least one measurable lesion were enrolled from August 2007 to April 2008 in a Phase II study. Treatment included vinorelbine 30 mg/m² i.v. days 1 and 8, and Lipoplatin 120 mg/m² days 1, 8 and 15. Cycles were repeated every 3 weeks for a total of 6 cycles. The primary objectives were response rate and time to treatment failure. In all, 45% of patients had one metastatic site, 30% had two and 25% had three or more. A total of 74 cycles were administered with a median number of 4 per patient. At the time of the analysis, 16 patients were evaluable for response. An objective tumor response was achieved in eight (50%) patients, with complete response in two (13%) patients. Six (38%) patients had SD. All patients (20) were evaluable for toxicity. Most adverse events were mild to moderate. No WHO grade 3 – 4 nephrotoxicity, asthenia or neuropathy was noted. Three (15%) patients developed hypomagnesemia; however, it was of no clinical significance. One (5%) patient presented grade 3 anemia and seven (35%) patients grade 3 – 4 neutropenia with only one episode of febrile neutropenia. The new combination of Lipoplatin and vinorelbine showed promising activity and good tolerance as first-line treatment for HER2/neu negative advanced or metastatic breast cancer [71].
- 720
- 725
- 730
- 735
- 740
- 745
- 750
- 755 **8.6 Lipoplatin-gemcitabine in cisplatin-treated NSCLC patients**
- A Phase II trial is evaluating response and toxicity in advanced NSCLC patients who underwent previously cisplatin-based chemotherapy; thus, this trial is addressing the efficacy of Lipoplatin plus gemcitabine in patients whose disease is refractory to classical cisplatin chemotherapy. Patients were treated with Lipoplatin 120 mg/m² days 1 and 8 plus gemcitabine 1000 mg/m² days 1 and 8 every 3 weeks; the study is in progress as of April 2009. Twenty-seven (77.8%) patients (21 males) were assessable for response and toxicity according to the WHO criteria of a median age of 70 years (41 – 78). Twenty-two (81.5%) patients were at stage IV at diagnosis; 14 (51.8%) patients had adenocarcinoma and 13 (48.2%) had squamous-cell carcinoma in histological type.
- 760
- 765
- 770
- 774 PR was observed in 6 (22.2%), SD in 5 (18.5%) and progressive disease in 16 (59.2%) patients.
- With respect to hematological toxicity grade 3 – 4 neutropenia was observed in six (22.2%) patients, grade 3

775 thrombocytopenia in one (3.7%) patient and grade 3
 anemia in one (3.7%) patient. Other toxicities included
 grade 3 – 4 nausea/emesis in nine (33.3%) patients, grade
 3 fever in nine (33.3%) patients and grade 3 nephrotoxicity
 in one (3.7%) patient. Further toxicities such as rash,
 780 constipation and peripheral neuropathy were rare and/or
 mild. Median overall time to tumor progression was
 14 weeks (3 – 50). The preliminary results of this continuing
 Phase II trial were encouraging in terms of response
 rate and toxicity [72]. Especially important is the fact that
 785 Lipoplatin seems to have activity in cisplatin-resistant
 tumors, something predicted previously from the liposomal
 nature of the drug; Lipoplatin was proposed to be able to
 treat cisplatin-resistant tumors with resistance arising at the
 cell membrane level and not at the level of DNA repair [12].
 790 It will be interesting to examine the gene expression profile
 of Ctr1, ATP7A, ATP7B cisplatin transporters as well as
 for ERCC1 and other DNA repair genes in white blood
 cells or in tumor specimens in the group of patients with
 PR, SD and progressive disease.

795

8.7 Lipoplatin, 5-FU and radiotherapy for locally advanced gastrointestinal adenocarcinoma

800 The objective of a Phase II study was to investigate the
 toxicity, response rates and overall survival of Lipoplatin
 radio-chemotherapy in locally advanced gastric adenocarcinomas,
 in those unable to undergo surgery and to test the radiosensitizing
 ability of Lipoplatin because of the concentration of its nanoparticles
 in tumors. Patients with locally advanced gastric cancer or gastric
 805 cancer inoperable for medical reasons or recurrent carcinomas of a
 performance status of 0 – 2 were recruited. Patients with previous
 radiotherapy, with an extensive metastatic disease or with
 uncontrolled brain metastasis were excluded.

810 Lipoplatin was given at a dose of 120 mg/m², 5-FU at
 400 mg/m² (day 1), while radiotherapy was given through
 3.5 Gy fractions on days 2, 3 and 4 in a 7-day schedule.
 Two groups of six patients received 4 and 5 consecutive
 cycles, respectively. Twelve of twenty planned patients in
 815 this study have completed treatment. No WHO grade 3 or
 4 nephrotoxicity, anemia, asthenia or neuropathy were noted,
 except of grade III neutropenia in 1 (8%) of 12 patients. A net
 improvement of the performance status (from a median of 1 – 0)
 was recorded at 2 months after the end of therapy. The response
 rates assessed with CT-scan, endoscopy and biopsies confirmed
 820 33% (2/6) complete remission and 3 (50%) of 6 PR in patients
 treated with four cycles and 4 (80%) of 5 complete remission
 in patients treated with five cycles [73].

825 Concurrent hypofractionated radiotherapy (4 – 5 Gy/
 fraction, 2 fractions a week) and 5-FU bolus 1 h before RT
 at doses of 300 mg/m² in patients suffering from recurrent
 or locally advanced inoperable colorectal cancer was an
 829 established scheme in this center [74].

9. Tumor targeting in human studies

830

Intravenous infusion of Lipoplatin to four patients (one with
 hepatocellular adenocarcinoma, two with gastric cancer, and
 one with colon cancer, Table 3) followed by a prescheduled
 surgery ~ 20 h later was used to show the accumulation of
 835 the drug in the lesion. During this study, tumor specimens
 were obtained during surgery but also adjacent noncancerous
 tissue; the specimens were first extracted in saline solution, a
 mild method that preserves cellular integrity, and the platinum
 that was solubilized was related to platinum trapped in
 840 tissues ('Trapped' in Table 3). Saline-insoluble material from
 tumor specimens was subsequently extracted in sodium dodecyl
 sulfate that dissolved membranes, nuclei, denaturing protein
 assemblies, RNA and DNA from chromatin; the sodium
 dodecyl sulfate-soluble fraction of the specimens revealed the
 845 amount of platinum that was bound to macromolecules
 ('Reacted' in Table 3). The ratio of platinum in tumor specimens
 versus platinum in the adjacent normal tissue revealed the
 concentration-fold of the nanoparticles in the cancer over
 normal tissue (Table 3). 850

Direct measurement of platinum levels by atomic absorption
 in the extracts from specimens from the excised tumor and the
 adjacent normal tissue as well as metastases (colon metastasis
 from a liver tumor, liver metastasis from a gastric cancer)
 showed that total platinum levels that reacted with
 855 macromolecules and caused damage to tissue were on the
 average 10 – 171 times higher in malignant tissue compared to
 the adjacent normal tissue; most effective targeting was
 observed in colon cancer with an accumulation up to 200-fold
 higher in colon tumors compared to normal colon tissue. Gas-
 860 tric tumor specimens accumulated the highest levels of drug
 than any other tissue and, thus, Lipoplatin may prove effective
 against stomach cancers in future clinical studies (Table 3) [29].

In conclusion, Lipoplatin was preferentially concentrated in
 the primary tumor and the metastases in human patients
 865 undergoing chemotherapy. High tumor levels were seen at
 about 20 h from infusion of the drug under conditions in
 which blood levels of Lipoplatin had dropped to below 1 mg/
 ml from Phase I study [22]. Targeting was proposed to take
 place at two levels: i) after i.v. injection, Lipoplatin was
 870 preferentially (40-times) concentrated into tumors by extravasation
 through the leaky tumor vasculature. To achieve this result,
 the nanoparticles of Lipoplatin are coated with PEG for long
 circulation and low clearance by macrophages. ii) Once inside
 the tumor, Lipoplatin nanoparticles were proposed to diffuse
 875 to the extracellular space and to be taken up more avidly by
 the cell membrane of the tumor cell compared to normal cell
 (five times more). This is supposed to arise from the avidity
 of tumor cells for nutrients (the lipid shell of Lipoplatin
 composed of lipids is mistaken as a nutrient) as well as by an
 enhanced diffusion of the nanoparticles with the cell membrane;
 to enhance uptake the nanoparticles the fusogenic lipid,
 880 DPPG, was used during formulation. These two mechanisms
 together contribute to an up to 200-fold higher 884

Table 3. Summary of human targeting by Lipoplatin.

Patient no. and specimen	Trapped (µgPt/g tissue)	Tumor Pt/normal tissue Pt	Reacted (µgPt/g tissue)	Tumor Pt/normal tissue Pt
No. 1 Liver tumor	5.18	0.31	33.18	10.50
No. 1 Normal liver tissue	16.45		3.16	
No. 1 Colon metastasis	4.44	74.00	2.17	27.12
No. 1 Normal colon tissue	0.06		0.08	
No. 2 Liver metastasis	34.51	2.04	96.64	24.16
No. 2 Normal liver tissue	16.94		4.00	
No. 3 Stomach tumor 1	44.17	16.86	220.45	55.53
No. 3 Stomach tumor 2	28.46	10.86	37.92	9.55
No. 3 Normal stomach tissue	2.62		3.97	
No. 4 Colon tumor 1	4.42	221.00	6.85	171.25
No. 4 Colon tumor 2	1.86	93.00	5.83	145.75
No. 4 Normal colon tissue	0.02		0.04	

Values in the column 'Trapped' or 'Reacted' are expressed in µg platinum (Pt)/g tissue measured by atomic absorption. The other two columns show the ratio (total platinum in tumor) versus (total platinum in the corresponding normal tissue).

Adapted from [29].

885 damage to cancer tissue compared to normal tissue and may
contribute to the low side effects of the drug.

10. Phase III studies

890 10.1 Lipoplatin plus gemcitabine versus cisplatin plus gemcitabine as first-line treatment in patients with NSCLC

895 A randomized multi-center Phase III non-inferiority clinical
study compares Lipoplatin 120 mg/m² on days 1, 8 and 15
900 plus gemcitabine 1 g/m² on days 1 and 8 in a 21-day cycle
(Arm A or Lipo/gem) with cisplatin 100 mg/m² on day 1
plus gemcitabine 1 g/m² on days 1 and 8 in a 21-day cycle
(Arm B or Cis/gem) as first-line treatment in patients with
905 NSCLC. Patients have disease evaluation after three and six
cycles and the planned number of patients is 200 in each
treatment arm. The primary end points are overall survival.
Secondary end points are toxicity, overall response rates,
910 progression-free survival and quality of life. Adverse events
are assessed using the WHO Common Toxicity Criteria
(CTC). Eligibility criteria included confirmed diagnosis of
inoperable or metastatic NSCLC, no previous chemotherapy,
WHO PS 0 – 1, and adequate end-organ function. Lipoplatin
was administered without hydration as a 6 h infusion in 1 l 5%
dextrose compared to patients receiving cisplatin who were
admitted to the hospital the day before treatment from pre-
hydration and had an extended stay for post hydration to
minimize adverse effects and enhance renal excretion of
cisplatin.

915 In a preliminary report on this non-inferiority Phase III
trial presented to ASCO [75], 59 patients were included of

whom 33 received the Lipo/gem and 26 the Cis/gem regi- 916
men. There were no grade 4 toxicities. Grade 3 toxicities
were observed in < 5% of the patients and were comparable
in the two groups, with the exception of neutropenia
(3% for Lipo/gem and 15% for Cis/gem) (Table 4). Grade 2 920
nephrotoxicity was reported for 6% of Lipo/gem patients
versus 19% of Cis/gem patients. Neurotoxicity was also mark-
edly less in the Lipo/gem arm. Particularly important might be
the significantly lower neuro- and nephro-toxicity of the Lip-
oplatin arm and its administration on an outpatient basis with 925
clear pharmacoeconomic benefits; Lipoplatin was administered
without pre- and post-hydration as a 6-h infusion.

An interim analysis of this trial on 101 patients of whom
60 received the Lipo/gem and 41 the Cis/gem regimen, with
a stratification for histological subtypes of NSCLC, showed 930
there was a significant reduction in nephrotoxicity, nausea/
vomiting, neurotoxicity and asthenia in the Lipo/gem com-
pared to Cis/gem treatment arms [76]. This study has
recruited > 280 patients and is expected to lead to a pivotal
EMEA study in the non-squamous histological subtypes of 935
NSCLC in 2009.

10.2 Lipoplatin plus paclitaxel versus cisplatin plus paclitaxel as first-line treatment in NSCLC

940 The use of a taxane in combination with a platinum compound
has become an acceptable standard as first-line treatment for
patients with advanced or metastatic NSCLC [77-79].

This randomized Phase III used 200 mg/m² Lipoplatin
plus 135 mg/m² paclitaxel administered on day 1 repeated 945
every 2 weeks (Lipo-Taxol or Arm A). Lipoplatin was infused
for 8 h in 1 l 5% dextrose. Arm B (Cis-Taxol) was 75 mg/m² 946

Table 4. Preliminary toxicity data from a randomized non-inferiority Phase III study.

	Lipoplatin arm (33 patients)	Cisplatin arm (26 patients)
Nephrotoxicity grade II	6.0	19.0
Nephrotoxicity grade III	0	4.5
Nausea and vomiting	0.0	6.8
Asthenia and anorexia	1.8	11.4
Anemia	5.3	2.3
Leucopenia	14.0	9.1
Neutropenia*	3.0	15.0
Thrombocytopenia	10.5	13.6
Neurotoxicity	+	+++

Numbers indicate percentage of patients.

Data were taken from [75].

*Neutrophils are more important than leucocytes for fighting infections; the fact that Lipoplatin does not cause neutropenia to the extent of cisplatin is a positive virtue of the drug.

Table 5. Summary of the preliminary toxicity results of the Phase III Lipoplatin plus paclitaxel versus cisplatin plus paclitaxel study.

	Toxicity	
	Arm A: Lipo-taxol	Arm B: Cis-taxol
Renal toxicity	3.70%	25.92%
Neurotoxicity grade I – II	Grade I – II only: 25.92%	Grade I – III: 44.44%
Nausea-vomiting	18.52%	25.92%
Myelotoxicity	Grade I – II only: 37.04%	Grade I – III: 62.96%

Data were taken from [80].

947 cisplatin (hydration of 2 l) and 135 mg/m² paclitaxel, administered every 2 weeks. One cycle was 14 days and the plan was to give nine cycles (treatments) per patient unless disease progression was detected before the ninth cycle.

950 The main objective of the study was to show that Lipoplatin was not inferior to cisplatin when combined with paclitaxel as first-line treatment as assessed by overall survival in a randomized group of patients with NSCLC at stage IIIB/IV (with locally advanced or metastatic disease) but that patients in the Lipoplatin/paclitaxel arm (Arm A) had a better toxicity profile and showed a better quality of life (EORTC questionnaire) compared to patients in the cisplatin/paclitaxel arm (Arm B). Secondary objectives of the study were to compare the time to tumor progression, 1-year survival and response rate between the two arms.

In a preliminary report of the study [80], 61 chemo-naïve 962 patients were recruited as of December 2006 and 54 patients were evaluable for response and toxicity, 27 in each arm. The median age was 65 (42 – 80). The toxicity data are 965 summarized in Table 5.

In the Lipo-Taxol arm, renal toxicity was observed in 1 (3.70%) patient, neurotoxicity grade I – II in 7 (25.92%) patients nausea-vomiting in 5 (18.52%) patients and myelotoxicity grade I – II in 10 (37.04%) patients. In the Cis-Taxol Arm, renal toxicity was observed in 7 (25.92%) 970 patients, neurotoxicity grade I – III in 12 (44.44%) patients nausea-vomit in 7 (25.92%) patients and myelotoxicity grade I – III in 17 (62.96%) patients. Thus, the toxicity differences were very important between the two arms. In 975 particular, the renal toxicity seemed to be sevenfold lower in the Lipoplatin arm. Also significantly lower was the neurotoxicity and myelotoxicity of grade III (totally absent in the Lipoplatin arm). It was concluded that the response rate was similar but toxicity and in particular nephrotoxicity, neuro- 980 toxicity and myelotoxicity were significantly lower in the Lipoplatin arm [80].

This Phase III was terminated successfully after treating 236 patients (of whom 229 were evaluable), 114 in arm A (Lipo-Taxol) and 115 in arm B (Cis-Taxol), respectively; the 985 data showed the non-inferiority of the Lipoplatin-paclitaxel combination compared to cisplatin-paclitaxel in the schedule described above but with statistically significant lower toxicities in the Lipoplatin-paclitaxel arm for nephrotoxicity, grade 3 and 4 leukopenia, grade 2 and 3 neuropathy, asthenia 990 (fatigue) and gastrointestinal toxicity (nausea/vomiting). There was no significant difference in median and overall survival as well as time to tumor progression between the two arms [81]. Patient cases from this study before and after treatment with Lipoplatin plus paclitaxel are shown in Figure 3. 995

10.3 Lipoplatin plus 5-FU versus cisplatin plus 5-FU against SCCHN

Cisplatin remains the reference drug in the induction chemotherapy setting for SCCHN when used in combination with 1000 5-FU. However, its clinical use is limited by its peripheral neuropathy, as well as renal and hematological toxicity, manifesting at increasing cumulative doses.

A randomized, multi-center Phase III trial against SCCHN was designed, in which conventional cisplatin or Lipoplatin 1005 were used in combination with 5-FU, to compare efficacy and safety profiles of both treatment arms. A pharmacokinetics study from this trial was published [82]. Inclusion criteria were: patients with histologically confirmed SCCHN (primary metastatic or patients with relapsed/progressive disease) with at least one measurable bidimensional lesion, 1010 between the age of 18 – 75 years, a performance status of at least Eastern Cooperative Oncology Group 3, an adequate bone marrow function (a peripheral absolute leukocyte count of at least 2500/mm³ and platelet count of at least 1015 100,000/mm³) and an adequate liver function, with a sufficient 1016

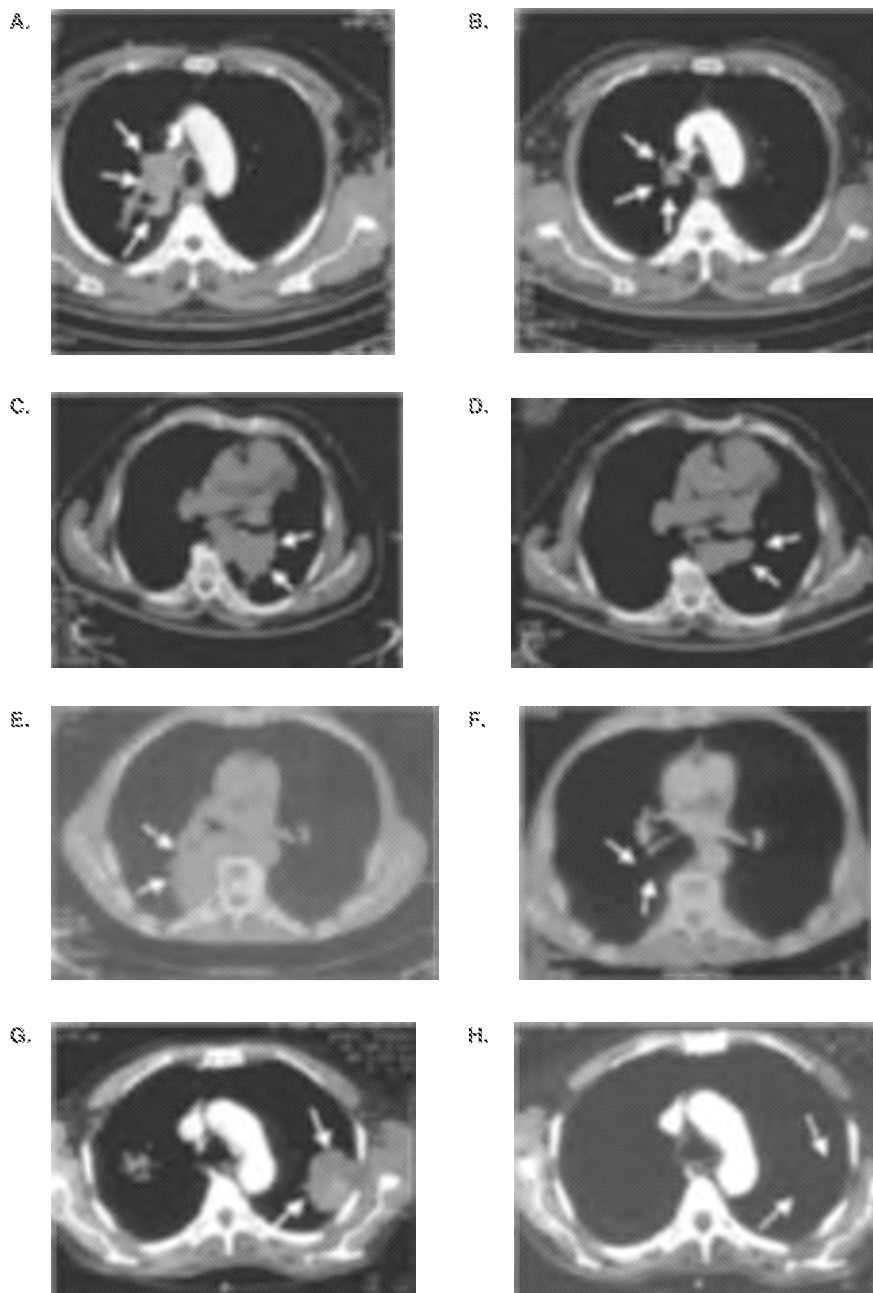


Figure 3. Patient cases from the Phase III study comparing Lipoplatin to cisplatin in combination with the same dose of paclitaxel documented with CT slices (with mediastinal window settings) before and after treatment. **A.** A low differentiated adenocarcinoma in the right upper lobe is present. **B.** The lesion was recorded as a partial response after four cycles of Lipoplatin–paclitaxel chemotherapy. **C.** A large adenocarcinoma cell tumor (arrows) in the left lower lobe. **D.** Follow-up scan taken after five cycles of Lipoplatin–paclitaxel treatment show reduction of volume of the lesion. **E.** CT section demonstrating a large tumor mass in the right lobe. **F.** Follow-up scan after nine cycles of Lipoplatin–paclitaxel treatment demonstrated a remarkable mass reduction. **G.** CT section demonstrating a large tumor mass in the left lobe. **H.** Follow-up scan after nine cycles of Lipoplatin–paclitaxel treatment showed mass reduction

From [109] with permission from Gene Therapy Press.

- 1017 renal function (defined as creatinine clearance > 50 ml/min). Exclusion criteria included progression during 100 mg/(m² day) cisplatin-based chemotherapy, no progressive disease after 1020 chemotherapy or radiochemotherapy, < 3 weeks since previous surgery, pregnancy, active/unstable ischemic heart disease, Hepatitis B or C and use of nonstudy cancer therapy. Stratification criteria were primary metastatic disease, recurrent or progressive SCCHN, previous chemotherapy/no previous chemotherapy, previous cisplatin-based chemotherapy/previous non cisplatin-based chemotherapy and center.
- This study is using treatment with 100 mg/(m² day) Lipoplatin as a 4 h i.v. infusion (days 1, 8, 15) plus 1000 mg/(m² day) 5-FU (days 1 – 5 continuous infusion) every 21 days (one cycle) for six cycles (Arm A). The comparative arm (Arm B) uses 100 mg/(m² day) cisplatin with pre- and post-hydration (day 1) plus 1000 mg/(m² day) 5-FU (days 1 – 5 continuous infusion) every 21 days (one cycle) for six cycles.
- A dose reduction of cisplatin occurred from 100 to 1035 70 mg/m² when the creatinine clearance fell between 99 and 70 ml/min, leukopenia < 500/μl during the last cycle, neutropenic fever/infection during last cycle or thrombopenia < 50,000/μl during the last treatment cycle. Cisplatin was reduced to 50 mg/m² when the creatinine 1040 clearance fell between 69 and 50 ml/min or mucositis CTC grade 4 occurred. 5-FU was reduced in dose from 1000 to 500 mg/(m² day) when severe hand and foot syndrome or mucositis CTC grade 4 occurred. No dose reductions of Lipoplatin were performed.
- An interim analysis was reported [83] on 46 evaluable 1045 patients, 25 in the Lipoplatin/5-FU and 21 in the cisplatin/5-FU arm, respectively, after at least two cycles in both arms. The main end points for this interim analysis were hemato- and nephro-toxicity.
- Toxicity: Seven patients had to stop cisplatin therapy due 1050 to severe toxicity as compared to one patient in the Lipoplatin treatment arm. Severe hematotoxicity was more frequent in the cisplatin arm, with grade III and IV toxicity occurring in 31.7% of the patients treated with the cisplatin-based regimen versus 12% in the Lipoplatin-based regimen 1055 (Table 6). Grade IV leucopenia occurred in 22.2% of the patients treated with cisplatin/5-FU, whereas in the Lipoplatin/5-FU arm, 0% grade IV leucopenia occurred.
- One of most debilitating toxic side effects and a great 1060 impingement on the quality of life of cisplatin-based chemotherapies is neuropathy. Lipoplatin seems to reduce neurotoxicity profoundly. A total of 67% of the patients treated with the cisplatin regimen experienced grade I and II neuropathy compared to 27% in the Lipoplatin arm. More 1065 patients developed severe mucositis in the cisplatin-based regimen than in the Lipoplatin regimen: 33.3% of the patients treated with cisplatin suffered grade III or IV mucositis and mostly hospitalization was required, compared to only 8% in the Lipoplatin treatment arm. The renal toxicity 1070 profile of both drugs also showed marked differences: 23.8% of the treated patients suffered a significant reduction in 1072 kidney function, with a decrease in creatinine clearance below 50 ml/min in the cisplatin arm; furthermore, three patients 1075 suffered acute renal insufficiency in the cisplatin arm. In contrast, no grade III or IV renal toxicity occurred in patients treated with Lipoplatin. This continuing study has shown so far that the Lipoplatin formulation reduces both the hematological and non-hematological toxicity profiles of cisplatin to a clinically relevant extent when combined with 5-FU.
- The efficacy results showed 38.8% objective partial remission in the Lipoplatin arm versus 19% in the cisplatin arm. 1080 However, 64% of the patients achieved SD while being treated with Lipoplatin/5-FU, compared to 50% of the patients in the cisplatin/5-FU regimen. A total of 24% of the patients progressed while being treated with Lipoplatin/5-FU 1085 versus 14.3% of these treated with cisplatin/5-FU. A high rate of SD was observed in the Lipoplatin versus cisplatin arms (64 versus 50%); also the clinical benefit rate (SD + partial remission) was similar for the cisplatin (88.5%) and Lipoplatin combinations (83%), although there were more objective 1090 responses seen in the cisplatin arm. Because patients with advanced SCCHN have an increased risk of renal toxicity due to poor hydration, the observed reduction of side effects with cisplatin can help to preserve the dose density of chemotherapy, and thereby efficacy, and to improve the quality of life of 1095 these patients [83].
- Increasing the dose of Lipoplatin to its weekly recommended schedule of 120 mg/m² and further reducing its infusion rate to reduce toxicities might improve the efficacy results. The overall Lipoplatin dose in the LipoFU study is 300 mg/m² every 1100 21 days compared to 360 mg/m² every 21 days in the LipoGEM study (see above section 10.1). Also, the LipoFU trial recruits both chemo-naïve and previously treated patients compared to LipoGEM that recruits only chemo-naïve patients. Both 5-FU and gemcitabine belong to the class of antimetabolites 1105 according to the FDA classification.

11. Discussion

11.1 Clinical benefit of Lipoplatin in NSCLC

Lung cancer is the most common cause of cancer-related death in men and the second most common in women, while it is responsible for 1.3 million deaths worldwide annually and ~ 300,000 new cases in the EU. Approximately 80% of lung cancer cases are NSCLC and in > 70% of these cases, disease is diagnosed at a late stage, when already locally advanced or metastatic. NSCLC is a slow spreading malignancy that consists of three major subtypes, adenocarcinoma, squamous cell carcinoma and undifferentiated large cell carcinoma, with frequencies 50, 30 and 5%, respectively [84]. A preferred regimen for first-line treatment against NSCLC include gemcitabine and cisplatin in EU and carboplatin-paclitaxel in the US [85,86]. Cisplatin-gemcitabine-bevacizumab [87], vinorelbine-platinum [88] and cisplatin-pemetrexed [89] have also been tested as front line. In the second-line setting of NSCLC, docetaxel, pemetrexed and erlotinib are widely used [90] although further experimental 1126

Table 6. Hematological and non-hematological toxicities for cisplatin/5-FU regimen (n = 21) versus Lipoplatin/5-FU regimen (n = 25).

Grade	I		II		III		IV	
	Cisplatin	Lipoplatin	Cisplatin	Lipoplatin	Cisplatin	Lipoplatin	Cisplatin	Lipoplatin
% patients								
WBC	33.3	16.0	22.2	7.0	9.5	0.0	22.2	0.0
Platelets	19.0	8.0	14.3	0.0	4.8	0.0	0.0	0.0
Hemoglobin	33.3	20.0	38.9	16.0	9.5	16.0	0.0	0.0
Nausea	4.8	8.0	27.8	16.0	28.6	8.0	9.5	0.0
Mucositis	4.8	8.0	22.0	4.0	19.0	4.0	14.3	4.0
Diarrhea	9.5	0.0	9.5	4.0	19.0	4.0	0.0	0.0
Infection	0.0	0.0	9.5	12.0	28.6	28.0	14.3	0.0
Allergic reaction	0.0	0.0	0.0	8.0	0.0	0.0	0.0	4.0
Renal	9.5	12.0	28.6	40.0	23.8	0.0	0.0	0.0
Neuropathy	33.3	27.0	33.3	0.0	19.0	0.0	0.0	4.0

Data were taken from [83].

5-FU: 5-Fluorouracil; WBC: White blood cell.

1127 second-line treatments have been explored including gemcitabine-
1130 irinotecan [91]. Response rates of 20 – 40% can now be expected,
with a median survival of 8 – 11 months and a 1-year survival
rate of 30 – 40% [86,92].

1135 In the quest for new treatments the combination of beva-
cizumab, a humanized anti-VEGF monoclonal antibody,
with chemotherapy was shown to produce better outcomes
than chemotherapy alone in chemotherapy-naïve, advanced,
1140 non-squamous NSCLC patients. Indeed, The Eastern Coop-
erative Oncology Group study E4599 [86] on 878 patients
comparing paclitaxel/carboplatin with or without bevaciz-
umab was the first Phase III randomized trial to show a
survival benefit for carboplatin–paclitaxel plus bevacizumab
1145 over chemotherapy alone; the results of this study led the
FDA to approve this novel combination for first-line treat-
ment of patients with unresectable, locally advanced, recur-
rent or metastatic non-squamous NSCLC. The median
survival was 12.3 months in the group assigned to chemo-
therapy plus bevacizumab, as compared with 10.3 months
in the chemotherapy-alone group.

1150 In all preclinical and clinical studies described here, Lipopla-
tin displayed low renal toxicity. The mechanism of severe neph-
rotoxicity caused by cisplatin, but not carboplatin, oxaliplatin
and nedaplatin, is not fully understood. Emerging data showed
that the nephrotoxicity of platinum agents was closely associ-
ated with their renal accumulation, which was determined by
the substrate specificity of the OCT and MATE families;
1155 indeed, a luminal H⁺/organic cation antiporter, rMATE1 (mul-
tidrug and toxin extrusion) as well as human MATE1 and
hMATE2-K, stimulated the H⁺-gradient-dependent antiport of
oxaliplatin, but not of cisplatin in rat kidneys [93].

1159 A number of agents have been shown to ameliorate
experimental cisplatin nephrotoxicity; these include antioxidants

(e.g., melatonin, vitamin E, selenium and many others), 1160
modulators of nitric oxide (e.g., zinc histidine complex),
agents interfering with metabolic pathways of cisplatin (e.g.,
procaine HCl), diuretics (e.g., furosemide and mannitol),
and cytoprotective and antiapoptotic agents (e.g., amifos- 1165
tine and erythropoietin). On the contrary, nitric oxide syn-
thase inhibitors, spironolactone and gemcitabine, augment
cisplatin nephrotoxicity (reviewed in [94]).

11.2 Clinical benefit of Lipoplatin in other tumors

1170 The Phase II studies on pancreatic, breast and gastric cancers
are expected to promote Lipoplatin as an important drug to
the arsenal of chemotherapeutics. Two groups of advantages
of the drug are expected to help its promotion in the clinic:
i) lower nephrotoxicity and administration benefits (without
1175 hydration); and ii) concentration into tumors. Important
data are expected to be obtained from tumors of high vascu-
larization (e.g., gastric cancer) because of the proposed ability
of Lipoplatin nanoparticles to use the vascular system of the
tumor for extravasation. These studies will also provide infor-
mation on the combination drug that gives optimal anti- 1180
cancer results with Lipoplatin against a certain indication.
Gemcitabine, 5-FU, paclitaxel, vinorelbine and radiation
have been under evaluation so far. Of these, gemcitabine and
5-FU are from the antimetabolite class; paclitaxel and vno-
relbine are antimicrotubule agents; and radiation can inflict
1185 double strand breaks on the DNA. Each drug has also differ-
ent toxicity profile with gemcitabine, for example, displaying
myelotoxicity and paclitaxel neurotoxicity.

1190 The preliminary Phase II and III studies of Lipoplatin
reviewed here, as well as further planned studies, are expected
to establish Lipoplatin as an important chemotherapy drug
with a broad range of activity against epithelial malignancies. 1192

- 1193 tumor targeting (see below), lower side effects and with an improved quality of life and overall survival. Especially important, a breakthrough in the chemotherapy field using nanotechnologies is anticipated to be the efficacy of Lipoplatin, compared to cisplatin in randomized trials against the non-squamous histological types of NSCLC, as well as in pancreatic, breast and gastrointestinal cancers. A preliminary efficacy in the adenocarcinoma histological subtype of NSCLC showed 83% response/stabilization rate with Lipoplatin + gemcitabine compared to 54% in the cisplatin + gemcitabine treatment arm in a recently completed Phase II study.
- 1195
- 1200 Also eminent is its significant radiosensitizing ability, especially in brain metastases from NSCLC after concurrent radiation (Angel, Theagenion Anticancer Hospital, Thessaloniki, Greece, in preparation). Finally, pharmacoeconomic benefits arise from its i.v. infusion without pre- or post-hydration on an outpatient basis, with less use of hematopoietic factors and no hospitalization costs from chemotherapy complications. Furthermore, it has allowed administration of a higher total dose of cisplatin due to a highly reduced cumulative toxicity.
- 1205
- 1210
- 12. Conclusions and prospects**
- 1215
- 12.1 Liposomes and other nanomaterials in cancer**
- Liposomes can be used as carriers of peptide, protein and antigen-encoding DNA vaccines [95]. Liposomes may be effective vehicles to improve the delivery of antisense oligonucleotides to the liver for the therapy of hepatotropic viruses [96]. Phospholipid liposomes and charged nanoparticles can be mixed together using sonication to yield particle-stabilized liposomes that repel one another and do not fuse [97]. A nanoliposomal CPT-11 (irinotecan) formulation has been described with unprecedented drug loading efficiency and *in vivo* drug retention using a modified gradient loading method [98]. Drugs of poor water-solubility and high toxicity, such as camptothecin, can also benefit from nanotechnology formulations.
- 1220
- 1225
- Sterically stabilized liposomes have been used for various applications by others; such liposomes prevent opsonization and reticular endothelial system uptake. PEGylation is known to greatly enhance the longevity of proteins, liposomes and other molecules in blood circulation [99]. Naturally occurring polymers of N-acetylneuraminic acid (polysialic acids) are biodegradable, exhibit long half-lives in the blood circulation and have, therefore, been proposed as carriers of short-lived drugs and small peptides [100]. Poly-(lactide), poly-(lactide-co-glycolide) and poly-(lactide-co-caprolactone) microspheres have also been used for the encapsulation of 5-FU by spray drying and slow release for inhalation delivery system for adjuvant therapy of lung cancer [101]. Upgrading these promising technologies and products to successful clinical studies remains a difficult task.
- 1230
- 1235
- 1240
- 12.2 Possibilities of our technology**
- 1245
- 1247
- Cisplatin, one of the most widely used and most effective cytotoxic agents in the treatment of epithelial malignancies was encapsulated into 100 nm in diameter liposomes in a stable formulation, Lipoplatin. The present article reviews the clinical data using Lipoplatin and discusses the mechanisms of the liposomal formulation. One important issue contributing to the therapeutic efficacy of Lipoplatin results from its ability to target primary tumors and metastases and to cause a greater damage to tumor tissue compared to normal tissue. Tumor uptake of the Lipoplatin nanoparticles (Table 1, Figure 2) results from their preferential extravasation through the leaky vasculature of tumors. Furthermore, a higher uptake of Lipoplatin nanoparticles by tumors takes place presumably arising from a more avid phagocytosis by tumor cells compared to adjacent normal tissue in human studies. The two mechanisms result to an overall 10- to 400-fold higher intracellular uptake of total platinum in tumor cells compared to cells in normal tissue. Lipoplatin is currently under several Phase III evaluations.
- 1248
- 1250
- 1255
- 1260
- Antisense VEGF oligodeoxynucleotides formulated in cationic liposomes could downregulate the expression of VEGF and could inhibit the growth of tumors [102]; our liposomes as carriers of antisense VEGF could also combined with Lipoplatin nanoparticles to test efficacy in animal studies. Antiangiogenic agents alone cannot eradicate tumors completely and are combined with other therapy to enhance their effects. Flk-1, a soluble VEGF receptor, is a potent inhibitor of angiogenesis. Flk-1 gene therapy combined with cisplatin improved antitumor efficacy in animals [103]. Phage display peptide libraries led to the identification of peptides (for example, CTKNSYLMC) with affinity for gastric cancer vascular endothelial cells [104]. Peptides are proposed here to be attached at the end of PEG in Lipoplatin to target specific types of cancer vascular endothelial cells as second-generation Lipoplatin nanoparticles, thus, enhancing the antiangiogenesis potential of the drug.
- 1265
- 1270
- 1275
- 1280
- 12.3 The pharmacoeconomics of Lipoplatin**
- Lipoplatin is being administered on an outpatient basis without pre- or post-hydration and with clear pharmacoeconomic benefits over cisplatin that requires admittance of the patient to the hospital a day before and a day after treatment for pre- and post-hydration. Hospitalization costs are usually \$1000/day in most Western countries. Although a 6 – 8 h infusion is recommended to minimize adverse reactions, a 4 h infusion is being used in the Phase III SCCHN study to deliver a total dose of 100 mg/m² [83] and a 3 h infusion to deliver a total dose of 120 mg/m² [73]. In addition, there is less healthcare requirements for the recovery of patients from adverse reactions, especially nephro- and neuro-toxicity as well as less use of the expensive hematopoietic factors GM-CSF after administration of Lipoplatin compared to cisplatin. The expected increase in overall survival and improvement in the quality of life suggested from preliminary results (e.g., [70,75,76,80]) are also considered important benefits. Although, the pricing of Caelyx/Doxil over doxorubicin is about 20 – 27 times higher per mg on
- 1285
- 1290
- 1295
- 1300
- 1302

1303 the basis of the active pharmaceutical ingredient. Although
 1305 Lipoplatin has not received marketing authorization yet, its
 pricing takes into consideration its affordability for establishing
 it as a drug able to replace cisplatin in all world markets.

13. Expert opinion

1310 The present article reviews the features and possible clinical
 applications of a nanotechnology formulation for cisplatin.
 The advantages of the platform encapsulation technology
 for Lipoplatin are described; its proposed ability to cross the
 cell membrane barrier and to deliver its payload to the inter-
 1315 rior of the cell suggest a property close to that of a magic
 bullet. The same technology was also applied to a liposome
 formulation of oxaliplatin (Lipoxal™) that has completed
 successfully a Phase I study [105].

A similar technology has been applied to liposomal encap-
 1320 sulation of plasmids carrying therapeutic genes for gene
 therapy applications (Figure 2). So far, the human IL-12 has
 been tested in human trials expressed from a liposomally-
 encapsulated Semliki Forest virus; the completed Phase I
 study has proven safety, has determined the MTD and has
 1325 shown that repeated administration of the therapeutic lipovirus
 is feasible without immune reactions to the patient [106].
 Obviously, regimens integrating combination Lipoplatin che-
 motherapy with liposomal gene therapy would have the
 advantage of targeting both nanoparticles classes to similar
 1330 tissues *in vivo*, especially to primary solid tumors and metas-
 tases; a more potent anticancer effect is expected with the
 proposed nanoparticle combinations than using the drugs
 separately or in a nonliposomal form.

A putative antiangiogenic activity of Lipoplatin has been
 1335 shown in animal studies (Figure 2). This implies that Lip-
 oplatin particles are primarily targeted to tumors and tumor
 vasculature. However, mechanisms of cellular uptake of the
 Lipoplatin particles by tumors and normal tissue await fur-
 ther elucidation. To demonstrate fusion between Lipoplatin
 1340 and the cell membrane, we are using fluorescent lipids to
 label nanoparticles and show transfer of the label to mem-
 brane lipids in cells in culture with confocal microscopy.
 Continuing studies in our group are also using gene expres-
 sion profile in patients from comparative Phase III studies
 1345 before, during and at the end of treatment to assess mecha-
 nisms in responding versus non-responding patients. Studies
 can also be undertaken to determine the extent and nature of
 damage by Lipoplatin versus cisplatin at the DNA and other
 macromolecules.

1350 The dose-dense Lipoplatin administration is important for
 efficacy. A weekly schedule of 120 mg/m² allows a higher
 total dose to be administered, now that the low cumulative
 toxicity of the drug has been established from Phase III
 1355 studies. In a monotherapy study using 100 mg/m² every
 14 days against NSCLC, the efficacy was low and the side
 effects were negligible [107]; the total dose administered was
 1357 100 mg/m² every 2 weeks as monotherapy compared to

240 mg/m² every 2 weeks as combination therapy in 1358
 Phase II [76] and Phase III [76]. A dose-dense monotherapy
 study in advanced breast cancer is starting with dose 1360
 escalation from a weekly 120 mg/m².

Lipoplatin could be tested with drugs that have a mecha-
 nism of action complementing or synergizing its own. For
 example, ionizing radiation eliciting DNA strand breaks or
 taxanes stabilizing tubulin polymers might show a synergistic
 1365 effect with Lipoplatin even higher to that of cisplatin. Fur-
 thermore, Lipoplatin could be combined with a higher num-
 ber of other chemotherapy regimens to explore reduction in
 the overall toxicity of the combination therapy.

The advent of taxanes (paclitaxel, docetaxel) stabilizing 1370
 tubulin, molecules that can inhibit signaling and a number
 of new approaches such as those targeting apoptosis or DNA
 topoisomerases is revolutionizing cancer chemotherapy. A
 plethora of clinical trials in progress optimizes the different
 ways drugs can be administered; for example, the addition
 1375 of cisplatin or carboplatin to paclitaxel results in higher
 response rates than for each of the drugs as single agents [108].
 One could foresee application of nanotechnology and the
 extension of the Lipoplatin and Lipoxal formulations to
 taxanes and other molecules with tumor targeting abilities.
 1380 Such an achievement and its promotion to the clinic would
 increase the efficacy of chemotherapy while reducing the
 side effects. The end goal of an effective anticancer regimen
 should always be the improvement in the quality of life of
 the patient and an extension in overall survival. 1385

Acquired resistance to chemotherapy is a major hurdle.
 The major factor of resistance seems to be linked with trans-
 port of the chemotherapy drug across the cell membrane
 barrier. Lipoplatin was proposed to enter by direct fusion
 bypassing the Ctr1 copper transporter and other resistance
 1390 mechanisms at the cell membrane level; in such a case, the
 drug could find applications in cisplatin resistant tumors,
 also suggested from a Phase II study [72] (see section 8.6).

Lipoplatin is anticipated to successfully complete several
 Phase III studies and become an important addition to the arse-
 1395 nal of anticancer drugs. It is hoped that chemotherapy regimens
 integrating Lipoplatin will allow higher overall survival of
 patients suffering with non-small cell lung, pancreatic, head and
 neck, gastric and other cancers with lower side effects and
 improvement in quality of life compared to cisplatin regimens. 1400

Acknowledgements

The author thanks G Stathopoulos, C Kostmas, N Mylonakis,
 1405 I Angel, M Froudarakis, M Koukourakis, D Lütfner, K Possinger,
 B Lubrich, A Ravaioli, J Stathopoulos, G Deliconstantinos,
 A Athanasiou, S Kortaris, G Fountzilias, A Rapti, V Georgoulas,
 S Rigatos, G Tsakonas, N Ziras, P Mihalopoulou, A Bastas,
 A Provata, K Marosis, H Bitsakou, P Giamboukakis, J Dimitroulis,
 1410 G Tsoukalas, N Politis, S Lambali, T Grigoratou and D Antoniou
 for their contributions in the clinical development of
 Lipoplatin. 1412

1413 Declaration of interest

1415 T Boulikas has been supported by the European grants RIGHT:
 1417 LSH-CT-2005-005276, NanoBiopharmaceutics: NMP4-CT-2006-026723 and MYASTAID: LSHM-CT-2006-037833, by Regulon

AE as well as two grants from the Hellenic government (General Secretariat of Research and Development) for the clinical development of Lipoplatin, Lipoxal and LipoVIL12. The author is employed by Regulon; Regulon has also sponsored the clinical trials described in this review.

Bibliography

1. Boulikas T, Pantos A, Bellis E, Christofis P. Designing platinum compounds in cancer: structures and mechanisms [review]. *Cancer Therapy* 2007;5:537-83. Available from: www.cancer-therapy.org
2. Boulikas T, Tsogas I. Microtubule-targeted antitumor drugs: chemistry, mechanisms and nanoparticle formulations. *Gene Ther Mol Biol* 2008;1:343-87. Available from: www.gumb.org
3. Ribatti D. The discovery of antiangiogenic molecules: a historical review. *Curr Pharm Des* 2009;15:345-52
4. Choo AY, Blenis J. Not all substrates are treated equally: implications for mTOR, rapamycin-resistance and cancer therapy. *Cell Cycle* 2009;8:567-72
5. Kang MH, Reynolds CE. Bcl-2 inhibitors: targeting mitochondrial apoptotic pathways in cancer therapy. *Clin Cancer Res* 2009;15:1126-32
6. Al-Jasadi A, Chandana SR, Conley BA. Histone deacetylation: an attractive target for cancer therapy? *Drugs R D* 2008;9:369-83
7. Emanuele S, Lauricella M, Tesoriere G. Histone deacetylase inhibitors: apoptotic effects and clinical implications [review]. *Int J Oncol* 2008;33:637-46
8. Ashworth A. A synthetic lethal therapeutic approach: poly(ADP) ribose polymerase inhibitors for the treatment of cancers deficient in DNA double-strand break repair. *J Clin Oncol* 2008;26:3785-90
9. Sakamoto-Hojo ET, Balajee AS. Targeting poly (ADP) ribose polymerase I (PARP-1) and PARP-1 interacting proteins for cancer treatment. *Anticancer Agents Med Chem* 2008;8:402-16
10. Abreu PA, Dellamora-Orriz G, Leño-Ferreira LR, et al. DNA methylation: a promising target for the twenty-first century. *Expert Opin Ther Targets* 2008;12:1035-47
11. Stresmann C, Lyko F. Modes of action of the DNA methyltransferase inhibitors azacytidine and decitabine. *Int J Cancer* 2008;123:8-13
12. Boulikas T. Status of gene therapy in 1997: molecular mechanisms, disease targets, and clinical applications. *Gene Ther Mol Biol* 1998;1:1-172
13. Bachtarzi H, Stevenson M, Fisher K. Cancer gene therapy with targeted adenoviruses. *Expert Opin Drug Deliv* 2008;5:1231-40
14. Boulikas T. Low toxicity and anticancer activity of a novel liposomal cisplatin (Lipoplatin) in mouse xenografts. *Oncol Rep* 2004;12:3-12
15. Rosenberg B, VanCamp L, Trosko JE, Mansour VH. Platinum compounds: a new class of potent antitumor agents. *Nature* 1969;222:385-6
16. Sorenson C, Eastman A. Mechanism of cis-diamminedichloroplatinum (II)-induced cytotoxicity: role of G2 arrest and DNA double-strand breaks. *Cancer Res* 1988;48:4484-8
17. Garcia-del-Muro X, Maroto P, Gumà J, et al. Chemotherapy as an alternative to radiotherapy in the treatment of stage IIA and IIB testicular seminoma: a Spanish Germ Cell Cancer Group Study. *J Clin Oncol* 2008;26:5416-21
18. Hanigan MH, Devarajan R. Cisplatin nephrotoxicity: molecular mechanisms. *Cancer Therapy* 2003;1:47-61
19. Harmers FR, Gispert WH, Kleijt JP. Neurotoxic side-effects of cisplatin. *Eur J Cancer* 1991;27:372-6
20. Humes HD. Insights into oto-toxicity. Analogies to nephrotoxicity. *Ann NY Acad Sci* 1999;884:15-18
21. Kitada N, Takara K, Minogaki T, et al. Factors affecting sensitivity to antitumor platinum derivatives of human colorectal tumor cell lines. *Cancer Chemother Pharmacol* 2008;62:577-84
22. Stathopoulos GP, Boulikas T, Vougiouka M, et al. Pharmacokinetics and adverse reactions of a new liposomal cisplatin (Lipoplatin): phase I study. *Oncol Rep* 2005;13:589-95
23. Cabizon A, Tzemach D, Mak L, et al. Dose dependency of pharmacokinetics and therapeutic efficacy of pegylated liposomal doxorubicin (DOXIL) in murine models. *J Drug Target* 2002;10:539-48
24. Lasic DD, Martin FJ, Cabizon A, et al. Sterically stabilized liposomes: a hypothesis on the molecular origin of the extended circulation times. *Biochim Biophys Acta* 1991;1070:187-92
25. Yuan F, Leunig M, Huang SK, et al. Microvascular permeability and interstitial penetration of sterically stabilized (stealth) liposomes in a human tumor xenograft. *Cancer Res* 1994;54:3352-6
26. Huang SK, Martin FJ, Jay G, et al. Extravasation and transcytosis of liposomes in Kaposi's sarcoma-like dermal lesions of transgenic mice bearing the HIV tat gene. *Am J Pathol* 1993;143:16-4
27. Martin F, Boulikas T. The challenge of liposomes in gene therapy. *Gene Ther Mol Biol* 1998;1:173-214
28. Yuan F, Dellian M, Fukumura D, et al. Vascular permeability in a human tumor xenograft: molecular size dependence and cutoff size. *Cancer Res* 1995;55:3752-6
29. Boulikas T, Stathopoulos GP, Volakakis N, Vougiouka M. Systemic Lipoplatin infusion results in preferential tumor uptake in human studies. *Anticancer Res* 2005;25:3031-40
30. Boulikas T. Molecular mechanisms of cisplatin and its liposomally encapsulated form, Lipoplatin™. Lipoplatin™ as a chemotherapy and antiangiogenesis drug. *Cancer Ther* 2007;5:351-76
31. Vesl GJ, Griffin MJ, Price E, et al. A phase I study in paediatric patients to evaluate the safety and pharmacokinetics of SPI-77, a liposome encapsulated formulation of cisplatin. *Br J Cancer* 2001;84:1629-35
32. White SC, Lorigan P, Margison GB, et al. Phase II study of SPI-77 (sterically stabilised liposomal cisplatin) in advanced non-small-cell lung cancer. *Br J Cancer* 2006;95:822-8
33. Meerum Terwogt JM, Groenewegen G, Pluim D, et al. Phase I and pharmacokinetic study of SPI-77, a liposomal encapsulated dosage form of

- cisplatin. *Cancer Chemother Pharmacol* 2002;49:201-10
34. Vokos EE, Gordon GS, Mauer AM, et al. A phase I study of STEALTH cisplatin (SPI-77) and vinorelbine in patients with advanced non-small-cell lung cancer. *Clin Lung Cancer* 2000;2:123-32
 35. Kim ES, Lu C, Khuri FR, et al. A phase II study of STEALTH cisplatin (SPI-77) in patients with advanced non-small cell lung cancer. *Lung Cancer* 2001;34:427-32
 36. Rosenthal DI, Yom SS, Liu L, et al. A phase I study of SPI-077 (Stealth liposomal cisplatin) concurrent with radiation therapy for locally advanced head and neck cancer. *Invest New Drugs* 2002;20:343-9
 37. Harrington KJ, Lewanski CR, Northcote AD, et al. Phase I-II study of pegylated liposomal cisplatin (SPI-077) in patients with inoperable head and neck cancer. *Ann Oncol* 2001;12:493-6
 38. Matsumoto S, Tanaka T, Kurokawa H, et al. Effect of copper and role of the copper transporters ATP7A and CTR1 in intracellular accumulation of cisplatin. *Anticancer Res* 2007;27:2209-16
 39. Song IS, Savaraj N, Siddik ZH, et al. Role of human copper transporter Ctr1 in the transport of platinum-based antitumor agents in cisplatin-sensitive and cisplatin-resistant cells. *Mol Cancer Ther* 2004;3:1543-9. Erratum in: *Mol Cancer Ther* 2005;4:864
 40. Koepsell H, Lips K, Volk C. Polyspecific organic cation transporters: structure, function, physiological roles, and biopharmaceutical implications. *Pharm Res* 2007;24:1227-51
 41. Yonezawa A, Masuda S, Yokoo S, et al. Cisplatin and oxaliplatin, but not carboplatin and nedaplatin, are substrates for human organic cation transporters (SLC22A1-3 and multidrug and toxin extrusion family). *J Pharmacol Exp Ther* 2006;319:879-86
 42. Plasencia C, Martínez-Balibrea E, Martínez-Cardús A, et al. Expression analysis of genes involved in oxaliplatin response and development of oxaliplatin-resistant HT29 colon cancer cells. *Int J Oncol* 2006;29:225-35
 43. Safaie R, Larson BJ, Cheng TC, et al. Abnormal lysosomal trafficking and enhanced exosomal export of cisplatin in drug-resistant human ovarian carcinoma cells. *Mol Cancer Ther* 2005;4:1595-604
 44. Babik CA, Maryon EB, Kasza K, et al. Role of copper transporters in resistance to platinating agents. *Cancer Chemother Pharmacol* 2009;64:133-42
 45. Zisowsky J, Koegel S, Leyers S, et al. Relevance of drug uptake and efflux for cisplatin sensitivity of tumor cells. *Biochem Pharmacol* 2007;73:298-307
 46. Owatari S, Akune S, Komatsu M, et al. Copper-transporting P-Type ATPase, ATP7A, confers multidrug resistance and its expression is related to resistance to SN-38 in clinical colon cancer. *Cancer Res* 2007;67:4860-8
 47. Choi MK, Kim DD. Platinum transporters and drug resistance. *Arch Pharm Res* 2006;29:1067-73
 48. Negoro K, Yamano Y, Nakashima D, et al. Cross-resistance of platinum derivatives in H-1R, a cisplatin-resistant cell line. *Oncol Rep* 2009;21:443-9
 49. Yokoo S, Masuda S, Yonezawa A, et al. Significance of organic cation transporter 3 (SLC22A3) expression for the cytotoxic effect of oxaliplatin in colorectal cancer. *Drug Metab Dispos* 2008;36:2299-306
 50. Zhang S, Lovejoy KS, Shima JE, et al. Organic cation transporters are determinants of oxaliplatin cytotoxicity. *Cancer Res* 2006;66:8847-57
 51. Peklak-Scott C, Smitherman PK, Townsend AJ, Morrow CS. Role of glutathione S-transferase P1-1 in the cellular detoxification of cisplatin. *Mol Cancer Ther* 2008;7:3247-55
 52. Acehan D, Jiang X, Morgan DG, et al. Three-dimensional structure of the apoptosome: implications for assembly, procaspase-9 binding, and activation. *Mol Cell* 2002;9:423-32
 53. Wei Q, Dong G, Franklin J, Dong Z. The pathological role of Bax in cisplatin nephrotoxicity. *Kidney Int* 2007;72:53-62
 54. Zhu J, Yang Y, Wu J. Bcl-2 cleavages at two adjacent sites by different caspases promote cisplatin-induced apoptosis. *Cell Res* 2007;17:441-8
 55. Villedieu M, Briand M, Duval M, et al. Anticancer and chemosensitizing effects of 2,3-DCPE in ovarian carcinoma cell lines: link with ERK activation and modulation of p21 (WAF1/CIP1), Bcl-2 and Bcl-x(L) expression. *Gynecol Oncol* 2007;105:373-84
 56. Nehmé A, Baskaran R, Aebi S, et al. Differential induction of c-Jun NH2-terminal kinase and c-Abl kinase in DNA mismatch repair-proficient and -deficient cells exposed to cisplatin. *Cancer Res* 1997;57:3253-7
 57. Han Z, Hong L, Wu K, et al. Reversal of multidrug resistance of gastric cancer cells by downregulation of Akt1 with Akt1 siRNA. *J Exp Clin Cancer Res* 2006;25:601-6
 58. Villar J, Quadri HS, Song J, et al. PCPH/ENTPD5 expression confers to prostate cancer cells resistance against cisplatin-induced apoptosis through protein kinase Calpha-mediated Bcl-2 stabilization. *Cancer Res* 2009;69:102-10
 59. Devarajan P, Tarabishi R, Mishra J, et al. Low renal toxicity of Lipoplatin compared to cisplatin in animals. *Anticancer Res* 2004;24:2193-200
 60. Marr AK, Kurzman ID, Vail DM. Preclinical evaluation of a liposome-encapsulated formulation of cisplatin in clinically normal dogs. *Am J Vet Res* 2004;65:1474-8
 61. Fedier A, Poyer C, Perucchini D, et al. Mlh1-deficient tumor cells are resistant to lipoplatin, but retain sensitivity to lipoxal. *Anticancer Drugs* 2006;17:315-23
 62. Fedier A, Erdmann R, Boulikas T, Fink D. Potential of the Akt inhibitor LY294005 to antagonize the efficacy of Cisplatin against HCT116 tumor cells in a DNA mismatch repair-dependent manner. *Int J Oncol* 2006;29:1303-10
 63. Arienti C, Tesi A, Ravaioli A, et al. Activity of lipoplatin in tumor and in normal cells in vitro. *Anticancer Drugs* 2003;19:983-90
 64. Froudarakis ME, Pataka A, Pappas P, et al. Phase I trial of Lipoplatin and gemcitabine as a second-line chemotherapy in patients with non-small cell lung carcinoma. *Cancer* 2008;113:2752-60
 65. Karpathiou G, Argiana E, Koutsopoulos A, Froudarakis ME. Response of a patient with pleural and peritoneal mesothelioma after second-line chemotherapy with Lipoplatin and gemcitabine. *Oncology* 2007;73(5-6):426-9
 66. Sathopoulos GP, Boulikas T, Rigatos SK, et al. Liposomal cisplatin combined with gemcitabine in pretreated advanced cancer patients. Phase I-II study. *Ann Oncol* 2003;13:25
 67. Sathopoulos GP, Androulakis N, Souglakos J, et al. Present treatment and

- future expectations in advanced pancreatic cancer. *Anticancer Res* 2008;28:1303-8
68. Stathopoulos GR, Boulikas T, Vougiouka M, et al. Liposomal cisplatin combined with gemcitabine in pretreated advanced pancreatic cancer patients: a phase I-II study. *Oncol Rep* 2006;15:1201-4
 69. Available from: <http://www.emea.europa.eu/pdfs/human/comp/opinion/16785007en.pdf>
 70. Mylonakis N, Athanasiou A, Ziras N, et al. Phase II study of liposomal cisplatin (Lipoplatin) plus gemcitabine versus cisplatin plus gemcitabine as 1st line treatment in inoperable (stage IIIB/IV) non-small cell lung cancer (NSCLC). Submitted
 71. Farhat FS, Nasser A, Ibrahim K, et al. Preliminary results of a phase II study of Lipoplatin (Liposomal Cisplatin) - Vinorelbine combination as first line treatment in HER2/neu negative advanced breast cancer [abstract # 550699]. 31st Annual San Antonio Breast Cancer Symposium: 2008
 72. Aneviavis S, Pataka A, Kouliarsis G, et al. A phase II trial of Lipoplatin-gemcitabine in patients with advanced NSCLC: preliminary results. *Eur Respir J* 2008;32:762s
 73. Koukourakis MI, Giannomanolaki A, Pirakoudis M, et al. Concurrent liposomal cisplatin (Lipoplatin™), 5-Fluorouracil and PET. Concurrent liposomal cisplatin (Lipoplatin Radiotherapy for the treatment of locally advanced gastric cancer: a phase I/II study. Submitted
 74. Skarlatos J, Kosma L, Koukourakis M, et al. Hypofractionated radiotherapy with concurrent 5-fluorouracil radiointensification for recurrent or locally advanced colorectal cancer. A phase II study. *Int J Colorectal Dis* 1996;11:206-10
 75. Boulikas T, Mylonakis N, Sarikos G, et al. Superiority of Lipoplatin™ plus gemcitabine compared to cisplatin plus gemcitabine as first-line treatment against NSCLC: Preliminary results of a randomized, multicenter phase III trial. ASCO Abstract ID: 33204 (1-5 June 2007, Chicago, Illinois, USA)
 76. Kosmas C, Angel J, Athanasiou A, et al. Interim Phase III analysis of Lipoplatin plus Gemcitabine versus Cisplatin plus Gemcitabine in advanced NSCLC. Abstract number: E13-1858. Submitted to ECCO 15 - 34th ESMO Multidisciplinary Congress, Berlin, 20-24 Sept 2009
 77. Kim SW, Suh C, Lee SD, et al. Weekly low dose paclitaxel and cisplatin as first-line chemotherapy for advanced non-small cell lung cancer. *Lung Cancer* 2003;41:221-6
 78. Rigas JR. Taxane-platinum combinations in advanced non-small cell lung cancer: a review. *Oncologist* 2004;9(Suppl 2):16-23
 79. Gridelli C, Aapro M, Ardizzoni A, et al. Treatment of advanced non-small-cell lung cancer in the elderly: results of an international expert panel. *J Clin Oncol* 2005;23:3125-37
 80. Stathopoulos GR, Michalopoulou P, Antoniou D, et al. Liposomal cisplatin and paclitaxel versus cisplatin and paclitaxel in advanced NSCLC. ASCO Annual Meeting Proceedings Part 1. *J Clin Oncol* 2007;25:7684
 81. Stathopoulos GR, Antoniou D, Dimitroulis J, et al. Liposomal cisplatin combined with paclitaxel versus cisplatin and paclitaxel in non-small-cell lung cancer. Submitted
 82. Jehn CE, Boulikas T, Kourvetaris A, et al. Pharmacokinetics of liposomal cisplatin (lipoplatin) in combination with 5-FU in patients with advanced head and neck cancer: first results of a phase III study. *Anticancer Res* 2007;27:471-5
 83. Jehn CE, Boulikas T, Kourvetaris A, et al. First safety and response results of a randomized phase III study with liposomal platin in the treatment of advanced squamous cell carcinoma of the head and neck (SCCHN). *Anticancer Res* 2008;28:3961-4
 84. Ginsberg MS, Grewal RK, Heslan RT. Lung cancer. *Radiol Clin North Am* 2007;45:21-4
 85. Crino L, Scagliotti G, Marangolo M, et al. Cisplatin-gemcitabine combination in advanced non-small-cell lung cancer: a phase II study. *J Clin Oncol* 1997;15:297-303
 86. Sandler A, Gray R, Perry MC, et al. Paclitaxel-carboplatin alone or with bevacizumab for non-small-cell lung cancer. *N Engl J Med* 2006;355:2542-50
 87. Reck M, von Pawel J, Zatloukal P, et al. Phase III trial of cisplatin plus gemcitabine with either placebo or bevacizumab as first-line therapy for nonsquamous non-small-cell lung cancer: AVAIL. *J Clin Oncol* 2009;27:1227-34
 88. Gao G, Jiang J, Liang X, et al. A meta-analysis of platinum plus gemcitabine or vinorelbine in the treatment of advanced non-small-cell lung cancer. *Lung Cancer* 2009 In Press
 89. Scagliotti GV, Parikh B, von Pawel J, et al. Phase III study comparing cisplatin plus gemcitabine with cisplatin plus pemetrexed in chemotherapy-naïve patients with advanced-stage non-small-cell lung cancer. *J Clin Oncol* 2008;26:3543-51
 90. Tassinari D, Carloni F, Santelmo C, et al. Second line treatments in advanced platinum-resistant non small cell lung cancer. A critical review of literature. *Rev Recent Clin Trials* 2009;4(1):27-33
 91. Kosmas C, Tsavaris N, Syrigos K, et al. A phase I-II study of bi-weekly gemcitabine and irinotecan as second-line chemotherapy in non-small cell lung cancer after prior taxane + platinum-based regimens. *Cancer Chemother Pharmacol* 2007;59:51-9
 92. Felip E, Rosell R. Pemetrexed as second-line therapy for advanced non-small-cell lung cancer (NSCLC). *Ther Clin Risk Manag* 2008;4:579-85
 93. Yokoo S, Yonezawa A, Masuda S, et al. Differential contribution of organic cation transporters, OCT2 and MATE1, in platinum agent-induced nephrotoxicity. *Biochem Pharmacol* 2007;74:477-87
 94. Ali BH, Al Moundhari MS. Agents ameliorating or augmenting the nephrotoxicity of cisplatin and other platinum compounds: a review of some recent research. *Food Chem Toxicol* 2006;44:1173-83
 95. Gregoriadis G, McCormack B, Obrenovic M, et al. Vaccine entrapment in liposomes. *Methods* 1999;19:156-62
 96. Soti PN, Brown D, Saffie R, et al. Biodistribution, stability, and antiviral efficacy of liposome-entrapped phosphorothioate antisense oligodeoxynucleotides in ducks for the treatment of chronic duck hepatitis B virus infection. *Hepatology* 1998;28:1402-10
 97. Zhang L, Granick S. How to stabilize phospholipid liposomes (using nanoparticles). *Nano Lett* 2006;6:694-8
 98. Drummond DC, Noble CO, Gao Z, et al. Development of a highly active nanoliposomal irinotecan using a novel intraliposomal stabilization strategy. *Cancer Res* 2006;66:3271-7

99. Martin F, Boulikas T. The challenge of liposomes in gene therapy. *Gene Ther Mol Biol* 1998;1:173-214
100. Gregoriadis G, Fernandes A, Mital M, McCormack B. Polysialic acids: potential in improving the stability and pharmacokinetics of proteins and other therapeutics. *Cell Mol Life Sci* 2000;57:1964-9
101. Huzman CJ, Elmquist WF, Wartenberg LW, Wiedmann TS. Development of a respirable, sustained release microcarrier for 5-fluorouracil I: In vitro assessment of liposomes, microspheres, and lipid coated nanoparticles. *J Pharm Sci* 2006;95:1114-26
102. Li YY, Qian GS, Huang GJ, et al. Enhancement of antiangiogenic effects of human canstatin with a hypoxia-regulated transgene vector in lung cancer model. *Cancer J* 2006;12:136-46
103. Wang R, Zhang XW, Wang CQ, et al. Systemic inhibition of tumor growth by soluble Flk-1 gene therapy combined with cisplatin. *Cancer Gene Ther* 2006;13(10):940-7
104. Liang S, Lin T, Ding J, et al. Screening and identification of vascular-endothelial-cell-specific binding peptide in gastric cancer. *J Mol Med* 2006;84:764-73
105. Stathopoulos GR, Boulikas T, Kourvetaris A, Stathopoulos I. Liposomal oxaliplatin in the treatment of advanced cancer: a phase I study. *Anticancer Res* 2006;26:1489-94
106. Stathopoulos GR et al. A Phase I study of the liposomal Semliki Forest virus expressing the human IL-12 gene in cancer patients. In preparation
107. Ravaioli A, Papi M, Pasquini E, et al. Lipoplatin monotherapy: A phase II trial of second-line treatment of metastatic non-small-cell lung cancer. *J Chemother* 2009;21:86-90
108. Ranson M, Thatcher N. Paclitaxel: a hope for advanced non-small cell lung cancer? *Expert Opin Investig Drugs* 1999;8:837-48
109. Lazarioti F, Boulikas T. Diagnostic and Therapeutic Efficacy of Imaging Modalities in Non-Small Cell Lung Cancer (NSCLC): experience from a Phase III clinical study using tumor targeted Lipoplatin nanoparticles. *Cancer Ther* 2008;6:629-46. Available from: www.cancer-therapy.org

Affiliation

Tem Boulikas^{1,2,3} PhD

¹Address for correspondence

¹Regulon, Inc., 715 N. Shoreline Blvd.,

Mountain View, CA 94043 and

Regulon AE,

Grigoriou Afentiou 7, Alikos,

Athens 17455, Hellas, Greece

²Editor,

Gene Therapy and Molecular Biology

(www.gtmb.org)

³Editor,

Cancer Therapy (www.cancer-therapy.org)

Tel: +30 210 9858454; Fax: +30 210 9858453;

E-mail: temi@regulon.org

Liposomes as nanomedical devices

Giuseppina Bozzuto^{1,2}
Agnese Molinari²

¹Chemical Methodology Institute, CNR, ²Department of Technology and Health, Istituto Superiore di Sanità, Rome, Italy

Abstract: Since their discovery in the 1960s, liposomes have been studied in depth, and they continue to constitute a field of intense research. Liposomes are valued for their biological and technological advantages, and are considered to be the most successful drug-carrier system known to date. Notable progress has been made, and several biomedical applications of liposomes are either in clinical trials, are about to be put on the market, or have already been approved for public use. In this review, we briefly analyze how the efficacy of liposomes depends on the nature of their components and their size, surface charge, and lipidic organization. Moreover, we discuss the influence of the physicochemical properties of liposomes on their interaction with cells, half-life, ability to enter tissues, and final fate *in vivo*. Finally, we describe some strategies developed to overcome limitations of the “first-generation” liposomes, and liposome-based drugs on the market and in clinical trials.

Keywords: liposomes, nanomedicine, drug delivery, ultrastructure

Introduction

Liposomes were discovered by Alec D Bangham in the 1960s at the Babraham Institute, University of Cambridge, and consist of single or multiple concentric lipid bilayers encapsulating an aqueous compartment (Figure 1).^{1,2} The first formulations were composed solely of natural lipids; at present they can include natural and/or synthetic lipids and surfactants. They have the capability of entrapping both lipophilic and hydrophilic agents, in the lipid membrane and in the aqueous core, respectively. The size of these nearly spherical lipid vesicles can range from a few nanometers to several micrometers. However, liposomes applied to medical use range between 50 and 450 nm.³

Liposomes seem to be an almost ideal drug-carrier system, since their morphology is similar to that of cellular membranes and because of their ability to incorporate various substances. Therefore, for the last 50 years liposomes have been widely investigated and they continue to be the subject of intense research. They are valued for their biological and technological advantages as optimal delivery systems for biologically active substances, both *in vitro* and *in vivo*, and are considered to be the most successful drug-carrier system known to date.⁴ During the two last decades, notable progress has been made, and several biomedical applications of liposomes are either in clinical trials or are about to be put on the market, while others have already been approved for public use.⁵

Therefore, the goal of this review is not to undertake an exhaustive report on the plethora of data published on liposomes since their first synthesis in the 1960s, but to focus on some points that play a key role in the development of liposomal formulation for therapy.

We briefly analyze how the efficacy of liposomes depends on the physicochemical properties of their membranes, on the nature of their components, and on their size,

Correspondence: Giuseppina Bozzuto
Department of Technology and Health,
Istituto Superiore di Sanità, 299 Viale
Regina Elena, Rome 00161, Italy
Tel +39 06 4990 2228
Fax +39 06 4990 2137
Email giuseppina.bozzuto@iss.it



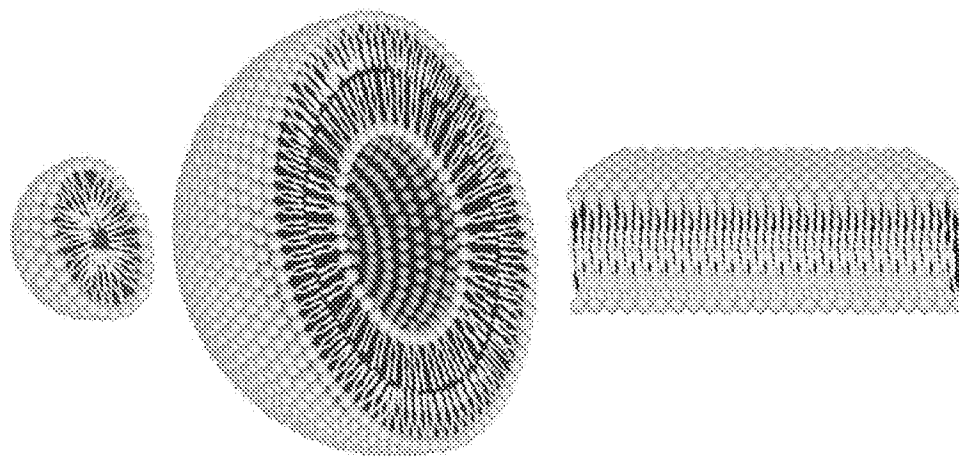


Figure 1 Representation of the steric organization of a micelle (left), a liposome (center), and a lipid bilayer (right). Whereas liposomes are composed of a lipid bilayer, micelles are constructed of one lipid layer in which the apolar section turns inward and the polar heads interact with the environment. These two different organizations mean that the space enclosed in the micelles is much more limited to that available in liposomes.

Note: Adapted from Bitounis D, Fanciullino R, Iliadis A, Ciccolini J. Optimizing druggability through liposomal formulations: new approaches to an old concept. *ISRN Pharm*. 2012;2012:738432.¹¹

surface charge, and lipid organization. In addition, we discuss how the physicochemical properties of liposomes influence their stability in the bloodstream, their ability to enter various tissues, their interaction with cells, and their final fate in vivo. We also describe some strategies developed to overcome the limitations of the “first-generation” liposomes, and how this has been crucial in opening the way from the laboratory bench to clinical trials or to the market.

The physicochemistry of liposomes

The adequacy of liposomes as a carrier system for drugs strictly depends on the physicochemical properties of their membranes, on the nature of their components, on their size, surface charge, and lipid organization.⁶

Liposomes are mainly composed of phospholipids, amphiphilic molecules that have a hydrophilic head and two apolar hydrophobic chains. When phospholipids are dispersed in aqueous solutions, due to their amphipathic nature they have a strong tendency to form membranes.⁷ On the one hand, their polar heads prefer to interact with the aqueous environment; on the other, their long apolar aliphatic chains promote interaction with one another. In aqueous solution, these dual properties favor the formation of two lipid layers. The hydrophobic chains of each layer face each other and constitute a lipophilic inner compartment that acts as a permeability barrier, both inward and outward. Hydrophobic interactions are behind the formation of these lipid bilayers, and van der Waals forces keep the long hydrocarbon tails together, thus strengthening this architecture. Lastly, hydrogen bonds and polar interactions between the water molecules of the aqueous environment and the polar heads

of lipids stabilize this organization. The final organization of lipids depends on their nature, concentration, temperature, and geometric form.⁸ If ions or molecules are present during the formulation process, they can be encapsulated inside these membranes.

Liposomes can be classified on the basis of the preparation method (reverse-phase evaporation vesicles or vesicle extruded technique), size (small, intermediate, or large), and lamellarity (uni-, oligo-, and multilamellar vesicles). The formation of unilamellar vesicles (ULVs) or multilamellar vesicles (MLVs) depends on the synthesis methods and postformation processing used for their preparation (refer to the “Methods for the preparation of liposomes” section for more details). Since ULVs (one lipid bilayer, 50–250 nm) enclose a large aqueous core, they are ideally suited for the encapsulation of hydrophilic drugs. On the other hand, MLVs (two or more concentric lipid bilayers organized like an onion-skin, 1–5 μm) preferentially entrap lipid-soluble drugs.⁹ In addition to the ability to entrap drugs with different solubility characteristics, it has been hypothesized that ULVs and MLVs have different release kinetics. In general, MLVs are formed more easily at larger hydrodynamic diameters, and thus have greater entrapped volume than ULVs. As a result, unilamellar liposomes with a hydrodynamic diameter of 130 nm exhibit a much faster release rate than MLVs with two to three lamellar bilayers and a hydrodynamic diameter of 250 nm.^{10,11} The difference in the release rate is due overall to the number of phospholipid bilayer that it have to cross before being released.

The ongoing interest of researchers in liposome characteristics, such as stability, pharmacokinetic properties, and

therapeutic efficacy, has led to second-generation liposomes by the modulation of lipid composition, size, and the charge of the vesicle. The addition of cholesterol to the lipid bilayer of liposomes reduces their permeability and increases their *in vivo* and *in vitro* stability, because the presence of cholesterol induces a dense packing of phospholipids and inhibits their transfer to high-density lipoprotein (HDL) and low-density lipoprotein (LDL). In fact, cholesterol is a hydrophobic molecule and preferentially interacts with the core of the membrane, thus stabilizing it. Further, cholesterol can be used to anchor other molecules, such as polyethylene glycol (PEG) or deoxyribonucleic acid (DNA), to the liposomes for their application in biosensing or as "stealth" drug carriers¹² (reviewed in Hosta-Rigan et al).¹³ Finally, the use of phosphatidylcholine with saturated fatty acyl chains and materials that stretch the transition temperature beyond 37°C offered even greater stabilization.¹⁴ For prolongation of the *in vivo* liposome circulation time, a milestone is the inclusion of hydrophilic carbohydrates or polymers, such as monosialoganglioside (G_{M1}) and PEG in liposome composition. G_{M1} decreases the blood proteins absorbed on the liposomal surface and improves the half-life of liposomes in the blood.^{15,16} Similarly, the PEGylation of the liposomal carrier proved to extend the blood-circulation time while diminishing the uptake by the reticuloendothelial system (RES). Further, by modifying the PEG-molecule terminus, liposomes can be actively addressed with specific ligands or monoclonal antibodies (more details are reported in the section "Pharmacokinetics of liposomes").¹⁷

Methods for the preparation of liposomes

There are many different methods for the preparation of liposomes. The choice of the appropriate method depends on several factors: 1) the physicochemical characteristics of the liposome components and those of the drug to be loaded; 2) the toxicity and the concentration of the loaded substance; 3) the type of the medium in which the liposomes are dispersed; 4) the additional processes during the application/delivery of the liposomes; 5) the size and the half-life desired for the successful application; and 6) the costs, reproducibility, and applicability regarding large-scale production for clinical purpose and good manufacturing practice-relevant issues.¹⁶⁻²⁰

One of the most widely used techniques for liposome-manufacture preparation is the thin-film hydration or Bangham method.^{21,22} Briefly, this method involves dissolution of the lipid in an organic solvent, evaporation of the solvent, and the dispersion of the obtained lipid film in

aqueous media. The drug to be entrapped can be included in the aqueous media (for hydrophilic drugs) or in the lipid film (for lipophilic drugs). However, the encapsulation efficiency of water-soluble drugs is low (5%–15%). Moreover, this method produces large and nonhomogeneous MLVs that require sonication or extrusion processes to be produced in homogeneous small ULVs.

The reverse-phase evaporation and solvent-injection methods provide hydration of the lipids directly from an organic solvent, and achieve an aqueous suspension of MLVs and ULVs, respectively.²³⁻²⁵ The use of these methods is affected by the solubility of lipids in the organic solvent and the elimination of the latter from the products. Nevertheless, these procedures guarantee higher encapsulation efficiency than thin-film hydration.

The detergent-depletion method involves the hydration of a lipid film with a detergent solution and leads to the formation of large MLVs.^{22,26,27} This method is rarely used, because it needs long preparation time and poor trapping efficiency. On the contrary, the dehydration–rehydration technique described by Kirby and Gregoriadis provides high drug-encapsulation efficiency and is widely used in nanomedicine. This procedure induces the fusion of preformed vesicles by means of dehydration and controlled rehydration.²⁸

To ensure the desired size, lamellarity, and homogeneity properties of liposomes manufactured with the aforementioned techniques, postformation processing is required. The most common methods for postformation processing are sonication, extrusion, and high-pressure homogenization. Sonication is used to reduce the size of the vesicles and give energy to lipid suspension. This can be obtained by applying an ultrasonic irradiation to the suspensions of MLVs.²⁹ The resulting small ULVs are purified by ultracentrifugation. The membrane-extrusion method reduces the size of the liposomes (large ULVs or MLVs) by passing them through a membrane filter with a defined pore size.³⁰⁻³² The high-pressure homogenization is a fluid mechanical process that involves the subdivision of vesicles into smaller sizes and occurs in a special homogenizing valve.³³

Since industrial-scale production of liposomes has become a reality, the range of liposome-preparation methods has been extended by a number of techniques. Among these are the heating method, spray-drying, freeze-drying, supercritical reverse-phase evaporation, and several modified ethanol-injection techniques that are increasingly attractive, as extensively reviewed in Laouini et al.³⁴

Finally, the microfluidic-based method is an emerging technology for liposome synthesis that allows strict control

of the lipid-hydration process. Microfluidics is a method to manipulate liquid flows in channels with dimensions of tens to hundreds of micrometers.^{35,36} The characteristic of laminar flow and rapid and tunable mixing has some advantages in liposome formation over traditional methods, such as thin-film hydration and reverse-phase evaporation. In continuous microfluidic flow systems, precise control of liposome size and size distribution can be implemented by controlling flow and mixing conditions. However, the problem of scaling up liposome production needs to be addressed during the implementation of microfluidic technology for practical application. Additionally, the ultrafine structure of liposomes produced with the microfluidic method needs to be further investigated.³⁷

Microfluidic remote loading for rapid single-step liposomal drug preparation has been recently reported. In this method, microfluidic-directed formation of liposomes is combined with in-line sample purification and remote drug loading for single-step, continuous-flow synthesis of nanoscale vesicles containing high concentrations of stably loaded drug compounds. Using an on-chip microdialysis element, the system enables rapid formation of large transmembrane pH and ion gradients, followed by immediate introduction of amphipathic drugs for real-time remote loading into the liposomes. The microfluidic process enables in-line formation of drug-laden liposomes with drug:lipid molar ratios of up to 1.3, and a total on-chip residence time of approximately 3 minutes, representing a significant improvement over conventional bulk-scale methods, which require hours to days for combined liposome synthesis and remote drug loading. The microfluidic platform may be further optimized to support real-time generation of purified liposomal drug formulations with high concentrations of drugs and minimal reagent waste for effective liposomal drug preparation at or near the point of care.³⁸

Real-time, highly sensitive, and low-cost monitoring of drug-loading and delivery dynamics in different pharmaceutical and biomedical environments could be very useful both for pharmaceutical manufacturing and for quality-assurance assays applied to liposomal formulations. Currently, the techniques used to investigate liposomal structures and their stability in different environments, as well as drug-loading and -delivery mechanisms, operate basically off-line and/or with prepared sampling. Organic electrochemical transistors (OECTs), promising devices for applications in bioelectronics and nanomedicine, have been recently proposed as ideally suitable for sensing and real-time monitoring of liposome-based structures. These systems seem to be particularly suited for real-time monitoring of liposomes in solution. OECTs

are sensitive devices for detecting liposomes on a wide dynamic range down to 10^{-5} mg/mL (with a lowest detection limit, assessed in real-time monitoring, of 10^{-7} mg/mL), thus matching the needs of typical drug-loading/drug-delivery conditions. Furthermore, OECTs proved to be able to sense and discriminate successive injections of different liposomes, and so could be good candidates in quality-control assays or in the pharmaceutical industry.³⁹

Parameters including shape, size, surface features, and lamellarity strongly influence the biological behavior of liposomes. Therefore, they have to be extensively characterized prior to their use in order to ensure in vitro and in vivo performance. Liposome shape can be assessed using electron microscopy techniques. Lamellarity of liposomes can be determined by using negative staining and/or freeze-fracturing for transmission electron microscopy (TEM) and P-31 nuclear magnetic resonance analysis.⁴⁰

Several techniques are available for the determination of size and size distribution, among which the most widely applied include dynamic light scattering (DLS), size-exclusion chromatography, and field-flow fractionation (FFF).⁴¹⁻⁴⁴ Various microscopy techniques, including cryo-TEM, have also been found useful for the characterization of liposome size.^{45,46}

DLS measures the time-dependent fluctuations in the intensity of scattered light, which occur because particles (liposomes) in a suspension undergo random Brownian motion due to collisions between suspended particles and solvent molecules. An analysis of the intensity fluctuations allows the determination of the distribution of the diffusion coefficients of the liposomes, which are converted into a size distribution using established theories. DLS is a simple and rapid method, but it provides an average property of liposome bulk.

On the contrary, electron microscopy techniques, such as cryo-TEM and TEM using freeze-fracturing, provide a precise determination of liposome size, since they allow for the visualization of single liposomes and can resolve particles of varying size. The result is exact information about the profile of the liposome population over the whole range of sizes. Unfortunately, these techniques are very expensive and require specific equipment.⁴⁵ Another microscopic technique utilized to analyze liposome morphology and size is atomic force microscopy, which provides information with high resolution on the three-dimensional profile of liposomes without removing them from their native environment.^{47,48}

Size-exclusion chromatography is a technique that can separate and quantify liposome populations by exploiting

the time-based resolution of hydrodynamic size. The process of separation is based on large-particle elution before that of smaller particles. The large particles are left out from the internal pore volume of the porous substrate used in this technique, and are eluted more quickly from the column.^{45,49}

FFF is a separation technique based on the laminar flow of particles in a solution, and uses a semipermeable membrane that allows only the carrier fluid to pass through the membrane. FFF separates liposomes based on size, and can separate materials over a wide colloidal size range while maintaining high resolution.⁵⁰

Liposomes as nanocarriers for drug delivery

Despite considerable progress in recent years, the diagnosis and treatment of various diseases, especially cancer, continue to present constraints, such as low sensitivity or specificity, drug toxicity, and severe side effects. In particular, many therapeutic agents have a very narrow window, i.e. the therapeutic dose is not much lower than a toxic one. In many cases, the employment of an appropriate drug carrier can reduce the toxicity by changing the temporal and spatial distribution of a drug.

Since they were first described in the 1960s, liposomes have long been recognized as drug-delivery vehicles. They are very appropriate for this aim, due to their biocompatibility and biodegradability.⁹ Due to their nature, liposomes are in fact considered safe nanocarriers. However, the addition of nonphysiological additives can induce chemical modifications that are useful to improve efficacy in drug delivery but potentially toxicogenic.

In addition to being biocompatible, all liposomes have in common a structure that gives them the ability to contain both hydrophilic and hydrophobic drugs. The encapsulation of the active form of a drug into the lipid bilayer protects it against naturally occurring phenomena, such as enzymatic degradation and immunologic and chemical inactivation. Therefore, liposomes prevent a drug from being metabolized prior to reaching target tissues, and simultaneously they minimize exposure of healthy tissue to the encapsulated drug during its circulation in the blood. Both of these effects contribute to increase the therapeutic index. In fact, high levels of the active form of a drug are delivered to the tumor site so that the expected cytotoxic effect can be achieved. Meanwhile, any undesirable side effects of the encapsulated drug are substantially reduced when compared to the free form.

The delivery of the encapsulated drug depends on the nature of the lipid bilayer, the size of the drug molecules, their partition coefficient in oil/water, and their interactions with the lipid membrane. The mechanism and extent of liposome-delivery is also strongly influenced by the nature and density of the charge (ζ -potential) of the liposome surface (refer to the "Charged liposomes for drug delivery" section for more details).

The encapsulation efficiency of a molecule in a liposome depends on its polarity and partition coefficient, which also determines its localization in the liposomal membrane. If a drug is hydrophobic in nature, it resides in the acyl hydrocarbon chain of the liposome, and hence encapsulation is dependent on the properties of the acyl chains of the liposome, such as length and packing density. It is also expected that the encapsulation efficiency of hydrophobic molecules is influenced by changes in the drug-to-lipid ratio. On the other hand, if a drug is polar/hydrophilic, it tends to localize in the aqueous core or adjacent to the water-lipid interface, near the polar head groups of the liposome. Therefore, its encapsulation efficiency does not exhibit a strong dependence on the drug-to-lipid ratio. On the contrary, the introduction of hydrophilic chains in the liposome surface favors greater entrapment of hydrophilic molecules when compared with hydrophobic molecules.⁵¹

Drugs loaded in liposomes are not bioavailable; they only become bioavailable when they are released. Therefore, optimizing the release rate of a liposome-vehicle drug is strategic to reach a level within its therapeutic window and at a sufficient rate for a sufficient period to have optimal therapeutic activity. On the other hand, premature drug release should be avoided. To overcome this inconvenience, several experimental approaches have been pursued, either by modifying the lipid bilayer or entrapping drugs suitable for the purpose.

Switching from a fluid-phase phospholipid bilayer to a solid-phase bilayer, e.g. by incorporating cholesterol (bilayer-tightening effect) or sphingomyelin into liposomes, the retaining of cargo into liposomes is increased.⁵²⁻⁵⁴ Another approach to control the release rate of entrapped substances is to choose drugs with physical characteristics favoring retention in the lipid nanovector. Similarly to biological membranes, liposomes have high permeability to hydrophobic drugs and low permeability to hydrophilic drugs. Anti-cancer drugs of high hydrophilicity retained in the aqueous internal compartment of liposomes (albeit with low trapping efficiency) are slowly released from the liposomes over several hours to several days.^{55,56} Drugs of high hydrophobicity

efficiently inserted into the fatty acyl chain region of the lipid bilayer can be easily released. Retention of highly hydrophobic drugs, such as paclitaxel, in liposomes is problematic, and many formulations and their pharmacokinetics have been studied to increase drug–liposome associations.⁵⁷

Many anticancer drugs are of intermediate solubility and readily partition between the liposome bilayer and the exterior or interior aqueous phase, resulting in their rapid release from liposomes. However, manipulation of the interior pH of the liposomes or the formation of molecular complexes within the liposomes can result in excellent retention of weak bases, such as doxorubicin (Dox) or daunorubicin, in liposomes.^{58,59} Drug retention can be improved by loading drugs to achieve high intraliposomal drug concentrations above their solubility limits, thus enhancing precipitation, or by encapsulating polyanions, such as dextran sulfate.^{60,61} Drugs that are not weak bases, such as docetaxel, can be converted to weak-base prodrugs, thus allowing encapsulation and liposomal retention.⁶²

Liposomes should store, protect, and transfer substantial quantities of drugs while being well tolerated in patients receiving the cure. These unique characteristics could provide for an improved biopharmaceutical profile through reduced toxicity, favorable pharmacokinetic behavior, and an enhanced therapeutic index in comparison to the free-form drug. Liposomes as drug-delivery systems could show several advantages over conventional dosage forms, particularly for parenteral (ie, local or systemic injection or infusion), topical, and pulmonary routes of administration.

Several clinical studies have demonstrated that liposomal encapsulation of drugs typically leads to a change in toxicity profiles. When used in clinical settings, liposomal treatments proved to improve patient outcome dramatically, reducing some of the side effects associated with chemotherapy, such as cardiotoxicity, nausea, and vomiting, when compared to unencapsulated drugs.^{63,64} Therapeutic activity of vincristine, widely used in the treatment of a number of human carcinomas, significantly increased after its encapsulation in appropriately designed liposomal systems. In fact, vincristine sulfate-liposome injection improved the therapeutic index by facilitating increased dose intensification, while maintaining a predictable and manageable safety profile. This effect is a consequence of a lower clearance and a higher area under the curve compared with conventional free vincristine sulfate.⁶⁵ In the field of antimicrobial agents, liposomal amphotericin B showed better tolerance and higher efficacy than the antibiotic amphotericin B deoxycholate. At present, liposomal amphotericin B is the drug of choice for the treatment of

patients with disseminated histoplasmosis and acquired immunodeficiency syndrome (AIDS).⁶⁶ Nystatin entrapped in pH-sensitive liposomes enhanced anticryptococcal efficacy in a murine model.⁶⁷

Antitumoral anthracyclines, such as Dox, daunorubicin, and epirubicin, achieve highly efficient encapsulation. Liposomal anthracyclines proved to be effective and showed reduced cardiotoxicity when compared to free agents, either as a single agent or in combination with other drugs.^{68,69} A meta-analysis study compared the safety and toxicity of liposomal Dox versus conventional anthracyclines. Both liposomal Dox and PEGylated liposomal Dox (PLD) showed favorable toxicity profiles, with better cardiac safety and less myelosuppression, alopecia, nausea, and vomiting compared with conventional anthracyclines, making them a favorable choice over conventional anthracyclines in elderly patients, patients with risk factors for cardiac disease, and patients with prior use of anthracyclines.⁷⁰

Among the pharmaceutical options available for treatment of ovarian cancer, increasing attention has been progressively focused on PLD, whose unique formulation prolongs the persistence of the drug in the circulation and potentiates intratumor accumulation. PLD has become a major component in the routine management of epithelial ovarian cancer (extensively reviewed in Pisano et al).⁷¹ Nonrandomized Phase II trials of PLD in platinum-resistant ovarian cancer patients documented the biological activity of this agent in this clinical setting, with objective response rates of approximately 10%–20% being reported in several trials.^{72–74} Data indicated that palmar–plantar erythrodysesthesia (hand–foot syndrome), toxic acral erythema, and mucositis were the most common toxicities of PLD, reported in up to 50% of treated patients. Although not life-threatening, palmar–plantar erythrodysesthesia can negatively impact quality of life, and it is a major cause of both dose reduction and treatment discontinuation.^{75,76} As regards cardiac toxicity, in several trials PLD formulation has been related to a better safety profile compared to conventional Dox.⁷⁷ Compared to the 7.5% incidence of irreversible cardiotoxicity at cumulative doses of 400–550 mg/m² reported with Dox, most of the studies of PLD showed a lower incidence of cardiac failure even at doses higher than 500 mg/m².^{78–80} In a prospective trial performed on patients with advanced gynecological malignancies treated with PLD, cardiac safety was further assessed at histology (endomyocardial biopsies), showing no myocardial damage in patients treated with PLD (median PLD dose of 708 mg/m²).⁸¹ Therefore, the optimal cardiac safety profile of PLD may allow prolonged treatment. Encouraging results

from a Phase II trial in AIDS-related Kaposi's sarcoma patients treated with PLD up to a 2,360 mg/m² cumulative dose have been reported.⁸² In metastatic breast cancer patients also, doses greater than 450 mg/m² were not associated with a significant decrease in left ventricular ejection fraction from baseline compared to conventional Dox.⁸⁰ In a relapsed ovarian cancer patient responding to second-line chemotherapy, maintenance therapy with PLD for more than 1 year was reported to be safe by Andreopoulou et al with no cardiac events reported.⁸³

Effect of size on liposome fate

Pathological tissues, such as inflammatory or solid tumor tissues, are characterized by increased vascular permeability.⁸⁴ The enhanced permeation and retention (EPR) effect is the phenomenon characterizing malignant tissues by which nanocarriers of an appropriate size can pass through tumor-vessel walls and enter the neoplastic lesion (Figure 2). More particularly, solid tumors that undergo angiogenesis develop a discontinuous endothelium, with large fenestrations allowing molecules of up to approximately 4,000 kDa, or 500 nm, to enter the interstitial space.^{85,86} Liposomes can satisfy the size conditions needed to pass through tumor vessels and concentrate in the target site. This mechanism represents the major targeting principle for intravenously administered long-circulating liposomes. However, because no specific targeting ligands are used to interact with the tumor target site, this tumor-localization process is referred to as "passive targeting."

This passive targeting depends on the mechanical and physical properties of liposomes. More importantly, once liposomes have entered the tumoral tissue, they are retained from the malfunctioning lymphatic system. Therefore, after its release, the drug encapsulated into liposomal carriers can exert its therapeutic effect.⁹

The overall size of the liposome-based drugs is an essential physical aspect that determines the clinical successes of the nanocarriers. Experimenting with variations in liposomal size, researchers observed that liposomes smaller than 100 nm in diameter interacted less with plasma proteins, evaded capture by the RES, had a longer half-life in the blood, and accumulated passively at the tumoral site.⁵ Conversely, it was found that larger liposomes were eliminated more rapidly from blood circulation and did not escape RES uptake. On the other hand, it was observed that small liposomes had reduced drug-storage capacities.¹⁷

Even if the size of these drug-delivery systems can be easily modulated, theoretically an ideal liposome designed for

the delivery of chemotherapeutics should be of 50–100 nm in diameter. The lower size limit (50 nm) should prevent intravenous-based nanocarriers from randomly penetrating normal vessel walls while in circulation.⁸⁷ However, an upper size limit to these systems could also exist. In order to gain access to tumor tissue, nanocarriers should retain the ability to extravasate from vessels through the large vascular fenestrations (250 nm or larger) that are present in and around tumor sites and are attributed to ongoing angiogenesis.^{84,87,88} At the tissue level, many nanomedicine products attempt to target sites passively through the EPR effect, with feature sizes typically in the 100–200 nm range, but particles up to 400 nm have demonstrated extravasation and accumulation in tumors (although this is an extreme case). However, when size is increased, capture by the RES also increases.^{68,89} For example, a previous study reported that PEGylated liposomes 250 nm in diameter were removed from circulation more than twice as fast as liposomes 100 nm in diameter with similar lipid composition.⁹⁰ This is particularly problematic, since it is imperative that liposomes loaded, eg, with an antitumoral agent, will remain in circulation until they accumulate within tumor tissue and release the active molecule at a concentration sufficient to exert a therapeutic effect.

Pharmacokinetics of liposomes

The pharmacokinetics of liposomes focuses on their distribution throughout the body fluids and tissues and their metabolism. The latter mainly includes liposome chemical degradation and excretion, which is achieved through their uptake and clearance by the RES.

As mentioned previously, one important goal of the design of a new liposomal carrier is the modulation of the pharmacokinetic profiles of a drug. The advantages of liposomal-based drugs should be greater solubility of the cargo, increased half-life, selective delivery to the site of action, improved therapeutic index, and the ability to overcome resistance against chemotherapeutics. When a therapeutic agent is loaded into liposomes, it adopts the carrier's pharmacokinetics until it is delivered. As a result, liposomes modify both the tissue distribution and the rate of clearance of the loaded drug.⁹¹ The pharmacokinetics of liposomal-based drugs depends on the physicochemical characteristics of the lipid vehicle, such as lipid composition, size, membrane lipid packing, steric stabilization, surface charge, dose, and route of administration. It has been reported that the primary sites of accumulation of carrier-mediated agents are the tumor, liver, and spleen, compared with noncarrier formulations. Factors affecting the pharmacokinetic and pharmacodynamic

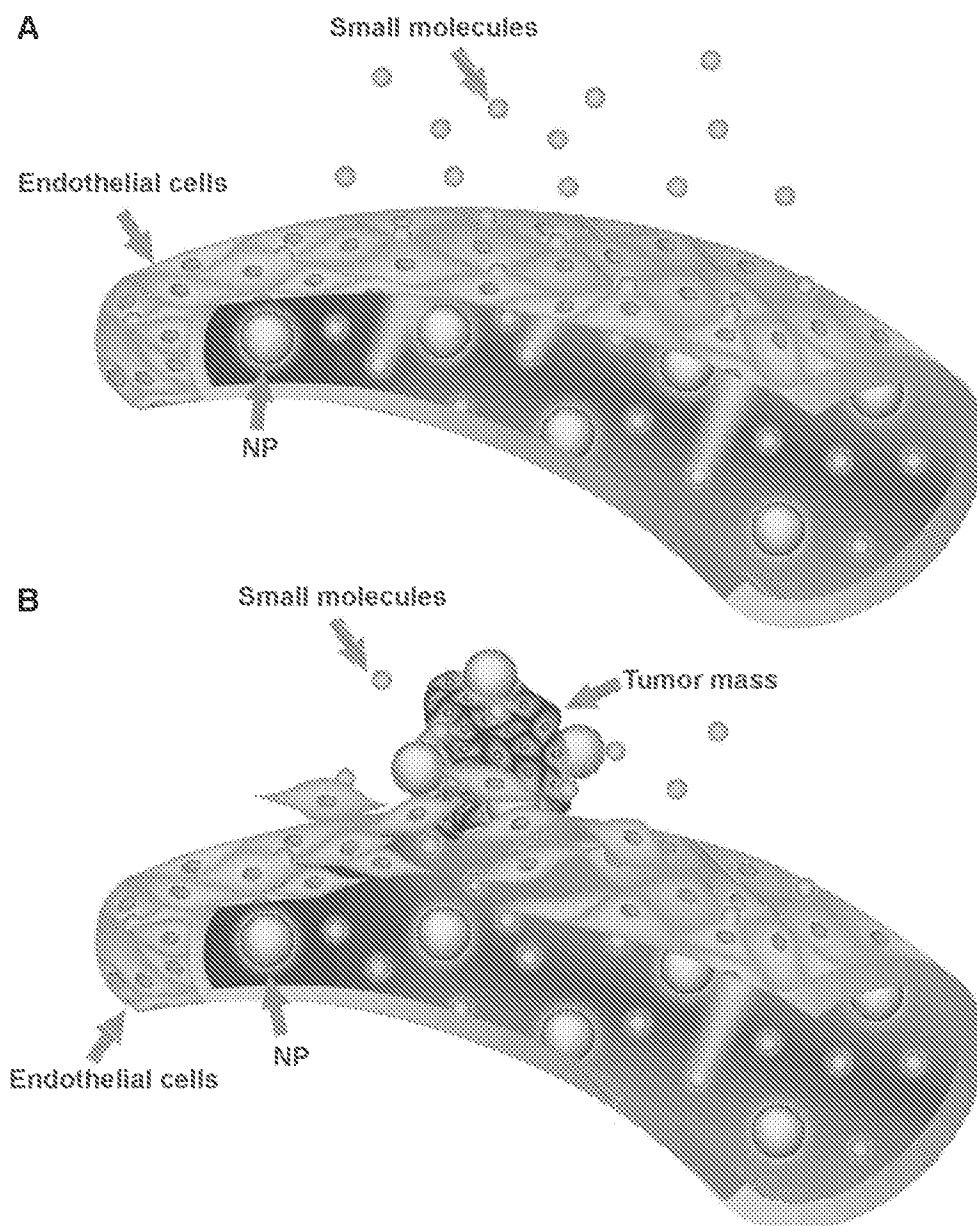


Figure 2 Targeting of nanomedicines by the enhanced permeability and retention (EPR) effect.

Notes: Differences between normal (A) and tumor (B) vessels are depicted. Tumor vessels contain large fenestrations between the endothelial cells; this structural characteristic allows the nanoparticles (NPs) to reach the matrix and the tumor cells by the EPR effect. Conversely, normal tissue contains tightly joined endothelial cells; this prevents the diffusion of NPs outside the blood vessels.

variability of these agents remain unclear, but most likely include the RES.⁶²

Once inside the organism, liposomes' stability in the bloodstream, as well as their capacity to enter target tissues, determines the fate of liposomes. During their circulation in the blood, liposomes meet plasma proteins, such as opsonins and HDLs and LDLs. Opsonins include various protein types, like immunoglobulins and fibronectin, which help RES recognize and eliminate liposomes. Blood carrying HDL and LDL interacts with liposomes and reduces their stability.

The interaction with lipoproteins causes lipid transfers and rearrangements on the surface of liposomes. This frequently induces lipid depletion, liposome breakdown, and rapid release of the cargo to the plasma.⁵ By modulation of lipid composition, this effect can be avoided (see later in this paper for more details).

After interaction with target cells, the delivery of the encapsulated drug depends on the nature of the lipid bilayer, the size of the drug molecules, their partition coefficient in oil/water, and their interactions with the lipid membrane.

The final fate of the drug, ie, the extracellular fluid or the cytoplasm of the target cell, depends on the molecular architecture, mechanism of release, and the composition of the carrier.⁹³

Elimination of liposomes takes place in different ways. The first involves absorption of plasma proteins on the surface of liposomes and then their recognition by the RES. This event results in the excretion of the cargo at the hepatic level and its subsequent metabolism by Kupffer cells. In the second way, liposomes are metabolized by splenic macrophages. Finally, after their accumulation, they are metabolized and eliminated by the target tissues.^{5,92,93}

Despite all the hopes invested in conventional liposomes, they have presented various problems and pharmacological implications over the years. A major drawback of conventional liposomes is their quick capture by the RES.⁹⁴ Liposomes are mainly accumulated in the liver and the spleen, due to their generous blood irrigation and the abundance of tissue-resident phagocytic cells.^{63,92,93} This is extremely advantageous in the case of local infections: the high concentration of antimicrobial agents in the RES can help treat infective pathogens. However, during chemotherapy, it may lead to partial depletion of the macrophages and interfere with the important host-defense functions of this cell type.⁹⁵ On the other hand, the marked increase in retention and accumulation of liposomal drugs in such organs as the spleen and the liver may lead to the delayed removal of lipophilic anticancer drugs from the circulation.⁹⁶

A number of different strategies were then tested in the following years in order to overcome the aforementioned limitations, giving rise to a "second generation" of liposomes. The best strategy was described in the early 1990s, when experiments carried out by several groups of scientists demonstrated that PEGylation of the liposome surface was able to improve the stability and circulation time of liposomes dramatically after intravenous administration, by rendering the liposomes invisible to macrophages.³⁰ These "long-circulating liposomes" were then named Stealth liposomes because of their ability to evade the immune system; this results in a significant increase in blood-circulation time *in vivo*.⁹⁷⁻⁹⁹

PEG is a linear or branched polyether diol with many useful properties, such as biocompatibility, solubility in aqueous and organic media, lack of toxicity, very low immunogenicity and antigenicity, and good excretion kinetics. These properties permit the employment of PEG in a variety of applications, including the biomedical field, after US Food and Drug Administration (FDA) approval for internal administration (<http://www.accessdata.fda.gov/scripts/cder/drugsatfda>).

PEG chains protect liposomes from mononuclear phagocytic system cells by building a protective, hydrophilic film on the liposomal surface. Their presence prevents the interaction of liposomes with other molecules, such as various serum components. One possible explanation for the impaired interaction is the PEG-induced "steric hindrance." The mechanism of steric hindrance by the PEG-modified surface has been thoroughly examined.¹⁰⁰ The water molecules form a structured shell through hydrogen bonding to the ether oxygen molecules of PEG. The tightly bound water forms a hydrated film around the particle and repels the protein interactions.¹⁰¹ In addition, the presence of PEG on the surface may also increase the hydrodynamic size of the particle, decreasing its clearance, a process that is dependent on molecular size as well as particle volume.¹⁰²

PEG-bearing liposomes are not opsonized or affected by complement components, and consequently evade capture by mononuclear phagocytic system cells.^{103,104} Finally, the presence of PEG in liposome formulations prevents aggregation, favors the formation of small, monodisperse particles, and increases the EPR effect, due to the extended circulation time and escape from the RES.¹⁰⁵

The practical consequences of these phenomena are evident when the biopharmaceutical profiles of Stealth liposomes and conventional liposomes are contemplated. Stealth liposomes have a longer half-life (which leads to longer blood-circulation times), low systemic plasma clearance, and low volume of distribution (minimal interaction with nondiseased tissue). This results in multiple-fold greater area-under-the-curve values (drug concentration-time profile) and improved tissue distribution (targeting of target sites).⁹⁹

The advantage of PEGylation is credible when the relative half-lives of non-PEGylated and PEGylated liposomes are compared. In fact, the half-life of liposomes after PEGylation increases from a few hours to 45 hours.¹⁰⁶ Therefore, it is not surprising that the clinically approved antitumoral drug Doxil® is PEGylated in order to improve tumor-site accumulation of the drug.¹⁰⁷ However, while PEG coating increases liposome-circulation times, it could also negatively influence the uptake by target cells due to PEG-induced steric hindrance.⁹⁷

Although clinically useful activity has been demonstrated, currently available liposome-based therapies do not exhibit active targeting at the cellular level. Existing FDA-approved liposome technologies against cancer rely on passive accumulation through the EPR effect.¹⁰⁸ In other words, these nanomedicines possess no functionality to actuate release other than passive efflux from the liposome

at the tumor site. However, this uncontrolled, passive release in some cases results in suboptimal pharmacokinetics or reduced efficacy, as observed with cisplatin-loaded liposomes.^{109–111} An additional level of sophistication and specificity for the target cell can be achieved through ligand-mediated targeting, which is defined as active targeting. The goal is to develop platforms with improved biodistribution, pharmacokinetic properties, and active targeting. The properties of such targeted liposomes can be modulated and adapted to different needs. Peptides, carbohydrates, glycoproteins, receptor ligands, monoclonal antibodies, and growth factors have been applied as ligands. Ligand-targeted liposomes can selectively recognize the antigens or the receptors located on the surface of target cells. Due to this high selectivity toward cancer cells, almost all of the administered liposomal drug would accumulate at the tumor site, leaving uninjured healthy bystander cells. That way, the required dose for the expected cytotoxic effect will be significantly smaller when compared to nontargeted therapies: this contributes to a better therapeutic index, with higher drug efficacy and fewer side effects.^{112–115}

As extensively reviewed in Noble et al¹¹⁶ ligand-targeted liposomes have demonstrated improved efficacy over passively targeted equivalents through enhanced targeting and intracellular uptake, but they have raised new challenges, such as hindered diffusion and penetration through the target tissue, immune recognition, and deactivation of targeting through the nonspecific binding of serum proteins. As a result, ligand-targeted liposome systems have not demonstrated consistently successful outcomes in preclinical settings, and other studies are necessary to address issues related to their efficiency.¹¹⁶

Charged liposomes

When a liposome interacts with a cell, the delivery of the drug and its distribution in the target cell can occur in several ways. Liposomes can adsorb into the membrane of cells, where the lipid bilayer of the carrier is degraded by enzymes, such as lipases, or by mechanical strain. This leads to the release of the active ingredients into the extracellular fluid, where they can diffuse through the cell membrane and cytoplasm. However, the latter process cannot easily occur when the loaded molecules are hydrophilic. A second way requires the fusion of the liposomal membrane with the plasma membrane of the target cell: this phenomenon causes the release of liposomal content directly into the cytoplasm. The third and most frequent way is receptor-mediated endocytosis. This process only regards vesicles of a maximum

diameter of 150 nm and active ingredients that can endure the acidic environment of lysosomes, where liposomes are enzymatically processed. Phagocytosis can also occur, but involves liposomes of a diameter larger than 150 nm. These large liposomes are phagocytosed by specialized cells of the immune system, such as macrophages, monocytes, and Kupffer cells (Figure 3).^{5,84,117}

The mechanism and extent of liposome–cell interaction is strongly influenced by the nature and density of the charge of the liposomes surface. By changing the lipid composition, both of these parameters can be modified. The liposomes can include charged components that confer them an overall neutral, positive, or negative charge. Lack of surface charge (neutral liposomes) increases the aggregation of liposomes, reducing their physical stability. Moreover, neutral liposomes do not interact significantly with cells, and this causes drug release from the liposomes in the extracellular space.^{118,119} On the other hand, charged liposomes present numerous advantages compared with neutral liposomes. For example, the presence of a charge on the surface induces electrostatic repulsion among liposomes by creating a ζ -potential, positive or negative, that

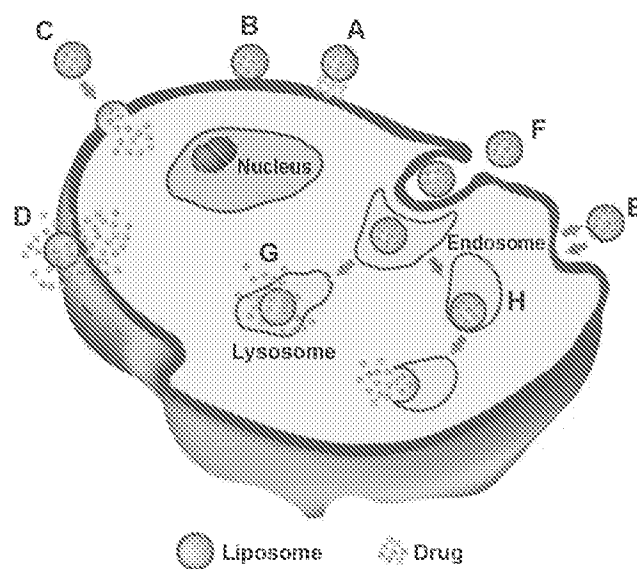


Figure 3 Liposome–cell interaction.

Notes: Liposomes loaded with a drug interact with the cell, binding to the surface through receptors (A). Adsorption onto the plasma membrane can also occur by electrostatic interactions (B). The delivery of the cargo into the cell cytoplasm can take place through different modes. Lipid nanocarriers fuse with the plasma membrane and discharge drugs into the cell (C). After the interaction with the cell, the structure of the liposome bilayer can be affected and the cargo is released (D). Exchange of carrier-lipid components with the cell membrane can also occur (E). Liposomes internalized by endocytosis (F) can have different fates depending on physicochemical characteristics. Endosomes fuse with lysosomes (G); in this case, the low pH induces the degradation of the liposome membrane and the drug is released. Endosomes follow another route (H): liposomes release their cargo after fusion or the destabilization of the endocytic vesicle.

prevents their aggregation and flocculation. Moreover, a high electrostatic surface charge could promote the interaction of liposomes with cells.

The literature includes several studies carried out on the potential use of charged liposomes for biomedical applications. However, the great majority of these studies focused on positively charged liposomes, due to the encouraging results obtained in *in vitro* and *in vivo* experimentations.

Negatively charged liposomes are generally constituted by anionic lipids, such as dimyristoyl phosphatidylglycerol and dipalmitoyl phosphatidylglycerol. Literature data show that the negative liposomes, due to their electrostatic properties, are less stable than neutral and positive liposomes when injected into the blood circulation. In fact, anionic liposomes rapidly interact with the biological system subsequently to their opsonization with complement and other circulating proteins.¹²⁰⁻¹²² Such an interaction has at least two acute consequences: a rapid uptake by the RES, and toxic effects, such as pseudoallergy that is manifested as vasoconstriction, pulmonary hypertension, dyspnea, and drop in circulating platelets and leukocytes.¹²³ For this reason, anionic liposomes have not been widely used as drug-delivery systems for intravenous administration. Moreover, several studies examining the effect of negative and positive charge on the adjuvant activities of liposomes have been carried out, but the results obtained were rather conflicting and inconclusive.¹²⁴⁻¹²⁷ However, in recent years, there has been increased interest in developing charged liposomes as carriers for transdermal drug delivery, due to their enhanced penetration properties through the skin.¹²⁸ To clarify the effect of the surface charge on percutaneous absorption, histological studies revealed that the negatively charged liposomes diffused to the dermis and the lower portion of hair follicles through the stratum corneum and the follicles much more quickly than the positive vesicles. Therefore, the rapid penetration of negatively charged liposomes would contribute to increased permeation of drugs through the skin.¹²⁹

Cationic liposomes (CLPs), first described in 1987 by Felgner et al are typically used for gene delivery, based on the electrostatics between positively charged lipids and negatively charged nucleic acids.¹³⁰ They consist of natural neutral phospholipids and positively charged lipids. Commonly used neutral phospholipids include dioleoyl phosphatidylethanolamine (DOPE) or dioleoyl phosphatidylcholine, and are in most cases required for the stabilization of the liposome/DNA complex. A variety of lipid formulations with a positive charge are already on the market, such as DC-cholesterol HCl, (3 β -[*N*-(*N*',*N*'-dimethylaminoethane)-carbonyl]

cholesterol hydrochloride), DOTAP (1,2-dioleoyl-3-trimethylammonium-propane [chloride salt]), DOBAQ (*N*-[4-carboxybenzyl]-*N*,*N*-dimethyl-2,3-bis(oleoyloxy)propan-1-aminium), DDAB (dimethyldioctadecylammonium [bromide salt]), and MLV5 (*N*1-[2-((15)-1-[(3-aminopropyl)amino]-4-[di(3-amino-propyl)amino]butylearboxamido)ethyl]-3,4-di[oleoyloxy]-benzamide), and many others are under development.

In the case of CLP-cell interaction, the endocytic pathway seems to be the preferential route of internalization. The pathway of internalization is of the utmost importance in the final fate of the drug loaded in the lipid carriers, as, eg, in the case of drugs sensitive to an acidic environment. Both the interaction with the cell membrane and the pathway of internalization are strictly dependent on the physicochemistry of liposomes. Morphological and ultrastructural studies are invaluable tools to study the mechanisms of liposome-cell interaction and analyze at nanoresolution the temporal and spatial parameters involved. As an example, morphological and ultrastructural studies by the freeze-fracturing technique on the interaction of CLPs with tumor cells are reported in Figures 4 and 5. In these experiments, CLPs formulated as described in Bombelli et al were used.¹³¹ Freeze-fracturing is an election technique used to study plasma-membrane architecture and its modifications occurring upon the interaction with xenobiotics, microbial agents, nanomaterials, and so on. As shown by the replica

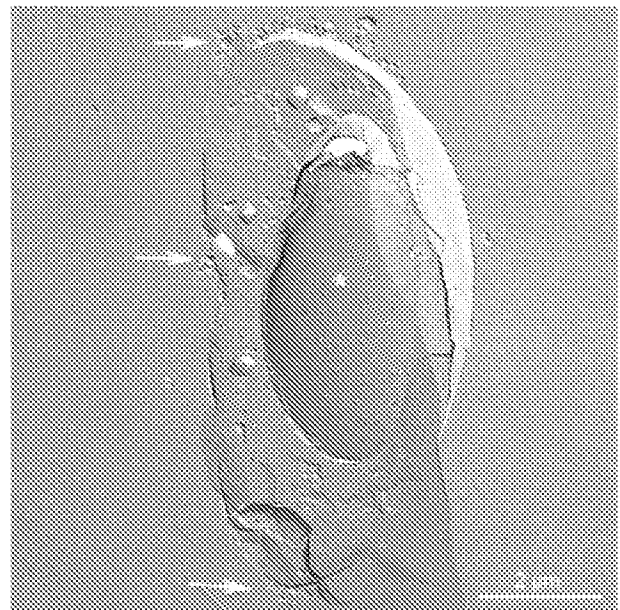


Figure 4 Replica of a cryofixed and cross-fractured human glioblastoma cell, interacting with dimyristoyl-*sn*-glycero-phosphatidylcholine liposomes. Liposomes appear mainly clustered on a pole of the cell (arrows). The fracture passes through the cytoplasm, and reveals the nucleus (asterisk) and the cytoplasmic organelles (arrowhead).

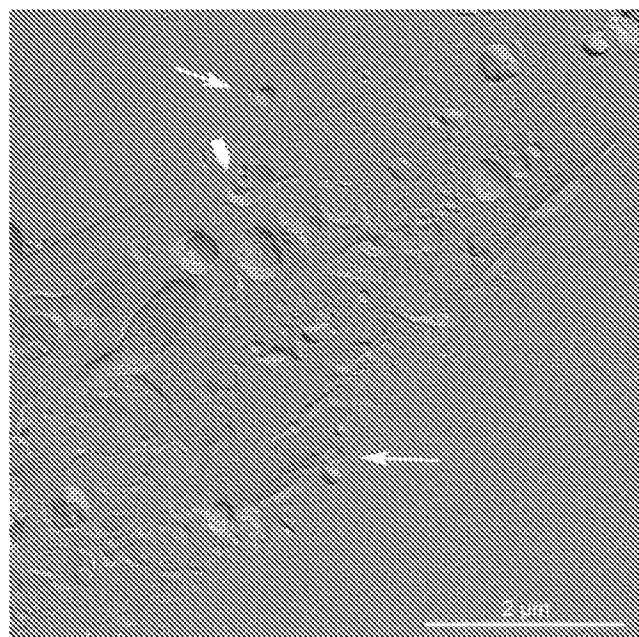


Figure 5 Replica of a cryofixed and cross-fractured human glioblastoma cell, interacting with dimyristoyl-*sn*-glycero-phosphatidylcholine liposomes. Liposomes (arrows) appear in the extracellular space and the cytoplasm of the cell. Some of them are interacting with cytoplasmic organelles (arrowhead).

performed on cryofixed and cross-fractured samples, before being internalized, CLPs appear clustered on the plasma membrane of the glioblastoma cell. The capping phenomenon strongly suggests the involvement of an endocytic pathway (Figure 4). The replica of cross-fractured tumor cells allows the visualization of liposomes interacting with cytoplasmic organelles, very likely endosomes (Figure 5).

Since the overall positive charge of CLPs enhances the transfection of anionic animal target cells, liposome/DNA complexes are commonly used for delivering genes. However, preclinical and clinical results encourage the use of CLPs for the delivery of antitumoral agents to the tumor vasculature. In fact, it has been demonstrated that the presence of anionic sites in angiogenic endothelial cells (such as anionic phospholipids, proteoglycans, hyperglycosylated and hypersialylated membrane proteins, and so on) makes newly formed tumor vessels selective targeting sites for CLPs. It has been reported that such drugs as paclitaxel, Dox, and oxaliplatin carried by CLPs showed enhanced antitumor efficacy associated with a reduced functionality of the tumor microvasculature.^{132,133} Campbell et al demonstrated that the presence of a positive charge on liposomes is needed to improve their interactions with the glycoproteins of the endothelial cell membranes.¹³⁴ These data support the use of CLPs to target cytotoxic drugs preferentially to the tumor vascular endothelium, and to achieve long circulation half-lives.¹³⁵

An important goal of CLPs is to cross the blood-brain barrier (BBB) and achieve brain drug concentration. The BBB is composed of specific structures formed by brain-capillary endothelial cells and basement membrane, sheathed with astrocytic end-feet. BBB impedes drug penetration into the central nervous system, and for this reason many brain drug-delivery strategies have focused on crossing it. The mechanism by which CLPs have been shown to cross the BBB easily is either absorptive-mediated transcytosis or receptor-mediated transcytosis. Both mechanisms are triggered by the electrostatic interaction between liposome cationic components and membrane anionic microdomains of the brain's capillary endothelial cells.¹³⁶

Even if an increased amount of cationic lipids in liposomes may enhance affinity for angiogenic endothelial cells and the subsequent anticancer effect, some points need to be considered. The increased positive charge on the unshielded CLP surface could result in their aggregation in the bloodstream through electrostatic interactions with anionic species in the blood, in an enhanced uptake by the RES, and in reduced accumulation in the tumor.^{122,133,137-141} These effects negatively influence the fate and therapeutic efficacy of CLPs *in vivo*.

Even in the case of CLPs, PEG protects from circulating proteins, improving their plasma clearance and enhancing their anticancer effects. PEG-modified CLPs have also been shown to improve oligonucleotide loading and delivery and the solubility of various therapeutic agents.^{142,143}

The use of CLPs may improve the efficacy and intrinsic safety of photodynamic therapy, a protocol that involves the administration of a photosensitizer and its irradiation in light of the appropriate wavelength (near infrared radiation) to excite and activate it and to induce the formation of cytotoxic species. In fact, liposomes can efficiently solubilize hydrophobic photosensitizers, thus increasing the photoactive population. Further, they can improve the accumulation in tumors and the pharmacokinetics of the photosensitizer, thus reducing the side effect of skin photosensitization due to poor target specificity.¹⁴⁴ In our studies, CLPs formulated with dimyristoyl-*sn*-glycero-phosphatidylcholine (DMPC) and the cationic gemini surfactant (*S,S*)-2,3-dimethoxy-1,4-bis(*N*-hexadecyl-*N,N*-dimethylammonio)butane bromide 1a (DMPC/1a) was developed to deliver the photosensitizer *m*-tetrahydroxyphenylchlorin (*m*-THPC) to human colon adenocarcinoma and glioblastoma cells.^{131,145} The presence of gemini surfactant strongly influenced the interaction of liposomes with the cell membrane and the delivery efficacy of CLPs. It significantly increased the cell uptake of *m*-THPC

and the cytotoxic effect of the photosensitizer after the irradiation, when compared with the related pharmaceutical formulation Foscan.¹⁴⁶ A subsequent study demonstrated that the stereochemistry of the gemini spacer strongly influenced the physicochemistry of liposomal formulations and the final intracellular fate of the loaded drug.¹⁴⁶

Stimuli-responsive liposomes

Conventional and long-circulating liposomes may present a slow release of the loaded drug or may be unable to fuse with the endosome after internalization. To overcome these problems, stimuli-responsive liposomes have been developed. Lipids in these liposomes generally include a triggerable component that is responsible for gating the stability and/or permeability of the lipid bilayer. Stimuli-responsive liposomes are capable of reacting when triggered by stimuli from target tissues (pH, redox potential) or applied from outside the organism (hyperthermia, ultrasound, and [electro]magnetic field).^{147,148} pH-sensitive, redox potential-sensitive, temperature-sensitive, magnetic field-sensitive, and ultrasound-sensitive liposomes have been produced.

The development of pH-sensitive liposomes was planned after the consideration that some pathological tissues, including tumors or areas of inflammation and infection, display an acidic environment compared with normal tissues.¹⁴⁹ A pH-sensitive liposome is generally stable at physiological pH, but can be subjected to destabilization and acquire fusogenic properties under acid conditions, thus leading to the release of its aqueous contents.¹⁵⁰ To achieve the pH-sensitive release of liposome content, liposomes are formulated with pH-sensitive components. After being endocytosed in an intact form, these fuse with the endovacuolar membrane as a result of the lower pH inside the endosome, and release their contents into the cytoplasm. Long-circulating PEGylated pH-sensitive liposomes, despite having decreased pH sensitivity, still effectively deliver their contents into the cytoplasm.¹⁵¹

Redox potential-sensitive liposomes take advantage of the high redox-potential difference that exists between the reducing intracellular space and the oxidizing extracellular space. Redox potential-sensitive liposomes release their content inside cells when disulfide bonds present in lipids or other components are reduced by glutathione to thiol groups. Consequently, the integrity of the liposome structure, which is maintained under normal conditions by disulfide bonds, is compromised, and the entrapped cargo can be released. Endogenous triggering of liposomal payload release by overexpressed enzyme activity in affected tissues offers the possibility of active and site-specific release. Redox-triggered

content release from liposomes was reported when applying liposomes made from quinone-DOPE (Q-DOPE) lipids. Complete payload release occurs upon their redox activation when the quinone head group possesses a "trimethyl-locked" quinone redox switch, attached to the N-terminus of DOPE lipids, that undergoes a cleavage event upon two-electron reduction.¹⁵² The authors expect that Q-DOPE liposomes and their variants will be important in treating diseases with associated tissues that overexpress quinone reductases, such as cancers and inflammatory diseases, because the quinone redox switch is a known substrate for this group of reductase.¹⁵²

Thermosensitive liposomes have been widely investigated since 1978.¹⁵³ In the last decade, there has been increased interest in delivery mediated by temperature-sensitive liposomes, in part due to advances in image-guided hyperthermia applicators. Temperature-sensitive liposomes in combination with heating the target region can selectively enhance the bioavailability of the drug locally while minimizing systemic exposure. Temperature-sensitive liposomes promptly discharge their cargo upon heating (within seconds to minutes), while at body temperature the payload is somewhat stably encapsulated.^{154–156} Temperature-sensitive liposomes release their encapsulated drugs at the melting-phase transition temperature (T_m) of the lipid bilayer. At this T_m , the lipid membrane changes its permeability because of the transition from the gel to the liquid crystalline phase.^{157,158} Temperature-sensitive liposomes frequently include dipalmitoylphosphatidylcholine as the key component, because the gel-to-liquid crystalline phase transition occurs for these lipids at 41°C, as extensively reviewed in Kono.¹⁵⁹

Temperature-sensitive liposomes have been successfully applied in both preclinical and clinical studies in combination with heat-based thermal therapies, including radiofrequency ablation, ultrasound hyperthermia, and microwave hyperthermia.^{160–163}

A formulation based on these thermosensitive liposomes took the brand name ThermoDox® and was further developed by Celsion Corporation. ThermoDox liposomes can be triggered to release their payload by any heat-based treatment, such as radiofrequency thermal ablation, microwave hyperthermia, and high-intensity-focused ultrasound.¹⁵⁷

A complete regression of local cancer using temperature-sensitive liposomes combined with ultrasound-mediated hyperthermia was recently reported by Kheirrolomoom et al.¹⁶⁴ These authors employed temperature-sensitive liposomes containing lysolipid, loaded with a pH-sensitive complex formed by Dox and copper, ie, CuDox. The complex remains associated at neutral pH, but dissociates to give free Dox

in lower-pH environments. The resulting liposomes were injected intravenously into a syngeneic murine breast cancer model. Successively, the intravascular release of the drug was triggered by ultrasound. The entire tumor was insonified for 5 minutes prior to drug administration and 20 minutes after drug injection. A single-dose administration of CuDox lysolipid-containing temperature-sensitive liposomes (LTSLs) combined with insonation suppressed tumor growth. Moreover, after twice-weekly treatment over a period of 28 days, a complete response was achieved in which the NDJ tumor cells and the tumor interstitium could no longer be detected. All mice treated with ultrasound combined with CuDox LTSLs survived, and the tumor was undetectable at 8 months posttreatment. Iron- and copper-laden macrophages were observed at early time points following treatment with this temperature-sensitive formulation. Systemic toxicity indicators, such as cardiac hypertrophy, leukopenia, and weight and hair loss, were not detected with CuDox LTSLs after the 28-day therapy.¹⁶¹

Liposomes in theranostics

Nanotechnology gives the opportunity to assemble therapeutic and diagnostic agents as a single theranostic platform, ie, a molecular platform that simultaneously integrates diagnosis and therapy.¹⁶⁵⁻¹⁶⁹ The main goal is to diagnose and treat the diseases at their earliest stage. A theranostic platform is multifunctional in nature, able to detect and specifically deliver therapeutic agents to the diseased cells with the help of targeting ligands and biomarkers.¹⁶⁸⁻¹⁷¹

Liposomes are a valid platform for theranostic nanomedicine, owing to their size, hydrophobic and hydrophilic character, biocompatibility, biodegradability, low toxicity, and immunogenicity. In 2007, the concept of liposome-nanoparticle hybrids was presented by Al-Jamal and Kostarelos as a general methodology to be used as a platform for the delivery of novel nanoparticles. Such hybrid constructs present great opportunities to engineer theranostic nanoscale delivery systems.¹⁷² Liposome-nanoparticle hybrids can be designed by embedding, encapsulation, or conjugation of nanoparticles onto various types of liposomes. The theranostic potential of such hybrids is illustrated in Al-Jamal and Kostarelos.¹⁷³ The authors described, in particular, Dox-loaded, lipid bilayer-embedded quantum-dot vesicle hybrids capable of chemotherapy (cytotoxic activity of Dox) and optical imaging (embedded quantum dots).

For imaging purposes, nanosize diagnostic agents can be entrapped within the theranostic liposomes, and the therapeutic agent can be either encapsulated in the core or embedded in the lipophilic bilayer shell.¹⁷³⁻¹⁷⁸ For example,

for magnetic resonance imaging, superparamagnetic iron oxides can either be coated with a lipid layer (small magnetoliposomes [MLs]) or several superparamagnetic iron oxides or gadolinium(III) chelates can be entrapped into the aqueous core of liposomes (large MLs). These large MLs provide additional cargo space for drug encapsulation, into either the core or the lipid membrane, rendering MLs (theranostic agents).^{179,180} Multimodal imaging properties have been obtained by loading quantum dots or fluorescent dyes, such as calcein, into the lipid membrane of liposomes. For example, recently, Li et al constructed a multifunctional liposome containing gadolinium-DOTA lipids for magnetic resonance imaging, a lipidized near-infrared dye for near-infrared fluorescence imaging, Dox loading for therapeutic activity, and radiolabeling with ^{99m}Tc and ⁶⁴Cu for single-photon emission computed tomography and positron-emission tomography imaging. These liposomes were applied *in vivo* to a squamous cell carcinoma of head and neck tumor xenograft in nude rats after intratumoral injection.¹⁸¹

Muthu et al prepared tocopheryl polyethylene glycol 1000 succinate-coated theranostic liposomes containing Dox and quantum dots with and without targeting moieties.¹⁸² Folic acid was used as the targeting probe to target folate receptors overexpressing MCF-7 breast cancer cell lines. Along similar lines, Wen et al developed quantum dots and apomorphine-incorporated theranostic liposomes to eliminate uptake by the liver and to enhance brain targeting.¹⁸³ In their most recent work, Wen et al prepared theranostic liposomes loaded with quantum dots, camptothecin, and irinotecan for simultaneous bioimaging and drug delivery.¹⁸⁴

Smith et al used heat-sensitive liposomes with modified HER2 affisomes (HER2⁺ affisomes).¹⁸⁵ Affibody[®] affinity ligands are innovative protein-engineering technologies. The liposomes were either loaded with rhodamine phosphatidylethanolamine and calcein or with Dox. HER2⁺ cells and HER2⁻ cells were both incubated with the liposomes.¹⁸⁶

As stated by Svenson, even if liposomes are an ideal platform for theranostics, several issues remain to be addressed. Nanocarrier polydispersity is an issue for clinical translation and regulatory approval of nanocarriers. Random entrapment and surface conjugation of diagnostic and therapeutic agents into liposomes or other nanocarriers is a tempting and easily achievable approach. However, the polydispersity of the resulting nanocarriers and questionable reproducibility of the approach will create high hurdles for clinical translation and regulatory approval. Adding active targeting ligands to a nanocarrier not only adds at least another step to its production but also adds to polydispersity, complicates regulatory

evaluation and approval, increases the costs of goods, and can have negative biological outcomes because of multivalency binding and enhanced recognition by the RES with reduced circulation time.¹⁸⁷

Liposomes on the market or in clinical trials

Doxil (100 nm) was the first pharmaceutical product in a PEGylated liposomal formulation that received FDA approval (1995) for the treatment of chemotherapy-refractory Kaposi's sarcoma in AIDS patients, and more recently for recurrent epithelial ovarian cancer.¹⁸⁸ Currently, several liposome-based drugs are approved for clinical practice; many others are still in the various stages of clinical trials (Tables 1 and 2).¹⁸⁹ Most liposomal drug formulations, such as Doxil and Myocet® (190 nm), have been approved for intravenous application.¹⁹⁰ Generally, liposome products have a longer circulating half-life when compared with respective unencapsulated drugs. The time of circulation in the blood depends on size, charge density, fluidity of the lipid bilayer, or coating by PEG. For the delivery of surface antigens derived from the influenza virus (Inflexal® V) or hepatitis A (Epaxal®), intramuscular delivery has been approved. Inflexal V and Epaxal are both vaccine products: it has been reported that cell-mediated and humoral immune response is potentiated when viral membrane proteins or peptide antigens are incorporated into liposomes.^{191,192} For the administration of liposomal vaccines, oral delivery has also been considered; however, this is more problematic, due to the potential for liposome breakdown following exposure to bile salts. Therefore, injections remain the best route of administration for therapeutic peptides.¹⁹³ Since the first liposomal pharmaceutical product, Doxil, liposomes have been widely utilized as carriers for various therapeutic agents in clinical trials (extensively reviewed in Chang and Yeh).¹⁸⁹ Until now, virosomes (Epaxal and Inflexal V), CLPs (EndoTAG1-1®), PEGylated liposomes (Doxil and Lipodox), and temperature-sensitive liposomes (ThermoDox) have been considered for clinical use. In contrast with the liposome-based drugs on the market, liposome-based drugs in clinical trials display a large variety of loaded drugs (eg, cisplatin, BLP25 lipopeptide, Grb2 antisense oligodeoxynucleotide, bacteriophage T4 endonuclease 5) for several therapeutic applications (from topical delivery systems to portable aerosol delivery systems). As previously described, PEGylation may extend the blood-circulation time of liposomes, modify drug distribution in the body, and hence reduce related adverse effects (eg, cardiotoxicity). However, a significant

incidence of stomatitis in clinical trials contemplating the use of PEGylated liposomes (Doxil and Lipodox) has been reported.¹⁸⁹

In addition, it has been observed that some of the new-generation liposomes demonstrated only comparable or even poor therapeutic efficiency when they were compared with relative free drugs or conventional vesicles in clinical trials. In comparison with Doxil, ThermoDox showed a significant decrease of Dox accumulation in mouse tumors at 24 hours after administration.^{162,189} EndoTAG-1 plus gemcitabine showed beneficial survival and efficacy in a randomized controlled Phase II clinical trial in advanced pancreatic cancer and triple receptor-negative breast cancer.¹⁹⁴ In addition, a positive efficacy trend of the EndoTAG-1 combination therapy for triple receptor-negative breast cancer was reported by MediGene (<http://www.medigene.com>). SPI-77, the first liposomes loaded with cisplatin, showed limited clinical efficacy in a Phase II clinical trial of advanced non-small-cell lung cancer. On the other hand, the same formulation induced increased cisplatin tumor accumulation in preclinical models.¹⁹⁵ Similarly to SPI-77, a Phase II study demonstrated that liposomal anamycin had no detectable antitumor activity in the treatment of Dox-resistant breast cancer.¹⁹⁶

Conclusion

Due to their biocompatibility and biodegradability, liposomes were the first drug-delivery system approved for clinical purposes. Despite their long history in the field of research and development, there are still unresolved problems that limit their ultimate therapeutic outcome.

The advantages of liposomal-based drugs should be greater solubility of the cargo, increased half-life, selective delivery to the site of action, and the ability to overcome resistance against chemotherapeutics. The consequential pharmacokinetic changes could result in a reduction of adverse effects and an improvement in the therapeutic index of the encapsulated drugs. To reach these therapeutic outcomes, liposomes were firstly modified (PEGylated) in order to solve pharmacological challenges, such as destabilization by blood lipoproteins, uptake by RES, and rapid clearance from blood circulation.

PEGylated liposomes have been approved and are on the market, but their clinical success is hampered by some limitations, such as a lack of specificity. To increase their target-specificity and the amount of released therapeutic agent at the site of disease, stimuli-sensitive liposomes and multifunctional carriers for theranostics have been designed.

However, the transfer to large-scale production and to the clinic of these liposomal formulations suffers drawbacks,

Table 1 Liposomes on market or in clinical trials

Product name	Drug	Indication	Route of injection	Nanoscale dimensions (nm)	Status	References
Abeicet	Amphotericin B	Fungal infections	Intravenous	1,600–11,000	Approved	197–200
AmBisome	Amphotericin B	Fungal infections	Intravenous	45–80	Approved	197–199,201
Amphocil	Amphotericin B	Fungal infections	Intravenous	110–114	Approved	202,203
DaunoXome	Daunorubicin citrate	Kaposi sarcoma	Intravenous	45	Approved	197,198,204,205
DepoCyt	Cytarabine	Lymphomatous meningitis	Intravenous	20	Approved	197–200
Doxil	Doxorubicin	Kaposi's sarcoma	Intravenous	87	Approved	197–199,206,207
Visudyne	Verteporfin	PDT sensitizer	Intravenous	100	Approved	197,199,208
Evacet	Doxorubicin	Ovarian cancer	Intravenous	150	Approved	199,209
Lipo-Dox	Doxorubicin	Solid tumors	Intravenous	20	Approved	210
Epaxal	Inactivated hepatitis A virus (strain RG-38)	Hepatitis A	Intramuscular		Approved	211
Inflexal	Inactivated hemagglutinin of influenza virus strains A and B	Influenza	Intramuscular		Approved	211
DepoDur	Morphine sulfate	Pain management	Epidural		Approved	212,213
Nyotran	Nystatin	Solid tumors	Intravenous	110–135	Terminated	214,215
Alcrest	Vinorelbine	Solid tumors	Intravenous	100	Investigational	216,217
AmBil	Amphotericin B	Fungal infections	Intravenous	130	Investigational	213,218
Aroplatin	Cisplatin and its analog	Colorectal neoplasms	Intravenous/ Intrapleural		Investigational	219–221
ATI-1123	Docetaxel	Solid tumors	Intravenous	60–80	Investigational	222,223
Atragen	Tretinoin	Solid tumors	Intravenous		Investigational	224,225
Atu027	siRNA	Solid tumors	Intravenous	120	Investigational	226–228
BAY 79-4980	Kogenate FS	Hemophilia a	Intravenous	80–110	Investigational	229,230
BP-100-1.01	Grb-2	Leukemia	Intravenous		Investigational	231
BP-100-1.02	Bcl-2	Lymphoma	Intravenous		Investigational	232
BP-100-2.01	siRNA	Ovarian cancer	Intravenous		Investigational	232
Brakiva	Topotecan	Solid tumors	Intravenous	100	Investigational	233,217
CPX-1	Irinotecan	Solid tumors	Intravenous	100	Investigational	234,235
CPX-351	Cytarabine and daunorubicin	Acute myeloid leukemia	Intravenous	100	Investigational	235,236
C-VI SA bikDD	BikDD	Pancreatic cancer	Intravenous	405	Investigational	237,238
Doxisome	Doxorubicin	Solid tumors	Intravenous		Investigational	213
EndoTAG-1	Paclitaxel	Solid tumors	Intravenous	180–200	Investigational	239,240
I HL-305	Irinotecan	Solid tumors	Intravenous	100	Investigational	241
I NGN-401	DOTAP: Chol-fus1	Lung cancer	Intravenous	375	Investigational	198,242
JVRS-100	Immunostimulatory DNA	Leukemia	Intravenous	120	Investigational	243,244
L-annamycin	Annamycin	Acute lymphocytic leukemia	Intravenous	150	Investigational	245,246
LE-DT	Docetaxel	Solid tumors	Intravenous	<200	Investigational	247
LE-M	Mitoxantrone	Solid tumors	Intravenous	<200	Investigational	247,248
LEP-ETU	Paclitaxel	Solid tumors	Intravenous	150	Investigational	249,250
LE-rafAON	LErafAON-ETU	Neoplasms	Intravenous	400	Investigational	251–253
LE-SN38	SN-38	Solid tumors	Intravenous	150–200	Investigational	254,255
L-Grb-2	Grb2 antisense oligodeoxynucleotide	Leukemia	Intravenous	90	Investigational	256,257
Lipoplatin	Cisplatin and its analog	Solid tumors	Intravenous	110	Investigational	258–260
Liposomal alendronate	Alendronate	Coronary artery stenosis	Intravenous	148–180	Investigational	261
Lipotecan	Camptothecin	Solid tumors	Intravenous	180–200	Investigational	213,262,263

Abbreviations: PDT, photodynamic therapy; siRNA, small interfering ribonucleic acid; DOTAP, 1,2-dioleoyl-3-trimethylammonium-propane (chloride salt); Chol, cholesterol; DNA, deoxyribonucleic acid; LErafAON, liposome-entrapped, end-modified raf antisense oligonucleotide; ETU, easy to use.

Table 2 Liposomes on market or in clinical trials

Product name	Drug	Indication	Route of injection	Nanoscale dimensions (nm)	Status	References
Lipovaxin-MM	Vaccine	Melanoma	Intravenous	240	Investigational	264,265
Lipostin	Prostaglandin	Peripheral vascular disease	Intravenous	100–200	Investigational	266
L-MTP-PE	L-MTP-PE	Osteosarcoma	Intravenous	710	Investigational	267,268
Marqibo	Vincristine	Solid tumors	Intravenous	100	Investigational	217,269
MBP-426	Oxaliplatin	Solid tumors	Intravenous	180	Investigational	239,270,271
MBP-Y003	Methotrexate	Lymphoma	Intravenous		Investigational	271
MBP-Y004	Docetaxel	Solid tumors	Intravenous		Investigational	271
MBP-Y005	Gemcitabine	Solid tumors	Intravenous		Investigational	271
MCC-465	Doxorubicin	Stomach cancer	Intravenous	143	Investigational	239,272
Myocet	Doxorubicin citrate	Breast cancer	Intravenous	190	Investigational	197,198,273
Nanocort	Prednisolone	Rheumatoid arthritis	Intravenous	<150	Investigational	274
NanoVNB	Vinorelbine	Colon cancer	Intravenous	95, 2	Investigational	213,275
ONCO-TCS™	Vincristine	Solid tumors	Intravenous	120	Investigational	276,277
OSI-211	Lurtotecan	Solid tumors	Intravenous	100–200	Investigational	278
PEP02	Irinotecan	Solid tumors	Intravenous	100	Investigational	279
PNT2258	Oligonucleotide	Cancer	Intravenous	100	Investigational	280
RVCLUV	Ropivacaine	Anesthetic	Intravenous	130	Investigational	281
SapC-DOPS	Sapoin C	Solid tumors	Intravenous	190	Investigational	282–284
S-CKD602	Camptothecin analog	Advanced malignancies	Intravenous	100	Investigational	285
Stimuvax	BLP25 vaccine	Solid tumors	Intravenous	150–580	Investigational	286
ThermoDox	Doxorubicin, lyso-thermosensitive	Solid tumors	Intravenous	175	Investigational	287,288
TKM-ApoB	siRNA	Hypercholesterolemia	Intravenous	120	Investigational	289,290
TKM-Ebola	siRNA	Ebola	Intravenous		Investigational	291
TKM-PLK1	siRNA	Solid tumors	Intravenous		Investigational	291
Dimericine	T4N5	Precancerous condition	Topical	200	Investigational	292,293
Lip glucantime	Meglumine antimoniate	Cutaneous leishmaniasis	Topical	400	Investigational	294
NanoDOX™	Doxycycline monohydrate	Foot ulcer, diabetic	Topical	200–350	Investigational	295,296
T4N5 liposomal lotion	Bacteriophage T4 endonuclease 5	Skin cancers	Topical		Investigational	297,298
AeroLEF	Fentanyl	Pain relief	Aerosol		Investigational	299
Arikace	Amikacin	Cystic fibrosis	Aerosol	375	Investigational	300
L9NC	L9NC	Solid tumors	Aerosol	100–300	Investigational	301
VaxiSome	Vaccine	Influenza	Intramuscular		Investigational	302
CAF01	Vaccine	Tuberculosis	Intramuscular	450	Investigational	303
RTS S/AS02	FMP2.1/AS02A	Malaria	Intramuscular	20	Investigational	197,304
CFTR gene liposome	CFTR gene	Cystic fibrosis	Nasal		Investigational	305
OX-NLA	Cetirizine HCl	Allergic rhinitis	Nasal		Investigational	306,307
pGT-1 gene liposome	pGT-1 gene	Cystic fibrosis	Nasal		Investigational	308
DPX-0907	Cancer vaccine	Neoplasms	Subcutaneous		Investigational	309
I L-2 LI PO	Interleukin 2	Melanoma	Subcutaneous		Investigational	310
FLCLUV	Prilocaine	Dental anesthesia	Interstitial	400	Investigational	311,312
L-CsA	Cyclosporine	Bronchiolitis obliterans	Interstitial	40–50	Investigational	313,314
Telintra	TLK199 HCl	Myelodysplastic syndromes	Oral		Investigational	315

Abbreviations: L-MTP-PE, liposome-encapsulated muramyl tripeptide phosphatidylethanolamine; siRNA, small interfering ribonucleic acid.

such as instability, polydispersity, toxicity at repeated administration, and capability of inducing immunostimulation and complement activation. The precise control of liposome size and distribution can be optimized by new preparation methods, such as microfluidic-based methods and microfluidic remote loading (rapid single-step liposomal drug preparation). For pharmaceutical manufacturing and for quality-assurance assays, we can foresee progress in automation and control of processes of conventional liposomes as well as multifunctional liposomes. OECTs have been recently proposed for real-time monitoring of liposome-based structures.

The increase of complexity of liposomal formulation even more needs accurate *in vitro* and *in vivo* preclinical studies before transfer to the clinic. The analysis of physicochemical characteristics, toxicity, hemato-compatibility, delivery, and therapeutic efficiency is mandatory. Dialogue between scientists, clinicians, and industry is indispensable in the design phase of new liposomal formulations to increase the success rate for liposomes as nanomedical formulations.

Acknowledgments

We would like to thank Giuseppe Formisano for his technical assistance with the freeze-fracturing technique and Cosimo Curiano for the graphics (Figures 1–3).

Disclosure

The authors report no conflicts of interest in this work.

References

- Bangham AD, Horne RW. Negative staining of phospholipids and their structural modification by surface-active agents as observed in the electron microscope. *J Mol Biol.* 1964;8:660–668.
- Bangham AD, Hill MW, Miller NG. Preparation and use of liposomes as models of biological membranes. In: Korn ED, editor. *Methods in Membrane Biology*. Vol 1. New York: Plenum; 1974:1–68.
- Etheridge ML, Campbell SA, Erdman AG, Haynes CL, Wolf SM, McCullough J. The big picture on nanomedicine: the state of investigational and approved nanomedicine products. *Nanomedicine.* 2013;9:1–14.
- Felice B, Prabhakaran MP, Rodríguez AP, Ramakrishna S. Drug delivery vehicles on a nano-engineering perspective. *Mater Sci Eng C Mater Biol Appl.* 2014;41:178–195.
- Fanciullino R, Ciccolini J. Liposome-encapsulated anticancer drugs: still waiting for the magic bullet? *Curr Med Chem.* 2009;16:4361–4373.
- Fuliss LE, DuPont JA, Gratton S, DeSimone J. Imparting size, shape, and composition control of materials for nanomedicine. *Chem Soc Rev.* 2006;35:1095–1104.
- Papahadjopoulos D, Kimelberg HK. Phospholipid vesicles (liposomes) as models for biological membranes: their properties and interactions with cholesterol and proteins. In: *Progress in Surface Science*. Vol. Oxford: Pergamon; 1973:141–149.
- Frolov VA, Shnyrova AV, Zimmerberg J. Lipid polymorphisms and membrane shape. *Cold Spring Harb Perspect Biol.* 2011;3:a004747.
- Immordino ML, Dosio F, Cattel L. Stealth liposomes: review of the basic science, rationale, and clinical applications, existing and potential. *Int J Nanomedicine.* 2006;1:297–315.
- Betageri GV, Parsons DL. Drug encapsulation and release from multilamellar and unilamellar liposomes. *Int J Pharm.* 1992; 81:235–241.
- Niven RW, Speer M, Schreier H. Nebulization of liposomes. II. The effects of size and modeling of solute release profiles. *Pharm Res.* 1991;8: 217–221.
- Schechter E. Aspects structuraux et fonctionnels. In: Schechter E, Rossignol B, editors. *Biochimie et Biophysique des Membranes*. Paris: Dunod; 2002.
- Hosta-Rigau L, Zhang Y, Teo BM, Postma A, Städler B. Cholesterol – a biological compound as a building block in bionanotechnology. *Nano-scale.* 2013;5:89–109.
- Bitounis D, Fanciullino R, Iliadis A, Ciccolini J. Optimizing drugability through liposomal formulations: new approaches to an old concept. *ISRN Pharm.* 2012;2012:738432.
- Milla F, Dosio F, Cattel L. PEGylation of proteins and liposomes: a powerful and flexible strategy to improve the drug delivery. *Curr Drug Metab.* 2012;13:105–109.
- Gabizon A, Papahadjopoulos D. Liposome formulations with prolonged circulation time in blood and enhanced uptake by tumors. *Proc Natl Acad Sci U S A.* 1988;85:6949–6953.
- Allen TM. Long-circulating (Stealth) liposomes: therapeutic applications. In: Puisieux F, Couvreur P, Delattre J, Devissaguet JP, editors. *Liposomes: New Systems and New Trends in Their Applications*. Paris: Editions de Santé; 1995:125–155.
- Gómez-Hens A, Fernández-Romero JM. Analytical methods for the control of liposomal delivery systems. *Trends Analyt Chem.* 2006;25: 167–178.
- Mozafari MR, Johnson C, Hatziamoniou S, Demetzos C. Nanoliposomes and their applications in food nanotechnology. *J Liposome Res.* 2008;18: 309–327.
- Wagner A, Vorauer-Uhl K. Liposome technology for industrial purposes. *J Drug Deliv.* 2011;2011:591325.
- Bangham AD, Standish MM, Watkins JC. Diffusion of univalent ions across the lamellae of swollen phospholipids. *J Mol Biol.* 1965; 13: 238–252.
- New RC. Preparation of liposomes. In: New RC, editor. *Liposomes: A Practical Approach*. New York: Oxford University Press; 1990.
- Szoka F, Papahadjopoulos D. Procedure for preparation of liposomes with large internal aqueous space and high capture by reverse-phase evaporation. *Proc Natl Acad Sci U S A.* 1978;75:4194–4198.
- Batzri S, Korn ED. Single bilayer liposomes prepared without sonication. *Biochim Biophys Acta.* 1973;298:1015–1019.
- Deamer D, Bangham AD. Large volume liposomes by an ether vaporization method. *Biochim Biophys Acta.* 1976;443:629–634.
- Lasch J, Weissig V, Brandl M. Preparation of liposomes. In: Torchilin V, Weissig V, editors. *Liposomes: A Practical Approach*. New York: Oxford University Press; 2003.
- Brunner J, Skrabal P, Hausser H. Single bilayer vesicles prepared without sonication physicochemical properties. *Biochim Biophys Acta.* 1976;455:322–331.
- Kirby C, Gregoriadis G. Dehydration-rehydration vesicles: a simple method for high-yield drug entrapment in liposomes. *Nat Biotechnol.* 1984;2:979–984.
- Woodbury DJ, Richardson ES, Grigg AW, Welling RD, Knudson BH. Reducing liposome size with ultrasound: bimodal size distributions. *J Liposome Res.* 2006;16:57–80.
- Hope MJ, Bally MB, Webb G, Cullis PR. Production of large unilamellar vesicles by a rapid extrusion procedure – characterization of size distribution, trapped volume and ability to maintain a membrane-potential. *Biochim Biophys Acta.* 1985;812:55–65.
- Berger N, Sachse A, Bender J, Schubert B, Brandl M. Filter extrusion of liposomes using different devices: comparison of liposome size, encapsulation efficiency, and process characteristics. *Int J Pharm.* 2001; 223:55–68.
- MacDonald RC, MacDonald RI, Menco BP, Takeshita K, Subbarao NK, Hu LR. Small volume extrusion apparatus for preparation of large, unilamellar vesicles. *Biochim Biophys Acta.* 1991;1061:297–303.

33. Bachmann D, Brandl M, Gregoriadis G. Preparation of liposomes using a mini-lab 8.30 H high-pressure homogenizer. *Int J Pharm*. 1993;91:69–74.
34. Laouini A, Jaafar-Maalej C, Limayem-Blouza I, Silar S, Charcosset C, Fessi H. Preparation, characterization and applications of liposomes: state of the art. *J Colloid Sci Biotechnol*. 2012;1:147–168.
35. Stone HA, Stroock AD, Adjari A. Engineering flows in small devices: microfluidics toward a lab-on-a-chip. *Annu Rev Fluid Mech*. 2004;36:381–411.
36. Whitesides GM. The origins and the future of microfluidics. *Nature*. 2006;442:368–373.
37. Yu B, Lee RJ, Lee LJ. Microfluidic methods for production of liposomes. *Methods Enzymol*. 2009;465:129–141.
38. Hood RR, Vreeland WN, DeVoe DL. Microfluidic remote loading for rapid single-step liposomal drug preparation. *Lab Chip*. 2014;14:3359–3367.
39. Tarabeila G, Balducci AG, Coppède N, et al. Liposomes sensing and monitoring by organic electrochemical transistors integrated in microfluidics. *Biochim Biophys Acta*. 2013;1830:4374–4380.
40. Lasic DD. Magnetic resonance methods in the studies of liposomes. *Bull Magn Reson*. 1991;13:3–13.
41. Ostrovsky N. Liposome size measurements by photon correlation spectroscopy. *Chem Phys Lipids*. 1993;64:45–56.
42. Palmer AF, Wingert P, Nickels J. Atomic force microscopy and light scattering of small unilamellar actin-containing liposomes. *Biophys J*. 2003;85:1233–1247.
43. Grabielle-Madefmont C, Lesieur S, Ollivon M. Characterization of loaded liposomes by size exclusion chromatography. *J Biochem Biophys Methods*. 2003;56:189–217.
44. Moon MH, Giddings JC, Pharm J. Size distribution of liposomes by flow field-flow fractionation. *J Pharm Biomed Anal*. 1993;11:911–920.
45. Ruozi B, Belletti D, Tombesi A, et al. AFM, ESEM, TEM, and CLSM in liposomal characterization: a comparative study. *Int J Nanomedicine*. 2011;6:557–563.
46. Frederik PM, Hubert DH. Cryoelectron microscopy of liposomes. *Methods Enzymol*. 2005;391:431–448.
47. Jass J, Tjärnhage T, Pau G. Atomic force microscopy imaging of liposomes. *Methods Enzymol*. 1993;367:199–213.
48. Ruozi B, Tosi G, Forni F, et al. Atomic force microscopy and photon correlation spectroscopy: two techniques for rapid characterization of liposomes. *Eur J Pharm Sci*. 2005;25:81–89.
49. Ruysschaert T, Marque A, Duteyrat JL, Lesieur S, Winterhalter M, Fournier D. Liposome retention in size exclusion chromatography. *BMC Biotechnol*. 2005;10:5–11.
50. Korgel BA, Van Zanten JH, Monbouquette HG. Vesicle size distributions measured by flow field-flow fractionation coupled with multiangle light scattering. *Biophys J*. 1998;74:3264–3272.
51. Mohan A, Narayanan S, Sethuraman S, Krishnan UM. Novel resveratrol and 5-fluorouracil coencapsulated in pegylated nanoliposomes improve chemotherapeutic efficacy of combination against head and neck squamous cell carcinoma. *Biomed Res Int*. 2014;2014:424239.
52. Storm G, Roerdink FH, Steerenberg PA, de Jong WH, Crommelin DJ. Influence of lipid composition on the antitumor activity exerted by doxorubicin-containing liposomes in a rat solid tumor model. *Cancer Res*. 1987;47:3366–3372.
53. McIntosh TJ. The effect of cholesterol on the structure of phosphatidylcholine bilayers. *Biochim Biophys Acta*. 1978;513:43–58.
54. Cullis PR, Hope MJ. The bilayer stabilizing role of sphingomyelin in the presence of cholesterol: a 31P NMR study. *Biochim Biophys Acta*. 1980;597:533–542.
55. Defrise-Quertain F, Chatelain P, Delmelle M, et al. Model studies for drug entrapment and liposome stability. In: Gregoriadis G, editor. *Liposome Technology*. Boca Raton (FL): CRC; 1984:1–17.
56. Allen TM, Mehra T, Hansen C, Chiu YC. Stealth liposomes: an improved sustained release system for 1-beta-D-arabinofuranosylcytosine. *Cancer Res*. 1992;52:2431–2439.
57. Fahr A, van Hoogevest P, May S, Bergstrand N, Leigh ML. Transfer of lipophilic drugs between liposomal membranes and biological interfaces: consequences for drug delivery. *Eur J Pharm Sci*. 2005;26:251–265.
58. Mayer LD, Baily MB, Cullis PR. Uptake of adriamycin into large unilamellar vesicles in response to a pH gradient. *Biochim Biophys Acta*. 1986;857:123–126.
59. Forssten EA, Malé-Brune R, Adler-Moore JP, et al. Fluorescence imaging studies for the disposition of daunorubicin liposomes (DaunoXome) within tumor tissue. *Cancer Res*. 1996;56:2066–2075.
60. Johnston MJ, Edwards K, Karlsson G, et al. Influence of drug-to-lipid ratio on drug release properties and liposome integrity in liposomal doxorubicin formulations. *J Liposome Res*. 2008;18:145–157.
61. Drummond DC, Noble CO, Guo Z, Hong K, Park JW, Kirpotin DB. Development of a highly active nanoliposomal irinotecan using a novel intraliposomal stabilization strategy. *Cancer Res*. 2006;66:3271–3277.
62. Zhigaltsev IV, Winters G, Srinivasulu M, et al. Development of a weak-base docetaxel derivative that can be loaded into lipid nanoparticles. *J Control Release*. 2010;144:332–340.
63. Zamboni WC. Concept and clinical evaluation of carrier mediated anticancer agents. *Oncologist*. 2008;13:248–260.
64. Lasic DD. Novel applications of liposomes. *Trends Biotechnol*. 1998;16:307–321.
65. Silverman JA, Reynolds L, Deitcher SR. Pharmacokinetics and pharmacodynamics of vincristine sulfate liposome injection (VSLI) in adults with acute lymphoblastic leukemia. *J Clin Pharmacol*. 2013;53:1139–1145.
66. Moen MD, Lyseng-Williamson KA, Scott LJ. Liposomal amphotericin B: a review of its use as empirical therapy in febrile neutropenia and in the treatment of invasive fungal infections. *Drugs*. 2009;69:361–392.
67. Nasti TH, Khan MA, Owais M. Enhanced efficacy of pH sensitive nystatin liposomes against *Cryptococcus neoformans* in murine model. *J Antimicrob Chemother*. 2006;57:349–352.
68. Drummond DC, Meyer O, Hong K, Kirpotin DB, Papahadjopoulos D. Optimizing liposomes for delivery of chemotherapeutic agents to solid tumors. *Pharmacol Rev*. 1999;51:691–743.
69. Lao J, Madani J, Puértolas T, et al. Liposomal doxorubicin in the treatment of breast cancer patients: a review. *J Drug Deliv*. 2013;2013:456409.
70. Rafiqyath SM, Rasul M, Lee B, Wei G, Lamba G, Liu D. Comparison of safety and toxicity of liposomal doxorubicin vs. conventional anthracyclines: a meta-analysis. *Exp Hematol Oncol*. 2012;1:10.
71. Pisano C, Cecere SC, Di Napoli M, et al. Clinical trials with pegylated liposomal doxorubicin in the treatment of ovarian cancer. *J Drug Deliv*. 2013;2013:898146.
72. Gordon AN, Granai CO, Rose PG, et al. Phase II study of liposomal doxorubicin in platinum- and paclitaxel-refractory epithelial ovarian cancer. *J Clin Oncol*. 2009;18:3093–3100.
73. Katsumata N, Fujiwara Y, Kamura T, et al. Phase II clinical trial of pegylated liposomal doxorubicin (JNS002) in Japanese patients with mullerian carcinoma (epithelial ovarian carcinoma, primary carcinoma of fallopian tube, peritoneal carcinoma) having a therapeutic history of platinum-based chemotherapy: a phase II study of the Japanese Gynecologic Oncology Group. *Jpn J Clin Oncol*. 2008;38:777–785.
74. Markman M, Kennedy A, Webster K, Peterson G, Kulp B, Belinson J. Phase 2 trial of liposomal doxorubicin (40 mg/m²) in platinum/paclitaxel-refractory ovarian and fallopian tube cancers and primary carcinoma of the peritoneum. *Gynecol Oncol*. 2000;78:369–372.
75. Lotem M, Hubert A, Lyass O, et al. Skin toxic effects of polyethylene glycol-coated liposomal doxorubicin. *Arch Dermatol*. 2000;136:1475–1480.
76. Alberts DS, Muggia FM, Carmichael J, et al. Efficacy and safety of liposomal anthracyclines in phase I/II clinical trials. *Semin Oncol*. 2004;31:53–90.
77. Gabizon AA. Liposomal anthracyclines. *Hematol Oncol Clin North Am*. 1994;8:431–450.

78. Von Hoff DD, Layard MW, Basa P, et al. Risk factors for doxorubicin-induced congestive heart failure. *Ann Intern Med.* 1979;91:710-717.
79. Batist G, Ramakrishnan G, Rao CS, et al. Reduced cardiotoxicity and preserved antitumor efficacy of liposome-encapsulated doxorubicin and cyclophosphamide compared with conventional doxorubicin and cyclophosphamide in a randomized, multicenter trial of metastatic breast cancer. *J Clin Oncol.* 2001;19:1444-1454.
80. O'Brien ME, Wigler N, Inbar M, et al. Reduced cardiotoxicity and comparable efficacy in a phase III trial of pegylated liposomal doxorubicin HCl (CAELYX/Doxil) versus conventional doxorubicin for first-line treatment of metastatic breast cancer. *Ann Oncol.* 2004;15:440-449.
81. Gabizon AA, Lyass O, Berry GJ, Wildgust M. Cardiac safety of pegylated liposomal doxorubicin (Doxil/Caelyx) demonstrated by endomyocardial biopsy in patients with advanced malignancies. *Cancer Invest.* 2004;22:663-669.
82. Mustafa MH. Decreased risk of cardiotoxicity with long-term use of Doxil/Caelyx at high lifetime cumulative doses in patients with AIDS-related Kaposi/Es sarcoma (KS). Poster presented at: ASCO Annual Meeting 2001; May 12-15, 2001; San Francisco, CA.
83. Andreopoulou E, Gaiotti D, Kim E, et al. Pegylated liposomal doxorubicin HCl (PLD; Caelyx/Doxily) experience with long-term maintenance in responding patients with recurrent epithelial ovarian cancer. *Ann Oncol.* 2007;18:716-721.
84. Torchilin V. Tumor delivery of macromolecular drugs based on the EPR effect. *Adv Drug Deliv Rev.* 2011;63:131-135.
85. Hashizume H, Balak P, Morikawa S, et al. Openings between defective endothelial cells explain tumor vessel leakiness. *Am J Pathol.* 2000;156:1363-1380.
86. Yuan F, DeLian M, Fukumura D, et al. Vascular permeability in a human tumor xenograft: molecular size dependence and cutoff size. *Cancer Res.* 1995;55:3752-3756.
87. Brown S, Khan DR. The treatment of breast cancer using liposome technology. *J Drug Deliv.* 2012;2012:212965.
88. Roberts WG, Delaat I, Nagane M, Huang S, Cavenee WK, Palade GE. Host microvasculature influence on tumor vascular morphology and endothelial gene expression. *Am J Pathol.* 1998;153:1239-1248.
89. O'Neal DP, Hirsch LR, Halas NJ, Payne JD, West JL. Photo-thermal tumor ablation in mice using near infrared-absorbing nanoparticles. *Cancer Lett.* 2004;209:171-176.
90. Woodle MC, Matthay KK, Newman MS, et al. Versatility in lipid compositions showing prolonged circulation with sterically stabilized liposomes. *Biochim Biophys Acta.* 1992;1105:193-200.
91. Gabizon A, Shmeeda H, Barenholz Y. Pharmacokinetics of PEGylated liposomal doxorubicin: review of animal and human studies. *Clin Pharmacokinet.* 2003;42:419-436.
92. Ishida T, Harashima H, Kiwada H. Liposome clearance. *Biosci Rep.* 2002;22:197-224.
93. Sempie SC, Harasym TO, Clow KA, Anselmi SM, Klimuk SK, Hope MJ. Immunogenicity and rapid blood clearance of liposomes containing polyethylene glycol-lipid conjugates and nucleic acid. *J Pharmacol Exp Ther.* 2005;312:1026-1026.
94. Gabizon AA, Shmeeda H, Zalipsky S. Pros and cons of the liposome platform in cancer drug targeting. *J Liposome Res.* 2006;16:175-183.
95. Daemen T, Hofstede G, Ten Kate MT, Bakker-Woudenberg JA, Scherphof GL. Liposomal doxorubicin-induced toxicity: depletion and impairment of phagocytic activity of liver macrophages. *Int J Cancer.* 1995;61:716-721.
96. Juliano RL, Stamp D. Pharmacokinetics of liposome-encapsulated anti-tumor drugs. Studies with vinblastine, actinomycin D, cytosine arabinoside, and daunomycin. *Biochem Pharmacol.* 1978;27:21-27.
97. Gabizon AA. Stealth liposomes and tumor targeting: one step further in the quest for the magic bullet. *Clin Cancer Res.* 2001;7:223-225.
98. Bedu-Addo FK, Tang P, Xu Y, Huang L. Effects of polyethyleneglycol chain length and phospholipid acyl chain composition on the interaction of polyethyleneglycol-phospholipid conjugates with phospholipid: implications in liposomal drug delivery. *Pharm Res.* 1996;13:710-717.
99. Photos PI, Bacakova L, Discher B, Bates FS, Discher DE. Polymer vesicles in vivo: correlations with PEG molecular weight. *J Control Release.* 2003;90:323-334.
100. Harris JM, editor. *Poly(Ethylene Glycol) Chemistry: Biotechnical and Biomedical Applications.* New York: Plenum;1992.
101. Graf R, Domb A, Quellec P, et al. The controlled intravenous delivery of drugs using PEG-coated sterically stabilized microspheres. *Adv Drug Deliv Rev.* 1995;16:215-233.
102. Moghimi SM, Hedeman H, Muir IS, Illum L, Davis SS. An investigation of the filtration capacity and the fate of large filtered sterically-stabilized microspheres in rat spleen. *Biochim Biophys Acta.* 1993;1157:233-240.
103. Harris JM, Martin NE, Modi M. PEGylation: a novel process for modifying pharmacokinetics. *Clin Pharmacokinet.* 2001;40:539-551.
104. Wu H, Ramanathan RK, Zamboni BA, et al. Population pharmacokinetics of PEGylated liposomal CKD-602 (S-CKD602) in patients with advanced malignancies. *J Clin Pharmacol.* 2011;52:180-194.
105. Heyes J, Hall K, Taylor V, Lenz R, MacLachlan I. Synthesis and characterization of novel poly(ethylene glycol)-lipid conjugates suitable for use in drug delivery. *J Control Release.* 2006;112:280-290.
106. Allen TM. Liposomes. Opportunities in drug delivery. *Drugs.* 1997;54:8-14.
107. Gabizon AA. PEGylated liposomal doxorubicin: metamorphosis of an old drug into a new form of chemotherapy. *Cancer Invest.* 2001;19:424-436.
108. Dawidczyk CM, Kim C, Park JH, et al. State-of-the-art in design rules for drug delivery platforms: lessons learned from FDA-approved nanomedicines. *J Control Release.* 2014;187:133-144.
109. Andresen TL, Jensen SS, Jørgensen K. Advanced strategies in liposomal cancer therapy: problems and prospects of active and tumor specific drug release. *Prog Lipid Res.* 2005;44:68-97.
110. Barenholz Y. Liposome application: problems and prospects. *Curr Opin Colloid Interface Sci.* 2011;6:66-77.
111. Bandak S, Goren D, Horowitz A, Tzemach D, Gabizon A. Pharmacological studies of cisplatin encapsulated in long-circulating liposomes in mouse tumor models. *Anticancer Drugs.* 1999;10:911-920.
112. Asai T, Oku N. Angiogenic vessel-targeting DDS by liposomalized oligopeptides. *Methods Mol Biol.* 2010;605:335-347.
113. Gabizon A, Tzemach D, Gorin J, et al. Improved therapeutic activity of folate-targeted liposomal doxorubicin in folate receptor-expressing tumor models. *Cancer Chemother Pharmacol.* 2010;66:43-52.
114. Garg A, Tisdale AW, Haidari E, Kakkoli E. Targeting colon cancer cells using PEGylated liposomes modified with a fibronectin-mimetic peptide. *Int J Pharm.* 2009;366:201-210.
115. Vingerhoeds MHJ, Haisma HJ, van Muijen M, van de Rijt RB, Crommelin DJ, Storm G. A new application for liposomes in cancer therapy. Immunoliposomes bearing enzymes (immuno-enzymosomes) for site-specific activation of prodrugs. *FEBS Lett.* 1993;336:485-490.
116. Noble GT, Stefaniek JF, Ashley JD, Kiziltepe T, Bilgicler B. Ligand-targeted liposome design: challenges and fundamental considerations. *Trends Biotechnol.* 2014;32:32-45.
117. Fanciullino R, Giacomelli S, Aubert C, et al. Development of stealth liposome formulation of 2'-deoxyinosine as 5-fluorouracil modulator: in vitro and in vivo study. *Pharm Res.* 2005;22:2051-2057.
118. Senior JH, Trimble KR, Maskiewicz R. Interaction of positively charged liposomes with blood: implications for their application in vivo. *Biochim Biophys Acta.* 1991;1070:173-179.
119. Zhao W, Zhuang S, Qi KR. Comparative study of the in vitro and in vivo characteristics of cationic and neutral liposomes. *Int J Nanomedicine.* 2011;6:3087-3098.
120. Harashima H, Matsuo H, Kiwada H. Identification of proteins mediating clearance of liposomes using a liver perfusion system. *Adv Drug Delivery Rev.* 1998;32:61-79.
121. Miller CR, Bondurant B, McLean SD, McGovern KA, O'Brien DF. Liposome-cell interactions in vitro: effect of liposome surface charge on the binding and endocytosis of conventional and sterically stabilized liposomes. *Biochemistry.* 1998;37:12875-12883.

122. Cullis PR, Chonn A, Semple SC. Interactions of liposome and lipid-based carrier systems with blood proteins: relation to clearance behavior in vivo. *Adv Drug Delivery Rev.* 1998;32:3-17.
123. Campbell PI. Toxicity of some charged lipids used in liposome preparations. *Cytobios.* 1983;37:21-26.
124. Allison AG, Gregoriadis G. Liposomes as immunological adjuvants. *Nature.* 1974;252:252.
125. Nakanishi T, Kimisawa J, Hayashi A, et al. Positively charged liposome functions as an efficient immunoadjuvant in inducing cell-mediated immune response to soluble proteins. *J Control Release.* 1999;61:233-240.
126. Afrin F, Rajesh R, Anam K, Gopinath M, Pal S, Ali N. Characterization of *Leishmania donovani* antigens encapsulated in liposomes that induce protective immunity in BALB/c mice. *Infect Immun.* 2002;70:6697-6706.
127. Badiee A, Jaafari MR, Khamesipour A, et al. The role of liposome charge on immune response generated in BALB/c mice immunized with recombinant major surface glycoprotein of *Leishmania* (rgp63). *Exp Parasitol.* 2009;121:362-369.
128. González-Rodríguez ML, Rabasco AM. Charged liposomes as carriers to enhance the permeation through the skin. *Expert Opin Drug Deliv.* 2011;8:857-871.
129. Ogiso T, Yamaguchi T, Iwaki M, Tanino T, Miyake Y. Effect of positively and negatively charged liposomes on skin permeation of drugs. *Drug Target.* 2001;9:49-59.
130. Felgner PL, Gadek TR, Holm M, et al. Lipofection: a highly efficient lipid-mediated DNA transfection procedure. *Proc Natl Acad Sci U S A.* 1987;84:7413-7417.
131. Bombelli C, Caracciolo G, Di Profio P, et al. Inclusion of a photosensitizer in liposomes formed by DMPC/gemini surfactant: correlation between physicochemical and biological features of the complexes. *J Med Chem.* 2005;48:4882-4891.
132. Strieth S, Eichhorn ME, Sauer B, et al. Neovascular targeting chemotherapy: encapsulation of paclitaxel in cationic liposomes impairs functional tumor microvasculature. *Int J Cancer.* 2004;110:117-124.
133. Wu J, Lee A, Lu Y, Lee RJ. Vascular targeting of doxorubicin using cationic liposomes. *Int J Pharma.* 2007;337:329-335.
134. Campbell RB, Fukumura D, Brown EB, et al. Cationic charge determines the distribution of liposomes between the vascular and extravascular compartments of tumors. *Cancer Res.* 2002;62:6831-6836.
135. Campbell RB, Ying B, Kuesters GM, Hemphill R. Fighting cancer: from the bench to bedside using second generation cationic liposomal therapeutics. *J Pharm Sci.* 2009;98:411-429.
136. Schnyder A, Huwyler J. Drug transport to brain with targeted liposomes. *NeuroRx.* 2005;2:99-107.
137. Krasnici S, Werner A, Eichhorn ME, et al. Effect of the surface charge of liposomes on their uptake by angiogenic tumor vessels. *Int J Cancer.* 2003;105:561-567.
138. Stamatatos L, Leventis R, Zuckermann MJ, Silvius JR. Interactions of cationic lipid vesicles with negatively charged phospholipid vesicles and biological membranes. *Biochemistry.* 1988;27:3917-3925.
139. Litzinger DC, Brown JM, Wala I, et al. Fate of cationic liposomes and their complex with oligonucleotide in vivo. *Biochim Biophys Acta.* 1996;1281:139-149.
140. McLean JW, Fox EA, Bahuk P, et al. Organ-specific endothelial cell uptake of cationic liposome-DNA complexes in mice. *Am J Physiol.* 1997;273:H387-H404.
141. Dass CR. Improving anti-angiogenic therapy via selective delivery of cationic liposomes to tumour vasculature. *Int J Pharm.* 2003;267:1-12.
142. Meyer O, Kirpotin D, Hong K, et al. Cationic liposomes coated with polyethylene glycol as carriers for oligonucleotides. *J Biol Chem.* 1998;273:15621-15627.
143. Gursel I, Gursel M, Ishii KJ, Klinman DM. Sterically stabilized cationic liposomes improve the uptake and immunostimulatory activity of CpG oligonucleotides. *J Immunol.* 2001;167:3324-3328.
144. Skupin-Mrugalska P, Piskorz J, Goslinski T, Mielcarek J, Konopka K, Düzgünes N. Current status of liposomal porphyrinoid photosensitizers. *Drug Discov Today.* 2013;18:776-784.
145. Molinari A, Bombelli C, Mannino S, et al. m-TRPC-mediated photodynamic therapy of malignant gliomas: assessment of a new transfection strategy. *Int J Cancer.* 2007;121:1149-1155.
146. Bombelli C, Stringaro A, Borozzi S, et al. Efficiency of liposomes in the delivery of a photosensitizer controlled by the stereochemistry of a gemini surfactant component. *Mol Pharm.* 2010;7:130-137.
147. Torchilin V. Multifunctional and stimuli-sensitive pharmaceutical nanocarriers. *Eur J Pharm Biopharm.* 2009;71:431-444.
148. Perche F, Torchilin VP. Recent trends in multifunctional liposomal nanocarriers for enhanced tumor targeting. *J Drug Deliv.* 2013;2013:705265.
149. Gullino PM, Grantham FH, Smith SH, Haggerty AC. Modifications of the acid-base status of the internal milieu of tumors. *J Natl Cancer Inst.* 1965;34:857-869.
150. Simões S, Moreira JN, Fonseca C, Düzgünes N, de Lima MC. On the formulation of pH-sensitive liposomes with long circulation times. *Adv Drug Deliv Rev.* 2004;56:947-965.
151. Caldeira de Araújo Lopes S, Vinícius Melo Novais M, Salviano Teixeira C, et al. Preparation, physicochemical characterization, and cell viability evaluation of long-circulating and pH-sensitive liposomes containing ursolic acid. *Biomed Res Int.* 2013;2013:467147.
152. Ong W, Yang Y, Cruciano AC, McCarley RL. Redox-triggered contents release from liposomes. *J Am Chem Soc.* 2008;130:14739-14744.
153. Yatvin MB, Weinstein JN, Dennis WH, Blumenthal R. Design of liposomes for enhanced local release of drugs by hyperthermia. *Science.* 1978;202:1290-1293.
154. Needham D, Dewhurst MW. The development and testing of a new temperature-sensitive drug delivery system for the treatment of solid tumors. *Adv Drug Deliv Rev.* 2001;53:285-305.
155. Li L, ten Hagen TL, Schipper D, et al. Triggered content release from optimized stealth thermosensitive liposomes using mild hyperthermia. *J Control Release.* 2010;143:274-279.
156. Kong G, Anyarambhata G, Petros WP, et al. Efficacy of liposomes and hyperthermia in a human tumor xenograft model: importance of triggered drug release. *Cancer Res.* 2000;60:6950-6957.
157. Thanou M, Gedroyc W. MRI-guided focused ultrasound as a new method of drug delivery. *J Drug Deliv.* 2013;2013:616197.
158. Evans E, Needham D. Physical properties of surfactant bilayer membranes: thermal transitions, elasticity, rigidity, cohesion, and colloidal interactions. *J Phys Chem.* 1987;91:4219-4228.
159. Kono K. Thermosensitive polymer-modified liposomes. *Adv Drug Deliv Rev.* 2001;53:307-319.
160. Gasselhuber A, Dröher MR, Negussie A, Wood BJ, Rattay F, Haemmerich D. Mathematical spatio-temporal model of drug delivery from low temperature sensitive liposomes during radiofrequency tumour ablation. *Int J Hyperthermia.* 2010;26:499-513.
161. Foon RT, Borys N. Lyso-thermosensitive liposomal doxorubicin: a novel approach to enhance efficacy of thermal ablation of liver cancer. *Expert Opin Pharmacother.* 2009;10:333-343.
162. Dromi S, Frenkel V, Luk A, et al. Pulsed-high intensity focused ultrasound and low temperature-sensitive liposomes for enhanced targeted drug delivery and antitumor effect. *Clin Cancer Res.* 2007;13:2722-2727.
163. Hauck ML, LaRue SM, Petros WP, et al. Phase I trial of doxorubicin-containing low temperature sensitive liposomes in spontaneous canine tumors. *Clin Cancer Res.* 2006;12:4004-4010.
164. Kheirrolomoom A, Lai CY, Tam SM, et al. Complete regression of local cancer using temperature-sensitive liposomes combined with ultrasound-mediated hyperthermia. *J Control Release.* 2013;172:266-273.
165. Wang LS, Chuang MC, Ho JA. Nanotheranostics - a review of recent publications. *Int J Nanomedicine.* 2012;7:4679-4695.
166. Sumer B, Gao J. Theranostic nanomedicine for cancer. *Nanomedicine (Lond).* 2008;3:37-140.
167. Deveza L, Choi J, Yang F. Therapeutic angiogenesis for treating cardiovascular diseases. *Theranostics.* 2012;2:801-814.
168. Janib SM, Moses AS, MacKay JA. Imaging and drug delivery using theranostic nanoparticles. *Adv Drug Deliv Rev.* 2010;2:1052-1063.

169. Yu MK, Park J, Jon S. Targeting strategies for multifunctional nanoparticles in cancer imaging and therapy. *Theranostics*. 2012;2:3–44.
170. Xie J, Lee S, Chen X. Nanoparticle-based theranostic agents. *Adv Drug Deliv Rev*. 2010;62:1064–1079.
171. Ye Y, Chen X. Integrin targeting for tumor optical imaging. *Theranostics*. 2011;1:102–126.
172. Al-Jamal WT, Kostarelos K. Liposome-nanoparticle hybrids for multimodal diagnostic and therapeutic applications. *Nanomedicine (Lond)*. 2007;2:85–98.
173. Al-Jamal WT, Kostarelos K. Liposomes: from a clinically established drug delivery system to a nanoparticle platform for theranostic nanomedicine. *Acc Chem Res*. 2011;44:1094–1104.
174. Nie Y, Ji L, Ding H, et al. Cholesterol derivatives based charged liposomes for doxorubicin delivery: preparation, in vitro and in vivo characterization. *Theranostics*. 2012;2:1092–1103.
175. Leung SJ, Romanowski M. Light-activated content release from liposomes. *Theranostics*. 2012;2:1020–1036.
176. Torchilin VP. Recent advances with liposomes as pharmaceutical carriers. *Nat Rev Drug Discov*. 2005;4:145–160.
177. Papahadjopoulos D, Allen TM, Gabizon A, et al. Sterically stabilized liposomes – improvements in pharmacokinetics and anti-tumor therapeutic efficacy. *Proc Natl Acad Sci U S A*. 1991;88:11460–11464.
178. Al-Jamal WT, Al-Jamal KT, Tian B, et al. Lipid-quantum dot bilayer vesicles enhance tumor cell uptake and retention in vitro and in vivo. *ACS Nano*. 2008;2:408–418.
179. Soenen SJ, Vande Veide G, Ketkar-Atre A, Himmelreich U, De Cuyper M. Magnetoliposomes as magnetic resonance imaging contrast agents. *Wiley Interdiscip Rev Nanomed Nanobiotechnol*. 2011;3:197–211.
180. Kamaly N, Miller AD. Paramagnetic liposome nanoparticles for cellular and tumour imaging. *Int J Mol Sci*. 2010;11:1759–1776.
181. Li S, Goins B, Zhang L, Bao A. Novel multifunctional theranostic liposome drug delivery system: construction, characterization, and multimodality MR, near-infrared fluorescent, and nuclear imaging. *Bioconjug Chem*. 2012;23:1322–1332.
182. Muthu MS, Kulkarni SA, Raju A, Feng SS. Theranostic liposomes of TPGS coating for targeted co-delivery of docetaxel and quantum dots. *Biomaterials*. 2012;33:3494–3501.
183. Wen CJ, Zhang LW, Al-Suwayeh SA, Yen TC, Fang JY. Theranostic liposomes loaded with quantum dots and apomorphine for brain targeting and bioimaging. *Int J Nanomedicine*. 2012;7:1599–1611.
184. Wen CJ, Sung CT, Aljuffali IA, Huang YJ, Fang JY. Nanocomposite liposomes containing quantum dots and anticancer drugs for bioimaging and therapeutic delivery: a comparison of cationic, PEGylated and deformable liposomes. *Nanotechnology*. 2013;24:325101.
185. Smith B, Lyakhov I, Loomis K, et al. Hyperthermia-triggered intracellular delivery of anticancer agent to HER2(+) cells by HER2-specific antibody (ZHER2-GS-Cys)-conjugated thermosensitive liposomes (HER2(+) affisomes). *J Control Release*. 2011;153:187–194.
186. Löfdahl J, Feldwisch J, Tolmachev V, Carlsson J, Ståhl S, Frejd FY. Antibody molecules: engineered proteins for therapeutic, diagnostic and biotechnological applications. *FEBS Lett*. 2010;584:2670–1680.
187. Svenson S. Theranostics: are we there yet? *Mol Pharm*. 2013;10:848–856.
188. Barenholz Y. Doxil® – the first FDA-approved nano-drug: lessons learned. *J Control Release*. 2012;160:117–134.
189. Chang HJ, Yeh MK. Clinical development of liposome-based drugs: formulation, characterization, and therapeutic efficacy. *Int J Nanomedicine*. 2012;7:49–60.
190. Mross K, Niemann B, Massing U, et al. Pharmacokinetics of liposomal doxorubicin (ILC-D99; Myocet) in patients with solid tumors: an open-label, single-dose study. *Cancer Chemother Pharmacol*. 2004;54:514–524.
191. Stegmann T, Morselt HW, Booy FP, van Breemen JF, Scherphof G, Wilschut J. Functional reconstitution of influenza virus envelopes. *EMBO J*. 1987;6:2651–2659.
192. Glöck R, Mischler R, Brantschen S, Just M, Althaus B, Cryz SJ Jr. Immunopotentiating reconstituted influenza virus virosome vaccine delivery system for immunization against hepatitis A. *J Clin Invest*. 1992;90:2491–2495.
193. Shaji J, Patole V. Protein and peptide drug delivery: oral approaches. *Indian J Pharm Sci*. 2008;70:269–277.
194. Löhr JM, Haas SL, Bechstein WO, et al. Cationic liposomal paclitaxel plus gemcitabine or gemcitabine alone in patients with advanced pancreatic cancer: a randomized controlled phase II trial. *Ann Oncol*. 2012;23:1214–1222.
195. White SC, Lorigan P, Margison GP, et al. Phase II study of SPI-77 (sterically stabilized liposomal cisplatin) in advanced non-small-cell lung cancer. *Br J Cancer*. 2006;95:822–828.
196. Booser DJ, Esteva FJ, Rivera E, et al. Phase II study of liposomal irinotecan in the treatment of doxorubicin-resistant breast cancer. *Cancer Chemother Pharmacol*. 2002;50:6–8.
197. Wagner V, Dullaart A, Bock AK, Zweck A. The emerging nanomedicine landscape. *Nat Biotechnol*. 2006;24:1211–1218.
198. Bawa R. Nanoparticle-based therapeutics in humans: a survey. *NLB*. 2008;5:135–155.
199. Faraji AH, Wipf P. Nanoparticles in cellular drug delivery. *Bioorg Med Chem*. 2009;17:2950–2962.
200. Sigma-Tau Pharmaceuticals, Inc. – Products (Website). Available from: http://www.sigmatau.com/products/abelcet_rx.asp. Accessed Sep 04, 2013.
201. Ambisome (amphotericin B) liposome for injection (Website). Available from: <http://www.ambisome.com/>. Accessed Sep 03, 2013.
202. Tollefmar J, Ringden O. Lipid formulations of amphotericin B. Less toxicity but at what economic cost? *Drug Saf*. 1995;13:207–218.
203. Samaritan Pharmaceuticals (Website). Available from: <http://www.samaritanpharma.com/amphocil/>. Accessed Sep 03, 2013.
204. Griese N, Blaschke G, Boos J, Hempel G. Determination of free and liposome-associated daunorubicin and daunorubicinol in plasma by capillary electrophoresis. *J Chromatogr A*. 2002;979:379–388.
205. DaunoXome (Website). Available from: <http://daunoxome.com/>. Accessed Sep 05, 2013.
206. Bao A, Goins B, Klipper R, Negrato G, Phillips WT. Direct ^{99m}Tc labeling of pegylated liposomal doxorubicin (Doxil) for pharmacokinetic and non-invasive imaging studies. *J Pharmacol Exp Ther*. 2004;308:419–425.
207. Doxil (Website). Available from: <http://www.doxil.com/>. Accessed Sep 05, 2013.
208. Visudyne (Website). Available from: <http://www.visudyne.com/>. Accessed Sep 05, 2013.
209. Muggia FM. Liposomal encapsulated anthracyclines: new therapeutic horizons. *Curr Oncol Rep*. 2001;3:156–162.
210. TLC – Product (Website). Cited: 2011 Mar 31. Available from: <http://www.ticbio.com/en/product.html>
211. Cruccell (Website). Available from: <http://www.cruccell.com/Products>. Accessed Oct 2, 2013.
212. Patil SD, Burgess DJ. Liposomes, design and manufacturing. In: Burgess DJ, editor. *Injectable Dispersed Systems: Formulation, Processing and Performance (Drugs and The Pharmaceutical Sciences Series)*. New York: Marcel Dekker; 2005:249–303.
213. Pacira Pharmaceuticals, INC – Products (Website). Cited: 2013 Sep 3. Available from: <http://www.pacira.com/products/depodar.php>
214. NCT00002742. Antifungal therapy for fever and neutropenia in patients receiving treatment for hematologic cancer (Clinical Trial). ClinicalTrials.gov.
215. Moribe K, Maruyama K. Pharmaceutical design of the liposomal antimicrobial agents for infectious disease. *Curr Pharm Des*. 2002;8:441–454.
216. NCT00364676. Study of Vinorelbine liposomes injection for advanced solid tumors, non Hodgkin's lymphoma or Hodgkin's disease (Clinical Trial). ClinicalTrials.gov.
217. Talon Therapeutics, Inc. (Website). Talon product portfolio. Available from: <http://www.talonx.com/pipeline.php>. Accessed Sep 03, 2013.

218. NCT01652859. An bioequivalence study to compare two 2 mg/mL liposomal Amphotericin B injections in healthy subjects (Clinical Trial). ClinicalTrials.gov.
219. NCT00643199. A safety and effectiveness study of aroplatin in patients with advanced colorectal cancer resistant to standard therapies (Clinical Trial). ClinicalTrials.gov.
220. Lu C, Perez-Soler R, Piperdi B, et al. Phase II study of a liposome-entrapped cisplatin analog (L-NDDP) administered intrapleurally and pathologic response rates in patients with malignant pleural mesothelioma. *J Clin Oncol*. 2005;23:3495-3501.
221. Dragovich T, Mendelson D, Kurtin S, Richardson K, Von Hoff D, Hoos A. A Phase 2 trial of the liposomal DACH platinum L-NDDP in patients with therapy-refractory advanced colorectal cancer. *Cancer Chemother Pharmacol*. 2006;58:759-764.
222. NCT01041235. Safety study of a liposomal docetaxel formulation in patients with solid tumors who have failed previous therapies (Clinical Trial). ClinicalTrials.gov.
223. Azaya Therapeutics Products (Website). Available from: <http://www.azayatherapeutics.com/about-us/products>. Accessed Sep 06, 2013.
224. NCT00605969. Liposomal tretinoin in treating patients with recurrent or refractory Hodgkin's disease (Clinical Trial). ClinicalTrials.gov.
225. Manconi M, Sinico C, Valenti D, Loy G, Fadda AM. Niosomes as carriers for tretinoin-Preparation and properties. *Int J Pharm*. 2002;34:237-248.
226. Ateku M, Schulz P, Keil O, et al. A10027, a liposomal small interfering RNA formulation targeting protein kinase N3, inhibits cancer progression. *Cancer Res*. 2008;68:9788.
227. Li L, Shen Y. Overcoming obstacles to develop effective and safe siRNA therapeutics. *Expert Opin Biol Ther*. 2009;9:609-619.
228. Silence Therapeutics (Website). Available from: <http://silence-therapeutics.com/pipeline/pre-clinical-development/>. Accessed Sep 06, 2013.
229. NCT00245297. Study of the efficacy of human recombinant factor VIII (Kogenate FS) reconstituted in pegylated liposomes (Clinical Trial). ClinicalTrials.gov.
230. Powell J, Nugent D, Harrison J, et al. Safety and pharmacokinetics of a recombinant factor VIII with pegylated liposomes in severe hemophilia A. *J Thromb Haemost*. 2008;6:277-283.
231. NCT01159028. Clinical trial of L-Grb-2 antisense oligonucleotide in CML, AML, ALL and MDS (Clinical Trial). ClinicalTrials.gov.
232. Bio-Path Holdings, Inc (Website). Available from: <http://www.bio-pathholdings.com/pdf/factsheetv1.pdf>. Accessed Sep 06, 2013.
233. NCT00765973. Topotecan liposomes injection for small cell lung cancer (SCLC), ovarian cancer and other advanced solid tumors (Clinical Trial). ClinicalTrials.gov.
234. NCT00361842. Multicenter study Of CPX-1 (irinotecan HCl: Floxuridine) liposome injection in patients with advanced colorectal cancer (Clinical Trial). ClinicalTrials.gov.
235. Mayer LD, Janoff AS. Optimizing combination chemotherapy by controlling drug ratios. *Mol Interv*. 2007;7:216-223.
236. NCT00875693. A novel sequential treatment of salvage and reduced intensity conditioning (RIC) chemotherapy for allogeneic stem-cell transplantation (SCT) for primary refractory and relapsed acute myelogenous leukemia (AML) (Clinical Trial). ClinicalTrials.gov.
237. NCT00968604. C-VISA BikDD: liposome in advanced pancreatic cancer (Clinical Trial). ClinicalTrials.gov.
238. Xie X, Xia W, Li Z, et al. Targeted expression of BikDD eradicates pancreatic tumors in noninvasive imaging models. *Cancer Cell*. 2007;12:52.
239. Matsumura Y. Preclinical and clinical studies of anticancer drug-incorporated polymeric micelles. *J Drug Target*. 2007;15:507-517.
240. Thurston G, McLean JW, Rizen M, Baluk P, Haskell A, Murphy TJ, et al. Cationic liposomes target angiogenic endothelial cells in tumors and chronic inflammation in mice. *J Clin Invest*. 1998;101:1401-1413.
241. NCT00364143. Safety study of IHL-305 (Irinotecan Liposome Injection) to treat advanced solid tumors (Clinical Trial). ClinicalTrials.gov.
242. NCT00059605. Phase I study of IV DOTAP: cholesterol-Fusi in non-small-cell lung cancer (Clinical Trial). ClinicalTrials.gov.
243. NCT00860522. JVR5-100 for the treatment of patients with relapsed or refractory leukemia (Clinical Trial). ClinicalTrials.gov.
244. Chang S, Warner J, Liang L, Fairman J. A novel vaccine adjuvant for recombinant flu antigens. *Biologicals*. 2009;37:141-147.
245. NCT00721063. Study of Liposomal Amphotericin in Patients With Refractory or Relapsed Acute Lymphocytic Leukemia (Clinical Trial). ClinicalTrials.gov.
246. Booser DJ, Esteve FX, Rivera E, et al. Phase II study of liposomal amphotericin in the treatment of doxorubicin-resistant breast cancer. *Cancer Chemother Pharmacol*. 2002;50:6-8.
247. Neopharm, Inc. Products -- Neopharm (Website). Available from: www.neopharm.com/products/. Accessed Sep 06, 2013.
248. NCT00024492. Study of Liposome Encapsulated Mitoxantrone (LEM) in Patients With Advanced Cancer (Clinical Trial). ClinicalTrials.gov.
249. NCT01190982. Efficacy and safety study of LEP-ETU to treat metastatic breast cancer (Clinical Trial). ClinicalTrials.gov.
250. Zhang JA, Anyarambhatla G, Ma L, et al. Development and characterization of a novel Cremophor EL free liposome-based paclitaxel (LEP-ETU) formulation. *Eur J Pharm Biopharm*. 2005;59:177-187.
251. NCT00024648. Study to determine maximum tolerated dose of LerafAON combined with radiotherapy in patients with advanced malignancies (Clinical Trial). ClinicalTrials.gov.
252. NCT00035867. Study of TLK199 HCl liposomes for injection in myelodysplastic syndrome (Clinical Trial). ClinicalTrials.gov.
253. Rudin CM, Marshall JL, Huang CH, et al. Delivery of a liposomal c-raf-1 antisense oligonucleotide by weekly bolus dosing in patients with advanced solid tumors. *Clin Cancer Res*. 2004;10:72447-7251.
254. NCT00104754. Liposomal SN-38 in treating patients with small cell lung cancer (Clinical Trial). ClinicalTrials.gov.
255. Zhang JA, Xuan T, Parmar M, et al. Development and characterization of a novel liposome-based formulation of SN-38. *Int J Pharm*. 2004;270:93-107.
256. NCT01159028. Clinical trial of L-Grb-2 antisense oligonucleotide in CML, AML, ALL and MDS (Clinical Trial). ClinicalTrials.gov.
257. Tari AM, Gutiérrez-Puente Y, Monaco G, et al. Liposome-incorporated Grb2 antisense oligodeoxynucleotide increases the survival of mice bearing bcr-abl-positive leukemia xenografts. *Int J Oncol*. 2007;31:1243-1250.
258. Fantini M, Gianni L, Santelmo C, et al. Lipoplatin treatment in lung and breast cancer. *Chemother Res Pract*. 2011;2011:125192.
259. Stathopoulos GP, Boulikas T, Vougiouka M, et al. Pharmacokinetics and adverse reactions of a new liposomal cisplatin (Lipoplatin): phase I study. *Oncol Rep*. 2005;13:589-595.
260. Farhat FS, Temraz S, Kattan J, et al. A phase II study of lipoplatin (liposomal cisplatin)/vinorelbine combination in HER-2/ neu-negative metastatic breast cancer. *Clin Breast Cancer*. 2011;11:384-389.
261. NCT00739466. Biorest Liposomal Alendronate With Stenting sTudy (BLAST) (Clinical Trial). ClinicalTrials.gov.
262. NCT00747474. Phase I study of intravenous LipotecanR (TL388 HCl for Injection) in patients with advanced solid tumors (Clinical Trial). ClinicalTrials.gov.
263. Huang ZR, Hua SC, Yang YL, Fang JY. Development and evaluation of lipid nanoparticles for camptothecin delivery: a comparison of solid lipid nanoparticles, nanostructured lipid carriers, and lipid emulsion. *Acta Pharmacol Sin*. 2008;29:1094-1102.
264. NCT01052142. Safety study of a liposomal vaccine to treat malignant melanoma (Clinical Trial). ClinicalTrials.gov.
265. Herringson TP, Altin JG. Convenient targeting of stealth siRNA-lipoplexes to cells with chelator lipid-anchored molecules. *J Control Release*. 2009;139:229-238.

266. NCT000537116. Prostaglandin E1 (Lipostin) treatment with lower limb angioplasty for peripheral arterial occlusive disease (Clinical Trial). *ClinicalTrials.gov*.
267. NCT00631631. L-MTP-PE for high-risk osteosarcoma (Clinical Trial). *ClinicalTrials.gov*.
268. Jain V, Vyas SP, Kohli DV. Well-defined and potent liposomal hepatitis B vaccines adjuvanted with lipophilic MDP derivatives. *Nanomedicine*. 2009;5:334-344.
269. NCT00144963. Liposomal Vincristine plus Dexamethasone in patients with relapsed or refractory acute lymphoblastic leukemia (Clinical Trial). *ClinicalTrials.gov*.
270. NCT00964080. Study of MBP-426 in Patients with second line gastric, gastroesophageal, or esophageal adenocarcinoma (Clinical Trial). *ClinicalTrials.gov*.
271. MebioPharm -- Product and Technologies (Website). Available from: <http://www.mebiopharm.com/english/pro.html>. Accessed Sep 06, 2013.
272. Hamaguchi T, Matsumura Y, Nakanishi Y, Muro K, Yamada Y, Shimada Y, et al. Antitumor effect of MCC-465, pegylated liposomal doxorubicin tagged with newly developed monoclonal antibody GAH, in colorectal cancer xenografts. *Cancer Sci*. 2004;95:608-613.
273. NCT00294996. Trial of Myocet in Metastatic Breast Cancer (Clinical Trial). *ClinicalTrials.gov*.
274. NCT01039103. Nanocort in acute exacerbation of relapsing-remitting Multiple Sclerosis (MS). (Clinical Trial). *ClinicalTrials.gov*.
275. Chow T-H, Lin Y-Y, Hwang J-J, Wang H-E, Tseng Y-L, Pang VF, et al. Therapeutic efficacy evaluation of ¹¹¹In-labeled PEGylated liposomal vinorelbine in murine colon carcinoma with multimodalities of molecular imaging. *J Nucl Med*. 2009;50:2073-2081.
276. NCT00038207. Liposomal Vincristine for pediatric and adolescent patients with relapsed malignancies (Clinical Trial). *ClinicalTrials.gov*.
277. Gebnon KA, Tolcher A, Diab AR, et al. Phase I study of liposomal vincristine. *J Clin Oncol*. 1999;17:697-705.
278. NCT00046787. Efficacy and safety study of OSI-211 (Liposomal Lurtotecan) to treat recurrent small cell lung cancer (Clinical Trial). *ClinicalTrials.gov*.
279. NCT00940758. Phase I and pharmacokinetic study of biweekly PEP02 in mCRC refractory to 1st-line oxaliplatin base therapy (Clinical Trial). *ClinicalTrials.gov*.
280. NCT01191775. A Study of PNT2258 in patients with advanced solid tumors (Clinical Trial). *ClinicalTrials.gov*.
281. NCT01054547. Topical formulations of liposomal local anesthetics (Clinical Trial). *ClinicalTrials.gov*.
282. Bexion Pharmaceuticals (Website). Available from: <http://www.bexionpharma.com/>. Accessed Sep 06, 2013.
283. Qi X, Chu Z, Mahller YY, Stringer KF, Witte DP, Cripe TP. Cancer-Selective targeting and cytotoxicity by liposomal-coupled lysosomal saposin C Protein. *Clin Cancer Res*. 2009;15:5840-5851.
284. Wojton J, Chu Z, Mathsyaraja H, et al. Systemic Delivery of SapC-DOPS Has Antiangiogenic and Antitumor Effects Against Glioblastoma. *Mol Ther*. 2013;21:1517-1525.
285. NCT00177281. Safety study of S-CKD602 in patients with advanced malignancies. (Clinical Trial). *ClinicalTrials.gov*.
286. NCT00157209. Phase IIb randomized controlled study of bhp25 liposome vaccine for immunotherapy of non-small cell lung cancer (Clinical Trial). *ClinicalTrials.gov*.
287. NCT00617981. Phase 3 Study of ThermoDox with Radiofrequency Ablation (RFA) in treatment of Hepatocellular Carcinoma (HCC) (Clinical Trial). *ClinicalTrials.gov*.
288. Celsion Corporation (Website). Available from: http://celsion.com/docs/pipeline_overview. Accessed Sep 06, 2013.
289. NCT00927459. Study to evaluate the safety, tolerability, pharmacokinetics (PK), and pharmacodynamics (PD) of liposomal siRNA in subjects with high cholesterol (Clinical Trial). *ClinicalTrials.gov*.
290. Rossi J. RNAi therapeutics: SMALPing siRNAs in vivo. *Gene Ther*. 2006;13:583-584.
291. Tekmira Pharmaceuticals Corporation-Products (Website). Available from: <http://www.tekmirapharm.com/Programs/Products.asp>. Accessed Sep 06, 2013.
292. NCT00089180. T4N5 liposomal lotion in preventing the recurrence of nonmelanoma skin cancer in patients who have undergone a kidney transplant (Clinical Trial). *ClinicalTrials.gov*.
293. Cafardi JA, Elmets CA. T4 endonuclease V: review and application to dermatology. *Expert Opin Biol Ther*. 2008;8:829-838.
294. NCT01050777. Efficacy of topical liposomal form of drugs in cutaneous leishmaniasis (Clinical Trial). *ClinicalTrials.gov*.
295. NCT00764361. Safety Study of Topical Doxycycline Gel for Adult Diabetic Lower Extremity Ulcers (Clinical Trial). *ClinicalTrials.gov*.
296. Nanotherapeutics -- Products (Website). Available from: http://www.nanotherapeutics.com/?q=products_nanodox. Accessed Sep 06, 2013.
297. NCT00089180. T4N5 liposomal lotion in preventing the recurrence of nonmelanoma skin cancer in patients who have undergone a kidney transplant (Clinical Trial). *ClinicalTrials.gov*.
298. Yarosh D, Klein J, O'Connor A, Hawk J, Rafal E, Wolf P. Effect of topically applied T4 endonuclease V in liposomes on skin cancer in xenoderma pigmentosum: a randomised study. *Xenoderma pigmentosum study group. Lancet*. 2001;357:926-929.
299. NCT00709254. Study of single and multiple doses of inhaled AeroLEF (Liposome-Encapsulated Fentanyl) in healthy subjects (Clinical Trial). *ClinicalTrials.gov*.
300. NCT00775138. A Study to Determine the Safety and Tolerability of Arikace™ Versus Placebo in Patients Who Have Bronchiectasis
301. NCT00492141. Aerosol L9-NC and temozolomide in ewing's sarcoma (Clinical Trial). *ClinicalTrials.gov*.
302. NCT00915187. Safety and immunogenicity study of intramuscular CCS/C-adjuvanted influenza vaccine in elderly (Clinical Trial). *ClinicalTrials.gov*.
303. NCT00922363. Trial on the safety of a new liposomal adjuvant system, CAF01, when given with the tuberculosis subunit vaccine Ag85B-ESAT-6 as two injections with two months interval to healthy adult volunteers (Clinical Trial). *ClinicalTrials.gov*.
304. NCT00460525. Phase II AMA-I malaria vaccine FMP2.1/AS02A trial in mali (Clinical Trial). *ClinicalTrials.gov*.
305. NCT00004806. Phase I Study of liposome-mediated gene transfer in patients with cystic fibrosis (Clinical Trial). *ClinicalTrials.gov*.
306. NCT00533637. Taste and local tolerance study of NLA nasal spray in patients with allergic rhinitis (Clinical Trial). *ClinicalTrials.gov*.
307. Orexo AB -- OX-NLA (Website). Available from: <http://www.orexo.com/en/Portfolio/OX-NLA/>. Accessed Sep 05, 2013.
308. NCT00004471. Phase I pilot study of gene therapy for cystic fibrosis using cationic liposome mediated gene transfer (Clinical Trial). *ClinicalTrials.gov*.
309. NCT01095848. A phase I safety study of a cancer vaccine to treat HLA-a2 positive advanced stage ovarian, breast and prostate cancer (Clinical Trial). *ClinicalTrials.gov*.
310. NCT00004104. Vaccine therapy plus interleukin-2 with or without interferon alfa-2b in treating patients with stage III melanoma (Clinical Trial). *ClinicalTrials.gov*.
311. NCT01073371. Anesthetic efficacy of liposomal prilocaine in maxillary infiltration anesthesia (Clinical Trial). *ClinicalTrials.gov*.
312. Saia Ceruda CM, Tofoli GR, de Brito Junior RB, et al. Stability and local toxicity evaluation of a liposomal prilocaine formulation. *J Liposome Res*. 2008;18:329-339.
313. NCT01334892. L-CsA in the prevention of bronchiolitis obliterans syndrome (BOS) in lung transplant (LT) patients (Clinical Trial). *ClinicalTrials.gov*.
314. Behr J, Zimmermann G, Baumgartner R, et al. Lung deposition of a liposomal cyclosporine A inhalation solution in patients after lung transplantation. *J Aerosol Med Pulm Drug Deliv*. 2009;22:121-130.
315. NCT00035867. Study of TLK199 HCl liposomes for injection in myelodysplastic syndrome (Clinical Trial). *ClinicalTrials.gov*.

International Journal of Nanomedicine

Dovepress

Publish your work in this journal

The International Journal of Nanomedicine is an international, peer-reviewed journal focusing on the application of nanotechnology in diagnostics, therapeutics, and drug delivery systems throughout the biomedical field. This journal is indexed on PubMed Central, MedLine, CAS, SciSearch®, Current Contents®/Clinical Medicine,

Journal Citation Reports/Science Edition, EMBase, Scopus and the Elsevier Bibliographic databases. The manuscript management system is completely online and includes a very quick and fair peer-review system, which is all easy to use. Visit <http://www.dovepress.com/testimonials.php> to read real quotes from published authors.

Submit your manuscript here: <http://www.dovepress.com/info/submit/submit-international-journal-of-nanomedicine-journal>

Review

Liposomal Formulations in Clinical Use: An Updated Review

Upendra Bulbake [†], Sindhu Doppalapudi [†], Nagavendra Kommineni and Wahid Khan ^{*}

Department of Pharmaceutics, National Institute of Pharmaceutical Education and Research,
Hyderabad 500037, India; upendra.bulbake@gmail.com (U.B.); dsdoppalapudisindhu@gmail.com (S.D.);
nagavendra.kommineni@gmail.com (N.K.)

^{*} Correspondence: wahid@niperhyd.ac.in

[†] These authors contributed equally to this work.

Academic Editor: Murali Mohan Yallapu

Received: 16 January 2017; Accepted: 23 March 2017; Published: 27 March 2017

Abstract: Liposomes are the first nano drug delivery systems that have been successfully translated into real-time clinical applications. These closed bilayer phospholipid vesicles have witnessed many technical advances in recent years since their first development in 1965. Delivery of therapeutics by liposomes alters their biodistribution profile, which further enhances the therapeutic index of various drugs. Extensive research is being carried out using these nano drug delivery systems in diverse areas including the delivery of anti-cancer, anti-fungal, anti-inflammatory drugs and therapeutic genes. The significant contribution of liposomes as drug delivery systems in the healthcare sector is known by many clinical products, e.g., Doxil[®], Ambisome[®], DepoDur[™], etc. This review provides a detailed update on liposomal technologies e.g., DepoFoam[™] Technology, Stealth technology, etc., the formulation aspects of clinically used products and ongoing clinical trials on liposomes.

Keywords: liposomes; therapeutics; drug delivery; liposome technology; nanotechnology; clinical trials; marketed products

1. Introduction

The concept of liposomal drug delivery system has revolutionised the pharmaceutical field. Alec Bangham, in 1961 [1], first described liposomes. Since then active research in the field of liposomes have been carried out and their applications are now well established in various areas, such as drug, biomolecules and gene delivery [2]. Liposomes are spherical vesicles characterised by a bilayer of lipids with an internal aqueous cavity. Liposome structural components are phospholipids or synthetic amphiphiles incorporated with sterols, such as cholesterol, to influence membrane permeability. Thin-film hydration is the most widely used preparation method for liposomes, in which lipid components with or without a drug are dissolved in an organic solvent. The solvent will be evaporated by rotary evaporation followed by rehydration of the film in an aqueous solvent. The other methods include reverse-phase evaporation, freeze-drying and ethanol injection [2]. Techniques like membrane extrusion, sonication, homogenization and/or freeze-thawing are being employed to control the size and size distribution. Liposomes can be formulated and processed to differ in size, composition, charge and lamellarity.

Due to extensive developments in liposome technology, a number of liposome-based drug formulations are available for human use and many products are under different clinical trials. Encapsulation of drugs in liposomes (as shown in Figure 1) enhanced the therapeutic indices of various agents, mainly through alterations in their pharmacokinetics and pharmacodynamics. Drugs with different solubility can be encapsulated in liposomes, hydrophobic drugs have affinity to the phospholipid bilayer and hydrophilic drugs are entrapped in the aqueous cavity. The first successful

milestone in liposome-based products was the introduction of Doxil® to the U.S. market in 1995 for the treatment of patients with ovarian cancer and AIDS-related Kaposi's sarcoma after the failure of prior systemic chemotherapy or intolerance to such therapy. Gabizon and Barenholz commenced the development of Doxil® in Israel and the USA [3]. It was the first nano-sized liposomal product to obtain regulatory approval. Later, NeXstar Pharmaceuticals USA also developed a liposomal product, DaunoXome®, for the delivery of daunorubicin (DNR), which was approved by the U.S. FDA in 1996 for the management of advanced HIV-associated Kaposi's sarcoma. Subsequently, a few more products have become available for the management of various cancers. These products includes Depocyt® by SkyPharma Inc., Myocet® by Elan Pharmaceuticals, Mepact® by Takeda Pharmaceutical and Marqibo® by Talon Therapeutics. Recently, a fluorouracil and leucovorin combination therapy-based product was approved for metastatic adenocarcinoma of the pancreas. This product is marketed as Onivyde™ by Merrimack Pharmaceuticals, Inc. Although cancer was the most widely explored area in terms of clinically approved products of liposomes, liposomal products were also developed for other diseases (Figure 2). For fungal infections, the U.S. FDA approved Amphotec® and Ambisome® in 1996 and 1997, respectively. Treatment of fungal infections has benefited since the development of these liposomal formulations of Amphotericin B (AmB). Also, liposomes have become important carrier systems in vaccine development and interest in liposomal vaccines have markedly increased because of the development of products Epaxal® and Inflexal® V. Both products are developed by Crucell, Berna Biotech for vaccination against hepatitis and influenza, respectively.

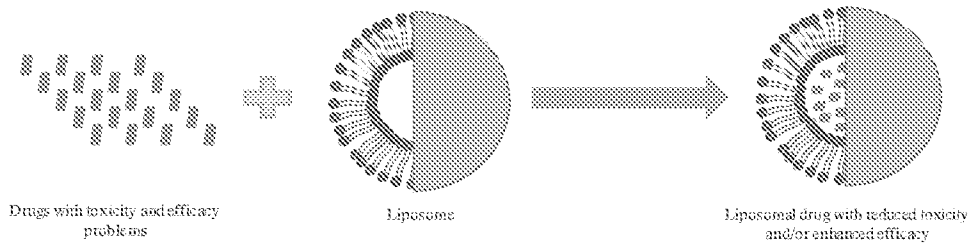


Figure 1. Schematic representation showing the advantages of formulating drugs in liposomes.

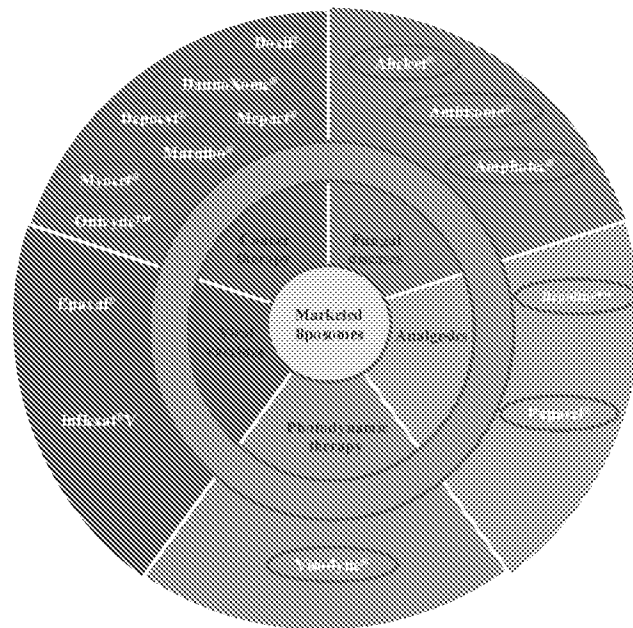


Figure 2. Therapeutic areas covered by liposome-based products.

This review gives a concise picture of various liposome-based products available in the market and liposome technologies (Stealth liposome technology, DepoFoam™ technology, Thermosensitive liposomes and Non-PEGylated liposomes) involved in the development of these products. Liposome-based products under ongoing clinical trials as monotherapy or in combination with other agents/therapies are also covered.

2. Liposome Technologies for Delivery of Therapeutics

This section emphasises the liposome technologies specifically developed for the preparation of clinically used liposome-based products. Each technology offers unique characteristics in an attempt to optimise drug delivery by protecting the unique properties of the therapeutic agent while minimizing its drawbacks.

2.1. Stealth Liposome Technology

Stealth technology has been explored in developing a drug delivery system that makes their detection by the mononuclear phagocyte system difficult. In this technology, strands of the polymer(s) are attached to drug molecules or a system that can improve the safety and efficacy of the therapeutic agents. Generally, polyethylene glycol (PEG) is used as a polymer and the process is called PEGylation. In general, PEGylation is attained by the incubation of a reactive derivative of PEG with the target moiety. Covalent linkage of liposome to a PEG protects the active moiety from the recipient's immune system, which results in reduced immunogenicity and antigenicity. It also produces alterations in the physicochemical properties of the active moiety, including changes in the hydrodynamic size, which further reduce its renal clearance and thereby prolongs its circulatory time (Figure 3). Also, it provides hydrophilicity to hydrophobic drugs and reduces dosage frequency. These changes do not diminish efficacy and show reduced toxicity [4]. Furthermore, due to the leaky nature of the tumour vasculature, nano-sized formulations with prolonged circulatory time show enhanced permeation and retention (EPR) and slowly accumulate in the tumour bed. This technology provided a very successful liposome-based product namely Doxil® as an intravenous injection for the management of advanced ovarian cancer, multiple myeloma and HIV-associated Kaposi's sarcoma. This technology helps to achieve a customised dosage profile.

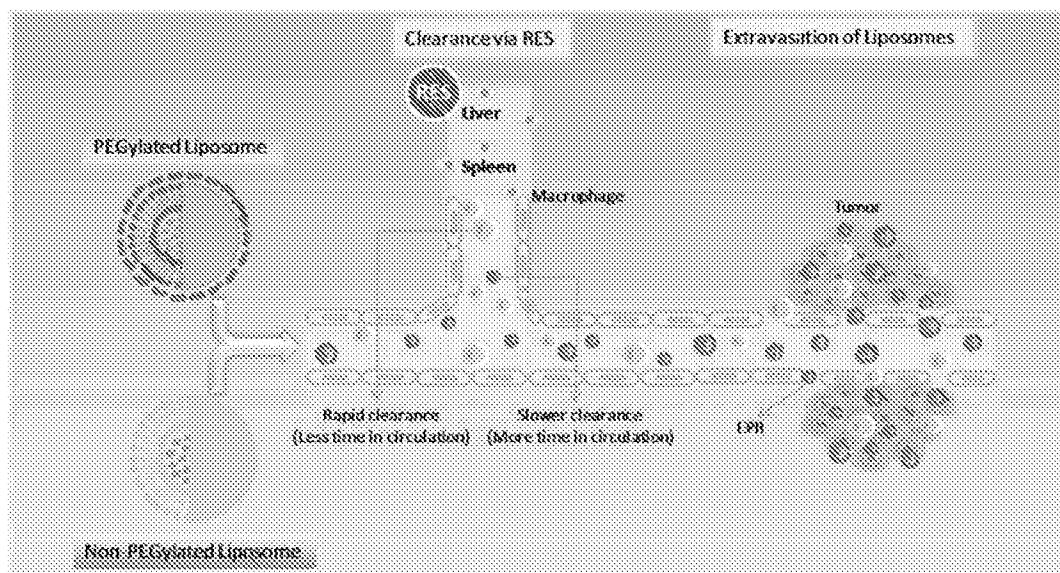


Figure 3. Pharmacokinetics of PEGylated liposomes and Non-PEGylated liposomes.

2.2. Non-PEGylated Liposome Technology

Non-PEGylated liposome (NPL) is a unique drug-delivery system that came as a breakthrough in cancer therapy by offering the benefits of PEGylated-liposome while eliminating the side effects associated with PEG such as hand-foot syndrome (HFS). NPL Doxorubicin (NPLD) injection provides a better safety profile over conventional DOX and Doxil[®]. NPLD not only reduces the cardiac toxicity associated with DOX, but also the dose-limiting toxicity linked with the use of Doxil[®], such as HFS. This is achieved by a combination of specific composition and a unique manufacturing process of the NPLD liposome, which gives it the desired physicochemical properties. The NPLDs have an increased circulation time and less cardiotoxicity as compared with conventional DOX. Since NPLD do not have a PEG coating, they are not associated with the painful HFS, which is a dose-limiting adverse event with PEG-DOX [5]. Myocet[®] is a NPLD manufactured by Elan Pharmaceuticals, Princeton, NJ, approved in Europe and Canada for the management of metastatic breast cancer in combination with cyclophosphamide.

2.3. DepoFoam[™] Liposome Technology

DepoFoam[™] is a proprietary, extended-release drug delivery technology introduced by Pacira Pharmaceuticals, Inc., Parsippany, NJ, USA. DepoFoam[™] is the core technology behind several marketed products such as Depocyt[®], DepoDur[™] and Exparel[®]. DepoFoam[™] technology encapsulates drugs in its multivesicular liposomal platform without modification of their molecular structure. The multivesicular liposomes releases drug(s) over a required period of time ranging from 1 to 30 days. DepoFoam[™] consists of microscopic spheroids (3–30 μm) with granular structure and single-layered lipid particles composed of a honeycomb of numerous nonconcentric internal aqueous chambers containing the bounded drug (Figure 4). Each particle contains numerous non-concentric aqueous chambers bounded by a single bilayer lipid membrane. Each chamber is partitioned from the adjacent chambers by bilayer lipid membranes composed of synthetic analogs of naturally existing lipids (DOPC, DPPC, cholesterol, triolein etc) [6]. Upon administration, DepoFoam[™] particles release the drug over a period of hours to weeks following erosion and/or reorganization of the lipid membranes. DepoFoam[™] technology improved the properties of both small and large molecules. This technology considerably improved patient care by providing a remarkable solution for medications that require frequent multiple injections and have a short period of action or side effects.

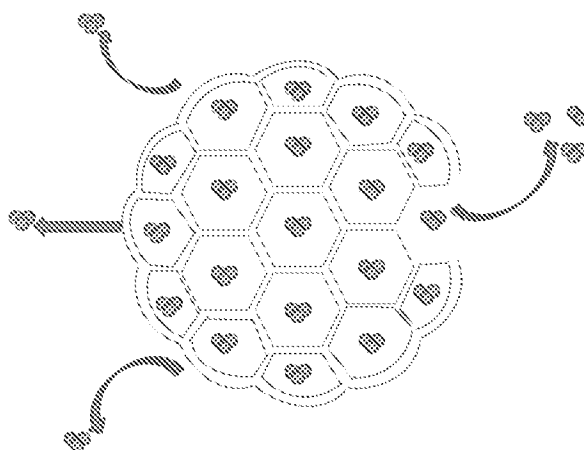


Figure 4. Spheroid and granular structure of a DepoFoam[™] particle.

2.4. Lysolipid Thermally Sensitive Liposome (LTSL) Technology

Thermosensitive liposomes have been studied for drug release at sites of elevated temperature. Generally, lipids, e.g., DPPC, MSPC, with a transition temperature between 40 and 45 °C have

been used in the preparation of these liposomes. These novel liposomes are being developed to exhibit temperature-dependent release of encapsulated drug(s). Local tissue temperature is generally elevated to 42 °C by radiofrequency ablation, a technique based on the application of radiofrequency. Lipid components present in the liposome undergo a gel to liquid transition at elevated temperatures, making it more permeable, and thus releasing the drug. Moreover, application of local hyperthermia causes leakage of blood vessels within tumours, thereby increasing accumulation of liposomes in the tumour. ThermoDox[®] of Celsion Corporation is being tested in phase III clinical trial uses LTSL (lysolipid thermally sensitive liposome) technology to encapsulate DOX for the treatment of various solid tumours. For ThermoDox[®], this technology allows a 25 times greater concentration of the drug in the treatment area than intravenous (i.v.) DOX. Also, DOX concentration increases significantly in the circulation when compared to other liposomally encapsulated DOX [7].

3. Clinically Available Liposome-Based Products

Comprehensive information related to clinically available liposome-based products is provided in this section. Currently, there are good numbers of liposome-based drugs available for human use. Most of the liposomal drug formulations are available for intravenous and intramuscular (i.m.) applications. A brief summary of these products is given in Table 1.

3.1. Liposomes for Cancer Therapy

3.1.1. Doxil[®]

Doxil[®], a formulation containing DOX hydrochloride, is the first FDA-approved nano drug delivery system based on PEGylated liposome technology. Sequus Pharmaceuticals, USA originally developed Doxil[®] in 1995 as an i.v. injection for the management of advanced ovarian cancer, multiple myeloma and HIV-associated Kaposi's sarcoma. Single-dose vials of 20 mg/10 mL and 50 mg/25 mL are available and administered at a starting rate of 1 mg/min through i.v. infusion to minimise the risk of infusion reactions.

Doxil[®] liposomes are composed of high phase-transition-temperature (T_m) phospholipid hydrogenated soy phosphatidylcholine (HSPC), cholesterol and *N*-(carbonyl-methoxypolyethylene glycol 2000)-1,2-distearoyl-*sn*-glycero-3-phosphoethanolamine sodium salt (MPEG-DSPE) in a molar ratio of 56:38:5 [8]. More drug retention was obtained because of the optimum proportion of cholesterol and HSPC, which forms a non-flexible bilayer at 37 °C and below 37 °C. DSPE is incorporated into the bilayer of the liposomes to supply a reactive functional group for the hydrophilic PEG chains (molecular weight 2000) to covalently bind to the DSPE head that elongates into water phases both inner and outer. The overall lipid content of Doxil[®] is nearly 16 mg/mL and 2 mg/mL is the DOX concentration [9]. DOX is located within the hydrophilic core of the liposomes in the form of DOX-sulphate complex [3]. More than 90% of DOX is encapsulated in the minuscule, unilamellar, vesicular stealth liposomes of 80 to 100 nm size [3]. A high and stable drug/lipid ratio was obtained through the remote loading approach (Figure 5) (first developed by Barenholz [3]) by a transmembrane gradient of ammonium sulphate: [(NH₄)₂SO₄] liposome >> [(NH₄)₂SO₄] medium that serves as a driving force for the efficient and stable loading of amphipathic weak bases into preformed liposomes [10,11]. This remote drug loading approach allows for systematic accumulation of DOX inside the liposome hydrophilic core (about 15,000 DOX molecules/vesicle), with most of the drug (>90%) present as a crystalline-like precipitate that is free from osmotic effects and thus contributes to the stability of the entrapment [12,13]. This approach is based on formulating liposomes that show a transmembrane gradient, which serves as a driving force for the remote loading of amphipathic weak base drugs. This loading technology allows higher retention with less drug efflux in circulation, while providing acceptable rates of drug distribution in tissues [14].

Table 1. Clinically used liposome-based products.

SN	Clinical Products (Approval Year)	Administration	Active Agent	Lipid/Lipid:Drug Molar Ratio	Indication	Company
1.	Doxil® (1995)	i.v.	Doxorubicin	HSPC:Cholesterol:PEG 2000-DSPE (56:39:5 molar ratio)	Ovarian, breast cancer, Kaposi's sarcoma	Seqirus Pharmaceuticals
2.	Danoxone® (1996)	i.v.	Danorubicin	DSPE and Cholesterol (2:1 molar ratio)	AIDS-related Kaposi's sarcoma	Noxstar Pharmaceuticals
3.	Depocyt® (1996)	Spinal	Cytarabine/Ara-C	DGPC, DPPG, Cholesterol and Trolen	Neoplastic meningitis	SkyPharma Inc.
4.	Myocet® (2000)	i.v.	Doxorubicin	EPC:Cholesterol (55:45 molar ratio)	Combination therapy with cyclophosphamide in metastatic breast cancer	Elan Pharmaceuticals
5.	Mepact® (2004)	i.v.	Mifampride	DOPS:POPC (3:7 molar ratio)	High-grade, resectable, non-metastatic osteosarcoma	Takeda Pharmaceutical Limited
6.	Margibo® (2012)	i.v.	Vincristine	SM:Cholesterol (69:30 molar ratio)	Acute lymphoblastic leukemia	Talon Therapeutics, Inc.
7.	Onivyde™ (2015)	i.v.	Irinotecan	DSPE:DMPEG-2000:DSPE (3:2:0.015 molar ratio)	Combination therapy with fluorouracil and leucovorin in metastatic adenocarcinoma of the pancreas	Merrimack Pharmaceuticals Inc.
8.	Abelcet® (1995)	i.v.	Amphotericin B	DMPC:DMPG (7:3 molar ratio)	Invasive severe fungal infections	Sigma-Tau Pharmaceuticals
9.	Ambisome® (1997)	i.v.	Amphotericin B	HSPC:DSPE:Cholesterol:Amphotericin B (26.8:33.4 molar ratio)	Presumed fungal infections	Astellas Pharma
10.	Atroplotec® (1996)	i.v.	Amphotericin B	Cholesteryl sulphate:Amphotericin B (1:1 molar ratio)	Severe fungal infections	Ben Venue Laboratories Inc.
11.	Viscotyne® (2000)	i.v.	Verteporphin	Verteporphin:DMPC and EPC (1:5 molar ratio)	Cholesterol neovascularization	Novartis
12.	DepoDur™ (2004)	Epidural	Morphine sulfate	DOPC, DPPG, Cholesterol and Trolen	Pain management	SkyPharma Inc.
13.	Eparex® (2011)	i.v.	Epirivacaine	DEPC, DPPG, Cholesterol and trimyristin	Pain management	Patrice Pharmaceuticals, Inc.
14.	Eparal® (1995)	i.m.	Inactivated hepatitis A virus (strain HGSB)	DOPC:DOPE (75:25 molar ratio)	Hepatitis A	Crossid, Beigba Biotech
15.	Inflvac® V (1997)	i.m.	Inactivated haemagglutinins of Influenza virus strains A and B	DOPC:DOPE (75:25 molar ratio)	Influenza	Crossid, Beigba Biotech

i.v. (intravenous), i.m. (intramuscular); HSPC (hydrogenated soy phosphatidylcholine); PEG (polyethylene glycol); DSPE (distearyl-sn-glycero-phosphoethanolamine); DSPC (distearylphosphatidylcholine); DGPC (dioleoylphosphatidylcholine); DPPG (dipalmitoylphosphatidylglycerol); EPC (egg phosphatidylcholine); DOPS (dioleoylphosphatidylserine); POPC (palmitoyloleoylphosphatidylcholine); SM (sphingomyelin); MPEG (methoxy polyethylene glycol); DMPC (dimyristoyl phosphatidylcholine); DMFG (dimyristoyl phosphatidylglycerol); DSPG (distearylphosphatidylglycerol); DEPC (diercylphosphatidylcholine); DOPE (dioleoyl-sn-glycero-phosphoethanolamine).

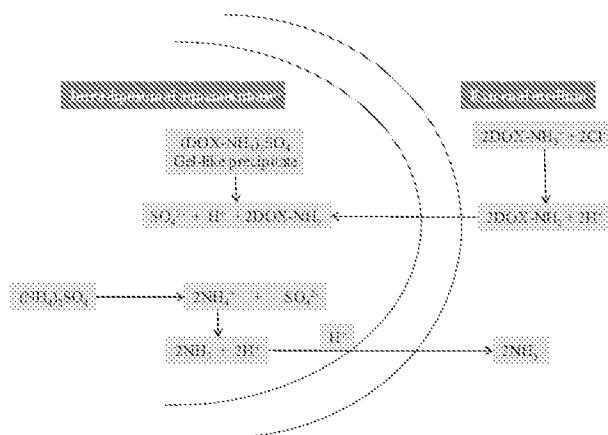


Figure 5. Remote loading approach of DOX into the intraliposomal aqueous phase. Liposomes are prepared at the desired concentration of ammonium sulphate. The gradient was formed by removing the ammonium sulphate from the external liposome medium. Intraliposomal NH_4^+ dissociates into NH_3 and H^+ , NH_3 escape from the liposome and H^+ is retained in the liposome water phase. DOX HCl is added to the liposome dispersion at a temperature above the phase transition of the liposomal lipids. DOX, a cationic amphiphile, is present in equilibrium between an ionised and a non-ionised form. The latter form commutes across the liposome bilayer and becomes ionised once exposed to the internal H^+ environment, and forms a salt with the SO_4^{2-} anions.

To examine the pharmacokinetics of DOX, Gabizon et al. reported a pilot clinical trial study on 15 cancer patients. In this study Doxil[®] was compared with the free DOX, at doses of 25 mg/m² and 50 mg/m². This study showed that Doxil[®] showed a much lower volume of distribution (4 L) compared to the free drug (254 L). Moreover, the clearance of Doxil[®] (0.1 L/h) was much lower compared to the free drug (45 L/h). Doxil[®] showed biphasic clearance phase with half-lives of 2 h and 45 h, which shows association of almost all the circulating DOX with the liposome. Doxil[®] showed 4–16 times higher concentration of DOX in the tumour of patients using the product [15]. Doxil[®] has shown the ability to clinically reduce cardiotoxicity, a side effect of free DOX treatment, because encapsulated DOX is not bioavailable at cardiac muscle cells and the myocardium [16].

3.1.2. DaunoXome[®]

DaunoXome[®], a DNR citrate liposomal formulation, is a germ-, pyrogen- and preservative-free product in a single-dose vial for i.v. infusion. NeXstar Pharmaceuticals, USA, developed DaunoXome[®] in 1996 for the management of HIV-associated Kaposi's sarcoma [17]. Each single-dose vial contains approximately 50 mg of DNR base enclosed in liposomes composed of 168 mg cholesterol and 704 mg distearoylphosphatidylcholine (DSPC). The aqueous dispersion of these liposomes (25 mL/vial) contains 2125 mg sucrose, 94 mg glycine and 7 mg calcium chloride dihydrate. Liposomes are neutrally charged with a bilayer composed of DSPC and cholesterol at 2:1 molar ratio and a mean particle size of approximately 45 nm. The lipid:drug weight ratio is 18.7:1 (total lipid:DNR base), which is equivalent to 10:5:1 molar ratio of DSPC:Cholesterol:DNR [18]. The specific lipidic formulation of DNR has been shown to form liposomes with excellent physical strength, improving the stability of entrapped DNR from fast metabolism and also minimising its protein binding [19]. Because of the small size and comparative neutrality of DaunoXome[®] particles, reticulo-endothelial system (RES) uptake is diminished, leading to extended drug circulation [20].

Liposomal DNR with increasing dosage for safety, pharmacokinetics and potential efficacy in patients with HIV-associated Kaposi's sarcoma was evaluated by Gill et al. [21]. They found that DaunoXome[®] at a dose range between 40 and 60 mg/m² was most efficacious. The mean plasma area under the curve (AUC) obtained from these results ranges from 114.91 to 120.1 $\mu\text{g h}^{-1} \text{mL}^{-1}$ [21,22].

These results represent an 11–12-fold increase over conventional DNR and reflect the steady nature of the liposomal carrier, as reported in murine model systems [20,21]. Similarly, elimination is significantly low in DaunoXome[®]-treated patients as compared to conventional DNR treated patients (10.5 vs. 233 mL/min, respectively) [22,23]. These two properties together increased the half-life of DaunoXome[®] between 4–5.6 h in comparison with free DNR \approx 0.77 h [21,22]. The data shown indicate that DaunoXome[®] has an improved pharmacokinetic profile in comparison with free DNR.

3.1.3. Depocyt[®]

Depocyt[®], a liposomal product containing cytarabine/Ara-C (Enzon Corporation, Piscataway, NJ, USA), was developed by SkyePharm Inc. (previously DepoTech Pharmaceuticals, La Jolla, CA, USA). Depocyt[®] is a pyrogen-free, parenteral suspension of the antimetabolite Ara-C, developed for the treatment of neoplastic meningitis (NM) by controlled release of Ara-C. Depocyt[®] is a slow-release formulation developed by encapsulating the aqueous drug solution in multivesicular particles with a granular structure known as DepoFoam[™]. DepoFoam[™] technology consists of microscopic spherical particles (3–30 μ m) and is suitable for encapsulating hydrophilic compounds such as Ara-C. These lipid foam-based particles are comprised of 96% aqueous foam and 4% biodegradable lipid [6]. The architecture of multivesicular DepoFoam[™] particles provides a comparatively high drug-loading ability. They are bigger than standard unilamellar or multilamellar liposomes. The residues of lipid foam are biodegradable and metabolised by the usual metabolic pathways for triglycerides, phospholipids and cholesterol. Each vial contains 50 mg of Ara-C encapsulated in DepoFoam[™] liposomes at a concentration of 10 mg/mL. Each 5-mL vial contains 50 mg Ara-C, 22 mg cholesterol, 6 mg triolein, 28.5 mg dioleoylphosphatidylcholine (DOPC) and 5 mg dipalmitoylphosphatidylglycerol (DPPG) suspended in 0.9% preservative-free saline. The Depocyt[®] suspension is maintained at a final pH of 5.5 to 8.5. Due to the higher density of DepoFoam[™] particles than that of the suspending medium, these particles have a tendency to settle at the bottom over time, and therefore the suspension require gentle agitation to re-suspend the particles before injection [6]. The recommended adult dosage of Ara-C is 50 mg (5 mL Depocyt[®]) once every two weeks.

A phase I/II clinical trials for ventricular and lumbar-administrated Depocyt[®] pharmacokinetic studies was initiated, in which cytotoxic CSF Ara-C levels were maintained for more than 14 days in both the lumbar and ventricular fluid regardless of the site of drug administration [24]. The terminal half-life of intraventricular Depocyt[®] was 141 h, whereas that of standard Ara-C was 3.4 h [25]. In another clinical study Depocyt[®] was compared to methotrexate in patients with solid tumour neoplastic meningitis and results revealed similar response rates. Also, Depocyt[®] significantly increased the phase to neurological progression and the effectiveness of Ara-C is a function of both the concentration and duration of exposure. Depocyt[®] has the ability to destroy tumour cells more effectively in the meninges and CSF than standard Ara-C formulations [26].

3.1.4. Myocet[®]

Myocet[®] is a nonpegylated liposomal DOX that has been approved in combination with cyclophosphamide for first-line treatment of patients with breast cancer. Myocet[®] (Elan Pharmaceuticals, Princeton, NJ, USA) was developed to reduce the cardiotoxicity of DOX while maintaining its anti-tumour efficacy [27]. Myocet[®] liposomes are about 150 to 250 nm in size and contains cholesterol and the acidic egg phosphatidylcholine (EPC) in a molar ratio of 45:55. The drug to lipid ratio is about 0.27. The larger size of these liposomes makes them easily recognised by the mononuclear phagocyte system (MPS). The large size of vesicles also minimises their exposure to normal tissues, due to which some acute and chronic toxicities were diminished [28]. Active loading for amphipathic weak bases was employed for the development of Myocet[®] liposomes. Blank liposomes were prepared in an acidic citrate buffer (pH 4.0, 300 mM citrate) followed by the addition of sodium carbonate to increase the pH outside these liposomes to approximately 7.3. Finally, these liposomes are incubated with DOX and slightly heated briefly. As a result, DOX goes across the lipid bilayer and becomes protonated

inside the liposomal aqueous core. The negatively charged membrane-associated lipids serve to form “ion pairs” with DOX (which is positively charged at a physiological pH), which favours entry of DOX into the liposome [29]. Once DOX becomes protonated, it has trouble crossing the lipid bilayer, which results in entrapment efficiencies of more than 99% [30].

Myocet[®] was compared with free DOX in preclinical toxicity studies performed on Beagle dogs, in which Myocet[®] has shown a better toxicity profile than free DOX [28]. Harasym and co-workers reported the highest tumour concentrations were 2–3 times higher for Myocet[®] as compared to free DOX in a solid tumour model and for the ascitic model the maximal level in tumour drug exposure was 10 times higher for Myocet[®] as compared to free DOX [31]. These results encouraged the selection of Myocet[®] for clinical studies. A phase I clinical study was performed on 38 patients with refractory solid tumours, in which Myocet[®] and free DOX were given through i.v. injection at same dose. The study demonstrated reduced myelosuppression and gastrointestinal adverse effects due to Myocet[®] as compared with free DOX [30]. In a phase III clinical study in patients with metastatic breast cancer, Myocet[®] demonstrated similar response rates and progression-free survival times. Furthermore, the occurrence of cardiac events and congestive heart failure was significantly lower for Myocet[®] [32]. Batist and co-workers [33] conducted another multicentric designed clinical trial in patients with metastatic breast cancer, in which a Myocet[®] (60 mg/m²) and cyclophosphamide (600 mg/m²) combination was compared with a free DOX and cyclophosphamide combination at the same dose. The results showed equivalent efficacy with minimal toxicity due to a combination of Myocet[®] with cyclophosphamide.

3.1.5. Mepact[®]

Mepact[®] is a mifamurtide (MFT) containing liposomes commercialised by Takeda Pharmaceutical Company Limited, previously IDM Pharma SAS. Mepact[®] designated as an ‘orphan’ drug by the European Medicines Agency (EMA) in 2004 and it was the first drug approved for the management of high-grade, resectable, non-metastatic bone tumours combined with postoperative combination chemotherapy in children, adolescents and young adults who have gone through full macroscopic surgical resection. Mepact[®] contains <100 nm multilamellar vesicles of liposome encapsulated muramyl tripeptide phosphatidylethanolamine (L-MTP-PE) [34]. MTP-PE is a fabricated lipophilic derivative of muramyl dipeptide (MDP) (a naturally occurring constituent of bacterial cell walls) and it is a conjugate of MTP and dipalmitoylphosphatidylethanolamine (DPPE). Muramyl dipeptide activates monocytes, macrophages and cytokines like tumour necrosis factor alpha, interleukin-1b, interleukin-6, interleukin-8 and interleukin-12. Synthetic lipids used in the preparation of Mepact[®] liposomes, i.e., dioleoyl-phosphatidylserine (DOPS) and 1-palmitoyl-2-oleoyl-phosphatidylcholine (POPC), are at a 3:7 molar ratio (1g total lipid/vial) with MTP-PE (4 mg/vial) [35]. The anti-osteosarcoma effects produced by MFT *in vivo* are due to an immune response against osteosarcoma lung metastases, even though the drug showed no cytotoxicity towards normal or tumour cells *in vitro*. Macrophage cells possess a “flipped phosphatidyl serine” to the external membrane after apoptosis from chemotherapy; therefore, phosphatidyl serine containing lipids provides the signal to these cells and thus both mifamurtide’s active and inactive constituents target the immune cells of the lungs [36].

The pharmacological parameters of liposomal MFT were characterised in healthy adults and in patients with high-risk, metastatic and recurrent osteogenic sarcoma [37]. The results showed that single MFT at a single 4 mg dose can be safely given to healthy adult volunteers and that pharmacokinetic variability is less for MFT [the coefficient of variation (% CV) in both the AUC and the maximal concentration (C_{max}) was less than 30%]. A phase III clinical trial of L-MTP-PE given in addition to the usual combination chemotherapy conducted in children and young adults with osteogenic sarcoma showed an increase in six-year net survival from 70% to 78% [38].

3.1.6. Marqibo[®]

Marqibo[®], vincristine (VCR) sulfate liposomal injection (VSLI), developed by Talon Therapeutics, Inc. USA, was approved for the treatment of adult patients with Philadelphia chromosome-negative

(Ph⁻) acute lymphoblastic leukaemia (ALL) with second or greater relapse or whose disease has advanced after two or more anti-leukaemia therapies. Each vial contains 5 mg/31 mL (0.16 mg/mL) VCR sulphate for a single dose. VCR is encapsulated in an aqueous interior core of sphingomyelin/cholesterol liposome called optisomes [39]. These optisomes were specifically developed to promote the higher loading and holding of VCR. Also, these optisomes increase the circulation time of enclosed VCR and slowly release the drug into the tumour vasculature. These factors lead to enhanced activity due to the high concentration of encapsulated drug in target tissues. Sphingomyelin (SM) and cholesterol at a molar ratio of approximately 60:40 (mol:mol) are present in the VSLI, with an approximate liposome mean diameter of 100 nm. The SM/Cholesterol lipid constituent and the small mean particle diameter of the VSLI liposome contribute to low protein binding, which results in a prolonged circulation time for the liposome. More than 95% of the drug is encapsulated in the liposomes [40].

Marqibo[®] has prolonged plasma circulation compared with free VCR and passively targets VCR to tumours by discharging through the fenestrations that characterise the tumour neovasculature [41]. A phase II clinical trial, single-arm open study in patients with relapsed or refractory aggressive non-Hodgkin lymphoma, analysed the efficacy and safety of Marqibo[®] as a single agent. Marqibo[®] was given at approximately twice the dose intensity of standard-free VCR. Patients in this study demonstrated a comparable toxicity profile to standard-free VCR [42].

3.1.7. Onivyde[™]

Onivyde[™], an irinotecan (IRI) liposome injection, is a product of Merrimack Pharmaceuticals Inc. approved in 2015. Onivyde[™] coupled with leucovorin and fluorouracil is indicated for the management of patients with metastatic adenocarcinoma of the pancreas that showed disease progression after gemcitabine-based therapy. Onivyde[™] is formulated with a water-soluble semisynthetic IRI hydrochloride trihydrate, a topoisomerase inhibitor, into a liposomal dispersion. Onivyde[™] liposomes are unilamellar lipid bilayer vesicles with a mean diameter of 110 nm that encapsulates IRI in a gelated or precipitated state as the sucrose octasulphate salt using an ion-exchange/titration method in aqueous space. Onivyde[™] was prepared by a novel method, i.e., intra-liposomal drug stabilization technology, which encapsulates drug into long circulating liposome-based nano-vesicles [43]. In this technology, polymeric or nonpolymeric highly charged anions and intra-liposomal trapping agents like polyphosphate or sucrose octasulfate were used. A high-pKa polyalkylamine gradient was utilised in this technology. This facilitates the encapsulation of IRI at a high drug:lipid ratio (more than 800 g IRI per mol of phospholipid) within the liposomes. The half-life of drug release in the system was also shown to be increased up to 56.8 h. The vesicle is composed of DSPC, cholesterol and methoxy-terminated polyethylene glycol (MW 2000)-distearoylphosphatidyl ethanolamine (MPEG-2000-DSPE) in the ratio of 3:2:0.015, which encapsulated more than 90% of the drug [44].

Liposomal IRI was compared with free IRI using human colon (HT29) and breast (BT474) cancer xenograft models. Liposomal IRI showed significantly enhanced cytotoxic activity due to exponentially higher drug loading and extended drug retention in vivo [43]. A randomised, open-label NAPOLI-1 clinical trial was conducted on patients with metastatic pancreatic adenocarcinoma whose cancer had progressed after consuming the chemotherapeutic agent gemcitabine or a gemcitabine-based therapy demonstrated efficacy and safety of Onivyde[™]. The patients in the study who consumed fluorouracil/leucovorin with Onivyde[™] survived 6.1 months on average, compared with 4.2 months on average for patients who consumed either fluorouracil or leucovorin. In another study patients who consumed fluorouracil/leucovorin with Onivyde[™] had an average delay of 3.1 months in the amount of time required for tumour progression compared with 1.5 months for those who consumed either fluorouracil or leucovorin [45].

3.2. Liposomes for Fungal Infections

3.2.1. Abelcet®

Abelcet®, amphotericin B (AmB) lipid complex formulation, is a sterile, preservative-free suspension for i.v. infusion. Sigma-Tau Pharmaceuticals developed Abelcet® in 1995 for the treatment of invasive fungal infections refractory to conventional AmB desoxycholate therapy or when renal impairment or unacceptable toxicity precludes use conventional AmB. Abelcet® is a unique formulation, combined with two phospholipids in a 1:1 drug:lipid weight ratio; the stoichiometry of the molecular complex that forms between AmB and lipid is also nearly a 1:1 drug:lipid molar ratio. The lipid comprises of dimyristoyl phosphatidylcholine (DMPC) and dimyristoyl phosphatidylglycerol (DMPG) combined in a 7:3 molar ratio. The concentration of the drug in the complex is from about 25 to about 50 mol % [46]. Abelcet®, when seen in a freeze-fracture electron microscope, appeared as ribbon-like structures [47], consisting of stable drug-phospholipid single layers or rosettes of large and variable size (1 to 10 nm diameter) [48]. In spite of the high concentration of AmB in the Abelcet®, there is immediate release of AmB into the system following infusion. Pharmacokinetic studies demonstrate that there is deposition in the RES [49]. This “depot” form releases the drug at local sites of infection, may be through the action of lipase [50].

Multiple doses of Abelcet® (5 mg/kg/day for five to seven days) vs. AmB deoxycholate (0.6 mg/kg/day for 42 days) were compared. Maximum plasma concentration of about 1.7 ± 0.8 vs. 1.1 ± 0.2 µg/mL, AUC 14 ± 7 vs. 17.1 ± 5 µg·h/mL, clearance 436 ± 188.5 vs. 38 ± 15 mL/h·kg, volume of distribution 131 ± 57.7 vs. 5 ± 2.8 L/kg and half-life 173.4 ± 78 vs. 91.1 ± 40.9 h were reported for Abelcet® and AmB deoxycholate, respectively. The high clearance and large volume of distribution values from the blood of AmB following the administration of Abelcet® possibly indicate uptake by tissues. The long terminal elimination half-life apparently indicates a slow redistribution from tissues. Even though AmB is cleared slowly, there is a low concentration in the blood after multiple dosing [51].

3.2.2. Ambisome®

Ambisome® liposome for injection is a sterile, non-pyrogenic freeze-dried product for i.v. infusion. It is a product of Astellas Pharma USA approved in 1997. Ambisome® is approved for the treatment of serious, life-threatening fungal infections including leishmaniasis, aspergillosis, blastomycosis, coccidioidomycosis in febrile, neutropenic patients and a certain form of meningitis in people infected with HIV. Ambisome® is also prescribed for the treatment of invasive systemic infections caused by *Aspergillus*, *Candida*, or *Cryptococcus* in patients those cannot tolerate conventional AmB therapy or renally impaired patients.

In Ambisome®, charged complexes were observed between positively charged mycosamine of AmB and the negatively charged distearoylphosphatidylglycerol (DSPG). It also showed hydrophobic interactions with cholesterol constituents of the lipid membrane, due to which AmB gets incorporated tightly within the liposomal membrane. The lipid bilayer of Ambisome® is composed of hydrogenated soy phosphatidylcholine, cholesterol, DSPG and AmB in a 2:1:0.8:0.4 molar ratio [52]. The stability of the liposomal membrane in Ambisome® is achieved by employing saturated (rigid) phospholipids and a charged phospholipid (phosphatidylglycerol) in combination with cholesterol. Interaction between AmB with the cholesterol is direct and occurs via its sterol binding region, which also plays a role in stabilization. Ambisome® liposomes small size (100 nm) provides prolonged circulation in the plasma, along with in vivo stabilization. The content of Ambisome® was kept low, i.e., about 10% by weight, which helps in maintaining a ‘true’ liposomal formulation [53].

Preclinical data reports showed negligible haemolysis caused by Ambisome® [53]. Ambisome® demonstrated increased safety in animal models with systemic fungal infection. It was tolerated at doses higher than those of conventional AmB and possessed a higher therapeutic index [52]. Ambisome® was also shown to retain the pharmacological properties of AmB for a broad range of

fungi, including *Candida*, *Cryptococcus*, *Aspergillus*, *Blastomyces* and *Paracoccidioides* in various preclinical studies [52]. Although Ambisome[®] has a different plasma pharmacokinetic profile than lipid complex formulations [54], it remains in the plasma compartment for a longer duration, resulting in higher plasma levels compared to conventional AmB. On the other hand, the lipid complexes get rapidly cleared. Ambisome[®] still accumulates mainly in MPS-related tissues like the liver and spleen in spite of its slow clearance [55].

3.2.3. Amphotec[®]

Amphotec[®], AmB cholesteryl sulphate complex for injection is a parenteral freeze dried lipid-based formulation to receive US FDA approval. Ben Venue Laboratories Inc., Bedford, OH, USA developed Amphotec[®] in 1996 for the treatment of serious fungal infections and leishmaniasis in patients where renal disease or higher toxicity prevents the use of AmB in efficacious doses and in patients with systemic aspergillosis where previous AmB deoxycholate therapy has failed. Guo et al. first prepared a novel drug dosage form based on the particular interaction of AmB with sterols. The sodium salt of cholesteryl sulphate (CS), a naturally existing metabolite of cholesterol, forms a thermodynamically stable colloidal complex with AmB at a 1:1 drug to lipid molar ratio. Amphotec[®] is composed totally of uniform small spherical unilamellar lipid vesicles less than 100 nm in size [56]. Amphotec[®] forms a colloidal suspension of microscopic disc-shaped particles when reconstituted in an aqueous solvent. The rigidity of the lipid components offers stability to the bilayer structures [56]. When compared with a conventional AmB formulation, this unique colloidal formulation of AmB reduces haemolysis, acute toxicity and lipoprotein binding [56]. It may be that the reduction of renal toxicity is because of the strong interaction of AmB with the cholesteryl sulphate of the formulation, which decreases the amount of free AmB in circulation.

The increased safety profile of Amphotec[®] (above conventional AmB) was demonstrated in repeated animal studies, which showed a 5–8-fold reduction in renal toxicity as compared to conventional AmB. Amphotec[®] gets eliminated quickly from the circulation, mainly from MPS tissues, where it accumulates in a comparatively non-toxic form [57,58]. In a Phase I clinical trial, Amphotec[®] was shown to be safe at doses higher than conventional AmB, with an identical pattern of acute adverse effects with decreased renal toxicity [59]. Amphotec[®] at different doses of up to 8 mg/kg/day exhibited high response rates against fungal infections like candidiasis, aspergillosis and coccidioidomycosis in patients who were unresponsive or hypersensitive to conventional AmB treatment in various clinical trials [60,61]. Therefore, Amphotec[®] was significantly less nephrotoxic than conventional AmB and could be given to patients with renal diseases.

3.3. Liposomes for Photodynamic Therapy

Visudyne[®]

Visudyne[®], a product of Novartis AG, Switzerland, is the first light-activated drug available for the treatment of patients with predominantly classic subfoveal choroidal neovascularization due to age-related macular degeneration (AMD). Visudyne[®] was designed to eradicate the abnormal blood vessels in the eye related with conditions such as the wet form of macular degeneration. Visudyne[®] contains verteporfin (VPF), a synthetic chlorine-like porphyrin, which has a light absorption peak at 692 nm and is utilised as a photosensitiser for photodynamic therapy (PDT). Photodynamic therapy may offer selective eradication of the neovascular membrane while producing minimal damage to retinal and choroidal tissues. This treatment modality uses low-intensity light at a wavelength within the absorption band of the injected dye to irradiate photosensitised tissues and cause local cytotoxic effects by photochemical reactions. Visudyne[®] liposome is a unilamellar phospholipid vesicle based on lipids DMPC and egg phosphatidyl glycerol (EPG). The molar ratio of photosensitiser and mixture of phospholipids is about 1:8.0 and the size of the liposomes is between 150 and 300 nm [62].

The lipophilicity of VPF resulted in 100% efficiency of incorporation into the liposome. In addition, it is readily reconstituted to a stable liquid form and results in accurate concentration.

Biodistribution studies for liposomal VPF and aqueous VPF showed slightly higher accumulation of VPF in tumour tissue with liposomal VPF than with aqueous VPF. Clearance rates were found to be almost equivalent, i.e., half-lives of 16.1 h for liposomal VPF and 16.9 h for aqueous VPF. In a bioassay in tumour-bearing mice, when PDT was administered 3 h after i.v. administration of liposomal VPF and aqueous VPF preparation, the former was superior to the aqueous VPF preparation. In vitro plasma distribution studies demonstrated the distribution of liposomal VPF and free VPF as $91.1\% \pm 0.3\%$ and $49.1\% \pm 2.6\%$, respectively. [63]. Age-related macular degeneration with PDT analysis was the subject of two phase III clinical studies, where liposomal VPF was compared with placebo. Photodynamic therapy with VPF liposomes in selected patients with neovascular AMD lessened the possibility of moderate and severe vision loss. These advantages were retained for at least 24 months of follow-up [64].

3.4. Liposomes for Pain Management

3.4.1. DepoDur™

Epidural morphine sulphate sustained-release liposome injection DepoDur™ is a novel drug of SkyePharma, San Diego, CA, approved in 2004. DepoDur™ is intended for administration before surgery or following clamping of the umbilical cord during a caesarean section. It has been employed as a single-dose administration at the lumbar level by the epidural route.

DepoDur™ is composed of multivesicular lipid-based particles with median diameter in the range of 17 to 23 μm . Each vial contains 10 mg/mL of morphine sulphate encapsulated into liposomes that are further dispersed in a 0.9% sodium chloride preservative-free suspension. Phospholipids and other ingredients are cholesterol, 3.3 mg/mL; DOPC, 4.2 mg/mL; DPPG, 0.9 mg/mL; tricaprilyn, 0.3 mg/mL; and triolein, 0.1 mg/mL [65]. In DepoDur™ formulation, morphine is encapsulated in lipid foam by DepoFoam™ Technology. The lipid foam encapsulation of morphine permits sustained release of morphine into the epidural space for a longer time. This foam is characterised by a specific multivesicular structure of micron-size, nonconcentric aqueous chambers that encapsulate the active drug. It ruptures in a time-dependent fashion to release the encapsulated drug into the epidural space and the constituents of the foam was designed to release the morphine for a 48-h period [66].

In preclinical studies, Kim et al. observed that the release of morphine sulphate was sustained from DepoFoam™. These liposomes were given epidurally in rats and compared with systemically given morphine sulphate. Results showed that a single dose of sustained-release morphine sulphate through the epidural route was sufficient to achieve a similar onset time of maximum analgesia. It also provides significantly prolonged analgesia compared to systemic morphine sulphate. The maximal concentration for sustained-release morphine was 6% in serum and 32% in cerebrospinal fluid (CSF) compared with systemic morphine sulphate. Furthermore, a 30-fold increase in the CSF terminal half-life was detected for sustained-release morphine [67]. A pilot study was conducted in which a single dose of extended-release epidural morphine (EREM) could provide safe and effective post-operative pain relief after total hip arthroplasty under spinal anaesthesia [68]. Patients received EREM 10, 20 or 30 mg and the other group received conventional epidural morphine. The use of EREM results in decreased total fentanyl requirements, longer time to rescue and lower pain ratings over 48 h of study.

3.4.2. Exparel®

Exparel®, a bupivacaine extended-release liposome injection, is a new liposomal local anaesthetic formulation. Pacira Pharmaceuticals, Inc. has developed Exparel®, approved by the U.S. FDA in 2011. Exparel® is designed for extended release of the drug up to 72 h. Exparel® is a multivesicular liposomal formulation of bupivacaine based on Depofoam™ technology, being developed for postsurgical analgesia [69]. Exparel® contains a novel phospholipid excipient, dierucoylphosphatidylcholine (DEPC),

which is unique to this product and has not previously been included in other DepoFoam™-based approved products, e.g. DepoDur™ and DepoCyt® [70]. Other lipid components present in Exparel® are cholesterol, DPPG and tricaprylin. The median diameter of the liposome particles ranges from 24 to 31 µm [70].

Subcutaneous (s.c.) administration of 20 mL of 2% bupivacaine liposomes vs. 20 mL of 0.5% plain bupivacaine in human volunteers was compared by Davidson et al. [71]. The C_{max} values found between the two groups i.e., vs. 0.83 ± 0.34 vs. 0.87 ± 0.45 µg/mL in liposomal and plain groups, respectively, show no difference in spite of a 4-fold higher bupivacaine dose. The terminal half-life increases by 9.8-fold in the liposomal bupivacaine group i.e., 1294 ± 860 vs. 131 ± 58 min. A phase II multi-centre clinical trial confirmed the 7-fold increase in t_{max} in the liposomal bupivacaine group compared with the plain bupivacaine group, which was attributed to the sustained release of liposomal bupivacaine [72].

3.5. Liposomes for Viral Infections

3.5.1. Epaxal®

Epaxal® is the first virosome-adjuvanted vaccine for hepatitis A (HAV). It was the first product based on the liposomal vaccine or virosome technology developed and patented by Crucell Berna Biotech, Switzerland. Epaxal® has a high tolerability and the absence of aluminium and thiomersal in this vaccine allows for intradural or s.c. administration since it causes fewer adverse local effects compared with conventional aluminium-adsorbed vaccines. Epaxal® is highly effective after administration of the first dose, offering protective immunity for a limited duration. It provides immunity for up to 20 years following the second booster dose [73]. In contrast to liposomes, virosomes contain viral envelope glycoproteins intercalated in the phospholipid bilayer membrane. The HAV vaccine Epaxal® is based on formalin-deactivated RG-SB strain HAV particles, which are combined to the surface of virosomes. Virosomes are spherical vesicles composed of phospholipids, lecithin, phosphatidylcholine and phosphatidylethanolamine. They form unilamellar vesicles of approximately 150 nm in diameter. The lipid components of Epaxal® virosomes are 1,2-Dioleoyl-sn-glycero-3-phosphoethanolamine (DOPE) and DOPC present in a molar ratio of 25:75 [74]. The RG-SB HAV strain was produced on an MRC-5 human diploid cell culture and then the virus was purified from disrupted cells by ultrafiltration. HAV was deactivated by treatment with formalin and then attached to the virosome surface. This structure facilitates the delivery of the HAV antigen to immunocompetent cells owing to the properties of fusion-active glycoproteins [75]. A well-designed clinical trial study on adults [76] and children aged 1.5 to 6 years [77] demonstrated the efficacy, tolerability and immunogenicity of Epaxal®. After a booster vaccination with Epaxal® in adults, more than 95% of subjects were protected from HAV infection for more than 20 years [78]. In general, details on pharmacokinetic properties of vaccines have not been extensively reported.

3.5.2. Inflexal® V

Inflexal® V, an inactivated, virosomal-adjuvanted influenza vaccine, was developed and patented by the Crucell Berna Biotech, Switzerland. Inflexal® V is composed of haemagglutinin surface molecules of the influenza viruses, which are kept on the double membrane of lecithin-phospholipid liposomes. Inflexal® V contains 15 µg haemagglutinin each of influenza A and B virus strains. Inflexal® V virosomes are prepared by a combination of natural and synthetic phospholipids after the removal of influenza surface glycoproteins, neuraminidase (NA) and hemagglutinin (HA) by detergent treatment. The phospholipids of Inflexal® V virosomes are composed of 70% lecithin and 20% cephalin as structural components. Cephalin additionally stimulates B cells independently of T-cell determinants and can bind hepatitis A antigen. Inflexal® V contains 10% envelope phospholipids in the molar ratio of 75:25 DOPC:DOPE [79]. The resulting virosomes are spherical, unilamellar vesicles with approximately 150 nm mean diameter. Due to the low viral and avian protein content, they

are almost non-immunogenic phospholipids vesicles. The superior immunogenicity of Inflexal[®] V vs. conventional influenza vaccines has shown statistically significant improvement above other vaccines [80]. The superior immunogenicity and tolerability of Inflexal[®] V has also been shown by a comparison with Influvac, a subunit vaccine [81].

4. Liposomal Formulations in Clinical Trials

Intensive research on lipid carriers has led to the development of many new liposomal formulations for the management of various ailments. Figure 6 represents various products undergoing clinical trial investigation along with their current development phase and indication. Table 2 shows details of different liposomal products in terms of liposome composition, indication and route of administration.

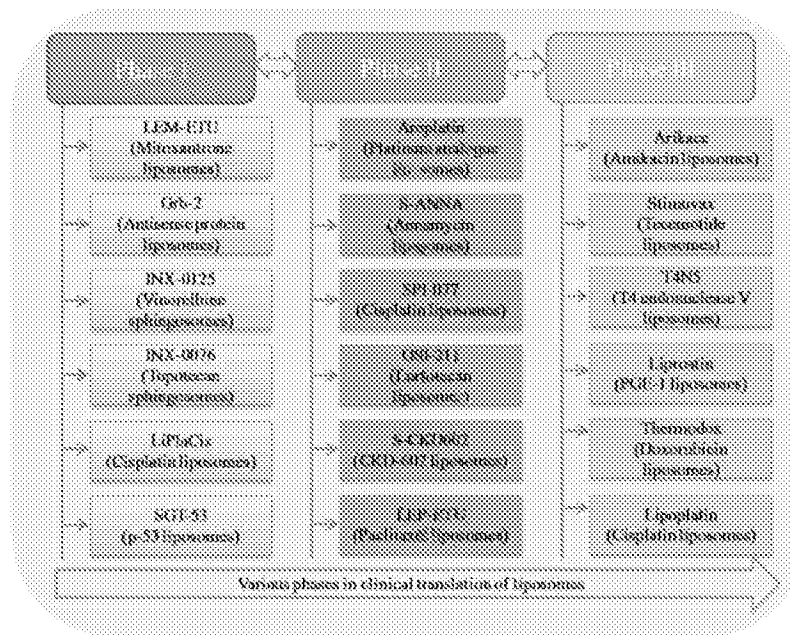


Figure 6. Liposomes present under different phases of clinical trial investigation.

4.1. Phase III

4.1.1. Arikace[™]

Arikace[™] (Transave, Inc.,) is a prolonged release amikacin (AMK) liposomal formulation for inhalation, developed using advanced pulmonary liposome technology. AMK is classified as belonging to the aminoglycoside class antibiotics, which act by inhibiting the production of bacterial proteins. It is indicated in the treatment of certain serious bacterial infections [82]. Transave, Inc. developed Arikace[™] for site-specific treatment of serious lung infections. Arikace[™] received orphan drug status from the FDA in the United States and the European Medicines Agency in Europe for the treatment of *Pseudomonas aeruginosa* (PsA) infections in patients with Cystic Fibrosis (CF). Product also received orphan drug status by FDA for *Pseudomonas*-associated non-CF bronchiectasis therapy. Transave Inc. got merged with Insmed Inc. in 2010 and the combined company filed for its orphan status with FDA and European Medicines Agency in 2011 for lung infections due to non-TB Mycobacteria (NTM). The product at present is in phase III clinical trials for these indications [83].

AMK is entrapped into liposomes (0.2–0.3 μm) composed of neutral, biocompatible lipids, i.e., DPPC and cholesterol. Arikace[™] has been administered once daily at different doses ranging from 70 to 560 via an electronic nebuliser (eFlow[®]). This device ensures the delivery of small droplet

sizes (1–5 μ) to facilitate more efficient distribution in the lungs. The formulation enables the penetration of the drug into biofilm and sustains the release of AMK in the lungs with minimal systemic exposure. The liposomal formulation achieved high lung C_{max} , AUC, $t_{1/2}$ and improved AUC:MIC ratio. It resulted in the potential inhibition of PsA pathogens, including its resistant isolates. Moreover, virulence factors secreted by PsA facilitated the further release of AMK from Arikace™ [84].

Toxicology studies in dogs and rats performed for a period of 3–6 months supported long-term clinical studies. Phase II blinded and placebo-controlled as well as multi-cycle open-label studies were performed in CF patients with chronic PsA infection for 28 days on and 56 days off cycle with once a day administration of the drug. Changes in Pulmonary Function Testing (PFT), Forced Expiratory Volume (FEV) and Colony-Forming Units (CFU) were considered as end-points of the study. Positive results were obtained from phase II studies, where there was a clinically significant improvement in lung function at the end of treatment. The observed clinical effect was dose-dependent, whereby the group that received a 560-mg dose showed a significant increase in FEV of 17.6% compared to the placebo. The product was well tolerated and no considerable difference was observed in adverse events between the Arikace™-treated and placebo groups. In summary, once a day administration of Arikace™ in CF patients with PsA infections demonstrated safety, tolerability, biologic activity and efficacy [85]. Similarly, in a randomised multi-centre study of Arikace™ in patients with NTM lung infections, a change from baseline on the semi-quantitative scale and NTM culture conversion to negative were taken as end-points. Liposomal AMK showed statistical significance in culture conversion compared to the placebo. The data obtained from clinical trials of Arikace™ confirmed the magnitude and sustained improvement of lung function. Arikace™ may be an advancement in terms of treatment options for CF patients with PsA lung infections as well as patients with NTM lung infections [86].

4.1.2. Stimuvax®

Stimuvax®, earlier known by the name BLP25 liposome vaccine, is a therapeutic vaccine indicated for certain types of cancer expressing Tumour-Specific Antigens (TSA). This cancer vaccine incorporates an antigenic lipo-peptide, i.e., Tecemotide (TCM), in a liposomal delivery system. TCM targets mucin 1 (MUC1), which is overexpressed in different cancer cells, including breast, prostate, non-small cell lung cancer (NSCLC) and colorectal cancer. MUC1 gets abnormally glycosylated when a cell becomes cancerous in nature. Stimuvax, upon targeting TSA, triggers a cellular immune reaction which leads to immune rejection of tumours that have the MUC1 antigen. Although it is referred to as a cancer vaccine, it does not actually prevent cancer but aids in enhancing the life expectancy of cancer patients. The product was initially developed by Cancer Research UK and was taken forward by Oncothyreon, Inc. (formerly known as Biomira, Inc.) [87]. In 2008, Merck KgaA acquired the product rights to Oncothyreon. Stimuvax® showed a positive response, i.e., a significant increase in life expectancy from 13.3 to 30.6 months, in its phase II trials. As a shocking disclosure in the field of cancer research, Stimuvax® faced failure in phase III trials as the vaccine did not meet its primary or secondary end-points of the study, which led to its termination [88].

The liposomal vaccine is composed of synthetic MUC1 lipopeptide (antigen), monophosphoryl lipid A (immunoadjuvant), cholesterol, DMPC and DPPC lipids. This vaccine is a lyophilised powder, which contains 300 μ g of TCM and 150 μ g of monophosphoryl lipid A per vial. Patients are treated with a 300 mg/m² cyclophosphamide i.v. dose followed by weekly s.c. injections of Stimuvax® for eight consecutive weeks in a phase II study. Vaccination with Stimuvax® stimulates immune-response-mediated, MUC1-specific cytotoxic T lymphocytes (CTL), which destroys cancer cells [89,90].

A positive outcome was obtained in stage III and IV NSCLC patients in an early-stage trial with Stimuvax®. It was the first product belonging to the class of cancer vaccines that entered advanced clinical trial phase III. Three worldwide phase III clinical trials, namely START (Stimulating Targeted Antigenic Responses to NSCLC), INSPIRE (Stimuvax® trial In Asian NSCLC Patients: Stimulating Immune REsponse) and STRIDE (STimulating Immune Response In aDvanced brEast cancer), were

initiated and sponsored by EMD Serono for Stimuvax[®]. Although the START study failed to meet its primary end-point, there was significant survival advantage in the subgroup of patients, which led to the START 2 and INSPIRE trials [91]. However, the product failed to meet its primary or secondary end-points, which led to the unfortunate termination of the Stimuvax[®] trial. In 2014, the company announced that it was discontinuing its worldwide clinical trials associated with TCM [88].

4.1.3. T4N5

T4N5 liposomal lotion, also known as bacteriophage T4 endonuclease V in liposomal lotion or Dimericine (DMC), has been developed to deliver DNA repair enzyme topically in Xeroderma pigmentosum patients [92]. This is a genetic disease making the individual susceptible to skin cancer. The liposomal lotion has also been reported to reduce the incidence of pre-malignant actinic keratosis by 68% and basal cell carcinoma by 30%. It is a lead product of ACI Dermatics, Inc., and the product received fast track designation in 2007 for Xeroderma pigmentosum in the USA. Upon administration of T4N5 lotion, T4-bacteriophage endonuclease V, a DNA repair enzyme, makes its entry into dermal cells. T4N5 then enters cell nuclei, where it attaches and incises pyrimidine dimers, which leads to catalysis of the first step of the cellular excision repair pathway. This further prevents pyrimidine dimers that inhibit DNA replication, which are produced within duplex DNA upon ultraviolet (UV) exposure. In vitro and in vivo studies showed that DMC improves the repair of UV-irradiation-associated DNA [92,93].

T4N5 liposomes are composed of egg lecithin and these are known to act by two different mechanisms, i.e., via removal of cyclobutane pyrimidine type DNA dimers or by restoring p53 gene function [94]. Phase I and phase II trials of DMC indicated for the prevention of skin cancer in Xeroderma pigmentosum patients were completed. However, phase III trials of this product were terminated in 2009. Although it seemed to be promising until phase II, the lack of expected clinical outcomes led to the termination of the T4N5 liposomes trial [95].

4.1.4. Liprostin[™]

Liprostin[™], or prostaglandin E-1 (PGE-1)-encapsulated liposomes, has been developed for the therapy of various cardiovascular diseases such as restenosis subsequent to angioplasty. Restenosis is associated with re-blockage of blood vessels in heart and legs following catheter intervention, which is a very expensive medical issue. PGE-1 is known to act as a potent vasodilator, platelet inhibitor, anti-inflammatory and anti-thrombotic agent [96]. Liprostin[™] has been developed by Endovasc Ltd., a biopharmaceutical company focused on developing liposomes for generic products that have safety and efficacy. The company has three patents covering the use of Liprostin[™] in various cardiovascular ailments. Liprostin[™] improved the drug dynamics and improved the therapeutic index of various ailments including occlusive disease, limb salvage, claudication and arthritis [97]. Endovasc has been granted a conditional waiver by the FDA for clinical trials. AngioSoma acquired Liprostin[™] in 2016 and phase II trials of the product were completed with excellent outcomes in peripheral vascular disorders, i.e., intermittent claudication. The company is planning a phase III trial for the product in treatment of intermittent claudication. This is the first clinical research trial where a vasoactive hormone like PGE1 has been used as an adjunct treatment along with angioplasty procedure [98]. The development of this product will have a significant, positive impact in terms of symptomatic relief by preventing blood vessel re-blockage.

4.1.5. ThermoDox[®]

ThermoDox[®], the only responsive liposomal formulation in clinical trials, is the temperature-sensitive liposomal formulation of approved drug DOX [99]. ThermoDox[®] has been developed by Celision Corporation, a leading oncology firm focused on the development of innovative anti-cancer drugs. It is indicated in primary liver cancer (hepatocellular carcinoma) and also recurring chest wall breast cancer. These liposomes are composed of DPPC, Myristoylstearyl phosphatidylcholine (MSPC) and

1,2-distearoyl-sn-glycero-3-phosphoethanolamine-*N*-[amino(polyethylene glycol)-2000] (DSPE-PEG-2000). Three component lipids have been combined to attain the specific function and specific material properties associated with lipids, i.e., sharp thermal transition and rapid onset of membrane permeability [99]. This specific combination leads to the development of proprietary heat-activated DOX liposomes. The phase transition temperature of DPPC is 41.5 °C, and it undergoes phase change at 42 °C, which can be attained clinically by local hyperthermia. The addition of MSPC to the composition accelerates drug release by a slight reduction in the transition temperature of DPPC, while DSPE-PEG-2000 enhances the circulation time of liposomes. The presence of PEG lipid also helps in attaining lysolipid-induced permeability at a faster rate. The potential of stimulating drug release in tumour targeting has been realised with ThermoDox[®] [100,101].

ThermoDox[®] is administered by the i.v. route in combination with Radio-Frequency Ablation (RFA) [102]. This product can also be used in combination with microwave hyperthermia or high-intensity focused ultrasound [103]. Local hyperthermia (39.5–42 °C) induced by RFA release the encapsulated DOX from liposomes and attains high drug concentrations in the targeted tumour. ThermoDox[®] achieved 25-fold higher drug concentration in the target site than a normal i.v. infusion and 5-fold higher drug concentration compared to standard DOX liposomes. Enhanced release of DOX from liposomes is due to grain boundary permeabilisation at the phase transition temperature [104]. This product received orphan drug designation from the European Commission, USA orphan drug status and FDA fast track designation for the treatment of hepatocellular carcinoma. Currently, phase III trials (HEAT study) are being evaluated in patients with primary liver cancer, which is non-resectable. A phase III heat study has received regulatory agency support in 11 countries worldwide. Other clinical trials associated with the product are OPTIMA (treatment of hepatocellular carcinoma with ThermoDox with standardised RFA) and TARDOX (targeted chemotherapy using focused ultrasound for liver tumours) [105,106].

4.1.6. Lipoplatin[™]

Lipoplatin[™] is a proprietary liposomal formulation of Cisplatin (CPT), an FDA-approved, commercially available cytotoxic agent. CPT has been categorised under DNA cross-linking agents or DNA synthesis inhibitors. The product has been introduced as Lipoplatin[™] for the treatment of pancreatic cancer and Nanoplatin[™] for lung cancer. This product has been developed by Regulon Inc., an oncology-focused drug delivery firm aimed at developing improved versions of leading chemotherapy drugs [107]. Lipoplatin[™] is composed of lipids including DPPG, soy PC, MPEG-DSPE lipid conjugate and cholesterol. CPT liposomes have been indicated against various indications, i.e., pancreatic cancer, non-small cell lung cancer, testicular and ovarian carcinoma, head and neck cancer as well as bladder cancer. Encapsulation of CPT into liposomes offer various advantages in terms of high encapsulation efficiency, long-term circulation in vivo, ability to attain 200-fold higher concentration in tumours compared to CPT alone and ability to penetrate the cell membrane [108].

Lipoplatin[™] has been used in combination with gemcitabine in pancreatic cancer [109], while it has been used in combination with pemetrexed in NSCL. The product is presently in phase I trials for malignant pleural effusion, phase II trials for breast cancer and gastric cancer, phase II/III trials for pancreatic cancer and phase III trials for NSCL [110]. Lipoplatin[™] has considerably reduced the adverse effects associated with CPT including renal toxicity, peripheral neuropathy, ototoxicity and myelotoxicity [111]. The European Medicines Agency granted orphan drug status to this product for pancreatic cancer treatment.

4.2. Phase II

4.2.1. Aroplatin[™]

Aroplatin[™] (L-NDDP, AR 726) is a chemotherapeutic platinum analogue *cis*-(*trans*-R,R-1,2-diaminocyclohexane) bis (neodecanoato) platinum (II) (NDDP) encapsulated liposomal product.

This is the first liposomal platinum formulation to enter into clinical trials and the loaded analogue is structurally similar to Eloxatin (Oxaliplatin; Sanofi Aventis). These platinum analogues exhibit tumour cell cytotoxicity by forming inter- and intra-strand cross-links of DNA, thereby inhibiting its synthesis [112,113]. DMPC- and DMPG-composed multilamellar liposomes were prepared to encapsulate NDDP analogues. The liposomal formulation accumulates NDDP to a great extent in target sites when compared to CPT. The analogue, when delivered by L-NDDP, inhibits the emergence of liver metastasis of reticulosarcoma in mice, proving the formulation to be beneficial compared to the drug alone. The improved activity of liposomal formulation has been attributed to intraliposomal activation by reaction with DMPG. Liposomal formulation improved the bioavailability of NDDP and reduced its toxicity profile [114].

L-NDDP has been developed by Agenus Inc., while Aronex Pharmaceuticals procured the ownership for investigational new drug application of Aroplatin™. The product received orphan drug designation for malignant mesothelioma from the U.S. FDA. In 2002, a phase II monotherapy trial was completed for the product towards indication of metastatic colorectal cancer [115]. In 2002, a phase I/II trial of Aroplatin™ was completed for advanced solid malignancies. However, in 2005, after a phase I dose escalation trial of the product, as the maximum tolerated dose had been reached, the trial was closed and no further internal development of the product has been pursued. Besides the results observed from clinical trials, the imprecise chemical composition along with the instability of the drug in liposomes led to the termination of its clinical investigation. Almost 50% degradation of the complex was observed after reconstitution, where neodecanoic acid gets hydrolysed, which results in the further inactivation of drug [116].

4.2.2. Liposomal Annamycin

Liposomal annamycin (L-Annamycin, Annamycin-LF, S-ANNA) is a liposomal formulation encapsulating the semi-synthetic DOX analogue annamycin. Liposomal vesicles of annamycin are composed of DMPC and DMPG in a 7:3 molar ratio. This liposomal composition allowed higher entrapment of the drug as well as flexibility in the selection of formulation, which delivers a higher proportion of drug to tumour [117]. This therapeutic moiety acts by DNA intercalation and the inhibition of topoisomerase II, further inhibiting DNA replication and protein synthesis. This formulation is also found to circumvent multidrug-resistance transporters, including p-glycoprotein. L-Annamycin has been developed to avoid the cardiotoxicity associated with available anthracyclines and is found to be less toxic with improved anti-tumour activity. Unmet medical need in the areas of acute myeloid leukaemia or acute lymphoid leukaemia necessitate the need for this product development [118,119]. This product has been developed by Aronex Pharmaceuticals and in 2015, Moleculin Biotech, Inc. made an agreement to acquire the rights for clinical stage development of L-Annamycin.

The product completed phase I and phase II trials in patients with refractory or relapsed acute lymphocytic leukaemia [120]. Both trials showed fewer dose-limiting toxicities compared to DOX and also improvement with respect to the clearance of leukaemic blasts [121]. Moleculin Biotech, Inc. has been planning accelerated approval of the product for acute myeloid leukaemia. The company also intends to apply for its orphan drug status in the USA for acute myeloid leukaemia.

4.2.3. SPI-077

Liposomal CPT (SPI-077) is a formulation that encapsulates CPT within liposomal vesicles composed of a 51:44:5 molar ratio of hydrogenated soybean PC, cholesterol and *N*-(carbamoyl-methoxypolyethylene glycol 2000)-1, 2-distearoyl-*sn*-glycero-3-phospho-ethanolamine sodium salt [10]. The formulation contains 14 µg of CPT/mg of lipid in 110-nm liposomal vesicles. The clinical efficacy of CPT is limited by intrinsic resistance and systemic toxicity. STEALTH®, a (sterically stabilised) liposomal formulation of CPT (SPI-077), showed significant improvement in preclinical models, with appreciably greater tumour growth delay than CPT [122]. This is the first CPT liposomal formulation that entered clinical stage development. The product has been developed by Alza Corporation for

the treatment of lung, head and neck cancer. The product is currently in phase II clinical trials, while pre-clinical trials showed that SPI-077 exhibited improvement of stability, prolonged circulation time, enhanced anti-tumour effect and decreased side effects compared with the free drug [123]. However, in clinical trials, the formulation failed to demonstrate efficacy, which may be due to incomplete release of the drug from liposomes at the target site.

4.2.4. OSI-211

OSI-211 is a next-generation cytotoxic and liposomal formulation of lurtotecan (LRT) (OSI-211, NX 211), a novel topoisomerase I inhibitor that has applications in ovarian, head and neck cancer. The liposomes are composed of a 2:1 molar ratio of HSPC and cholesterol and the product is currently in phase II clinical trials. OSI Pharmaceuticals developed liposomes of LRT, which is another water-soluble camptothecin analogue [96]. The product demonstrated a 9%–67% increased drug accumulation in tumour accumulation in comparison to a drug delivered in 5% dextrose in preclinical trials. This product is being developed with the goal of developing a competitor to topotecan with superior efficacy and an equivalent or better toxicity profile for refractory ovarian cancer. OSI-211 showed a similar toxicity profile in a randomised phase II clinical trial when compared with topotecan in relapsed ovarian cancer treatment. The study of this formulation is ongoing in alternate patient populations or in alternate schedules [124].

4.2.5. S-CKD602

S-CKD602 is a pegylated liposomal formulation encapsulated with potent topoisomerase I inhibitor (CKD-602), developed by the Alza Corporation. This formulation has been associated with a long circulation property that assists in the improvement of AUC. CKD-602 is a semi-synthetic analogue of camptothecin, which, when encapsulated into liposomes, increased the AUC 50-fold compared to non-liposomal CKD-602 [125]. The STEALTH liposomes of the camptothecin analogue (CKD-602) are composed of a lipid bilayer with MPEG linked phospholipids on the outer surface. The inclusion of MPEG lipids into liposomes imparts properties of prolonged plasma circulation and improved drug delivery into tumours compared to conventional liposomes [113]. In preclinical studies conducted with these liposomes, there is a 3–10-fold increase in therapeutic index compared to the non-liposomal formulation. S-CKD602, presently under phase II trial investigation, exhibited an interesting property of greater distribution in fat compared to muscle tissue, which varies according to the body composition of a patient [126].

4.2.6. LE-SN38

LE-SN38 is a liposomal product encapsulated with SN-38, which is an IRI active metabolite (Camptostar[®], Pfizer, Inc.) that has been developed by NeoPharm Labs Ltd. [127]. Camptostar[®] is a chemotherapeutic prodrug indicated for advanced colorectal cancer [128]. LE-SN38 is formulated by using NeoLipid[®] patented technology with the goal of delivering the active drug without the need for conversion, which further minimises the variability and optimises the dose with minimum side effects. It is composed of a 50:40:10 molar ratio of DOPC, cholesterol and cardiolipin and a drug to lipid ratio of 1:18 [127]. LE-SN38 improved the pharmacodynamic profile of a relatively insoluble compound, SN38, in parallel with an improved safety and efficacy profile when compared with the pro-drug version. The product demonstrated safety and tolerability in its phase I trial investigation. SN-38, when delivered via liposomes, achieved similar blood levels and a systemic effect comparable to or greater than Camptostar[®]. The product is currently undergoing phase II clinical trial investigation for patients with metastatic colorectal cancer [129].

4.2.7. LEP-ETU

LEP-ETU is a liposomal formulation of paclitaxel (PTX); ETU in the code represents an easy-to-use formulation. PTX is a well-established therapeutic moiety used for ovarian cancer therapy. It is

also developed by NeoPharm Labs using its proprietary NeoLipid[®] technology. These liposomes are composed of a 90:5:5 molar ratio of DOPC, cholesterol and cardiolipin and a final total lipid to drug molar ratio of 33:1. This formulation achieved a maximum of 85% entrapment efficiency of PTX [130]. This technology eliminates the use of cremophor, which in turn circumvents the limitations and adverse effects associated with Taxol[®] treatment. The clinical trial development of this formulation has been sponsored by Insys Therapeutics, Inc. and has an FDA-approved orphan drug designation for ovarian cancer therapy. Entrapment of PTX in liposomes demonstrated reduced toxicity with similar efficacy when compared with Taxol[®]. Pharmacokinetic data in patients are in correlation with preclinical data, which suggests comparable properties between LEP-ETU and Taxol[®] [131,132]. The product is presently under phase II clinical trial investigation.

4.2.8. Endotag-I

Endotag-I is another PTX liposomal formulation composed of cationic lipid dioleoyloxypropyltrimethylammonium (DOTAP) and neutral lipid (DOPC) [DOTAP:DOPC:PTX in 50:47:3]. This product has been developed by Medigene, which has an agreement with SynCore Biotechnology Co. for the complete technology transfer of EndoTAG[®] [133,134]. These liposomal vesicles, being cationic in nature, interact with negatively charged endothelial cells required for tumour angiogenesis. PTX released from Endotag[®]-I attacks the activated and dividing endothelial cells of a tumour, thus damaging the tumour blood supply without affecting healthy tissue. This mechanism of EndoTAG[®] prevents angiogenesis in the tumour and thereby inhibits tumour growth. The anti-cancer efficacy of PTX, along with inhibition of tumour vasculature via vascular targeting of cationic liposomes, is the major mechanism behind the efficacy of EndoTAG[®] in breast and pancreatic cancer therapy. The product is currently under phase II clinical trial investigation, where it showed prolonged survival rates when used along with gemcitabine in patients with pancreatic adenocarcinoma [135].

4.2.9. Atragen[®]

Atragen[®] is an all-trans retinoic acid encapsulated liposome composed of tretinoin, DMPC, and soybean oil with 2 mg of tretinoin/mL. All-trans retinoic acid is a protein synthesis inhibitor or retinoic acid receptor agonist that acts by affecting gene expression, leading to cell differentiation and a reduction in cell proliferation. Retinoic acid also inhibits telomerase, which leads to the shortening of telomeres that leads to apoptosis of tumour cells [136]. This product has been developed by Aronex Pharmaceuticals for acute promyelocytic leukaemia and other hematologic malignancies [137]. The encapsulation of retinoic acid into liposomes improves the half-life of intravenously administered tretinoin. The clinical development (Phase II) of Atragen[®] has been designed to determine its potential towards management of hormone-resistant prostate cancer, renal cell carcinoma and acute myelogenous leukaemia [138].

4.3. Phase I

Apart from liposomal formulations listed under phase III and phase II trials, some liposomes like LEM-ETU, liposomal Grb-2, INX-0125, INX-0076 etc., are currently undergoing phase I clinical trial investigation. LEM-ETU is a liposomal formulation entrapped with Mitoxantrone, composed of a 90:5:5 molar ratio of DOPC, cholesterol and cardiolipin [139]. The product has been developed by NeoPharm's NeoLipid liposome technology for the management of various cancers [140]. The co-lipid cardiolipin plays a key role in drug entrapment as this negatively charged diphosphatidyl glycerol lipid forms an electrostatic interaction with loaded moiety. This in turn leads to higher drug loading capability compared to other liposome formulations [141]. This product has been developed for the treatment of leukaemia, breast, stomach, liver and ovarian cancers. Liposomal Grb-2 is a liposomal formulation entrapped with antisense oligodeoxynucleotide growth factor receptor bound protein 2 (Grb-2). This protein possesses potent antineoplastic activity that acts by inhibition of cancer cell proliferation [142]. This has been developed by Bio-Path holdings for the treatment of breast cancer and various types of

leukaemia. Overexpression of the Grb2 protein and amplification of the GRB2 gene have been reported in human cancer cell lines. Liposomal Grb-2, also known as BP-100-1.01, is a DOPC-incorporated antisense oligonucleotide formulation developed to inhibit the production of the growth factor receptor-bound protein-2 (Grb-2) [143]. The safety, maximum tolerated dose, optimal therapeutic dose and anticancer activity of liposomal Grb-2 have been investigated for the treatment of relapsed or refractory acute myeloid leukaemia. A dose range of 5 mg/m² to 90 mg/m² is well tolerated in these patients, with no product-related toxicities. Grb-2 target protein downregulation and promising anti-leukaemia activity were demonstrated in this study [144]. Liposomal formulations have been developed that incorporate sphingomyelin and saturated fatty acid chains in the cholesterol-rich liposomes [145].

INX-0125 (sphingosine-encapsulated vinorelbine tartrate) and INX-0076 (sphingosine-encapsulated topotecan), which come under the category of sphingosomes, have been developed by Inex Pharmaceuticals and are undergoing phase I investigation. Both the liposome formulations are composed of cholesterol and SM in a 45:55 molar ratio and are indicated for advanced solid tumours [113]. INX-0125 has been developed for the treatment of Hodgkin's disease and non-Hodgkin's lymphoma. Sphingosomal encapsulation is a novel platform for targeted liposomal drug delivery, which is capable of increasing tumour targeting significantly and improves the duration of exposure for loaded anticancer agents. This also demonstrated an improved dose intensity without any increase in toxicity in preclinical trials [146]. Another product developed by the sphingosomal platform, INX-0076, encapsulates topotecan, which is a camptothecin analogue. This liposomal platform protects the drug from *in vivo* degradation, which has been demonstrated in preclinical trials and can specifically accumulate at target sites. This in turn increases the efficacy and reduces the dose compared to the free drug. Both the abovementioned sphingosomal formulations have been developed for advanced solid tumours [147].

Other products currently in phase I/II include PLK1 siRNA (TKM-080301) indicated for neuroendocrine tumours, PKN3 siRNA (Ato027) for pancreatic cancer and DOX (2B3-101) for solid tumours. TKM 080301 is a stable nucleic acid lipid particle (SNALP)-encapsulated siRNA targeting PLK1. This siRNA is targeted against polo-like kinase 1 (PLK1), a protein that plays a key role in tumour cell proliferation. Inhibition of PLK1 expression prevents tumour cell growth and thereby inhibits cancer cell proliferation. This product was evaluated in patients with gastrointestinal neuroendocrine tumours and adrenocortical carcinoma [148]. PKN3 siRNA is a lipoplex formulation containing siRNA directed against protein kinase N3 (PKN3). This is encapsulated in catiogenic and fusogenic lipids and demonstrated potential antineoplastic activity. Upon delivery, PKN3 siRNAs bind to PKN3 mRNAs and inhibit translation and expression of the PKN3 protein. Extensive preclinical studies demonstrated the anti-metastatic effect by targeting systemic vasculature in a prostate cancer model [149,150]. 2B3-101 is a PEGylated liposomal DOX formulation that targets patients with brain metastases [151]. Targeting brain tumours is challenging due to the limitation posed by the blood-brain barrier (BBB) as it restricts the entry of endogenous molecules as well as xenobiotics. The technology behind the development of 2B3-101 is termed G-technology, which is based on safe receptor biology in humans. It is the most flexible technology for the encapsulation of various molecules, i.e., high and low molecular weight drugs as well as hydrophilic and lipophilic compounds without any modifications of the payload [152]. This product is developed based on glutathione PEGylation, where glutathione enhances the delivery of encapsulated moiety across the BBB [153].

Products including CEBPA siRNA (MTL-CEBPA) for liver cancer, Docetaxel (ATI-1123) for solid tumours, Vinorelbine (Alocrest) for breast and lung cancers, CPT (LiPlaCis) for advanced solid tumours, DOX (MCC-465) for metastatic stomach cancer, p53 gene (SGT-53) for various solid tumours etc., were also in phase I clinical trial investigation [154]. Other products currently undergoing phase I trials, their lipid compositions and indications are listed in Table 2.

Table 2. Liposomal formulations present in clinical trials.

SN	Products	Administration	Active Agent	Lipid Composition	Indication	Company
Phase III						
1	Acikase	Aerosol delivery	Amikacin	DMPC and cholesterol	Long infections	Transave Inc.
2	Rintavaz	s.c.	Tecemotide	Cholesterol, DMPC, DPPC	Non-small cell lung cancer	Oncothyreon Inc.
3	1315 liposomal lotion	Topical	T4 endonuclease V	Egg lecithin	Xeroderma pigmentosum	AGI Dermatics Inc.
4	Liprosin	i.v.	Prostaglandin E 1 (PGE 1)	Unknown	Restenosis after angioplasty	Endovase Inc.
5	ThermdDox	i.v.	Doxorubicin	DPPC, Myristoylseryl phosphatidylcholine and DSPC-N-(amino)polysilylene glycol-2000	Hepatocellular carcinoma and also recurring chest wall breast cancer	Celsion
6	Lipoptatin	i.v.	Cisplatin	DEPG, soy phosphatidyl choline, mPEG-distearyl phosphatidylethanolamine lipid conjugate and cholesterol	Non-small cell lung cancer	Regeneron Inc.
Phase II						
7	Atropofin	i.v.	Platinum analogue cis-(trans-R,R'-1,2-bis(oxo)cyclohexane) bis (neodecanoato) platinum (II)	DMPC and DMPC	Metastatic colorectal cancer	Agenos Inc.
8	Liposomal anastrozole	i.v.	Semi-synthetic dioxotubacin analogue anastrozole	DMPC and DMPC	Relapsed or refractory acute myeloid leukaemia	Aronex Pharmaceuticals
9	SP-877	i.v.	Cisplatin	Soybean phosphatidylcholine, cholesterol	Lung, head and neck cancer	Alza Corporation
10	OSI-211	i.v.	Losifotecan	HSPC and cholesterol	Ovarian, head and neck cancer	OSI Pharmaceuticals
11	S-CKD662	i.v.	Potent topoisomerase I inhibitor	Phospholipids covalently bound to mPEG	Cancer	Alza Corporation
12	TE-SN38	i.v.	Irinotecan's active metabolite	DOPC, cholesterol and cardiolipin	Advanced colorectal cancer	NeoPharm Labs Ltd
13	LEP-ETU	i.v.	Paclitaxel	DOPC, cholesterol and cardiolipin	Cancer	NeoPharm Labs Ltd.
14	Endotag-1	i.v.	Paclitaxel	DOTAP, DOPC, Paclitaxel	Breast and pancreatic cancers	Medigene
15	Abraxen	i.v.	All-trans retinoic acid	DMPC and soybean oil	Hormone-resistant prostate cancer, renal cell carcinoma and acute myelogenous leukaemia	Aronex Pharmaceuticals

Table 2. Cont.

SN	Products	Administration	Active Agent	Lipid Composition	Indication	Company
Phase I						
16.	LEM-FYU	i.v.	Mitomycin	DOPC, cholesterol and cardiolipin	Various cancers	Neodharma Labs Ltd
17.	Liposomal Grb-2	i.v.	Antisense oligodeoxynucleotide growth factor receptor bound protein 2 (Grb-2)	Unknown	Hereditary malignancies	Bio-Path Holdings
18.	BNX-0125	i.v.	Vincristine tartrate	Cholesterol and sphingomyelin	Advanced solid tumours	Ineo Pharmaceuticals
19.	BNX-0076	i.v.	Topotecan	Cholesterol and sphingomyelin	Advanced solid tumours	Ineo Pharmaceuticals
20.	TKM-060201	Hepatic intra-arterial administration	PLK1 siRNA	Unique LNP technology (formerly referred to as stable nucleic acid lipid particles or SNALP)	Neuroendocrine tumours	Tekmira Pharmaceuticals
21.	Ab027	i.v.	FKNS siRNA	ALIOFECT01	Pancreatic cancer	SiGene Therapeutics
22.	Z63-191	i.v.	Doxorubicin	Glutathione PEGylated liposomes	Solid tumours	Z-NBB therapeutic
23.	MYL-CYBPA	i.v.	CYBPA siRNA	SMARTICLES [®] liposomal nanoparticles	Liver cancer	siRNA Therapeutics
24.	ATI-1123	i.v.	Docetaxel	Protein stabilizing liposomes (PSL [®])	Solid tumours	Azaya therapeutic
25.	UPhacis	i.v.	Cisplatin	The lipid composition of the UPhacosomes is tailored to be specifically sensitive to degradation by the sPLA2 enzyme	Advanced solid tumours	Oncology Venture
26.	MCC-465	i.v.	Doxorubicin	DPPC, cholesterol and maleiminated palmitoyl phosphatidyl ethanolamine; immunoliposomes tagged with PEG and the Fab [®] /2 fragments of human monoclonal antibody G4H	Metastatic stomach cancer	Mitsubishi Tanabe Pharma Corporation
27.	SGT-53	i.v.	p53 gene	Cationic lipids complexed with plasmid DNA encoding wild-type p53 tumour suppressor protein	Various solid tumours	SynerGene Therapeutics
28.	Alocresit	i.v.	Vinorelbine	Sphingomyelin/cholesterol (OPTISOME [®])	Breast and lung cancers	Spectrum Pharmaceuticals

DMPC (Dimyristoyl phosphatidylglycerol); DPPC (Dipalmitoyl phosphatidylcholine); DPPG (Dipalmitoyl phosphatidylglycerol); DMPC (dimyristoyl phosphatidylcholine); HSPC (hydrogenated soy phosphatidylcholine); PEG (polyethylene glycol); mPEG (methoxy polyethylene glycol); DOPC (dioleoylphosphatidylcholine); DSPE (distearoyl-sn-glycero-phosphoethanolamine); i.v. intravenous.

5. Conclusions

Liposomes made their successful entry into the market in 1995 with the development of the PEGylated liposomal formulation Doxil[®]. Since its entry, there has been no looking back for these delivery systems, which have been explored for various diseases ranging from cancer treatment to pain management. The main advantages of liposomes include: control over pharmacokinetics' and pharmacodynamics' properties, improved bioavailability and limited toxicity. Together these confer on liposomes the ability to overcome the limitations of conventional therapy. Different types of liposomes, e.g., PEGylated liposomes (Lipodox), temperature sensitive liposomes (ThermoDox), cationic liposomes (EndoTAG-1) and liposomal vaccines (Epaxal and Inflexal V), demonstrate the intense research on liposomes. Several liposomes were successfully translated into the clinic and other liposomal formulations are in different phases of clinical investigation. Although many of these products have been proven to be beneficial in preclinical trials, only formulations that show efficacy in clinical trials will make their way into the clinic. In summary, the liposomes currently in clinical trials may provide benefits to the diversified patient population for various therapeutic applications.

Conflicts of Interest: The authors declare no conflict of interest.

References

1. Bangham, A.; Standish, M.M.; Watkins, J. Diffusion of univalent ions across the lamellae of swollen phospholipids. *J. Mol. Biol.* **1965**, *13*, 238–252. [CrossRef]
2. Torchilin, V.; Weissig, V. *Liposomes: A Practical Approach*; Oxford University Press: Kettering, UK, 2003; pp. 77–101.
3. Barenholz, Y.C. Doxil[®]—The first FDA-approved nano-drug: Lessons learned. *J. Control. Release* **2012**, *160*, 117–134. [CrossRef] [PubMed]
4. Veronese, F.M.; Harris, J.M. Introduction and overview of peptide and protein pegylation. *Adv. Drug Deliv. Rev.* **2002**, *54*, 453. [PubMed]
5. Leonard, R.; Williams, S.; Tulpule, A.; Levine, A.; Oliveros, S. Improving the therapeutic index of anthracycline chemotherapy: Focus on liposomal doxorubicin (Myocet[™]). *Breast* **2009**, *18*, 218–224. [CrossRef] [PubMed]
6. Murry, D.J.; Blaney, S.M. Clinical pharmacology of encapsulated sustained-release cytarabine. *Ann. Pharmacother.* **2000**, *34*, 1173–1178. [CrossRef] [PubMed]
7. Slingerland, M.; Guchelaar, H.-J.; Gelderblom, H. Liposomal drug formulations in cancer therapy: 15 Years along the road. *Drug Discov. Today* **2012**, *17*, 160–166. [CrossRef] [PubMed]
8. Working, P.; Dayan, A. Pharmacological-toxicological expert report. CAELYX (Stealth liposomal doxorubicin HCl). *Hum. Exp. Toxicol.* **1996**, *15*, 751. [PubMed]
9. Gabizon, A.; Shmeeda, H.; Barenholz, Y. Pharmacokinetics of pegylated liposomal doxorubicin. *Clin. Pharmacokinet.* **2003**, *42*, 419–436. [CrossRef] [PubMed]
10. Barenholz, Y. Liposome application: Problems and prospects. *Curr. Opin. Colloid Interface Sci.* **2001**, *6*, 66–77. [CrossRef]
11. Barenholz, Y.; Haran, G. Efficient Loading and Controlled Release of Amphipathic Molecules. U.S. Patent No. 5,316,771, 31 May 1994.
12. Lasic, D.; Frederik, P.; Stuart, M.; Barenholz, Y.; McIntosh, T. Gelation of liposome interior A novel method for drug encapsulation. *FEBS Lett.* **1992**, *312*, 255–258. [CrossRef]
13. Lasic, D.; Čeh, B.; Stuart, M.; Guo, L.; Frederik, P.; Barenholz, Y. Transmembrane gradient driven phase transitions within vesicles: Lessons for drug delivery. *Biochim. Biophys. Acta (BBA) Biomembr.* **1995**, *1239*, 145–156. [CrossRef]
14. Gabizon, A.A. Liposome circulation time and tumor targeting: Implications for cancer chemotherapy. *Adv. Drug Deliv. Rev.* **1995**, *16*, 285–294. [CrossRef]
15. Gabizon, A.; Catane, R.; Uziely, B.; Kaufman, B.; Safra, T.; Cohen, R.; Martin, E.; Huang, A.; Barenholz, Y. Prolonged circulation time and enhanced accumulation in malignant exudates of doxorubicin encapsulated in polyethylene-glycol coated liposomes. *Cancer Res.* **1994**, *54*, 987–992. [PubMed]
16. Batist, G. Cardiac safety of liposomal anthracyclines. *Cardiovasc. Toxicol.* **2007**, *7*, 72–74. [CrossRef] [PubMed]

17. Petre, C.E.; Dittmer, D.P. Liposomal daunorubicin as treatment for Kaposi's sarcoma. *Int. J. Nanomed.* **2007**, *2*, 277.
18. Allen, T.M.; Martin, R.J. Advantages of liposomal delivery systems for anthracyclines. In *Seminars in Oncology*; Elsevier: Amsterdam, The Netherlands, 2004.
19. Forssen, E.A.; Ross, M.E. DaunoXome[®] treatment of solid tumors: Preclinical and clinical investigations. *J. Liposome Res.* **1994**, *4*, 481–512. [CrossRef]
20. Forssen, E.A.; Coulter, D.M.; Proffitt, R.T. Selective in vivo localization of daunorubicin small unilamellar vesicles in solid tumors. *Cancer Res.* **1992**, *52*, 3255–3261. [PubMed]
21. Gill, P.S.; Espina, B.M.; Muggia, F.; Cabriales, S.; Tulpule, A.; Esplin, J.A.; Liebman, H.A.; Forssen, E.; Ross, M.E.; Levine, A.M. Phase I/II clinical and pharmacokinetic evaluation of liposomal daunorubicin. *J. Clin. Oncol.* **1995**, *13*, 996–1003. [CrossRef] [PubMed]
22. Fumagalli, L.; Zucchetti, M.; Parisi, L.; Viganò, M.G.; Zecca, B.; Careddu, A.; D'Incalci, M.; Lazzarin, A. The pharmacokinetics of liposomal encapsulated daunorubicin are not modified by HAART in patients with HIV-associated Kaposi's sarcoma. *Cancer Chemother. Pharmacol.* **2000**, *45*, 495–501. [CrossRef] [PubMed]
23. Alberts, D.S.; Bachur, N.R.; Holtzman, J.L. The pharmacokinetics of daunomycin in man. *Clin. Pharmacol. Ther.* **1971**, *12*, 96–104. [CrossRef] [PubMed]
24. Chamberlain, M.C.; Kormanik, P.; Howell, S.B.; Kim, S. Pharmacokinetics of intralumbar DTIC-101 for the treatment of leptomeningeal metastases. *Arch. Neurol.* **1995**, *52*, 912–917. [CrossRef] [PubMed]
25. Kim, S.; Chatelut, E.; Kim, J.C.; Howell, S.B.; Cates, C.; Kormanik, P.A.; Chamberlain, M.C. Extended CSF cytarabine exposure following intrathecal administration of DTIC 101. *J. Clin. Oncol.* **1993**, *11*, 2186–2193. [CrossRef] [PubMed]
26. Glantz, M.J.; Jaekle, K.A.; Chamberlain, M.C.; Phuphanich, S.; Recht, L.; Swinnen, L.J.; Maria, B.; LaFollette, S.; Schumann, G.B.; Cole, B.F. A randomized controlled trial comparing intrathecal sustained-release cytarabine (DepoCyt) to intrathecal methotrexate in patients with neoplastic meningitis from solid tumors. *Clin. Cancer Res.* **1999**, *5*, 3394–3402. [PubMed]
27. Balazsovits, J.; Mayer, L.; Bally, M.; Cullis, P.; McDonnell, M.; Ginsberg, R.; Falk, R. Analysis of the effect of liposome encapsulation on the vesicant properties, acute and cardiac toxicities, and antitumor efficacy of doxorubicin. *Cancer Chemother. Pharmacol.* **1989**, *23*, 81–86. [CrossRef] [PubMed]
28. Kanter, P.; Bullard, G.; Pilikiewicz, F.; Mayer, L.; Cullis, P.; Pavelic, Z. Preclinical toxicology study of liposome encapsulated doxorubicin (TLC D-99): Comparison with doxorubicin and empty liposomes in mice and dogs. *In Vivo* **1992**, *7*, 85–95.
29. Sparano, J.A.; Winer, E.P. Liposomal anthracyclines for breast cancer. In *Seminars in Oncology*; Elsevier: Amsterdam, The Netherlands, 2001.
30. Cowens, J.; Creaven, P.; Greco, W.; Brenner, D.; Tung, Y.; Ostro, M.; Pilikiewicz, F.; Ginsberg, R.; Petrelli, N. Initial clinical (phase I) trial of TLC D-99 (doxorubicin encapsulated in liposomes). *Cancer Res.* **1993**, *53*, 2796–2802. [PubMed]
31. Harasym, T.O.; Cullis, P.R.; Bally, M.B. Intratumor distribution of doxorubicin following iv administration of drug encapsulated in egg phosphatidylcholine/cholesterol liposomes. *Cancer Chemother. Pharmacol.* **1997**, *40*, 309–317. [CrossRef] [PubMed]
32. Harris, L.; Batist, G.; Belt, R.; Rovira, D.; Navari, R.; Azarnia, N.; Welles, L.; Winer, E. Liposome-encapsulated doxorubicin compared with conventional doxorubicin in a randomized multicenter trial as first-line therapy of metastatic breast carcinoma. *Cancer* **2002**, *94*, 25–36. [CrossRef] [PubMed]
33. Batist, G.; Ramakrishnan, G.; Rao, C.S.; Chandrasekharan, A.; Gutheil, J.; Guthrie, T.; Shah, P.; Khojasteh, A.; Nair, M.K.; Hoelzer, K. Reduced cardiotoxicity and preserved antitumor efficacy of liposome-encapsulated doxorubicin and cyclophosphamide compared with conventional doxorubicin and cyclophosphamide in a randomized, multicenter trial of metastatic breast cancer. *J. Clin. Oncol.* **2001**, *19*, 1444–1454. [CrossRef] [PubMed]
34. Alphandéry, E.; Grand-Dewyse, P.; Lefevre, R.; Mandawala, C.; Durand-Dubief, M. Cancer therapy using nanoformulated substances: Scientific, regulatory and financial aspects. *Expert Rev. Anticancer Ther.* **2015**, *15*, 1233–1255. [CrossRef] [PubMed]
35. Vail, D.M.; MacEwen, E.G.; Kurzman, I.D.; Dubielzig, R.R.; Helfand, S.C.; Kisseberth, W.C.; London, C.A.; Obradovich, J.E.; Madewell, B.R.; Rodriguez, C.O. Liposome-encapsulated muramyl tripeptide phosphatidylethanolamine adjuvant immunotherapy for splenic hemangiosarcoma in the dog: A randomized multi-institutional clinical trial. *Clin. Cancer Res.* **1995**, *1*, 1165–1170. [PubMed]

36. Anderson, P.; Tomaras, M.; McConnell, K. Mifamurtide in osteosarcoma—A practical review. *Drugs Today* **2010**, *46*, 327–337. [CrossRef] [PubMed]
37. Anderson, P.; Meyers, P.; Kleinerman, E.; Oliva, C.; Liu, Y. Mifamurtide (L-MTP-PE) for metastatic and recurrent osteosarcoma (OS): Survival and safety profile from a patient access study. In *Annals of Oncology*; Oxford University Press: Oxford, UK, 2012.
38. Meyers, P.A.; Schwartz, C.L.; Krailo, M.D.; Healey, J.H.; Bernstein, M.L.; Betcher, D.; Ferguson, W.S.; Gebhardt, M.C.; Goorin, A.M.; Harris, M. Osteosarcoma: The addition of muramyl tripeptide to chemotherapy improves overall survival—A report from the Children's Oncology Group. *J. Clin. Oncol.* **2008**, *26*, 633–638. [CrossRef] [PubMed]
39. Webb, M.; Harasym, T.; Masin, D.; Baily, M.; Mayer, L. Sphingomyelin-cholesterol liposomes significantly enhance the pharmacokinetic and therapeutic properties of vincristine in murine and human tumour models. *Br. J. Cancer* **1995**, *72*, 896. [CrossRef] [PubMed]
40. Johnston, M.J.; Semple, S.C.; Klimuk, S.K.; Edwards, K.; Eisenhardt, M.L.; Leng, B.C.; Karlsson, G.; Yanko, D.; Cullis, P.R. Therapeutically optimized rates of drug release can be achieved by varying the drug-to-lipid ratio in liposomal vincristine formulations. *Biochim. Biophys. Acta (BBA) Biomembr.* **2006**, *1758*, 55–64. [CrossRef] [PubMed]
41. Krishna, R.; Webb, M.S.; Ornge, G.S.; Mayer, L.D. Liposomal and nonliposomal drug pharmacokinetics after administration of liposome-encapsulated vincristine and their contribution to drug tissue distribution properties. *J. Pharmacol. Exp. Ther.* **2001**, *298*, 1206–1212. [PubMed]
42. Rodriguez, M.; Pytlik, R.; Kozak, T.; Chhanabhai, M.; Gascoyne, R.; Lu, B.; Deitcher, S.R.; Winter, J.N. Vincristine sulfate liposomes injection (Marqibo) in heavily pretreated patients with refractory aggressive non-Hodgkin lymphoma. *Cancer* **2009**, *115*, 3475–3482. [CrossRef] [PubMed]
43. Drummond, D.C.; Noble, C.O.; Guo, Z.; Hong, K.; Park, J.W.; Kirpotin, D.B. Development of a highly active nanoliposomal irinotecan using a novel intraliposomal stabilization strategy. *Cancer Res.* **2006**, *66*, 3271–3277. [CrossRef] [PubMed]
44. Hong, K.; Drummond, D.C.; Kirpotin, D. Liposomes Useful for Drug Delivery. U.S. Patent No. US20160030341 A1, 4 February 2016.
45. Wang-Gillam, A.; Li, C.-P.; Bodoky, G.; Dean, A.; Shan, Y.-S.; Jameson, G.; Macarulla, T.; Lee, K.-H.; Cunningham, D.; Blanc, J.F. Nanoliposomal irinotecan with fluorouracil and folinic acid in metastatic pancreatic cancer after previous gemcitabine-based therapy (NAPOLI-1): A global, randomised, open-label, phase 3 trial. *Lancet* **2016**, *387*, 545–557. [CrossRef]
46. Lister, J. Amphotericin B lipid complex (Abelcet[®]) in the treatment of invasive mycoses: The North American experience. *Eur. J. Haematol.* **1996**, *56*, 18–23. [CrossRef]
47. Madden, T.; Janoff, A.; Cullis, P. Incorporation of amphotericin B into large unilamellar vesicles composed of phosphatidylcholine and phosphatidylglycerol. *Chem. Phys. Lipids* **1990**, *52*, 189–198. [CrossRef]
48. Janoff, A.; Boni, L.; Popescu, M.; Minchey, S.; Cullis, P.R.; Madden, T.; Taraschi, T.; Gruner, S.; Shyamsunder, E.; Tate, M. Unusual lipid structures selectively reduce the toxicity of amphotericin B. *Proc. Natl. Acad. Sci. USA* **1988**, *85*, 6122–6126. [CrossRef] [PubMed]
49. Olsen, S.J.; Swerdel, M.R.; Blue, B.; Clark, J.M.; Bonner, D.P. Tissue distribution of amphotericin B lipid complex in laboratory animals. *J. Pharm. Pharmacol.* **1991**, *43*, 831–835. [CrossRef] [PubMed]
50. Janoff, A.; Perkins, W.; Saletan, S.; Swenson, C. Amphotericin B lipid complex (ABLC[™]): A molecular rationale for the attenuation of amphotericin B related toxicities. *J. Liposome Res.* **1993**, *3*, 451–471. [CrossRef]
51. Adedoyin, A.; Bernardo, J.F.; Swenson, C.E.; Bolsack, L.E.; Horwith, G.; DeWit, S.; Kelly, E.; Klasterksy, J.; Sculier, J.-P.; DeValeriola, D. Pharmacokinetic profile of ABELCET (amphotericin B lipid complex injection): Combined experience from phase I and phase II studies. *Antimicrob. Agents Chemother.* **1997**, *41*, 2201–2208. [PubMed]
52. Adler-Moore, J.F.; Proffitt, R.T. Development, characterization, efficacy and mode of action of Ambisome, a unilamellar liposomal formulation of amphotericin B. *J. Liposome Res.* **1993**, *3*, 429–450. [CrossRef]
53. Woodle, M.C.; Storm, G. *Long Circulating Liposomes: Old Drugs, New Therapeutics*; Springer Science & Business Media: Berlin, Germany, 1998.

54. Walsh, T.J.; Yeldandi, V.; McEvoy, M.; Gonzalez, C.; Chanock, S.; Freifeld, A.; Seibel, N.I.; Whitcomb, P.O.; Jarosinski, P.; Boswell, G. Safety, tolerance, and pharmacokinetics of a small unilamellar liposomal formulation of amphotericin B (AmBisome) in neutropenic patients. *Antimicrob. Agents Chemother.* **1998**, *42*, 2391–2396. [PubMed]
55. Boswell, G.; Buell, D.; Bekersky, I. AmBisome (liposomal amphotericin B): A comparative review. *J. Clin. Pharmacol.* **1998**, *38*, 583–592. [CrossRef] [PubMed]
56. Guo, L.S.; Fielding, R.M.; Lasic, D.D.; Hamilton, R.L.; Mufson, D. Novel antifungal drug delivery: Stable amphotericin B-cholesteryl sulfate discs. *Int. J. Pharm.* **1991**, *75*, 45–54. [CrossRef]
57. Fielding, R.; Singer, A.; Wang, L.; Babbar, S.; Guo, L. Relationship of pharmacokinetics and drug distribution in tissue to increased safety of amphotericin B colloidal dispersion in dogs. *Antimicrob. Agents Chemother.* **1992**, *36*, 299–307. [CrossRef] [PubMed]
58. Wang, L.H.; Fielding, R.M.; Smith, P.C.; Guo, L.S. Comparative tissue distribution and elimination of amphotericin B colloidal dispersion (Amphoci[®]) and Fungizone[®] after repeated dosing in rats. *Pharm. Res.* **1995**, *12*, 275–283. [CrossRef] [PubMed]
59. Sanders, S.W.; Buchi, K.; Goddard, M.; Lang, J.; Tolman, K. Single-dose pharmacokinetics and tolerance of a cholesteryl sulfate complex of amphotericin B administered to healthy volunteers. *Antimicrob. Agents Chemother.* **1991**, *35*, 1029–1034. [CrossRef] [PubMed]
60. White, M.H.; Anaissie, E.J.; Kusne, S.; Wingard, J.R.; Hiemenz, J.W.; Cantor, A.; Gurwith, M.; Mond, C.D.; Mamelok, R.D.; Bowden, R.A. Amphotericin B colloidal dispersion vs. amphotericin B as therapy for invasive aspergillosis. *Clin. Infect. Dis.* **1997**, *24*, 635–642. [PubMed]
61. Bowden, R.A.; Cays, M.; Gooley, T.; Mamelok, R.D.; van Burik, J.-A. Phase I study of amphotericin B colloidal dispersion for the treatment of invasive fungal infections after marrow transplant. *J. Infect. Dis.* **1996**, *173*, 1208–1215. [CrossRef] [PubMed]
62. Strong, H.A.; Levy, J.; Huber, C.; Fsadni, M. Vision through Photodynamic Therapy of the Eye. U.S. Patent No. US5910510 A, 8 June 1999.
63. Richter, A.M.; Waterfield, E.; Jain, A.K.; Canaan, A.J.; Allison, B.A.; Levy, J.G. Liposomal delivery of a photosensitizer, benzoporphyrin derivative monoacid ring A (BPD), to tumor tissue in a mouse tumor model. *Photochem. Photobiol.* **1993**, *57*, 1000–1006. [CrossRef] [PubMed]
64. Bressler, N.M. Photodynamic therapy of subfoveal choroidal neovascularization in age-related macular degeneration with verteporfin: One-year results of 2 randomized clinical trials—TAP report 1. *Arch. Ophthalmol.* **1999**, *117*, 1329–1345.
65. Alam, M.; Hartrick, C.T. Extended-Release Epidural Morphine (DepoDur[™]): An Old Drug with a New Profile. *Pain Pract.* **2005**, *5*, 349–355. [CrossRef] [PubMed]
66. Hartrick, C.; Manvelian, G. Sustained-Release Epidural Morphine (DepoDur[™]): A Review. *Today's Ther. Trends* **2004**, *22*, 167–180.
67. Kim, T.; Murdande, S.; Gruber, A.; Kim, S. Sustained-release morphine for epidural analgesia in rats. *J. Am. Soc. Anesthesiol.* **1996**, *85*, 331–338. [CrossRef]
68. Viscusi, E.R.; Kopacz, D.; Hartrick, C.; Martin, G.; Manvelian, G. Single-dose extended-release epidural morphine for pain following hip arthroplasty. *Am. J. Ther.* **2006**, *13*, 423–431. [CrossRef] [PubMed]
69. Angst, M.S.; Drover, D.R. Pharmacology of drugs formulated with DepoFoam[™]. *Clin. Pharmacokinet.* **2006**, *45*, 1153–1176. [CrossRef] [PubMed]
70. Richard, B.M.; Rickert, D.E.; Newton, P.E.; Ott, L.R.; Haan, D.; Brubaker, A.N.; Cole, P.L.; Ross, P.E.; Rebelatto, M.C.; Nelson, K.G. Safety evaluation of EXPAREL (DepoFoam bupivacaine) administered by repeated subcutaneous injection in rabbits and dogs: Species comparison. *J. Drug Deliv.* **2011**. [CrossRef] [PubMed]
71. Davidson, E.M.; Barenholz, Y.; Cohen, R.; Haroutiunian, S.; Kagan, L.; Ginosar, Y. High-dose bupivacaine remotely loaded into multivesicular liposomes demonstrates slow drug release without systemic toxic plasma concentrations after subcutaneous administration in humans. *Anesth. Analg.* **2010**, *110*, 1018–1023. [CrossRef] [PubMed]
72. Miller, H.; Terem, T.; Kheladze, K.; Mosidze, B. A single administration of depobupivacaine (TM) intraoperatively provides three-day analgesia and reduction in use of rescue opioids in patients undergoing hemorrhoidectomy. In *Diseases of the Colon & Rectum*; Lippincott Williams & Wilkins: Philadelphia, PA, USA, 2009.

73. Clarke, P.D.; Adams, P.; Ibáñez, R.; Herzog, C. Rate, intensity, and duration of local reactions to a virosome-adsjuvanted vs. an aluminium-adsorbed hepatitis A vaccine in UK travellers. *Travel Med. Infect. Dis.* **2006**, *4*, 313–318. [CrossRef] [PubMed]
74. Zylberberg, C.; Matosevic, S. Pharmaceutical liposomal drug delivery: A review of new delivery systems and a look at the regulatory landscape. *Drug Deliv.* **2016**, *23*, 1–11. [CrossRef] [PubMed]
75. Bungener, L.; Serre, K.; Bijl, L.; Leserman, L.; Wilschut, J.; Daemen, T.; Machy, P. Virosome-mediated delivery of protein antigens to dendritic cells. *Vaccine* **2002**, *20*, 2287–2295. [CrossRef]
76. Ambrosch, F.; Wiedermann, G.; Jonas, S.; Althaus, B.; Finkel, B.; Glück, R.; Herzog, C. Immunogenicity and protectivity of a new liposomal hepatitis A vaccine. *Vaccine* **1997**, *15*, 1209–1213. [CrossRef]
77. Perez, O.M.; Herzog, C.; Zellmeyer, M.; Loáisiga, A.; Frösner, G.; Egger, M. Efficacy of virosome hepatitis A vaccine in young children in Nicaragua: Randomized placebo-controlled trial. *J. Infect. Dis.* **2003**, *188*, 671–677. [CrossRef] [PubMed]
78. Bovier, P.; Bock, J.; Loutan, L.; Farinelli, T.; Glueck, R.; Herzog, C. Long-term immunogenicity of an inactivated virosome hepatitis A vaccine. *J. Med. Virol.* **2002**, *68*, 489–493. [CrossRef] [PubMed]
79. Gluck, R.; Metcalfe, I. New technology platforms in the development of vaccines for the future. *Vaccine* **2002**, *20*, 10–16. [CrossRef]
80. Gluck, R.; Mischler, R.; Finkel, B.; Que, J.; Cryz, S.; Scarpa, B. Immunogenicity of new virosome influenza vaccine in elderly people. *Lancet* **1994**, *344*, 160–163. [CrossRef]
81. Conne, P.; Gauthey, L.; Vernet, P.; Althaus, B.; Que, J.U.; Finkel, B.; Glück, R.; Cryz, S.J. Immunogenicity of trivalent subunit versus virosome-formulated influenza vaccines in geriatric patients. *Vaccine* **1997**, *15*, 1675–1679. [CrossRef]
82. Li, Z.; Zhang, Y.; Wurtz, W.; Lee, J.K.; Malinin, V.S.; Durvas-Krishnan, S.; Meers, P.; Perkins, W.R. Characterization of nebulized liposomal amikacin (Arikace™) as a function of droplet size. *J. Aerosol Med. Pulm. Drug Deliv.* **2008**, *21*, 245–254. [CrossRef] [PubMed]
83. Clancy, J.P. Clinical trials of lipid-associated aerosolized amikacin: The arikace™ story. In *Pediatric Pulmonology*; Wiley-Liss Div John Wiley & Sons Inc.: Hoboken, NJ, USA, 2009.
84. Bilton, D.; Pressler, T.; Fajac, J.; Clancy, J.P.; Sands, D.; Minic, P.; Cipolli, M.; LaRosa, M.; Galeva, I.; Sole, A.A. Phase 3 efficacy and safety data from randomized, multicenter study of liposomal amikacin for inhalation (ARIKACE) Compared with TOBI in cystic fibrosis patients with chronic infection due to *Pseudomonas Aeruginosa*. *Pediatr. Pulmonol.* **2013**, *48*, 207–453.
85. Clancy, J.; Dupont, L.; Konstan, M.W.; Billings, J.; Fustik, S.; Goss, C.H.; Lymph, J.; Minic, P.; Quittner, A.; Rubenstein, R. Phase II studies of nebulised Arikace in CF patients with *Pseudomonas aeruginosa* infection. *Thorax* **2013**, *68*, 818–825. [CrossRef] [PubMed]
86. Gupta, R.; Daley, C.L.; Winthrop, K.L.; Ruess, S.; Addrizzo-Harris, D.J.; Flume, P.; Dorgan, D.; Salathe, M.A.; Olivier, B.; Brown-Elliott, A. A randomized, double-blind, placebo-controlled study of liposomal amikacin for inhalation (Arikace®) in patients with recalcitrant nontuberculous mycobacterial lung disease. In *C27. Diagnosis and Treatment of Nontuberculous Mycobacteria Infections*; American Thoracic Society: New York, NY, USA, 2014; p. 4126.
87. Timmerman, L. Oncothyreon Marches on with ‘Son of Stimuvax’ Cancer Vaccine. Available online: <http://www.xconomy.com/seattle/2012/04/10/oncothyreon-marches-on-with-son-of-stimuvax-cancer-vaccine/> (accessed on 27 March 2017).
88. Kroemer, G.; Zitvogel, L.; Galluzzi, L. Victories and deceptions in tumor immunology: Stimuvax®. *Oncimmunology* **2013**, *2*, e23687. [CrossRef] [PubMed]
89. Bradbury, P.A.; Shepherd, F.A. Immunotherapy for lung cancer. *J. Thorac. Oncol.* **2008**, *3*, S164–S170. [CrossRef] [PubMed]
90. Vergati, M.; Intrivici, C.; Huen, N.-Y.; Schlom, J.; Tsang, K.Y. Strategies for cancer vaccine development. *BioMed Res. Int.* **2010**, *2010*, 1–13. [CrossRef] [PubMed]
91. Cart, S.; Alert, N.P.R. Merck KCaA Starts Stimuvax Phase III Study INSPIRE in Asian Patients with Advanced NSCLC. Available online: <http://www.businesswire.com/news/home/20091210005488/en/Merck-KCaA-Starts-Stimuvax-Phase-III-Study> (accessed on 27 March 2017).
92. Zahid, S.; Brownell, I. Repairing DNA damage in xeroderma pigmentosum: T4N5 lotion and gene therapy. *J. Drugs Dermatol.* **2008**, *7*, 405–408. [PubMed]

93. Yarosh, D.B.; Kibitel, J.T.; Green, L.A.; Spinowitz, A. Enhanced unscheduled DNA synthesis in UV-irradiated human skin explants treated with T4N5 liposomes. *J. Investig. Dermatol.* **1991**, *97*, 147–150. [CrossRef] [PubMed]
94. Wolf, P.; Müllegger, R.R.; Soyer, H.P.; Hofer, A.; Smolle, J.; Horn, M.; Cerroni, L.; Hofmann-Wellenhof, R.; Kerl, H.; Maier, H. Topical treatment with liposomes containing T4 endonuclease V protects human skin in vivo from ultraviolet-induced upregulation of interleukin-10 and tumor necrosis factor- α . *J. Investig. Dermatol.* **2000**, *114*, 149–156. [CrossRef] [PubMed]
95. Cafardi, J.A.; Elmets, C.A. T4 endonuclease V: Review and application to dermatology. *Expert Opin. Biol. Ther.* **2008**, *8*, 829–838. [CrossRef] [PubMed]
96. Chang, H.-I.; Yeh, M.-K. Clinical development of liposome-based drugs: Formulation, characterization, and therapeutic efficacy. *Int. J. Nanomed.* **2012**, *7*, 49–60.
97. Summers, D.; Ruff, D.; Smalling, R.; Cardoza, D.; Dottavio, D.; Lasic, D. Administration of liprostin (TM) for the treatment of critical limb ischemia (CLI) and peripheral arterial disease (PAD). In *Journal of Liposome Research*; Marcel Dekker Inc.: New York, NY, USA, 2003.
98. Li, J.; Wang, B.; Wang, Y.; Wu, F.; Li, P.; Li, Y.; Zhao, L.; Cui, W.; Ding, Y.; An, Q. Therapeutic effect of liposomal prostaglandin E1 in acute lower limb ischemia as an adjuvant to hybrid procedures. *Exp. Ther. Med.* **2013**, *5*, 1760–1764. [PubMed]
99. Chen, J.; He, C.-Q.; Lin, A.-H.; Gu, W.; Chen, Z.-P.; Li, W.; Cai, B.-C. Thermosensitive liposomes with higher phase transition temperature for targeted drug delivery to tumor. *Int. J. Pharm.* **2014**, *475*, 408–415. [CrossRef] [PubMed]
100. Mylonopoulou, E.; Arvanitisa, C.D.; Bazan-Peregrino, M.; Arora, M.; Coussios, C.C. Ultrasonic activation of thermally sensitive liposomes. In Proceedings of the 9th International Symposium on Therapeutic Ultrasound: Istu—2009, Aix-en-Provence, France, 24–26 September 2009; AIP Publishing: New York, NY, USA, 2010.
101. Puri, A. Phototriggerable liposomes: Current research and future perspectives. *Pharmaceutics* **2013**, *6*, 1–25. [CrossRef] [PubMed]
102. Wood, B.; Poon, R.; Neeman, Z.; Eugeni, M.; Locklin, J.; Dromi, S.; Kachala, S.; Probhakar, R.; Hahne, W.; Libutti, S. Phase I study of thermally sensitive liposomes containing doxorubicin (ThermoDox) given during radiofrequency ablation (RFA) in patients with unresectable hepatic malignancies. In Proceedings of the Gastrointestinal Cancers Symposium, Orlando, FL, USA, 19–21 January 2007; The American Society of Clinical Oncology: Alexandria, VA, USA, 2007.
103. Dromi, S.; Quijano, J.; Xie, J.; Frenkel, V.; Wood, B.; Li, K. Pulsed-high intensity focused ultrasound (HIFU) enhanced delivery of Doxorubicin using heat sensitive liposome (Thermodox TM). In Proceedings of the 91st Annual Meeting of the Radiological Society of North America, Chicago, IL, USA, 27 November–2 December 2005.
104. Palazzi, M.; Maluta, S.; Dall'Oglio, S.; Romano, M. The role of hyperthermia in the battle against cancer. *Tumori* **2010**, *96*, 902. [PubMed]
105. Mura, S.; Nicolas, J.; Couvreur, P. Stimuli-responsive nanocarriers for drug delivery. *Nat. Mater.* **2013**, *12*, 991–1003. [CrossRef] [PubMed]
106. Egusquiaguirre, S.P.; Igarua, M.; Hernández, R.M.; Pedraz, J.L. Nanoparticle delivery systems for cancer therapy: Advances in clinical and preclinical research. *Clin. Transl. Onco.* **2012**, *14*, 83–93. [CrossRef] [PubMed]
107. Boulikas, T. Clinical overview on Lipoplatin™: A successful liposomal formulation of cisplatin. *Expert Opin. Investig. Drugs* **2009**, *18*, 1197–1218. [CrossRef] [PubMed]
108. Sotiriou-Rigatos, E.D.; Viliotou, V.; Stathopoulos, J.G. Pharmacokinetics and adverse reactions of a new liposomal cisplatin (Lipoplatin): Phase I study. *Oncol. Rep.* **2005**, *13*, 589–595.
109. Stathopoulos, G.P.; Boulikas, T.; Vougiouka, M.; Rigatos, S.K.; Stathopoulos, J.G. Liposomal cisplatin combined with gemcitabine in pretreated advanced pancreatic cancer patients: A phase I-II study. *Oncol. Rep.* **2006**, *15*, 1201–1204. [CrossRef] [PubMed]
110. Mylonakis, N.; Athanasiou, A.; Ziras, N.; Angel, J.; Rapti, A.; Lampaki, S.; Politis, N.; Karanikas, C.; Koemas, C. Phase II study of liposomal cisplatin (Lipoplatin™) plus gemcitabine versus cisplatin plus gemcitabine as first line treatment in inoperable (stage IIIb/IV) non-small cell lung cancer. *Lung Cancer* **2010**, *68*, 240–247. [CrossRef] [PubMed]
111. Boulikas, T.; Stathopoulos, G.P.; Volakakis, N.; Vougiouka, M. Systemic Lipoplatin infusion results in preferential tumor uptake in human studies. *Anticancer Res.* **2005**, *25*, 3031–3039. [PubMed]

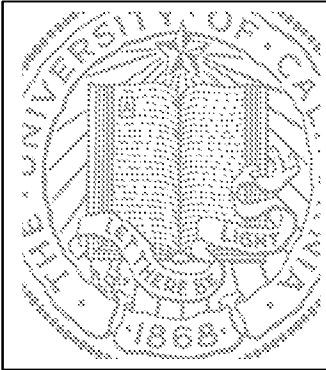
112. Harper, B.W.; Krause-Heuer, A.M.; Grant, M.P.; Manohar, M.; Garbutcheon-Singh, K.B.; Aldrich-Wright, J.R. Advances in platinum chemotherapeutics. *Chem. Eur. J.* **2010**, *16*, 7064–7077. [CrossRef] [PubMed]
113. Immordino, M.L.; Dosio, F.; Cattel, L. Stealth liposomes: Review of the basic science, rationale, and clinical applications, existing and potential. *Int. J. Nanomed.* **2006**, *1*, 297.
114. Farrell, N.P. Platinum formulations as anticancer drugs clinical and pre-clinical studies. *Curr. Top. Med. Chem.* **2011**, *11*, 2623–2631. [CrossRef]
115. Dragovich, T.; Mendelson, D.; Hoos, A.; Lewis, J.; Kurtin, S.; Richardson, K.; von Hoff, D. 268 A phase II trial of aroplatin (L-NDDP), a liposomal DACH platinum, in patients with metastatic colorectal cancer (CRC)—a preliminary report. *Eur. J. Cancer Suppl.* **2003**, *1*, S82–S83. [CrossRef]
116. Jakupec, M.; Galanski, M.; Keppler, B. Tumour-inhibiting platinum complexes—State of the art and future perspectives. In *Reviews of physiology, Biochemistry and Pharmacology*; Springer: New York, NY, USA, 2003; pp. 1–53.
117. Zou, Y.; Friebe, W.; Perez-Soler, R. Lyophilized preliposomal formulation of the non-cross-resistant anthracycline annamycin. Effect of surfactant on liposome formation, stability and size. *Cancer Chemother. Pharmacol.* **1996**, *39*, 103–108. [CrossRef] [PubMed]
118. Wasan, K.M.; Perez-Soler, R. Distribution of free and liposomal annamycin within human plasma is regulated by plasma triglyceride concentrations but not by lipid transfer protein. *J. Pharm. Sci.* **1995**, *84*, 1094–1100. [CrossRef] [PubMed]
119. Zou, Y.; Ling, Y.H.; Van, N.T.; Friebe, W.; Perez-Soler, R. Antitumor activity of free and liposome-entrapped annamycin, a lipophilic anthracycline antibiotic with non-cross-resistance properties. *Cancer Res.* **1994**, *54*, 1479–1484. [PubMed]
120. Pui, C.-H.; Jeha, S. New therapeutic strategies for the treatment of acute lymphoblastic leukaemia. *Nat. Rev. Drug Discov.* **2007**, *6*, 149–165. [CrossRef] [PubMed]
121. Wetzler, M.; Thomas, D.A.; Wang, E.S.; Shepard, R.; Ford, L.A.; Helfner, T.L.; Parekh, S.; Andreeff, M.; O'Brien, S.; Kantarjian, H.M. Phase I/II trial of nanomolecular liposomal annamycin in adult patients with relapsed/refractory acute lymphoblastic leukemia. *Clin. Lymphoma Myeloma Leuk.* **2013**, *13*, 430–434. [CrossRef] [PubMed]
122. Harrington, K.J.; Rowlinson-Busza, G.; Syrigos, K.N.; Vile, R.G.; Uster, P.S.; Peters, A.M.; Stewart, J.S.W. Pegylated liposome-encapsulated doxorubicin and cisplatin enhance the effect of radiotherapy in a tumor xenograft model. *Clin. Cancer Res.* **2000**, *6*, 4939–4949. [PubMed]
123. Zamboni, W.C.; Gervais, A.C.; Egorin, M.J.; Schellens, J.H.; Zuhowski, E.G.; Pluin, D.; Joseph, E.; Hamburger, D.R.; Working, P.K.; Colbern, G. Systemic and tumor disposition of platinum after administration of cisplatin or STEALTH liposomal-cisplatin formulations (SPI-077 and SPI-077 B103) in a preclinical tumor model of melanoma. *Cancer Chemother. Pharmacol.* **2004**, *53*, 329–336. [CrossRef] [PubMed]
124. Tomkinson, B.; Bendele, R.; Giles, F.J.; Brown, E.; Gray, A.; Hart, K.; LeRay, J.D.; Meyer, D.; Pelanne, M.; Emerson, D.L. OSI-211, a novel liposomal topoisomerase I inhibitor, is active in SCID mouse models of human AML and ALL. *Leuk. Res.* **2003**, *27*, 1039–1050. [CrossRef]
125. Yu, N.Y.; Conway, C.; Pena, R.L.; Chen, J.Y. STEALTH[®] liposomal CKD-602, a topoisomerase I inhibitor, improves the therapeutic index in human tumor xenograft models. *Anticancer Res.* **2007**, *27*, 2541–2545. [PubMed]
126. Zamboni, W.C.; Strychor, S.; Joseph, E.; Walsh, D.R.; Zamboni, B.A.; Parise, R.A.; Tonda, M.E.; Ning, Y.Y.; Ingbers, C.; Eiseman, J.L. Plasma, tumor, and tissue disposition of STEALTH liposomal CKD-602 (S-CKD602) and nonliposomal CKD-602 in mice bearing A375 human melanoma xenografts. *Clin. Cancer Res.* **2007**, *13*, 7217–7223. [CrossRef] [PubMed]
127. Zhang, J.A.; Xuan, T.; Parmar, M.; Ma, L.; Ugwu, S.; Ali, S.; Ahmad, I. Development and characterization of a novel liposome-based formulation of SN-38. *Int. J. Pharm.* **2004**, *270*, 93–107. [CrossRef] [PubMed]
128. Gupta, V.; Su, Y.S.; Samuelson, C.C.; Liebes, L.F.; Chamberlain, M.C.; Hofman, F.M.; Schönthal, A.H.; Chen, T.C. Irinotecan: A potential new chemotherapeutic agent for atypical or malignant meningiomas. *J. Neurosurg.* **2007**, *106*, 455–462. [CrossRef] [PubMed]
129. Maroun, J.; Jonker, D.; Seymour, L.; Goel, R.; Vincent, M.; Kocha, W.; Cripps, C.; Fisher, B.; Lister, D.; Maipage, A. A National Cancer Institute of Canada Clinical Trials Group Study—IND. 135: Phase I/II study of irinotecan (camptosar), oxaliplatin and raltitrexed (tomudex)(COT) in patients with advanced colorectal cancer. *Eur. J. Cancer* **2006**, *42*, 193–199. [CrossRef] [PubMed]

130. Zhang, J.A.; Anyarambhatla, G.; Ma, L.; Ugwu, S.; Xuan, T.; Sardone, T.; Ahmad, I. Development and characterization of a novel Cremophor® EL free liposome-based paclitaxel (LEP-ETU) formulation. *Eur. J. Pharm. Biopharm.* **2005**, *59*, 177–187. [CrossRef] [PubMed]
131. Tan, A.; Hanauske, A.; Gelderblom, H.; Scheulen, M.; van Warmerdam, L.; Rosing, H.; Fetterly, G.; Shu, V.; Sherman, J.; Rubin, E. Results of a clinical pharmacokinetic (PK) bioequivalence (BE) study of liposomal paclitaxel (LEP-ETU) versus paclitaxel (T) in patients with advanced cancer. In *Journal of Clinical Oncology*; American Society of Clinical Oncology: Alexandria, VA, USA, 2006.
132. Slingerland, M.; Guchelaar, H.-J.; Rosing, H.; Scheulen, M.E.; van Warmerdam, L.J.; Beijnen, J.H.; Gelderblom, H. Bioequivalence of Liposome-Entrapped Paclitaxel Easy-To-Use (LEP-ETU) formulation and paclitaxel in polyethoxylated castor oil: A randomized, two-period crossover study in patients with advanced cancer. *Clin. Ther.* **2013**, *35*, 1946–1954. [CrossRef] [PubMed]
133. Eichhorn, M.E.; Ischenko, I.; Luedemann, S.; Strieth, S.; Pappan, A.; Werner, A.; Bohnenkamp, H.; Guenzi, E.; Preissler, G.; Michaelis, U. Vascular targeting by EndoTAG™-1 enhances therapeutic efficacy of conventional chemotherapy in lung and pancreatic cancer. *Int. J. Cancer* **2010**, *126*, 1235–1245. [CrossRef] [PubMed]
134. Schuch, G. EndoTAG-1. *MediGene. Curr. Opin. Investig. Drugs* **2005**, *6*, 1259. [PubMed]
135. Lohr, M.; Haas, S.; Bechstein, W.; Bodoky, G.; Maerten, A.; Fischbach, W.; Lilla, C.; Mescheder, A.; Pap, A.; Fölsch, U. A phase II trial of cationic liposomal paclitaxel in combination with gemcitabine in patients with unresectable pancreatic cancer. In Proceedings of the ASCO Gastrointestinal Cancers Symposium, San Francisco, CA, USA, 15–17 January 2009.
136. Wallace, T.L.; Larson, J.L.; Bazemore, S.A.; Wilson, C.W.; Cossum, P.A. The nonclinical safety evaluation of the anticancer drug ATRAGEN® (Liposomal all-trans-retinoic acid). *Int. J. Toxicol.* **2000**, *19*, 33–42. [CrossRef]
137. Douer, D.; Estey, E.; Santillana, S.; Bennett, J.M.; Lopez-Bernstein, G.; Boehm, K.; Williams, T. Treatment of newly diagnosed and relapsed acute promyelocytic leukemia with intravenous liposomal all-transretinoic acid. *Blood* **2001**, *97*, 73–80. [CrossRef] [PubMed]
138. Dutta, R.C. Drug carriers in pharmaceutical design: Promises and progress. *Curr. Pharm. Des.* **2007**, *13*, 761–769. [CrossRef] [PubMed]
139. Wicki, A.; Witzigmann, D.; Balasubramanian, V.; Huwyler, J. Nanomedicine in cancer therapy: Challenges, opportunities, and clinical applications. *J. Control. Release* **2015**, *200*, 138–157. [CrossRef] [PubMed]
140. Ahmad, A.; Wang, Y.-F.; Ahmad, I. Separation of liposome-entrapped mitoxantrone from nonliposomal mitoxantrone in plasma: Pharmacokinetics in mice. *Methods Enzymol.* **2005**, *391*, 176–185. [PubMed]
141. Tayi, W.; Cheng, K. Advanced drug delivery in cancer therapy. In *Advanced Drug Delivery*; Mitra, C.H.L.A., Cheng, K., Eds.; John Wiley & Sons: Hoboken, NJ, USA, 2013.
142. Tari, A.M.; Gutiérrez-Puente, Y.; Monaco, G.; Stephens, C.; Sun, T.; Rosenblum, M.; Belmont, J.; Arlinghaus, R.; Lopez-Berestein, C. Liposome-incorporated Grb2 antisense oligodeoxynucleotide increases the survival of mice bearing bcr-abl-positive leukemia xenografts. *Int. J. Oncol.* **2007**, *31*, 1243–1250. [PubMed]
143. Ashizawa, A.T.; Cortes, J. Liposomal delivery of nucleic acid-based anticancer therapeutics: BP-100-1.01. *Expert Opin. Drug Deliv.* **2015**, *12*, 1107–1120. [CrossRef] [PubMed]
144. Ohanian, M.; Kantarjian, H.M.; Ravandi, F.; Borthakur, G.; Garcia-Manero, G.; Andreeff, M.; Jabbour, E.; Konopleva, M.; Lim, M.; Pierce, S. Safety, Pharmacokinetics, and Efficacy of BP-100-1.01 (Liposomal Grb-2 Antisense Oligonucleotide) in Patients with Refractory or Relapsed Acute Myeloid Leukemia (AML), Philadelphia Chromosome Positive Chronic Myelogenous Leukemia (CML), Acute Lymphoblastic Leukemia (ALL), and Myelodysplastic Syndrome (MDS). *Blood* **2015**, *126*, 3801–3801.
145. Singh, R.; Kumari, P.; Kumar, S. Nanotechnology for enhanced bioactivity of bioactive phytochemicals. In *Nutrient Delivery*; Grumezescu, A.M., Ed.; Elsevier: Amsterdam, The Netherlands, 2016.
146. Torchilin, V.P. Multifunctional, stimuli-sensitive nanoparticulate systems for drug delivery. *Nat. Rev. Drug Discov.* **2014**, *13*, 813–827. [CrossRef] [PubMed]
147. Egusquiaguirre, S.P.; Pedraz, J.L.; Hernandez, R.M.; Igartua, M. Nanotherapeutic platforms for cancer treatment: From preclinical development to clinical application. In *Nanoarchitectonics for Smart Delivery and Drug Targeting*; Grumezescu, A., Holban, A.M., Eds.; Elsevier: Amsterdam, The Netherlands, 2016; pp. 813–869.
148. Lee, J.-M.; Yoon, T.-J.; Cho, Y.-S. Recent developments in nanoparticle-based siRNA delivery for cancer therapy. *BioMed Res. Int.* **2013**. [CrossRef] [PubMed]

149. Zuckerman, J.E.; Davis, M.E. Clinical experiences with systemically administered siRNA-based therapeutics in cancer. *Nat. Rev. Drug Discov.* **2015**, *14*, 843–856. [CrossRef] [PubMed]
150. Resnier, F.; Montier, T.; Mathieu, V.; Benoit, J.-P.; Passirani, C. A review of the current status of siRNA nanomedicines in the treatment of cancer. *Biomaterials* **2013**, *34*, 6429–6443. [CrossRef] [PubMed]
151. Gaillard, P.J.; Appeldoorn, C.C.; Dorland, R.; van Kregten, J.; Manca, E.; Vugts, D.J.; Windhorst, B.; van Dongen, G.A.; de Vries, H.E.; Maussang, D. Pharmacokinetics, brain delivery, and efficacy in brain tumor-bearing mice of glutathione PEGylated liposomal doxorubicin (2B3-101). *PLoS ONE* **2014**, *9*, e82331. [CrossRef]
152. Gaillard, P.J.; Visser, C.C.; Appeldoorn, C.C.; Rip, J. Enhanced brain drug delivery: Safely crossing the blood-brain barrier. *Drug Discov. Today Technol.* **2012**, *9*, e155–e160. [CrossRef] [PubMed]
153. Birngruber, T.; Raml, R.; Gladdines, W.; Gatschelhofer, C.; Gander, E.; Ghosh, A.; Kroath, T.; Gaillard, P.J.; Pieber, T.R.; Sinner, E. Enhanced Doxorubicin Delivery to the Brain Administered Through Glutathione PEGylated Liposomal Doxorubicin (2B3-101) as Compared with Generic Caelyx[®]/Doxil[®]—A Cerebral Open Flow Microperfusion Pilot Study. *J. Pharm. Sci.* **2014**, *103*, 1945–1948. [CrossRef] [PubMed]
154. Danhier, F. To exploit the tumor microenvironment: Since the EPR effect fails in the clinic, what is the future of nanomedicine? *J. Control. Release* **2016**, *244*, 108–121. [CrossRef] [PubMed]



© 2017 by the authors. Licensee MDPI, Basel, Switzerland. This article is an open access article distributed under the terms and conditions of the Creative Commons Attribution (CC BY) license (<http://creativecommons.org/licenses/by/4.0/>).



**A Phase I Study of CED of Liposomal-Irinotecan Using Real-Time Imaging
With Gadolinium In Patients With Recurrent High Grade Glioma
NCT02022644**

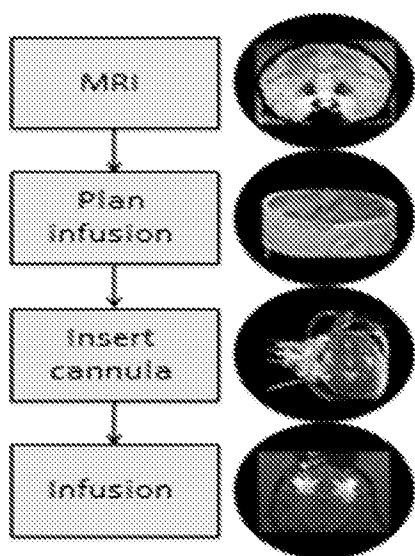
N. A. Butowski, S. Han, J. W. Taylor, M. K. Aghi, M. Prados, S. M. Chang, J. L. Clarke, K. Bankiewicz, D. C. Drummond, J. Fitzgerald

contact: Nicholas.Butowski@UCSF.edu poster 68b

INTRODUCTION

- Chemotherapy for brain tumors is limited by poor activity and compromised delivery
- Convection Enhanced Delivery (CED) improves chemotherapy delivery by utilizing a pressure gradient to distribute macromolecules to clinically significant volumes of tissue.
 - ✓ Bypasses Blood-Brain Barrier
 - ✓ Direct intra-tumoral drug delivery avoids plasma dilution and minimizes systemic exposure
 - ✓ Larger distribution volume than obtained by diffusion (cm vs. mm)
 - ✓ Studies comparing routes of delivery (CED v IV) showed superior anti-tumor activity of CED
- CED of nanoliposomal irinotecan has been optimized in rat, dog, and primate models at UCSF.
- The highly stabilized liposome-encapsulated irinotecan has advantages when used with the CED approach.
 - Due to the large size, when administered by CED the liposomal particle uniformly distributes throughout the brain with a volume of distribution that correlates linearly with the volume of drug administered
 - Designed to release irinotecan slowly over an extended period (T1/2=56 h), dramatically increasing the temporal exposure of the tumor to the chemotherapy
- Real time CED is important because previous studies utilizing CED showed promise but limited activity due to the following challenges:
 - 1) accumulation of drug in cells nearest the injection site leading to non-uniform distribution
 - 2) suboptimal pk within the tumor attributed to delivering free drug resulting in high but transient exposure with corresponding toxicity
 - 3) an inability to confirm efficient intracranial drug exposure within the tumor since MR image guided delivery was not available
- Real time CED with MRI = Seeing is believing
 - ✓ Guidance and confirmation of cannula placement
 - ✓ Detection of reflux, leakage, hemorrhage
 - ✓ Confirmation of delivery

Background: Integrated CED Platform For Imaged Delivery of Therapeutics to Brain Tumors



Imaging

Diagnostic pre-infusion
Measurement of porous expansion

+ Software

DTI-based simulation (with Brainlab)
Shape fitting for inverse planning

+ Hardware =

Acute iMRI CED (with Surgivision)
In-dwelling CED (with BrainLab, Renishaw)

= real-time placement and adjustment of the CED cannula with real-time CED infusion of study drug into the brain.

- critical for achieving optimal exposure of the intracranial tumor to the drug while minimizing systemic exposure

METHODS

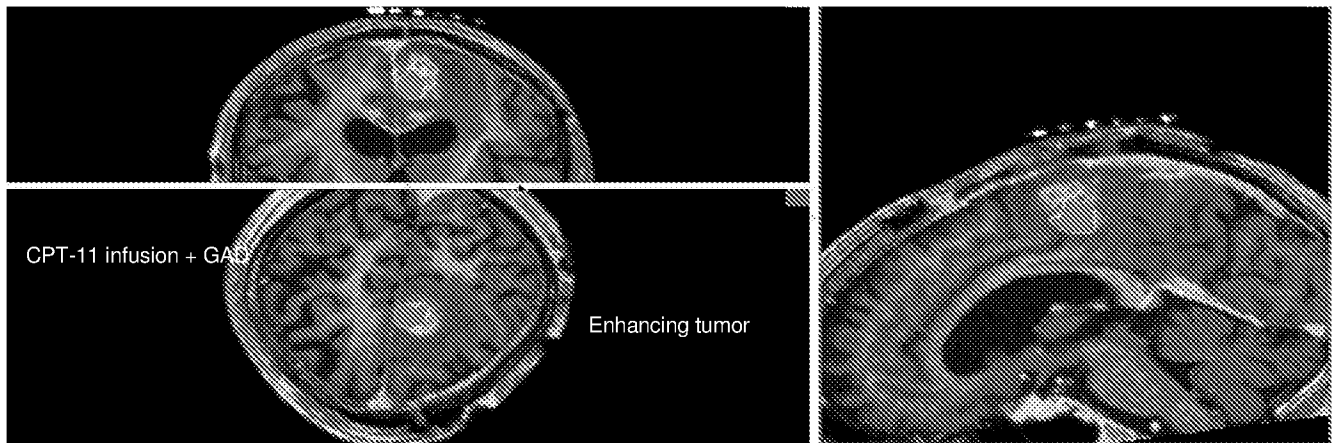
- NIH R21 supported, single center prospective 3+3 dose escalating, single arm phase I trial
 - Primary endpoint: safety and tolerability
 - Secondary endpoint: Optimization of real time CED, OS, PFS, imaging response.
- Eligibility: patients with recurrent grade 3 or 4 glial tumors
- Patients fall into 4 dose escalation groups based on dose and tumor volume as seen in the table.

Group	Dose	Tumor volume	Infusion Volume	Irinotecan conc.	Infusion Time
1	20 mg	1-4 cm ³	1.0 ml	20 mg/ml	2-3 h
2	40 mg	1-4 cm ³	1.0 ml	40 mg/ml	2-3 h
3	60 mg	2-5 cm ³	1.5 ml	40 mg/ml	3-4 h
4	80 mg	2-6 cm ³	2.0 ml	40 mg/ml	3-4 h

- Four-level dose escalation: 20 mg, 40 mg, 60 mg, and 80 mg given via 1 to 3 catheters surgically placed in an intra-tumoral location.
- Concentration of gadoteridol (ProHance) will be 2 mM for all dose groups
- Maximum total volume infused will be 1.0 ml for two lowest dose groups, 1.5 ml for the third dose group, and 2.0 ml for the highest dose group.

RESULTS

- 1st patient treated on October 17, 2104
- 3 patients have received treatment to date without a DLT
 - Patient #3 treated 2/13/2015
- 2 of the 3 enrolled patients have had tumor progression outside of treated volume
- All patients followed through the 30 day tox period and then for secondary endpoints
 - 0 patients off-study 2° to toxicity
 - 2 off-study for disease progression
- Cohort 2 currently enrolling



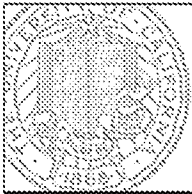
Summary

Further safety, efficacy, and imaging response results will be presented at future meetings

Although the principle of CED is not novel, this study represents device and procedural advancements for the application of CED that will increase the precision, reliability, and safety of directly delivering drugs to brain tumors.

Though regulatory agencies counseled the above design, it is possible that a single treatment may only lead to transient clinical benefit.

Data gained herein will enable an expanded clinical program, including a study using repeated dosing.



A Phase I Study of CED of Liposomal-Irinotecan Using Real-Time Imaging With Gadolinium In Patients With Recurrent High Grade Glioma

N. A. Butowski, S. Han, J. W. Taylor, M. K. Aghi, M. Prados, S. M. Chang, J. L. Clarke, K. Bankiewicz, D. C. Drummond, J. Fitzgerald

contact: Richard.Butowski@UTD.edu; poster 656

INTRODUCTION

- Chemotherapy for brain tumors is limited by poor solubility and compromised delivery
- Convection Enhanced Delivery (CED) improves chemotherapy delivery by utilizing a pressure gradient to distribute macromolecules to clinically significant volumes of tissue.
 - ✓ Bypasses blood-brain barrier
 - ✓ Direct intra-tumoral drug delivery avoids plasma dilution and minimizes systemic exposure
 - ✓ Larger distribution volume than obtained by diffusion (cm vs. mm)
 - ✓ Studies comparing routes of delivery (CED v IV) showed superior anti-tumor activity of CED
- CED of nonliposomal irinotecan has been optimized in rat, dog, and primate models at UICF.
- The highly stabilized liposome-encapsulated irinotecan has advantages when used with the CED approach.
 - Due to the large size, when administered by CED the liposomal particles uniformly distribute throughout the tumor with a volume of distribution that compares favorably with the volume of drug administered
 - Designed to release irinotecan slowly over an extended period (14-21 d), differentially increasing the temporal treatment of the tumor to the chemotherapy
- Real time CED is important because previous studies utilizing CED showed promise but limited activity due to the following challenges:
 - 1) accumulation of drug in cells nearest the injection site leading to non-uniform distribution
 - 2) suboptimal pH within the tumor attributed to delivering free drug resulting in high but transient exposure with corresponding toxicity
 - 3) an inability to confine sufficient intratumoral drug exposure within the tumor since MR image guided delivery was not available
- Real time CED with real-time imaging is allowing
 - guidance and confirmation of cannula placement
 - detection of reflux, leakage, hemorrhage
 - confirmation of delivery

Poster Board # 656

Background: Integrated CED Platform For Imaged Delivery of Therapeutics to Brain Tumors



METHODS

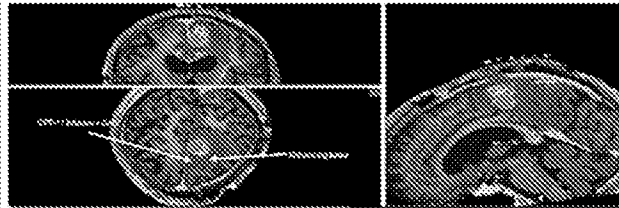
- NIA R21 supported, single center prospective 3rd dose-escalating, single arm phase I trial
- Primary endpoint: safety and tolerability
- Secondary endpoint: Optimization of real time CED, QI, TFS, imaging response.
- Eligibility: patients with recurrent grade 3 or 4 glioblastoma
- Patients fall into 4 dose escalation groups based on dose and tumor volume as seen in the table.

Group	Dose	Mean volume	Median volume	Maximum volume	Minimum time
1	20 mg	14.0 ml	12 ml	30 ml	2.5 h
2	40 mg	14.0 ml	12 ml	30 ml	2.5 h
3	80 mg	26.0 ml	16 ml	40 ml	3.5 h
4	80 mg	26.0 ml	16 ml	40 ml	3.5 h

- Four-level dose-escalation: 20 mg, 40 mg, 80 mg, and 80 mg given via 1 to 3 catheters surgically placed in an intra-tumoral location
- Concentration of gadoteridol (ProHance) will be 2 mM for all dose groups
- Maximum total volume infused will be 1.0 ml for two lowest dose groups, 1.5 ml for the third dose group, and 2.0 ml for the highest dose group.

RESULTS

- 1st patient treated on October 17, 2014
- 3 patients have received treatment to date without a DLT
- Patient #3 treated 2/11/2015
- 2 of the 3 enrolled patients have had tumor progression outside of treated volume
- All patients followed through the 30 day toxic period and then for secondary endpoints
- 0 patients off-study 2nd to toxicity
- 1 off-study for disease progression
- Cohort 2 currently enrolling



Summary

Further safety, efficacy, and imaging response results will be presented at future meetings

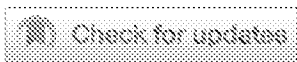
Although the principle of CED is not novel, this study represents device and procedural advancements for the application of CED that will increase the precision, reliability, and safety of directly delivering drugs to brain tumors.

Though regulatory agencies considered the above design, it is possible that a single treatment may only lead to transient clinical benefit.

Data gained herein will enable an expanded clinical program, including a study using repeated dosing.

CENTRAL NERVOUS SYSTEM TUMORS

A phase I study of convection-enhanced delivery of nanoliposomal irinotecan using real-time imaging in patients with recurrent high grade glioma.



[Nicholas A. Butowski](#) , [Seunggu Han](#) , [Jennie Webster Taylor](#) , [Manish K. Aghi](#) , [Michael Prados](#) , [Susan Marina Chang](#) [Jennifer Leigh Clarke](#) , [Krys Bankiewicz](#) , [Daryl C. Drummond](#) , [Jonathan Fitzgerald](#)

University of California, San Francisco, San Francisco, CA; UC San Francisco, San Francisco, CA; Merrimack Pharmaceuticals, Inc., Lincoln, MA; Merrimack Pharmaceuticals, Inc., Cambridge, MA

[Show Less](#)

[Abstract Disclosures](#)

Abstract

TPS2081

Background: Cytotoxic drug delivery to high grade glioma (HGG) is limited by the blood brain barrier (BBB). Convection-enhanced delivery (CED) improves chemotherapy delivery by utilizing fluid convection, obviating the challenges of crossing the BBB while minimizing systemic toxicity. CED of a highly concentrated formulation of nanoliposomal irinotecan (MM-398, nal-IRI) has been optimized in animal models of brain tumors and shows superior anti-tumor activity compared to systemic delivery. A major advance in the application of CED is the development of real time CED, which utilizes an interventional MRI suite to visualize the CED process with the aid of a co-convected contrast agent, and thus allows for real time monitoring of drug delivery to the target. **Methods:** With support from a R21 grant, a Phase I study of CED of concentrated nal-IRI using real-time imaging in patients with recurrent HGG is currently open for enrollment. This is a 3+3 dose escalation trial, with dose levels of 20 mg, 40 mg, 60 mg, and 80 mg of nal-IRI, given via up to 3 catheters surgically placed in an intra-tumoral location. The MRI contrast agent gadoteridol (2 mM) will be co-infused via the same catheters. Interim safety, efficacy, and imaging response results will be presented. From the imaging data, the correlation of pre-infusion modeling of drug distribution with post-infusion imaging will be analyzed. This will also allow for determination of the total volume of distribution to volume of infusion (Vd:Vi) ratio for each infusion. Clinical trial information: NCT02022644.

HOME / ... / C / CAELYX

Caelyx

(doxorubicin)

DIN (Drug Identification Number)

02238389 CAELYX 2MG/ML INJECTION

About this Medication

.....
How does this medication work? What will it do for me?

.....
What form(s) does this medication come in?

.....
How should I use this medication?

.....
Who should NOT take this medication?

.....
What side effects are possible with this medication?

.....
Are there any other precautions or warnings for this medication?

.....
What other drugs could interact with this medication?

How does this medication work? What will it do for me?

Doxorubicin belongs to the group of cancer-fighting medications known as *antineoplastics*, and specifically to the family of antineoplastics called *anthracyclines*. Doxorubicin prevents the growth of cancer cells by interfering with the genetic material DNA, which is necessary for reproduction of cells.

Doxorubicin is used to **treat many types of cancer**, including cancers of the blood (e.g., leukemia), bone, breast, ovaries, testicles, thyroid, head and neck, bladder, stomach and soft tissues, Hodgkin's disease, lung cancer, non-Hodgkin's lymphoma, Wilm's tumour, and neuroblastomas.

This medication may be available under multiple brand names and/or in several different forms. Any specific brand name of this medication may not be available in all of the forms or approved for all of the conditions discussed here. As well, some forms of this medication may not be used for all of the conditions discussed here.

Your doctor may have suggested this medication for conditions other than those listed in these drug information articles. If you have not discussed this with your doctor or are not sure why you are being given this medication, speak to your doctor. **Do not stop receiving this medication without consulting your doctor.**

What form(s) does this medication come in?

Each mL of a sterile, translucent, red liposomal dispersion, contains doxorubicin HCl 2 mg in a pegylated liposomal formulation in water for injection and a pH of 6.0 to 7.0. *Nonmedicinal ingredients:* the STEALTH liposome carriers are composed of N-(carbamoyl-methoxypolyethylene glycol 2000)-1,2-distearoyl-sn-glycero-3-phosphoethanolamine sodium salt (MPEG-DSPE) 3.19 mg/mL, fully hydrogenated soy phosphatidylcholine (HSPC) 9.58 mg/mL, and cholesterol 3.19 mg/mL. Each mL also contains 2 mg of ammonium sulfate, 1.55 mg of histidine as a buffer, hydrochloric acid and/or sodium hydroxide for pH control, and 94 mg of sucrose to maintain isotonicity. Greater than 90% of the drug is encapsulated in the STEALTH liposomes.

How should I use this medication?

The recommended dose of doxorubicin varies according to the specific condition being treated, the response to therapy, the other medications being used, and body size. Doxorubicin is usually injected into a vein through a specially prepared site on your skin.

Less often, it is administered into the bladder or into an artery. **The most common dosing schedule is one dose every 21 days.** Some dosing schedules call for smaller doses of the medication to be administered for 3 consecutive days every 4 weeks.

It is important this medication be given exactly as recommended by your doctor. If you miss an appointment to receive doxorubicin, contact your doctor as soon as possible to reschedule your appointment.

Very careful handling of this medication is required. Doxorubicin should only be given by health care professionals familiar with the use of chemotherapy medications used to treat cancer. It is always given under the supervision of a doctor in a hospital or similar setting with access to sterile equipment for preparation.

This medication will be stored at the hospital or clinic in the refrigerator and protected from light.

Do not dispose of medications in wastewater (e.g. down the sink or in the toilet) or in household garbage. Ask your pharmacist how to dispose of medications that are no longer needed or have expired.

Who should NOT take this medication?

Do not use this medication if you:

- are allergic to doxorubicin, any component of the container, or any ingredients of the medication
- are allergic to other similar cancer-fighting medications (e.g., epirubicin, daunorubicin, mitoxantrone, mitomycin)
- have a history of severe heart disease
- have already been treated with the maximum allowable lifetime dose of any anthracycline or anthracenedione medications (e.g., daunorubicin, doxorubicin, epirubicin, idarubicin, or mitoxantrone)

- have low blood cell counts caused by previous treatment with other cancer medications or radiation therapy
- have decreased heart function
- have severe heart rhythm problems
- have had a recent myocardial infarction (heart attack)
- have severe liver function impairment

In addition, doxorubicin should not be given directly into the bladder if tumours have penetrated the bladder wall, if blood in the urine or bladder infections are present, or if there is inflammation of the bladder.

What side effects are possible with this medication?

Many medications can cause side effects. A side effect is an unwanted response to a medication when it is taken in normal doses. Side effects can be mild or severe, temporary or permanent.

The side effects listed below are not experienced by everyone who takes this medication. **If you are concerned about side effects, discuss the risks and benefits of this medication with your doctor.**

The following side effects have been reported by at least 1% of people taking this medication. Many of these side effects can be managed, and some may go away on their own over time.

Contact your doctor if you experience these side effects and they are severe or bothersome. Your pharmacist may be able to advise you on managing side effects.

- changes in menstrual periods
- changes to the skin and nails
- diarrhea
- hot flashes
- increased sensitivity of skin to light
- loss of appetite

- nausea and vomiting
- reddish urine (not blood) – this is normal, and lasts 1 to 2 days after each dose
- temporary total loss of hair (returns after treatments end)
- tiredness

Although most of the side effects listed below don't happen very often, they could lead to serious problems if you do not check with your doctor or seek medical attention.

Check with your doctor as soon as possible if any of the following side effects occur:

- pain, redness, swelling at the place of injection
- signs of anemia (e.g., feeling weak, dizzy, or short of breath)
- signs of bleeding (e.g., bloody nose, blood in urine, coughing blood, cuts that don't stop bleeding)
- signs of a blood clot in blood vessels, such as sudden vision change or dizziness, chest pain, pain and swelling in one leg muscle
- signs of dehydration (e.g., decreased urine, dry skin, dry and sticky mouth, sleepiness, dizziness, headache, thirst, confusion)
- signs of an infection (e.g., fever over 38°C, chills or sweating, sore throat, coughing, redness or swelling around a cut, wound or catheter site, painful or difficult urination, unusual vaginal itching or discharge)
- skin rash, itching, tingling
- sores in the mouth and on the lips

Seek immediate medical attention if *any* of the following occur:

- signs of a severe allergic reaction (i.e., abdominal cramps, difficulty breathing, hives, nausea and vomiting, or swelling of the face and throat)
- signs of digestive tract bleeding or inflammation (e.g., black, tarry stools, blood in urine or vomit, or any other unusual bleeding or bruising)
- signs of changing heart function (e.g., fast or irregular heartbeat, shortness of breath, swelling of feet and lower legs)

- o signs of shock (e.g., cold, clammy skin; rapid, shallow breathing)

Some people may experience side effects other than those listed. Check with your doctor if you notice any symptom that worries you while you are taking this medication.

Are there any other precautions or warnings for this medication?

Before you begin using a medication, be sure to inform your doctor of any medical conditions or allergies you may have, any medications you are taking, whether you are pregnant or breast-feeding, and any other significant facts about your health. These factors may affect how you should use this medication.

Blood clotting: This medication can reduce the number of platelet cells in the blood. Platelets help the blood to clot, and a shortage could make you bleed more easily. Tell your doctor if you see any signs that your blood is not clotting as quickly as normal. Symptoms may include black and tarry stools, blood in the urine, easy bruising, or cuts that won't stop bleeding.

Fertility: Doxorubicin can cause changes to sperm in men and may cause ovulation to stop during treatment in women. Both men and women appear to regain fertility after doxorubicin treatment is complete. Women and men receiving doxorubicin should use effective birth control methods.

Heart problems: This medication increases the risk of heart problems such as abnormal heart rhythm, congestive heart failure, and a weakened heart (*cardiomyopathy*). Some of these problems occur early in treatment, while others occur later in treatment. People with existing heart disease, those who have had radiotherapy, people who have been treated with this medication in the past, and people who are taking certain medications that act on the heart are more at risk of these problems. Your doctor will monitor you closely for these problems.

Infection: As well as killing cancer cells, doxorubicin can reduce the number of cells that fight infection in the body (white blood cells). If possible, avoid contact with people with contagious infections. Tell your doctor if you begin to notice signs of an infection, such as fever or chills, severe diarrhea, shortness of breath, prolonged dizziness, headache, stiff neck, weight loss, or listlessness. Your doctor will do regular blood tests to monitor the number of specific types of blood cells in your blood.

Liver function: Decreased liver function or liver disease can cause this medication to build up in the body, causing side effects. People with impaired liver function may require lower doses of this medication. This medication should not be used by people who have severe liver impairment. If you have reduced liver function, discuss with your doctor how this medication may affect your medical condition, how your medical condition may affect the dosing and effectiveness of this medication, and whether any special monitoring is needed.

Secondary leukemia: There is some evidence to suggest that people who receive treatment with doxorubicin are at slightly increased risk of developing leukemia. This risk is increased when doxorubicin is given along with other anticancer medications or with radiotherapy. Talk to your doctor if you have concerns.

Tumour Lysis Syndrome: Doxorubicin, like many other cancer medications, causes many cancer cells to be suddenly killed when treatment is first started. This can overwhelm the body with waste products from the cells. When this happens, you may experience nausea, shortness of breath, notice cloudy urine or joint pain. This is called *tumour lysis syndrome*. Your doctor may prescribe some medications to help your body get rid of the waste products.

Pregnancy: This medication should not be used during pregnancy unless the benefits outweigh the risks. If you become pregnant while taking this medication, contact your doctor immediately.

Breast-feeding: This medication passes into breast milk. If you are a breast-feeding mother and are taking doxorubicin, it may affect your baby. Talk to your doctor about whether you should continue breast-feeding.

Children: Children who receive doxorubicin are at an increased risk of developing leukemia. Children may also be more susceptible to effects of this medication on the heart.

What other drugs could interact with this medication?

There may be an interaction between doxorubicin and any of the following:

- abiraterone acetate
- amiodarone
- amphotericin B
- apalutamide
- aprepitant

- azole antifungals (e.g., fluconazole, itraconazole, voriconazole)
- BCG
- bicalutamide
- bosentan
- bupropion
- calcium channel blockers (e.g., diltiazem, verapamil)
- carbamazepine
- carvedilol
- cinacalcet
- clozapine
- cobicistat
- conivaptan
- cyclosporine
- darifenacin
- deferasirox
- deferiprone
- denosumab
- digoxin
- dipyridamole
- duloxetine
- echinacea
- elagolix
- enzalutamide
- fingolimod

- flibanserin
- grapefruit juice
- hepatitis C antivirals (e.g., asunaprevir, daclatasvir, ledipasvir, velpatasvir)
- HIV non-nucleoside reverse transcriptase inhibitors (NNRTIs; e.g., delavirdine, efavirenz, etravirine, nevirapine)
- HIV protease inhibitors (e.g., atazanavir, indinavir, ritonavir, saquinavir)
- idelalisib
- isoniazid
- leflunomide
- lomitapide
- macrolide antibiotics (e.g., clarithromycin, erythromycin)
- mefloquine
- mifepristone
- mirabegron
- modafinil
- natalizumab
- other anthracycline cancer medications (e.g., daunorubicin, idarubicin)
- other cancer medications (e.g., cyclophosphamide, doxorubicin, irinotecan, paclitaxel)
- oxcarbazepine
- phenobarbital
- phenytoin
- pimecrolimus
- primidone
- protein kinase inhibitors (e.g., crizotinib, dabrafenib, imatinib, lapatinib, nilotinib, sunitinib)
- quinidine

- quinine
- rifabutin
- rifampin
- roflumilast
- sarilumab
- certain selective serotonin reuptake inhibitors (SSRI's; e.g., fluoxetine, paroxetine, sertraline)
- sirolimus
- St. John's wort
- stiripentol
- tacrolimus
- ticlopidine
- tocilizumab
- tranylcypromine
- tricyclic antidepressants (e.g., clomipramine, desipramine, imipramine)
- vaccines
- zidovudine

If you are taking any of these medications, speak with your doctor or pharmacist.

Depending on your specific circumstances, your doctor may want you to:

- stop taking one of the medications,
- change one of the medications to another,
- change how you are taking one or both of the medications, or
- leave everything as is.

An interaction between two medications does not always mean that you must stop taking one of them. Speak to your doctor about how any drug interactions are being managed or should be managed.

Medications other than those listed above may interact with this medication. Tell your doctor or prescriber about all prescription, over-the-counter (non-prescription), and herbal medications you are taking. Also tell them about any supplements you take. Since caffeine, alcohol, the nicotine from cigarettes, or street drugs can affect the action of many medications, you should let your prescriber know if you use them.

All material copyright MediResource Inc. 1996 – 2021. Terms and conditions of use. The contents herein are for informational purposes only. Always seek the advice of your physician or other qualified health provider with any questions you may have regarding a medical condition. Source: www.medbroadcast.com/drug/getdrug/Caelyx

Synergistic Antitumor Activity of Capecitabine in Combination with Irinotecan

Shousong Cao, Farukh A. Durrani, Youcef M. Rustum

Abstract

5-Fluorouracil (5-FU) and capecitabine alone and in combination with irinotecan/oxaliplatin are clinically active in the treatment of colorectal and other solid tumors. Studies of the antitumor activity and toxicity of capecitabine or irinotecan alone and in combination with each other, were compared with 5-FU and raltitrexed in human tumor xenografts of colorectal and squamous cell carcinoma of the head and neck using clinically relevant schedules. Antitumor activity and toxicity were evaluated in nude mice bearing human colon carcinomas of HCT-8 and HT-29 and in head and neck squamous cell carcinomas of A253 and FaDu xenografts using the maximum tolerable dose of single-agent capecitabine, 5-FU, or raltitrexed, or each of the drugs in combination with irinotecan. Mice were treated with capecitabine and irinotecan alone or in combination using 2 different schedules: (1) capecitabine orally once a day for 7 days and a single dose of irinotecan (50 mg/kg intravenously [I.V.]), with each drug alone or in combination, and (2) capecitabine orally 5 days a week for 3 weeks and irinotecan 50 mg/kg (I.V. injection) once a week for 3 weeks, with each drug alone or in combination. For comparative purposes, the antitumor activity of single-agent capecitabine, 5-FU, or raltitrexed, or each drug in combination with irinotecan was carried out at its maximum tolerated dose (MTD) using a 3-week schedule. Results indicated that HT-29 and A253 xenografts were de novo resistant (no cure) to capecitabine and irinotecan alone at the MTD, whereas HCT-8 and FaDu xenografts were relatively more sensitive, yielding 10%-20% cures. The combination of irinotecan/capecitabine was much more active than either drug alone against all 4 tumor models. The cure rates were increased from 0 to 20% in A253 and HT-29 xenografts and from 10%-20% to 80%-100% in HCT-8 and FaDu tumor xenografts, respectively. Irinotecan/capecitabine had clear advantage over irinotecan/5-FU and irinotecan/raltitrexed in efficacy and selectivity in that they were more active and less toxic. The extent of synergy with irinotecan/capecitabine appears to be tumor-dependent and independent of the status of p53 expression. The potential impact of the preclinical results on clinical practice for the use of these drugs in combination needs clinical validation.

Clinical Colorectal Cancer, Vol. 4, No. 5, 336-343, 2005

Key words: Combination therapy, 5-Fluorouracil, p53, Raltitrexed, Synergistic interaction, Xenograft

Introduction

The fluorinated pyrimidines 5-fluorouracil (5-FU) and fluorodeoxyuridine have been the standard drugs for treatment of advanced colorectal carcinoma, as well as several other malignancies including head and neck cancer.¹ 5-Fluorouracil-based chemotherapy plays an important role with proven benefits with regard to relapse-free survival in adju-

vant head and neck squamous cell carcinoma (HNSCC) and colorectal cancers. Historically, 5-FU used as a secondary agent in advanced HNSCC has a response rate averaging 15% and a median survival time of < 1 year in colorectal cancer.²⁻³ Therapy with 5-FU and leucovorin has increased tumor response in patients with colorectal cancer; however, severe side effects such as diarrhea, mucositis, and neutropenia were observed.⁴⁻⁷

Over the past 2 decades, attempts have been made to improve on the therapeutic efficacy of 5-FU by optimizing schedule, modulation of its intracellular metabolism, and developing new and more specific thymidylate synthase (TS) inhibitors (raltitrexed, pemetrexed, and ZD9331). Based on consideration of the biochemical pathway of 5-FU activation

Grace Cancer Drug Center, Roswell Park Cancer Institute, Buffalo, NY

Submitted: Sep 8, 2004; Revised: Nov 2, 2004; Accepted: Nov 8, 2004

Address for correspondence: Shousong Cao, MD, Roswell Park Cancer Institute, Elm and Carlton Sts, Buffalo, NY 14263

Fax: 716-345-8857; e-mail: shousong.cao@roswellpark.org

Electronic forwarding or copying is a violation of US and International Copyright Laws.

Authorization to photocopy items for internal or personal use, or the internal or personal use of specific clients, is granted by Cancer Information Group.

ISSN #1533-0028, provided the appropriate fee is paid directly to Copyright Clearance Center, 222 Rosewood Drive, Danvers, MA 01923 USA 978-750-8400.

and the site of 5-FU action, several oral fluoropyrimidines (uracil/tegafur, S-1, and capecitabine) are under preclinical and clinical development.⁸⁻¹⁵ Capecitabine was approved by the US Food and Drug Administration (FDA) for the treatment of patients with breast and colorectal cancer. Capecitabine is an orally administered fluoropyrimidine carbamate primarily metabolized by thymidine phosphorylase (TP). It is converted to 5-FU by 3 enzymatic steps (Figure 1), initially metabolized by carboxylesterase in the liver to 5'-deoxy-5-fluorocytidine, then converted by cytidine deaminase, which is expressed at higher concentration in tumors than normal tissues, to 5'-deoxy-5-fluorouridine and doxifluridine; it is finally converted to 5-FU by TP. 5-Fluorouracil is eliminated rapidly from the plasma with a half life of < 10 minutes^{16,17} and is also inactivated by dihydropyrimidine dehydrogenase in normal and tumor tissues.¹⁸ In tumor tissues with significantly high levels of TP, the 5-FU concentrations in tumors derived from capecitabine was significantly higher than in tumor treated with 5-FU.¹⁹ Furthermore, the tumor-plasma ratio of 5-FU derived from capecitabine was 127.¹⁹ Preclinical studies in model systems demonstrated the antitumor efficacy and selectivity of capecitabine against various murine and human tumors.^{14,20,21}

Irinotecan is a potent inhibitor of topoisomerase I, a nuclear enzyme that plays a critical role in DNA replication and transcription. Irinotecan accomplishes this by causing transient single-strand DNA breaks that release the torsional strain caused by the synthesis of a new strand of DNA or RNA around a double helix. Camptothecins target this topoisomerase I-DNA complex (also known as the cleavable complex) and, when bound, inhibit reannealing of the parent DNA, thereby halting nucleic acid synthesis and leading to cell death.^{22,23} Irinotecan is converted by carboxylesterases to its more active metabolite, SN-38.²² Irinotecan alone or in combination with 5-FU is active clinically and approved by the FDA for the treatment of colorectal cancer.²⁴⁻²⁶

In this study, we evaluated the antitumor activity and toxicity of capecitabine and irinotecan alone and in combination using clinically relevant daily and weekly schedules against various human tumor xenografts and compared the antitumor efficacy of the combination of irinotecan/capecitabine with those of irinotecan/5-FU and irinotecan/raltitrexed.

Materials and Methods

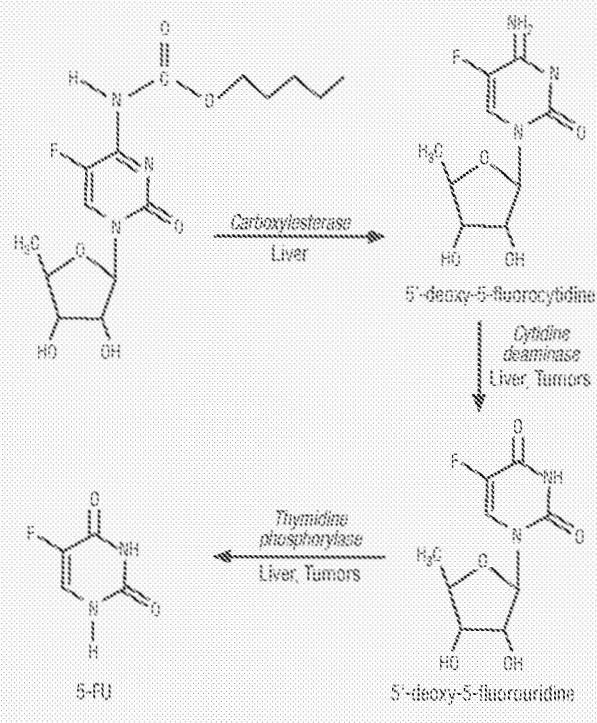
Animals

Female athymic nude mice with a body weight of 20-25 g and aged 8-12 weeks were kept 5 mice per cage with water and food ad libitum according to an institutionally approved protocol.

Tumors

The human colorectal tumor xenografts HCT-8 (poorly differentiated, relatively drug-sensitive) and HT-29 (moderately differentiated, relatively drug-resistant) were used; and HNSCC xenografts FaDu (poorly differentiated, relatively drug-sensitive) and A253 (well differentiated, relatively drug-

Figure 1 Capecitabine's Chemical Structure and Metabolic Pathway



resistant) were used. The cell lines were maintained as a monolayer in RPMI 1640 supplemented with 10% fetal bovine serum. Xenografts were initially established by implanting cultured cells ($\times 10^6$) subcutaneously and passed several generations by transplanting approximately 50 mg nonnecrotic tumor tissue subcutaneously.

Tumor Measurement

Two axes of the tumor (L, longest axis in mm; W, shortest axis in mm) were measured with a vernier caliper. Tumor weight (in mg) was calculated as: $1/2 (L \times W^2)$. Relative tumor volume (%) was calculated by actual tumor weight (ATW) divided by initial tumor weight (ITW; day 0) as follows: $ATW/ITW \times 100\%$. Measurements were taken once a day during the first 10 days and 3-4 times a week thereafter.

Drugs

Capecitabine was dissolved in sterile saline solution before use at a final concentration of 20 mg/mL. Irinotecan was a ready-to-use clinical formulation solution in 5-mL vials containing 100 mg of drug (20 mg/mL). 5-Fluorouracil was a solution of 50 mg/mL vials and diluted in sterile saline solution.

Drug Doses and Schedules

Capecitabine was administered orally using a 20-gauge feeding needle to administer a 0.2-0.5-mL/dose solution once daily for 7 days or 5 days a week with 2 days rest for 3 weeks. Irinotecan was administered by a single intravenous

Regimen	Schedule	MTD
Irinotecan	I.V. weekly for 3 weeks	100 mg/kg
Capecitabine	Oral daily for 7 weeks	600 mg/kg
Capecitabine	Oral 5 days per week for 3 weeks	400 mg/kg
5-FU	I.V. weekly for 3 weeks	100 mg/kg
Raltitrexed	I.V. weekly for 3 weeks	60 mg/kg
Irinotecan/ Capecitabine	I.V. for 1 week	50 mg/kg
	Orally daily for 7 weeks	600 mg/kg
Irinotecan/ Capecitabine	I.V. weekly for 3 weeks	50 mg/kg
	Orally 5 days per week for 3 weeks	400 mg/kg
Irinotecan/5-FU	I.V. weekly for 3 weeks	50 mg/kg
		50 mg/kg
Irinotecan/ Raltitrexed	I.V. weekly for 3 weeks	50 mg/kg
		30 mg/kg

From 3-4 independent experiments, 15-20 mice were treated for each group.

(I.V.) injection (via the animal's tail vein) or once a week for 3 weeks. For the combination of irinotecan and capecitabine, 2 treatment schedules were used: (1) a single irinotecan injection of 50 mg/kg followed 24 hours later by oral capecitabine (600 mg/kg) daily for 7 days; (2) weekly irinotecan 50 mg/kg followed 24 hours later by oral capecitabine (400 mg/kg) for 5 days a week for 3 weeks. For the weekly combination of irinotecan (50 mg/kg) with 5-FU (50 mg/kg) or raltitrexed (30 mg/kg), the 2 drugs were simultaneously administered I.V. once a week for 3 weeks. Each experimental group contained 5 mice per experiment, and each experiment was repeated ≥ 2 times.

Maximum Tolerated Dose and Toxicity Evaluation

The maximum tolerated dose (MTD) was defined as the maximum dose that caused no drug-related lethality and which produced animal body weight loss of < 20% of original weight. The kinetics of drug-induced toxicities (body weight loss and lethality) were determined daily for a minimum of 4 weeks and observed ≥ 2 times a week thereafter.

Antitumor Activity

Drug treatments were initiated 7-8 days after tumor transplantation when tumor weights reached approximately 200-250 mg (mm³) as described previously.^{27,28} Antitumor activity was assessed by tumor growth inhibition, which is mean tumor weight (MTW) of the treated group (TG) relative to the untreated control group (CG) and calculated as: (MTW TG - MTW CG) / MTW CG \times 100. The tumor growth inhibition is calculated on day 12, the day the animals in the control group had to be killed because of large tumors (approximately 2000 mg). The tumor doubling time was defined as the mean time for the tumor to reach twice

its initial weight (determined at the beginning of treatment or day 0).

Tumor response was expressed as a partial response (PR) when tumor weight was temporarily reduced by $\geq 50\%$ and as a complete response (CR) when tumor was undetectable by palpation for 90 days after therapy (ie. cure), at which time the animals were killed. The response rate was expressed as the percentage of animals with responding tumors in the group. In general, tumors in mice with a PR recurred within 2 weeks after treatment termination; however, tumors rarely (< 5% of cases) recurred after a CR was achieved. As a general policy, animals were killed when the tumor weight reached 2000 mg. All studies were performed in accordance with institutional animal care and use committee and under an approved institute protocol.

Results

Determination of Maximum Tolerated Doses

To determine the MTD of capecitabine, nude mice with or without xenografted tumors were treated orally according to 1 of 2 alternate schedules: (1) once a day for 7 days or (2) 5 days a week for 3 weeks. When 5-FU or raltitrexed was combined with irinotecan, mice were treated by I.V. injection once a week for 3 weeks (on day 0 of each cycle).

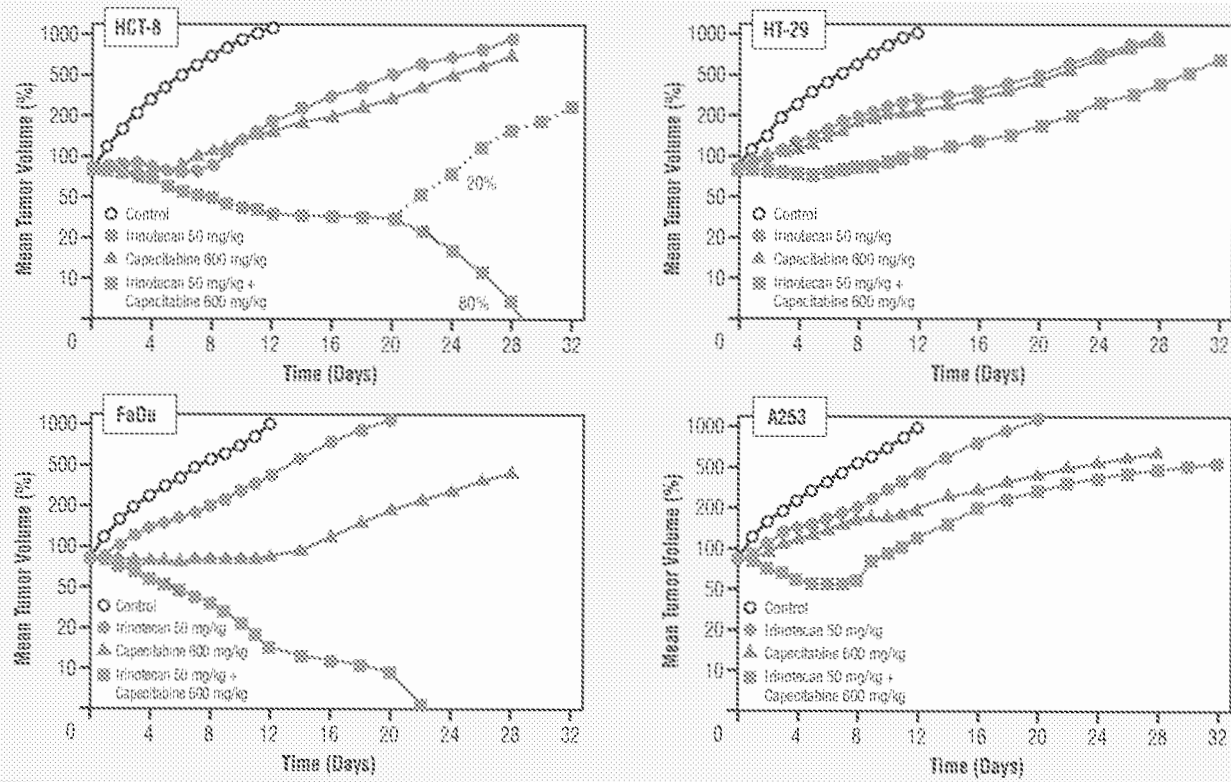
The MTDs of capecitabine were 600 mg/kg per day when mice were treated for 7 days and 400 mg/kg per day when mice were treated for 5 days a week (Table 1). The MTDs of irinotecan, 5-FU, and raltitrexed were 100 mg/kg, 100 mg/kg, and 60 mg/kg per week for 3 weeks, respectively. With the combination of irinotecan/capecitabine, the MTDs were 50/600 mg/kg and 50/400 mg/kg for daily and weekly schedules, respectively. With the combination of irinotecan/5-FU and irinotecan/raltitrexed, the MTDs were 50/50 mg/kg and 50/30 mg/kg per week for 3 weeks, respectively. Unlike 5-FU or raltitrexed in combination with irinotecan, the MTD of capecitabine can be administered (Table 1).

Antitumor Activity of Daily Capecitabine and Irinotecan Alone or in Combination

The data in Figures 2 and 3 summarize the antitumor activity of capecitabine (600 mg/kg) administered orally once a day for 7 days with or without a single dose of irinotecan (50 mg/kg I.V.) in nude mice bearing xenografts tumors of HCT-8 and HT-29 and head/neck xenografts of FaDu and A253. As a single agent, irinotecan at 50 mg/kg was only slightly active against all 4 tumor xenografts, with 52%-62% tumor growth inhibition without a CR or PR. Whereas daily capecitabine 600 mg/kg for 1 week was modestly active as a single agent against HT-29 and A253 xenografts, with 69% and 79% tumor growth inhibition, respectively, without achieving CR and PR, it was more active against HCT-8 and FaDu xenografts: mice with HCT-8 tumors exhibited a 10% PR and 10% CR and mice with FaDu tumors exhibited a 20% PR and 20% CR.

In terms of tumor growth inhibition, the combination of capecitabine/irinotecan was much more active than either

Figure 2 Kinetics of the Antitumor Activity of Human Tumor Xenografts Treated with Single-Dose Irinotecan and Daily Capecitabine



Kinetics of the antitumor activity of human tumor xenografts treated with irinotecan (I.V. once) and capecitabine (orally daily for 7 days) alone and in combination. Each treatment group had 15-20 mice in total from 3-4 independent experiments.

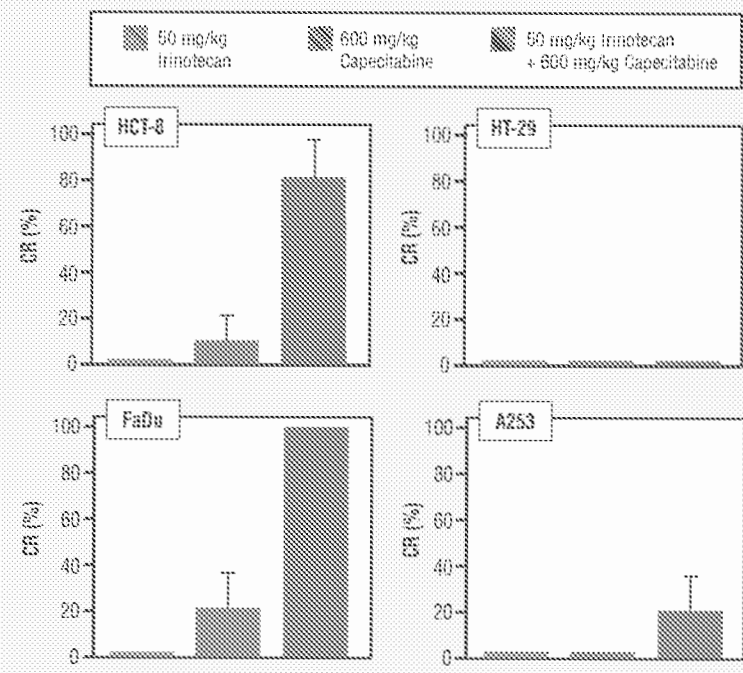
drug alone against all 4 tumor models (Figure 2). However, greater tumor growth inhibition and CR rates were apparent in HCT-8 and FaDu tumor xenografts, with 80% and 100% of cure rates achieved, respectively (Figure 3).

Antitumor Activity of Weekly Capecitabine and Irinotecan Alone or in Combination

We evaluated a clinically relevant schedule of capecitabine administered orally 5 days a week for 3 weeks with or without weekly irinotecan (50 mg/kg, I.V. injection) against the 4 human tumor models (Figures 4 and 5). The data show that single-agent capecitabine at 400 mg/kg per day (MTD) for 5 days per week for 3 weeks had similar antitumor activity as capecitabine 600 mg/kg daily for 7 days against the 4 xenografted tumors, with 66%-92% tumor growth inhibition. No mice exhibited CR and PR with single-agent capecitabine with the exception of mice bearing FaDu xenografts, which exhibited 20% PR and 20% CR.

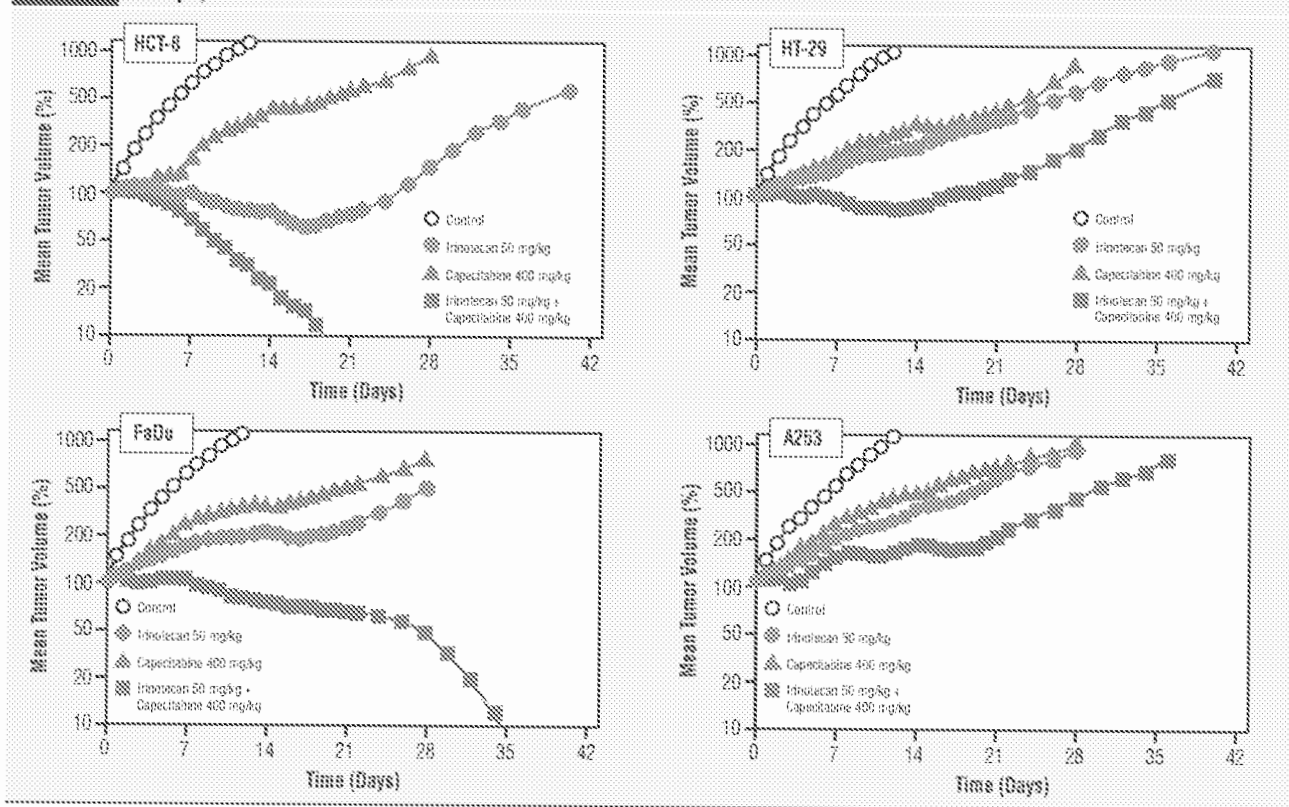
Single-agent irinotecan 50 mg/kg (50% of the MTD) every week was more active against the 4 tumor xenografts than a single dose. In-

Figure 3 Complete Tumor Regression with Irinotecan and Capecitabine



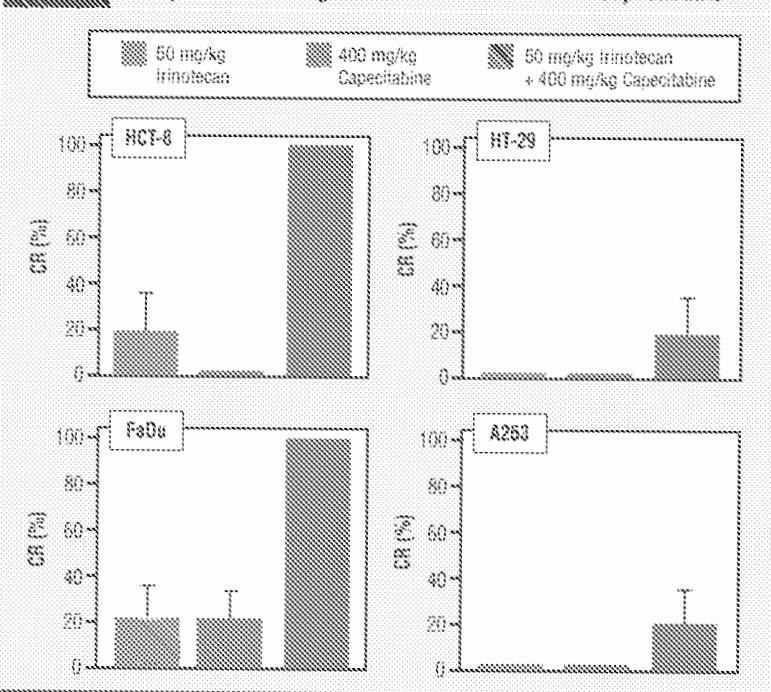
Complete tumor regression (cure) produced by irinotecan (I.V. once) and oral capecitabine (daily for 7 days) alone and in combination in nude mice bearing human tumor xenografts. Each treatment group had 15-20 mice in total from 3-4 independent experiments.

Figure 4 Kinetics of the Antitumor Activity Human Tumor Xenografts Treated with 3 Weekly Doses of Irinotecan and Capecitabine for 5 Days per Week for 3 Weeks



Kinetics of the antitumor activity of human tumor xenografts treated with irinotecan (i.v. weekly for 3 weeks) and capecitabine (orally 5 days per week for 3 weeks) alone and in combination. Each treatment group had 15-20 mice in total from 3-4 independent experiments.

Figure 5 Complete Tumor Regression with Irinotecan and Capecitabine



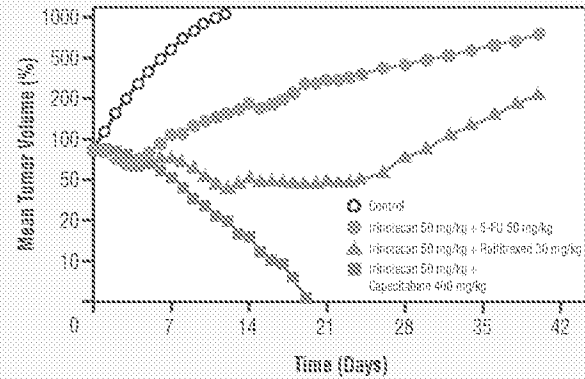
Complete tumor regression (cure) produced by with irinotecan (i.v. weekly for 3 weeks) and capecitabine (orally 5 days per week for 3 weeks) alone and in combination in nude mice bearing human tumor xenografts. Each treatment group had 15-20 mice in total from 3-4 independent experiments.

creasing the irinotecan dose to the MTD (100 mg/kg per week for 3 weeks) slightly increased the antitumor activity against all 4 tumor xenografts and also enhanced host toxicity (data not shown).

The combination of capecitabine and irinotecan was much more active than either drug alone against all 4 tumor models tested, achieving 20% PR and 20% CR in both of the relatively resistant tumors derived from HT-29 and A253. Most impressive is that all the treated animals in the HCT-8 and FaDu tumor xenograft groups were cured (100% CR; Figure 5).

Comparative Antitumor Activity and Toxicity of Irinotecan Combinations at the MTD Using Weekly Schedule Against HCT-8 or FaDu Tumor Xenografts

We chose the weekly 21-day schedule to compare the antitumor activity and toxicity of irinotecan/capecitabine with irinotecan/5-FU or irinotecan/capecitabine at the MTD against HCT-8 and FaDu tumor xenografts.

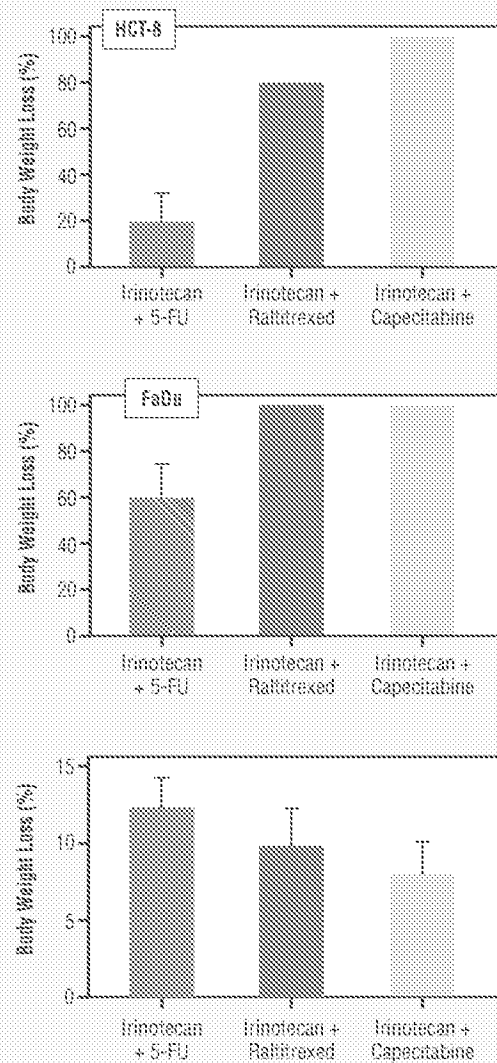
Figure 6 Antitumor Activity with Combination Regimens at Maximum Tolerated Dose

Comparative antitumor activity of the combination of irinotecan/5-FU, irinotecan/raltitrexed, or irinotecan/capecitabine at their MTDs with weekly $\times 3$ schedule in nude mice bearing human tumor HCT-8 colon tumor xenografts. Each treatment group had 15-20 mice in total from 3-4 independent experiments.

The data in Figures 6 and 7 summarize the antitumor activity and toxicity of irinotecan/capecitabine, irinotecan/5-FU, and irinotecan/raltitrexed. The data showed that irinotecan/capecitabine is more active than irinotecan/5-FU or irinotecan/raltitrexed against HCT-8 tumors (Figures 6 and 7) and more active than irinotecan/5-FU and equally effective as irinotecan/raltitrexed against FaDu xenografts (Figure 7) in terms of cure rates. Of interest, unlike the combinations of irinotecan/5-FU and irinotecan/raltitrexed, which significantly increase toxicity with 100% lethality when 5-FU and raltitrexed were used at the MTD, the doses of 5-FU and raltitrexed had to be reduced to 50% of each drug. In contrast, capecitabine can be administered at the MTD in combination with irinotecan without increasing host toxicity.

Discussion

Despite significant advances in the treatment of colorectal cancer and HNSCC in recent years, therapeutic selectivity remains a major obstacle to curative therapy. 5-Fluorouracil (a TS inhibitor) and irinotecan (a topoisomerase-I inhibitor) are active agents in treatment of colorectal cancer and HNSCC. However, toxicities such as diarrhea, myelosuppression, and stomatitis and drug resistance limit the effectiveness when they are used alone or in combination. Selective activation of a 5-FU prodrug in tumor tissues may be a useful approach for reducing drug-induced toxicity and increasing antitumor efficacy. Studies herein were performed to determine the antitumor efficacy of capecitabine and irinotecan alone or in combination against human colorectal and HNSCC models with clinically relevant schedules. Our earlier studies with the combination of irinotecan and 5-FU in rats and in nude mice bearing human tumor xenografts had demonstrated that the antitumor activity is highly sequence-dependent, with the sequence of irinotecan administered 24 hours before 5-FU being superior to the other sequences tested.^{29,30}

Figure 7 Antitumor Activity and Toxicity of Combination Weekly Regimens

Comparative antitumor activity and toxicity of the combination of irinotecan/5-FU, irinotecan/raltitrexed, or irinotecan/capecitabine with weekly $\times 3$ schedule in nude mice bearing human tumor HCT-8 colon and FaDu head and neck tumor xenografts. Each treatment group had 15-20 mice in total from 3-4 independent experiments.

In the current study, irinotecan was given 24 hours before capecitabine using 2 different schedules. The data herein demonstrate that the combination of irinotecan and capecitabine is much more active than each drug alone against both colorectal cancer models and both HNSCC tumor models with daily and weekly schedules. However, the models that were most sensitive to irinotecan/capecitabine combination were the HCT-8 and FaDu tumors, whereas the A253 and HT-29 tumors are relatively resistant to the therapy. With the daily schedule, the cure rate of the combination was increased from 0-10% to 80% in HCT-8, from 0 to 20% in A253, and from 0-20% to 100% in FaDu. With the weekly schedule, the cure rate was increased from 0 to 20% in HT-

29 and A253. In contrast, 100% cures rates resulted from the combination in the HCT-8 and FaDu xenografts. The weekly schedule was more active than the daily schedule with irinotecan and the combination.

The reason for different sensitivity with the irinotecan/capecitabine combination in the 4 tumor models tested have yet to be determined. Histologic analysis in our laboratory showed that HCT-8 and FaDu are poorly differentiated with relative higher cyclin A index (36%-37%), whereas A253 is well differentiated with a cyclin A index of 22% and HT-29 is moderately differentiated with a cyclin A index of 29%.³⁰ Thus, it is possible that with the MTD of the combination and the well-differentiated tumor xenografts, insufficient drug concentration will reach the target. In fact, support for this hypothesis has recently been confirmed with use of higher doses of irinotecan combined with selenium.³¹

Irinotecan/capecitabine is more active and less toxic than irinotecan/5-FU or irinotecan/raltitrexed. Unlike the combination of irinotecan with 5-FU or raltitrexed, capecitabine could be administered at its MTD in combination with irinotecan. In addition, capecitabine is an orally bioavailable agent.

Markers associated with tumor response to 5-FU include TS, TP, and dihydropyrimidine dehydrogenase, a 5-FU degradative enzyme. In general, tumors with lower TS and TP enzyme levels had a higher response rate to treatment than tumors with only low TS or TP expression.³² The favorable toxicity profile with capecitabine compared with 5-FU results at least in part from the final conversion step of capecitabine to 5-FU that occurred mainly in the tumor. The 5-FU concentration in the tumor was reported to be much higher than those in plasma and normal tissues.²⁰

The mechanisms whereby irinotecan may potentiate the antitumor efficacy of 5-FU and capecitabine are not yet fully understood. Results from our laboratory and other investigators indicate that a higher S-phase fraction is associated with improved drug response against cultured tumor cell lines and human tumor xenografts.³³⁻³⁵ The effect of irinotecan and 5-FU on cell cycle distribution and the S phase fraction in HCT-8 tumor xenograft was investigated. The data indicate that irinotecan, but not 5-FU, increased the number of cells in S-phase from 23% to 57%.³⁰ This effect is drug-specific, because topotecan (another topoisomerase-I inhibitor) did not produce a similar effect.³⁰ So the synergy between irinotecan and capecitabine may be primarily caused by cell cycle synchronization in S-phase by irinotecan, resulting in a sensitization of the tumor cells to subsequent treatment with capecitabine.

In summary, these studies with human colorectal and HNSCC tumor xenograft models clearly demonstrated that irinotecan significantly potentiated the antitumor efficacy of capecitabine without increasing the toxicity. Although the combination of irinotecan/capecitabine was more active against all 4 tumor models tested, the most sensitive tumors were FaDu and HCT-8. The different response to the therapy with different tumors may be associated with tumor differentiation status and/or the cyclin A index. The HCT-8 and

FaDu tumors are poorly differentiated and have a higher cyclin A index. The combination of irinotecan/capecitabine is more active and less toxic, with a higher therapeutic index than irinotecan/5-FU or irinotecan/raltitrexed. Because these studies were carried out using clinically active drug combinations and schedules, the therapeutic benefit achieved in these preclinical models could have significant impact on clinical value.

References

1. Pinedo HM, Peters GJ. 5-Fluorouracil: biochemistry and pharmacology. *J Clin Oncol* 1983; 6:1653-1664.
2. Hughes RS, Frenkel E. The role of chemotherapy in head and neck cancer. *Am J Clin Oncol* 1997; 20:449-461.
3. Advanced Colorectal Cancer Meta-Analysis Project. Modulation of fluorouracil by leucovorin in patients with advanced colorectal cancer: Evidence in terms of response rate. *J Clin Oncol* 1992; 10:896-903.
4. Rustum YM, Cao S, Zhang Z. Rationale for treatment design: biochemical modulation of 5-fluorouracil by leucovorin. *Cancer J Sci Am* 1998; 4:12-18.
5. Petrelli N, Herrera L, Rustum Y, et al. A prospective randomized trial of 5-fluorouracil and methotrexate in previously untreated patients with advanced colorectal carcinoma. *J Clin Oncol* 1987; 5:1559-1565.
6. Petrelli N, Douglass HOJ, Herrera L, et al. The modulation of fluorouracil with leucovorin in metastatic colorectal carcinoma: A prospective randomized phase III trial. *J Clin Oncol* 1989; 7:1419-1426.
7. Poon MA, O'Connell MJ, Weiland HS, et al. Biochemical modulation of fluorouracil with leucovorin: confirmatory evidence of improved therapeutic efficacy in advanced colorectal cancer. *J Clin Oncol* 1991; 9:1967-1972.
8. Cao S, Frank C, Shirasaka T, Rustum YM. 5-Fluorouracil prodrug: role of anabolic and catabolic pathway modulation in therapy of colorectal cancer. *Clin Cancer Res* 1995; 1:839-845.
9. Malik STA, Talbot D, Clarke PI, et al. Phase II trial of UFT in advanced colorectal and gastric cancer. *Br J Cancer* 1992; 62:1023-1025.
10. Douillard JY, Hoff PM, Skillings JR, et al. Multicenter phase III study of uracil/tegafur and oral leucovorin versus fluorouracil and leucovorin in patients with previously untreated metastatic colorectal cancer. *J Clin Oncol* 2002; 20:3605-3616.
11. Shirasaka T, Nakano K, Takechi T, et al. Antitumor activity of 1 M tegafur-0.4 M 5-chloro-2,4-dihydropyridino-1 M potassium oxonate (S-1) against human colon carcinoma orthotopically implanted into nude rats. *Cancer Res* 1996; 56:2602-2606.
12. Cao S, Lu K, Toth K, et al. Persistent induction of apoptosis and suppression of mitosis as the basis for curative therapy with S-1, an oral 5-Fluorouracil prodrug in a colorectal tumor model. *Clin Cancer Res* 1999; 5:267-274.
13. Cohen SJ, Leichman CG, Yeslow G, et al. Phase I and pharmacokinetic study of once daily oral administration of S-1 in patients with advanced cancer. *Clin Cancer Res* 2002; 8:2116-2122.
14. Ishikawa T, Utoh M, Sawada N. Tumor selective delivery of 5-fluorouracil by capecitabine, a new oral fluoropyrimidine carbamate in human cancer xenografts. *Biochem Pharmacol* 1998; 55:1091-1093.
15. Hoff PM. Capecitabine as first-line treatment for colorectal cancer (CRC): integrated results of 1207 patients (pts) from 2 randomized, phase III studies. On behalf of the capecitabine CRC study group. *Ann Oncol* 2000; 11:60.
16. Reigner B, Blesch K, Weidekamm E. Clinical pharmacokinetics of capecitabine. *Clin Pharmacokinet* 2001; 40:85-104.
17. Fraile RJ, Baker LH, Buroker TR, et al. Pharmacokinetics of 5-fluorouracil administered orally, by rapid intravenous and by slow infusion. *Cancer Res* 1980; 40:2223-2228.
18. Hoggie GD, Sommadossi JP, Gross DS, et al. Clinical pharmacokinetics of 5-fluorouracil and its metabolites in plasma, urine and bile. *Cancer Res* 1987; 47:2203-2206.
19. Diasio RB, and Harris BE. Clinical pharmacology of 5-fluorouracil. *Clin Pharmacokinet* 1989; 16:215-237.

20. Ishikawa T, Utoh M, Sawada N, et al. Xeloda (capecitabine): an orally available tumor-sensitive fluoropyrimidine carbamate. *Proc Am Soc Clin Oncol* 1997;16:208 (Abstract #796).
21. Cao S, Li K, Ishitsuka H, Rustum YM. Antitumor efficacy of capecitabine against fluorouracil-sensitive and -resistant tumors. *Proc Am Soc Clin Oncol* 1997; 16:226 (Abstract #795).
22. Kawato Y, Aonuma M, Hirota Y, et al. Interacellular roles of SN-38, a metabolite of the camptothecin derivative CPT-11, in the antitumor effect of CPT-11. *Cancer Res* 1991; 51:4187-4191.
23. Wiseman LR, Markham A. Irinotecan. A review of its pharmacological properties and clinical efficacy in the management of advanced colorectal cancer. *Drugs* 1996; 52:606-623.
24. Conti JA, Kemeny NE, Saltz LB, et al. Irinotecan is an active agent in untreated patients with metastatic colorectal cancer. *J Clin Oncol* 1996; 14:709-715.
25. Rougier P, Bugat R, Douillard JY, et al. Phase II study of irinotecan in the treatment of advanced colorectal cancer in chemotherapy-naïve patients and patients pretreated with fluorouracil-based chemotherapy. *J Clin Oncol* 1997; 15:251-260.
26. Vanhoefler U, Harstick A, Kohne CH, et al. Phase I study of a weekly schedule of irinotecan, high-dose leucovorin, and fluorouracil as first-line chemotherapy in patients with advanced colorectal cancer. *J Clin Oncol* 1999; 17:907-913.
27. Cao S, Abraham A, Nair MG, et al. Polyglutamylated dihydrofolate reductase inhibitor g-methylene-10-deazaaminopterin is not essential for antitumor activity. *Clin Cancer Res* 1996; 2:707-712.
28. Cao S, McGuire JJ, Rustum YM. Antitumor activity of ZD1694 (Tomudex) against human head and neck cancer in nude mouse models: role of dosing schedule and plasma thymidine. *Clin Cancer Res* 1999; 5:1925-1934.
29. Cao S, Rustum YM. Synergistic Antitumor activity of Irinotecan in combination with 5-Fluorouracil in *ras* bearing advanced colorectal cancer: Role of drug sequence and dose. *Cancer Res* 2000; 60:3717-3721.
30. Azrak RG, Cao S, Slocum HK, et al. Therapeutic synergy between irinotecan and 5-fluorouracil against human tumor xenografts. *Clin Cancer Res* 2004; 10:1158-1167.
31. Cao S, Durrani FA, and Rustum YM. Selective modulation of the therapeutic efficacy of anticancer drugs by selenium containing compounds against human tumor xenografts. *Clin Cancer Res* 2004; 10:2561-2569.
32. Metzger R, Danenberg KD, Leichman CG, et al. High basal level gene expression of thymidine phosphorylase (plate-derived endothelial cell growth factor) in colorectal tumors is associated with non-response to 5-fluorouracil. *Clin Cancer Res* 1998; 4:2371-2376.
33. Yin MB, Hapke G, Wu J, et al. Chk1 signaling pathways that mediated G2/M checkpoint in relation to the cellular resistance to the novel topoisomerase I poison BNP1350. *Biochem Biophys Res Commun* 2002; 295:435-444.
34. Yin MB, Guo B, Vanhoefler U, et al. Characterization of protein kinase chk1 essential for the cell cycle checkpoint after exposure of human head and neck carcinoma A253 cells to a novel topoisomerase I inhibitor BNP1350. *Mol Pharmacol* 2000; 57:453-459.
35. Kolfschoten GM, Hulscher TM, Pinedo HM, et al. Drug resistance features and S-phase fraction as possible determinants for drug response in a panel of human ovarian cancer xenografts. *Br J Cancer* 2000; 83:921-927.

A Gold Nanoparticle Bouquet held on plasma membrane: An ultrasensitive dark-field imaging approach for Cancer Cell Analysis

 Yue Cao[✉], Jie Wang, Qiao-Yan Jiang, Li Hu, You-Jia Yu, Yan-Fang Yu, Feng Chen[✉]

Department of Forensic Medicine, Nanjing Medical University, Nanjing, Jiangsu, 211166, PR China.

✉ Corresponding author: E-mails: ycao@njmu.edu.cn (Yue Cao); E-mail: fchen@njmu.edu.cn (Feng Chen).

 © The author(s). This is an open access article distributed under the terms of the Creative Commons Attribution License (<https://creativecommons.org/licenses/by/4.0/>). See <http://ivyspring.com/terms> for full terms and conditions.

Received: 2019.11.12; Accepted: 2020.06.08; Published: 2020.06.20

Abstract

Rational: p53 is suppressing tumor protein correlated with the cell cycle factors and apoptosis. Here, a gold nanoparticle bouquet is designed for an ultrasensitive dark-field imaging approach for cancer cell analysis.

Methods: AuNP60/APBA is functionalized by a gold nanoparticle bouquet-plasmonic 60 nm gold nanoparticles. And consistent APBA can be held on the plasma membrane. After 13 nm gold nanoparticles are functionalized with mannose (AuNP13/MN), the AuNP60/APBA gold nanoparticles are captured. The absorption spectrum of aggregation gold nanoparticles (AuNPs) shifts to near-infrared (NIR) region which can be observed under dark-field microscopy (DFM) and is treated the subsequent with photothermal therapy.

Results: The results that MCF-7 cells were successfully destroyed under the near-infrared (NIR) irradiation and the intracellular WTp53 increased while the MTP53 decreased. These results indicated that p53 is the key molecule in the apoptosis signaling pathway. Photothermal therapy can stimulate the MTP53 in the cell signal conductive pathway.

Conclusion: This work offers a new method for intracellular p53 analysis and a potential targeted cancer treatment.

Key words: gold nanoparticle bouquet, dark-field imaging, p53, cancer cell, photothermal therapy

Introduction

Noble metal nanoparticles, peculiarly gold nanoparticles (AuNPs), keep attracting much attention due to its excellent biocompatibility and picturesque optical properties [1-5]. AuNP is an attractive nanomaterial candidate with resonant absorption and excitation of incident light to induce strong local surface plasmon resonance (LSPR) [6,7]. With the continuous development of dark-field hyperspectral imaging (DFM) and plasmon resonance scattering spectrum, the impact of plasmonic nanoparticles has been successfully applied in biosensing [6], single particle analysis [8], colorimetric biosensors [9], and single-cell monitoring [10]. On one

hand, AuNPs has a strong absorption capacity and high heat conversion efficiency, which was also inspired by the AuNPs' plasma properties and excellent tolerability [11]. Although AuNP-based light therapies for cancer have been widely reported [12-14], these methods lack the ability to do cell surface photothermal therapy or track cancer marker p53. In this field, it's worth emphasizing that how flexibility to design new-style AuNP-based photothermal reagents for high sensitivity and selectivity of cancer therapy. On the other hand, taken the clinical trials consideration the clinical trials, it is expected that the photothermal emission of

absorption of long-wave light in the near-infrared (NIR) region can further penetrate the tissue [15,16]. To accomplish this target, AuNPs of varying forms and sizes have been prepared for NIR illumination and attained a good therapeutic effect [17]. Regrettably, these nanoparticles cannot fixedly aggregate on the cell membrane since they can easily be endocytosed into cells. This prompted us to design an intelligent system that assembled on the surface of cancer cells after the small-sized AuNPs (The diameter of which is less than 20 nm) capture the 60 nm gold which is immobilized on the cell membrane. The system can form a gold nanobeam, whose absorbing light is in the near-infrared region, for subsequent photothermal therapy.

Human p53 is a tumor-suppressing protein that controls cell dividing cycle and apoptosis (programmed cell death) by controlling tumor progression [18]. There is a central specific DNA-binding domain in present human WTp53 (wild-type p53 protein) [19]. The DNA-binding center region of p53 protein loses binding capacity due to extensive mutation in p53 gene in various types of cancer cells [20]. Abnormal expression of MTP53 (mutant-type p53 protein) can serve as an important carcinogenesis stimulus [21]. Thus far, various methods for detecting endogenous p53 have been reported, including enzyme-linked immunosorbent assay (ELISA) [22], immunohistochemically assay [23], electrophoretic mobility shift assay [24], and ds-DNA consensus binding biosensing assay [25]. Despite the favorable detection limit and sensitivity of these methods, none of these methods linked at the relationship between photothermal therapy and p53 protein signaling pathways. Hence, it is urgently needed to design *in situ* analysis strategies for photothermal therapy of cell membrane surface to analyzing the changes of p53 protein in cells.

To investigate whether the gold nanoparticle bouquet can downregulate MTP53 during photothermal therapy, the gold nanoparticle bouquet (AuNP60/APBA-AuNP13/MN) was designed through dual functionalization of a single 3-aminophenyl boronic acid (APBA) assembled on the surface of gold nanoparticles (AuNP60) with amine-gold links to construct AuNP60/APBA. APBA binds to mannan-conjugated gold nanoparticles (AuNP13/MN) [26,27]. The AuNP60/APBA, which is a plasmonic AuNP, can held on the plasma membrane through the competitive reaction of cell surface SA with AuNP13/MN. Thus SA can replace AuNP13/MN and bound to AuNP60/APBA. AuNPs absorption can be transferred to near-infrared by polymerization. They can not only can be viewed

under dark-field hyperspectral imaging (DFM), but also be used for the subsequent photothermal therapy. It is showed that MCF-7 cells were successfully broke under-near-infrared (NIR) irradiation. And the intracellular WTp53 increased while the MTP53 decreased (Figure 1). These results indicated that p53 is the key molecule in the apoptosis signaling pathway. Photothermal therapy can stimulate the MTP53 in the cell signal conductive pathway. This research affords a new strategy for studying intracellular p53 analysis through photothermal therapy on the cell surface and finds a potential *in-situ* treatment against cancer.

Experimental Section

Sample Preparation for the Detection with Dark-Field Microscopy (DFM) and Scattering Spectroscopy

The AuNPs that were used for DFM images were fixed on the surface of the glass sheet. The glass sheet was sonicated in ethanol and then washed with pure water. The clean glass sheet was dried, and the AuNP solution was deposited on the surface to evaluate the DFM detection. To image cells that had absorbed AuNPs, the cell suspension ($1\text{ mL}, 1 \times 10^6\text{ mL}^{-1}$) was seeded in each culture dish (the bottom is glass sheet) and cultured overnight. Then, 30 μL of the AuNP-60/APBA was added to each dish and incubated for various times at 37 °C. Furthermore, the dishes were washed twice and immersed in PBS for DFM imaging. Then, 50 μL of the AuNP-wrapped mannan was added to each dish. The AuNP-scattered light was split using a grating, and the scattering spectra of the samples were recorded by CCD spectrometer.

Supporting Information (Experimental Section).

Result and Discussion

Characterization of the gold nanoparticle bouquet

The preparation of 60 nm AuNPs is by the method previously reported [28]. The AuNPs were modified APBA and could identify the sialic acid SA site. The mannan-conjugated 13 nm AuNPs were synthesized through a one-pot synthetic process with mannose-polysaccharide mannan as stabilizer and NaBH₄ as the reducing reagent.[29]. The image of AuNP60/APBA was taken by transmission electron microscopy (TEM). We can see from Figure 2A-1 that the average size of the AuNP60/APBA nanoparticles is 60 nm and it distributes evenly. Figure 2A-2 indicates that the diameter of the AuNP13/MN diameter is 18 nm, which is consistent with the

dynamic light scattering (DLS) result of 18 nm and is 5 nm larger than the naked AuNPs synthesized under the same condition without the presence of mannan (Figure 2C). TEM images of the AuNP60/APBA incubated with AuNP13/MN at different concentrations were shown in Figure 2 A-3, Figure 2B, B-1, B-2, B-3, B-4, B-5. The AuNP13/MN, AuNP60/APBA and AuNP60/APBA-AuNP13/MN nanoparticles presented a negative zeta potential (Figure S1). As shown in Supporting Information Figure S2, green spots (AuNPs) were observed from the DFM image. The modified AuNP60/APBA still has green spots, which means that the diameters of the AuNP60/APBA and the bald AuNPs are the same. The UV-Vis spectrum of the AuNP60/APBA showed a characteristic peak at 535 nm, which red shifted to 548 nm after added AuNP13/MN (322 nm) was conjugated on their surface, which demonstrated the successful connection of the AuNP13/MN and

AuNP60/APBA (Figure 2D). The average amount of APBA assembled on each nanoparticles was measured to be around 1.44×10^6 . The concentration-dependent temperature increase of AuNP60/APBA-AuNP13/MN nanoparticles bouquent was detected with the extension of laser illumination time, as indicated in Figure S3A. After 50 min of irradiation, the temperature of AuNP60/APBA-AuNP13/MN aqueous solution was increased to 42°C at the maximum concentration of 10 nm (Figure S3B). Then, the photothermal conversion efficiency (η) of AuNP60/APBA-AuNP13/MN nanoparticles bouquent exposed to 680 nm lasers for 500 s was performed and the photothermal conversion efficiency value of AuNP60/APBA-AuNP13/MN nanoparticles bouquent was calculated to be 40.6%.^[60] (The detailed process is provided in the Supporting Information.

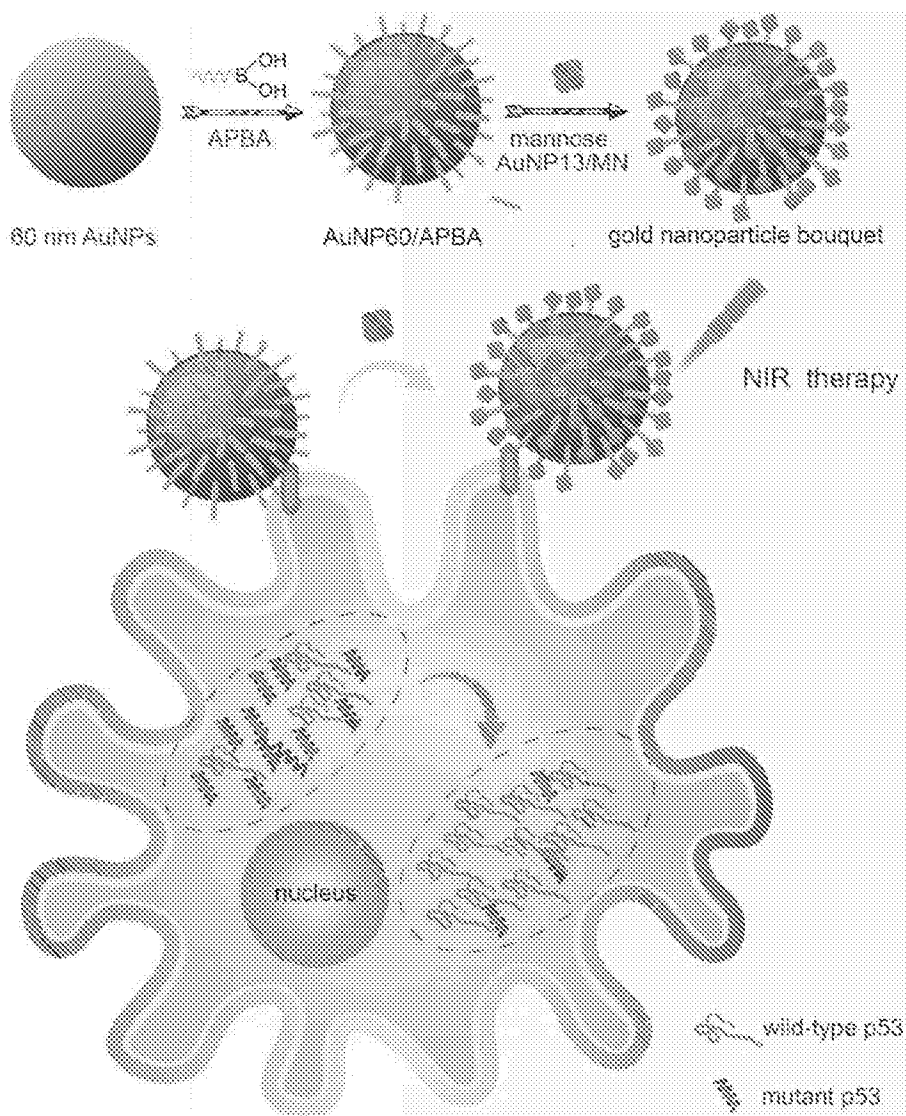


Figure 1. A schematic illustration of a gold nanoparticle bouquet (AuNP60/APBA-AuNP13/MN) for *in situ* analysis of in-tracellular WTp53 and MTP53.

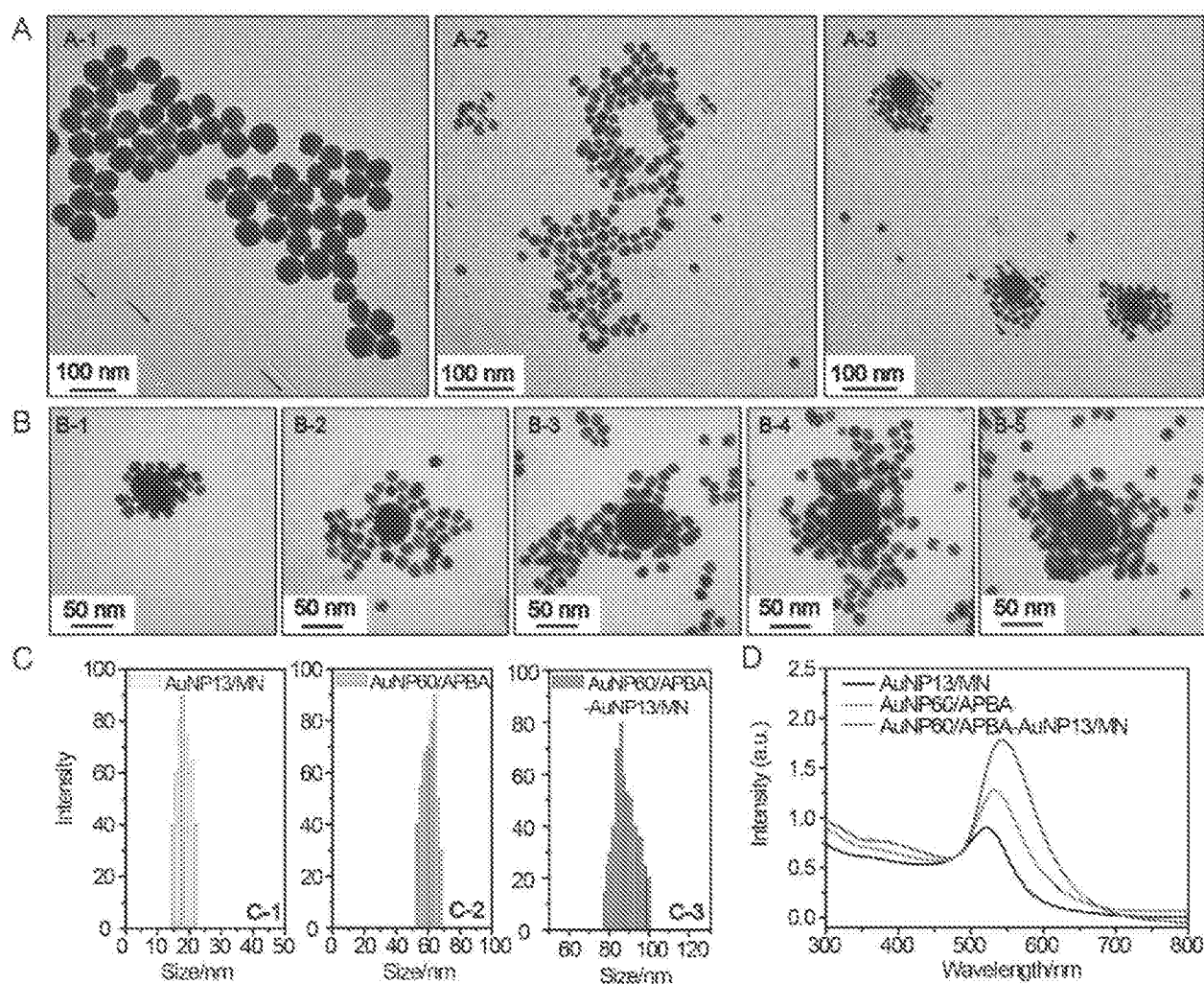


Figure 2. (A) TEM image of the prepared AuNP60/APBA (A-1), AuNP13/MN (A-2) and AuNP60/APBA-AuNP13/MN (A-3). (B) TEM images of the AuNP60/APBA incubated with AuNP13/MN at different concentration (final AuNP13/MN concentration: 2, 4, 6, 8 and 10 nM from (B-1) to (B-5)). (C) Dynamic light scattering (DLS) result of the prepared AuNP13/MN, AuNP60/APBA and AuNP60/APBA-AuNP13/MN. (D) UV-Vis spectra of AuNP13/MN, AuNP60/APBA and AuNP60/APBA-AuNP13/MN.

***In situ* Dark Imaging of the gold nanoparticle bouquet**

To optimize the incubation time for the binding reaction between AuNP60/APBA and AuNP13/MN in solution, the DFM images were recorded at different time points after a series of AuNP13/MN solution (50 μ L) were incubated with AuNP60/APBA (30 μ L, 5 μ M) at 37°C. As shown in Supporting Information Figure S4, the color of AuNPs by degrees changed from green to orange and stopped changing after 100 min, which demonstrated the aggregation of AuNP13/MN and AuNP60/APBA-triggered. A series of different concentrations of AuNP13/MN solutions were incubated with AuNP60/APBA (30 μ L, 5 μ M) solution according to the optimum reaction time. Figure 3A demonstrated this by the fact that the color was green at a low concentration and the peak of the scattering spectrum was basically the same as that

of the control group (Figure 3Aa, g1). The interaction between the AuNP60/APBA and the increase of AuNP13/MN concentration caused a dramatic color change to yellow and then orange and the scattering peak shifted from 550 nm to 610 nm upon the AuNP13/MN and AuNP60/APBA conjugation (Figure 3A b-f, g2-g6). Therefore, we developed an expedient quantification approach for AuNP60/APBA DFM images processed with AuNP13/MN at different concentrations. Corresponding statistical scattering spectral peak of the AuNP60/APBA was determined using the Gaussian function (Figure 3B). The distribution histogram showed the relationship between the AuNP60/APBA and different concentrations of the AuNP13/MN.

***In vitro* Studies**

MCF-7 cells (1 mL, 1×10^6 mol·L⁻¹) were planted in a petri dish for intracellular testing. After the

adding of 30 μL AuNP60/APBA, DFM images were obtained at different time points. Only a small amount of AuNP60/APBA particles were observed in the first 30 min. After 1 h, significantly more AuNP60/APBA nanoparticles appeared on cell membrane surface. The number of AuNP60/APBA increased with the extended incubation time until reached the plateau after 2 h (Supporting Information, Figure S5). MCF-7 cells incubated with different concentrations of AuNP13/MN were analyzed by DFM imaging and scattering spectroscopy at 2h optimum incubation time (Figure 4). From Figure 4 A1-A3, the AuNP60/APBA nanoparticles bouquet had a green color and has a peak scattering spectrum at approximately 520 nm (Figure 4, A4-A6), which indicated no AuNP13/MN in the MCF-7 cells. However, with increasing doses of AuNP13/MN, the color of AuNP60/APBA nanoparticle bouquet became orange in the DFM images (Figure 4, B3, C3, D3), and the scattering peak gradually redshifted from 520 nm to 610 nm little by little (Figure 4, B4-B6; C4-C6; D4-D6), after incubation with different concentration of the AuNP13/MN for 2 h, these changes indicated that the formation of AuNP60/APBA nanoparticle bouquet depends on the

dose-dependent increase of AuNP13/MN in intracellular.

In addition, after the intracellular DFM images, the feasibility of p53 apoptotic signalling pathway based on the AuNP60/APBA nanoparticle bouquet was applied by MCF-7 cell-free extracts. The change of p53 level in MCF-7 cells was studied by using AuNP60/APBA nanoparticle bouquet as a simulation drug through NIR irradiation. After incubated with AuNP60/APBA for 2 h, the MCF-7 cells ($1 \text{ mL}, 1 \times 10^6 \text{ mL}^{-1}$) extracts were added with different amounts of AuNP13/MN solution for 12h. A p53 pan ELISA kit (KeyGen Biotech. Co. Ltd., Nanjing, China) was used to detect the level of total p53 (Wtp53 and Mtp53), extraction of the above cell extracts for testing and establishment of the standard calibration curve (Supporting Information, Figure S6, Figure S7). After drug treatment, the total p53 level was increased, while the Mtp53 level gradually declined (Figure 5A), which indicated through NIR irradiation of AuNP60/APBA-AuNP13/MN nanoparticle bouquet ability to stimulate the Mtp53 in cell signal conductive pathway.

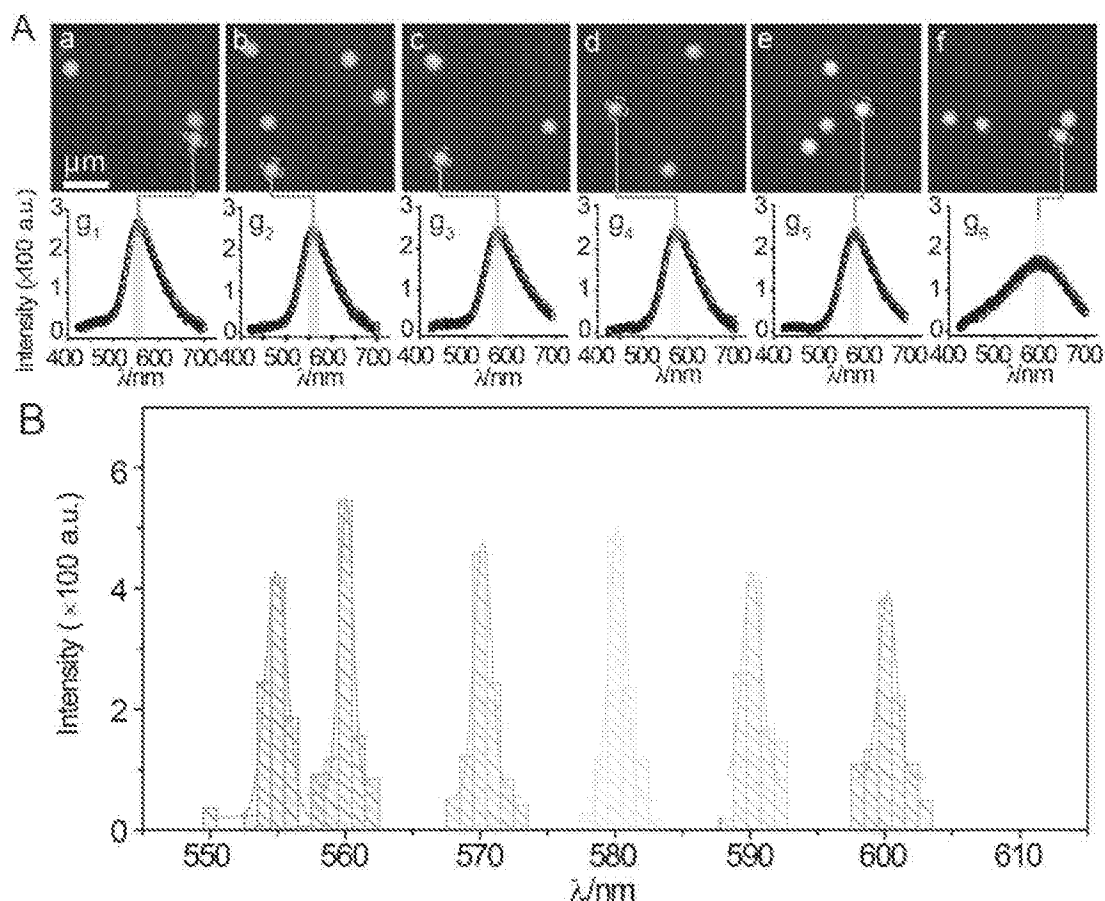


Figure 3. (A) DFM images of 30 μL AuNP60/APBA incubated with 50 μL AuNP13/MN for 100 min with different concentrations (final AuNP13/MN concentration: 0, 2, 4, 6, 8 and 10 nM from (a) to (f), g1)-g6); Corresponding scattering spectra of AuNP60/APBA observed in DFM images. (B) Corresponding statistical graph of AuNP60/APBA in DFM images a-f in (A).

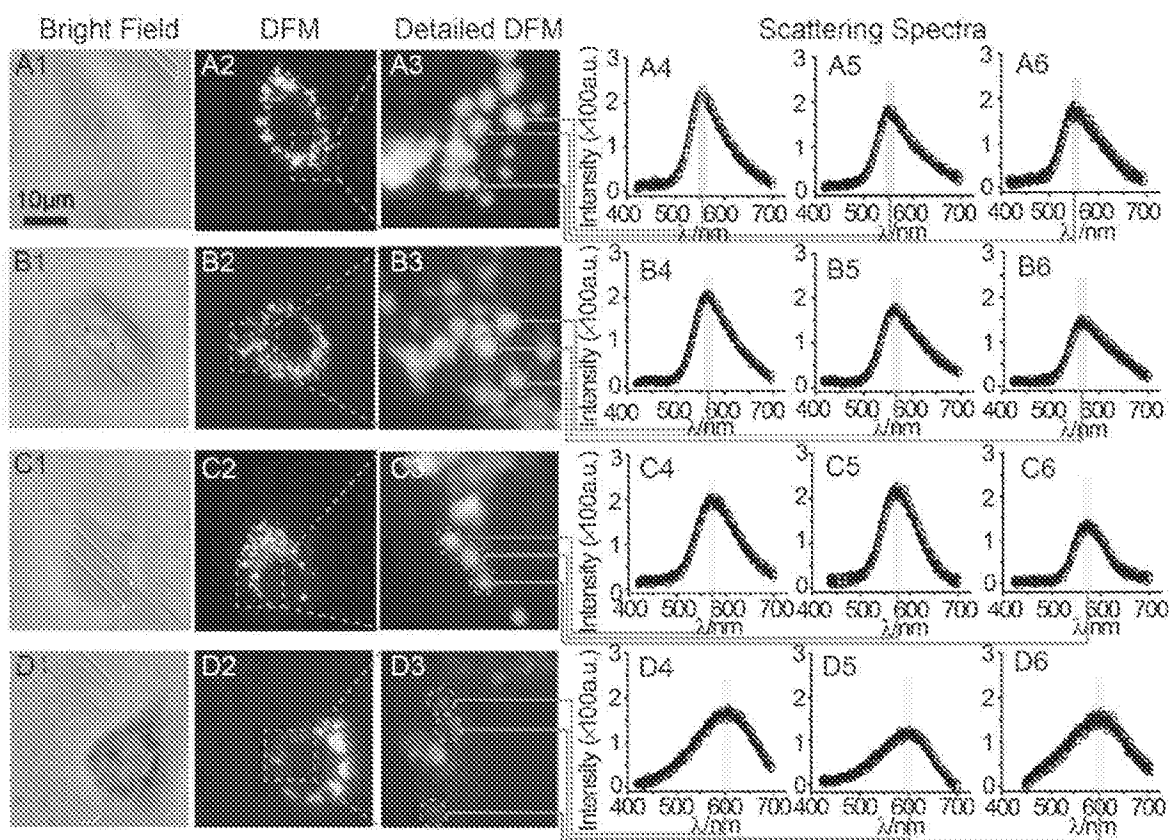


Figure 4. DFM images of 30 μ L AuNP60/APBA incubated with a single MCF-7 cell (treated with 0, 2, 5 and 10 nM AuNP13/MN from A to D) for 100 min. (A1-D1: bright field, A2-D2: DFM images; A3-D3: Detailed DFM, A4-6-D4-6: corresponding scattering spectra).

To demonstrate that photothermal therapy using AuNP60/APBA-AuNP13/MN nanoparticle bouquet could adjust MTP53 content, WTP53 and MTP53 in the MCF-7 cell extracts were collected respectively for measurement after the therapy. The result showed that the expression of WTP53 was upregulated while the expression of MTP53 was downregulated. The identification of WTP53 and MTP53 in HBE cells, a non-tumor cell line, was used as control-experiment (Figure 5B). P53 levels were normal in the HBE cells, but MTP53 levels were abnormal in MCF-7 cells. At the same time, when the AuNP60/APBA-AuNP13/MN nanoparticle bouquet was added to MCF-7 cells for photothermal treatment, the MTP53 levels have been decreased by a half and the number of WTP53 increased by one times (Figure 5B). The results indicate that photothermal therapy can stimulate the MTP53 in the cell signal conductive pathway and the cells enter normal apoptosis state.

The above results have successfully proved that the proposed binary system can efficiently bind AuNP probe on the surface of living cells to form a polymer in the presence of AuNP13/MN. MCF-7 cells were used as a model to investigate whether the aggregates could be applied to kill tumor cells under NIR photothermal therapy. After incubation with the

different concentrations of AuNP60/APBA nanoparticle bouquet for 12 h, the cells were irradiated with a laser (680 nm, 0.5 W cm⁻², 37 °C). The absorbances were examined to ascertain the relative cell activity. Cell viability remained at 90 % in the dark (Supporting Information, Figure S8), suggesting that AuNP60/APBA nanoparticle bouquet were biocompatible in cell experiments. However, after 20 min of NIR irradiation, morphological changes of cells (Figure S9) and the apoptotic MCF-7 cells burst, which demonstrated that AuNP60/APBA nanoparticle bundles were capable of killing cancer cells under NIR illumination in a cell biocompatibility assay system (Figure S8). Meanwhile, consistent with the results from the MTT assay, EdU incorporation assay (Figure 5C and 5D) and TUNEL assay (Figure 5E and 5F) revealed that the proliferation of MCF-7 cells was reduced while the apoptosis was increased in light group. TEM images showed the AuNP60/APBA-AuNP13/MN nanoparticle bouquet in MCF-7 cell surface (Figure S10). Overall, these results revealed that AuNP60/APBA-AuNP13/MN nanoparticle bouquet combined with illumination showing an excellent anti-tumor effect on human MCF cells.

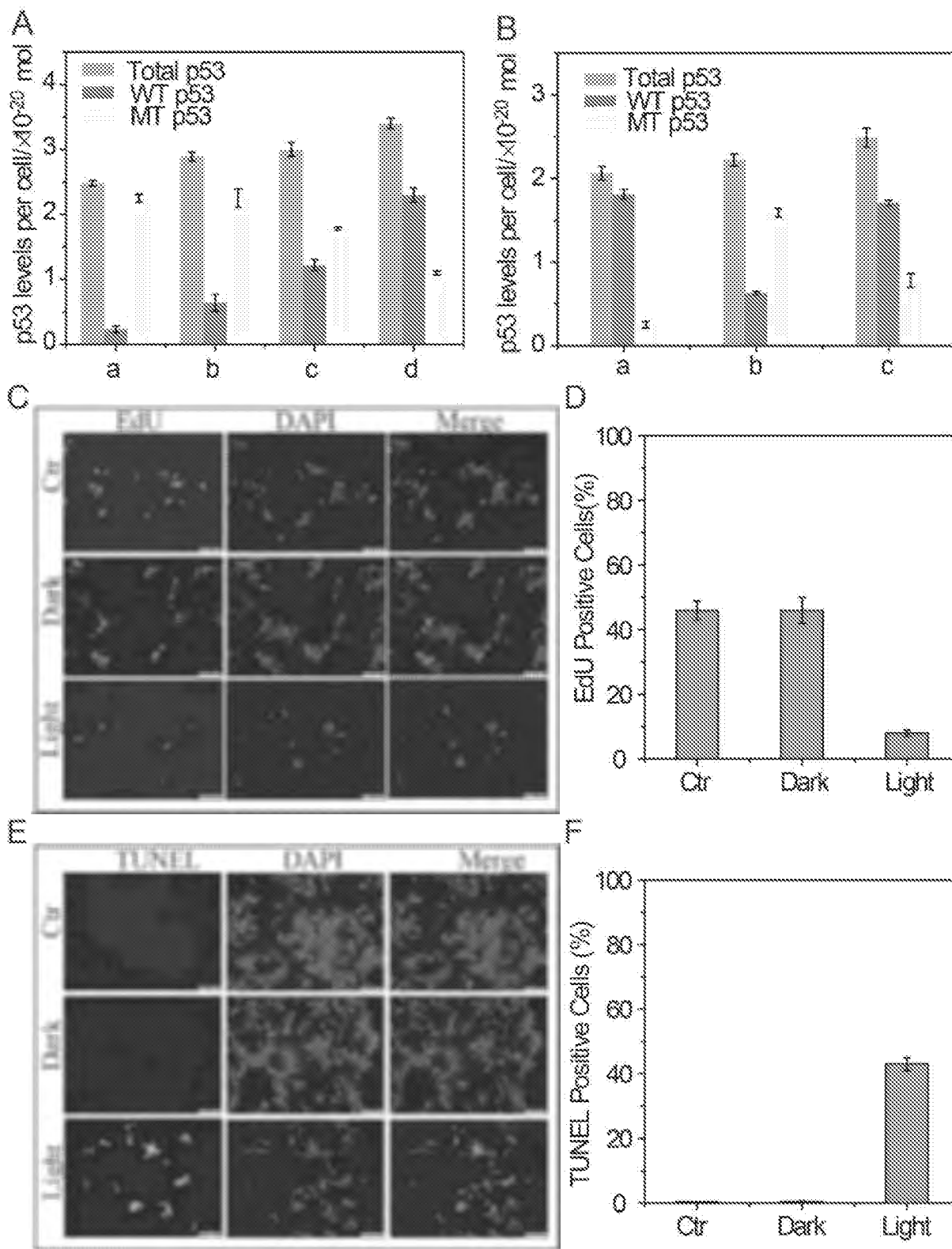


Figure 8. (A) p53 levels (total p53, WTp53 and MTp53) in MCF-7 cell (detected from cell extracts collected from MCF-7 cells treated with: AuNP60/APBA contain (no. 2, 5, 10 nm) AuNP13/MN from A to D. (B) p53 levels (total p53, WTp53 and MTp53) in (A: HBE cells; B: MCF-7 cells; C: Added AuNP60/APBA-AuNP13/MN nanoparticle bouquet to MCF-7 cells. (C) EdU incorporation assay in MCF-7 cells. Scale bars = 50 μm. (D) Quantitative measurement of EdU positive cells showed in C. (E) TUNEL assay in MCF-7 cells. Scale bars = 50 μm. (F) Quantitative measurement of TUNEL positive cells showed in E. Results are representative of at least 3 separate experiments and expressed as mean ± SE.

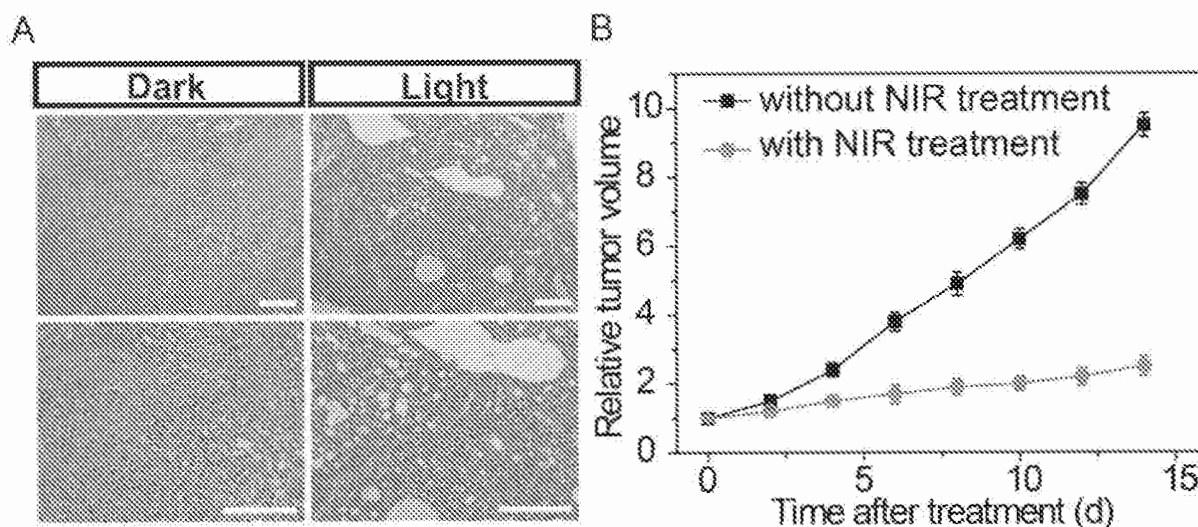


Figure 6. (A) Histological observation of the tumor tissues without and with NIR treatment hypodermic injection of the gold nanoparticle bouquet after 7 days. (B) Change of tumor volume with or without NIR treatment for 2 weeks. Scale bars, 200 μ m.

In vivo Studies

On the basis of former cell NIR studies, we further established a binary system to monitor the effects of NIR therapeutic in living mice. Feminine pathogen free (5-6 weeks) BALB/c nude mice were used as tumor models. Under isoflurane anesthesia, MCF-7 cells in the logarithmic growth stage were injected subcutaneously into the flanks of the nude mice. Then, the AuNP60/APBA-AuNP13/MN nanoparticle bouquet solution was hypodermically injected into the tumor-bearing mice. The nanoparticle bouquet could efficiently arrival the tumor region, mice with the MCF-7 tumor were treated with a NIR laser (power of 0.5 W cm^{-2}) irradiation for 30 min to treatment, while mice without NIR treatment were served for control. As shown in Figure 6, after 7 days of NIR treatment, the tumor status was monitored. Histological examination was carried out to observe the tumor tissues. The tumor tissue sections were clearly necrotic, while the control group showed no apparent cell destruction (Figure 6B). The results show that the proposed system NIR therapy has an obvious therapeutic effect on tumor tissue.

Conclusion

In this work, we designed the AuNP60/APBA-AuNP13/MN nanoparticle bouquet to research the p53 in cells signal conductive pathway by photothermal therapy. The developed plasmonic AuNP60/APBA and AuNP13/MN sample can be easily prepared and had good biocompatibility. The AuNP60/APBA-wrapped AuNP13/MN readily entered living cells to do photothermal therapy.

Evidently, the color changes are caused by the conjugation of AuNP60/APBA and AuNP13/MN, the formation of AuNP60/APBA-AuNP13/MN nanoparticle bouquet was observed, the changes of the p53 level in cells were studied through NIR irradiation. Thus, results showed that the intracellular WTP53 content increases while the MTP53 content decreases. The method is applicable to detect the changes of p53 level in cells during AuNP60/APBA-AuNP13/MN nanoparticle bouquet photothermal therapy, which is helpful to clarify the role of p53 in cell biological events. Thus, this capability demonstrates the effectiveness of the method for performing intracellular p53 analysis to target cancer therapy.

Supplementary Material

Supplementary figures.

<http://www.ntno.org/v04p0201s1.pdf>

Acknowledgements

We acknowledge Professor Yi-Tao Long's great help for establishing the dark-filed instrument system and providing the data analysis software. This research was supported by the National Natural Science Foundation of China (21904068, 81922041, 81570378 and 81772020), the Science and Technology of Jiangsu Province China (BK20170048), Jiangsu university natural science research program (19KJB150014), and Jiangsu Specially Appointed Professor program, Introduction of talent research start fund of Nanjing Medical University (NMUR2019007).

Competing Interests

The authors have declared that no competing interest exists.

References

- Jiang Y, Shi M-L, Liu Y, Wan S, Cui C, Zhang L-Q, Tan W-H. Aptamer/AuNP Biosensor for Colorimetric Profiling of Exosomal Proteins. *Angew. Chem. Int. Ed.* 2017, 56(39): 11916-11920. doi: 10.1002/anie.201703807.
- Qi G-H, Zhang Y, Xu S-P, Li C-P, Wang D-D, Li H-J, and Jin Y-D. Nucleus and mitochondria targeting Theranostic Plasmonic Surface-Enhanced Raman Spectroscopy Nanoprobes as a Means for Revealing Molecular Stress Response Differences in hyperthermia cell death between cancerous and normal cells. *Anal. Chem.* 2018, 90(22):13356-13364. doi.org/10.1021/acs.analchem.8b03034.
- Huang P, Luo J, Li W-W, Rong P-F, Wang Z, Wang S-J, Wang X-P, Sun X-L, Aronova M, Niu G, Leapman R-D, Nie Z-H, Chen X-Y. Biodegradable gold nanovesicles with an ultrastrong plasmonic coupling effect for photoacoustic imaging and photothermal. *Angew. Chem. Int. Ed.* 2013, 52(52):13958-13964. doi: 10.1002/anie.201308986
- Alouf M and El-Sayed M-A. A Real-Time surface enhanced Raman spectroscopy study of plasmonic photothermal cell death using targeted gold nanoparticles. *J. Am. Chem. Soc.* 2016, 138(4): 1258-1264. doi: 10.1021/jacs.5b10997.
- Cheng X-J, Sun R, Yin L, Chai Z-F, Shi H-B, and Cao M-Y. Light-triggered assembly of gold nanoparticles for photothermal therapy and photoacoustic imaging of tumors *in vivo*. *Adv. Mater.* 2017, 29(6): 1604894-1604900. doi: 10.1002/adma.201604894.
- Lopez-Marzo A-M, Hoyos-de-la-Torre R, Baldrich E. NaNO₃/NaCl oxidant and Polyethylene glycol (PEG) capped gold nanoparticles (AuNPs) as a novel green route for AuNPs detection in electrochemical biosensors. *Anal. Chem.* 2018, 90(6):4010-4018. doi: 10.1021/acs.analchem.7b05150.
- Kim J, Oh S-Y, Shukla S, Hong S-B, Heo N-S, Bajpai V-K, Chun H-S, Jo C-H, Choi B-G, Huh Y-S, Han Y-K. Heteroassembled gold nanoparticles with sandwich-immunoassay LSPP chip format for rapid and sensitive detection of hepatitis B virus surface antigen (HBsAg). *Biosens. & Bioelectron.* 2018, 107:118-122. doi: 10.1016/j.bios.2018.02.019.
- Yu R-J, Ying Y-L, Cao R, Long Y-T. Confined Nanopipette Sensing: From Single Molecules, Single Nanoparticles to Single Cells. *Angew. Chem. Int. Ed.* 2019, 58(12):3706-3714. doi: 10.1002/anie.201803229.
- Aldewachi H, Chalabi T, Woodroffe M-N, Riddlebank N, Sharrack B, Gardiner P. Gold Nanoparticle-Based Colorimetric Biosensors. *Nanoscale* 2018, 10(1): 18-33. doi.org/10.1039/C7NR06367A.
- Qian B-C, Cao Y, Long Y-T. Dual-Targeting Nanovesicles for *In situ* Intracellular Imaging of and Discrimination between Wild-type and Mutant p53. *Angew. Chem. Int. Ed.* 2015, 55(2):719-723. doi: 10.1002/anie.201510142.
- Jing C, Gu Z, Ying Y-L, Li D-W, Zhang L, Long Y-T. Chrominance to Dimension. A Real-Time Method for Measuring the Size of Single Gold Nanoparticles. *Anal. Chem.* 2012, 84(10):4284-4291. doi: 10.1021/ac203118g.
- Kim J, Jo C, Lim W, Jung S, Lee Y-M, Lim J, Lee H, Lee J, Kim W-J. Programmed Nanoparticle-Loaded Nanoparticles for Deep-Penetrating 3D Cancer Therapy. *Adv. Mater.* 2018, 30(29):1707557-1707563. doi: 10.1002/adma.201707557.
- Wang J, Zhang Y, Jin N, Mao C-B, Yang M-Y. Protein-Induced Gold Nanoparticle Assembly for Improving the Photothermal Effect in Cancer Therapy. *ACS Appl. Mater. Interfaces* 2019, 11(12):11126-11143. doi: 10.1021/acsami.8b21488.
- Jin R-H, Liu Z-N, Bai Y-K, Zhou Y-S, Gooding J-J, Chen X. Core-Satellite Mesoporous Silica-Gold Nanotheranostics for Biological Stimuli Triggered Multimodal Cancer Therapy. *Adv. Funct. Mater.* 2018, 28(31): 1801961-1801969. doi.org/10.1002/adfm.201801961.
- Choi C-K, Kim Y-T, E, Zhuo X-L, Liu Y, Pak C-Y, Liu X-D, Fse Y-L, S, Wang J-F, and Choi C-H. Dopamine-mediated assembly of citrate-capped plasmonic nanoparticles into stable core-shell nanoworms for intracellular applications. *ACS Nano* 2019, 13(5):5864-5884. doi: 10.1021/acsnano.8b01591.
- Belhout S.A, Baptista F.R, Devereux S.J, Parker A.W, Ward A. D and Quinn S.J. Preparation of polymer gold nanoparticle composite with tunable plasmon coupling and their application as SEFS substrates. *Nanoscale*, 2019, 11(42): 19084-19094. doi.org/10.1039/C9NR03014E.
- Shen N, Yan F, Pang J-X, Cao Z, Al-Kali A, Haynes C-L, Litzow M-E, Liu S-J. HDL-AuNPs-BMS nanoparticle conjugates as molecularly targeted therapy for leukemia. *ACS Appl. Mater. Interfaces* 2018, 10(17):14454-14462. doi: 10.1021/acsami.8b01696.
- Fornesello M-L, Annunziata C, Fornesello A-L, Buonaguro L, Buonaguro F-M. Human Oncoviruses and p53 Tumor Suppressor Pathway Deregulation at the Origin of Human Cancers. *Cancers* 2018, 10(7):3892-3901. doi: 10.3390/cancers10070210.
- He F, Borchers W, Song T-J, Wei X, Das M, Chen L-H, Daughdrill G-W, Chen J-D. Interaction between p53 N terminus and core domain regulates specific and nonspecific DNA binding. *PNAS* 2019, 116(18): 8859-8868. doi: 10.1073/pnas.1903077116.
- Aggarwal M, Saxena R, Asif N, Sinclair E, Tan J, Cruz J, Berry D, Kallakury B, Pham Q, Wang T-T-Y, Chung F-L. p53 mutant-type in human prostate cancer cells determines the sensitivity to phenethyl isothiocyanate induced growth inhibition. *J. Exp. Clin. Oncol.* 2019; 36(1):307-324. doi: 10.1186/s12046-019-1267-z.
- Greenblatt M-S, Bennett W-F, Hollstein M, Harris C-C. Mutations in the p53 Tumor Suppressor Gene: Clues to Cancer Etiology and Molecular Pathogenesis. *Cancer Res.* 1994, 54(18):4835-4878.
- Maritschegg B, Heinzl N, Wilson S, Deyckmar B, Niebuhr M, Klammeth L, Holzer B, Kozel K, Concin N, Zollinger R. Polymer-ligand-based ELISA for robust, high throughput, quantitative detection of p53 aggregates. *Anal. Chem.* 2018, 90(26): 13273-13279. doi: 10.1021/acs.analchem.8b02373.
- Cole A-J, Dwight T, Gill A-J, Dickson Y-A, Zhu Y, Clark-son A, Gard C-B, Maidens J, Valmadre S, Clifton-Bligh P, Marsh D-J. Assessing mutant p53 in primary high-grade serous ovarian cancer using immunohistochemistry and massively parallel sequencing. *Scientific Reports* 2016; 6:26191-26203. doi: 10.1038/srep26191.
- Ream J-A, Lewis L-K, Lewis K-A. Rapid agarose gel electrophoretic mobility shift assay for quantitating protein-RNA interactions. *Anal. Biochem.* 2016; 511:36-41. doi: 10.1016/j.jab.2016.07.027.
- Qian B-C, Cao Y, Zhao L-J, Gu Z, Long Y-T. A Two-Stage Dissociation System for Multilayer Imaging of Cancer Biomarker-Synergic Networks in Single Cells. *Angew. Chem. Int. Ed.* 2017, 56(17):4802-4805. doi: 10.1002/anie.201702415.
- Deshpande N, Ramesh A, Nandi D, Nguyen A, Brouillard A, Kulkarni A. Supramolecular polysaccharide nanotheranostics that inhibit cancer cell growth and monitor targeted therapy response. *Nanotheranostics* 2020, 4(2):156-172. doi: 10.7150/ntno.44705.
- Cheung C-C, Lu, Ma G-L, Karatasos K, Seitsonen J, Ruokolainen J, Koffi C-R, H Hassan A.F.M, Al-Jama W T. Liposome-templated indocyanine green J-aggregates for *in vivo* near infrared imaging and stable photothermal heating. *Nanotheranostics* 2020, 4(2):91-106. doi: 10.7150/ntno.41737. eCollection 2020.
- Cao Y, Xie T, Qian B-C, Long Y-T. Plasmon Resonance Energy Transfer: Coupling between Chromophore Molecules and Metallic Nanoparticles. *Small* 2017, 13(2): 1318-1322. doi: 10.1002/smll.201601955.
- Han E, Ding L, Ju H-X. Highly Sensitive Fluorescent Analysis of Dynamic Glycan Expression on Living Cells Using Glyconanoparticles and Functionalized Quantum Dots. *Anal. Chem.* 2011, 83(18): 7006-7012. doi: 10.1021/ac201488x.
- Liu Y, Ai K, Liu J, Deng M, He Y, Lu L. Dopamine-Melanin Colloidal Nanospheres: An Efficient Near-Infrared Photothermal Therapeutic Agent for *In vivo* Cancer Therapy. *Adv. Mater.* 2013, 25(9): 1353-1359. doi: 10.1002/adma.201204603.

Research Paper

Sphingomyelin Liposomes Containing Porphyrin-phospholipid for Irinotecan Chemophototherapy

Kevin A Carter¹, Dandan Luo¹, Aida Razi², Jumin Geng¹, Shuai Shao¹, Joaquin Ortega², Jonathan F Lovell¹✉

1. Department of Biomedical Engineering, University at Buffalo, State University of New York, Buffalo, NY, 14260.

2. Department of Biochemistry and Biomedical Sciences and M. G. DeGroot Institute for Infectious Diseases Research, McMaster University, Hamilton, ON L8S4L8, Canada.

✉ Corresponding author: jlovell@buffalo.edu

© Ivyspring International Publisher. Reproduction is permitted for personal, noncommercial use, provided that the article is in whole, unmodified, and properly cited. See <http://ivyspring.com/terms-for-terms-and-conditions>.

Received: 2016.03.30; Accepted: 2016.06.24; Published: 2016.10.01

Abstract

Porphyrin-phospholipid (PoP) liposomes can entrap anti-cancer agents and release them in response to near infrared (NIR) light. Doxorubicin, when remotely loaded via an ammonium sulfate gradient at a high drug-to-lipid ratio, formed elongated crystals that altered liposome morphology and could not be loaded into liposomes with higher PoP content. On the other hand, irinotecan could also be remotely loaded but did not form large crystals and did not induce liposome elongation. The loading, stability, and NIR light-triggered release of irinotecan in PoP liposomes was altered by the types of lipids used and the presence of PEGylation. Sphingomyelin, which has been explored previously for liposomal irinotecan, was found to produce liposomes with relatively improved serum stability and rapid NIR light-triggered drug release. PoP liposomes composed from sphingomyelin, cholesterol and 2 molar percent PoP rapidly released irinotecan in vivo in response to NIR irradiation as monitored by intravital microscopy and also induced effective tumor eradication in mice bearing MIA Paca-2 subcutaneous tumor xenografts.

Key words: liposomes, chemophototherapy, irinotecan

Introduction

Liposomes have been used successfully as pharmaceutical carriers for anti-cancer agents [1,2]. Encapsulating chemotherapy agents in liposomes can reduce non-specific toxicity, and enhance the therapeutic effects of the drug [3,4]. Most of the nanoparticles currently being used for the treatment of solid tumors rely on the enhanced permeability and retention (EPR) effect for drug accumulation in the tumor [4,5]. This effect allows particles of a specific size range to passively accumulate due to the leaky nature of blood vessels in tumors [6–8]. Doxil[®], a long circulating PEGylated liposomal form of doxorubicin takes advantage of this effect. PEGylated liposomes circulate for extended durations, which in turn allows for more passive accumulation of the drug in the tumor [5–9]. While the EPR effect can be exploited for the treatment of certain tumors clinically, the success of drug delivery strategies which rely on the EPR

effect has been limited. This is due to other factors such as high interstitial fluid pressure, poor vascularization in the tumor, tumor heterogeneity, and poor drug bioavailability [10–13]. Several strategies have been proposed to overcome these limitations including active targeting, and site specific release of nanoparticle-encapsulated drugs, with varying degrees of success [14–18]. Site-specific triggered drug release is of interest as it provides the ability to increase the bioavailability of nanoparticle encapsulated drugs at the tumor site improving the efficacy of the treatment. The use of light to induce enhanced drug deposition is an emerging area of research [19–26]. Such combination of chemotherapy and phototherapy; chemophototherapy, is a developing treatment modality for solid tumors. [27] Porphyrins and other tetrapyrroles are promising candidates for phototherapy applications.[28–30] We

have recently found that porphyrin-phospholipids are well-suited to be used for theranostic applications, including chemophototherapy [31–40].

It was shown that PEGylated liposomes containing porphyrin-phospholipid (PoP) enable near infrared (NIR) light-triggered drug release and have a significant therapeutic effect on tumor xenografts using different types of PoP including 2-[1-hexyloxyethyl]-2-devinyl pyropheophorbide-*a* (HPPH-lipid) [31,32] and pyropheophorbide-*a* (pyro-lipid) [33]. At a high PoP molar percentage in the liposome bilayer, HPPH-lipid was originally shown to be more effective at entrapping both dyes and the anti-cancer drug doxorubicin (Dox) than pyro-lipid [31,34]. However, follow-up studies have shown that pyro-lipid, when used with specific liposomal formulations at lower PoP molar percentage in the bilayer, gives rise to greater serum stability. While liposomes made with pyro-lipid were more stable than HPPH-lipid, the amount of pyro-lipid which could be used while retaining Dox loading capacity was limited by the cholesterol content [33]. With lower cholesterol content (i.e. 35 mol. %) Dox could not be loaded into liposomes containing more than 2 mol. % pyro-lipid whereas liposomes made with 45 mol. % cholesterol could be loaded with Dox with up to 8 mol. % pyro-lipid. The exact reason for this trend was not ascertained, however the physical stress imparted on the bilayer due to large Dox exerting physical pressure may be responsible. With high amounts of Dox loading into liposomes, the morphology is known to convert from spherical to ellipsoid [41–43]. This stretching may cause the bilayer of liposomes containing higher amounts of pyro-lipid to become destabilized.

Irinotecan hydrochloride (IRT, CPT-11) is a water soluble topoisomerase I inhibitor which gets converted to its active form SN-38 *in vivo* [44]. Liposomal irinotecan has been shown to be effective. [45,46] It is used clinically in both its free and liposomal form [47,48]. Unlike Dox, IRT does not form large elongated crystals when actively loaded [49,50]. Here we show that, IRT can be loaded in sphingomyelin liposomes and be used for light-triggered drug release and anti-tumor effective chemophototherapy.

2. Methods

2.1 Liposome preparation

Unless otherwise noted, lipids were purchased from Avanti Polar Lipids, and other materials were obtained from Sigma. 1,2-distearoyl-sn-glycero-3-phosphocholine (DSPC, Avanti #850365P), cholesterol (Avanti #700000P), 1,2-distearoyl-sn-glycero-3-

phosphoethanolamine-N-[methoxy(polyethylene glycol)-2000] (DSPE-PEG-2K, Avanti #880120P), and Sphingomyelin (SPM, # Coatsome NM-10, NOF America) were used. Pyro-lipid was synthesized as previously reported [34]. Liposomes were made by dissolving the lipids (100 mg) of the indicated compositions in 1 mL of ethanol at 60°C and 4 mL of 250 mM ammonium sulfate (60°C) was added to the ethanol solution. The liposomes were then extruded 10 times in a high pressure nitrogen extruder (Northern Lipids) using stacked (80, 100 and 200 nm) polycarbonate membranes at 60°C. Free ammonium sulfate and ethanol were removed by dialysis with a 10% sucrose, 10 mM histidine (pH 6.5) solution overnight. IRT (LC Laboratories # I-4122) or Dox (LC Laboratories # D-4000) were loaded into the liposomes by mixing the liposomes and drug in the indicated ratios and incubating the solution for 60 minutes at 60°C. For serum stability studies, liposomes were made with either SPM:pyro-lipid:chol (53:2:45), or with SPM:DSPE-PEG2000:pyro-lipid:chol (48:5:2:45), or with DSPC:DSPE-PEG2000:pyro-lipid:chol (48:5:2:45).

2.2 Liposome characterization

Liposome size and zeta potential were measured by dynamic light scattering in a NanoBrook 90 plus PALS instrument. Sizes were measured in PBS and zeta potential in a 1 mM NaCl solution. Loading efficiency was characterized by running the samples through a Sephadex G-75 column and collecting 24 × 1 mL fractions. The loading efficiency was determined by the amount of drug fluorescence in the liposome-containing fractions. IRT fluorescence was measured an excitation of 370 nm and emission of 435 nm using a TECAN Safire fluorescent microplate reader. Stability was tested in 50% bovine serum at 37°C. IRT fluorescence was measured at the indicated time points and the % release was calculated using the formula $\text{Release} = (F_{\text{final}} - F_{\text{initial}}) / (F_{\text{TX-100}} - F_{\text{initial}}) \times 100\%$, where $F_{\text{TX-100}}$ is the fluorescence value when the liposomes are lysed with 0.25% Triton X-100.

2.3 Light release experiments

Release tests were conducted at 37°C in 50% bovine serum unless otherwise noted. Liposome samples were diluted 1000 times and irradiated using a 665 nm diode laser (RPMC laser, LDX-3115-665) at a fluence rate of ~310 mW/cm². IRT release was measured in real time in a fluorometer (FTI) and the percent release was calculated by the formula $\text{Release} = (F_{\text{final}} - F_{\text{initial}}) / (F_{\text{TX-100}} - F_{\text{initial}}) \times 100\%$

2.4 Cryo-TEM

Holey carbon grids (c-flat CF-2/2-2C-T) were treated with chloroform for ~ 10 hours and then glow

discharged at 5 mA for 15 seconds immediately before the application of the sample. IRT- and Dox PoP-liposomes at a concentration of ~20 mg/mL (lipid) were diluted 10x with water. Approximately 4 μ L of the diluted preparation were deposited on the electron microscopy grid. Vitrification of samples was performed in a Vitrobot (FEI) by blotting the grids once for 15 seconds and with 0 offset before they were plunged into liquid ethane. Temperature and relative humidity during the vitrification process were maintained at 25 °C and 100%, respectively. The grid was loaded into the FEI Tecnai F20 electron microscope operated at 200kV using a Gatan 626 single tilt cryo-holder. Images were collected in a Gatan K2 Summit direct detector device camera at a nominal magnification 25,000X, which produced images with a calibrated pixel size of 1.45Å. The detector was used in counting movie mode with five electrons per pixel per second with 15 second exposures and 0.5 seconds per frame. This method produced movies containing 30 frames with an exposure rate of one electron per square angstrom per frame. Movies were collected using a defocus range of -1 to -2.5 μ m. Frames were aligned using the program `alignframesleastsquares_list.exe` and averaged into a single micrograph with the `shiftframes_list.exe` program available from the website of Dr. John Rubinstein. These programs perform whole frame alignment of the movies using previously published motion correction algorithms [51]. A de-noising filter using Photoshop was applied to the entire image to obtain the figures shown.

2.5 Animal studies

Procedures performed were approved by the University at Buffalo Institutional Animal Care and Use Committee. 5×10^6 Mia Paca-2 cells (obtained from ATCC) were injected in the right flank female nude mice (5 weeks, Jackson Labs, #007850). When tumor volumes reached 5-7 mm in diameter, mice bearing Mia Paca-2 tumors were grouped as follows: 1) Saline, Free IRT, PoP(IRT)-laser, PoP(empty)+laser, PoP(IRT)+laser (n=5-7 mice per group). Mice were injected with 15 mg/kg free IRT, PoP(IRT) or empty PoP-liposomes of an equivalent PoP dose. 10-15 minutes following injection, mice in the +laser groups were treated with a 665 nm laser for 16 min. 40 sec. at a fluence rate of 300 mW/cm². Tumor volumes were measured 2-3 times per week and volumes were calculated using the equation $Volume = \pi \times L \times W \times H / 6$ where L, W and H represent the length, width and height respectively. The mice were sacrificed when the tumor volume reached 10 times the initial size.

For intravital imaging, female nude mice were injected with IRT-loaded PoP liposomes (10 mg/kg)

or co-injected with standard liposomes and empty PoP liposomes for an equivalent IRT or pyro-lipid dose. The mice were anesthetized using isoflurane and one ear of the mouse was treated with a 665 nm laser for 16.4 minutes at a fluence rate of 300 mW/cm². Following the laser treatment both the treated and untreated ears were imaged using a fluorescent microscope (EVOS FL Auto). IRT was imaged using a DAPI filter cube (357 nm excitation; 477 nm emission) and pyro was imaged with a custom filter cube (400 nm excitation; 679 nm emission).

2.7 Statistical analysis

Kaplan-Meier survival curves were analyzed using Graphpad prism (Version 5.01) software. Groups were compared by Log-rank (Mantel-Cox) test. Differences were considered significant at $p < 0.05$. Median survival was defined as the time at which the survival curve crossed the 50% survival point.

3. Results and Discussion

3.1 Drug loading and release

We recently reported a long-circulating stealth liposomal Dox formulation that contained a small amount of pyro-lipid and exhibited similar pharmacokinetics to the pyro-lipid free liposomes, while being effective for chemophototherapy [33]. However, there was a maximum amount of pyro-lipid which could be added to the liposomes before Dox loading became impossible. To examine if this phenomenon occurred with irinotecan (IRT), liposomes were prepared with DSPC:DSPE-PEG2000:Cholesterol (molar ratio 60:5:35) and pyro-lipid was titrated in, replacing DSPC. As expected, Dox could not be loaded into liposomes containing more than 2 mol. % pyro-lipid; IRT however did not show such limitations and could be loaded into liposomes containing as much as 15 mol. % pyro-lipid. (Fig 1A). The NIR light-triggered release of IRT was tested using 2 mol. % pyro, which was previously found to be the optimum for Dox release [33]. NIR-induced IRT release was compared to Dox release in 50% serum, and was found to be substantially faster (Fig 1B). To help understand these differences between IRT and Dox, cryo-transmission electron microscopographs of IRT and Dox loaded PoP liposomes comprising DSPC:DSPE-PEG2000:Pyro-lipid:Cholesterol (molar ratio 58:5:2:35) were examined. The images showed that IRT loaded liposomes did not form large elongated crystals like Dox, nor did they have an effect on the shape of the liposomes. Instead, IRT formed precipitates that occupied the entirety of the liposomes core (Fig 2).

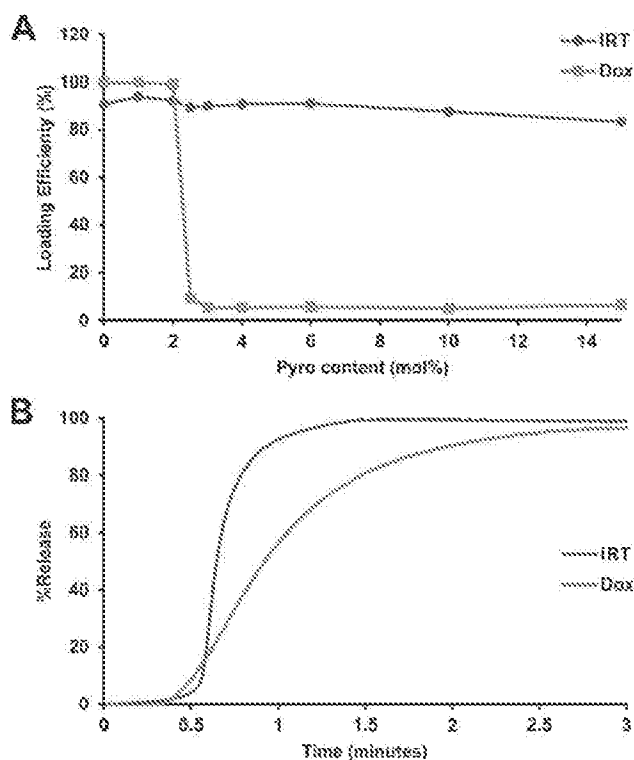


Figure 1: Drug loading and light-triggered release. **A)** Pyro lipid was titrated into liposomes consisting of DSPC:DSPE-PEG2000:Chol (molar ratio 60:5:35), replacing DSPC. Using this formulation Dox cannot be loaded above 2 mol. % while IRT does not demonstrate such a limitation. Data represent the average of 3 experiments (Dox data in figure A was adapted from ref. [33]). **B)** Light-induced release of Dox and IRT under 665 nm irradiation from liposomes containing 2% pyro-lipid.

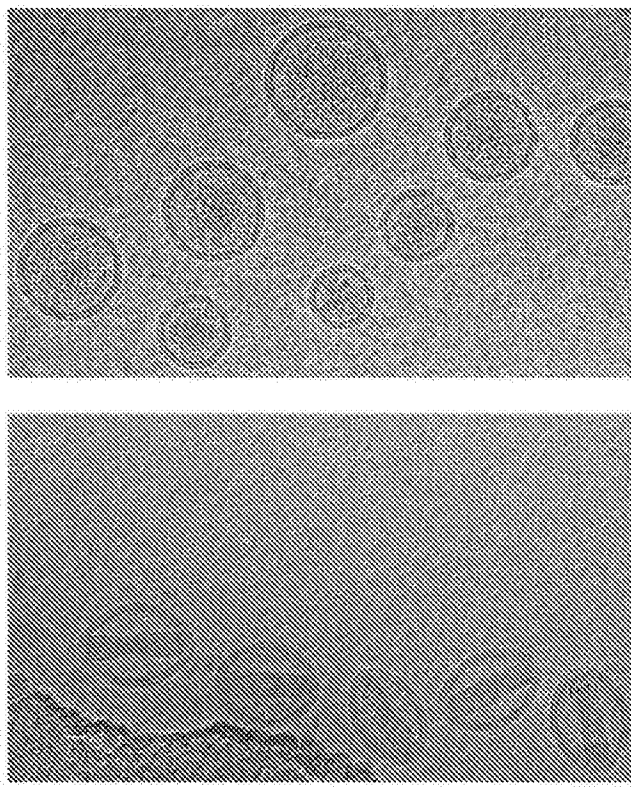


Figure 2: Effects of drug loading on liposome morphology. Cryo-TEM images of IRT (top) and Dox (bottom) loaded via an internal ammonium sulfate gradient in P α P-liposomes consisting of [DSPC:DSPE-PEG2000:Pyro-lipid:Chol] [58:5:2:35]. IRT liposomes show aggregates in the core while Dox shows linear crystals which cause the liposomes to stretch. A 50 nm scale bar is shown.

This demonstrates that IRT did not alter the shape of the liposomes. It also suggests that the poor loading of Dox in pyro-lipid containing liposomes is likely caused by destabilization of the bilayer as a consequence of the stretching induced by the formation of Dox crystals. It additionally suggests that the faster release of IRT may be due to more diffused drug aggregates inside the liposome which can dissolve more readily when the liposome bilayer is permeabilized by NIR light.

3.2 Formulation Optimization

While the formulation used in the imaging and initial experiments was stable in 50% serum when loaded with Dox, it was not stable when loaded with IRT. To address this, the cholesterol content was increased to 45 mol. % to produce more stable liposome bilayers. However, this did not significantly improve the stability. IRT is known to be prone to poor stability in liposomes [44]. One method which has been shown to enhance the stability of drug loaded liposomes is the use sphingomyelin (SPM) in place of DSPC [52,53]. To assess the effect of SPM on stability, liposomes made with SPM and DSPC were compared. DSPC liposomes were prepared using DSPC:DSPE-PEG2000:Pyro-lipid:Chol (48:5:2:45), and

SPM liposomes with SPM:DSPE-PEG2000:Pyro-lipid:Chol (48:5:2:45). The DSPC liposomes had >90% loading, whereas the SPM liposomes loaded only ~75% IRT. To verify how the absence of PEG would impact loading, we tested the loading of a PEG free SPM formulation; SPM:Pyro-lipid:Chol (53:2:45). Similar to the DSPC formulation, this formulation showed >90% loading (Fig 3A). The stability of the three formulations was compared by incubating the samples in 50% serum at 37°C. The DSPC formulation showed more than 50% release after 3 hours while both formulations with SPM had less than 30% (Fig 3B). Light triggered release experiments of IRT from these liposomes showed that the PEG-free SPM formulation had the fastest release rate, releasing most of the drug in less than 60 seconds. The PEGylated SPM formulation took 3 minutes to achieve the same results, while the DSPC formulation was significantly slower (Fig 3C). The observed lag time at the initiation of light-triggered release is likely related to initial disruption of the actively loaded IRT-sulfate aggregates inside the liposomes. Since the PEG-free SPM formulation showed good loading, greater serum stability, and faster release compared to the DSPC containing liposomes it was selected to be used for *in vivo* tests. All of the liposomes had similar

sizes and zeta potential with the exception of the SPM:Pyro-lipid:Chol liposomes which had a less negative zeta potential (Supporting Fig S3). To better understand the release properties, IRT release was tested under various conditions including different serum content, fluence rates and irradiation conditions. The light-triggered release rate was found to increase with increasing serum concentration, suggesting the presence of serum proteins help to destabilize the bilayer during release (Supporting Fig S2A). Laser treatment was essential for rapid drug release, with release starting when the laser was applied and stopping when the laser was stopped (Supporting Fig S2B), a phenomena which has previously been described for PoP liposomes. [31] IRT release was also found to be a function of total applied fluence rate, requiring approximately 20 J/cm² to achieve 90% release. (Supporting Fig S2C)

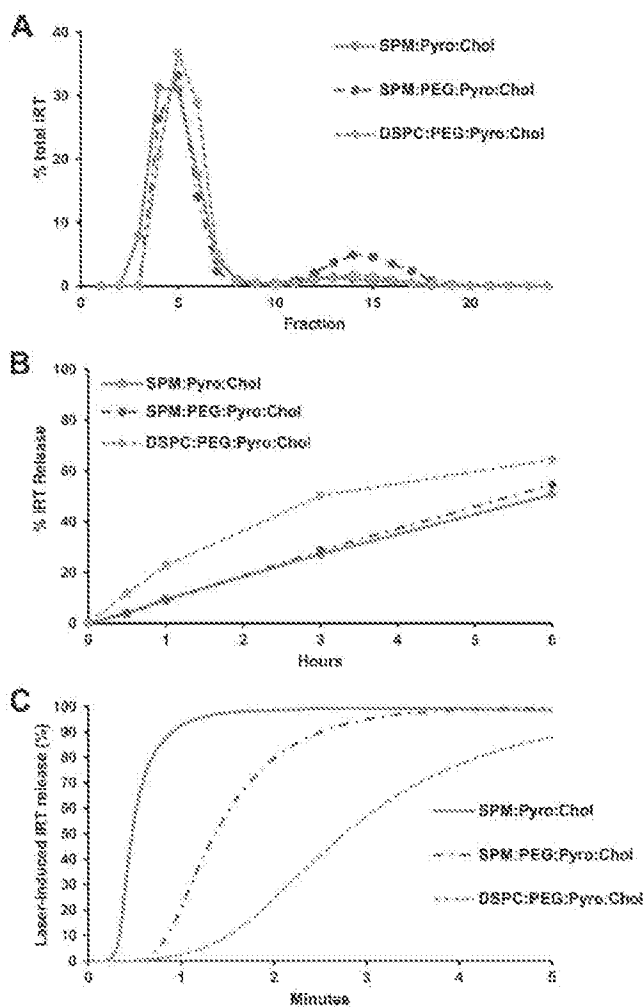


Figure 3: Development of a PoP IRT formulation. Liposomes were made with SPM:pyro-lipid:chol (53:2:45), SPM:DSPE-PEG2000:pyro-lipid:chol (48:5:2:45), or DSPE:DSPE-PEG2000:pyro-lipid:chol (48:5:2:45). **A)** IRT loading was quantified via gel filtration with a Sephadex G-75 column **B)** Stability tests in 50% adult bovine serum at 37°C. **C)** NIR-induced IRT release in 50% adult bovine serum showed SPM liposomes had faster release rate, with the PEG free formulation releasing the quickest.

3.3 Intravascular, light-triggered IRT release

We have previously shown that the efficacy of PoP liposomes is due to a combination of an vascular photodamage-related enhanced drug uptake and light-triggered release [32]. However, the extent of light-triggered drug release occurring in the vasculature was not determined, as the release rate of Dox was relatively slow. To determine whether or not vascular release was possible with this formulation, we studied the effects of laser treatment on drug release in the ears of mice as this allows for easy treatment and microscope imaging. Nude mice were injected with 10 mg/kg IRT loaded liposomes and treated on one ear. To demonstrate release was a result of laser treatment, IRT fluorescence was monitored in real time. Immediately following injection mice were anaesthetized and placed on the microscope stage and one ear treated with a laser. Mice treated with IRT PoP showed an increase in IRT fluorescence than those treated with Empty PoP + IRT liposomes ([SPM:Pyro-lipid:Chol] [53:2:45]) when the laser was turned on. (Fig 4A; Additional File 2: video 1 and Additional File 3: video 2). Interestingly, this fluorescence decreased over time while the pyro PoP fluorescence remained relatively constant (Fig 4B). This suggests that the IRT was released from the liposomes and was either diffusing throughout the treated region or being washed out. While there was a difference in the IRT fluorescence between the treated and untreated ears no such difference was observed for pyro (Supporting Fig S3). Drug release began immediately following the start of laser treatment. This is demonstrated by a significant increase in IRT fluorescence. Over time, the fluorescence levels reached a maximum after which fluorescence began to decrease. After the end of laser treatment, the fluorescence decreased to the levels similar to the initial. However further studies are required to determine if this decrease was due to the IRT washing out or due to photobleaching from prolonged light exposure. It is most likely to be washout as the physiology of the ear vasculature and tissues may not allow for retention of the drug.

To further demonstrate that the increase in fluorescence observed was due to drug release and not liposome accumulation, pyro-lipid free liposomes ([DSPE:DSPE-PEG2000:Chol] [55:5:45]) loaded with IRT was co-injected with empty PoP-liposomes ([SPM:Pyro-lipid:Chol] [53:2:45]). The results showed no significant increase in the IRT fluorescence compared to the no laser control (Figure S4 in the Supporting Information).

3.4 Chemophototherapy efficacy

To study the efficacy of the liposomes nude mice bearing Mia PaCa-2 tumors were injected with 15 mg/mL of free or PoP-liposome encapsulated IRT or equivalent (PoP) doses of empty liposomes and treated 10-15 minutes' post injection with a 665 nm laser at a fluence rate of 300 mW/cm² for 16 minutes, 40 seconds (300 J/cm²). As shown in Fig 5, mice treated with free IRT (median survival 18 days) showed no significant improvement over the saline control (median survival 17 days), while mice receiving IRT loaded PoP-liposomes with and without laser treatment and empty PoP-liposomes with laser showed statistically significant improvement over the saline control ($P < 0.01$). Mice receiving laser treatment and IRT-loaded PoP-liposomes showed complete tumor regression in all but one mouse (80% cure rate). Mice receiving only IRT-loaded PoP-liposomes without laser treatment and empty PoP-liposome with laser treatment had median survival times of 29 days and 42 (with 17 % cured) days respectively. There was no statistically significant difference between these two groups; however, there was a significant difference between each group and the IRT loaded PoP-liposomes and laser treatment ($P < 0.05$).

Individual tumor growth curves are shown in Figure S5 in the Supporting Information. This demonstrates a synergistic effect between the laser treatment and drug delivery which together produce an overall effective chemophototherapy treatment. Photodynamic therapy is known to be able to enhance the permeability of nanoparticles in tumor vasculature and affect blood flow [54–56]. We have previously shown that both effects are present in tumors treated with Dox PoP-liposomes [33] and would expect similar effects to be present in IRT PoP liposomes. The results of the survival study for IRT PoP liposomes are similar to that of Dox PoP liposomes with the empty +laser and Dox PoP -laser having equal efficacy and the Dox/IRT PoP liposomes showing significantly greater efficacy. The improved efficacy of the IRT-PoP +laser can be attributed to a synergistic effect between the drug and the photodynamic effects similar to that previously observed for Dox PoP liposomes. Microscopy images of tumors treated with IRT PoP with and without laser show that tumors receiving laser treatment had a greater and more homogeneous distribution of IRT (Supporting Fig S6).

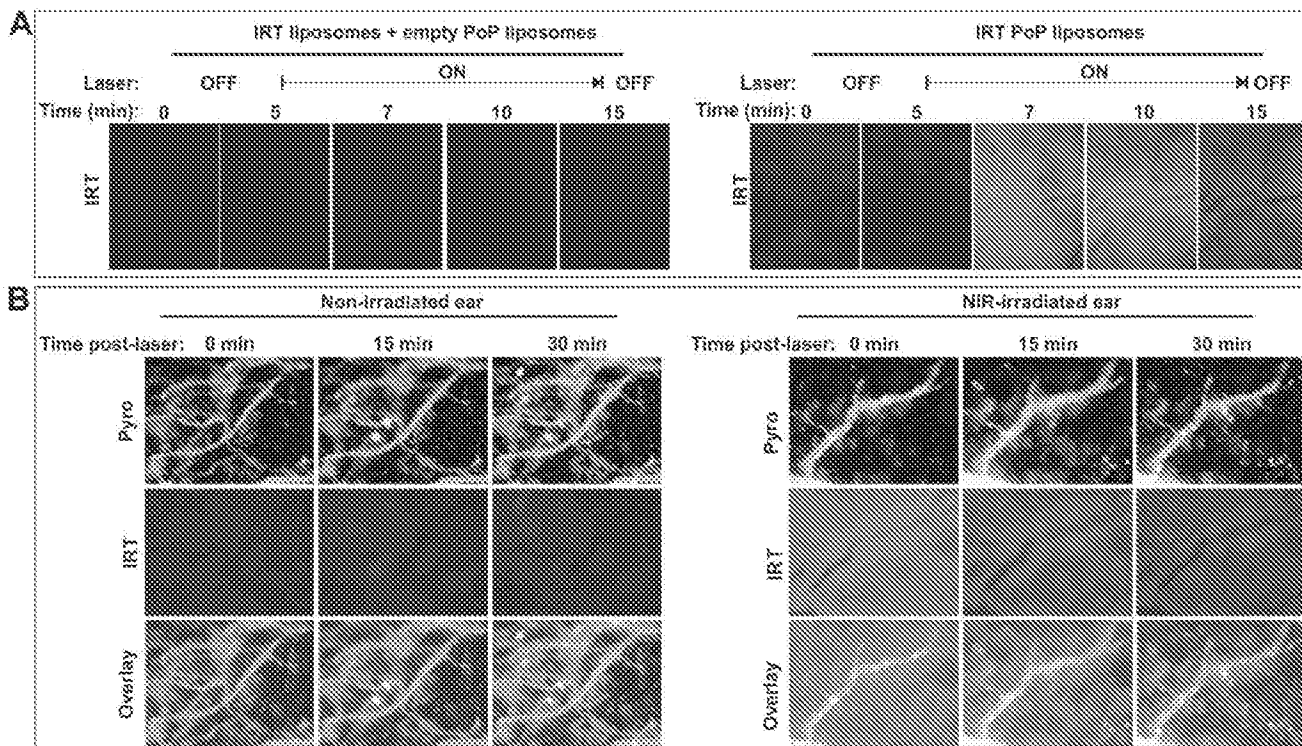


Figure 4: Intravascular light-triggered IRT release. Mice were injected with SPM:pyro-lipid:cholesterol liposomes loaded with IRT (10 mg/kg IRT), anesthetized and treated on one ear with a 665 nm laser at a fluence rate of 300 mW/cm². **A)** IRT fluorescence was measured during treatment in mice injected with both empty PoP-liposomes and PoP-free IRT loaded liposomes (left) or IRT loaded PoP liposomes (right). **B)** Pyro-lipid and IRT fluorescence were also monitored immediately following a 10 minute phototreatment.

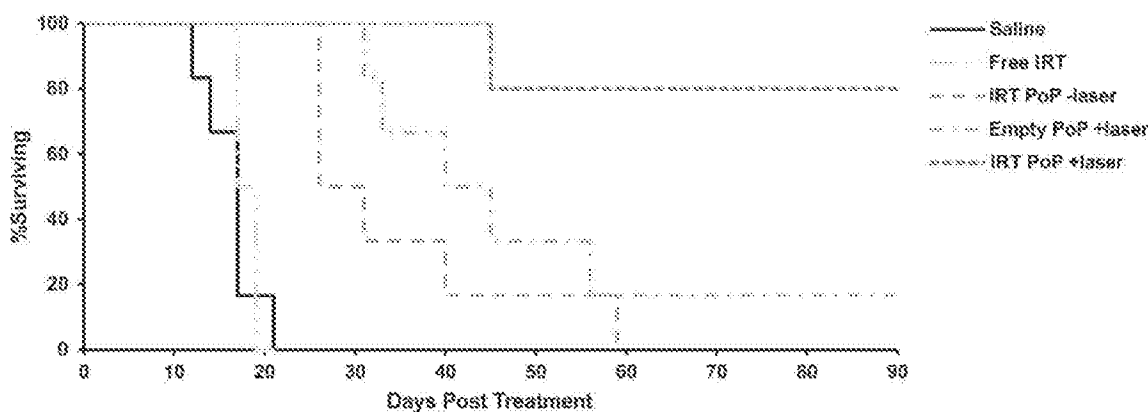


Figure 5: Kaplan-Meier survival curves for nude mice bearing Mia PaCa-2 tumors phototreated shortly after IV injection. Mice were IV injected with saline, 15 mg/kg free IRT, 15 mg/kg IRT-loaded PoP liposomes or equivalent PoP doses of empty liposomes. 10 minutes following injection, mice in the +laser groups were treated with a 665 nm laser at a fluence rate of 300 mW/cm² for 16 min, 40 sec. (360 J/cm²). Mice were given a single treatment and sacrificed when the tumors grew more than 10 times initial size. n= 5-7 mice per group.

Conclusion

We demonstrated that IRT can be loaded into liposomes with higher pyro-lipid content, whereas that was not possible for Dox. This is likely linked to the morphology of the liposomes following loading, and the avoidance of bilayer stretching by IRT. While IRT was loaded effectively into PoP liposomes, IRT loaded liposomes were not as stable as Dox loaded liposomes. IRT has been reported to be unstable in liposomes and strategies are being developed to increase stability and efficacy [44,49,50,57-59]. In this work, we substituted the DSPC used in our previous formulation with sphingomyelin, increased the cholesterol content and omitted PEG. This approach resulted in liposomes with a modest increase in serum stability. Although the liposomes were not highly serum stable, when subjected to NIR light treatment, they rapidly released the drug and effectively suppressed tumor growth. Taken together, we conclude that IRT PoP liposomes are promising for chemophototherapy approaches.

Supplementary Material

Additional File 1:

Figures S1-S6. <http://www.thno.org/v06p2329s1.pdf>

Additional File 2:

Video 1. <http://www.thno.org/v06p2329s2.wmv>

Additional File 3:

Video 2. <http://www.thno.org/v06p2329s3.wmv>

Acknowledgments

This work was supported by the National Institutes of Health (R01EB017270 and DP5OD017898).

Competing Interests

The authors have declared that no competing

interest exists.

References

1. Torchilin VP. Recent advances with liposomes as pharmaceutical carriers. *Nat. Rev. Drug Discov.* 2005;4:145-60.
2. Peer D, Karp JM, Hong S, Farokhzad OC, Margalit R, Langer R. Nanocarriers as an emerging platform for cancer therapy. *Nat. Nanotechnol.* 2007;2:751-60.
3. Wang AZ, Langer R, Farokhzad OC. Nanoparticle Delivery of Cancer Drugs. *Annu. Rev. Med.* 2012;63:185-98.
4. Allen TM, Cullis PR. Drug Delivery Systems: Entering the Mainstream. *Science.* 2004;303:1818-22.
5. Maruyama K. Intracellular targeting delivery of liposomal drugs to solid tumors based on EPR effects. *Adv. Drug Deliv. Rev.* 2011;63:161-9.
6. Fang J, Nakamura H, Maeda H. The EPR effect: Unique features of tumor blood vessels for drug delivery, factors involved, and limitations and augmentation of the effect. *Adv. Drug Deliv. Rev.* 2011;63:136-51.
7. Torchilin V. Tumor delivery of macromolecular drugs based on the EPR effect. *Adv. Drug Deliv. Rev.* 2011;63:131-5.
8. Maeda H. Macromolecular therapeutics in cancer treatment: The EPR effect and beyond. *J. Controlled Release.* 2012;164:138-44.
9. Barenholz Y. Doxil® -- The first FDA-approved nano-drug: Lessons learned. *J. Controlled Release.* 2012;169:117-34.
10. Manzoer AA, Lindner LH, Landon CD, Park J-Y, Simunek AJ, Dreher MR, et al. Overcoming Limitations in Nanoparticle Drug Delivery: Triggered, Intravascular Release to Improve Drug Penetration into Tumors. *Cancer Res.* 2012;72:5566-75.
11. Prabhakar U, Maeda H, Jain RK, Sevick-Muraca EM, Zamboni W, Farokhzad OC, et al. Challenges and Key Considerations of the Enhanced Permeability and Retention Effect for Nanomedicine Drug Delivery in Oncology. *Cancer Res.* 2013;73:2412-7.
12. Jain RK, Stylianopoulos T. Delivering nanomedicine to solid tumors. *Nat. Rev. Clin. Oncol.* 2010;7:653-64.
13. Bertrand M, Wu J, Xu X, Kamaly N, Farokhzad OC. Cancer nanotechnology: The impact of passive and active targeting in the era of modern cancer biology. *Adv. Drug Deliv. Rev.* 2014;66:2-25.
14. Mills JK, Needham D. Targeted drug delivery. *Expert Opin. Ther. Pat.* 1999;9:1499-513.
15. Koo OM, Rubinstein I, Onyiah H. Role of nanotechnology in targeted drug delivery and imaging: a concise review. *Nanomedicine Nanotechnol. Biol. Med.* 2005;1:199-212.
16. Freeman AI, Mayhew E. Targeted drug delivery. *Cancer.* 1986;58:570-83.
17. Ganta S, Devalapally H, Shahiwala A, Amiji M. A review of stimuli-responsive nanocarriers for drug and gene delivery. *J. Controlled Release.* 2008;126:187-204.
18. Luo D, Carter KA, Lovell JF. Nanomedical engineering: shaping future nanomedicines. *Wiley Interdiscip. Rev. Nanomed. Nanobiotechnol.* 2015;7:169-88.
19. You J, Zhang C, Li C. Exceptionally High Payload of Doxorubicin in Hollow Gold Nanospheres for Near-Infrared Light-Triggered Drug Release. *ACS Nano.* 2010;4:1933-41.
20. Timko BP, Kohane DS. Prospects for near-infrared technology in remotely triggered drug delivery. *Expert Opin. Drug Deliv.* 2014;11:1681-5.
21. Araki T, Ogawara K, Suzuki H, Kawai R, Watanabe T, Ono T, et al. Augmented EPR effect by photo-triggered tumor vascular treatment improved therapeutic efficacy of liposomal paclitaxel in mice bearing tumors with low permeable vasculature. *J. Controlled Release.* 2015;200:106-14.

22. Fomina N, Sankaranarayanan J, Almutairi A. Photochemical mechanisms of light-triggered release from nanocarriers. *Adv. Drug Deliv. Rev.* 2012;64:1905–20.
23. Zhen Z, Tang W, Chen H, Lin X, Todd T, Wang C, et al. RGD-Modified Apolipoprotein Nanoparticles for Efficient Drug Delivery to Tumors. *ACS Nano*. 2013;7:4830–7.
24. He C, Liu D, Lin W. Self-Assembled Core-Shell Nanoparticles for Combined Chemotherapy and Photodynamic Therapy of Resistant Head and Neck Cancers. *ACS Nano*. 2015;9:991–1003.
25. Spring BC, Sears RB, Zheng LZ, Mai Z, Watanabe R, Sherwood ME, et al. A photoactivable multi-inhibitor nanoliposome for tumour control and simultaneous inhibition of treatment escape pathways. *Nat. Nanotechnol.* 2016;11:578–87.
26. Yen H-C, Cabral H, Mi F, Yoh K, Matsumoto Y, Liu X, et al. Light-Induced Cytosolic Activation of Reduction-Sensitive Camptothecin-Loaded Polymeric Micelles for Spatiotemporally Controlled *In Vivo* Chemotherapy. *ACS Nano*. 2014;8:11591–602.
27. Luo D, Carter KA, Miranda D, Lovell JF. Chemophototherapy: An Emerging Treatment Option for Solid Tumors. *Adv. Sci.* 2016.
28. Huang H, Song W, Rieffel J, Lovell JF. Emerging applications of porphyrins in photomedicine. *Front Phys* 2015;3:23.
29. Zhang Y, Lovell JF. Porphyrins as theranostic agents from prehistoric to modern times. *Theranostics*. 2012;2:905–15.
30. Zhang Y, Lovell JF. Recent applications of phthalocyanines and naphthalocyanines for imaging and therapy. *Wiley Interdiscip. Rev. Nanomed. Nanobiotechnol.* 2016.
31. Carter KA, Shao S, Hoopes MJ, Luo D, Ahsan E, Grigoryants VM, et al. Porphyrin-phospholipid liposomes permeabilized by near-infrared light. *Nat. Commun.* 2014; 5:3546.
32. Luo D, Carter KA, Razi A, Geng J, Shao S, Lin C, et al. Porphyrin-phospholipid liposomes with tunable leakiness. *J. Controlled Release*. 2015;220:484–94.
33. Luo D, Carter KA, Razi A, Geng J, Shao S, Gimble D, et al. Doxorubicin encapsulated in stealth liposomes conferred with light-triggered drug release. *Biomaterials*. 2016;73:193–202.
34. Lovell JF, Jin CS, Huynh E, Jin H, Kim C, Rubinstein JL, et al. Porphyrin nanovesicles generated by porphyrin bilayers for use as multimodal biophotonic contrast agents. *Nat. Mater.* 2011;10:324–32.
35. Carter KA, Wang S, Geng J, Luo D, Shao S, Lovell JF. Metal Chelation Modulates Photo-therapeutic Properties of Mitoxantrone-Loaded Porphyrin-Phospholipid Liposomes. *Mol. Pharm.* 2016;13:420–7.
36. Shao S, Geng J, Ah Yi H, Gogia S, Neelamegham S, Jacobs A, et al. Functionalization of cobalt porphyrin-phospholipid bilayers with his-tagged ligands and antigens. *Nat. Chem.* 2015;7:438–46.
37. Kress J, Rohrbach DJ, Carter KA, Luo D, Shao S, Lei S, et al. Quantitative imaging of light-triggered doxorubicin release. *Biomed. Opt. Express*. 2015;6:3546–55.
38. Rieffel J, Chen F, Kim J, Chen G, Shao W, Shao S, et al. Hexamodal Imaging with Porphyrin-Phospholipid-Coated Upconversion Nanoparticles. *Adv. Mater.* 2015;27:1785–90.
39. Luo D, Li N, Carter KA, Lin C, Geng J, Shao S, et al. Rapid Light-Triggered Drug Release in Liposomes Containing Small Amounts of Unsaturated and Porphyrin-Phospholipids. *Small*. 2016;12:3039–47.
40. Lovell JF, Jin CS, Huynh E, MacDonald TD, Cao W, Zheng C. Enzymatic Regioselection for the Synthesis and Biodegradation of Porphyrin Nanovesicles. *Angew. Chem. Int. Ed.* 2012;51:2429–33.
41. Fritze A, Hens F, Kimpfler A, Schubert R, Peschka-Süss R. Remote loading of doxorubicin into liposomes driven by a transmembrane phosphate gradient. *Biochim. Biophys. Acta BBA - Biomembr.* 2006;1758:163–40.
42. Lasic DD, Frederik PM, Stuart MCA, Barenholz Y, McIntosh TJ. Gelation of liposome interior: A novel method for drug encapsulation. *FEBS Lett.* 1992;312:255–8.
43. Andriyanov AV, Koren E, Barenholz Y, Goldberg SN. Therapeutic Efficacy of Combining PEGylated Liposomal Doxorubicin and Radiofrequency (RF) Ablation: Comparison between Slow-Drug-Releasing, Non-Thermo-sensitive and Fast-Drug-Releasing, Thermo-sensitive Nano-Liposomes. *PLoS ONE*. 2014;9:e92555.
44. Chou T-H, Chen S-C, Chu I-M. Effect of Composition on the stability of liposomal irinotecan prepared by a pH gradient method. *J. Biosci. Bioeng.* 2003;95:405–8.
45. Messerer CL, Ramsay EC, Waterhouse D, Ng P, Simms B-M, Harasym N, et al. Liposomal Irinotecan Formulation Development and Therapeutic Assessment in Murine Xenograft Models of Colorectal Cancer. *Clin. Cancer Res.* 2004;10:6638–49.
46. Drummond DC, Noble CO, Guo Z, Hong K, Park JW, Kirpotin DB. Development of a Highly Active Nanoliposomal Irinotecan Using a Novel Intraliposomal Stabilization Strategy. *Cancer Res.* 2006;66:3271–7.
47. Mathijssen RHJ, Aijphen RJ van, Verweij J, Loos WJ, Nooter K, Stoter G, et al. Clinical Pharmacokinetics and Metabolism of Irinotecan (CPT-11). *Clin. Cancer Res.* 2001;7:2182–94.
48. Chang H-I, Yeh M-K. Clinical development of liposome-based drugs: formulation, characterization, and therapeutic efficacy. *Int. J. Nanomedicine*. 2012;7:49–60.
49. Ramsay E, Alnajim J, Anantha M, Taggar A, Thomas A, Edwards K, et al. Transition Metal-Mediated Liposomal Encapsulation of Irinotecan (CPT-11) Stabilizes the Drug in the Therapeutically Active Lactone Conformation. *Pharm. Res.* 2006;23:2799–808.
50. Wei H, Song J, Li H, Li Y, Zhu S, Zhou X, et al. Active loading liposomal irinotecan hydrochloride: Preparation, *in vitro* and *in vivo* evaluation. *Asian J. Pharm. Sci.* 2013;8:307–11.
51. Li X, Mooney P, Zheng S, Booth CR, Braumfeld MB, Gubbens S, et al. Electron counting and beam-induced motion correction enable near-atomic-resolution single-particle cryo-EM. *Nat. Methods*. 2013;10:584–90.
52. Webb MS, Harasym TC, Masin D, Bally MB, Mayer LE. Sphingomyelin-cholesterol liposomes significantly enhance the pharmacokinetic and therapeutic properties of vincristine in murine and human tumour models. *Br. J. Cancer*. 1995;72:896–904.
53. Tardi P, Choice E, Masin D, Redelmeier T, Bally M, Madden TD. Liposomal encapsulation of irinotecan enhances anticancer efficacy in murine and human xenograft models. *Cancer Res.* 2006;66:3389–93.
54. Snyder JW, Greco WR, Bellnier DA, Vaughan L, Henderson BW. Photodynamic therapy: a means to enhanced drug delivery to tumors. *Cancer Res.* 2003;63:8126–31.
55. Sano K, Nakajima Y, Choyke PL, Kobayashi H. Markedly Enhanced Permeability and Retention Effects Induced by Photo-immunotherapy of Tumors. *ACS Nano*. 2013;7:717–24.
56. Zhen Z, Tang W, Chuang Y-J, Todd T, Zhang W, Lin X, et al. Tumor Vasculature Targeted Photodynamic Therapy for Enhanced Delivery of Nanoparticles. *ACS Nano* 2014;8:6004–13.
57. Modrak DE, Rodriguez MD, Goldenberg DM, Lew W, Elumenthal RD. Sphingomyelin enhances chemotherapy efficacy and increases apoptosis in human colonic tumor xenografts. *Int. J. Oncol.* 2002;20:379–84.
58. Krauze ME, Noble CO, Kawaguchi T, Drummond D, Kirpotin DB, Yamashita Y, et al. Convection-enhanced delivery of nanoliposomal CPT-11 (irinotecan) and PEGylated liposomal doxorubicin (Doxil) in rodent intracranial brain tumor xenografts. *Neuro-Oncol.* 2007;9:392–403.
59. Hattori Y, Shi L, Ding W, Koga K, Kawano K, Hakoshima M, et al. Novel irinotecan-loaded liposome using phytic acid with high therapeutic efficacy for colon tumors. *J. Controlled Release*. 2009;136:30–7.

Antiemetic Efficacy of Dexamethasone Therapy in Patients Receiving Cancer Chemotherapy

Peter A. Cassileth, MD; Edward J. Lusk, PhD; Susan Torri, RN; Nancy DiNubile, RN; Stanton L. Gerson, MD

To assess the value of high-dose dexamethasone therapy in preventing the gastrointestinal (GI) side effects of chemotherapy, a randomized double-blind study was conducted in women receiving outpatient therapy for breast cancer. Single-dose dexamethasone sodium phosphate (10 mg) or placebo was administered intravenously in 57 trials in 22 women immediately before chemotherapy. Questionnaires (administered before therapy and 24 hours later) were compared for evidence of nausea, vomiting, and anorexia produced by chemotherapy. No GI intolerance to chemotherapy was noted in 24 (83%) of the 29 dexamethasone trials v 16 (57%) of the 28 placebo trials. Dexamethasone trials produced the following results: no side effects in 50% (14/29), insomnia the night after chemotherapy in 21% (6/29), an increase in energy levels in 24% (7/29), and an improvement in mood in 14% (4/29). High-dose dexamethasone therapy has useful application in alleviating the emetic effects of cancer chemotherapy.

(Arch Intern Med 1983;143:1347-1349)

The management of chemotherapy-induced nausea and vomiting continues to be a major problem in the treatment of patients with cancer.^{1,2} Because of the limited effectiveness of standard antiemetics, eg, the phenothiazines,³ other approaches have been tried, eg, metoclopramide hydrochloride⁴ and tetrahydrocannabinol.⁵ Our observations and the pilot study reports of others^{6,7} suggest that high-dose glucocorticoid administration ameliorates the nausea and vomiting of cancer chemotherapy. The following randomized double-blind study of intravenous (IV) dexamethasone sodium phosphate therapy v placebo was conducted to evaluate the efficacy of dexamethasone therapy.

PATIENTS AND METHODS

Women with breast cancer who were receiving outpatient chemotherapy in the hematology-oncology section of the Hospital of the University of Pennsylvania, Philadelphia, were eligible for this study. Patients were excluded from the study if they (1) were more than 70 years old, (2) had anticipatory vomiting before chemotherapy, and (3) had diabetes mellitus, peptic ulcer disease,

Chemotherapy	No. of Trials	
	Dexamethasone-Treated Group	Placebo-Treated Group
Cyclophosphamide, methotrexate sodium, and fluorouracil	26	25
Doxorubicin hydrochloride and vinorelbine sulfate	1	3
Mitomycin	2	0
Total	29	28

congestive heart failure, infection, hypertension, or a previous adverse reaction to corticosteroids. Twenty-two women were enrolled from May through November 1981. The study was approved by the University of Pennsylvania's Human Studies Committee and informed consent was obtained. Patients were eligible for rerandomization with each subsequent chemotherapy treatment unless they declined. In all, 57 trials were conducted in the 22 patients.

A randomized, double-blind, study design was employed. Dexamethasone sodium phosphate in 1-mL vials (10 mg/mL) and identical 1-mL vials containing only the carrier vehicle were used. The vials were coded from a table of random numbers before delivery to us. One milliliter was withdrawn from a vial, diluted to a total volume of 10 mL in physiological saline, and administered slowly IV during three to five minutes immediately before IV chemotherapy. The IV dilution and slow push were deliberately performed to avoid the perineal and groin discomfort that transiently appears if high-dose glucocorticoids are rapidly injected. Patients were given prochlorperazine maleate tablets or rectal suppositories for use in the event of nausea or vomiting subsequent to chemotherapy.

A questionnaire, administered by the nurses, was used to assess the patient's baseline status in the 24-hour period before chemotherapy. Appetite and nausea were each assessed on a scale of 1 (none) to 4 (severe) and the number of episodes of emesis, number of doses of prochlorperazine used, and the duration of nausea were recorded. Alterations in emotional status or mood, abdominal complaints, edema or fullness, allergic responses, and abnormalities in vision, taste, or sensation were also recorded. Twenty-four hours after chemotherapy, the patient was contacted at home by telephone by the nurses. The questionnaire was readministered to determine the patient's status in the 24 hours since chemotherapy.

Accepted for publication Feb 23, 1983.

From the Hematology-Oncology Section, Department of Medicine (Drs Cassileth and Gerson and Mrs Torri and DiNubile) and the Biostatistics Program of the Cancer Center (Dr Lusk), University of Pennsylvania, Philadelphia.

Reprint requests to the Hospital of the University of Pennsylvania, 3406 Spruce St, Philadelphia, PA 19104 (Dr Cassileth).

Table 2.—Gastrointestinal (GI) Intolerance to Chemotherapy in Trials of Patients Receiving Dexamethasone Therapy v Placebo

	Dexamethasone-Treated Group		Placebo-Treated Group	
	Success	Failure*	Success	Failure*
Total trials	34	5	16	12
Cyclophosphamide, methotrexate, sodium, and fluorouracil therapy	21	5	16	9
Doxorubicin hydrochloride and vincristine sulfate therapy	1	0	0	3
Mitomycin therapy	2	0	0	0
GI manifestations				
Nausea only		2		9
Vomiting only		1		0
Nausea and vomiting		0		4
Used antiemetics		3		7

*Any trial was rated a failure if nausea, vomiting, or anorexia occurred or if a single antiemetic medication was used by the patient.

Table 3.—Side Effects in Randomized Patients

Side Effect	Dexamethasone* (28 Trials)	Placebo (28 Trials)
No change	14	16
Insomnia	6	0
Metallic taste	1	3
Elevated mood	4	1
Depressed mood	0	4
Increased energy	7	0
Abdominal discomfort	1	3
Headache	0	1

*Some patients recorded more than one alteration.

The questionnaire results were reviewed blindly by two of us (S.L.G. and P.A.C.) who were not involved in the administration of the drugs or the questionnaires. The success or failure in preventing chemotherapy-induced nausea, anorexia, and vomiting was assessed by comparing the results recorded for the 24 hours preceding and following chemotherapy. A trial was rated a success only if nausea or anorexia did not ensue or increase during the 24 hours after chemotherapy and if vomiting did not occur. Otherwise, the trial was rated a failure. If a single prochlorperazine dose was used by the patient, the trial was rated as a failure.

Fifty-seven trials were conducted in 22 different patients. Fifty-one trials were conducted in 18 patients receiving standard cyclophosphamide, methotrexate, and fluorouracil¹ chemotherapy; two trials were performed in one patient receiving mitomycin therapy (10 mg/sq m IV) and four trials in three patients receiving a combination of doxorubicin hydrochloride (30 mg/sq m) and vincristine sulfate (1 mg) IV. Table 1 gives the distribution of trials involving dexamethasone therapy v placebo. Patients in the dexamethasone-treated group ranged in age from 30 to 70 years (median age, 52 years), while patients in the placebo-treated group were aged from 29 to 66 years (median age, 54 years).

RESULTS

Eleven patients exited from the study after a single trial and asked to be treated with dexamethasone at subsequent

chemotherapy. Of these eleven patients, six patients had received dexamethasone therapy (five patients had no nausea or vomiting and one had vomiting requiring a single dose of prochlorperazine therapy). The other five patients had received placebo and experienced nausea and/or vomiting after chemotherapy. Thus, ten of these 11 patients correctly assessed the antiemetic effects of dexamethasone therapy and the lack of benefit from placebo. Four other patients had two trials each and refused subsequent rerandomization. Of these four patients, two patients received dexamethasone therapy on both trials (one patient had no nausea or vomiting on either occasion, and one patient had one success and one failure); one patient received dexamethasone therapy initially (success) followed by placebo (failure); and one patient received placebo both times (one failure and one success). Only seven patients were willing to continue rerandomization beyond two trials. One patient participated for eight trials, receiving dexamethasone therapy six times (all successes) and placebo twice (one success and one failure).

The data from the analysis of the pretherapy and post-therapy questionnaire results are given in Table 2 for patients receiving dexamethasone therapy or placebo. Overall, 24 (83%) of the 29 dexamethasone trials were free of GI intolerance to chemotherapy compared with 16 (57%) of the 28 placebo trials. One patient experienced vomiting in only one of the 29 dexamethasone trials, whereas four different patients suffered vomiting in the 28 placebo trials. The success rate for the dexamethasone-treated group was significantly higher than for the placebo-treated group ($P < .025$). Analysis also showed that the results of the study were independent of age or race of the patients or the cycle of the combined cyclophosphamide, methotrexate, and fluorouracil therapy (first or second week of the monthly cycle).

Potential side effects of therapy were assessed on a separate part of the questionnaire administered before and after chemotherapy. Table 3 lists the results of any change in the patients' status on the day of chemotherapy for the dexamethasone-treated and placebo-treated groups. In seven of the 29 dexamethasone trials, patients noted an increased level of energy ("more pep") often associated with insomnia during the night after chemotherapy. In the placebo-treated group, three of the 28 trials were associated with vague abdominal distress, and four of the 28 trials were linked with depressed mood.

COMMENT

Agents previously reported to be useful in ameliorating the nausea and vomiting of chemotherapy include tetrahydrocannabinol^{2,3} and high-dose metoclopramide,⁴ both of which have limitations. To be effective, tetrahydrocannabinol requires a prior positive experience with marijuana and the development of a "high," and it produces dysphoric effects in patients aged older than 40 years (which includes the majority of patients with cancer). High-dose metoclopramide therapy has sedative and extrapyramidal side effects.

The results of this study clearly show the efficacy of a single injection of high-dose dexamethasone therapy in suppressing the nausea and vomiting of outpatient IV chemotherapy for breast cancer. That the cyclophosphamide, methotrexate, and fluorouracil regimen does not cause intense nausea is apparent from the fact that a number of placebo trials were counted as successes, ie, no nausea, vomiting, or anorexia resulted from the chemotherapy. In contrast, in the four trials of patients receiving doxorubicin and vincristine therapy, drugs with higher emetic activity,⁵ the one dexamethasone trial was judged a

success and the other three even more striking. Dexamethasone therapy in trials of chemotherapy suggested previously. Dexamethasone therapy caused no side effects in trials. Moreover, with no side effects caused a pleasant improvement in patient population. A single dose was used in the nauseating than prochlorperazine, such

1. Seigel LL, Losa RW. *Ann Intern Med*.
2. Laska J, Laska J. *Am J Surg*.
3. Frytak S. *Br J Cancer*.
4. Gralla RJ. *Int J Radiat Oncol Biol Phys*.
5. Sullivan SE. *Cancer Chemother Pharmacol*.

six patients had nausea and/or vomiting. The other five patients had nausea and/or vomiting. These 11 patients received dexamethasone. Four of the 11 patients had no subsequent recurrence of nausea and/or vomiting. One patient had received dexamethasone twice (one success).

therapy and post-therapy or placebo. The 28 trials were free of vomiting in 16 (57%) patients, whereas four (14%) placebo trials resulted in vomiting. The 28 placebo trials were assessed on a 24-hour follow-up. The 28 trials were

in ameliorating nausea and vomiting. High-dose dexamethasone

the efficacy of dexamethasone therapy in the outpatient setting. The cyclophosphamide regimen does not support the fact that dexamethasone is more effective than the chemotherapy agents with higher doses was judged as

success and the three placebo trials a failure. We believe an even more striking demonstration of the efficacy of dexamethasone therapy would have appeared with additional trials of chemotherapy regimens with high emetic activity as suggested previously.^{1,3}

Dexamethasone administration in this single-dose protocol caused no ill-effects except for insomnia in 21% (6/29) of trials. Moreover, almost half of the trials were associated with no side effects; 24% (7/29) of the dexamethasone trials caused a pleasant increase in energy levels and 14% (4/29) an improvement in mood. This single-dose application thus offers a significant benefit without apparent hazard in the patient population studied.

A single dose of dexamethasone before chemotherapy was used in this study. With regimens more potentially nauseating than cyclophosphamide, methotrexate, and fluorouracil, such as those that include cisplatin, additional

injections of dexamethasone and other antiemetic drugs may be necessary after chemotherapy administration to control nausea and vomiting. A recommended antiemetic for use in chemotherapy, high-dose metoclopramide,⁶ is twice as expensive as dexamethasone for equivalent antiemetic doses. We believe that high-dose dexamethasone therapy has useful application in alleviating the nausea and vomiting induced by cancer chemotherapy. Its relative efficacy compared with metoclopramide therapy needs to be tested in blind clinical trials.

This investigation was supported in part by grant CA-16520 from the National Cancer Institute, National Institutes of Health, Bethesda, Md, and a grant from Organon Inc, West Orange, NJ.

Organon Inc provided 1-mL vials of carrier vehicle. Richard Halberger, PhD, helped in the original study design. Kathy Munda, RN, and Brenda Cline, RN, obtained the 24-hour follow-up questionnaire information. Debora Brant prepared the manuscript.

References

1. Seigel LJ, Longo DL: The control of chemotherapy-induced emesis. *Ann Intern Med* 1981;95:352-359.
2. Lasdo J, Lucas VS Jr: Emesis as a critical problem in chemotherapy. *J Clin Oncol*. *N Engl J Med* 1981;305:948-949.
3. Frytak S, Moertel CG: Management of nausea and vomiting in the cancer patient. *JAMA* 1981;245:393-396.
4. Gralla RJ, Itri LM, Fishb S, et al: Antiemetic efficacy of high-dose metoclopramide: Randomized trials with placebo and prochlorperazine in patients with chemotherapy-induced nausea and vomiting. *N Engl J Med* 1981;305:995-998.
5. Sallan SE, Cronin C, Zelen M, et al: Antiemetics in patients receiving chemotherapy for cancer. A randomized comparison of delta-9-tetrahydrocannabinol and prochlorperazine. *N Engl J Med* 1980;302:135-138.
6. Rich WM, Abdulhayoglu Q, Di Saia PH: Methylprednisolone as an antiemetic during cancer chemotherapy: A pilot study. *Gynecol Oncol* 1980;9:133-138.
7. Aspro MS, Alberts DS: Dexamethasone as an antiemetic in patients treated with cisplatin, letter. *N Engl J Med* 1981;303:330.
8. Lee BJ: Methylprednisolone as an antiemetic, letter. *N Engl J Med* 1981;304:486.
9. Aspro MS, Alberts DS: High-dose dexamethasone for prevention of cisplatin-induced vomiting. *Cancer Chemother Pharmacol* 1981;7:11-14.
10. Canellos GP, Pineski SJ, Taylor SB III, et al: Combination chemotherapy for metastatic breast carcinoma: Prospective comparison of multiple drug therapy with L-phenylalanine mustard. *Cancer* 1976;38:1883-1886.

Volume tightly bound

**This is the best copy
available**

Clinical Pharmacokinetics of Irinotecan

Guy G. Chabot

Pharmacology Laboratory (URA 147 CNRS), Gustave-Roussy Institute, Villejuif, France

Contents

Summary	245
1. Historical Notes	246
2. Chemistry and Drug Administration	247
3. Mechanism of Action	248
4. Preclinical Activity	248
5. Clinical Toxicity and Anticancer Activity	249
5.1 Toxicity	249
5.2 Anticancer Activity	249
6. Pharmacokinetics	249
6.1 Analysis in Biological Materials	249
6.2 Metabolism	250
6.3 Pharmacokinetics of Irinotecan	251
6.4 Pharmacokinetics of SN-38	252
6.5 Pharmacokinetics of SN-38 Glucuronide	253
6.6 Pharmacokinetics of the Metabolite APC	253
6.7 Interconversion of Lactone and Carboxylate Forms <i>In vivo</i>	253
6.8 Protein Binding	253
6.9 Absorption	253
6.10 Distribution	253
6.11 Excretion	253
6.12 Pharmacokinetics of Irinotecan and SN-38 after Repeated Dosage	254
6.13 Influence of Physiopathological Conditions on Pharmacokinetics	254
6.14 Influence of Cotreatments on the Pharmacokinetics of Irinotecan	254
7. Pharmacokinetic-Pharmacodynamic Relationships	255
7.1 Toxicities	255
7.2 Antitumoural Responses	255
8. Conclusions and Perspectives	256

Summary

This article reviews the clinical pharmacokinetics of a water-soluble analogue of camptothecin, irinotecan (CPT-11 or 7-ethyl-10-[4-(1-piperidino)-1-piperidino]-carbonyloxy-camptothecin). Irinotecan, and its more potent metabolite SN-38 (7-ethyl-10-hydroxy-camptothecin), interfere with mammalian DNA topoisomerase I and cancer cell death appears to result from DNA strand breaks caused by the formation of cleavable complexes.

The main clinical adverse effects of irinotecan therapy are neutropenia and diarrhoea. Irinotecan has shown activity in leukaemia, lymphoma and the following cancer sites: colorectum, lung, ovary, cervix, pancreas, stomach and breast.

Following the intravenous administration of irinotecan at 100 to 350 mg/m², mean maximum irinotecan plasma concentrations are within the 1 to 10 mg/L

range. Plasma concentrations can be described using a 2- or 3-compartment model with a mean terminal half-life ranging from 5 to 27 hours. The volume of distribution at steady-state (V_{ss}) ranges from 136 to 255 L/m², and the total body clearance is 8 to 21 L/h/m².

Irinotecan is 65% bound to plasma proteins. The areas under the plasma concentration-time curve (AUC) of both irinotecan and SN-38 increase proportionally to the administered dose, although interpatient variability is important. SN-38 levels achieved in humans are about 100-fold lower than corresponding irinotecan concentrations, but these concentrations are potentially important as SN-38 is 100- to 1000-fold more cytotoxic than the parent compound.

SN-38 is 95% bound to plasma proteins. Maximum concentrations of SN-38 are reached about 1 hour after the beginning of a short intravenous infusion. SN-38 plasma decay follows closely that of the parent compound with an apparent terminal half-life ranging from 6 to 30 hours. In human plasma at equilibrium, the irinotecan lactone form accounts for 25 to 30% of the total and SN-38 lactone for 50 to 64%.

Irinotecan is extensively metabolised in the liver. The biperidinocarbonyloxy group of irinotecan is first removed by hydrolysis to yield the corresponding carboxylic acid and SN-38 by carboxyesterase. SN-38 can be converted into SN-38 glucuronide by hepatic UDP-glucuronyltransferase.

Another recently identified metabolite is 7-ethyl-10-[4-N-(5-aminopentanoic acid)-1-piperidino]-carbonyloxy-camptothecin (APC). This metabolite is a weak inhibitor of KB cell growth and a poor inducer of topoisomerase I DNA-cleavable complexes (100-fold less potent than SN-38). Numerous other unidentified metabolites have been detected in bile and urine. The mean 24-hour irinotecan urinary excretion represents 17 to 25% of the administered dose. Recovery of SN-38 and its glucuronide in urine is low and represents 1 to 3% of the irinotecan dose. Cumulative biliary excretion is 25% for irinotecan, 2% for SN-38 glucuronide and about 1% for SN-38.

The pharmacokinetics of irinotecan and SN-38 are not influenced by prior exposure to the parent drug. The AUC of irinotecan and SN-38 correlate significantly with leuco-neutropenia and sometimes with the intensity of diarrhoea. Certain hepatic function parameters have been correlated negatively with irinotecan total body clearance. It was noted that most tumour responses were observed at the highest doses administered in phase I trials, which indicates a dose-response relationship with this drug. In the future, these pharmacokinetic-pharmacodynamic relationships will undoubtedly prove useful in minimising the toxicity and maximise the likelihood of tumour response in patients.

This review looks at the clinical pharmacology of irinotecan (CPT-11) with a special focus on pharmacokinetic-pharmacodynamic relationships. These relationships may prove useful in the clinical management of irinotecan, i.e. they could guide the drug administration in order to minimise toxicity and optimise the tumour response rate in patients.

1. Historical Notes

The plant alkaloid camptothecin was first isolated and characterised by Wall et al.^[1] from an Oriental tree, *Camptotheca acuminata*. The compound has shown significant antitumour activity in various experimental tumour models. However,

because of the severe toxicities encountered during the early clinical development of camptothecin, administered as the soluble sodium salt (thus as the carboxylate or inactive form), this compound was not developed further.^[2-4] In the late 1980s the camptothecin analogues attracted renewed interest because of the identification of the enzyme DNA topoisomerase I as a cellular target of this class of drugs^[5-7] and also because of the overexpression of topoisomerase I in human colon adenocarcinoma and other malignancies.^[8,9] Novel camptothecin derivatives have, therefore, been synthesised^[3,4] including irinotecan,^[10] (fig. 1), topotecan^[11] and 9-aminocamptothecin,^[12] among the most studied so far.

2. Chemistry and Drug Administration

Irinotecan [7-ethyl-10-[4-(1-piperidino)-1-piperidino]-carbonyloxy-camptothecin] exhibits improved water solubility compared with camptothecin. It differs from camptothecin by 2 substitutions: an ethyl group at position 7 of the B ring and a 4-piperidinopiperidine group at position 10 of the A

ring (fig. 1). Ring E containing the lactone, and the α -hydroxyl group at position 20, are both essential for the stabilisation of topoisomerase I-DNA adducts.^[6,13] The camptothecins undergo a reversible pH-dependent hydrolysis of the E ring lactone which yields a carboxylate form (or, α,β -dihydroxycarboxylic acid). Only the closed lactone form, which predominates in an acidic environment, is considered active.

Irinotecan is a yellow crystalline powder, soluble in water and glacial acetic acid, partially soluble in chloroform and slightly soluble in methanol. The molecular weight of the hydrochloride trihydrate salt is 677 (free base: 587). The formulation usually consists of D-sorbitol, lactic acid and sodium hydroxide for pH = 3.5. The solution for intravenous administration is presented in 2 or 5ml vials containing 40 or 100mg of the drug, respectively. The required dose is further diluted in 250ml of 0.9% sodium chloride in water, or 5% dextrose in water, and administered as an intravenous infusion. The diluted solution is stable for 12 hours at 15 to 20°C, or 4 days at 2 to 8°C.

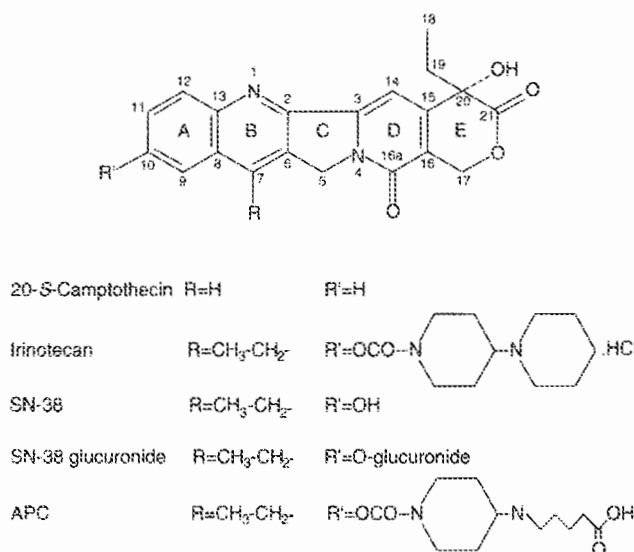


Fig. 1. Chemical structures of 20-S-camptothecin, the water-soluble analogue irinotecan (CPT-11, or 7-ethyl-10-[4-(1-piperidino)-1-piperidino]-carbonyloxy-camptothecin) and its metabolites, SN-38 (7-ethyl-10-hydroxy-camptothecin), SN-38 glucuronide and APC (7-ethyl-10-[4-N-(5-aminopentanoic acid)-1-piperidino]carbonyloxy-camptothecin).

3. Mechanism of Action

Irinotecan, and its more cytotoxic metabolite SN-38 (7-ethyl-10-hydroxy-camptothecin) [fig. 1], interfere with mammalian DNA topoisomerase I in a fashion similar to camptothecin.^[5,7] Cell death appears to result from the DNA strand breaks caused by the formation of cleavable complexes.^[5,14-16] Although the intracellular role of SN-38 appears determinant for irinotecan activity,^[17,18] a study has shown that the sensitivity of human colon cancer cells is mostly determined by topoisomerase I activity and not by carboxylesterase activity needed to produce SN-38.^[19] In addition, irinotecan-induced apoptosis appears to require the presence of both the cytoplasm and the nucleus.^[20] Resistance to the camptothecins involves decreased activity of the target enzyme DNA-topoisomerase I^[21-24] and/or mutation of the enzyme with decreased binding of the drug.^[25]

Although some correlation is observed between camptothecin-induced topoisomerase I-cleavable complexes and growth inhibition in certain colon carcinoma cell lines, other cell lines display marked growth inhibition difference with minimal differences in cleavable complexes and S-phase fraction, which suggest that other parameters downstream from the cleavable complexes are also critical for camptothecin cytotoxicity.^[26] The lack of cross-resistance of the camptothecins with drugs affected by the multidrug resistance phenotype appears as a major asset of this class of drug.^[27]

Irinotecan is frequently referred to as a prodrug because: (i) its metabolite, SN-38, has a cytotoxic activity which is 100- to 1000-fold greater than that of the parent compound *in vitro*;^[17,18,23] (ii) and the SN-38 concentrations required to cause topoisomerase I inhibition and DNA-single strand breaks are >250 times those of irinotecan.^[17] Whether or not irinotecan is simply the prodrug of SN-38, however, does not seem as simple as it first appears, since *in vitro* data have shown that irinotecan possesses its own growth inhibitory properties.^[28]

It was recently demonstrated that the 4-piperidinopiperidine leaving group during the hydrolysis of irinotecan to SN-38 is itself involved in

irinotecan cytotoxicity.^[29] Also, the sensitivity of human tumour xenografts *in vivo* appears independent of their *in vitro* production of SN-38.^[30] In addition, cellular carboxylesterase activity that yield SN-38 does not relate to irinotecan sensitivity.^[19] Moreover, *in vivo* data have shown that at maximum tolerated doses, irinotecan administration is more effective against human tumour xenografts in nude mice than SN-38 administration.^[30]

Another observation showing that irinotecan is solid tumour selective *in vitro*, compared with SN-38 which is equally toxic toward tumour cells and bone marrow cells, would also suggest that the parent compound is an active compound by itself.^[31] The above observations suggest that irinotecan itself plays a role in the antitumour activity and should not be considered as only the prodrug of SN-38.

4. Preclinical Activity

In vitro, irinotecan displays slight cytotoxic activity with an inhibitory concentrations for 50% of tumour cells (IC₅₀) ranging from 1.6 to 24 mg/L in murine P388 leukaemia cells and a number of human tumour cell lines of various tissue origin (breast, stomach, lung, colon, epidermoid carcinoma and leukaemia). As mentioned in section 3, the metabolite SN-38 is 100- to 1000-fold more cytotoxic than the parent compound with IC₅₀ values ranging from 2 to 14 µg/L.^[31] Cytotoxicity *in vitro* is time-dependent.

In animal models, irinotecan presents a good antitumour activity against various experimental tumour models of mouse or human origins, following intravenous, intraperitoneal and oral administration.^[10,30,31-34] Of particular importance, irinotecan has demonstrated remarkable activity against neuroblastomas, neuroectodermal and central nervous system tumour xenografts.^[34-37] In addition, irinotecan was found active against pleiotropic drug-resistant tumours and tumours resistant to another camptothecin analogue.^[34,38]

Table I. Summary of the phase I studies of irinotecan

Schedule	Dose	n	Dose-limiting toxicities	MTD (mg/m ²)	Phase II recommended dose	Dose intensity (mg/m ² /wk)	Reference
90 min IV weekly × 4wk q 6wk	50-180 mg/m ² /wk	32	Diarrhoea	150	150 mg/m ² /wk	100	42
90 min IV q 3wk	100-345 mg/m ²	32	Diarrhoea, neutropenia	240	240 mg/m ² /3wk	80	43
30 min IV weekly	50-150 mg/m ² /wk	17	Diarrhoea, neutropenia	100	100 mg/m ² /wk	100	40
30 min IV daily × 3d q 3wk	33-115 mg/m ²	46	Diarrhoea, neutropenia	115	100 mg/m ² /d	100	44
30-90 min IV weekly × 3wk q 4-5wk	50-145 mg/m ² /wk	59	Diarrhoea	145	115 mg/m ² /wk	69	45
30 min IV q 3wk ^a	100-750 mg/m ²	64	Neutropenia	600	350 mg/m ² /3wk	116	46
5d CIV q 3wk	5-40 mg/m ² /d	36	Diarrhoea	30	30 mg/m ² /d	50	41

a Use of high-dose loperamide to control diarrhoea.

Abbreviations: CIV = continuous intravenous infusion; d = day(s); IV = intravenous; MTD = maximum tolerated dose; n = number of patients; q = every; wk = week(s).

5. Clinical Toxicity and Anticancer Activity

5.1 Toxicity

Irinotecan phase I studies conducted in Japan,^[39-41] France and the US have explored various schedules of administration that ranged from 30-minute intravenous infusions for 3 days every 3 weeks to a 120-hour continuous intravenous infusion every 3 weeks (table I).^[40-46] The principal dose-limiting toxicities were delayed diarrhoea and neutropenia, which were non-cumulative, reversible and dose-related. Other adverse effects included an acute cholinergic syndrome during drug administration,^[47] nausea, vomiting and alopecia. Also frequently reported were weakness and asthenia which appeared dose-related.

The phase II recommended doses were 240 to 350 mg/m² every 3 weeks, 100 to 150 mg/m²/week every 3 to 5 weeks for the weekly schedule, and 30 mg/m² when administered as a continuous 5-day intravenous infusion every 3 weeks (table I). A recent feasibility study of higher dose-intensity administration of irinotecan has demonstrated that 500 mg/m² can be administered in good-risk and carefully monitored patients.^[48]

Differences in recommended doses between phase II studies can partly be explained by the ef-

fective control of diarrhoea with high dose loperamide administration in the Gustave-Roussy Institute study,^[46] which allowed the administration of higher irinotecan doses. Preclinical and clinical studies aiming at effectively controlling this adverse effect are ongoing.^[49-51]

5.2 Anticancer Activity

Early in phase I studies, irinotecan displayed some activity in various disease locations including colorectal, lung and cervical cancers.^[39-46] Also of importance, most investigators noted activity at the higher dosages administered, which is indicative of a dose-response relationship with this drug.

In phase II studies, irinotecan has demonstrated antitumour activity (partial and complete responses) in many cancer types^[52,53] including: colorectum,^[54-59] lung,^[60-62] cervix,^[63-65] pancreas,^[66,67] stomach^[68] and breast cancers.^[69,70] Activity has also been reported in leukaemias and lymphomas^[71,72] (table II).

6. Pharmacokinetics

6.1 Analysis in Biological Materials

High performance liquid chromatography methods are available to assay irinotecan and its metabolites in biological materials. All the assays ap-

Table II. Summary of the anticancer activity observed in early phase II irinotecan studies

Cancer type	n	Dose and schedule	Response rate (%)	References
Colorectal	178	350 mg/m ² /3wk	19	54
Colorectal	160	=125 mg/m ² /wk × 4	15-27	55-58
Colorectal	213	350 mg/m ² /3wk	18	59
Lung (NSCLC)	73	100 mg/m ² /wk	32	60
Lung (SCLC)	16	100 mg/m ² /wk	47	62
Cervical	40	350 mg/m ² /3wk	15-23	63
Cervical	55	125 mg/m ² /wk × 4	0-23	64, 65
Leukaemia/lymphoma	62	40 mg/m ² /d × 5 q 3-4wk	17-24	71
Leukaemia/lymphoma	13	40 mg/m ² /d × 3 q wk	38	72
Pancreas	35	100-150 mg/m ² /1-2wk	10	66
Pancreas	32	350 mg/m ² /3wk	9	67
Stomach	60	100-150 mg/m ² /1-2wk	23	68
Breast	29	350 mg/m ² /3wk	8	69
Breast	65	100-150 mg/m ² /1-2wk 200 mg/m ² /3-4 wk	14-20	70

Abbreviation: d = day(s); n = number of patients; NSCLC = non-small-cell lung cancer; q = every; SCLC = small-cell lung cancer; wk = week(s).

pear highly reproducible and sensitive. Depending on the specific needs of a particular experimental or clinical study it is possible to assay separately total irinotecan or SN-38 (i.e. carboxylate plus lactone forms)^[73] or simultaneously determine total irinotecan and SN-38.^[74] The simultaneous determination of the carboxylate and lactone forms of either compound was also reported.^[75-78] Monitoring of total irinotecan and SN-38 appears to essentially have the same clinical significance as the monitoring of the lactone form of either compound,^[79,80] since the fraction of lactone to total (i.e. lactone + carboxylate) is constant between patients.^[79,81]

6.2 Metabolism

Irinotecan is extensively metabolised in human liver to various metabolites. The bipiperidino-carbonylxy group of irinotecan is first removed by hydrolysis to yield the corresponding carboxylic acid and SN-38 (molecular weight 392) by a carboxylesterase (fig. 1).^[82,83] Liver carboxylesterases from several species have been compared and the human enzyme is among the least efficient at catalysing the biotransformation of irinotecan to SN-38.^[83]

Although purified human liver carboxylesterase can metabolise irinotecan to SN-38, the production is relatively inefficient and is enzyme deacylation rate-limited with a steady-state phase occurring after 15 to 20 minutes of incubation.^[84] The later phase follows Michaelis-Menten kinetics with an apparent K_m of 52.9 $\mu\text{mol/L}$ and a specific activity of 200 $\mu\text{mol/sec/mol}$.^[84] Although this de-esterification reaction can also take place in murine plasma, human plasma does not contain the carboxylesterase needed to achieve the formation of SN-38.

This carboxylesterase does not appear to be influenced by pretreatment with irinotecan, which implies that neither induction nor repression of this enzymatic system appears to take place after repeated administrations.^[85] This is of clinical importance since a change in irinotecan or SN-38 pharmacokinetics is not likely to occur as a function of rechallenge with the parent compound. Also of importance, this enzymatic system is not saturated at high doses, as shown by the proportional increase in SN-38 area under the concentration-time curve (AUC) and by the stability of the percentage of metabolite production in both plasma and urine.^[85] The metabolic ratio (percentage SN-38 AUC/irinotecan AUC) represents a mean value of 3% of the parent compound AUC.

Although loperamide, which can be used to alleviate irinotecan-induced diarrhoea, can interfere with the hydrolysis of the parent drug to SN-38 *in vitro*, it is unlikely to greatly influence the production of SN-38 *in vivo* since it is given at least 8 hours following irinotecan administration.^[84]

SN-38 can be further converted into SN-38 glucuronide (SN-38G) by hepatic UDP-glucuronyl-transferase^[86,87] (fig. 1). Compared with SN-38, SN-38G plasma concentrations are relatively high and this metabolite could be involved in the pharmacodynamics of the drug, e.g. in terms of intestinal toxicity,^[88] or in terms of exposure to the active metabolite SN-38 which will be excreted more or less rapidly, depending of the rate of formation of its glucuronide.

Another major metabolite of irinotecan is 7-ethyl-10-[4-N-(5-aminopentanoic acid)-1-piperidino]carbonyloxy-camptothecin (APC; molecular weight 618) which is the result of 2 oxidations, probably by a cytochrome P450 (CYP)^[89,90] (fig. 1). The metabolite APC is a weak inhibitor of KB cells growth and a poor-inducer of topoisomerase I DNA-cleavable complexes (100-fold less potent than SN-38).^[89] This metabolite is not further metabolised to SN-38.^[89]

Several other metabolites remain to be identified in humans, since at least 16 metabolites are detectable in human bile of which 8 are also found in urine.^[90] In addition to the above mentioned metabolites, other metabolites have been found:

- single oxidation of the terminal piperidine ring of irinotecan side chain, which eventually results in the formation of a primary amine
- oxidation of the camptothecin nucleus
- decarboxylation of irinotecan carboxylate form
- several metabolites resulting from combinations of these pathways.^[90]

Although the role of mono-oxygenases (probably the cytochrome P450) in irinotecan metabolism remains to be firmly established, it is likely to be based on the above mentioned information.^[89,90]

The high interpatient variability in the pharmacokinetics of irinotecan and SN-38 (details presented

below) could be due to pharmacogenetic factors, to induction or repression of certain metabolic routes or to variability in transport systems. Further knowledge of the metabolic routes of irinotecan will undoubtedly lead to a better understanding of the interindividual variability in pharmacokinetics and the pharmacodynamics of this compound.

6.3 Pharmacokinetics of Irinotecan

Upon administration of irinotecan at phase II recommended doses of 100 mg/m² (daily times 3 every 3 weeks; or weekly times 3 every 3 weeks) and 350 mg/m² (once every 3 weeks), the mean maximum irinotecan plasma concentrations achieved were within 2 and 10 mg/L (fig. 2) which is within the cytotoxic concentrations necessary to kill cancer cells *in vitro*. For example, the 50% growth inhibition concentration values for KB and L1210 cells are 1.1 and 5.5 mg/L, respectively.^[73]

It is of interest to note that the maximum plasma concentrations of irinotecan and AUCs previously observed in the mouse model^[33,73] at the highest nontoxic dosages are similar to the values obtained in humans at near toxic dosages.^[41-46,85,91,92] Rebound concentrations of irinotecan are frequently observed at about 30 minutes to 1 hour following

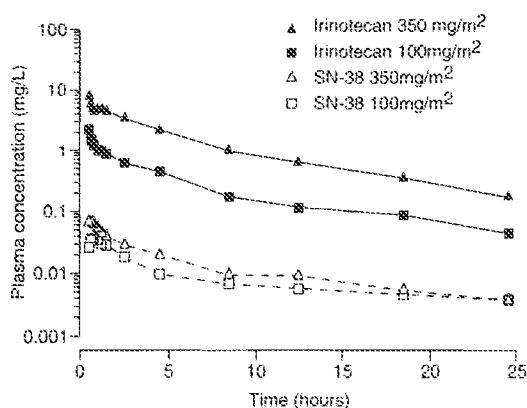


Fig. 2. Irinotecan mean plasma concentrations in patients^[85] at the phase II recommended doses of 350 mg/m² (once every 3 weeks) and 100 mg/m² (daily for 3 days every 3 weeks, or 3 times weekly every 3 weeks) in a 30-minute intravenous infusion.

Table III. Summary of the clinical pharmacokinetic of irinotecan and SN-38

Infusion time	n	irinotecan			SN-38	Reference
		$t_{1/2}$ (h)	CL (L/h/m ²)	V _{ss} (L/m ²)	$t_{1/2}$ (h)	
30 min	21	8.3	14.3	141	10.2	44
30 min	60	14.2	15	157	13.8	46
30-90 min	26	9.3	15	142	7.7	45
30 min	107	10.8	14.3	150	10.6	85
90 min	17	7.9	15.3		13.1	42
90 min	31	5.2	21.1 ^a	148	5.9	43
90 min	10	11.4	16.8	255	22.3	91
90 min	13	14.2	11.6	214	22.1	92
90 min	40	8.8	14.6	136	11.6	101
120h	24	27	7.9 ^b		30	41

a Converted to L/h/m².

b Average recalculated CL from the total dose (daily dose x 5, mg/m²) divided by the AUC, so as to obtain a value in L/h/m².

Abbreviations: CL = total body clearance; n = number of patients; $t_{1/2}$ = terminal half-life; V_{ss} = volume of distribution at steady-state.

the end of a short intravenous infusion, this suggests enterohepatic recycling of the drug. Following a short intravenous administration (30 to 90 minutes), the plasma concentrations can be described using a 2- or 3-compartment model with a mean terminal half-life ranging from 5 to 14 hours (table III).^[41-46,85,91,92] The total body clearance (CL) ranges from 12 to 17 L/h/m², and the volume of distribution at steady-state (V_{ss}) ranges from 141 to 255 L/m² (table III). When irinotecan is administered as a short intravenous infusion (30 to 90 minutes) at doses ranging from 33 to 750 mg/m², the AUC increases proportionally to the administered dose, indicating linear pharmacokinetics, although the interpatient variability is important.^[85]

The long disposition half-life of irinotecan could be of therapeutic advantage for this S-phase specific drug, not only by allowing a prolonged exposure time for tumour cells, but also by the combined effect of metabolic production of protracted cytotoxic concentrations of the metabolite SN-38.

6.4 Pharmacokinetics of SN-38

Since SN-38 is 100- to 1000-fold more potent *in vitro* than irinotecan, the pharmacokinetics of this important metabolite was determined early at the preclinical and clinical development of irino-

tecan. Although the metabolite SN-38 levels achieved in humans are about 100-fold lower than corresponding irinotecan concentrations (fig. 2), these SN-38 plasma levels are, however, well above the IC₅₀ values reported for KB and L1210 cells (0.37 and 3.6 µg/L, respectively) in preclinical studies.^[73]

It is also of interest that the maximum concentrations of SN-38 achieved in the mouse^[33,73] are about 20 times higher than in humans, which indicates that the mouse model metabolises irinotecan to a greater extent than humans. In humans, time to the maximum drug concentration (t_{max}) of SN-38 is reached at about 1 hour after the beginning of a short 30-minute intravenous infusion. The plasma decay of SN-38 follows closely that of the parent compound with an apparent terminal half-life of 6 to 22 hours (table III). As with the parent compound, SN-38 presents rebound concentrations at about 1 hour following the end of a short intravenous infusion which probably indicates enterohepatic recycling because SN-38 concentrations achieved in the bile are elevated. Since the AUC of SN-38 increases proportionally with the irinotecan dose,^[85] it obviously implies that higher irinotecan doses are more likely to elicit an antitumoural response given the high activity of the metabolite.

6.5 Pharmacokinetics of SN-38 Glucuronide

SN-38 is extensively glucuronidated to SN-38 glucuronide (SN-38G) and the plasma concentrations of this metabolite are higher than that of SN-38 since the AUC ratio of SN-38G/SN-38 is about 6.5 for the dose level of 350 mg/m².^[93] Saturation of glucuronidation may occur at weekly administration of 175 mg/m².^[88] The disposition profile of SN-38G follows closely the profiles of SN-38 and irinotecan with similar plasma concentration decay curves.^[94] The human UDP-glucuronosyltransferase isozyme responsible for SN-38 glucuronidation is the UGT isoform 1.1.^[95]

6.6 Pharmacokinetics of the Metabolite APC

The metabolite APC (7-ethyl-10-[4-N-(5-aminopentanoic acid)-1-piperidino]carbonyloxy-camptothecin)^[89] presents high plasma concentrations with a peak concentration at about 2 hours after the end of the infusion. APC concentrations are usually intermediate between those of irinotecan and SN-38G, and may even reach higher concentrations than the parent compound in some patients.^[94] Disposition curves of APC are similar to those of irinotecan.^[94]

6.7 Interconversion of Lactone and Carboxylate Forms *In Vivo*

Since only the lactone form of the camptothecins is thought to be active at their target topoisomerase I, the *in vivo* interconversion of the carboxylate and lactone forms of both irinotecan and SN-38 has been studied in patients.^[79,81] In human plasma, the ratio of irinotecan lactone to total irinotecan concentration is highest (66%) just after the end of infusion and gradually decreases to an equilibrium of 25 to 30% at 24 hours after the infusion. The metabolite SN-38 is 70 to 80% in its lactone form after the end of infusion and decreases to an equilibrium of 50 to 64% within 24 hours.^[79,81]

6.8 Protein Binding

At equilibrium, irinotecan is bound to plasma proteins *in vitro* to an extent of about 65% whereas SN-38 is bound to about 95%.^[96] The lactone form of irinotecan and SN-38 is more stable in the presence of human serum albumin.^[97] The stability of the irinotecan lactone form is enhanced by albumin as shown by an increased percentage of lactone form at equilibrium (from 13% without albumin, to 21% lactone with albumin). Likewise, the SN-38 lactone form is favoured in the presence of albumin at equilibrium, since 13% is in lactone form at equilibrium without albumin, whereas in its presence, 38% is in the lactone form.^[97]

The protein binding of the carboxylate and lactone forms of irinotecan appears similar, although it is significantly different for SN-38, i.e. SN-38 binds preferentially to albumin in its lactone form^[97] which probably plays a role in the stabilisation of this molecule *in vivo*.

6.9 Absorption

Irinotecan is active when administered orally in mice.^[33,34] To date, a phase I trial using orally administered irinotecan has been performed in humans and preliminary results indeed show absorption and activity of the drug via this route, although the precise bioavailability value is not presently known.^[98]

6.10 Distribution

Preclinical studies have shown that irinotecan and SN-38 reach cytotoxic concentrations in the tumour. Indeed the tumour decay of irinotecan and SN-38 is slower than the corresponding plasma concentrations.^[33] In humans, the hepatic distribution of irinotecan and its metabolites, as assessed by biliary excretion, appears important.^[86,89,100]

6.11 Excretion

The mean 24-hour irinotecan urinary excretion represents 17 to 25% of the administered dose. The recovery of SN-38 and its glucuronide in urine is low and represents 1 to 3% of the irinotecan dose.

Cumulative biliary excretion is 25% for irinotecan, 2% for SN-38G and 1% for SN-38.^[43,85,100] A substantial portion of the administered dose is still not accounted for in excretas, but the recent detection of many other unidentified metabolites in bile and urine will allow a more complete picture of irinotecan excretion.^[90]

6.12 Pharmacokinetics of Irinotecan and SN-38 after Repeated Dosage

The pharmacokinetics of irinotecan and SN-38 are not influenced by prior exposure to the parent drug. Also, the ratio of SN-38 AUC over irinotecan AUC is not affected by course number, indicating that there is no enzyme induction nor change in distribution as a function of course number. Similarly, and in agreement with plasma pharmacokinetics, urinary excretion of either compound is not significantly affected by course number.^[85]

6.13 Influence of Physiopathological Conditions on Pharmacokinetics

Since the characteristics of cancer patients may influence markedly the disposition of certain anticancer drugs,^[100] the possible influence of several patient characteristics on either irinotecan clearance or the metabolic ratio have been examined (percentage SN-38 AUC/irinotecan AUC).^[85] No relationship between CL nor the metabolic ratio, with the following physiological factors, has been found: age, height, bodyweight, body surface, race or gender.^[85,101]

Renal function (creatininaemia) does not influence irinotecan CL nor the metabolic ratio. Interestingly, certain hepatic function parameters have been correlated negatively with irinotecan CL, e.g. bilirubinaemia and γ -glutamyl transpeptidase.^[85] Also noteworthy, a significant positive correlation between the metabolic ratio (percentage SN-38 AUC/irinotecan AUC) and some liver function parameters were observed, e.g. bilirubinaemia, aspartate transferase (AST, formerly SGOT) and alanine transferase (ALT, formerly SGPT).^[85] The above observations are not only indicative of the hepatic metabolism of this drug, but they may

eventually lead to clinical dose adjustment based on hepatic function markers, obviously when more data are available to substantiate and extend these observations.

The increase in the metabolic ratio (percentage SN-38 AUC/irinotecan AUC) when certain hepatic function markers are high could be due to a low clearance value of irinotecan leading to a higher metabolic conversion due to a longer availability of the parent compound to the enzyme system involved in the SN-38 formation.

6.14 Influence of Cotreatments on the Pharmacokinetics of Irinotecan

Although irinotecan may be administered with drugs used to alleviate its adverse effects (e.g. diarrhoea and nausea/vomiting) or with other anticancer drugs to increase its anticancer efficacy [e.g. fluorouracil (5-fluorouracil), cisplatin and analogues, etoposide and taxoids], little is known about the possible clinical pharmacokinetic interactions.

To date, preclinical studies have indicated some potential drug interactions. In rats, the combination of irinotecan with valproic acid (valproate sodium), an inhibitor of glucuronidation, almost completely blocks the glucuronidation of SN-38 with a concomitant increase in SN-38 AUC, whereas irinotecan kinetics is unchanged.^[102] Phenobarbital pretreatment that induces UDP-glucuronosyltransferase activity leads to an increase in SN-38G AUC and also a reduction in both SN-38 and irinotecan AUCs.^[102] Cyclosporin can reduce the systemic clearance of irinotecan due to lowered biliary excretion in rats.^[103]

Drugs that may be used in combination with irinotecan were studied *in vitro* with regard to their potential interference with glucuronidation of SN-38 using human hepatic microsomes: of the various drugs studied, only morphine, paracetamol (acetaminophen) and loperamide caused a slight inhibition whereas no inhibition was observed with the other drugs tested [the antibiotic drugs amikacin, cotrimoxazole (trimethoprim/sulfamethoxazole), ciprofloxacin, rocephin and troleandomycin; the antineoplastic agent fluorouracil; antiemetic drugs

metoclopramide and ondansetron; or the anti-diarrhoeic drug acetorphan).^[87] Although these preclinical data may not be exactly transferable to the human situation, extra care should be taken in combining drugs that have shown interference with irinotecan.

In clinical studies, the interaction between irinotecan and fluorouracil is still controversial, as fluorouracil appeared to increase irinotecan AUC and decrease SN-38 AUC in 1 study,^[104] whereas other studies do not show such interaction.^[105,106] Irinotecan combined with etoposide is active in lung cancer^[92] and a drug interaction with this drug has been suggested.^[107] The combination of docetaxel and irinotecan does not lead to changes in the pharmacokinetics of both drugs and SN-38.^[108]

The combination of irinotecan with the platinum analogue oxaliplatin (LOHP) does not alter either drug pharmacokinetics (F. Lokiec, personal communication).

7. Pharmacokinetic-Pharmacodynamic Relationships

As already mentioned, monitoring of total irinotecan and SN-38 has essentially the same clinical significance as monitoring the lactone form of either compound,^[79,80] when pharmacokinetic-pharmacodynamic relationships are examined in clinical trials. In fact, since the fraction of lactone to total AUC appears to be constant between patients,^[79,81] monitoring the total form is probably a simpler alternative because it is more practical to assay in a clinical setting.

7.1 Toxicities

The relationships between certain pharmacokinetic parameters and the principal toxicities of irinotecan have been reported. Irinotecan AUC correlates significantly with the percentage decrease in white blood cells, and also with the decrease in neutrophils.^[42-46,85,92,93] In most studies, the more cytotoxic SN-38 AUC is also significantly correlated with the percentage decrease in white blood cells and neutrophils.^[41,43,85,93]

Inconsistent relationships have been reported between irinotecan AUC and the intensity of gastrointestinal toxicity (diarrhoea, nausea and vomiting). Those discrepancies may be due to the different patient populations studied, the number of patients included in studies and also the inherent difficulties in precisely measuring and grading these toxicities. The severity of diarrhoea is correlated in some studies with the peak plasma concentrations of SN-38^[109] and the AUC.^[85,109]

Other studies indicate a correlation of SN-38 glucuronidation and diarrhoea.^[88,101] To assess the relationship between gastrointestinal toxicity and the pharmacokinetics of irinotecan and its metabolites (SN-38 and its glucuronide), Gupta et al.^[88] have defined a biliary index of SN-38 which is the product of the relative area ratio of SN-38 to SN-38G, and the total AUC of irinotecan. Using this approach, higher biliary indices are observed in patients with most severe diarrhoea. The relatively higher index values are suggestive of higher biliary concentrations of SN-38 and are possibly due to low glucuronidation rates.^[88,101] This approach may be a useful pharmacokinetic tool in identifying patients likely to display severe diarrhoea.

7.2 Antitumoural Responses

It is worth noting that most tumour responses are observed at the highest doses administered in phase I and II trials, which indicates a dose-response relationship with this drug.^[48,85] This strongly suggests that high exposure (AUC) to this compound and its metabolite, is more likely to produce an antitumour effect. Therefore, any strategy aimed at controlling or alleviating irinotecan-related dose-limiting toxicities that would allow a higher dose to be administered, is likely to play a favourable role in the clinical antitumour activity of this compound. For example, irinotecan-induced neutropenia could be alleviated by the administration of recombinant human granulocyte colony-stimulating factor (rhG-CSF).^[92] In addition, the clinical management of diarrhoea not only appears feasible, but could allow higher doses of irinotecan to be administered.^[46,49,110] Ongoing phase II and

III trials will undoubtedly better define the relationships between irinotecan and/or SN-38 pharmacokinetics and anticancer activity with a more defined patient population, and also with optimal dosage and schedule.

8. Conclusions and Perspectives

The data reviewed here indicate that the pharmacokinetics of irinotecan are linear over a wide dose range (33 to 750 mg/m²), that the number of courses do not influence pharmacokinetics and that liver function appears to affect irinotecan clearance. Also of interest, the intensity of the major irinotecan-related toxicities (e.g. leuco-neutropenia and diarrhoea) correlate with irinotecan and SN-38 exposure. With regard to anticancer activity, it was also observed that the higher irinotecan doses produced tumour responses, which may indicate a dose-response relationship.

Future clinical trials aimed at further defining the pharmacokinetic-pharmacodynamic relationships may benefit from limited-sampling strategy^[110-114] which could allow the conduct of such studies with a minimal burden to the patient, the clinical and laboratory personnel. Moreover, the elucidation of major irinotecan metabolic pathways may lead to a better understanding of the mechanism of anticancer action and toxicity of this active drug. These pharmacokinetic-pharmacodynamic relationships will undoubtedly prove useful in the clinical management of this drug in order to minimise toxicity and maximise the likelihood of tumour response in patients.

Acknowledgements

I would like to thank all the clinical and laboratory personnel who contributed to the studies referred to in this review article. The following organisations made these studies possible: the Institut National de la Santé et de la Recherche Médicale (INSERM, Paris, France), the Centre National de la Recherche Scientifique (CNRS, Paris, France), Rhône-Poulenc Rorer Laboratories, S.A. (Antony, France) and the Association pour la Recherche sur le Cancer (Villejuif, France).

References

1. Wall ME, Wani MC, Cook CE, et al. Plant antitumor agents I. The isolation and structure of camptothecin, a novel alkaloidal leukemia and tumor inhibitor from *Camptotheca acuminata*. *J Am Chem Soc* 1966; 88: 3888-90
2. Potmesil M. Camptothecins: from bench research to hospital wards. *Cancer Res* 1994; 54: 1431-9
3. Wall ME, Wani MC. Camptothecin and analogs: from discovery to clinic. In: Potmesil M, Pineto H, editors. *Camptothecins: new anticancer agents*. Boca Raton (FL): CRC Press, Inc., 1995: 21-41
4. Wall ME, Wani MC. Camptothecin: discovery to clinic. *Ann N Y Acad Sci* 1996; 803: 1-12
5. Hsiang YH, Liu LF. Identification of mammalian DNA topoisomerase I as an intracellular target of the anticancer drug camptothecin. *Cancer Res* 1988; 48: 1722-6
6. Jaxel C, Kohn K, Wani MC, et al. Structure-activity study of the actions of camptothecin derivatives on mammalian topoisomerase I. Evidence for a specific receptor site and for a relation to antitumor activity. *Cancer Res* 1989; 49: 1465-9
7. Hsiang YH, Liu LF, Wall ME, et al. DNA topoisomerase I mediated DNA cleavage and cytotoxicity of camptothecin analogues. *Cancer Res* 1989; 49: 4835-9
8. Giovaneila BC, Stehlin JS, Wall ME, et al. DNA topoisomerase I-targeted chemotherapy of human colon cancer in xenografts. *Science* 1989; 246: 1046-8
9. Potmesil M, Hsiang YH, Liu LF, et al. Resistance of human leukemic and normal lymphocytes to drug-induced DNA cleavage and low levels of DNA topoisomerase II. *Cancer Res* 1988; 48: 3537-43
10. Kunimoto T, Nitta K, Tanaka T, et al. Antitumor activity of 7-ethyl-10-[4-(1-piperidino)-1-piperidino]-carbonyloxy-camptothecin, a novel water-soluble derivative of camptothecin, against murine tumors. *Cancer Res* 1987; 47: 5944-7
11. Kingsbury WD, Boehm JC, Jakas DR, et al. Synthesis of water-soluble (aminoalkyl) camptothecin analogues: inhibition of topoisomerase I and antitumor activity. *J Med Chem* 1991; 34: 98-107
12. Wani MC, Nicholas AW, Wall ME. Plant antitumor agents: 23. Synthesis and antileukemic activity of camptothecin analogues. *J Med Chem* 1986; 29: 2358-63
13. Hertzberg RP, Caranfa MJ, Hecht S. On the mechanism of topoisomerase I inhibition by camptothecin: evidence for binding to an enzyme-DNA complex. *Biochemistry* 1989; 28: 4629-38
14. Kessel D, Bosmann HB, Lohr K. Camptothecin effects on DNA synthesis in murine leukemia cells. *Biochem Biophys Acta* 1972; 269: 210-6
15. Wang JC. DNA topoisomerases. *Annu Rev Biochem* 1985; 54: 665-97
16. Liu LF. DNA topoisomerase poisons as antitumor drugs. *Annu Rev Biochem* 1989; 58: 351-75
17. Kawato Y, Aonuma M, Hirota Y, et al. Intracellular roles of SN-38, a metabolite of the camptothecin derivative, CPT-11, in the antitumor effect of CPT-11. *Cancer Res* 1991; 51: 4187-91
18. Ogasawara H, Nishio K, Kanzawa F, et al. Intracellular carboxylesterase activity is a determinant of cellular sensitivity to the antineoplastic agent KW-2189 in cell lines resistant to cisplatin and CPT-11. *Jpn J Cancer Res* 1995; 86: 124-9
19. Jansen WJ, Zwaer B, Huischer ST, et al. CPT-11 in human colon cancer cell lines and xenografts: characterization of cellular sensitivity determinants. *Int J Cancer* 1997; 70: 335-40

20. Suzuki A, Kato M. Chemotherapeutic agent CPT-11 induces the new expression of the apoptosis initiator to the cytoplasm. *Exp Cell Res* 1996; 227: 154-9
21. Woessner RD, Eng WK, Hofmann FA, et al. Camptothecin hyper-resistant P388 cells: drug-dependent reduction in topoisomerase I content. *Oncol Res* 1992; 4: 481-8
22. Gupta RS, Gupta R, Eng B, et al. Camptothecin-resistant mutants of chinese hamster ovary cells containing a resistant form of topoisomerase I. *Cancer Res* 1988; 48: 6404-10
23. Kanzawa F, Sugimoto Y, Minato K, et al. Establishment of a camptothecin analogue (CPT-11)-resistant cell line of human small cell lung cancer: characterization and mechanism of resistance. *Cancer Res* 1990; 50: 5919-24
24. Sugimoto Y, Tsukahara S, Oh-Hara T, et al. Decreased expression of DNA topoisomerase I in camptothecin-resistant tumor cell lines as determined by a monoclonal antibody. *Cancer Res* 1990; 50: 6925-30
25. Tamura H, Kohchi C, Yamada R. Molecular cloning of a cDNA of a camptothecin-resistant human DNA topoisomerase I and identification of mutation sites. *Nucleic Acids Res* 1991; 51: 1129-36
26. Goldwasser F, Bae I, Valenti M, et al. Topoisomerase I-related parameters and camptothecin activity in the colon carcinoma cell lines from the National Cancer Institute anticancer screen. *Cancer Res* 1995; 55: 2116-21
27. Chen AY, Yu C, Potmesil M, et al. Camptothecin overcomes MDR1-mediated resistance in human KB carcinoma cells. *Cancer Res* 1991; 51: 6039-44
28. Takeda S, Shimazoe T, Kuga H, et al. Camptothecin analog (CPT-11)-sensitive human pancreatic tumor cell line QGP-1N shows resistance to SN-38, an active metabolite of CPT-11. *Biochem Biophys Res Commun* 1992; 188: 70-7
29. Onishi Y, Oguro M, Kizaki H. A lymphoma cell line resistant to 4-piperidinopiperidine was less sensitive to CPT-11. *Cancer Chemother Pharmacol* 1997; 39: 473-8
30. Kawato Y, Furuta T, Aonuma M, et al. Antitumor activity of a camptothecin derivative, CPT-11, against human tumor xenografts in nude mice. *Cancer Chemother Pharmacol* 1991; 28: 192-8
31. Bissery MC, Vignaud F, Lavelle F, et al. Experimental antitumor activity and pharmacokinetics of the camptothecin analog irinotecan (CPT-11) in mice. *Anti-Cancer Drugs* 1996; 7: 437-60
32. Tanizawa A, Fujimori A, Fujimori Y, et al. Comparison of topoisomerase I inhibition, DNA damage, and cytotoxicity of camptothecin derivatives presently in clinical trials. *J Natl Cancer Inst* 1994; 86: 836-42
33. Lavelle F, Bissery MC, André S, et al. Preclinical evaluation of CPT-11 and its active metabolite SN-38. *Semin Oncol* 1996; 3 (1 Suppl.): 11-20
34. Houghton PJ, Cheshire PJ, Hallman JC, et al. Therapeutic efficacy of the topoisomerase I inhibitor 7-ethyl-10-(4-[1-piperidino]-1-piperidino)-carbonyloxy-camptothecin against human tumor xenografts: lack of cross-resistance *in vivo* in tumors with acquired resistance to the topoisomerase I inhibitor 9-dimethylaminomethyl-10-hydroxycamptothecin. *Cancer Res* 1993; 53: 2823-9
35. Vassal G, Terrier-Lacombe MJ, Bissery MC, et al. Therapeutic activity of CPT-11, a DNA-topoisomerase I inhibitor, against peripheral primitive neuroectodermal tumour and neuroblastoma xenografts. *Br J Cancer* 1996; 74: 537-45
36. Komuro R, Li P, Tsuchida Y, et al. Effects of CPT-11 (a unique DNA topoisomerase I inhibitor) on a highly malignant xenotransplanted neuroblastoma. *Med Pediatr Oncol* 1994; 23: 487-92
37. Hare CB, Eliou GB, Houghton PJ, et al. Therapeutic efficacy of the topoisomerase I inhibitor 7-ethyl-10-(4-[1-piperidino]-1-piperidino)-carbonyloxy-camptothecin against pediatric and adult central nervous system tumor xenografts. *Cancer Chemother Pharmacol* 1997; 38: 187-91
38. Tsuruo T, Matsuzaki T, Matsushita M, et al. Antitumor effect of CPT-11, a new derivative of camptothecin, against pleiotropic drug-resistant tumors *in vitro* and *in vivo*. *Cancer Chemother Pharmacol* 1988; 21: 71-4
39. Taguchi T, Wakui A, Hasegawa K. Phase I clinical study of CPT-11; Research Group of CPT-11. *Jpn J Cancer Chemother* 1990; 17: 115-20
40. Negoro S, Fukuoka M, Masuda N, et al. Phase I study of weekly intravenous infusion of CPT-11, a new derivative of camptothecin, in the treatment of advanced non-small cell lung cancer. *J Natl Cancer Inst* 1991; 83: 1164-8
41. Ohe Y, Sasaki Y, Shinkai T, et al. Phase I study and pharmacokinetics of CPT-11 with 5-day continuous infusion. *J Natl Cancer Inst* 1992; 84: 972-4
42. Rothenberg ML, Kuhn JG, Burris III HA, et al. Phase I and pharmacokinetic trial of weekly CPT-11. *J Clin Oncol* 1993; 11: 2194-204
43. Rowinsky EK, Grochow LB, Etinger DS, et al. Phase I and pharmacological study of the novel topoisomerase I inhibitor 7-ethyl-10-[4-(1-piperidino)-1-piperidino]carbonyloxy-camptothecin (CPT-11) administered as a ninety-minute infusion every 3 weeks. *Cancer Res* 1994; 54: 427-36
44. Catimel G, Chabot GG, Guastalla JP, et al. Phase I and pharmacokinetic study of irinotecan (CPT-11) administered daily for three consecutive days every three weeks in patients with advanced solid tumors. *Ann Oncol* 1995; 6: 133-40
45. de Forni M, Bugat R, Chabot GG, et al. Phase I and pharmacokinetic study of the camptothecin derivative irinotecan administered on a weekly schedule in cancer patients. *Cancer Res* 1994; 54: 4347-54
46. Abigeres D, Chabot GG, Armand JP, et al. Phase I and pharmacologic studies of the camptothecin analog irinotecan administered every 3 weeks in cancer patients. *J Clin Oncol* 1995; 13: 210-21
47. Gandia D, Abigeres D, Armand JP, et al. CPT-11-Induced cholinergic effects in cancer patients [letter]. *J Clin Oncol* 1993; 11: 196-7
48. Merrouche Y, Extra JM, Abigeres D, et al. High dose-intensity of irinotecan administered every 3 weeks in advanced cancer patients: a feasibility study. *J Clin Oncol* 1997; 15: 1050-6
49. Hagipantelli R, Saliba F, Misset JL, et al. Pathophysiology and therapy of irinotecan (CPT-11) induced delayed onset diarrhoea: a prospective assessment [abstract]. *Proc Am Soc Clin Oncol* 1995; 14: 464
50. Sakata Y, Suzuki H, Kamataki T. Preventive effect of TJ-14, a kampo medicine, on diarrhoea induced by irinotecan hydrochloride [in Japanese]. *Jpn J Cancer Chemother (Gan To Kagaku Ryoho)* 1994; 21: 1241-4
51. Takasuna K, Hagiwara T, Hirohashi M, et al. Involvement of -glucuronidase in intestinal microflora in the intestinal toxicity of the antitumor camptothecin derivative irinotecan hydrochloride (CPT-11) in rats. *Cancer Res* 1996; 56: 3752-7
52. Boisseau M, Guichard S, Canal P, et al. Irinotecan (CPT-11): current status and perspectives. *Expert Opin Investig Drugs* 1996; 5: 613-26
53. Rothenberg ML. CPT-11: an original spectrum of clinical activity. *Semin Oncol* 1996; 23 (1 Suppl. 3): 21-6
54. Armand JP, Ducreux M, Mahjoubi M, et al. CPT-11 (irinotecan) in the treatment of colorectal cancer. *Eur J Cancer* 1995; 31A: 1283-7

55. Shimada Y, Yoshino M, Wakui A, et al. Phase II study of CPT-11, a new camptothecin derivative, in metastatic colorectal cancer: CPT-11 Gastrointestinal Cancer Study Group. *J Clin Oncol* 1993; 11: 909-13
56. Conti JA, Kemeny NE, Saltz LB, et al. Irinotecan is an active agent in untreated patients with metastatic colorectal cancer. *J Clin Oncol* 1996; 14: 709-15
57. Shimada Y, Rougier P, Pitor H. Efficacy of CPT-11 (irinotecan) as a single agent in metastatic colorectal cancer. *Eur J Can* 1996; 3 (32A Suppl.): S13-7
58. Rothenberg ML, Eckardt JR, Burris III HA, et al. Phase II trial of irinotecan in patients with progressive or rapidly recurrent colorectal cancer. *J Clin Oncol* 1996; 14: 1128-35
59. Rougier P, Bugat R, Douillard JY, et al. Phase II study of irinotecan in the treatment of advanced colorectal cancer in chemotherapy-naïve patients and patients pretreated with fluorouracil-based chemotherapy. *J Clin Oncol* 1997; 15: 251-60
60. Fukuoka M, Nitani H, Suzuki A, et al. A phase II study of CPT-11, a new derivative of camptothecin, for previously untreated non-small cell lung cancer. *J Clin Oncol* 1992; 10: 16-20
61. Masuda N, Fukuoka M, Kusunoki Y, et al. CPT-11: a new derivative of camptothecin for the treatment of refractory or relapsed small-cell lung cancer. *J Clin Oncol* 1992; 10: 1225-9
62. Masuda N, Fukuoka M, Takada M, et al. CPT-11 in combination with cisplatin for advanced non-small-cell lung cancer. *J Clin Oncol* 1992; 10: 1775-80
63. Chevallier B, Lhomme C, Dieras V, et al. Phase II trial of CPT-11 in advanced cervical carcinoma [abstract]. *Proc Am Soc Clin Oncol* 1995; 14: 267
64. Potkul RK, Price VT, Bailey H, et al. Irinotecan (CPT-11) in advanced squamous cell carcinoma of the cervix (Phase II) [abstract]. *Proc Am Soc Clin Oncol* 1995; 14: 279
65. Verschraegen CF, Levy T, Kudelka AP, et al. Phase II study of irinotecan in prior chemotherapy-treated squamous cell carcinoma of the cervix. *J Clin Oncol* 1997; 15: 625-31
66. Sakata Y, Shimada Y, Yoshino M, et al. A late phase II study of CPT-11, irinotecan hydrochloride, in patients with advanced pancreatic cancer [in Japanese]. *Gan To Kagaku Ryoho* 1994; 21: 1039-46
67. Wagener DJ, Verdonk HE, Dirix LY, et al. Phase II trial of CPT-11 in patients with advanced pancreatic cancer, an EORTC early clinical trials group study. *Ann Oncol* 1995; 6: 129-32
68. Futatsuki K, Wakui A, Nakao I, et al. A late Phase II study of irinotecan hydrochloride (CPT-11) in advanced gastric cancer: CPT-11 Gastrointestinal Cancer Study Group [in Japanese]. *Gan To Kagaku Ryoho* 1994; 21: 1033-8
69. Bonnetterre J, Pion JM, Adenis A, et al. A Phase II study of a new camptothecin analog CPT-11 in previously treated advanced breast cancer patients [abstract]. *Proc Am Soc Clin Oncol* 1993; 12: 94
70. Taguchi T, Tominaga T, Ogawa M, et al. A late phase II study of CPT-11 (irinotecan) in advanced breast cancer, CPT-11 Study Group on Breast Cancer [in Japanese]. *Jpn J Cancer Chemother (Gan To Kagaku Ryoho)* 1994; 21: 1017-24
71. Ohno R, Okada K, Masaoka T, et al. An early phase II study of CPT-11: a new derivative of camptothecin for the treatment of leukemia and lymphoma. *J Clin Oncol* 1990; 8: 1907-12
72. Tsuda H, Takatsuki K, Ohno R, et al. Treatment of adult T-cell leukaemia-lymphoma with irinotecan hydrochloride (CPT-11): CPT-11 Study Group on Hematological Malignancy. *Br J Cancer* 1994; 70: 771-4
73. Kaneda N, Nagata H, Furuta T, et al. Metabolism and pharmacokinetics of the camptothecin analogue CPT-11 in the mouse. *Cancer Res* 1990; 50: 1715-20
74. Barilero I, Gandia D, Armand JP, et al. Simultaneous determination of the camptothecin analogue CPT-11 and its active metabolite SN-38 by high-performance liquid chromatography: application to plasma pharmacokinetic studies in cancer patients. *J Chromatogr Biomed Appl* 1992; 575: 275-80
75. Akimoto K, Goto A, Ohya K. Selective and sensitive determination of lactone and hydroxy acid forms of camptothecin and two derivatives (CPT-11 and SN-38) by high-performance liquid chromatography with fluorescence detection. *J Chromatogr* 1991; 588: 165-70
76. Rivory LP, Robert J. Reversed-phase high-performance liquid chromatographic method for the simultaneous quantitation of the carboxylate and lactone forms of the camptothecin derivative irinotecan, CPT-11, and its metabolite SN-38 in plasma. *J Chromatogr Biomed Appl* 1994; 661: 133-41
77. Warner DL, Burke TG. Simple and versatile high-performance liquid chromatographic method for the simultaneous quantitation of the lactone and carboxylate forms of camptothecin anticancer drugs. *J Chromatogr B Biomed Appl* 1997; 691: 161-71
78. Sumiyoshi H, Fujiwara Y, Ohune T, et al. High-performance liquid chromatographic determination of irinotecan (CPT-11) and its active metabolite (SN-38) in human plasma. *J Chromatogr B Biomed Appl* 1995; 670: 309-16
79. Sasaki Y, Yoshida Y, Sudoh K, et al. Pharmacological correlation between total drug concentration and lactones of CPT-11 and SN-38 in patients treated with CPT-11. *Jpn J Cancer Res* 1995; 86: 111-6
80. Sasaki Y, Hokusui H, Mizuno S, et al. A pharmacokinetic and pharmacodynamic analysis of CPT-11 and its active metabolite SN-38. *Jpn J Cancer Res* 1995; 86: 101-10
81. Rivory LP, Chatelet E, Canal P, et al. Kinetics of the in vivo interconversion of the carboxylate and lactone forms of irinotecan (CPT-11) and of its metabolite SN-38 in patients. *Cancer Res* 1994; 54: 6330-3
82. Tsuji T, Kaneda N, Kado K, et al. CPT-11 converting enzyme from rat serum: purification and some properties. *J Pharmacobiodyn* 1991; 14: 341-9
83. Satoh T, Hosokawa M, Atsumi R, et al. Metabolic activation of CPT-11, 7-ethyl-10-[4-(1-piperidino)-1-piperidino]carbonyloxy camptothecin, a novel antitumor agent, by carboxylesterase. *Biol Pharm Bull* 1994; 17: 662-4
84. Rivory LP, Bowles MR, Robert J, et al. Conversion of irinotecan (CPT-11) to its active metabolite, 7-ethyl-10-hydroxycamptothecin (SN-38), by human liver carboxylesterase. *Biochem Pharmacol* 1996; 52: 1103-11
85. Chabot GG, Abigeres D, Catimel G, et al. Population pharmacokinetics and pharmacodynamics of irinotecan (CPT-11) and active metabolite SN-38 during phase I trials. *Ann Oncol* 1995; 6: 141-51
86. Rivory LP, Robert J. Identification and kinetics of a beta-glucuronide metabolite of SN-38 in human plasma after administration of the camptothecin derivative irinotecan. *Cancer Chemother Pharmacol* 1995; 36: 176-9
87. Haaz MC, Rivory L, Jantet S, et al. Glucuronidation of SN-38, the active metabolite of irinotecan, by human hepatic microsomes. *Pharmacol Toxicol* 1997; 80: 91-6
88. Gupta E, Lestingi TM, Mick R, et al. Metabolic fate of irinotecan in humans: correlation of glucuronidation with diarrhoea. *Cancer Res* 1994; 54: 3723-5
89. Rivory LP, Riou JF, Haaz MC, et al. Identification and properties of a major plasma metabolite of irinotecan (CPT-11) isolated from the plasma of patients. *Cancer Res* 1996; 56: 3689-94

90. Lokiec F, Monegier du Sorbier B, Sanderink GJ. Irinotecan (CPT-11) metabolites in human bile and urine. *Clin Cancer Res* 1996; 2: 1943-9
91. Masuda N, Fukuoka M, Kudoh S, et al. Phase I and pharmacologic study of irinotecan in combination with cisplatin for advanced lung cancer. *Br J Cancer* 1993; 68: 777-82
92. Masuda N, Fukuoka M, Kudoh S, et al. Phase I and pharmacologic study of irinotecan and etoposide with recombinant human granulocyte colony-stimulating factor support for advanced lung cancer. *J Clin Oncol* 1994; 12: 1833-41
93. Canal P, Gay C, Dezeuze A, et al. Pharmacokinetics and pharmacodynamics of irinotecan during a phase II clinical trial in colorectal cancer. *J Clin Oncol* 1996; 14: 2688-95
94. Rivory LP, Haaz MC, Canal P, et al. Pharmacokinetic interrelationships of irinotecan (CPT-11) and its three major plasma metabolites in patients enrolled in phase I-II trials. *Clin Cancer Res* 1997; 3: 1261-6
95. Iyer L, King C, Tephly T, et al. UGT isoform 1.1 (UGT*1.1) glucuronidates SN-38, the active metabolite of irinotecan [abstract 707]. *Proc Am Soc Clin Oncol* 1997; 16: 201a
96. Data on file Rhône-Poulenc Rorer, S.A Antony, France
97. Burke TG, Mi Z. The structural basis of camptothecin interactions with human serum albumin: impact on drug stability. *J Med Chem* 1994; 37: 40-6
98. Burris H, Dietz A, Eckardt J, et al. A Phase I trial to evaluate orally administered irinotecan HCl (CPT-11) given daily X 5 every 3 weeks in patients with refractory malignancies [abstract]. *Proc Am Soc Clin Oncol* 1996; 15: 489
99. Lokiec F, Canal P, Gay C, et al. Pharmacokinetics of irinotecan and its metabolites in human blood, bile, and urine. *Cancer Chemother Pharmacol* 1995; 36: 79-82
100. Chabot GG. Factors involved in clinical pharmacology variability in oncology. *Anticancer Res* 1994; 14: 2269-72
101. Gupta E, Mick R, Ramirez J, et al. Pharmacokinetic and pharmacodynamic evaluation of the topoisomerase inhibitor irinotecan in cancer patients. *J Clin Oncol* 1997; 15: 1502-10
102. Gupta E, Wang X, Ramirez J, et al. Modulation of glucuronidation of SN-38, the active metabolite of irinotecan, by valproic acid and phenobarbital. *Cancer Chemother Pharmacol* 1997; 39: 440-4
103. Gupta E, Safa AR, Wang X, et al. Pharmacokinetic modulation of irinotecan and metabolites by cyclosporin A. *Cancer Res* 1996; 56: 1309-14
104. Sasaki Y, Ohtsu A, Shimada Y, et al. Simultaneous administration of CPT-11 and fluorouracil: alteration of the pharmacokinetics of CPT-11 and SN-38 in patients with advanced colorectal cancer. *J Natl Cancer Inst* 1994; 86: 1096-8
105. Grossin F, Barbault H, Benhammouda A, et al. A phase I pharmacokinetics study of concomitant CPT-11 and 5FU combination [abstract 1156]. *Proc Am Assoc Cancer Res* 1996; 37: 168
106. Saltz LB, Kanowitz J, Kemeny NE, et al. Phase I clinical and pharmacokinetic study of irinotecan, fluorouracil, and leucovorin in patients with advanced solid tumors. *J Clin Oncol* 1996; 14: 2959-67
107. Karato A, Sasaki Y, Shiraishi J, et al. Pharmacokinetic study in the dose escalation study of CPT-11 and VP-16 [abstract]. *Proc Am Assoc Cancer Res* 1993; 34: 2325
108. Couteau C, Lokiec F, Vernillet L, et al. Phase I dose-finding and pharmacokinetic (PK) study of docetaxel (D) in combination with irinotecan (I) in advanced solid tumors [abstract 709]. *Proc Am Soc Clin Oncol* 1997; 16: 202a
109. Kudoh S, Fukuoka M, Masuda N, et al. Relationship between the pharmacokinetics of irinotecan and diarrhoea during combination chemotherapy with cisplatin. *Jpn J Cancer Res* 1995; 86: 406-13
110. Mick R, Gupta E, Vokes EE, et al. Limited-sampling models for irinotecan pharmacokinetics-pharmacodynamics: prediction of biliary index and intestinal toxicity. *J Clin Oncol* 1996; 14: 2012-9
111. Chabot GG. Limited sampling models for simultaneous estimation of the pharmacokinetics of irinotecan and its active metabolite SN-38. *Cancer Chemother Pharmacol* 1995; 36: 463-72
112. Nakashima H, Lieberman R, Karato A, et al. Efficient sampling strategies for forecasting pharmacokinetic parameters of irinotecan (CPT-11): implication for area under the concentration-time curve monitoring. *Ther Drug Monit* 1995; 17: 221-9
113. Sasaki Y, Mizuno S, Fujii H, et al. A limited sampling model for estimating pharmacokinetics of CPT-11 and its metabolite SN-38. *Jpn J Cancer Res* 1995; 86: 117-23
114. Yamamoto N, Ramura T, Karato A, et al. CPT-11: population pharmacokinetic model and estimation of pharmacokinetics using the Bayesian method in patients with lung cancer. *Jpn J Cancer Res* 1994; 85: 972-7

Correspondence and reprints: Dr Guy G. Chabot, Pharmacology Laboratory (URA 147 CNRS), Gustave-Roussy Institute, 39 rue Camille-Desmoulins, F-94805 Villejuif, France. e-mail: gchabot@igr.fr

A Phase 1/2 Study Combining MM-151 + nal-IRI + 5-FU + Leucovorin in RAS/RAF Wild-Type Metastatic Colorectal Cancer

Emily Chan¹, Wael Harb², Kabir Mody⁴, Xiaoyu Jiang³, Ty McClure⁵, Jeffrey D. Kearns⁵, Andrea Valencia⁵, Jonathan Fitzgerald⁵, J. Marc Pipas⁵, Rachel Nering⁵, Lionel D. Lewis²

¹Vanderbilt University Medical Center, Nashville, TN; ²Horizon Oncology Center, Lafayette, IN;

³The Geisel School of Medicine at Dartmouth and The Norris Cotton Cancer Center, Lebanon, NH;

⁴Division of Medical Oncology at Mayo Clinic, Jacksonville, FL;

⁵Merrimack Pharmaceuticals, Inc, Cambridge, MA



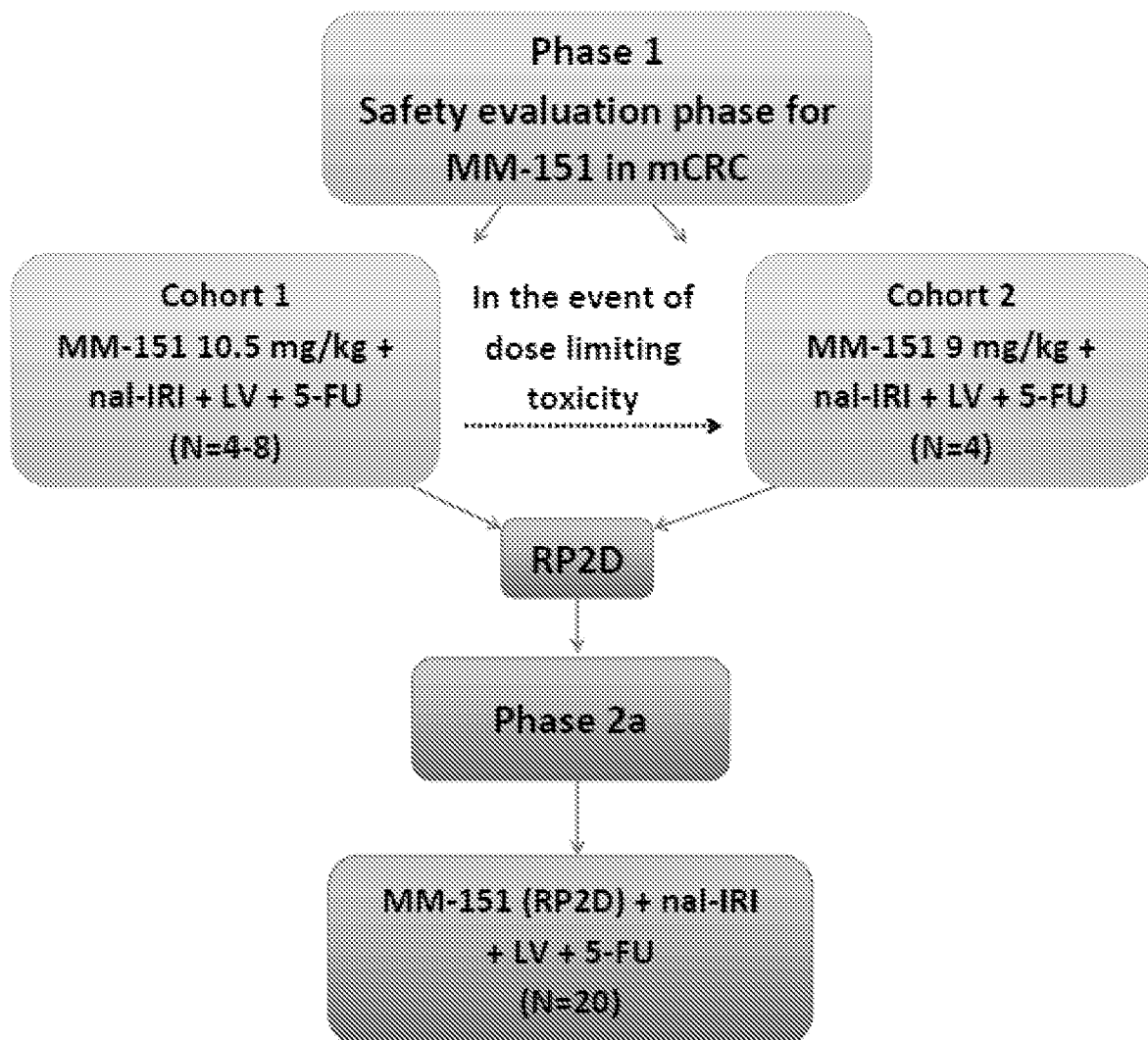
Abstract # 168108

Background

Colorectal cancer is a leading cause of cancer death worldwide and the third most common cancer in men and women. Despite recent approvals of new agents in refractory disease, there has been little change in the composition of first-line therapies in recent years, which generally include chemotherapy in combination with a biologic, either an EGFR-targeted antibody or a VEGF inhibitor. Investigational agents currently in development represent attempts to improve anti-neoplastic efficacy within these established drug classes.

MM-151 is an oligoclonal mixture of three IgG1, anti-EGFR antibodies designed to bind distinct non-overlapping EGFR epitopes and inhibit ligand-mediated signal amplification. MM-151's molecular composition enables antagonism of clinically relevant EGFR ligand mixtures, EGFR down-regulation and immune effector function (ADCC and CDC). Nal-IRI is a nanoliposomal formulation of irinotecan. In a randomized phase-III study (NAPOLI-1) of patients with metastatic pancreatic cancer previously treated with gemcitabine-based therapy, nal-IRI + 5-FU/LV demonstrated its safety and significant clinical activity, increasing overall survival (OS) and progression-free survival (PFS) relative to 5-FU/LV. The current study will characterize preliminary safety, initial efficacy and biomarker / pharmacodynamic profile of MM-151 + nal-IRI + 5-FU/LV in mCRC patients who are treatment naïve to an EGFR inhibitor and irinotecan-based chemotherapy.

Study Design



Phase 1: A modified toxicity probability interval (mTPI) approach will be used to evaluate safety and RP2D. Pre-determined DLT decision rules will guide the dose finding of MM-151. Nal-IRI + LV + 5-FU will be given at fixed doses.

Phase 2a: Efficacy, pharmacodynamics and additional safety data will be assessed.

Study Objectives

Phase 1:

- To determine the maximum tolerated dose, safety and tolerability of MM-151 + nal-IRI + 5-FU + LV in patients with mCRC that are RAS wild-type.
- To characterize the adverse event profile (including DLT's)
- To determine the pharmacokinetic parameters
- To determine the immunogenicity parameters

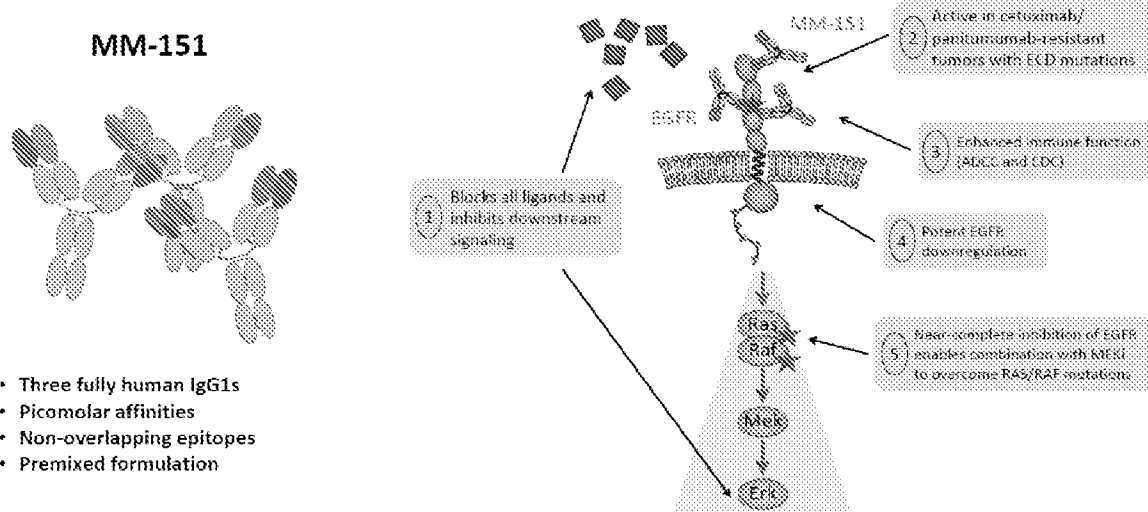
Phase 2a:

- To characterize initial efficacy in conjunction with levels of irinotecan and SN-38 measured in tissue
- To further characterize the adverse event profile
- To describe the observed objective response rate (ORR) and disease control rate
- To measure pretreatment and on-treatment levels of EGFR ligands
- To determine the pharmacokinetic parameters
- To determine the immunogenicity parameters

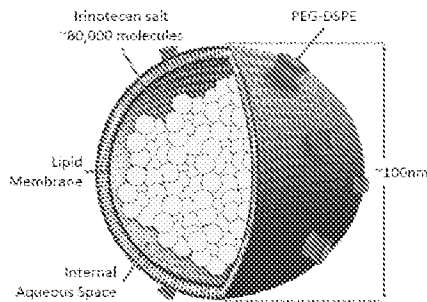
Exploratory:

- To assess the relationship between biomarkers from tissue, blood and/or urine with toxicity and efficacy parameters, including markers of the development of resistance to treatment

MM-151: Oligoclonal Anti-EGFR



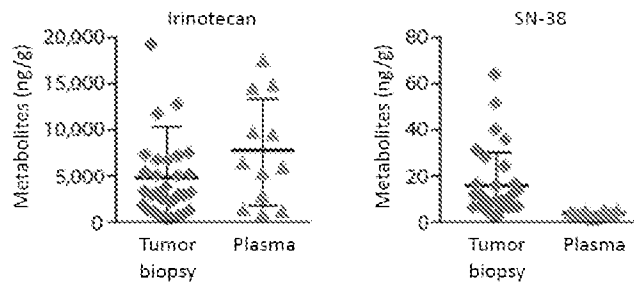
nal-IRI: liposomal formulation of irinotecan, a topoisomerase inhibitor



Key Attributes

- Sheltered and extended circulation of pro-drug within liposome
- Deposition in tumor through EPR effect
- Local activation and release of active drug
- Sustained levels of pro-drug and active drug in the tumor

Irinotecan and SN-38 levels 72 hours after nal-IRI treatment

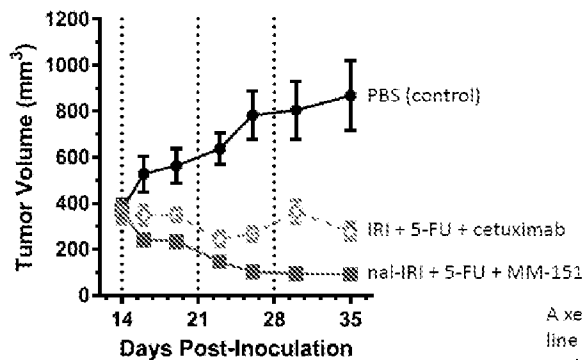


Preliminary data from a small pilot study across different cancer types showed higher levels of SN-38 found in tumor biopsies compared with plasma at 72 hours, suggesting local metabolic activation of irinotecan, which was contained in the liposomal nanoparticles, to SN-38.

Combination Rationale

Clinical Hypothesis: Improved delivery method of SN-38 combined with oligoclonal targeting of EGFR may result in improved clinical outcomes.

The Combination of [nal-IRI + 5-FU + MM-151] Demonstrates Superior Inhibition of Tumor Growth in a Preclinical Xenograft as Compared to the Combination of [IRI + 5-FU + cetuximab]



	in vivo Response at Day 35	
	FOI/IRI + Cetuximab	nal-IRI + 5-FU + MM-151
PR	5/10 (50%)	9/10 (90%)
SD	3/10 (30%)	1/10 (10%)
PD	2/10 (20%)	0/10

A xenograft experiment was performed with the LIM1215 colorectal cancer cell line to compare inhibition of tumor growth between (1) MM-151+ nal-IRI + 5-FU, and (2) cetuximab + IRI + 5-FU. Dosing was performed weekly as indicated by the stippled lines at Days 14, 21, and 28.

Key Eligibility Criteria

INCLUSION:

- Adults aged ≥ 18 years
- Pathologically confirmed, metastatic, unresectable colorectal adenocarcinoma
- For Phase 1 of the study, patients must be either treatment naive or have had no more than one prior line of therapy with an oxaliplatin-based regimen for metastatic disease
- For Phase 2a of the study, patients must have had no prior therapy for metastatic disease.

- Wild-type KRAS/NRAS genes as assessed in tumor tissue via extended RAS testing
- Histologic confirmed BRAF wild-type status of primary colorectal cancer or related metastasis
- ECOG Performance Score (PS) of 0 or 1
- Adequate hematologic parameters, and hepatic and renal function
- Patient must be willing to provide a pre-treatment biopsy as well as an on study biopsy.

EXCLUSION:

- Prior treatment with irinotecan or an EGFR inhibitor (patients in Phase 1b)
- History of any second malignancy in the last 3 years
- Clinically significant gastrointestinal disorders

Study Evaluations

Safety and Tolerability

- Safety evaluations, including AE and hospitalization reporting, routine labs will be collected throughout the study.
- AEs will be graded according to the NCI- Common Terminology Criteria for Adverse Events (CTCAE) version 4.0, and will be summarized according to severity and relatedness to treatment.

Pharmacokinetics

- Conducted for MM-151, nal-IRI and 5-FU

Biomarkers

- Analyses will be performed to further characterize and correlate potential biomarkers that may help to predict or evaluate efficacy (from plasma and tissue).
- Whole blood samples will be analyzed for identification of genomic alterations in cell-free DNA
- Whole blood and plasma sampling for biomarker analyses will occur serially
- Archived tissue, pre-treatment and on study biopsies will be collected to assess the deposition of nal-IRI within the tumor in comparison to baseline, chemo-sensitivity markers and their pharmacodynamic relationship to nal-IRI, the role of EGFR ligands and other pathway markers mutations as mediators of MM-151 sensitivity.

Efficacy

- Tumor response will be evaluated at least every 8 weeks according to RECIST, version 1.1

Summary

- **This phase 1/2 study will evaluate the safety and tolerability of MM-151 + nal-IRI + 5-FU + LV in RAS/RAF wild-type, unresectable, metastatic colorectal cancer.**
- **Robust biomarker analysis will help to characterize pharmacokinetics, immunogenicity, and intratumoral drug deposition.**
- **Preliminary efficacy of this novel combination in front-line mCRC will also be assessed.**
- **NCT NCT02785068**

We thank the participating investigators, patients, our colleagues and collaborators who contributed to the research that made this study possible.

Copies of this poster obtained through Quick Response (QR) Code are for personal use only and may not be reproduced without permission from ASCO® and the author of this poster.

Please contact rnering@merrimack.com with questions or comments.



Journal of Clinical Oncology®

An American Society of Clinical Oncology Journal

[Log In](#) [Submit](#) [E-Alerts](#) [Subscribe](#)

[OpenAthens/Shibboleth »](#)

ACCESS PROVIDED BY IPSEN LIMITED - THE LIBRARY


MENU

[Journal of Clinical Oncology](#) > [List of Issues](#) > [Volume 34, Issue 15, suppl.](#) >

Article Tools

GASTROINTESTINAL (COLORECTAL) CANCER

A phase 1b/2 study combining MM-151 + nal-IRI + 5-FU + leucovorin in RAS-wildtype metastatic colorectal cancer (mCRC).

 [Check for updates](#)

[Emily Chan](#), [Wael A. Harb](#), [Kabir Mody](#), [Xiaoyi Jiang](#), [Iy McClure](#), [Jeffrey D. Kearns](#), ...

[Show More](#)

[Abstract Disclosures](#)

Abstract

TPS3633

Background: Colorectal cancer is a leading cause of cancer death worldwide and the third most

OPTIONS & TOOLS

ADVERTISEMENT

[Export Citation](#)

[Track Citation](#)

[Add To Favorites](#)

[Rights & Permissions](#)

COMPANION ARTICLES

ADVERTISEMENT

No companion articles

ARTICLE CITATION

DOI:
10.1200/JCO.2016.34.15_suppl.TPS3633

Journal of Clinical Oncology 34, no. 15_suppl

Published online May 20, 2016.

WE RECOMMEND

UFT/LV combination based regimens with oxaliplatin or irinotecan as first line treatment for patients (pts)

common cancer in men and women. Despite recent approvals of new agents in refractory disease, there has been little change in the composition of first-line therapies in recent years, which generally include chemotherapy in combination with a biologic, either an EGFR-targeted antibody or a VEGF inhibitor.

Investigational agents currently in development represent attempts to improve anti-neoplastic efficacy within these established drug classes. MM-151 is a oligoclonal mixture of three IgG1, anti-EGFR antibodies designed to bind distinct non-overlapping EGFR epitopes and inhibit ligand-mediated signal amplification. MM-151's molecular composition enables antagonism of clinically relevant EGFR ligand mixtures, EGFR down-regulation and immune effector function (ADCC, CDC). Nal-IRI is a nanoliposomal formulation of irinotecan. In a randomized phase-III study (NAPOLI-1) of patients with metastatic pancreatic cancer previously treated with gemcitabine-based therapy, nal-IRI + 5-FU/LV demonstrated its safety and significant clinical activity, increasing overall survival (OS) and progression-free survival (PFS) relative to 5-FU/LV. The current study will characterize preliminary safety, initial efficacy and biomarker / pharmacodynamic profile of MM-151 + nal-IRI + 5-FU/LV in mCRC patients who are treatment naïve to an EGFR inhibitor or irinotecan-based chemotherapy. **Methods:** In the dose finding cohorts of this Phase 1b/2 study, a modified toxicity probability interval approach (mTPI) will be utilized to determine the maximum tolerated dose (MTD) of MM-151 in combination with nal-IRI, 5FU and leucovorin. Enrollment will be determined by the safety profile observed, with approximately 8-12 pts anticipated. In the Phase 2 portion of the study, approximately 20-30 pts will receive the combination at the defined MTD. The primary objectives of this phase of the study is to characterize initial efficacy, obtain additional safety data, and complete pharmacodynamic and biomarker evaluation through the collection of pre-treatment and on-study samples.

© 2016 by American Society of Clinical Oncology

with non resectable metastatic colorectal cancer (mCRC): Results of two multicentric phase II trials

J.-Y. Douillard, *J Clin Oncol*, 2016

Bevacizumab in combination with 5-FU/leucovorin improves survival in patients with metastatic colorectal cancer: A combined analysis
R. D. Mass et al., *J Clin Oncol*, 2016

Capecitabine (X) plus irinotecan (XELIRI) as first-line treatment for metastatic colorectal cancer (mCRC): Final safety findings from a phase II trial
Y. Z. Patt et al., *J Clin Oncol*, 2016

Phase Ib study of recombinant human Apo2L/TRAIL plus irinotecan and cetuximab or FOLFIRI in metastatic colorectal cancer (mCRC) patients (pts): Preliminary results
L. Yee, *J Clin Oncol*, 2016

Phase I study of weekly oxaliplatin (OXA) + 5-fluorouracil continuous infusion (FU CI) in patients (pts) with advanced colorectal cancer (CRC)
L. M. Pasetto et al., *J Clin Oncol*, 2016

Pharmacological Management of Colon Cancer
Michael Steinberg et al., *US Pharmacist*, 2009

FDA grants Braftovi-Mektovi plus Erbitux breakthrough therapy designation for colorectal cancer
Victor Sandor et al., *Healio*, 2018

In colorectal cancer, all KRAS mutations may not be created equal: A post-EMCC update

For more information,
Healio, 2011

Eli Lilly, Sermonix Pharma
Partner on Phase II Trial of
Drug Combo in Metastatic
Breast Cancer
Precision Oncology News,
2020

Powered by



WHAT'S POPULAR

Most Read

Most Cited

Venous
Thromboembolism
Prophylaxis and
Treatment in Patients
With Cancer: ASCO
Clinical Practice
Guideline Update
Key et al.

Management of
Immune-Related Adverse
Events in Patients
Treated With Immune
Checkpoint Inhibitor
Therapy: American
Society of Clinical
Oncology Clinical Practice
Guideline
Brahmer et al.

Prognostic Index for
Acute- and Lymphoma-
Type Adult T-Cell
Leukemia/Lymphoma
Katsuya et al.

Outpatient Management
of Fever and Neutropenia
in Adults Treated for
Malignancy: American
Society of Clinical
Oncology and Infectious
Diseases Society of
America Clinical Practice
Guideline Update
Taplitz et al.

Antiemetics: American
Society of Clinical



QUICK LINKS

Content

[Newest Articles](#)
[Archive](#)
[Meeting Abstracts](#)

Journal Information

[About](#)
[Editorial Roster](#)
[Contact Us](#)
[Permissions](#)

Resources

[Authors](#)
[Reviewers](#)
[Subscribers](#)
[Institutions](#)
[Advertisers](#)

Submit Your Manuscript

Subscribe to this Journal



ASCO FAMILY OF SITES

Journals

[Journal of Clinical
Oncology](#)
[JCO Oncology Practice](#)
[JCO Global Oncology](#)
[JCO Clinical Cancer
Informatics](#)
[JCO Precision Oncology](#)

Publications

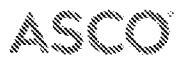
[ASCO Educational Book](#)
[ASCO Daily News](#)
[ASCO Connection](#)
[The ASCO Post](#)
[JCO OP DAIS](#)

Education

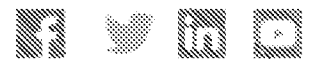
[ASCO eLearning](#)
[ASCO Meetings](#)
[Cancer.Net](#)

Other Sites

[ASCO.org](#)
[ASCO Author Services](#)
[ASCO Career Center](#)
[CancerLinq](#)
[Conquer Cancer
Foundation](#)
[TAPUR Study](#)



American Society of Clinical Oncology
2215 Mill Road, Suite 800, Alexandria, VA 22314
© 2020 American Society of Clinical Oncology



[Terms of Use](#) | [Privacy Policy](#) | [Cookies](#)



Published in final edited form as:

Nat Nanotechnol. ; 7(6): 383–388. doi:10.1038/nnano.2012.45.

Normalization of tumour blood vessels improves the delivery of nanomedicines in a size-dependent manner

Vikash P. Chauhan^{1,2,‡}, Triantafyllos Stylianopoulos^{1,3,‡}, John D. Martin^{1,4}, Zoran Popović⁵, Ou Chen⁵, Walid S. Kamoun¹, Mounji G. Bawendi⁵, Dai Fukumura¹, and Rakesh K. Jain¹

¹Edwin L. Steele Laboratory, Department of Radiation Oncology, Massachusetts General Hospital and Harvard Medical School, Boston, Massachusetts, USA.

²Harvard School of Engineering and Applied Sciences, Harvard University, Cambridge, Massachusetts, USA.

³Department of Mechanical and Manufacturing Engineering, University of Cyprus, Nicosia, Cyprus.

⁴Department of Chemical Engineering, Massachusetts Institute of Technology, Cambridge, Massachusetts, USA.

⁵Department of Chemistry, Massachusetts Institute of Technology, Cambridge, Massachusetts, USA.

Abstract

The blood vessels of cancerous tumours are leaky^{1–3} and poorly organized^{4–7}. This can increase the interstitial fluid pressure (IFP) inside tumours and reduce blood supply to them, which impairs drug delivery^{8–9}. Anti-angiogenic therapies – which “normalize” the abnormal blood vessels in tumours by making them less leaky – have been shown to improve the delivery and effectiveness of chemotherapeutics with low molecular-weights¹⁰, but it remains unclear whether normalizing tumour vessels can improve the delivery of nanomedicines. Here we show that repairing the abnormal vessels in mammary tumours, by blocking vascular endothelial growth factor (VEGF) receptor-2, improves the delivery of small nanoparticles (12nm diameter) while hindering the delivery of large nanoparticles (125nm diameter). We utilize a mathematical model to show that

Users may view, print, copy, download and text and data- mine the content in such documents, for the purposes of academic research, subject always to the full Conditions of use: http://www.nature.com/authors/editorial_policies/license.html#terms

[‡]Correspondence and requests for materials should be addressed to R.K.J. jain@steele.mgh.harvard.edu (R.K.J).

[‡]these authors contributed equally to this work

Author contributions

V.P.C. and R.K.J. conceived and designed the experiments. T.S. and R.K.J. designed and developed the mathematical model and its simulations. V.P.C., J.D.M., and O.C. performed the experiments. T.S. carried out the mathematical model simulations. V.P.C., T.S., J.D.M., and W.S.K. analyzed the data. Z.P., O.C., W.S.K., M.G.B., and D.F. contributed materials/analysis tools. V.P.C., T.S., and R.K.J. co-wrote the paper. All authors discussed the results and commented on the manuscript.

Additional information

Supplementary information accompanies this paper at www.nature.com/naturenanotechnology. Reprints and permission information is available online at <http://npg.nature.com/reprintsandpermissions/>.

Competing financial interests

The other authors declare no competing financial interests.

reducing vessel wall pore sizes through normalization decreases IFP in tumours, allowing small nanoparticles to enter them more rapidly. However, increased steric and hydrodynamic hindrances, also associated with smaller pores, make it more difficult for large nanoparticles to enter tumours. Our results further suggest that smaller (~12nm) nanomedicines are ideal for cancer therapy, owing to superior tumour penetration.

Elevated tumour IFP hinders drug delivery by abolishing fluid pressure gradients that produce rapid convective (flow-driven) penetration into tumours¹¹. This limits drug penetration across vessel walls into tumours (transvascular) and through tumour tissue (interstitial) to slow diffusion⁹. Anti-angiogenic therapies can repair tumour vessel abnormalities, such as large heterogeneous pores that facilitate leakiness, by inducing vessel maturation^{12–13}. This “vascular normalization” reduces IFP to induce convective penetration of molecules up to the size (~11 nm) of immunoglobulin-G (IgG) (Supplementary Tables 1 and 2)^{12–14}. Through normalization, anti-angiogenic therapies seem to benefit patients with colorectal¹⁵ and brain tumours^{16–17}, potentially through improved drug delivery, reduced chemoresistance, and immune reprogramming¹⁰. Whether normalizing vessels can improve the delivery of nanomedicines – ranging in size from 10–125nm – is not known. These slow-diffusing large therapeutics provide new hope for cancer treatment^{18–19} and would greatly benefit from convective delivery. Unfortunately, increased hydrodynamic and steric hindrance, from smaller vessel pores caused by normalization, may compromise the advantage from enhanced convection.

To determine how vascular normalization affects nanomedicine delivery, we studied whether the anti-VEGF-receptor-2 antibody DC101 modulates nanoparticle penetration rates in orthotopic mammary tumours *in vivo*. We used intravital multiphoton microscopy and a system of quantum dot-based nanoparticles with tunable size and fluorescence emission wavelength but identical surface chemistry as probes²⁰. With these tools, we measured the effects of DC101 on real-time delivery for particles of 12–125nm – the size range of approved nanomedicines. Using the resulting data, we applied a novel physiologically-based mathematical model for drug delivery to tumours to determine how anti-angiogenics affect pore size distributions. Furthermore, we utilized this model to study how pore size distributions can be therapeutically modulated to optimize delivery of different sizes of nanomedicines.

We found that a 5mg/kg dose of DC101 transiently decreases vessel diameter in orthotopic E0771 tumours – consistent with the structural vascular normalization “window” measured in mice^{12–13} and patients¹⁶ (Supplementary Fig. 1). We imaged nanoparticle delivery with or without DC101 in orthotopic 4T1 and E0771 mammary tumours (Fig. 1a, Supplementary Fig. 2). We quantified nanoparticle penetration rates as transvascular mass flux per unit vascular surface area and transvascular concentration difference, often termed the effective permeability²¹. Vascular normalization with 10mg/kg DC101 led to a 3.1-fold enhancement of transvascular flux in 4T1 tumours for the smallest (12nm) nanoparticles, with no improvement in penetration for the larger (60nm and 125nm) nanoparticles (Fig. 1b). Similarly, 5mg/kg DC101 led to 2.7-fold improvement in transvascular flux in E0771 tumours for the 12nm particles with no enhancement for the larger nanoparticles (Fig. 1c).

Some individual control tumours exhibited zero or near-zero penetration rates for the larger nanoparticles, with DC101 therapy apparently shutting down large nanoparticle delivery in several tumours (Fig 1b,c). Consistent with the structural normalization “window,” we characterized a functional normalization “window” for nanoparticle delivery. During treatment of mice bearing E0771 tumours with 5mg/kg DC101 every 3 days, the transvascular flux of 12nm particles was enhanced on days 2 and 5 but returned to baseline levels by day 8 (Fig. 2). Importantly, a 10mg/kg dose seemed to hinder nanoparticle delivery in E0771 tumours (Supplementary Fig. 3), suggesting a need for judicious dosing based on vascular sensitivity in each tumour and host.

To study how changes in vascular pore size distribution can bring about this complex size-dependent improvement in nanoparticle penetration rates, we developed a mathematical model of drug delivery to tumours (details in the Supplementary Information). The tumour vasculature is represented by a two-dimensional percolation network with one inlet and one outlet, which has been shown to resemble the vascular structure and function of tumours (Fig. 3a)^{6, 22}. It involves a series of interconnected nodes representing vessel segments. Each node is assigned a pore size, assuming a unimodal pore size distribution throughout the tumour vasculature based on previous studies^{1, 23}. We assume axial Poiseuille-type blood flow²⁴⁻²⁵. Drug exchange with the interstitial space follows Starling’s approximation for both diffusive and convective mass flux²⁴. Interstitial drug transport also occurs by diffusion and convection, with interstitial fluid flow driving convection calculated using Darcy’s law. We use pore theory for the transport of spherical particles through cylindrical pores²⁶⁻²⁷ to calculate the hindrances to diffusion and convection for each pore size²⁴. We first solve the steady state fluid problem requiring the net fluid accumulation at each node to be zero and determine the microvascular pressure (MVP) and IFP (Supplementary Figs. 4–6). Subsequently, we solve the transient drug delivery problem and calculate transvascular flux versus particle size as in the experiment. Model parameters were based on previous studies (Supplementary Tables 3 and 4).

Applying the model, we studied how changes in the mean and heterogeneity (standard deviation) of the vascular pore size distribution affect fluid pressure profiles and drug delivery in tumours. Consistent with previous studies, large heterogeneous pores result in elevated IFP in the centre of the tumour with no transvascular pressure difference, $\Delta P = MVP - IFP$ (Fig. 3b). Smaller, more homogenous pores produce low IFP with a non-zero ΔP – the result of vascular normalization – that induces convection (Fig. 3b). We simulated penetration rates for therapeutics from 1–250nm in size while varying mean pore sizes from 40–1000nm (diameter)¹ for homogenous, moderate, or heterogeneous pores corresponding to 20nm, 60nm, or 100nm pore size standard deviations respectively (area fractions held constant; Fig. 3c). Generally, smaller therapeutics (1–12nm) demonstrate the most rapid tumour penetration, while the largest therapeutics (125–250nm) did not appreciably leave the vasculature (Fig. 3d). Importantly, convection is dominant at small mean pore sizes. Increasing the mean pore size past a point (>140nm) hinders nanoscale therapeutic delivery due to rising IFP leading to limited convection, leaving diffusion dominant (Fig. 4a). This effect couples with increasing hydrodynamic and steric hindrance to transport as pore sizes approach therapeutic particle size (Fig. 4b). Therefore, each size of therapeutic has its own ideal mean pore size for maximal delivery to tumours. This ideal mean pore size becomes

larger with therapeutic size, though increasing pore size heterogeneity broadens these maxima towards smaller mean pore sizes for therapeutics larger than 12nm.

To investigate potential translational implications of these findings, we studied whether vascular normalization enhances the effectiveness of anti-cancer nanomedicines. We compared two clinically-used nanomedicines with widely varied sizes – Doxil, with a diameter of ~100nm, and Abraxane, which attains a size of ~10nm upon dilution in plasma (Supplementary Fig. 7). Considering the 5 day normalization window we characterized for nanoparticles, we treated mice bearing orthotopic E0771 mammary tumours with DC101 (5mg/kg) or non-specific IgG on days 0 and 3 while treating with Doxil (2mg/kg) or Abraxane (10mg/kg) on days 1–5 (Fig. 5a). We quantified the effect of each combination therapy based on the time to reach double the initial volume (Fig. 5b). While both Doxil and Abraxane monotherapy induced a similar growth delay, vascular normalization with DC101 enhanced the effectiveness of only the ~10nm Abraxane while not affecting that of the ~100nm Doxil.

Combining our experimental and simulated results, several conclusions can be made. The experiments suggest that vascular normalization with anti-angiogenic therapies will only enhance delivery and effectiveness for relatively small therapeutics – including small-molecule chemotherapeutics, biologics, and small nanoparticles. Together with the model, these data support the general, yet experimentally unproven, concept that vascular normalization reduces vessel pore sizes (Supplementary Fig. 8). This reduces IFP leading to a non-zero ΔP throughout tumours, an effect seen experimentally^{12, 15}, which our model shows can restore convective drug penetration. Unfortunately, smaller and more homogenous pores can also hinder transport for large therapeutics, resulting in diminished or unimproved tumour penetration for larger nanoparticles in both our experiments and simulations. The simulations also predict that remodelling vessels to increase pore sizes would enhance delivery for only the largest (>125nm) therapeutics, which are size-excluded by small pores. Perhaps most importantly, they show that tumour penetration rates decrease with increasing nanoparticle size – an effect most pronounced for tumours with smaller vessel pores, as with normalization.

Our findings emphasize the importance of size in nanomedicine design by demonstrating that 12nm particles penetrate tumours better than larger particles. Physical principles dictate that both diffusive and convective penetration – transvascular and interstitial – are faster for smaller particles^{8, 18, 26–27}. Importantly, most normal organs feature non-sinusoid continuous epithelium that may be either fenestrated or non-fenestrated with pore cutoff sizes of up to 6–12nm²⁸, suggesting that 12nm particles are the smallest that can take advantage of the enhanced permeability and retention (EPR) effect that leads to favourable toxicity profiles for nanomedicine¹⁹. Indeed, the smallest probe demonstrating selective delivery – a plurality of the injected dose reaching the tumour – through passive EPR is the ~11nm IgG²⁹. While vascular-targeted tumour-penetrating ligands can enhance nanoparticle penetration³⁰ and tumour cell-targeting can improve uptake and retention¹⁹, targeting ligands cannot fully overcome tumour penetration barriers made worse by large size⁸. Considering the superior mass flux into tumours and long circulation times for small nanoparticles, along with the large number of patients receiving normalizing anti-

angiogenics⁵, small size may represent an important new design constraint for anti-cancer nanomedicine.

Methods

Tumour models

Orthotopic mammary tumour models were prepared by implanting a small piece (1mm³) of viable tumour tissue from a source tumour animal into severe combined immunodeficient (SCID) mice bearing mammary fat pad chambers²¹. The tumours were allowed to grow to 3mm in diameter. All animal procedures were carried out following the Public Health Service Policy on Humane Care of Laboratory Animals and approved by the Institutional Animal Care and Use Committee of Massachusetts General Hospital.

Treatment

Mice were treated with 5 or 10mg/kg of DC101 (ImClone Systems), using non-specific rat IgG for control treatments, as a 5mg/mL solution by intraperitoneal injection on days 0, 3, and 6. Imaging studies were carried out on days 2, 5, and 8.

Nanoparticle synthesis

Nanoparticles were prepared and characterized as described previously²⁰.

In vivo imaging

A mixture of nanoparticles with diameters of 12nm (476nm emission), 60nm (540nm emission), and 125nm (625nm emission) was prepared for intravenous injection. Concentrations were adjusted with in vitro calibration to result in roughly equal photoluminescence intensity for all three nanoparticle samples under 800nm multiphoton excitation. Following retro-orbital injection of 200µL with these concentrations, multiphoton imaging was carried out as described previously²¹ on a custom-built multiphoton laser-scanning microscope using confocal laser-scanning microscope body (Olympus 300; Optical Analysis Corp.) and a broadband femtosecond laser source (High Performance MaiTai, Spectra-Physics). Image slices were taken at ~60mW at sample surface with depths from 0 -- 201µm, with 2.76µm steps and 2.76×2.76µm pixels. Mosaic images were taken in raster pattern using a motorized stage (H101, Prior Scientific, Inc.) and customized automation software (LabView, National Instruments). Imaging studies were performed with a 20X magnification, 0.95NA water immersion objective (Olympus XLUMPlanFI, 1-UB965, Optical Analysis).

Image analysis

Images were analyzed using custom analysis software developed in Matlab (The Mathworks) as described previously²¹. The analysis approach involved 3D vessel tracing to create vessel metrics and a 3D map of voxel intensity versus distance to the nearest vessel over time. Images were also corrected for sample movement over time with 3D image registration. The normalized transvascular flux was calculated using

$\frac{J_t}{S_v(C_v - C)} = P_{eff} = \lim_{t \rightarrow 0} \frac{\partial \int_0^R C(r)r dr}{\partial t (C_v - C)R}$, where J_t is the transvascular flux, S_v is the vessel surface area, C_v is the concentration of the probe in the vessel, C is the concentration of the probe immediately extravascular, P_{eff} is the effective permeability²¹, t is time after the initial image, r is the distance from the vessel central axis, and R is the vessel radius at that point along the vessel. Fluorescence intensities were used as these concentrations. The calculation was made as an average over the entire imaged volume for each tumour.

Model equations

Details of the model and corresponding equations are provided in the Supplementary Information section.

Tumour growth studies

E0771 mammary tumours were orthotopically implanted in female SCID mice. The mice were split into treatment groups, time-matched for time after implantation and size-matched for tumour volume at this time (110–111 mm³). The mice were treated at this initial size with 5mg/kg DC101 or non-specific IgG on days 0 and 3 by intraperitoneal injection. The mice were simultaneously treated with either 2mg/kg Doxil, with a diameter of ~100nm, or 10mg/kg Abraxane, with a diameter of ~10nm, on days 1–5 by retro-orbital injection. These relative doses are similar to the relative doses for these two nanomedicines in patients. The primary tumours were then measured every 3 days, beginning on day 0, using callipers. Tumour growth was quantified using the time for each to reach double its initial volume.

Statistical analysis

The data are presented as means with standard errors. Groups were compared using a Student's t-test, except for tumour growth data – for which we anticipated a non-normal distribution and used an (exact) Mann-Whitney U-test. In pairwise comparisons of groups in tumour growth experiments, P values were adjusted using Holm's method.

Supplementary Material

Refer to Web version on PubMed Central for supplementary material.

Acknowledgements

We thank Julia Kahn and Sylvie Roberge for technical assistance, James Baish for assistance with the mathematical model, and Marek Ancukiewicz for assistance with statistical analysis. We thank ImClone Systems for generously providing DC101. We gratefully acknowledge support from the National Institutes of Health (P01-CA080124, R01-CA126642, R01-CA115767, R01-CA096915, R01-CA085140, R01-CA098706, T32-CA073479), DoD Breast Cancer Research Innovator award (W81XWH-10-1-0016), and an FP7 Marie-Curie IRG grant (PIRG08-GA-2010-276894).

R.K.J. receives research support from Dyax, MedImmune, and Roche; is a consultant for Dyax and Noxxon; is on the Scientific Advisory Board for Enlight and SynDevRx; is on the Board of Trustees for H&Q Capital Management, and is a Co-founder of Xtuit.

References

1. Hobbs SK. Regulation of transport pathways in tumor vessels: role of tumor type and microenvironment. *Proc. Natl. Acad. Sci. USA.* 1998; 95:4607–4612. [PubMed: 9539785]
2. Nagy JA, Dvorak AM, Dvorak HF. VEGF-A and the induction of pathological angiogenesis. *Annu. Rev. Pathol.* 2007; 2:251–275. [PubMed: 18039100]
3. Yuan F, et al. Microvascular permeability and interstitial penetration of sterically stabilized (stealth) liposomes in a human tumor xenograft. *Cancer Res.* 1994; 54:3352–3356. [PubMed: 8012948]
4. Baish JW, et al. Scaling rules for diffusive drug delivery in tumor and normal tissues. *Proc. Natl. Acad. Sci. USA.* 2011; 108:1799–1803. [PubMed: 21224417]
5. Carmeliet P, Jain RK. Molecular mechanisms and clinical applications of angiogenesis. *Nature.* 2011; 473:298–307. [PubMed: 21593862]
6. Gazit Y, Berk DA, Leunig M, Baxter LT, Jain RK. Scale-invariant behavior and vascular network formation in normal and tumor tissue. *Phys. Rev. Lett.* 1995; 75:2428–2431. [PubMed: 10059301]
7. Nagy JA, Chang SH, Dvorak AM, Dvorak HF. Why are tumour blood vessels abnormal and why is it important to know? *Br. J. Cancer.* 2009; 100:865–869. [PubMed: 19240721]
8. Chauhan VP, Stylianopoulos T, Boucher Y, Jain RK. Delivery of Molecular and Nanoscale Medicine to Tumors: Transport Barriers and Strategies. *Annu. Rev. Chem. Biomol. Eng.* 2011; 2:281–298. [PubMed: 22432620]
9. Jain RK. Normalization of tumor vasculature: an emerging concept in antiangiogenic therapy. *Science.* 2005; 307:58–62. [PubMed: 15637262]
10. Goel S, et al. Normalization of the vasculature for treatment of cancer and other diseases. *Physiol. Rev.* 2011; 91:1071–1121. [PubMed: 21742796]
11. Jain RK, Baxter LT. Mechanisms of heterogeneous distribution of monoclonal antibodies and other macromolecules in tumors: significance of elevated interstitial pressure. *Cancer Res.* 1988; 48:7022–7032. [PubMed: 3191477]
12. Tong RT, et al. Vascular normalization by vascular endothelial growth factor receptor 2 blockade induces a pressure gradient across the vasculature and improves drug penetration in tumors. *Cancer Res.* 2004; 64:3731–3736. [PubMed: 15172975]
13. Winkler F, et al. Kinetics of vascular normalization by VEGFR2 blockade governs brain tumor response to radiation: role of oxygenation, angiopoietin-1, and matrix metalloproteinases. *Cancer Cell.* 2004; 6:553–563. [PubMed: 15607960]
14. Nakaham T, Norberg SM, Shalinsky DR, Hu-Lowe DD, McDonald DM. Effect of inhibition of vascular endothelial growth factor signaling on distribution of extravasated antibodies in tumors. *Cancer Res.* 2006; 66:1434–1445. [PubMed: 16452199]
15. Willett CG, et al. Direct evidence that the VEGF-specific antibody bevacizumab has antivascular effects in human rectal cancer. *Nature Med.* 2004; 10:145–147. [PubMed: 14745444]
16. Batchelor TT, et al. AZD2171, a pan-VEGF receptor tyrosine kinase inhibitor, normalizes tumor vasculature and alleviates edema in glioblastoma patients. *Cancer Cell.* 2007; 11:83–95. [PubMed: 17222792]
17. Sorensen AG, et al. Increased Survival of Glioblastoma Patients who Respond to Antiangiogenic Therapy with Elevated Blood Perfusion. *Cancer Res.* 2012; 72:402–407. [PubMed: 22127927]
18. Jain RK, Stylianopoulos T. Delivering nanomedicine to solid tumors. *Nat. Rev. Clin. Oncol.* 2010; 7:653–664. [PubMed: 20838415]
19. Peer D, et al. Nanocarriers as an emerging platform for cancer therapy. *Nature Nanotechnol.* 2007; 2:751–760. [PubMed: 18654426]
20. Popovic Z, et al. A nanoparticle size series for in vivo fluorescence imaging. *Angew. Chem. Int. Ed.* 2010; 49:8649–8652.
21. Chauhan VP, et al. Fluorescent Nanorods and Nanospheres for Real-Time In Vivo Probing of Nanoparticle Shape-Dependent Tumor Penetration. *Angew. Chem. Int. Ed.* 2011; 50:11417–11420.
22. Gazit Y, et al. Fractal characteristics of tumor vascular architecture during tumor growth and regression. *Microcirculation.* 1997; 4:395–402. [PubMed: 9431507]

23. Hashizume H, et al. Openings between defective endothelial cells explain tumor vessel leakiness. *Am. J. Pathol.* 2000; 156:1363–1380. [PubMed: 10751361]
24. Baish JW, Netti PA, Jain RK. Transmural coupling of fluid flow in microcirculatory network and interstitium in tumors. *Microvasc. Res.* 1997; 53:128–141. [PubMed: 9143544]
25. Pozrikidis C, Farrow DA. A model of fluid flow in solid tumors. *Am. Biomed. Eng.* 2003, 31:181–194. [PubMed: 12627826]
26. Bungay PM, Brenner H. The motion of a closely-fitting sphere in a fluid-filled tube. *Int. J. Multiphase Flow.* 1973; 1:25–56.
27. Deen WM. Hindered transport of large molecules in liquid-filled pores. *AIChE Journal.* 1987, 33:1409–1425.
28. Satia H. Physiologic upper limits of pore size of different blood capillary types and another perspective on the dual pore theory of microvascular permeability. *J. Angiogenes. Res.* 2010; 2:14. [PubMed: 20701757]
29. Matsumura Y, Maeda H. A New Concept for Macromolecular Therapeutics in Cancer Chemotherapy: Mechanism of Tumor-tropic Accumulation of Proteins and the Antitumor Agent Smancs. *Cancer Res.* 1986; 46:6387–6392. [PubMed: 2946403]
30. Ruoslahti E, Bhatia SN, Saylor MJ. Targeting of drugs and nanoparticles to tumors. *J. Cell Biol.* 2010; 188:759–768. [PubMed: 20231381]

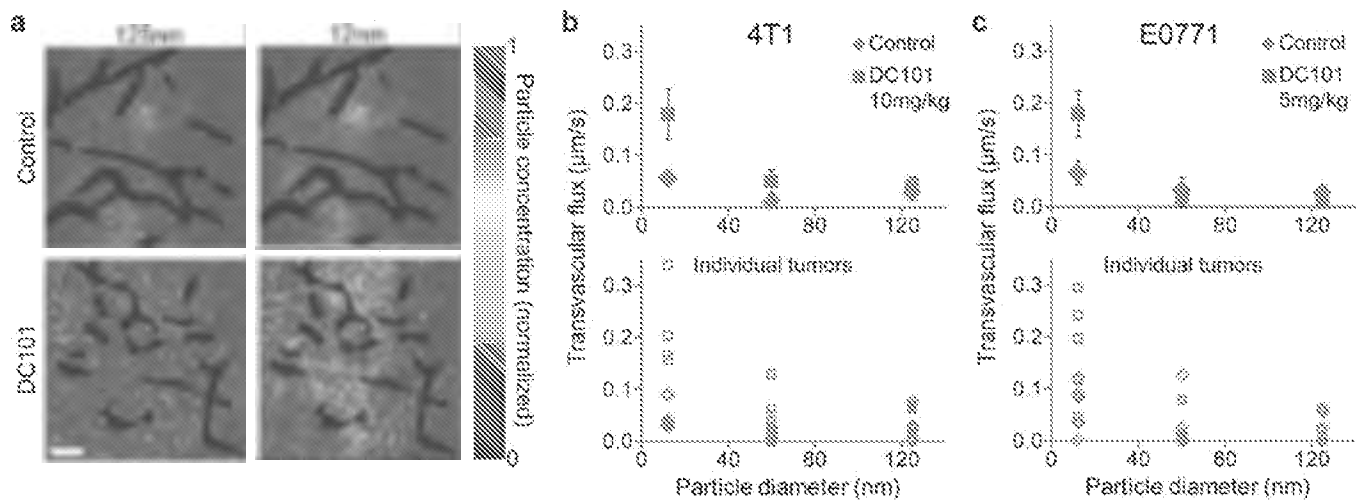


Figure 1. Effects of vascular normalization on nanoparticle delivery in tumours

a. Nanoparticle penetration versus particle size in orthotopic 4T1 mammary tumours in response to normalizing therapy with DC101. Nanoparticle concentrations – denoted by pseudocolour – are relative to initial intravascular levels, with vessels in black. Normalization improves 12nm particle penetration while not affecting 125nm penetration. Scale – 100µm. **b, c.** Penetration rates (transvascular flux) for nanoparticles in orthotopic 4T1 and E0771 mammary tumours in mice treated with 10mg/kg or 5mg/kg DC101, respectively. Closed symbols (top) denote averages by mouse, while open symbols (bottom) are individual tumours. Normalization improves the transvascular flux of 12nm particles on day 2 by a factor of 3.1 in 4T1 ($P = 0.042$, Student's t-test) and 2.7 in E0771 ($P = 0.049$, Student's t-test), while not improving delivery for larger nanoparticles. Normalization also reduces the flux of large nanoparticles to zero in several individual tumours. Animal number $n = 5$ for all groups.

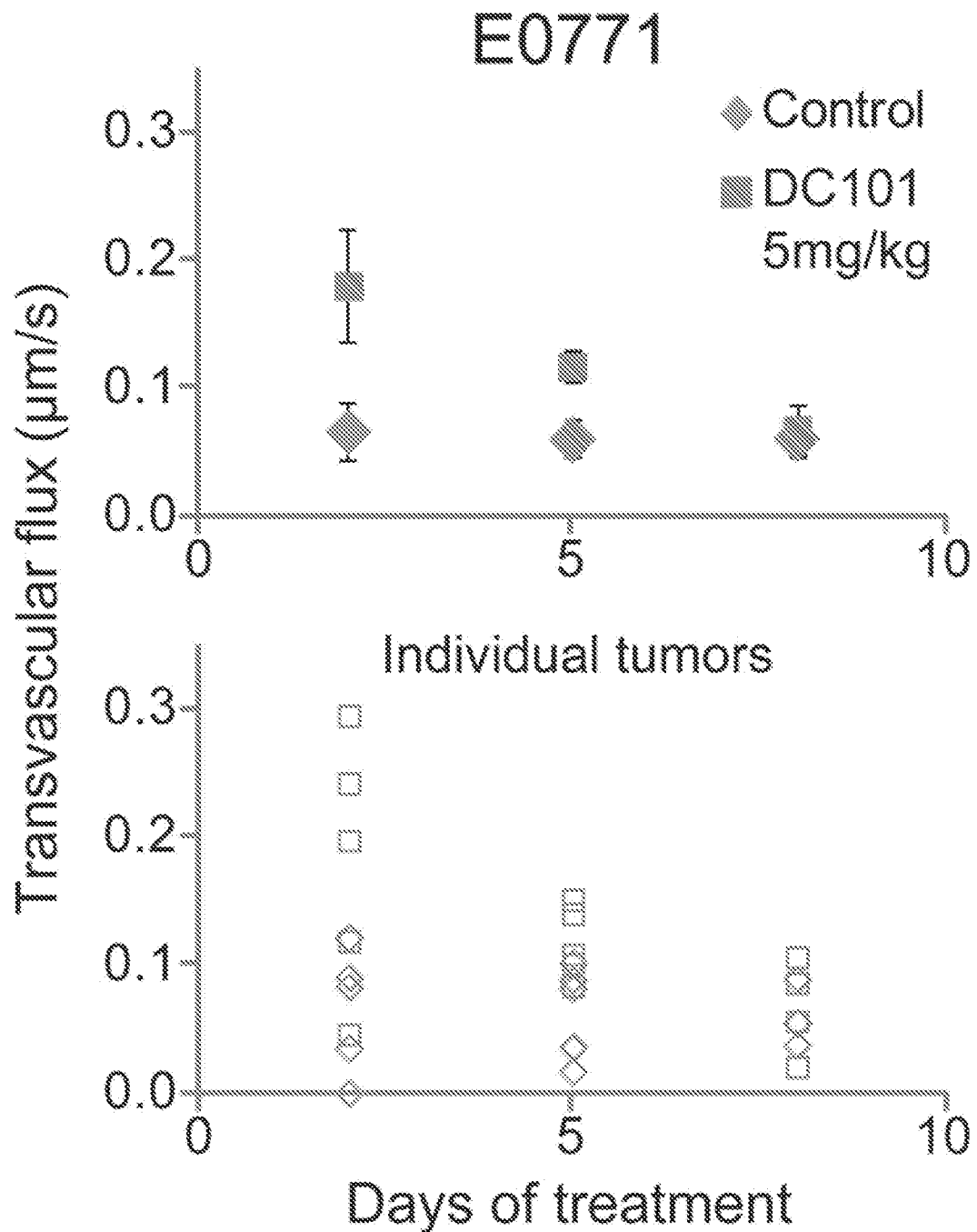


Figure 2. Functional vascular normalization “window” for nanomedicine delivery
 Penetration rates (transvascular flux) for 12nm nanoparticles in orthotopic E0771 mammary tumours. Measurements over an 8 day course of treatment with either 5mg/kg DC101 or non-specific rat IgG every 3 days starting on day 0. Closed symbols (top) denote averages by mouse, while open symbols (bottom) are individual tumours. Treatment with DC101 enhances nanoparticle transvascular flux on days 2 ($P = 0.049$, Student’s t-test) and 5 ($P = 0.017$, Student’s t-test), with no difference in the treatment groups by day 8. Animal number $n = 4-5$ for all groups.

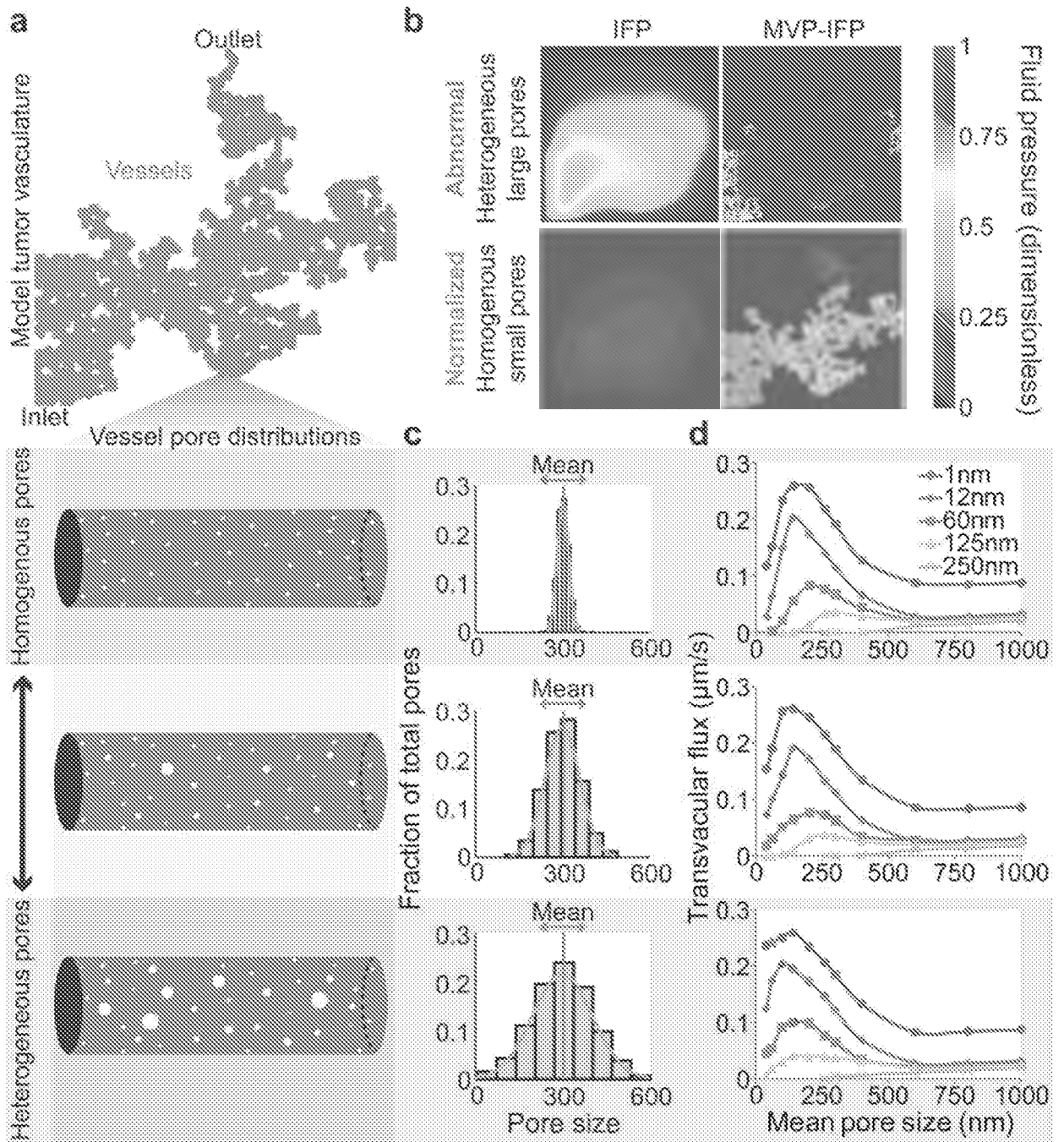


Figure 3. Mathematical model predictions of how changes in vascular pore size distribution affect delivery for different sizes of drugs
 a. Model tumour vasculature, formed as a percolation network, with a schematic of vessel pore structure. b. The effect of pore size distribution on fluid pressure. Large heterogeneous pores produce an elevated IFP that approaches the MVP, resulting in a near-zero transvascular pressure gradient (MVP – IFP) for central tumour vessels. Small homogenous pores result in a near-zero IFP and a high transvascular pressure gradient that can drive convective drug delivery. c. The mean pore size (diameter) and pore size standard deviation

are varied to predict how pore size changes affect drug delivery. Three standard deviations, at 20nm, 60nm, or 100nm, are selected to represent homogenous, moderate, and heterogeneous pores respectively. **d**, Simulations of transvascular flux versus mean pore size and pore size standard deviation for drugs from 1–250nm in diameter.

Author Manuscript

Author Manuscript

Author Manuscript

Author Manuscript

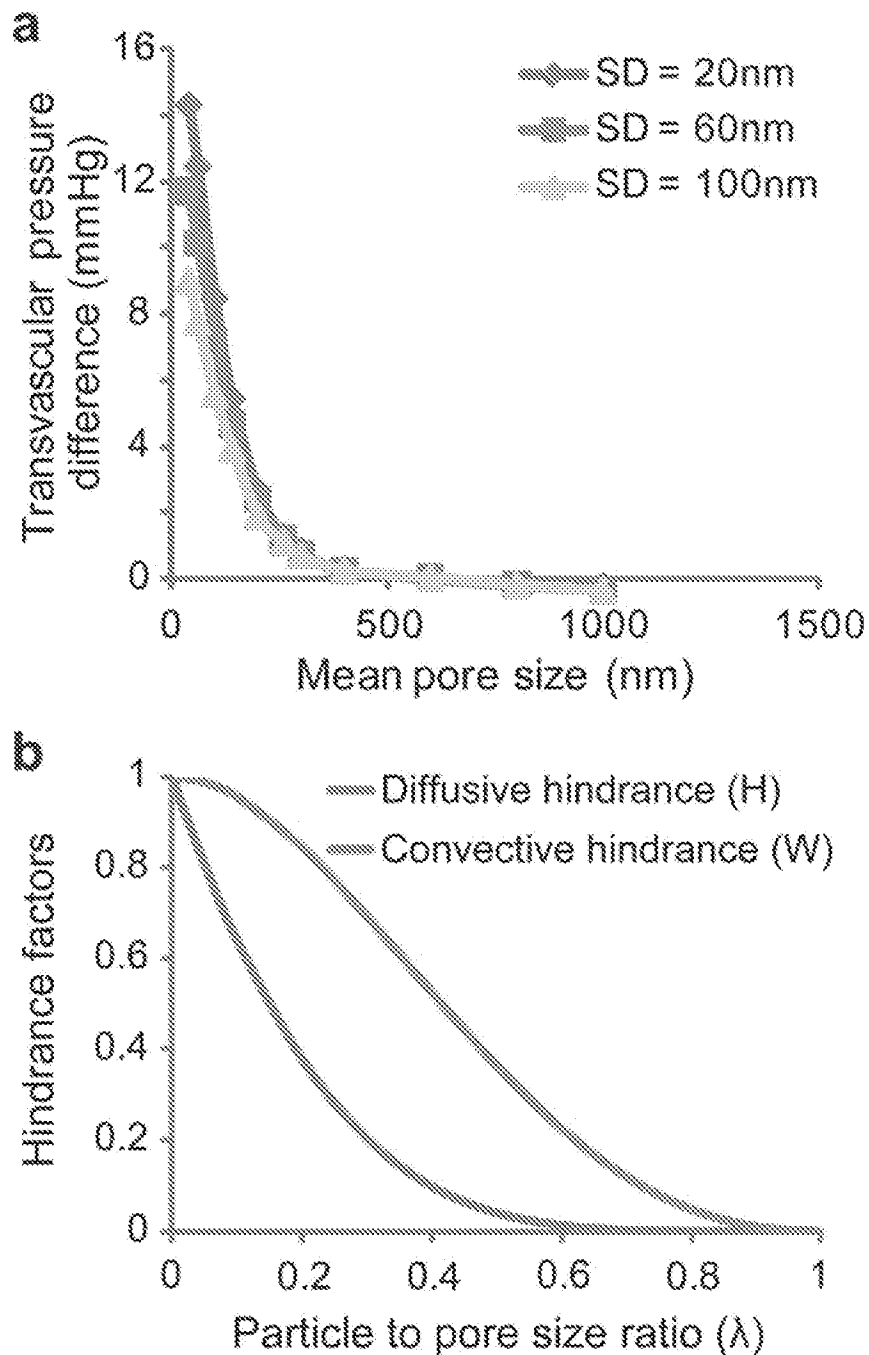


Figure 4. Dependence of the transvascular pressure gradient and transport hindrance on pore size

a, Transvascular pressure difference as a function of the vessel wall pore size. The plot presents the model predictions for three different standard deviations, namely 20, 60, and 100nm. The standard deviation of the distribution affects the transvascular pressure difference only for small pore sizes. For pore size distributions with a mean > 400 nm the pressure difference, and thus the fluid flux across the vessel wall, is practically zero. b, Hindrance factors for transport through pores versus particle to pore size ratio. The diffusive

(H) and convective (W) hindrance factors, which represent hydrodynamic and steric transport hindrance through pores, depend strongly on the particle to pore size ratio (λ). A hindrance factor of 1 indicates no hindrance, while that of zero denotes no transport whatsoever. Both diffusion and convection are increasingly hindered as particle size approaches pore size.

Author Manuscript

Author Manuscript

Author Manuscript

Author Manuscript

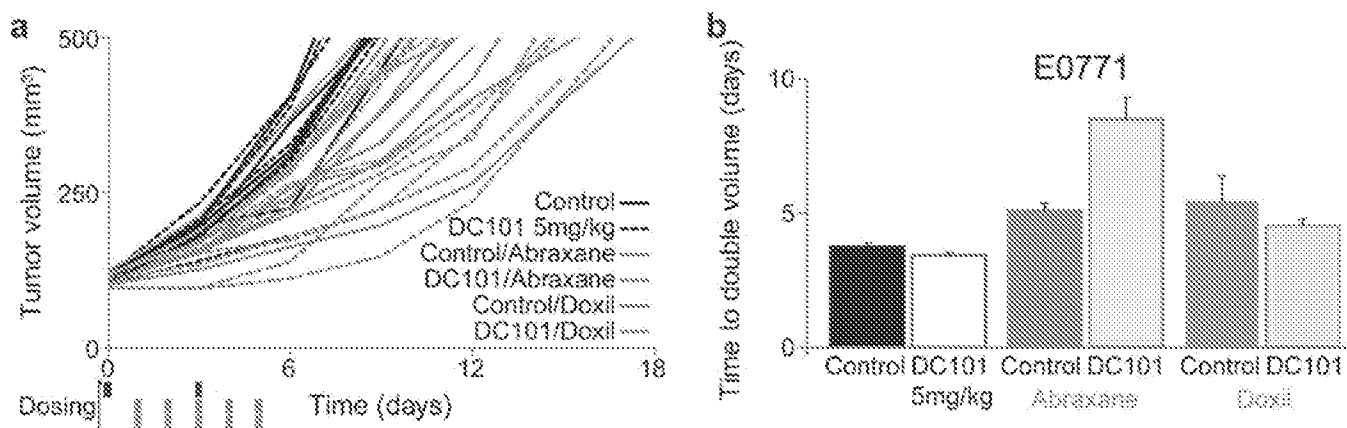


Figure 5. Improvement of cytotoxic nanomedicine effectiveness by vascular normalization
 a, Volumes of orthotopic E0771 mammary tumours in response to treatment with DC101 or non-specific rat IgG control (5mg/kg on days 0 and 3) in combination with either the ~10nm nanomedicine Abraxane (10mg/kg on days 1–5) or the ~100nm nanomedicine Doxil (2mg/kg on days 1–5). b, Quantification of tumour growth rates, based on the time to reach double the initial volume. Abraxane ($P = 0.040$, Mann-Whitney U-test) and Doxil ($P = 0.040$, Mann-Whitney U-test) monotherapy both induce growth delays versus the control treatment. Normalization with DC101 enhances the effectiveness of the ~10nm Abraxane ($P = 0.040$, Mann-Whitney U-test), but does not affect that of the ~100nm Doxil. Animal number $n = 4-5$ for all groups.

Improved pharmacokinetics and reduced toxicity of brucine after encapsulation into stealth liposomes: role of phosphatidylcholine

Jun Chen^{1*}
 Guo-jun Yan^{1,2*}
 Rong-rong Hu¹
 Qian-wen Gu¹
 Ming-lei Chen¹
 Wei Gu¹
 Zhi-peng Chen¹
 Bao-chang Cai^{1,2}

¹College of Pharmacy, ²Engineering Center of State Ministry of Education for Standardization of Chinese Medicine Processing, Nanjing University of Chinese Medicine, Nanjing, People's Republic of China

*These authors contributed equally to this project

Objective: Brucine was encapsulated into stealth liposomes using the ammonium sulfate gradient method to improve therapeutic index.

Materials and methods: Four brucine stealth liposomal formulations were prepared, which were made from different phosphatidylcholines (PCs) with different phase transition temperatures (T_m). The PCs used were soy phosphatidylcholine (SPC), dipalmitoyl phosphatidylcholine (DPPC), hydrogenated soy phosphatidylcholine (HSPC), and distearoyl phosphatidylcholine (DSPC). The stabilities, pharmacokinetics, and toxicities of these liposomal formulations were evaluated and compared.

Results: Size, zeta potential, and entrapment efficiency of brucine-loaded stealth liposomes (BSL) were not influenced by PC composition. In vitro release studies revealed that drug release rate increased with decreased T_m of PCs, especially with the presence of rat plasma. After intravenous administration, the area under the curve (AUC) values of BSL-SPC, BSL-DPPC, BSL-HSPC, and BSL-DSPC in plasma were 7.71, 9.24, 53.83, and 56.83-fold as large as that of free brucine, respectively. The LD_{50} values of brucine solution, BSL-SPC, BSL-DPPC, BSL-HSPC, and BSL-DSPC following intravenous injection were 13.17, 37.36, 37.69, 51.18, and 52.86 mg/kg, respectively. It was found in calcitonin retention experiments that the order of calcitonin retention in rat plasma was SPC < DPPC << HSPC < DSPC stealth liposomes.

Conclusion: PC composition could exert significant influence on the stabilities, pharmacokinetics, and toxicities of brucine-loaded stealth liposomes. DSPC or HSPC with T_m above 50°C should be used to prepare the stealth liposomal formulation for the intravenous delivery of brucine. However, it was found in the present paper that the pharmacokinetics and toxicity of BSL were not influenced by the PC composition when the T_m of the PC was in the range of -20°C to 41°C.

Keywords: brucine, stealth liposomes, phosphatidylcholine, pharmacokinetics, toxicity

Introduction

Brucine, originally isolated by Pelletier and Caventon in 1819 from *mux-vornica*,¹ is a white, odorless, crystalline solid with a molecular weight of 394.45. Antiproliferative and cytotoxic effects of brucine have been reported in HepG2,² SMMC-7721³ hepatoma cells, and multiple myeloma RPMI 8226 cell lines.⁴ Further study⁵ revealed that brucine produced time- and dose-dependent inhibition of MCF-7 cells in vitro and Ehrlich ascites carcinoma tumors in vivo, and that, furthermore, it could reduce peritoneal angiogenesis and microvessel density in vivo. Although brucine has been shown to possess an impressive preclinical profile in the pharmacological studies, severe central nervous system toxicity is the major obstacle to its clinical application. There is a narrow margin of safety between a therapeutic and a toxic dose. Higher

Correspondence: Bao-chang Cai
 College of Pharmacy, Nanjing University of Chinese Medicine, Nanjing 210046, People's Republic of China
 Tel +86 258 679 8281
 Fax +86 258 679 8281
 Email: robust2011@sina.com

doses of brucine will cause such symptoms as violent convulsion, significant increase in blood pressure, and even lethal poisoning.⁶

Liposomes have previously been used as carriers for antitumor drugs, and they have shown a significant effect in decreasing the extent and types of nonspecific toxicities. In addition, liposomes also increase the amount of drug that can be effectively delivered to the tumor. In the early 1990s, grafting polyethylene glycol (PEG) onto liposomes was invented to avoid the uptake of the mononuclear phagocyte system, resulting in improved pharmacokinetics *in vivo*. The term "stealth" was applied to these PEGylated liposomes because of their ability to evade interception by the mononuclear phagocyte system, much in the same way the stealth bomber is able to evade radar. The main properties of stealth liposomes are their significantly improved pharmacokinetics and thus enhanced residence in the blood.⁷ If brucine is encapsulated into the stealth liposomes, it mainly stays in the blood circulation since stealth liposomes cannot pass the biomembrane directly. Therefore, the distribution of brucine into the brain can be avoided and the acute toxicity of brucine can be reduced subsequently.

It is evident that the phosphatidylcholine (PC) used to prepare liposomes has a significant effect on the stability of the resulting liposomes. In the early 1980s, it was demonstrated that liposomes obtained from a PC with a high transition temperature (T_m) were more stable in the blood than liposomes prepared from a PC with a low T_m .⁸ PC is an important consideration with liposome stability, and the state of liposomes at physiological temperature, for instance, can be altered by the inclusion of PCs with different T_m s.

For stealth liposomes, different PCs possessing different T_m s have been used to prepare liposome formulations. Hydrogenated soy phosphatidylcholine (HSPC, $T_m = 50^\circ\text{C}$) was recently used to make flavopiridol-loaded stealth liposomes⁹ and its *in vivo* pharmacokinetics were significantly improved compared to the free drug. Dipalmitoyl phosphatidylcholine (DPPC) was used to prepare gemcitabine-loaded stealth liposomes and their antitumor activity at 5 mg/kg was equal to the free drug at the dose of 50 mg/kg.¹⁰ CKD-602, a camptothecin analogue, was encapsulated into stealth liposomes composed of distearoyl phosphatidylcholine (DSPC). Compared to the free drug, the AUC in plasma after intravenous administration of CKD-602-containing DPPC stealth liposomes increased about 22-fold.¹¹

Since stealth liposomes composed of different PCs with different T_m s were all reported to improve *in vivo* behavior,

it is necessary to evaluate the effect of PC on the stability, pharmacokinetic behavior, and toxicity of brucine-loaded stealth liposomes.

As for brucine, the stability of stealth liposomes is the key factor which is directly associated with toxicity. If the stealth liposomes are unstable in the blood circulation, brucine can be rapidly leaked from the carrier and distribution into the brain cannot be avoided. Therefore, PC composition seems to have a significant effect on the toxicity of brucine stealth liposomes following intravenous administration.

In the present paper, four different PCs – soy phosphatidylcholine (SPC), DPPC, HSPC, and distearoyl phosphatidylcholine (DSPC) – with T_m in the range of -20°C to 55°C were used to prepare brucine-loaded stealth liposomes (BSL). Their stabilities, pharmacokinetics, and acute toxicities were investigated and compared.

Materials and methods

Materials

SPC, DPPC, HSPC, DSPC, and 1,2-distearoyl-sn-glycero-3-phosphoethanolamine- N-(carbonyl-methoxypolyethylene glycol-2000) (DSPE-PEG2000) were purchased from Lipoid Corp (Ludwigshafen, Germany). Cholesterol was purchased from Huxing Biochemistry Reagent Company (Shanghai, China). Reference substances of brucine and the internal standard (IS) huperzine A were supplied by the National Institute for the Control of Pharmaceutical and Biological Products (Beijing, China). The purities of brucine (95.9%) and huperzine A (98.0%) were determined by high-performance liquid chromatography (HPLC) analysis. Brucine and calcein were obtained from Sigma-Aldrich (St Louis, MO). Sephadex G-50 was purchased from Pharmacia Biotech (Uppsala, Sweden). HPLC-grade acetonitrile was obtained from Tedia Company Inc. (Fairfield, OH). All other reagents were of analytical grade.

Animals

Male Sprague-Dawley rats, weighing 200–250 g, were purchased from Shanghai Slac Laboratory Animal Co, Ltd (Shanghai, China). Toxicity experiments were performed with male ICR mice, weighing 15–22 g, also obtained from the Slac Laboratory Animal Co, Ltd. The animals were acclimatized for at least 1 week in a 12-hour light/dark cycle with free access to standard food and water. According to the requirement of the National Act on the Use of Experimental Animals (People's Republic of China), the protocols of the animal experiments were approved by

the Animal Ethics Committee of Nanjing University of Chinese Medicine.

Preparation of liposomes

The BSLs were prepared by the ammonium sulfate gradient loading method as described previously.¹² Briefly, the mixture of PC, cholesterol and DSPC-PEG2000 at a molar ratio of 15:5:1 were dissolved in 2 mL ethanol and then injected into a solution of 5 mL 200 mol/L ammonium sulfate under magnetic stirring at 60°C. The ethanol was evaporated to no odor under vacuum, and then water was added to adjust the volume of final liposome suspension to 5 mL. To get homogenous liposome suspensions, liposomes were ultrasonically treated for 10 minutes, using a JY92-2 probe ultrasonicator (Xinzhi Biotechnology Co, Ltd, Ningbo, China) equipped with a tapered microtip. The resultant liposomes were filtered through a 0.22 µm micropore filter to remove the titanium fragments. The transmembrane ammonium sulfate gradient was created by four consecutive dialysis exchanges (2 hours at a time) against 100 mL of phosphate buffer solution (PBS) (pH = 7.4) at room temperature. Brucine in powder form in a drug/lipid mass ratio of 1:12 was added to liposomes at 60°C for 20 minutes.

A total of four formulations were prepared which were named BSL-SPC, BSL-DPPC, BSL-HSPC, and BSL-DSPC. The main difference among these formulations was PC composition (see Figure 1 for more information).

Vesicle size and zeta potential measurement

The particle sizes and zeta potentials of BSLs were evaluated in triplicate by dynamic light scattering (DLS), using a Zeta Potential Analyzer (Brookhaven Instruments Corporation, Holtsville, NY).

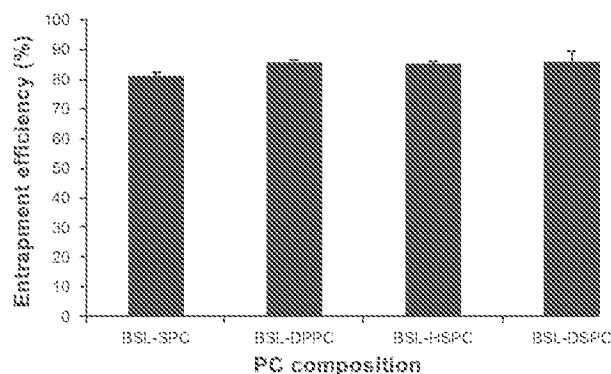


Figure 1 The characterization of brucine-loaded stealth liposomes with different PC composition.

Abbreviations: PC, phosphatidylcholine; BSL, brucine-loaded stealth liposome; SPC, soy phosphatidylcholine; DPPC, dipalmitoyl phosphatidylcholine; HSPC, hydrogenated soy phosphatidylcholine; DSPC, distearoyl phosphatidylcholine.

Entrapment efficiency

The entrapment efficiency (EE) was calculated by the percentage of brucine encapsulated in stealth liposomes relative to the total amount of brucine (encapsulated and free) in stealth liposome suspension. To determine the total amount of brucine in stealth liposome suspension, 0.5 mL brucine stealth liposome was disrupted by the addition of 2 mL ethanol-isopropanol (1:4, v/v) to form a clear solution. The concentration of brucine was assayed by UV spectroscopy (TU1300S, Puxi Instrument Company, Beijing, China) at 264 nm compared to a standard curve.

To completely remove nonentrapped drug, BSLs were passed through a Sephadex G50 column (1 × 27 cm; Pharmacia Biotech Corp., Uppsala, Sweden) equilibrated with PBS (pH 7.4). The resultant PBS fraction containing the stealth liposomes free of nonentrapped brucine was collected and the entrapped brucine concentration was determined as described above.

EE was calculated using the following equation:

$$\%EE = \text{encapsulated drug} / \text{total drug} \times 100\%$$

HPLC analysis of brucine in PBS

An HPLC system (Shimadzu Corporation, Kyoto, Japan) consisting of a LC-20AT pump and a SPD-20A UV-VIS detector was used for the assay of brucine. The mobile phase consisted of acetonitrile and buffer (10 mM sodium heptane sulfonate and 20 mM potassium dihydrogen phosphate, pH adjusted to 2.8 with 10% phosphonic acid). The ratio of acetonitrile/buffer (v/v) was adjusted to 24/76. Separation was carried out at 35°C using a reverse-phase C₁₈ column (Lichrospher, 5 µm, 4.6 mm × 250 mm, Hanbang Corp, Hunan, China). The detection wavelength was 264 nm and a flow rate of 1.0 mL/minute was employed. A sample volume of 20 µL was injected.

Calibration curves of brucine in PBS were linear in the range of 0.4–12.8 mg/L. The regression coefficient was 0.9994. Intra-day and inter-day precisions of brucine were no more than 1.50%.

Drug release study

The *in vitro* release of BSLs with different PC composition was analyzed according to the published method.¹³ Non-entrapped drug was removed from BSLs over a Sephadex G-50 column as described above before an *in vitro* release test. The BSL suspension (drug content: 2 mg) was placed in a dialysis bag with a molecular weight cut-off of 10,000. The dialysis bag was suspended in 100 mL isotonic PBS (pH 7.4) which was

incubated at 37°C under constant rotation at 500 rpm. At scheduled time intervals, aliquot samples were withdrawn and assayed for brucine content by HPLC as described above. The volume of dissolution medium was maintained at 100 mL throughout the experiment. To evaluate the effect of plasma albumin on drug release from stealth liposomes, brucine stealth liposome suspension combined with fresh rat plasma (1:1, v/v) was placed in the dialysis bag.

In vivo pharmacokinetic studies

Rats were randomized into groups of five and six. Five groups of rats were given a single dose of 2.5 mg/kg brucine solution (dissolved in PBS), BSL-SPC, BSL-DPPC, BSL-HSPC, and BSL-DSPC by tail vein injection. At predetermined intervals (5, 10, 20, 40, 60, 90, 120, 180, 240, and 360 minutes), the rats were anaesthetized using ether and blood samples were collected from the retro-orbital plexus into heparinized microfuge tubes. The blood samples were then immediately centrifuged at 10,000 rpm for 2 minutes to obtain the plasma samples, which were then stored at -20°C until HPLC analysis.

Sample preparation

Plasma samples were treated using the liquid-liquid extraction step described previously.¹³ Briefly, 100 μ L plasma were spiked with 10 μ L IS (40 μ g/mL loperazine A solution in methanol). 10 μ L of aqueous ammonia was added and the samples were basified. 3 mL n-hexane-dichloromethane-isopropanol (65:30:5, v/v/v) was then added. The mixture was vortex-mixed for 3 minutes and subsequently centrifuged for 10 minutes at 4000 rpm at ambient temperature. The organic layer was transferred into a glass tube and the residue was re-extracted in a similar manner. The combined organic layer was evaporated at 50°C under a gentle stream of nitrogen gas, until a completely dried residue was left. The residue was reconstituted in 100 μ L methanol and centrifuged for 5 minutes at 12,000 rpm. Finally, 50 μ L of the supernatant were injected into HPLC system for analysis.

HPLC analysis of plasma samples

HPLC analysis of treated plasma samples were performed using a HPLC-UV system (Shimadzu Corporation, Kyoto, Japan) consisting of a LC-20AT pump and a SPD-20A UV detector. Data was collected by a HPLC chromatography workstation (N2000, Intelligence and Information Institute of Zhejiang University, Hangzhou, China). Chromatographic separation was achieved on a Kromasil C₁₈ analytical column (4.6 mm \times 250 mm, 5 μ m,

Kromasil, Sweden) coupled with a C₁₈ guard cartridge (4.6 mm \times 10 mm, 5 μ m, Haubang Corp), maintained at 35°C. The mobile phase consisted of 24% acetonitrile and 76% buffer (isometric mixture of 10 mM sodium heptane sulfonate and 20 mM potassium dihydrogen phosphate, the pH value was adjusted to 2.8 with 10% phosphoric acid). The prepared mobile phase was filtered using a vacuum filter system equipped with 0.45 μ m filter and delivered at a flow rate of 1.0 mL/minute. The detection wavelength was set at 264 nm.

Statistical analysis and calculation of pharmacokinetic parameters

The chromatographic data were automatically processed to obtain the peak-area ratios of compound to IS and fitted to a weighted (1/C²) linear regression relationship. The pharmacokinetic parameters were calculated using non-compartmental analysis of data. The data are presented as means with standard deviations (SD) for the individual groups. Statistically significant differences were assessed by Student's *t*-test with the level of statistical significance set at *P* < 0.05.

The following pharmacokinetic parameters were calculated using noncompartmental analysis of data (Drug and Statistics version 2.0 Program, Shanghai, China): the area under the plasma concentration-time curve from time zero to time infinity (AUC_{0- ∞}), the area under the plasma concentration-time curve from time zero to the last time point (AUC_{0-*t*}), the total body clearance (Cl), the mean residence time (MRT), the terminal elimination half-life (t_{1/2}) and the apparent volume of distribution (V).

Acute toxicity test

Brucine was dissolved in pH 7.4 PBS and the resulting brucine solution was obtained. BSLs with different PC compositions had concentrations of 2.0 mg/mL and EEs higher than 80%. The maximal and minimal lethal doses were preliminarily estimated. The dosages for determination of the median lethal dose (LD₅₀) were then calculated and intravenously administered to five dosage groups (10 mice each). All mice were observed for general symptoms. The number of dead mice was recorded. LD₅₀, LD₅₀ and LD₁₀₀ values were calculated using the Bliss method.¹⁴

Evaluation of membrane permeability by calcein release measurements in vitro

Because the release of calcein from liposomes can be determined without the use of dialysis bags, calcein is usually

used to evaluate membrane stability. Calcein-loaded liposomes with different PC compositions were prepared by the thin film hydration method.¹⁵ The mixture of PC, cholesterol, and DSPE-PEG2000 at a molar ratio of 15:5:1 was dissolved in chloroform in a round-bottom flask. The solvent was evaporated using a rotary evaporator to form a thin layer of lipid in the flask. 5 mL of 90 mM calcein (pH 7.4) was added and the lipid mixture was hydrated at 60°C for 40 minutes to form multilamellar vesicles (MLV). MLVs were then sonicated using a JY92-2 probe ultrasonicator (Xinzhi Biotechnology Co, Ltd, Ningbo, China) equipped with a tapered microtip. The resulting liposomes were filtered through a 0.22 µm micropore filter to remove the titanium fragments. Unencapsulated calcein was removed by gel filtration using Sephadex G50 column (1 × 27 cm) with pH7.4 phosphate buffer saline (PBS) as eluent at a flow rate of 1 mL/minute.

Calcein-loaded liposomes (100 µL) were added to 2.9 mL rat plasma/PBS medium (1:1) and incubated at 37°C under constant stirring. At predetermined time points, aliquot samples were withdrawn and diluted. After rapid cooling in an ice-bath, the fluorescence of the sample was measured in a fluorimeter (F96S; Lengguang, Shanghai, China) using 490 nm excitation and 515 nm emission wavelengths. Complete release of calcein was achieved by the addition of Triton X-100 (Anresco LLC, Solon, OH) (final concentration, 1%). The percentage of calcein release at different time points was calculated using the following equation:

$$\% \text{release} = 100 \times (F_t - F_0) / (F_{100} - F_0)$$

Where F_t is the fluorescence at time point, F_0 is the initial fluorescence of calcein liposomes at the start of the incubation time, and F_{100} is the fluorescence of Triton X-100 treated samples.

Results and discussion

Characterization of brucine-loaded stealth liposomes

The particle sizes of BSL-SPC, BSL-DPPC, BSL-HSPC, and BSL-DSPC are shown in Figure 1. The PC composition had little effect on the size of BSLs. The polydispersity index was lower than 0.25 for all BSLs, indicating that liposome population was homogenous in size. The results of zeta potential measurements revealed that four liposomal formulations were all electric neutral.

The effect of PC composition on EE of stealth liposomes at a drug-to-lipid mass ratio of 1:12 is shown in Figure 2.

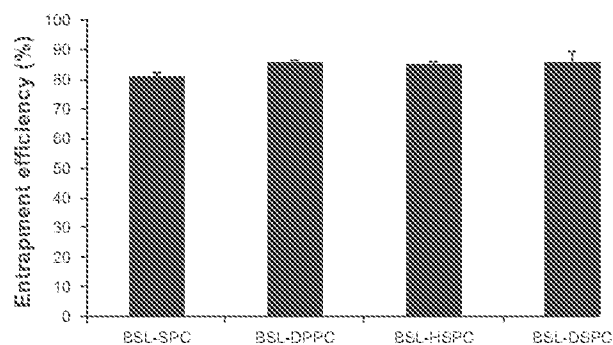


Figure 2 Effect of phosphatidylcholine composition on entrapment efficiency of brucine-loaded stealth liposomes.

Note: $n = 3$.

Abbreviations: BSL, brucine-loaded stealth liposomes; SPC, soy phosphatidylcholine; DPPC, dipalmitoyl phosphatidylcholine; HSPC, hydrogenated soy phosphatidylcholine; DSPC, distearoyl phosphatidylcholine.

The EE of BSLs was not influenced by PC composition and all EEs were higher than 80%.

Drug release in vitro

HPLC chromatograms are shown in Figure 3. The in vitro drug release profiles are shown in Figures 4 and 5. Without the existence of rat plasma, the drug release ratios of BSL-SPC, BSL-DPPC, BSL-HSPC, and BSL-DSPC in 10 hours were $10.52\% \pm 0.47\%$, $13.25\% \pm 0.81\%$, $6.08\% \pm 1.25\%$, and $6.43\% \pm 1.55\%$, respectively. With the presence of rat plasma, the release of brucine was accelerated dramatically and a large extent of drug release was observed. The retention of the loaded brucine in the stealth liposomes was more significantly dependent on PC compositions with different T_m . Most encapsulated brucine ($80.92\% \pm 1.94\%$) had been released from BSL-SPC. In comparison, the other three BSLs improved drug retention significantly. For BSLs with higher T_m , only $30.71\% \pm 5.23\%$, $15.56\% \pm 1.04\%$, and $17.34\% \pm 0.95\%$ released from BSL-DPPC, BSL-HSPC, and BSL-DSPC at 10 hours, respectively. It was evident that the extent of drug retention in BSLs corresponded to the T_m of PC, even though the release of BSL-DPPC was markedly higher than compared to BSL-SPC in the initial 4 hours.

For stealth liposomes, the effect of lipid composition on the stability in vitro was investigated. Irinotecan was encapsulated into HSPC, DSPC, or egg phosphatidylcholine (EPC)-based stealth liposomes and the drug leakage profiles of these liposome formulations were compared.¹⁶ Stealth liposomes that contained EPC of a lower T_m (approximately -20°C) were found to be highly unstable as about 95% irinotecan was leaked in 240 minutes. In contrast, liposomes that were composed of lipids with higher T_m (approximately 50°C – 60°C), HSPC and DSPC, were significantly more

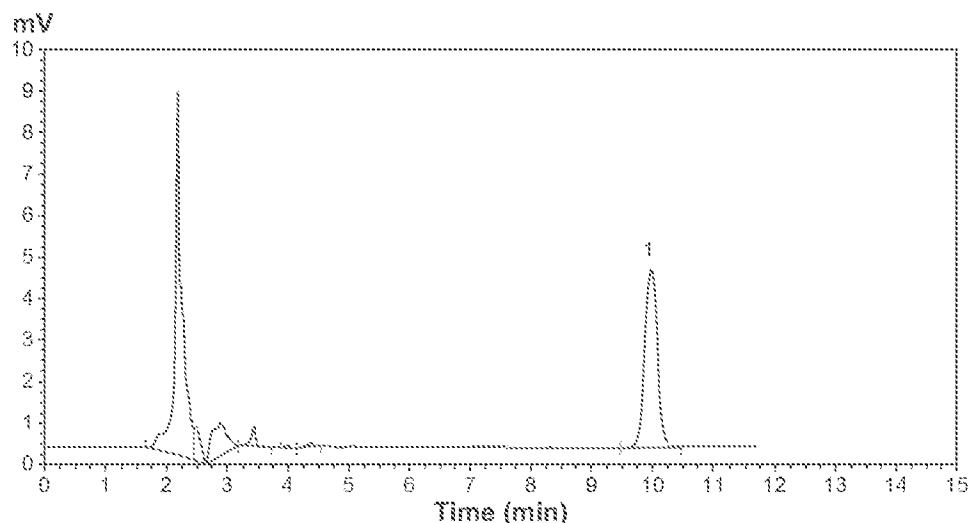


Figure 3 HPLC chromatographs of brucine in PBS.

Note: Peak 1 represents brucine.

Abbreviations: HPLC, high-performance liquid chromatography; PBS, phosphate buffer solution.

stable under the experimental condition. Only 50%–60% of the encapsulated drug was leaked in 240 minutes. It was concluded that the lipid membranes consisting of PCs with lower T_m exhibit higher fluidity compared to membranes consisting of PCs with higher T_m .

It should be noted that preparation methods influence the release profiles as well. For brucine-loaded HSPC liposomes prepared by ethanol-dripping method and ammonium sulfate gradient loading method, there were about 68%¹⁷ and 6% brucine (in the present paper) released into PBS after 10 hours.

In the present study, the stability of BSLs with different PC compositions was examined by drug release kinetics *in vitro*. The results of the drug release test without the presence of rat plasma revealed that nearly 85%–95% of the encapsulated drug was retained inside the liposomes in 10 hours. One possible explanation for the good drug retention is that brucine forms a gel-like precipitate with ammonium sulfate as doxorubicin does because of the lower solubility of the brucine sulfate salt formed in the intra-liposomal aqueous phase. It was well known that serum components destabilize liposomal membranes.¹⁸

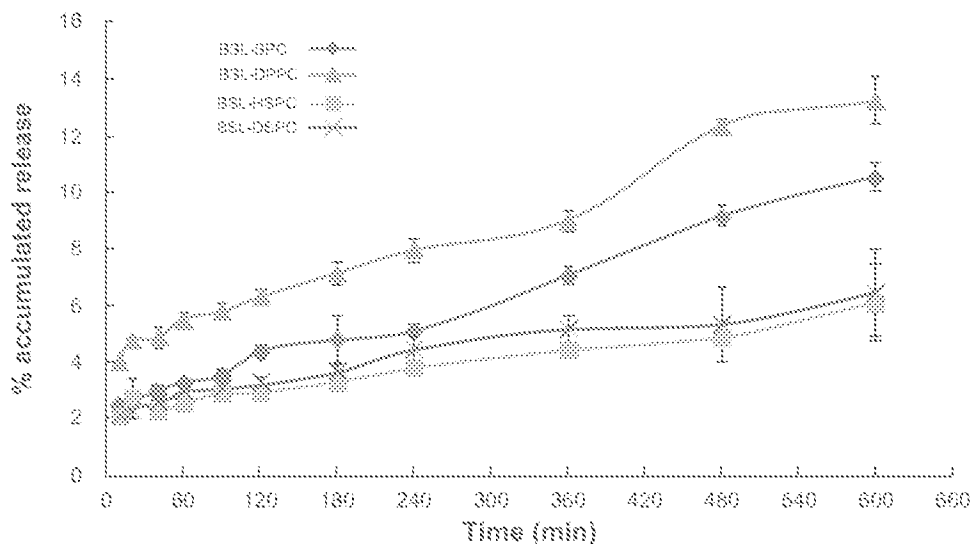


Figure 4 *in vitro* release profiles of brucine from brucine-loaded stealth liposomes with different phase transition temperature.

Note: mean \pm SD; n = 3.

Abbreviations: BSL, brucine-loaded stealth liposomes; SPC, soy phosphatidylcholine; DPPC, dipalmitoyl phosphatidylcholine; HSPC, hydrogenated soy phosphatidylcholine; DEPC, distearoyl phosphatidylcholine; SD, standard deviation.

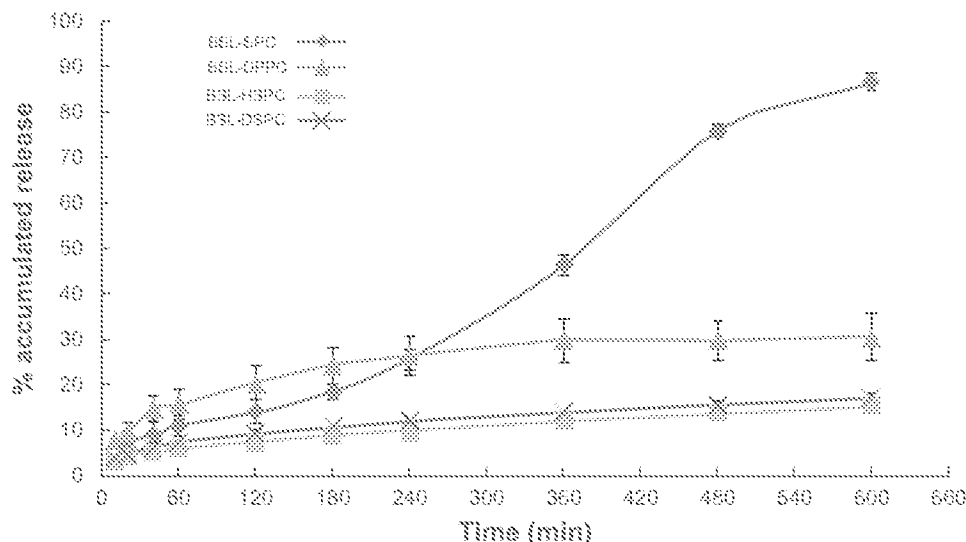


Figure 5 In vitro release profiles of brucine from brucine-loaded stealth liposomes with different phase transition temperature in the presence of rat plasma.

Notes: mean \pm SD, n = 3.

Abbreviations: BSL, brucine-loaded stealth liposomes; SPC, soy phosphatidylcholine; DPPC, dipalmitoyl phosphatidylcholine; HSPC, hydrogenated soy phosphatidylcholine; DSPC, distearoyl phosphatidylcholine; SD, standard deviation.

Phospholipids exchange and transfer to lipoproteins, which can destabilize and disintegrate liposomes. Therefore, with the presence of rat plasma, the release of brucine was significantly increased. Compared with BSL-SPC, the other three BSLs were proved to possess better drug retention. The good stability of BSLs with higher T_m may be attributed to the enhanced bilayer rigidity. Thus BSLs with higher T_m showed a significant decrease in release rate and an increase in resistance to release. However, if T_m was higher than

50°C, the PC composition effect on the stability of BSL was no longer significant.

In vivo pharmacokinetic studies

The semi-logarithmic plasma concentration-time profiles of brucine following intravenous administration of 2.5 mg/kg brucine solution and four BSLs are shown in Figure 6. The pharmacokinetic parameters are summarized in Table 1. As seen in Figure 6 and Table 1, after encapsulation into

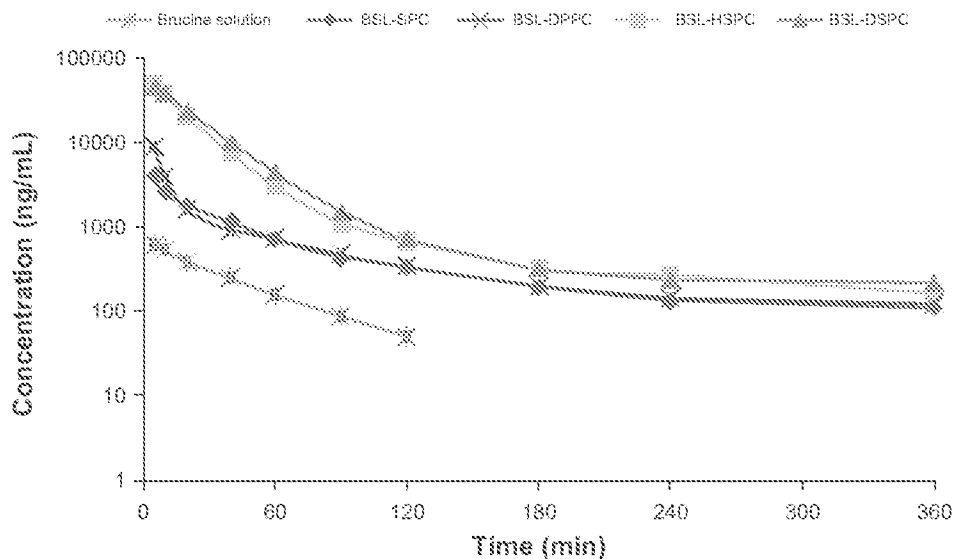


Figure 6 Plasma concentration-time profile of brucine after intravenous administration at a single dose of 2.5 mg/kg of brucine solution or brucine-loaded stealth liposomes with different phase transition temperature in rats.

Notes: n = 5.

Abbreviations: BSL, brucine-loaded stealth liposomes; SPC, soy phosphatidylcholine; DPPC, dipalmitoyl phosphatidylcholine; HSPC, hydrogenated soy phosphatidylcholine; DSPC, distearoyl phosphatidylcholine.

Table 1 Pharmacokinetic parameters of brucine after intravenous administration at a single dose of 2.5 mg/kg of brucine solution or brucine-loaded stealth liposomes with different phase transition temperature in rats

Parameters	Brucine solution	BSL-SPC	BSL-DPPC	BSL-HSPC	BSL-DSPC
AUC_{0-5} ($\mu\text{g}\cdot\text{min}\cdot\text{mL}^{-1}$)	29.78 \pm 5.18	242.22 \pm 146.67	300.85 \pm 201.07	1378.72 \pm 357.62	1450.00 \pm 378.74**
AUC_{0-24} ($\mu\text{g}\cdot\text{min}\cdot\text{mL}^{-1}$)	25.27 \pm 4.73	194.85 \pm 118.21	233.57 \pm 107.20	1360.24 \pm 330.07**	1436.17 \pm 377.23**
MRT/min	28.78 \pm 1.52	68.85 \pm 45.33	50.77 \pm 26.15	28.79 \pm 9.56**	28.206 \pm 3.84**
CL/FL ($\text{Kg}^{-1}\cdot\text{min}^{-1}$)	0.086 \pm 0.013	0.018 \pm 0.016	0.012 \pm 0.008	0.002 \pm 0.001*	0.002 \pm 0.001*
V/FL (Kg^{-1})	4.31 \pm 1.44	2.07 \pm 1.74	2.00 \pm 1.36	0.24 \pm 0.07*	0.19 \pm 0.10*
$t_{1/2}$ /min	34.93 \pm 11.44	100.86 \pm 43.66	103.74 \pm 49.87	89.13 \pm 25.07	71.95 \pm 32.37

Notes: n = 6; compared to BSL-SPC. *P < 0.05; **P < 0.001.

Abbreviations: BSL, brucine-loaded stealth liposomes; SPC, soy phosphatidylcholine; DPPC, dipalmitoyl phosphatidylcholine; HSPC, hydrogenated soy phosphatidylcholine; DSPC, distearoyl phosphatidylcholine; AUC_{0-t} , area under the curve from time 0 to time t; MRT, mean residence time; CL, total body clearance; V, volume of distribution; N, number; BSL, brucine-loaded stealth liposomes; P, probability.

stealth liposomes, the pharmacokinetics of brucine were significantly improved. In comparison with free brucine, the AUC_{0-5} of BSL-SPC, BSL-DPPC, BSL-HSPC, and BSL-DSPC increased 7.71-, 9.24-, 53.83-, and 56.83-fold, respectively. The $t_{1/2}$ values of BSLs were also increased. It was obvious that the pharmacokinetics of BSL-SPC and BSL-DPPC were similar and no statistical significance was found in all pharmacokinetic parameters of these two groups as shown in Table 1. It appeared that the pharmacokinetic characteristics of BSL were not influenced by the PC composition when the T_m of the PC was in the range of -20°C to 41°C . The pharmacokinetics of BSL-HSPC and BSL-DSPC with higher T_m were also similar. Compared to BSL-SPC and BSL-DPPC, BSL-HSPC and BSL-DSPC significantly increased AUC and remarkably reduced CI ($P < 0.05$). Therefore, the pharmacokinetics of BSL seemed to be

improved significantly with the increase of the T_m in the PC from 41°C to 50°C .

The relationship between the T_m of PC and the AUC_{0-5} of the corresponding BSLs after intravenous administration were shown in Figure 7. When the T_m of PC was higher than 50°C , the AUC of BSL composed of the corresponding PC was significantly increased compared to that of BSL with T_m under 41°C .

Although in vitro stability of stealth liposomes was intensively studied, the effect of PC composition on in vivo stability should also be investigated and revealed. The results of pharmacokinetics demonstrated that the AUC of BSLs with T_m above 50°C was significantly increased compared to those with T_m below 41°C . Therefore, for the development of BSL for the treatment of tumors, DSPC or HSPC with higher T_m should be taken into consideration.

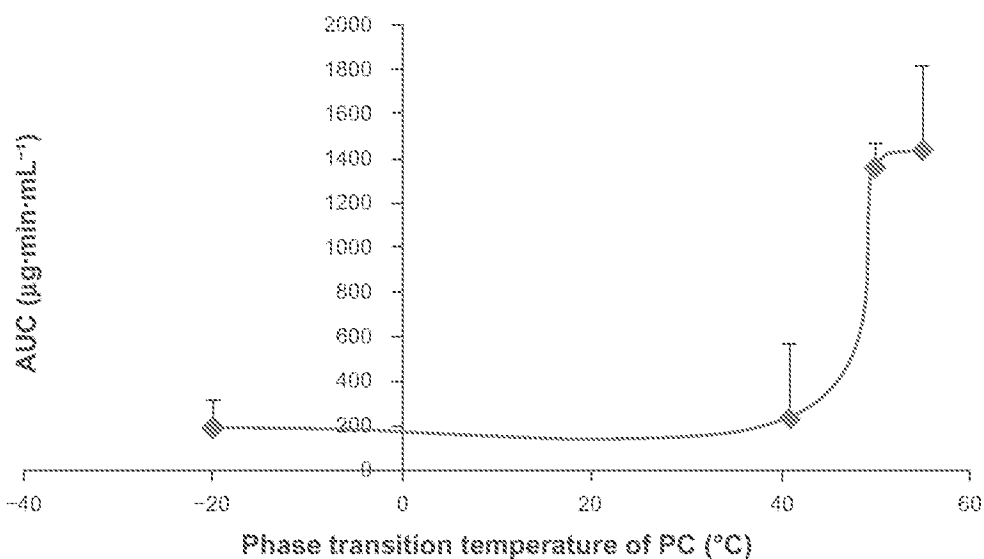


Figure 7 Relationship between the phase transition temperature of PC and the AUC_{0-5} of brucine-loaded stealth liposomes composed of the corresponding PC after intravenous administration at a single dose of 2.5 mg/kg to rats.

Note: n = 6.

Abbreviations: PC, phosphatidylcholine; AUC_{0-t} , area under the curve from time 0 to time (t).

Table 2 Toxic values (Bliss method) of intravenously administrated brucine solution or brucine-loaded stealth liposomes in mice

Formulations	LD ₅₀ (mg/kg)	LD ₁₀ (mg/kg)	LD ₁ (mg/kg)
Brucine solution	18.93	13.17	9.17
BSL-SPC	52.84	37.30	26.34
BSL-DPPC	57.27	37.69	24.81
BSL-HSPC	72.08	51.18	36.34
BSL-DSPC	73.30	52.86	38.11

Abbreviations: LD, median lethal dose; BSL, brucine-loaded stealth liposomes; SPC, soy phosphatidylcholine; DPPC, dipalmitoyl phosphatidylcholine; HSPC, hydrogenated soy phosphatidylcholine; DSPC, distearoyl phosphatidylcholine.

The higher concentration of BSLs in the bloodstream, as demonstrated by plasma AUC measurements, could lead to a higher brucine accumulation in the tumor by enhanced permeation and retention effects after intravenous administration.

It was surprising that MRT values of BSL-HSPC and BSL-DSPC were found to be lower than that of BSL-SPC. But the pharmacokinetic results were in accordance with the drug release profiles in rat plasma. It was generally assumed that the macrophage-resistant property of stealth liposomes is due to suppression in surface opsonization and protein absorption. However, evidence showed that stealth liposomes were also prone to opsonization particularly by the opsonic components of the complement system.¹⁹ Although opsonization was significantly restricted in the initial phase after intravenous administration, protein absorption might not be avoided in the later phase. Therefore, the accelera-

tion of clearance from the blood might lead to the reduced MRT values. However, because the liposomes are mainly uptaken by the liver and spleen, not including the brain, the toxicity of BSLs will not be affected.

Acute toxicity test

Table 2 shows a comparison of the acute toxicity of free brucine and different BSL formulations. The intravenous LD₅₀ of brucine solution was 13.17 mg/kg, while the LD₅₀ values of BSL-SPC, BSL-DPPC, BSL-HSPC, and BSL-DSPC were 37.30, 37.69, 51.18, and 52.86 mg/kg, respectively.

Severe central nervous system toxicity is the major obstacle to the clinical application of brucine. If it is encapsulated into the stealth liposomes, brucine mainly stays in the blood circulation since stealth liposomes cannot pass the biomembrane directly. Therefore, the distribution of brucine into the brain can be avoided and the acute toxicity of brucine can be reduced subsequently. However, if brucine can be easily released from the liposomes with lower T_m in the bloodstream, it can pass through the blood-brain barrier completely and rapidly. And the toxicity of BSL was increased subsequently.

It was obvious that the toxicity of brucine was significantly reduced after encapsulation into stealth liposomes. In addition, although plasma concentrations of brucine after intravenous administration of BSL-HSPC and BSL-DSPC were much higher than those after intravenous

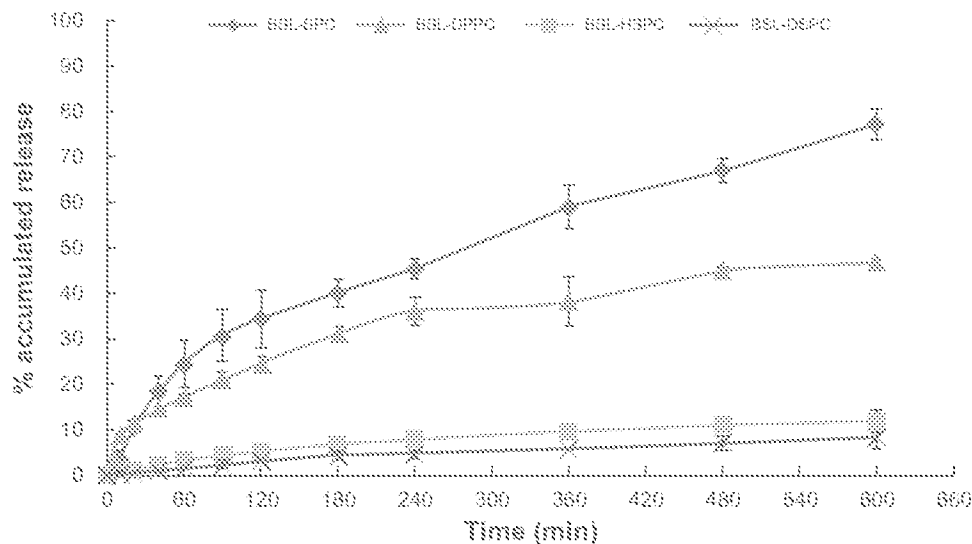


Figure 8 Calcein release from BSLs with different PC composition in rat plasma: PBS (1:1) at 37°C monitored at different time intervals in the range from 5 to 600 minutes.

Notes: mean ± SD, n = 3.

Abbreviations: BSL, brucine-loaded stealth liposomes; PC, phosphatidylcholine; PBS, phosphate buffered solution; SPC, soy phosphatidylcholine; DPPC, dipalmitoyl phosphatidylcholine; HSPC, hydrogenated soy phosphatidylcholine; DSPC, distearoyl phosphatidylcholine; SD, standard deviation.

administration of BSL-SPC and BSL-DPPC, the LD_{50} values were significantly increased. It demonstrated that brucine was mostly encapsulated into stealth liposomes in plasma due to higher stability of HSPC or DSPC stealth liposomes.

Evaluation of membrane permeability by calcein release measurements in vitro

The release of calcein was determined fluorometrically by measuring the increase of the fluorescence signal as a result of de-quenching. This has usually been used to characterize the membrane permeability of liposomes. A 90 mM solution of the fluorescent dye calcein was encapsulated into the liposomes. The concentration of the encapsulated dye is above its self-quenching concentration (12 μ M).¹² Consequently, the fluorescence is only observable upon dilution of the dye due to its release. This enabled monitoring of the release of entrapped material in situ by measuring the increase in the fluorescence signal intensity. The calcein release profiles from stealth liposomes with different PC composition are shown in Figure 8. At 10 hours, 77.18% \pm 3.35% calcein were released from SPC stealth liposomes. For liposomes with higher T_m , only 46.85% \pm 0.57%, 11.82% \pm 2.53%, and 8.39% \pm 2.55% calcein were released from DPPC, HSPC, and DSPC stealth liposomes at 10 hours, respectively. The order of calcein retention in 50% rat plasma was SPC < DPPC << HSPC < DSPC stealth liposomes. The results were in accordance with the results of in vitro brucine release tests.

Conclusion

In the present paper, the effects of PC (with different T_m) composition on stabilities, pharmacokinetics, and toxicities of BSLs were investigated. It was found that BSLs composed of PC with T_m above 50°C were more stable in vitro and in vivo. But if the T_m of the PC was lower than 41°C, the resulting BSL-SPC and BSL-DPPC were unstable in plasma in vitro and the AUC in vivo was less than one-fifth of that of BSL-HSPC or BSL-DSPC. The toxicity of BSL was in direct relationship with the PC composition. BSL-HSPC and BSL-DSPC with T_m above 50°C possessed lower toxicity compared to BSL-SPC and BSL-DPPC. In summary, our study indicated that DSPC or HSPC with T_m above 50°C should be used to prepare the stealth liposomal formulation for the targeted delivery of brucine because of high stability.

Acknowledgments

This work was financially supported by the National Nature Science Foundation of China (No 30701111, 81001644) and Guangdong Nature Science Foundation (10451040701004643).

Disclosure

The authors report no conflicts of interest. The authors alone are responsible for the content and writing of this paper.

References

- Philippe G, Angenot L, Tits M, Fr  d  rich M. About the toxicity of some *Strychnos* species and their alkaloids. *Toxicon*. 2004;44(4):405-416.
- Deng XK, Yin W, Li WD, et al. The anti-tumor effects of alkaloids from the seeds of *Strychnos nux-vomica* on HepG2 cells and its possible mechanism. *J Ethnopharmacol*. 2006;106(2):179-186.
- Yin W, Deng XK, Yin FZ, Zhang XC, Cai BC. The cytotoxicity induced by brucine from the seed of *Strychnos nux-vomica* proceeds via apoptosis and is mediated by cyclooxygenase 2 and caspase 3 in SMMC 7721 cells. *Food Chem Toxicol*. 2007;45(9):1706-1702.
- Rao PS, Kamanadham M, Prasad MN. Anti-proliferative and cytotoxic effects of *Strychnos nux-vomica* root extract on human multiple myeloma cell line - RPMI 8226. *Food Chem Toxicol*. 2009;47(2):283-283.
- Agarwal BS, Saraswati S, Mathur R, Pandey M. Cytotoxic and antitumor effects of brucine on Ehrlich ascites tumor and human cell line. *Life Sci*. 2011;89(5-6):147-158.
- Malone MH, St John-Allan KM, Bejar E. Brucine lethality in mice. *J Ethnopharmacol*. 1992;35(3):295-297.
- Zhang L, Han L, Sun X, Gao D, Qin J, Wang J. The use of PEGylated liposomes to prolong the circulation lifetime of silybinic acid B. *Fitoterapia*. February 25, 2012 [Epub ahead of print].
- Senior J, Gregoriadis G. Is half-life of circulating liposomes determined by changes in their permeability? *FEBS Lett*. 1982;145(1):109-114.
- Yang X, Zhao X, Phelps MA, et al. A novel liposomal formulation of flavopiridol. *Int J Pharm*. 2009;365(1-2):170-174.
- Paolino D, Cosco D, Ruscicchi L, et al. Gemcitabine-loaded PEGylated unilamellar liposomes vs GEMZAR: biodistribution, pharmacokinetic features and in vivo antitumor activity. *J Control Release*. 2010;144(2):144-150.
- Zamboni WC, Strychar S, Joseph E, et al. Plasma, tumor, and tissue distribution of STEALTH liposomal CKD-602 (8-CKD602) and nonliposomal CKD-602 in mice bearing A375 human melanoma xenografts. *Clin Cancer Res*. 2007;13(23):7217-7223.
- Chen J, Liu A, Chen Z, et al. Ammonium sulfate gradient loading of brucine into liposomes: effect of phospholipid composition on encapsulation efficiency and physicochemical properties in vitro. *Drug Dev Ind Pharm*. 2010;36(3):245-253.
- Chen J, Xiao HL, Hu RR, et al. Pharmacokinetics of brucine after intravenous and oral administration to rats. *Fitoterapia*. 2011;82(8):1302-1308.
- Rosello AP, Essigmann JM, Wogan GN. Rapid and accurate determination of the median lethal dose (LD50) and its error with a small sample. *J Toxicol Environ Health*. 1977;3:797-809.
- Djanashvili E, ten Hagen TL, Biang   R, Schipper D, Peters JA, Koning GA. Development of a liposomal delivery system for temperature-triggered release of a tumor targeting agent, Ln(III)-DOTA-phenylboronate. *Inorg Med Chem*. 2011;19(3):1123-1130.
- Chou TH, Chen SC, Chu IM. Effect of composition on the stability of liposomal irinotecan prepared by a pH gradient method. *J Biosci Bioeng*. 2003;95(4):405-402.

17. Qin XQ, Yuan Y, Liu CS, et al. Preparation of liposomal brucine and its pharmaceutical/pharmacodynamic characterization. *Acta Pharmacol Sin.* 2007;28(11):1851-1858.
18. Mercadal M, Domingo JC, Bermudez M, Mora M, De Madariaga MA. N-palmitoylphosphatidylethanolamine stabilizes liposomes in the presence of human serum: effect of lipid composition and system characterization. *Biochim Biophys Acta.* 1995;1235(2):281-288.
19. Moghimi SM, Szabeni I. Stealth liposomes and long circulating nanoparticles: critical issues in pharmacokinetics, opsonization and protein-binding properties. *Prog Lipid Res.* 2003;42(6):463-478.

International Journal of Nanomedicine

Publish your work in this journal

The International Journal of Nanomedicine is an international, peer-reviewed journal focusing on the application of nanotechnology in diagnostics, therapeutics, and drug delivery systems throughout the biomedical field. This journal is indexed on PubMed Central, Medline, CAS, SciSearch®, Current Contents®/Clinical Medicine,

Submit your manuscript for consideration at <http://www.dovepress.com/info/submit-your-manuscript-to-international-journal>

Dovepress

Journal Citation Reports/Science Edition, EMBase, Scopus and the Elsevier Bibliographic databases. The manuscript management system is completely online and includes a very quick and fair peer-review system, which is all easy to use. Visit <http://www.dovepress.com/testimonials.php> to read real quotes from published authors.

Electronic Acknowledgement Receipt

EFS ID:	42151132
Application Number:	15809815
International Application Number:	
Confirmation Number:	5137
Title of Invention:	Methods for Treating Metastatic Pancreatic Cancer Using Combination Therapies Comprising Liposomal Irinotecan and Oxaliplatin
First Named Inventor/Applicant Name:	Eliel Bayever
Customer Number:	153749
Filer:	Mary Rucker Henninger/Richard King
Filer Authorized By:	Mary Rucker Henninger
Attorney Docket Number:	263266-421428
Receipt Date:	12-MAR-2021
Filing Date:	10-NOV-2017
Time Stamp:	16:21:07
Application Type:	Utility under 35 USC 111(a)

Payment information:

Submitted with Payment	no
------------------------	----

File Listing:

Document Number	Document Description	File Name	File Size(Bytes)/ Message Digest	Multi Part /.zip	Pages (if appl.)
1	Transmittal Letter	2021-03-12_01208-0007-01US_IDS_Transmittal_as_filed.pdf	120456 <small>560132f9de0806c72c7254cd69a2dd40082cbede</small>	no	2

Warnings:

CSPC Exhibit 1109

Page 221 of 339

Information:					
2	Information Disclosure Statement (IDS) Form (SB08)	2021-03-12_01208-0007-01US-SB08_1_OF_6_as_filed.pdf	1060084	no	12
			26cba4311106b6f9f38875548031295e84ae2154		
Warnings:					
Information:					
3	Foreign Reference	CA2412790A1.pdf	7196959	no	49
			8d1b420c430328491304ce321f74bc0a461fa235		
Warnings:					
Information:					
4	Foreign Reference	CN101878229A.pdf	3458065	no	47
			fe9598630518b54eea7e04d3c21bc39b6c09cce4		
Warnings:					
Information:					
5	Foreign Reference	CN1829741A.pdf	5729231	no	76
			6ba4bab62b37d0e4cd0d31e38f2480d1efc02188		
Warnings:					
Information:					
6	Foreign Reference	CN1980637B.pdf	1431922	no	102
			f150492b3074f8d3e79eadd8c3734b6ff0ad133e		
Warnings:					
Information:					
7	Foreign Reference	WO2000023052A1.pdf	2329097	no	50
			7ff13294c52c1e27f44aeadd8c59b1a99297ca058		
Warnings:					
Information:					
8	Foreign Reference	WO2004017940A2.pdf	2254162	no	43
			de75ff5b057ade9ea7004ee5f026c230ff893ad0		
Warnings:					
Information:					

9	Foreign Reference	WO2004093795A2.pdf	5319222	no	113
			f00137088a06f521182bb51e67e87c6a8f3c4a1f		
Warnings:					
Information:					
10	Foreign Reference	WO2009040426A1.pdf	679307	no	75
			77b51aae64a1143f03244f308445657966dd4f14		
Warnings:					
Information:					
11	Foreign Reference	WO2010125462A2.pdf	1515025	no	32
			4dc8cb713c4adb75c6226d8c6a7af5c670660a87		
Warnings:					
Information:					
12	Foreign Reference	WO2011066684A1.pdf	1839350	no	38
			f5b6fbd541e46284981ae1814b3216cd4f39ee2e		
Warnings:					
Information:					
13	Foreign Reference	WO2012031293A1.pdf	2862680	no	50
			08be5f078a0e35230b5d79b7f4064110d2ee2a50		
Warnings:					
Information:					
14	Foreign Reference	WO2013138371A1.pdf	2630628	no	57
			2f6b4b42ca48fa782b0bb1571d68e3bedf4cc6ba		
Warnings:					
Information:					
15	Foreign Reference	WO2014157444A1.pdf	1506433	no	39
			6ac6d5c9c82b28fea80b27429fcb264650951a77		
Warnings:					
Information:					

16	Foreign Reference	WO2016168451A1.pdf	5035959	no	53
			64787baf220af3d25ddafa09cd88db1978c63e05		
Warnings:					
Information:					
17	Foreign Reference	WO2017066726A1.pdf	3725770	no	123
			fcfc9624f3a91d57c9c4c30cddd3c1bf085559e8		
Warnings:					
Information:					
18	Foreign Reference	WO2017172678A1.pdf	4501016	no	98
			c0bdd9f286eea04d745c46d7c425cce61a8981ec		
Warnings:					
Information:					
19	Foreign Reference	WO2018083470A1.pdf	4308348	no	90
			3116812a5aedede55b9a2bef66655467950499		
Warnings:					
Information:					
20	Foreign Reference	WO2005000900A1.pdf	5392054	no	93
			30bdf3e310e6473fee46b879f14caaaa83d18f6e		
Warnings:					
Information:					
21	Foreign Reference	WO2005107712A1.pdf	8275113	no	179
			0ee36d29f6c85647d3cac146f5667bb25ec95b7d		
Warnings:					
Information:					
22	Non Patent Literature	Abra_2002.pdf	63914	no	3
			b88dff9f81cd5830ba593fb39ad22ce4b8bdcb84		
Warnings:					
Information:					

23	Non Patent Literature	Alese_ASCO_GI_2018_poster.pdf	1341487	no	1
			9cb1ed4cf768e85975e491bc56c0c4a952e08d09		
Warnings:					
Information:					
24	Non Patent Literature	Alese_ASCO_GI_2018_abstract.pdf	1514158	no	5
			b26ccc20a2d47b55068928245672d873d55ae9a8		
Warnings:					
Information:					
25	Non Patent Literature	Allergriini_2008.pdf	148327	no	8
			51769712589964c4d04d79b8a35ba446b01de4eb		
Warnings:					
Information:					
26	Non Patent Literature	Alves_da_silva_2018.pdf	255186	no	9
			0973099bb2e6783124837f09af54e877553cbd9c		
Warnings:					
Information:					
27	Non Patent Literature	Anders_2019_presentation.pdf	306182	no	11
			3c93888652faee84485733da814ef3c5b1cd06c4		
Warnings:					
Information:					
28	Non Patent Literature	Anders_ASCO_2019_abstract.pdf	110252	no	2
			4024c7b92ed53fa90f5b49a607398928062ffcb8b		
Warnings:					
Information:					
29	Non Patent Literature	Anders_2019_abstract.pdf	57663	no	1
			8cbb4a66bdb916a183d067feb268962f951e2eb7		
Warnings:					
Information:					

30	Non Patent Literature	Andre_2007.pdf	139568	no	7
			68f5c77eb7c544f3f6569acfc25602e69f2d426		
Warnings:					
Information:					
31	Non Patent Literature	Aranda_2009.pdf	213156	no	7
			49f5ba02fb5f574c0777ebf4e9386068a9014ec7		
Warnings:					
Information:					
32	Non Patent Literature	Awasthi_AACR_2020_poster.pdf	3904300	no	6
			e0c1d3772b4839faf459b4323cea02365bc73854		
Warnings:					
Information:					
33	Non Patent Literature	Awasthi_AACR_2020_abstract.pdf	101831	no	2
			e313e45783befea84deb76f5470fdca3c70e3dd4		
Warnings:					
Information:					
34	Non Patent Literature	Barenholz_2014.pdf	4071529	no	89
			2733a6a0aa15734457cdc4c4cb36d552e654bc31		
Warnings:					
Information:					
35	Non Patent Literature	Barenholz_2012.pdf	526352	no	18
			1acc3123b67f6b4119487a8d108281ad625ac182		
Warnings:					
Information:					
36	Non Patent Literature	Barone_2007.pdf	117930	no	8
			258dbd5b273d12c9858d56c5aecfc2b91e0dcde3		
Warnings:					
Information:					

37	Non Patent Literature	Basu_2016.pdf	266417	no	8
			580bd4f33f8682743b1d4a6d84bd13f82d7ef4de		
Warnings:					
Information:					
38	Non Patent Literature	Batist_2009.pdf	901733	no	9
			719578014e914240608e4d290b6ef15f460564ac		
Warnings:					
Information:					
39	Non Patent Literature	Batist_2006.pdf	141470	no	2
			9d035bb7fb8e6f24726623957617936b7a2a1108		
Warnings:					
Information:					
40	Non Patent Literature	Batist_2007.pdf	1407271	no	5
			89e1da1e64533bd7a5609447f32f3e95dda57a9		
Warnings:					
Information:					
41	Non Patent Literature	Bendell_2012.pdf	411165	no	10
			28173dd6fab01ca04006274005ef281aee15cba1		
Warnings:					
Information:					
42	Non Patent Literature	Bernards_2018.pdf	4197836	no	7
			c6e6d9b0ec9f7ef67335bc3e920b6b852bd09342		
Warnings:					
Information:					
43	Non Patent Literature	Bernards_2017_poster.pdf	843467	no	5
			c4d7fe67731a6bec68f0a13dd29ec283347d1968		
Warnings:					
Information:					

44	Non Patent Literature	Boman_1993.pdf	498125	no	6
			3b546302b9b3508f75afb2c67aba42e4ff8a5f44		
Warnings:					
Information:					
45	Non Patent Literature	Borner_2005.pdf	81134	no	7
			cc74c4734934aa4061a29822cf5e22fb3d8a77bc		
Warnings:					
Information:					
46	Non Patent Literature	Boulikas_2009.pdf	619021	no	22
			e5b8dc26f114257632e8927f33a55c415b84da77		
Warnings:					
Information:					
47	Non Patent Literature	Bozzuto_2015.pdf	633772	no	25
			a40cf39c0b65a8526f8a9008064f0476a8245ab		
Warnings:					
Information:					
48	Non Patent Literature	Bulbake_2017.pdf	480794	no	33
			63ae9e48f733b89026748edbb830db1d65266aa4		
Warnings:					
Information:					
49	Non Patent Literature	Butowski_ASCO_2015_poster.pdf	1362338	no	4
			0c890ba11972696907066850b813a50f8111e084		
Warnings:					
Information:					
50	Non Patent Literature	Butowski_ASCO_2015_abstract.pdf	67143	no	2
			f133530d8378a7607b41d680c8f963c0e84f7aec		
Warnings:					
Information:					

51	Non Patent Literature	Caelyx.pdf	74162	no	11
			e3e3f75adbcbda2ece4ebb2ae89e360d07580bcc		
Warnings:					
Information:					
52	Non Patent Literature	Cao_2005.pdf	351264	no	8
			0236203adc0d7bc09ea49a20c4186f9cd985b4bd		
Warnings:					
Information:					
53	Non Patent Literature	Cao_2020.pdf	860963	no	9
			9c0b7e91854a962905bfd8b4eb090c44b2b90f3a		
Warnings:					
Information:					
54	Non Patent Literature	Carter_2016.pdf	880785	no	8
			86f69c759c274ac27a745c25339bd5cc1524455f		
Warnings:					
Information:					
55	Non Patent Literature	Cassileth_1983.pdf	1682578	no	4
			43dde20857c373de3ffe3b1bae2380257c1c4719		
Warnings:					
Information:					
56	Non Patent Literature	Chabot_1997.pdf	1008350	no	15
			94596a63220eca4b79814d27ad0c3602bcb69387		
Warnings:					
Information:					
57	Non Patent Literature	Chan_ASCO_2016_poster.pdf	2259953	no	7
			190f8d59dc40128005dda533b61ba0217da0a108		
Warnings:					
Information:					

58	Non Patent Literature	Chan_ASCO_2016_abstract.pdf	1347648	no	4
			1077c6b79639188cd03fdab2aff80ccb1650670		

Warnings:

Information:

59	Non Patent Literature	Chauhan_2012.pdf	541062	no	15
			ff4d4a4dd27fa5a835a4a4520f352268e1d202fd		

Warnings:

Information:

60	Non Patent Literature	Chen_J_2012.pdf	193571	no	11
			2003b36adaf626d7914e97c56b9eda20bbb4b0f		

Warnings:

Information:

Total Files Size (in bytes):			105154738		
-------------------------------------	--	--	-----------	--	--

This Acknowledgement Receipt evidences receipt on the noted date by the USPTO of the indicated documents, characterized by the applicant, and including page counts, where applicable. It serves as evidence of receipt similar to a Post Card, as described in MPEP 503.

New Applications Under 35 U.S.C. 111

If a new application is being filed and the application includes the necessary components for a filing date (see 37 CFR 1.53(b)-(d) and MPEP 506), a Filing Receipt (37 CFR 1.54) will be issued in due course and the date shown on this Acknowledgement Receipt will establish the filing date of the application.

National Stage of an International Application under 35 U.S.C. 371

If a timely submission to enter the national stage of an international application is compliant with the conditions of 35 U.S.C. 371 and other applicable requirements a Form PCT/DO/EO/903 indicating acceptance of the application as a national stage submission under 35 U.S.C. 371 will be issued in addition to the Filing Receipt, in due course.

New International Application Filed with the USPTO as a Receiving Office

If a new international application is being filed and the international application includes the necessary components for an international filing date (see PCT Article 11 and MPEP 1810), a Notification of the International Application Number and of the International Filing Date (Form PCT/RO/105) will be issued in due course, subject to prescriptions concerning national security, and the date shown on this Acknowledgement Receipt will establish the international filing date of the application.

IN THE UNITED STATES PATENT AND TRADEMARK OFFICE

In re Application of Inventors:

Eliel BAYEVER et al.

Application No.: 15/809,815

Filed: November 10, 2017

Title: Methods for Treating Metastatic
Pancreatic Cancer Using Combination
Therapies Comprising Liposomal
Irinotecan and Oxaliplatin

Group Art Unit: 1612

Examiner: Celeste A. RONEY

Confirmation No.: 5137

INFORMATION DISCLOSURE STATEMENT UNDER 37 C.F.R. § 1.97(b)

VIA EFS WEB

Commissioner for Patents
P.O. Box 1450
Alexandria, VA 22313-1450

Commissioner:

Pursuant to 37 C.F.R. §§ 1.56 and 1.97(b), Applicant brings to the attention of the Examiner the documents listed on the enclosed IDS Forms PTO/SB/08. This Information Disclosure Statement is being filed after the filing of a Request for Continued Examination on February 25, 2021 and to the undersigned's knowledge before the mailing of an Office Action on the merits.

Copies of the listed non-US patent publication documents are enclosed.

Applicant respectfully requests that the Examiner consider the listed documents and indicate that they have been considered by making appropriate notations on the enclosed form.

This submission does not represent that a search has been made or that no better art exists and does not constitute an admission that the listed documents are material or constitute "prior art." If the Examiner applies a cited document against any claim of the application and Applicant determines that the cited document does not constitute "prior art," Applicant reserves the right to present to the Office the relevant facts and law regarding the appropriate status of the document.

Applicant further reserves the right to take appropriate action to establish the patentability of the claimed invention over the cited documents, should the Examiner apply one or more of the documents against any of the claims of the present application.

Please charge any fee required for entry of this Information Disclosure Statement, or credit any overpayment, to Deposit Account No. 506488.

Respectfully submitted,

McNeill Baur PLLC

Dated: March 12, 2021

By: /Mary R. Henninger/
Mary R. Henninger
Reg. No. 56,992
Telephone: 404-891-1400

INFORMATION DISCLOSURE STATEMENT BY APPLICANT (Not for submission under 37 CFR 1.99)	Application Number	15809815
	Filing Date	2017-11-10
	First Named Inventor	Eliel Bayever
	Art Unit	1612
	Examiner Name	Celeste A. RONEY
	Attorney Docket Number	01208-0007-01US

U.S.PATENTS							Remove
Examiner Initial*	Cite No	Patent Number	Kind Code ¹	Issue Date	Name of Patentee or Applicant of cited Document	Pages,Columns,Lines where Relevant Passages or Relevant Figures Appear	
	1						

If you wish to add additional U.S. Patent citation information please click the Add button. Add

U.S.PATENT APPLICATION PUBLICATIONS							Remove
Examiner Initial*	Cite No	Publication Number	Kind Code ¹	Publication Date	Name of Patentee or Applicant of cited Document	Pages,Columns,Lines where Relevant Passages or Relevant Figures Appear	
	1						

If you wish to add additional U.S. Published Application citation information please click the Add button. Add

FOREIGN PATENT DOCUMENTS								Remove
Examiner Initial*	Cite No	Foreign Document Number ³	Country Code ² i	Kind Code ⁴	Publication Date	Name of Patentee or Applicant of cited Document	Pages,Columns,Lines where Relevant Passages or Relevant Figures Appear	T ⁵
	1							

If you wish to add additional Foreign Patent Document citation information please click the Add button Add

NON-PATENT LITERATURE DOCUMENTS								Remove
Examiner Initials*	Cite No	Include name of the author (in CAPITAL LETTERS), title of the article (when appropriate), title of the item (book, magazine, journal, serial, symposium, catalog, etc), date, pages(s), volume-issue number(s), publisher, city and/or country where published.						T ⁵

**INFORMATION DISCLOSURE
STATEMENT BY APPLICANT**
(Not for submission under 37 CFR 1.99)

Application Number		15809815
Filing Date		2017-11-10
First Named Inventor	Eliel Bayever	
Art Unit		1612
Examiner Name	Celeste A. RONEY	
Attorney Docket Number		01208-0007-01US

1	KRAUT E, et. al., Abstract 2017. "Final Results of a Phase I Study of Liposome Encapsulated SN-38 (LE-SN38): Safety, Pharmacogenomics, Pharmacokinetics, and Tumor Response," J Clin Oncol. 23(16_Suppl):2017 (2005), 3 printed pages.
2	KULKE M, et. al., "A Phase II Trial of Irinotecan and Cisplatin in Patients with Metastatic Neuroendocrine Tumors," Dig Dis Sci. 51(6):1033-8 (2006).
3	LAMICHHANE N, et. al., "Liposomes: Clinical Applications and Potential for Image-Guided Drug Delivery," Molecules. 23(2):288 doi: 10.3390/molecules2302028 (2018), 17 pages.
4	LARSEN A, et al., "Influence of Liposomal Irinotecan (nal-IRI) and Non-Liposomal Irinotecan, Alone and in Combination, on Tumor Growth and Angiogenesis in Colorectal Cancer (CRC) Models." Poster presented at the American Society of Clinical Oncology Gastrointestinal Cancers Symposium (ASCO GI), San Francisco, CA, January 18-20, 2018, 9 pages.
5	LARSEN A, et al., Abstract 771. "Influence of Liposomal Irinotecan (nal-IRI) and Non-Liposomal Irinotecan, Alone and in Combination, on Tumor Growth and Angiogenesis in Colorectal Cancer (CRC) Models," J Clin Oncol. 36(4_Suppl):711 DOI: 10.1200/JCO.2018.36.4_suppl.711 (2018), 2 printed pages.
6	Lecovorin Calcium package insert, Teva, revised 10/2009, 6 pages.
7	LEE H, et al., "(64)Cu-MM-302 Positron Emission Tomography Quantifies Variability of Enhanced Permeability and Retention of Nanoparticles in Relation to Treatment Response in Patients with Metastatic Breast Cancer," Clin Cancer Res. 23(15):4190-4202 (2017).
8	LEE H, et al., "A Gradient-Loadable (64)Cu-Chelator for Quantifying Tumor Deposition Kinetics of Nanoliposomal Therapeutics by Positron Emission Tomography," Nanomedicine. 11(1):155-65 (2015). Epub 2014.
9	LIU B, et al., "Mapping Tumor Epitope Space by Direct Selection of Single-Chain Fv Antibody Libraries on Prostate Cancer Cells," Cancer Res. 64(2):704-10 (2004).
10	LIU B, et al., "Recombinant Full-Length Human IgG1s Targeting Hormone-Refractory Prostate Cancer," J Mol Med (Berl). 85(10):1113-23 (2007).
11	LIU J-J, et al., "Simple and Efficient Liposomal Encapsulation of Topotecan by Ammonium Sulfate Gradient: Stability, Pharmacokinetic and Therapeutic Evaluation," Anticancer Drugs. 13(7):709-17 (2002).

**INFORMATION DISCLOSURE
STATEMENT BY APPLICANT**
(Not for submission under 37 CFR 1.99)

Application Number		15809815
Filing Date		2017-11-10
First Named Inventor	Eliel Bayever	
Art Unit		1612
Examiner Name	Celeste A. RONEY	
Attorney Docket Number		01208-0007-01US

12	LORUSSO P, et al., "Abstract CT325: Combination of the PARP Inhibitor Veliparib (ABT888) with Irinotecan in Patients with Triple Negative Breast Cancer: Preliminary Activity and Signature of Response." Proceedings: AACR 106th Annual Meeting, April 18-22, 2015, Philadelphia, PA (2015), 3 printed pages.
13	LUNDBERG B, et al., "Conjugation of Apolipoprotein B with Liposomes and Targeting to Cells in Culture," Biochim Biophys Acta. 1149(2):305-12 (1993).
14	MA W, et al., Abstract e13588. "Population Pharmacokinetics and Exposure-Safety Relationship of Nanoliposomal Irinotecan (MM-398, nal-IRI) in Patients With Solid Tumors," J Clin Oncol. 33(15_Suppl):e13588 DOI: 10.1200/jco.2015.33.15_suppl.e13588 (2015), 2 printed pages.
15	MABRO M, et. al., "A Phase II Study of FOLFIRI-3 (Double Infusion of Irinotecan Combined With LV5FU) After FOLFOX in Advanced Colorectal Cancer Patients," Br J Cancer. 94(9):1287-92 (2006).
16	MABRO M, et. al., "Bimonthly Leucovorin, Infusion 5-Fluorouracil, Hydroxyurea, and Irinotecan (FOLFIRI-2) for Pretreated Metastatic Colorectal Cancer," Am J Clin Oncol. 26(3):254-8 (2003).
17	MACKENZIE M, et. al., "A Phase I Study of OSI-211 and Cisplatin as Intravenous Infusions Given on Days 1, 2 and 3 Every 3 Weeks in Patients With Solid Cancers," Ann Oncol. 15(4):665-70 (2004).
18	MALET-MARTINO M and MARTINO R, "Clinical Studies of Three Oral Prodrugs of 5-Fluorouracil (Capecitabine, UFT, S-1): A Review," Oncologist. 7(4):288-323 (2002).
19	MAMOT C, et al., "Epidermal Growth Factor Receptor (EGFR)-Targeted Immunoliposomes Mediate Specific and Efficient Drug Delivery to EGFR- and EGFRvIII-Overexpressing Tumor Cells," Cancer Res. 63(12):3154-61 (2003).
20	MAMOT C, et al., "Liposome-Based Approaches to Overcome Anticancer Drug Resistance," Drug Resist Updat. 6(5):271-9 (2003).
21	MANCINI R and MODLIN J, "Chemotherapy Administration Sequence: A Review of the Literature and Creation of a Sequencing Chart," J Hematol Oncol Pharm. 1(1):17-25 (2011).
22	MARTIN L, et. al., "VEGF Remains an Interesting Target in Advanced Pancreas Cancer (APCA): Results of a Multi-Institutional Phase II Study of Bevacizumab, Gemcitabine, and Infusional 5-Fluorouracil in Patients With APCA," Ann Oncol. 23(11):2812-20 (2012).

**INFORMATION DISCLOSURE
STATEMENT BY APPLICANT**
(Not for submission under 37 CFR 1.99)

Application Number	15809815
Filing Date	2017-11-10
First Named Inventor	Eliel Bayever
Art Unit	1612
Examiner Name	Celeste A. RONEY
Attorney Docket Number	01208-0007-01US

23	MATHIJSEN R, et. al., "Clinical Pharmacokinetics and Metabolism of Irinotecan (CPT-11)," Clin Cancer Res. 7 (8):2182-94 (2001).
24	MATSUSAKA S, et. al., "Differential Effects of Two Fluorouracil Administration Regimens for Colorectal Cancer," Oncol Rep. 10(1):109-13 (2003).
25	MAYER L, et. al., "Ratiometric Dosing of Anticancer Drug Combinations: Controlling Drug Ratios After Systemic Administration Regulates Therapeutic Activity in Tumor-Bearing Mice," Mol Cancer Ther. 5(7):1854-63 (2006).
26	McNAMARA M, et al., "NET-02: A Multi-Centre, Randomized, Phase II Trial of Liposomal Irinotecan (nal-IRI) and 5-Fluorouracil (5-FU)/Folinic Acid or Docetaxel as Second-Line Therapy in Patients (pts) With Progressive Poorly Differentiated Extra-Pulmonary Neuroendocrine Carcinoma (PD-EP-NEC)." Poster presented at the 17th Annual European Neuroendocrine Tumor Society (ENETS) Conference for the Diagnosis and Treatment of Neuroendocrine Tumor Disease, Virtual Conference, March 11-13, 2020, 4 pages.
27	McNAMARA M, et al., Abstract P04. "NET-02: A Phase II Trial of Liposomal Irinotecan (nal-IRI) and 5-Fluorouracil (5-FU)/Folinic Acid or Docetaxel as Second-Line Therapy in Patients (pts) With Progressive Poorly Differentiated Extra-Pulmonary Neuroendocrine Carcinoma (PD-EP-NEC)," In Abstracts of the 17th Annual European Neuroendocrine Tumor Society (ENETS) Conference for the Diagnosis and Treatment of Neuroendocrine Tumor Disease, Virtual Conference, March 11-13, 2020, page 374.
28	MEERUM TERWOGT J, et. al., "Phase I and Pharmacokinetic Study of SPI-77, a Liposomal Encapsulated Dosage Form of Cisplatin," Cancer Chemother Pharmacol. 49(3):201-10 (2002).
29	MESSERER C, et. al., "Liposomal Encapsulation of Irinotecan and Potential for the Use of Liposomal Drug in the Treatment of Liver Metastases Associated with Advanced Colorectal Cancer," MS Thesis, University of British Columbia, 2000, 90 pages.
30	MIRTSCHING B, et al., "Irinotecan-induced Immune Thrombocytopenia," Am J Med Sci. 347(2):167-9 (2014).
31	MUNZONE E, "Adverse Side Effects Associated to Metronomic Chemotherapy," Presentation presented at Aiom Cancer Metronomic Therapy, February 26, 2016, Milan, 32 pages.
32	Myocet liposomal, Summary of product characteristics and labelling and package leaflet, European Medicines Agency, available at ema.europa.eu/en/documents/product-information/myocet-liposomal-previously-myocet-epar-product-information_en.pdf , Date of first authorisation: 13 July 2000, Date of latest renewal: 02 July 2010, 37 pages.
33	NAKAJIMA T, et. al., "Synergistic Antitumor Activity of the Novel SN-38-Incorporating Polymeric Micelles, NK012, Combined With 5-Fluorouracil in a Mouse Model of Colorectal Cancer, As Compared With That of Irinotecan Plus 5-Fluorouracil," Int J Cancer. 122(9):2148-53 (2008).

**INFORMATION DISCLOSURE
STATEMENT BY APPLICANT**
(Not for submission under 37 CFR 1.99)

Application Number	15809815
Filing Date	2017-11-10
First Named Inventor	Eliel Bayever
Art Unit	1612
Examiner Name	Celeste A. RONEY
Attorney Docket Number	01208-0007-01US

34	NARDI M, et. al., Abstract 14520. "Metronomic Irinotecan and Standard FOLFIRI Regimen as First-Line Chemotherapy in Metastatic Colorectal Cancer (MCRC). Final Results of Phase II Study," J Clin Oncol. 25(18_suppl):14520 (2007), 1 printed page.
35	National Cancer Institute, "Irinotecan Hydrochloride Liposome," Posted: October 27, 2015, Updated: March 28, 2019, available at cancer.gov/about-cancer/treatment/drugs/irinotecan-hydrochloride-liposome, 2 pages.
36	No authors listed. "5HT3-receptor Antagonists as Antiemetics in Cancer," Drug Ther Bull. 43(8):57-62 (2005).
37	NOBLE C, et al, "Development of Ligand-Targeted Liposomes for Cancer Therapy," Expert Opin Ther Targets. 8 (4):335-53 (2004).
38	NOORDHUIS P, et. al., "5-Fluorouracil Incorporation into RNA and DNA in Relation to Thymidylate Synthase Inhibition of Human Colorectal Cancers," Ann Oncol. 15(7):1025-32 (2004).
39	OGATA Y, et. al., "Dosage Escalation Study of S-1 and Irinotecan in Metronomic Chemotherapy against Advanced Colorectal Cancer," Kurume Med J. 56(1-2):1-7 (2009).
40	Oncology NEWS International, "Experts Debate Bolus vs Continuous Infusion 5-FU." February 1, 2003, Volume 12, Issue 2, 3 printed pages.
41	O'REILLY S, "Topotecan: What Dose, What Schedule, What Route?" Clin Cancer Res. 5(1):3-5 (1999).
42	PAL A, et. al., "Preclinical Safety, Pharmacokinetics and Antitumor Efficacy Profile of Liposome-Entrapped SN-38 Formulation," Anticancer Res. 25(1A):331-41 (2005).
43	PAPAHADJOPOULOS D, et al., "Targeting of Drugs to Solid Tumors Using Anti-HER2 Immunoliposomes," J Liposome Res. 8(4):425-42 (1998).
44	PAPAHADJOPOULOS D, et. al., "Sterically Stabilized Liposomes: Improvements in Pharmacokinetics and Antitumor Therapeutic Efficacy," Proc Natl Acad Sci USA. 88(24):11460-4 (1991).

**INFORMATION DISCLOSURE
STATEMENT BY APPLICANT**
(Not for submission under 37 CFR 1.99)

Application Number	15809815
Filing Date	2017-11-10
First Named Inventor	Eliel Bayever
Art Unit	1612
Examiner Name	Celeste A. RONEY
Attorney Docket Number	01208-0007-01US

45	PAPI M, et. al., "Clinically Approved PEGylated Nanoparticles Are Covered by a Protein Corona That Boosts the Uptake by Cancer Cells," <i>Nanoscale</i> . 9(29):10327-34 (2017).
46	PARK J, et al., "Anti-HER2 Immunoliposomes for Targeted Therapy of Human Tumors," <i>Cancer Lett.</i> 118(2):153-60 (1997).
47	PARK J, et al., "Development of Anti-p185HER2 Immunoliposomes for Cancer Therapy," <i>Proc Natl Acad Sci U S A.</i> 92(5):1327-31 (1995).
48	PARK J, et al., "Immunoliposomes for Cancer Treatment," <i>Adv Pharmacol.</i> 40:399-435 (1997).
49	PARK J, et al., "Sterically Stabilized Immunoliposomes: Formulations for Delivery of Drugs and Genes to Tumor Cells In Vivo," In <i>Targeting of Drugs 6: Strategies for Stealth Therapeutic Systems</i> , Gregoriadis G, et al., eds., Plenum Press, New York, pp. 41-47 (1998).
50	PARK J, et al., "Tumor Targeting Using Anti-HER2 Immunoliposomes," <i>J Control Release.</i> 74(1-3):95-113 (2001).

If you wish to add additional non-patent literature document citation information please click the Add button

EXAMINER SIGNATURE

Examiner Signature	<input type="text"/>	Date Considered	<input type="text"/>
--------------------	----------------------	-----------------	----------------------

*EXAMINER: Initial if reference considered, whether or not citation is in conformance with MPEP 609. Draw line through a citation if not in conformance and not considered. Include copy of this form with next communication to applicant.

¹ See Kind Codes of USPTO Patent Documents at www.USPTO.GOV or MPEP 901.04. ² Enter office that issued the document, by the two-letter code (WIPO Standard ST.3). ³ For Japanese patent documents, the indication of the year of the reign of the Emperor must precede the serial number of the patent document. ⁴ Kind of document by the appropriate symbols as indicated on the document under WIPO Standard ST.16 if possible. ⁵ Applicant is to place a check mark here if English language translation is attached.

INFORMATION DISCLOSURE STATEMENT BY APPLICANT (Not for submission under 37 CFR 1.99)	Application Number	15809815
	Filing Date	2017-11-10
	First Named Inventor	Eliel Bayever
	Art Unit	1612
	Examiner Name	Celeste A. RONEY
	Attorney Docket Number	01208-0007-01US

CERTIFICATION STATEMENT

Please see 37 CFR 1.97 and 1.98 to make the appropriate selection(s):

That each item of information contained in the information disclosure statement was first cited in any communication from a foreign patent office in a counterpart foreign application not more than three months prior to the filing of the information disclosure statement. See 37 CFR 1.97(e)(1).

OR

That no item of information contained in the information disclosure statement was cited in a communication from a foreign patent office in a counterpart foreign application, and, to the knowledge of the person signing the certification after making reasonable inquiry, no item of information contained in the information disclosure statement was known to any individual designated in 37 CFR 1.56(c) more than three months prior to the filing of the information disclosure statement. See 37 CFR 1.97(e)(2).

See attached certification statement.

The fee set forth in 37 CFR 1.17 (p) has been submitted herewith.

A certification statement is not submitted herewith.

SIGNATURE

A signature of the applicant or representative is required in accordance with CFR 1.33, 10.18. Please see CFR 1.4(d) for the form of the signature.

Signature	/Mary R. Henninger/	Date (YYYY-MM-DD)	2021-03-12
Name/Print	Mary R. Henninger	Registration Number	56992

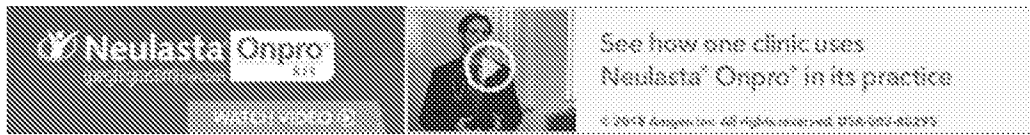
This collection of information is required by 37 CFR 1.97 and 1.98. The information is required to obtain or retain a benefit by the public which is to file (and by the USPTO to process) an application. Confidentiality is governed by 35 U.S.C. 122 and 37 CFR 1.14. This collection is estimated to take 1 hour to complete, including gathering, preparing and submitting the completed application form to the USPTO. Time will vary depending upon the individual case. Any comments on the amount of time you require to complete this form and/or suggestions for reducing this burden, should be sent to the Chief Information Officer, U.S. Patent and Trademark Office, U.S. Department of Commerce, P.O. Box 1450, Alexandria, VA 22313-1450. **DO NOT SEND FEES OR COMPLETED FORMS TO THIS ADDRESS. SEND TO: Commissioner for Patents, P.O. Box 1450, Alexandria, VA 22313-1450.**

Privacy Act Statement

The Privacy Act of 1974 (P.L. 93-579) requires that you be given certain information in connection with your submission of the attached form related to a patent application or patent. Accordingly, pursuant to the requirements of the Act, please be advised that: (1) the general authority for the collection of this information is 35 U.S.C. 2(b)(2); (2) furnishing of the information solicited is voluntary; and (3) the principal purpose for which the information is used by the U.S. Patent and Trademark Office is to process and/or examine your submission related to a patent application or patent. If you do not furnish the requested information, the U.S. Patent and Trademark Office may not be able to process and/or examine your submission, which may result in termination of proceedings or abandonment of the application or expiration of the patent.

The information provided by you in this form will be subject to the following routine uses:

1. The information on this form will be treated confidentially to the extent allowed under the Freedom of Information Act (5 U.S.C. 552) and the Privacy Act (5 U.S.C. 552a). Records from this system of records may be disclosed to the Department of Justice to determine whether the Freedom of Information Act requires disclosure of these records.
2. A record from this system of records may be disclosed, as a routine use, in the course of presenting evidence to a court, magistrate, or administrative tribunal, including disclosures to opposing counsel in the course of settlement negotiations.
3. A record in this system of records may be disclosed, as a routine use, to a Member of Congress submitting a request involving an individual, to whom the record pertains, when the individual has requested assistance from the Member with respect to the subject matter of the record.
4. A record in this system of records may be disclosed, as a routine use, to a contractor of the Agency having need for the information in order to perform a contract. Recipients of information shall be required to comply with the requirements of the Privacy Act of 1974, as amended, pursuant to 5 U.S.C. 552a(m).
5. A record related to an International Application filed under the Patent Cooperation Treaty in this system of records may be disclosed, as a routine use, to the International Bureau of the World Intellectual Property Organization, pursuant to the Patent Cooperation Treaty.
6. A record in this system of records may be disclosed, as a routine use, to another federal agency for purposes of National Security review (35 U.S.C. 181) and for review pursuant to the Atomic Energy Act (42 U.S.C. 218(c)).
7. A record from this system of records may be disclosed, as a routine use, to the Administrator, General Services, or his/her designee, during an inspection of records conducted by GSA as part of that agency's responsibility to recommend improvements in records management practices and programs, under authority of 44 U.S.C. 2904 and 2906. Such disclosure shall be made in accordance with the GSA regulations governing inspection of records for this purpose, and any other relevant (i.e., GSA or Commerce) directive. Such disclosure shall not be used to make determinations about individuals.
8. A record from this system of records may be disclosed, as a routine use, to the public after either publication of the application pursuant to 35 U.S.C. 122(b) or issuance of a patent pursuant to 35 U.S.C. 151. Further, a record may be disclosed, subject to the limitations of 37 CFR 1.14, as a routine use, to the public if the record was filed in an application which became abandoned or in which the proceedings were terminated and which application is referenced by either a published application, an application open to public inspections or an issued patent.
9. A record from this system of records may be disclosed, as a routine use, to a Federal, State, or local law enforcement agency, if the USPTO becomes aware of a violation or potential violation of law or regulation.



See how one clinic uses Neulasta[®] Onpro[™] in its practice

© 2016 Cengage Inc. All rights reserved. USA: 002-802373

Journal of Clinical Oncology[®]

An American Society of Clinical Oncology Journal



jco.org / dx.doi.org

ACCESS PROVIDED BY IPSEN LIMITED - THE LIBRARY

MENU SEARCH

Article Tools

DEVELOPMENTAL THERAPEUTICS: CYTOTOXIC CHEMOTHERAPY

Final results of a phase I study of liposome encapsulated SN-38 (LE-SN38): Safety, pharmacogenomics, pharmacokinetics, and tumor response

E. H. Kraut, M. N. Fishman, P. M. Lonussen, M. S. Gordon, E. H. Rubin, A. Haas...

Show More

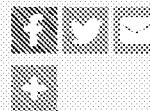
Abstract

2017

Background: The prodrug irinotecan is converted into its active moiety, SN-38, with wide interpatient variability, due in part to differential expression of cellular carboxylesterases responsible for prodrug hydrolysis. The enzyme UDP-glucuronosyltransferase 1A1 (UGT1A1) detoxifies SN-38 by metabolizing it to SN-38 glucuronide. Polymorphisms in the *UGT1A1* promoter lead to decreased expression of the enzyme and are associated with increased risk of irinotecan toxicity. **Methods:** This was a multi-center, dose-escalation study of Liposome Encapsulated SN-38 (LE-SN38) in patients with advanced cancer. To examine whether toxicities and appropriate dose levels might differ with *UGT1A1**28 genotype, patients were stratified prospectively. LE-SN38 was infused intravenously over 90 minutes every 21 days until disease progression or unacceptable toxicity occurred. Tumor progression was monitored radiographically after every 2 cycles. **Results:** Enrollment is complete; 75 patients were treated with LE-SN38. Screened patients had genotype frequencies of 42.4% homozygous wild-type (*WT/WT*), 45.1% heterozygous (*WT*/**28*), 10.9% homozygous variant (**28*/**28*), and 1.6% other. Across all genotypes the most frequent adverse events were fatigue, nausea, anorexia, diarrhea, and vomiting. Importantly, diarrhea was generally mild and self-limiting, and no late onset diarrhea was reported. DLTs of neutropenia/febrile neutropenia in *WT/WT* patients at 40

OPTIONS & TOOLS

- Export Citation
- Track Citation
- Add to Favorites
- Rights & Permissions



COMPANION ARTICLES

No companion articles

ARTICLE CITATION

DOI: 10.1200/JCO.2005.23.16_suppl.2017
Journal of Clinical Oncology 23, no. 16_suppl (June 01, 2005) 2017-2017.

Published online December 12, 2016.

PMID: 27266623

WE RECOMMEND

- Pharmacogenomic and pharmacokinetic assessment of liposome encapsulated SN-38 (LE-SN38) in advanced cancer patients
 E. H. Kraut et al. | *Clin Oncol*, 2016
- Phase I and pharmacokinetic (PK) study of JHL-305 (pegylated liposomal irinotecan) in patients with advanced solid tumors
 S. E. Jones, | *Clin Oncol*, 2016
- Dose-Finding and Pharmacokinetic Study to Optimize the Dosing of Irinotecan According to the UGT1A1 Genotype of Patients With Cancer



See how one clinic uses Neulasta[®] Onpro[™] in its practice

© 2016 Cengage Inc. All rights reserved. USA: 002-802373



In advanced research, you can't afford to miss a single issue. That's why you need JCO's Impact Factor. It's the only journal in the field that offers you the most comprehensive, up-to-date information on the latest research. **TRY IT TODAY!**

JCO's Impact Factor
26.245

Make an impact
 published with JCO

SUBMIT NOW

jco.org

mg/m² resulted in an MTD of 35 mg/m². No DLTs occurred in *28/*28 patients; accrual was halted at 20 mg/m² before the MTD was reached. PK results showed that *28/*28 patients had 2- to 3-fold greater drug exposure than WT/*28 or WT/WT patients at the same doses. Stable disease (≥4 cycles) was observed in 37% of patients. Conclusions: LE-5N38 was well tolerated in all patients, with no reported acute/delayed diarrhea. The MTD was not reached for *28/*28 patients. An MTD of 35 mg/m² LE-5N38 was found for WT/WT patients. Since WT/WT and WT/*28 patients did not appear to exhibit clinically significant differences in safety or PK profiles, this dose will be evaluated in both groups in a Phase II study of patients with colon cancer.

Author Disclosure

Employment or Ownership	Consultant or Advisory Role	Stock Ownership	Honoraria	Research Funding
NeoPharm				
American Society of Clinical Oncology				

Federica Innocenti et al., *J Clin Oncol*, 2015

Genotype-Driven Phase I Study of Irinotecan Administered in Combination With Fluorouracil/Leucovorin in Patients With Metastatic Colorectal Cancer
 Giuseppe Toffa et al., *J Clin Oncol*, 2016

UGT1A and Irinotecan Toxicity: Keeping It in the Family
 Janette M. Hoskins et al., *J Clin Oncol*, 2016

Efficacy and Safety of FOLFIRI With High-Dose Irinotecan in Metastatic Colorectal Cancer According to UGT1A 1 Genotype
[Practical Update](#), 2015

FDA Updates Label for Irinotecan with PGx Data
[Genomeweb](#), 2010

FDA Updates Label for Irinotecan with PGx Data
[Genomeweb](#), 2010

Clinical and Pharmacogenetic Determinants of 5-Fluorouracil/Leucovorin/Irinotecan Toxicity
[Practical Update](#), 2015

S-1 plus irinotecan: promising alternative treatment in NSCLC
[Health](#)

Powered by



WHAT'S POPULAR

Most Read Most Cited

Management of Immune-Related Adverse Events in Patients Treated With Immune Checkpoint Inhibitor Therapy
 American Society of Clinical Oncology Clinical Practice Guideline
 Brahmer et al.

Outpatient Management of Fever and Neutropenia in Adults Treated for Malignancy
 American Society of Clinical Oncology and Infectious Diseases Society of America Clinical Practice Guideline Update
 Taplitz et al.

Venous Thromboembolism Prophylaxis and Treatment in Patients With Cancer
 ASCO Clinical Practice Guideline Update
 Key et al.

Aspirineticin: American Society of Clinical Oncology Clinical Practice Guideline Update
Hesketh et al.

Comparison of an Oral Factor Xa Inhibitor With Low Molecular Weight Heparin in Patients With Cancer With Venous Thromboembolism: Results of a Randomized Trial (SELECT-D)
Young et al.



QUICK LINKS

Content

[Newest Articles](#)
[Archive](#)
[Meeting Abstracts](#)

Journal Information

[About](#)
[Editorial Board](#)
[Contact Us](#)
[Permissions](#)

Resources

[Authors](#)
[Reviewers](#)
[Subscribers](#)
[Institutions](#)
[Advertisers](#)

[Submit Your Manuscript](#)

[Subscribe to this Journal](#)



ASCO FAMILY OF SITES

Journals

[Journal of Clinical Oncology](#)
[JCO Oncology Practice](#)
[JCO Global Oncology](#)
[JCO Clinical Cancer Informatics](#)
[JCO Precision Oncology](#)

Publications

[ASCO Educational Book](#)
[ASCO Daily News](#)
[ASCO Connection](#)
[The ASCO Post](#)
[JCO OP DAIS](#)

Education

[ASCO University](#)
[ASCO Meetings](#)
[Cancer.Net](#)

Other Sites

[ASCO.org](#)
[ASCO Author Services](#)
[ASCO Career Center](#)
[CancerUnQ](#)
[Conquer Cancer Foundation](#)
[TAPUR Study](#)



American Society of Clinical Oncology
7315 Mill Road, Suite 800, Alexandria, VA 22314
© 2020 American Society of Clinical Oncology



[Terms of Use](#) | [Privacy Policy](#) | [Cookies](#)

A Phase II Trial of Irinotecan and Cisplatin in Patients with Metastatic Neuroendocrine Tumors

MATTHEW H. KULKE, MD,* BINGYAN WU, MS,† DAVID P. RYAN, MD,‡ PETER C. ENZINGER, MD,*
ANDREW X. ZHU, MD, PhD,‡ JEFFREY W. CLARK, MD,‡ CRAIG C. EARLE, MD,*
ANN MICHELINI, RN, MSN,* and CHARLES S. FUCHS, MD, MPH*§

The role of systemic chemotherapy in the treatment of patients with metastatic neuroendocrine tumors is controversial. While combination regimens containing cisplatin and etoposide have activity against more aggressive neuroendocrine tumor variants, such regimens appear to have little efficacy in patients with well-differentiated neuroendocrine tumor subtypes. The combination of irinotecan and cisplatin is active both against small cell lung cancer and in upper gastrointestinal malignancies but has not been prospectively evaluated in patients with metastatic neuroendocrine tumors. We therefore assessed the efficacy of an irinotecan/cisplatin combination in patients with this disease. Eighteen patients with metastatic neuroendocrine tumors (excluding small cell carcinoma) were treated with irinotecan, 65 mg/m², and cisplatin, 30 mg/m², administered weekly for 2 of every 3 weeks. Patients were followed for evidence of toxicity, response, and survival. The toxicities associated with this regimen were mild and included myelosuppression, nausea, and diarrhea. Only one radiologic response was observed among four patients with poorly differentiated neuroendocrine tumors. No radiologic responses were observed in 14 patients with well-differentiated tumors. The median overall survival duration of patients treated with this regimen was 11.4 months. We conclude that while the combination of irinotecan and cisplatin may have activity in aggressive neuroendocrine tumor subtypes, this combination is inactive in patients with well-differentiated neuroendocrine tumors.

KEY WORDS: pancreatic islet cell tumors; carcinoid tumors; neuroendocrine tumors; cisplatin; irinotecan.

There is no universally accepted, standard treatment for patients with metastatic neuroendocrine tumors. The use of somatostatin analogues to control symptoms of hormonal excretion has significantly improved the quality of life for such patients, but only rarely causes actual tu-

mor regression (1). Patients who do not respond or become refractory to somatostatin analogues may pursue a number of other treatment options, including resection of hepatic metastases, chemoembolization, and, in some cases, systemic administration of α -interferon or systemic chemotherapy.

Neuroendocrine tumors are generally subcategorized as either carcinoid tumors or pancreatic endocrine tumors and have been further classified according to their histologic appearance and clinical behavior. "Typical," or well-differentiated, neuroendocrine tumors are characterized by rare mitoses and generally pursue an indolent course. More aggressive neuroendocrine tumor variants have been variously described as "atypical" or "anaplastic" carcinoid tumors, as "neuroendocrine carcinomas," and as "poorly differentiated neuroendocrine tumors" (2-4). While the

Manuscript received May 9, 2005; accepted June 3, 2005.

From the Departments of *Medical Oncology and †Biostatistics, Dana-Farber Institute, ‡Division of Hematology/Oncology, Massachusetts General Hospital, and §Channing Laboratory, Brigham and Women's Hospital, Boston, Massachusetts, USA.

This work received financial support from Pfizer Corporation. M. H. Kulke is supported in part by NIH grants K23 CA 093401 and K30 HL04095 and gifts from Dr. Raymond and Beverly Sackler, the Stephen and Caroline Kauffer Fund for neuroendocrine tumor research, and the Caring for Carcinoid Foundation.

Address for reprint requests: Matthew Kulke, MD, Department of Adult Oncology, Dana-Farber Cancer Institute, 44 Binney Street, Boston, Massachusetts 02115, USA; matthew_kulke@dfci.harvard.edu.

nomenclature for these more aggressive variants differs, these tumors are generally characterized by the presence of >2 mitoses per high-powered field and areas of tumor necrosis, in the absence of frank histologic features of small cell carcinoma. Whereas treatment with systemic chemotherapy has yielded only mixed results in the treatment of typical neuroendocrine tumors, a regimen of cisplatin and etoposide commonly used in small cell lung carcinoma has been reported to be effective in treating patients with these more aggressive neuroendocrine tumor variants (3, 4).

Irinotecan, an inhibitor of DNA topoisomerase I, has activity against a wide range of human malignancies. When administered either as a single agent or in combination with 5-fluorouracil, treatment with irinotecan is associated with both radiologic responses and improved survival in patients with advanced colorectal cancer (5, 6). Following reports of synergy between irinotecan and cisplatin, cisplatin/irinotecan combinations have been widely utilized in the treatment of gastric, esophageal, and small cell lung cancer (7–9). In a large, randomized trial of 154 patients with advanced small cell lung cancer, treatment with a combination of irinotecan and cisplatin was shown to result in a longer median survival time than treatment with a standard combination of etoposide and cisplatin (10).

Small, retrospective studies have reported that cisplatin and irinotecan combinations may have activity in patients with high-grade neuroendocrine carcinomas; however, this combination has not been prospectively evaluated in neuroendocrine tumor patients with a broader range of histologies (11). We therefore undertook a phase II study in which 18 patients with metastatic neuroendocrine tumors were treated with irinotecan, 65 mg/m², and cisplatin, 30 mg/m², administered intravenously for 2 of every 3 weeks. Patients were followed for toxicity, response, and overall survival.

PATIENTS AND METHODS

Study Population. The study population consisted of patients with histologically confirmed, locally unresectable or metastatic neuroendocrine tumors. Patients were classified as having either well-differentiated neuroendocrine tumors (<2 mitoses per HPF) or poorly differentiated neuroendocrine tumors (≥ 2 mitoses per HPF and/or areas of necrosis). Patients with histologic features of small cell carcinoma were excluded. Prior treatment with chemotherapy was allowed. Patients may also have received prior treatment with chemoembolization or cryotherapy provided that the areas of disease used for tumor measurements were not affected by these treatments. Further inclusion criteria included Eastern Cooperative Oncology Group (ECOG) performance status ≤ 2 and life expectancy ≥ 12 weeks. Adequate hematologic parameters, renal function (serum creatinine ≤ 1.5 mg/dl), and hepatic function (bilirubin ≤ 2.0 mg/dl,

AST $\leq 5 \times$ ULN) were also required. Patients with either clinically apparent central nervous system metastases or carcinomatous meningitis, who had experienced a myocardial infarction in the past 6 months, who had serious medical or psychiatric illness, or who were pregnant or lactating were excluded from protocol treatment. Patients from the Dana-Farber Cancer Institute, Massachusetts General Hospital, and the Brigham and Women's Hospital were eligible for enrollment. All patients provided informed consent as required by the Institutional Review Boards of the respective institutions.

Treatment Program. Pretreatment evaluation included a medical history and physical examination, hematologic and biochemical analysis, and confirmation of the histologic diagnosis by a pathologist at one of the treating institutions. Baseline radiologic tumor measurements were obtained by chest x-ray and by abdominal CT scan.

Each treatment cycle consisted of irinotecan and cisplatin administered weekly for 2 weeks followed by a 1-week rest period. Treatment cycles were repeated every 3 weeks. Cisplatin was delivered at a starting dose of 30 mg/m² followed immediately after with irinotecan at a starting dose of 65 mg/m². Patients received prehydration with at least 500 ml of D5NS prior to administration of cisplatin and antiemetics at the discretion of the treating physician. Dose adjustments in irinotecan were made based on hematological, gastrointestinal (diarrhea), and other nonhematological grade 3 or higher toxicity. Patients who developed febrile neutropenia received a dose reduction of 10 mg/m² at the time of the next and all future treatment cycles. Treatment was held in patients who had an absolute neutrophil count of less than 1000/mm³ or a platelet count of less than 100,000/mm³ on the scheduled treatment day. Support with growth factors was not allowed on study except in the setting of hospitalization for febrile neutropenia. If their counts recovered within 1 week, they then received the same dose. If the counts did not recover within 1 week, the dose was reduced by 10 mg/m² once toxicity resolved. Patients with interval diarrhea of \geq grade 2 were evaluated weekly until it recovered to $<$ grade 1, at which time treatment was reinitiated with a dose reduction of 10 mg/m². Patients with other grade 3 or higher nonhematological toxicity had their doses held until toxicity resolved to grade 2 or lower and had the irinotecan dose reduced by 10 mg/m². Dose adjustments in cisplatin were made based on creatinine levels monitored prior to each dose. Patients with creatinine levels between 1.5 and 2.0 mg/dl received a dose reduction of 15 mg/m². Treatment was held in patients who had a creatinine level above 2.0 mg/dl. Doses that were held due to toxicity or that were missed were not given at a later time. All adverse events were documented and graded according to the National Cancer Institute Common Toxicity Criteria, Version 2.0.

Radiologic tumor assessments were performed every 9 weeks after initiation of treatment. Patients with evidence of response (complete or partial response) to treatment or stable disease remained on treatment until there was evidence of disease progression or unacceptable toxicity or the patients desired to have therapy discontinued. Radiologic response was classified according to the World Health Organization (WHO) criteria. Complete response required total resolution of all detectable disease lasting for at least 4 weeks. Partial response required a decrease of over 30% in the sum of the products of the largest perpendicular diameters of all measurable lesions, persisting for at least 4 weeks, without progression of any nonmeasurable sites and without the appearance of new sites of disease. Progressive disease included

TABLE 1. BASELINE PATIENT CHARACTERISTICS

Total number of patients	18
Median age	52 (range, 37–76)
Sex	
Male	10 (56%)
Female	8 (44%)
ECOG PS	
0	3 (16.7%)
1	14 (77.8%)
2	1 (5.6%)
Site of tumor origin	
Pancreas	6 (33%)
Small bowel	4 (22%)
Colon	3 (17%)
Rectum	2 (11%)
Lung	1 (5%)
Other/unknown	2 (11%)
Tumor histology	
Well differentiated (typical)	14 (78%)
Poorly differentiated	4 (22%)
Prior treatment	
Chemotherapy*	4 (22%)
Embolization	1 (5%)
Somatostatin analogues	2 (11%)
Baseline laboratory parameters	
WBC (k/ μ l)	6.9 (4.6–8.1)
Platelets (k/ μ l)	333 (141–637)
Creatinine (mg/dl)	0.8 (0.6–1.4)
SGOT (U/L)	37 (21–75)
Alkaline phosphatase (U/L)	100 (55–708)
Chromogranin A (ng/ml)	424 (5–1710)

*Prior chemotherapy regimens: streptozocin/doxorubicin (two patients), doxorubicin (one patient), and gemcitabine (one patient).

an increase of 20% or more in the sum of the products of the largest perpendicular diameters of one or more measurable lesions, the development of new lesions, or progression of nonmeasurable but evaluable sites of disease. Stable disease was defined as neither sufficient decrease to qualify for partial response nor sufficient increase to qualify for progressive disease.

Statistical Considerations. This Phase II study was originally designed with the primary endpoint of response rate in patients with advanced, unresectable neuroendocrine tumors. This was a two-stage design with a total of 32 eligible patients expected if activity was seen in the initial patient cohort. Because only one unconfirmed response was noted in the first 18 patients accrued, the study was terminated early due to lack of sufficient antitumor activity. Kaplan-Meier estimates were used for overall survival (OS) as well as progression-free survival (PFS).

RESULTS

A total of 18 patients were entered in the study at the three participating centers (Table 1). Patients ranged in age from 37 to 76 years, with a median age of 52 years. The number of males (10; 56%) and females (8; 44%) was similar. The majority of patients were experiencing symptoms from their disease: only 3 had an ECOG performance status of 0, 14 (78%) had a performance status of 1, and 1 (6%) had a status of 2. The tumor primary sites included the pancreas (33%), small bowel (22%), colon (17%), rec-

tum (11%), and lung (5%); 14 (78%) of the patients had typical, or well-differentiated, neuroendocrine tumors and 4 (22%) patients had poorly differentiated neuroendocrine tumors. Only four (22%) patients had received prior treatment with chemotherapy.

Eight patients (44%) required dose modifications of irinotecan due to treatment-related toxicity, and seven patients (39%) required dose modifications of cisplatin due to elevation of creatinine levels. The median number of complete or partial cycles that a patient received was 3.5, with a range of from 1 to 9 cycles. The total amount of irinotecan administered to each patient ranged from 65 to 845 mg/m² (median, 477.5 mg/m²), and the total amount of cisplatin ranged from 30 to 420 mg/m² (median, 225 mg/m²).

The treatment-related toxicities associated with irinotecan and cisplatin in this patient population were relatively mild (Table 2). The most common treatment-related toxicity was myelosuppression: grade 3 or 4 neutropenia occurred in 39% of patients. Cisplatin is often associated with significant nausea; however, grade 3 nausea or vomiting developed in only 22% of patients treated in the study. While treatment-related diarrhea was a common occurrence, it was generally not severe: grade 3 diarrhea developed in only one patient (5.6%), grade 2 diarrhea in two patients (11.2%), and grade 1 diarrhea in nine patients (50%).

Of the 18 patients treated, 15 were evaluable for radiologic response. The three nonevaluable patients discontinued study therapy prior to the time of their restaging studies. Only one patient (6.6%) had a partial radiologic response to therapy (Table 3). The response could not be confirmed due to sudden patient death of unknown cause. This patient had a poorly differentiated neuroendocrine tumor rather than a typical carcinoid tumor. Of the remaining patients, 11 had stable disease and 3 had progressive disease as their best response to therapy. Nine patients had elevated chromogranin A levels at baseline that were also subsequently evaluable for evidence of biochemical response. All nine evaluable patients had typical, well-differentiated neuroendocrine tumors: two experienced decreases in chromogranin A of more than 50%, three had stable chromogranin A levels (less than 50% decrease and less than 25% increase), and four had an increase in chromogranin A levels of more than 25% as their best response to treatment.

The median follow-up time for all patients was 11.4 months, with a range of 0.8 to 30 months. The Kaplan-Meier plots of overall survival and time to progression are given in Figures 1 and 2, respectively. The time to progression was 4.5 months (95% confidence interval, 2.9–10.3 months). The median overall survival was

TABLE 2. TREATMENT-RELATED TOXICITY

Toxicity	Maximum toxicity grade			
	1	2	3	4
Hemoglobin	8 (44.5%)	7 (38.9%)	—	—
Leukocytes	7 (38.9%)	4 (22.2%)	3 (16.7%)	—
Neutrophils/granulocytes	4 (22.2%)	2 (11.1%)	6 (33.3%)	1 (5.6%)
Platelets	5 (27.8%)	—	—	—
Fatigue	6 (33.3%)	6 (33.3%)	—	1 (5.6%)
Anorexia	6 (33.3%)	1 (5.6%)	1 (5.6%)	—
Constipation	7 (38.9%)	3 (16.7%)	1 (5.6%)	—
Dehydration	1 (5.6%)	—	—	—
Nausea	6 (33.3%)	6 (33.3%)	3 (16.7%)	—
Stomatitis/pharyngitis	2 (11.1%)	—	—	—
Vomiting	3 (16.7%)	5 (27.8%)	1 (5.6%)	—
Diarrhea	9 (50%)	2 (11.1%)	1 (5.6%)	—
Bilirubin	1 (5.6%)	—	—	—
SGOT (AST)	2 (11.1%)	—	—	—
Hyperglycemia	—	3 (16.7%)	—	—
Neuropathy-sensory	2 (11.1%)	—	—	—
Abdominal pain or cramping	4 (22.2%)	2 (11.1%)	1 (5.6%)	—
Dyspnea (shortness of breath)	2 (11.1%)	1 (5.6%)	—	—
Creatinine	4 (22.2%)	1 (5.6%)	—	—

11.4 months (95% confidence interval, 8.9 months; not estimable).

DISCUSSION

Our study shows that, while the combination of cisplatin and irinotecan may have activity in patients with poorly differentiated neuroendocrine tumors, it has little or no activity in patients with typical, well-differentiated histologies. Four patients in this study had poorly differentiated neuroendocrine tumors; of these, one patient had an unconfirmed partial response. Among the 14 patients with well-differentiated neuroendocrine tumors, none experienced radiologic tumor regression with treatment. Myelosuppression, nausea, and diarrhea were the most common treatment-related toxicities associated with this regimen but were rarely severe.

Patients with poorly differentiated neuroendocrine tumors have been previously reported to be more responsive to cytotoxic chemotherapy than patients with well-differentiated tumors. In an initial study, a combination of cisplatin and etoposide commonly used for small cell lung cancer was associated with an overall tumor response rate of 67% in 18 patients with "anaplastic" neuroendocrine

tumors (presumably analogous to the currently described poorly differentiated neuroendocrine tumors) but had little activity in more well-differentiated tumor subtypes (3). In a subsequent study of 36 patients with advanced neuroendocrine tumors, treatment with cisplatin and etoposide was associated with an overall radiologic response rate of 36% and a median survival time of 19 months. All patients enrolled in this study had either poorly differentiated histology or a rapidly progressing clinical course, suggesting that few, if any, of these patients had more classic, indolent carcinoid or pancreatic endocrine tumors (4). Irinotecan and cisplatin have not previously been prospectively studied in patients with neuroendocrine tumors; however, in a small, retrospective analysis, 6 (43%) of 14 patients with high-grade neuroendocrine carcinomas were reported to respond to this combination (11). Our finding that one of four patients (25%) with poorly differentiated neuroendocrine tumors responded to irinotecan and cisplatin is consistent with these prior findings.

In contrast to our observation in patients with poorly differentiated tumors, we found that the irinotecan and cisplatin combination had little or no activity in patients with well-differentiated, typical neuroendocrine tumors. No patients with typical carcinoid or pancreatic islet cell tumors experienced radiologic regression, and only 22% of the evaluable patients experienced improvement in biochemical parameters. The minimal efficacy of irinotecan and cisplatin in this setting is consistent with other studies of cytotoxic chemotherapy in patients with typical carcinoid tumors. The ECOG initially reported combined biochemical and radiologic responses in 33% of carcinoid patients treated with streptozocin and 5-fluorouracil (12).

TABLE 3. BEST RESPONSE TO THERAPY

Radiologic response	Number (%) of patients (n = 15 evaluable)
Complete response	0
Partial response	1 (6.6%)
Stable disease	11 (73.3%)
Progressive disease	3 (20%)

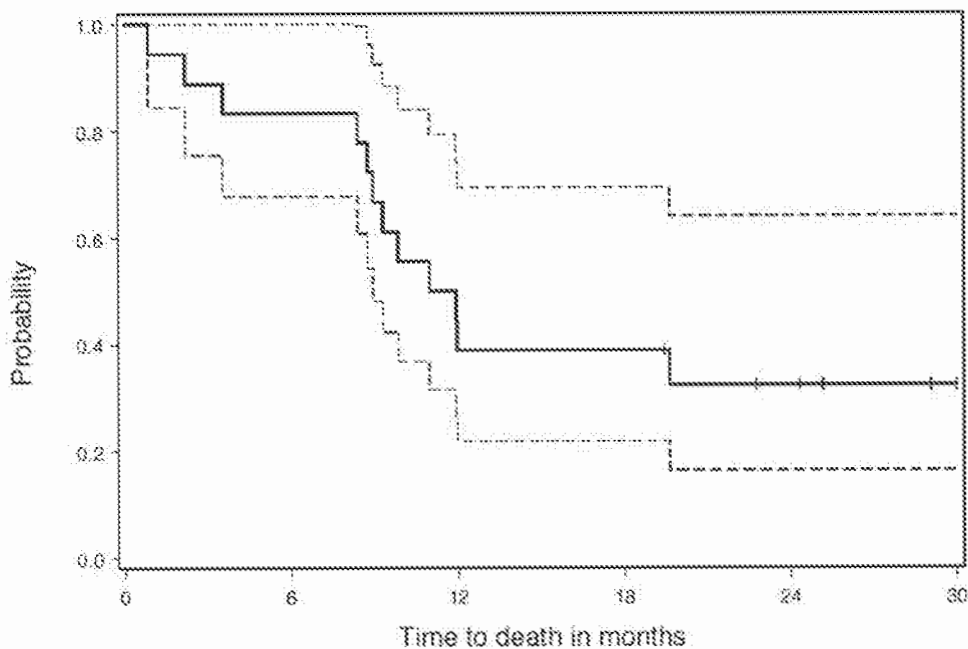


Fig 1. Overall survival time of neuroendocrine tumor patients treated with irinotecan and cisplatin.

The significant toxicity associated with this regimen led to a second study, in which the dosing interval was lengthened. In this follow-up trial the combined biochemical and radiologic response rate associated with streptozocin and 5-fluorouracil was 22%, and the median overall survival time only 14 months (13).

Other studies have suggested that pancreatic endocrine tumors may be somewhat more responsive to cytotoxic chemotherapy than are carcinoid tumors. In one randomized trial, a combination of streptozocin and doxorubicin was associated with a combined biochemical and radiologic response rate of 69% and a median overall survival

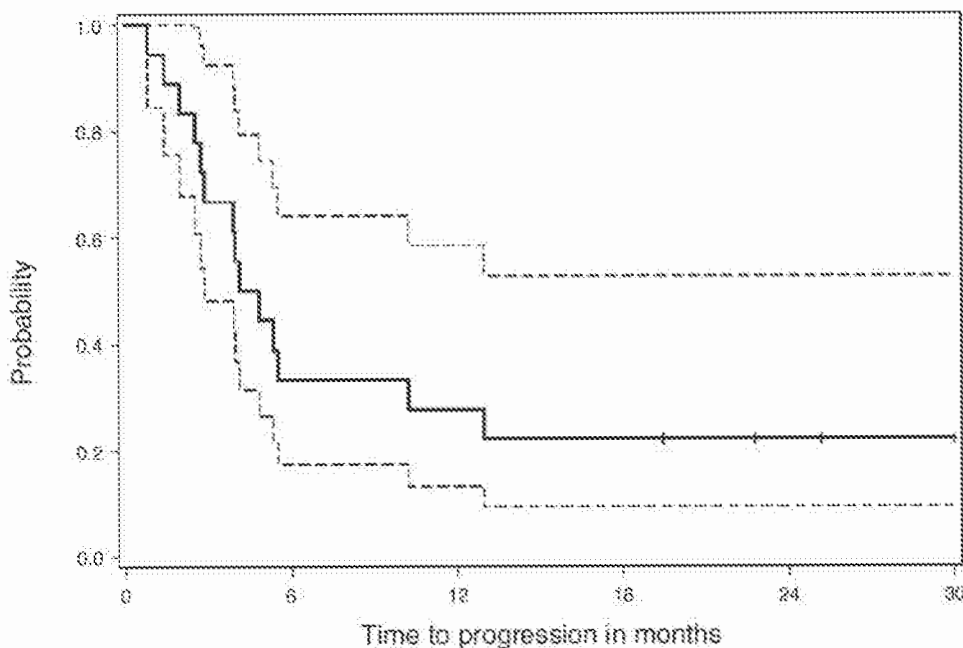


Fig 2. Time to progression of neuroendocrine tumor patients treated with irinotecan and cisplatin.

time of 20 months in patients with pancreatic islet cell tumors (14). Using standard radiologic response criteria, however, small retrospective series have reported response rates as low as 6% with this combination (15, 16). In the largest series reported to date, a three-drug combination of streptozocin, doxorubicin, and 5-fluorouracil was associated with an overall response rate of 39% and a 2-year overall survival rate of 74% in 84 patients with both locally advanced and metastatic pancreatic endocrine tumors (17). Although the number of pancreatic endocrine tumor patients in our study was small, the complete absence of activity associated with irinotecan and cisplatin in this patient subgroup suggests that streptozocin-based therapy may be superior to platinum-based therapy in patients with pancreatic endocrine tumors.

Relatively few other chemotherapeutic agents have been evaluated in the treatment of patients with metastatic neuroendocrine tumors. While dacarbazine (DTIC) has reported activity against both carcinoid and pancreatic endocrine tumors, high rates of nausea, vomiting, and myelosuppression have precluded its widespread use in this setting (18, 19). High-dose paclitaxel, administered with granulocyte-colony stimulating factor, has been associated with an objective radiologic response rate of only 8% in patients with advanced carcinoid and islet cell tumors (20). No objective radiologic responses were reported in phase II trials of docetaxel or gemcitabine (21, 22).

We conclude that the combination of cisplatin and irinotecan is relatively inactive in the treatment of patients with typical, well-differentiated neuroendocrine tumors. Our observation of activity in a patient with a poorly differentiated neuroendocrine tumor is consistent with previous reports that cisplatin-based regimens may be active against aggressive neuroendocrine tumor variants. Novel treatment strategies are clearly needed for patients with this disease.

REFERENCES

- DiBartolomeo M, Bajetta E, Buzzoni R, *et al*: Clinical efficacy of octreotide in the treatment of metastatic neuroendocrine tumors. *Cancer* 77:402-408, 1996
- Capella C, Heitz P, Hoffer H, Solcia E, Kloppel G: Revised classification of neuroendocrine tumors of the lung, pancreas and gut. *Virchows Arch* 425:547-560, 1995
- Moertel C, Kvols L, O'Connell M, Rubin J: Treatment of neuroendocrine carcinomas with combined etoposide and cisplatin: evidence of major therapeutic activity in the anaplastic variants of these neoplasms. *Cancer* 68:227-232, 1991
- Fjallskog M, Granberg D, Welin S, *et al*: Treatment with cisplatin and etoposide in patients with neuroendocrine tumors. *Cancer* 92:1101-1107, 2001
- Cunningham D, Pyrhonen S, James RD, *et al*: Randomised trial of irinotecan plus supportive care versus supportive care alone after fluorouracil failure for patients with metastatic colorectal cancer. *Lancet* 352(9138):1413-1418, 1998
- Saltz L, Cox J, Blanke C, *et al*: Irinotecan plus fluorouracil and leucovorin for metastatic colorectal cancer: Irinotecan Study Group. *N Engl J Med* 343:905-914, 2000
- Saltz L, Spriggs D, Schaaf L, *et al*: Phase I clinical and pharmacologic study of weekly cisplatin combined with weekly irinotecan in patients with advanced solid tumors. *J Clin Oncol* 16:3858-3865, 1998
- Iison DH, Saltz L, Enzinger P, *et al*: Phase II trial of weekly irinotecan plus cisplatin in advanced esophageal cancer. *J Clin Oncol* 17(10):3270-3275, 1999
- Kudo S, Fujiwara Y, Takada Y, *et al*: Phase II study of irinotecan combined with cisplatin in patients with previously untreated small-cell lung cancer. West Japan Lung Cancer Group. *J Clin Oncol* 16:1068-1074, 1998
- Noda K, Nishiwaki Y, Kawahara M, *et al*: Irinotecan plus cisplatin compared with etoposide plus cisplatin for extensive small-cell lung cancer. *N Engl J Med* 346:85-91, 2002
- Hou Z, Elasmir A, Lozano R, *et al*: A pilot study of irinotecan plus cisplatin in patients with metastatic high-grade neuroendocrine carcinoma. *Proc Am Soc Clin Oncol* 22:A1508, 2003
- Moertel C, Hanley J: Combination chemotherapy trials in metastatic carcinoid tumor and the malignant carcinoid syndrome. *Cancer Clin Trials* 2:327-334, 1979
- Engstrom P, Lavin P, Moertel C, Folsch E, Douglass H: Streptozocin plus fluorouracil versus doxorubicin in therapy for metastatic carcinoid tumor. *J Clin Oncol* 2:1255-1259, 1984
- Moertel C, Lefkopoulo M, Lipsitz S, Hahn R, Klaassen D: Streptozocin-doxorubicin, streptozocin-fluorouracil, or chlorozotocin in the treatment of advanced islet-cell carcinoma. *N Engl J Med* 326:519-523, 1992
- Cheng P, Saltz L: Failure to confirm major objective antitumor activity of streptozocin and doxorubicin in the treatment of patients with advanced islet cell carcinoma. *Cancer* 86:944-948, 1999
- McCollum A, Kulke M, Ryan D, *et al*: Lack of efficacy of streptozocin and doxorubicin in patients with advanced pancreatic endocrine tumors. *Am J Clin Oncol* 27:485-488, 2004
- Kouvaraki M, Ajani J, Hoff P, *et al*: Fluorouracil, doxorubicin, and streptozocin in the treatment of patients with locally advanced and metastatic pancreatic endocrine carcinomas. *J Clin Oncol* 22:4762-4771, 2004
- Bukowski R, Tangen C, Peterson R, *et al*: Phase II trial of dimethyltriazenoimidazole carboxamide in patients with metastatic carcinoid. *Cancer* 73:1505-1508, 1994
- Ramanathan R, Cnaan A, Hahn R, Carbone P, Haller D: Phase II trial of dacarbazine (DTIC) in advanced pancreatic islet cell carcinoma. Study of the Eastern Cooperative Oncology Group. *Ann Oncol* 112:1139-1143, 2000
- Anseli S, Pitot H, Burch P, Kvols L, Mahoney M, Rubin J: A phase II study of high-dose paclitaxel in patients with advanced neuroendocrine tumors. *Cancer* 91:1543-1548, 2001
- Kulke M, Kim H, Stuart K, *et al*: A phase II study of docetaxel in patients with metastatic carcinoid tumors. *Cancer Invest* 22:353-359, 2004
- Kulke M, Kim H, Clark J, *et al*: A phase II trial of gemcitabine for metastatic neuroendocrine tumors. *Cancer* 101:934-939, 2004

Review

Liposomes: Clinical Applications and Potential for Image-Guided Drug Delivery

Narottam Lamichhane ^{1,*}, Thirupandiyur S. Udayakumar ², Warren D. D'Souza ¹, Charles B. Simone II ¹, Srinivasa R. Raghavan ³, Jerimy Polf ¹ and Javed Mahmood ¹

¹ Department of Radiation Oncology, University of Maryland School of Medicine, Baltimore, MD 21201, USA; wdsouza@som.umm.edu (W.D.D.); CharlesSimone@umm.edu (C.B.S.I.); jpolf@umm.edu (J.P.); jmahmood@som.umaryland.edu (J.M.)

² Department of Radiation Oncology, University of Miami Miller School of Medicine, Miami, FL 33136, USA; tudayakumar@med.miami.edu

³ Department of Chemical and Biomolecular Engineering, University of Maryland, College Park, MD 20742, USA; sraghava@umd.edu

* Correspondence: narottamlamichhane@umm.edu; Tel.: +1-410-7062772

Received: 14 December 2017; Accepted: 26 January 2018; Published: 30 January 2018

Abstract: Liposomes have been extensively studied and are used in the treatment of several diseases. Liposomes improve the therapeutic efficacy by enhancing drug absorption while avoiding or minimizing rapid degradation and side effects, prolonging the biological half-life and reducing toxicity. The unique feature of liposomes is that they are biocompatible and biodegradable lipids, and are inert and non-immunogenic. Liposomes can compartmentalize and solubilize both hydrophilic and hydrophobic materials. All these properties of liposomes and their flexibility for surface modification to add targeting moieties make liposomes more attractive candidates for use as drug delivery vehicles. There are many novel liposomal formulations that are in various stages of development, to enhance therapeutic effectiveness of new and established drugs that are in preclinical and clinical trials. Recent developments in multimodality imaging to better diagnose disease and monitor treatments embarked on using liposomes as diagnostic tool. Conjugating liposomes with different labeling probes enables precise localization of these liposomal formulations using various modalities such as PET, SPECT, and MRI. In this review, we will briefly review the clinical applications of liposomal formulation and their potential imaging properties.

Keywords: liposomes; clinical applications; image guidance; radioisotopes; PET; SPECT; MRI

1. Introduction

Over the recent years of research innovation, drug delivery techniques have made a significant contribution to our understanding of drug tissue interactions. While many chemotherapeutic drugs and gene therapies have been developed in the last couple of decades, their efficacy is marred by toxicity and the inability to effectively reach the target site. The failure to deliver therapeutic agents at desired concentration to tumors derives from constraints that are innate to the tumor microenvironment or the bioactivity and bioavailability of therapeutic agents. Many tumors, such as pancreatic ductal adenocarcinoma (PDAC), harbor dense desmoplastic stroma that prevents therapeutic agents from effectively reaching the tumor cells [1]. In addition, increased interstitial fluid pressure (IFP) keeps the therapeutic agents at bay [2]. Low bioavailability due to elimination from circulation or biotransformation also contribute to impaired delivery of the therapeutic agents to the target site [3]. Mononuclear phagocyte system is very efficient at eliminating the therapeutic agents from circulation, hence impeding the delivery to the target site [2].

Challenges in drug delivery due to the limited diffusion of drugs as a result of high interstitial pressure and, rapid clearance of intravenously administered drugs by the systemic circulation hamper the adequate uptake of drugs in tumor regions [4,5]. These challenges associated with drug delivery have spurred research in the field of “drug delivery” aimed at developing methods that aid in delivery of the drugs/molecules to the target sites for improved clinical outcomes. Circumventing such problems is a major challenge in drug delivery vehicles. Research has primarily focused on increasing bioavailability while at the same time improving the targeting of the therapeutic agents to the tumor site. Drug delivery methods such as liposomes, micelles, dendrimers, etc. [6–9] have been widely investigated for their potential in a wide range of clinical applications. However, liposomes are one of the potentially most promising drug delivery vehicles. Liposomes are lipid vesicles consisting of one or more concentric lipid bilayers enclosing an aqueous space (Figure 1). Liposomes present an attractive delivery system because of the flexibility of changing their chemical composition, structure and colloidal size by modifying the preparation methods [10]. Liposomes can therefore be manufactured with different size, ranging from several nanometers to micrometers. Flexibility of formulation of liposomes with varying the choice of bilayer components allows liposomes to be either rigid and impermeable or permeable and less stable [11]. Surface modifications allows liposomes to be tailored for both diagnostic, therapeutic, as well as image-guided drug delivery. These unique advantages of liposomes over other nanocarriers offer solutions to many limitations in diagnosis, delivery and treatment management of human diseases [12].

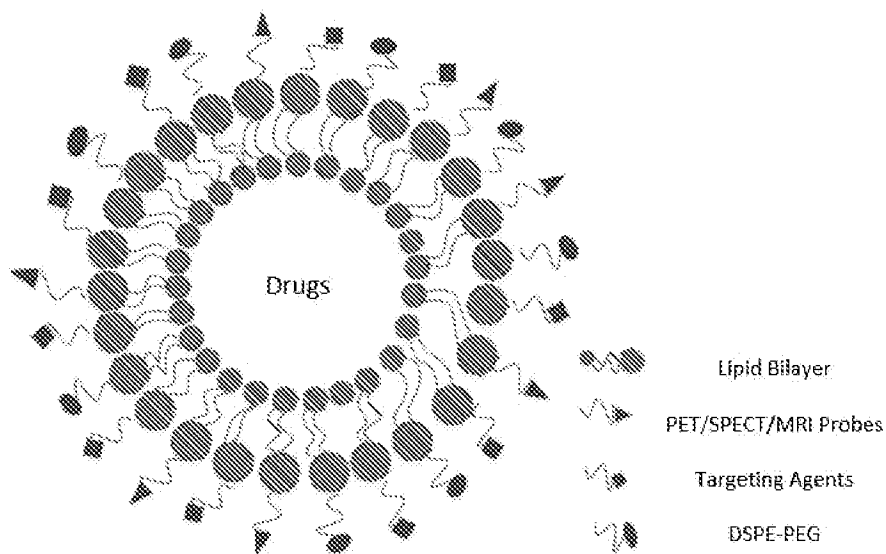


Figure 1. Schematics of a functionalized liposome.

Despite their attractive characteristics, liposomal delivery systems also have some drawbacks. Liposomal systems can trigger an acute hypersensitivity syndrome known as complement activation-related pseudoallergy (CARPA) as a result of the innate immune response [13]. Conventional liposomes are cleared rapidly from the circulation by the macrophages that are located mainly in the liver, spleen and bone marrow [14–16]. The use of modified flexible hydrophilic polymers such as polyethylene glycol (PEG), which provide a protective hydrophilic layer on the surface of the liposome reduces the clearance of liposomes from the reticuloendothelial system (RES) [17–19]. Such pegylated liposomes, also known as “stealth liposomes”, have prolonged circulation time [20,21] and an improved pharmacokinetic profile compared with that of a free drug [22]. Owing to their many properties liposomes have been investigated pre-clinically and clinically on many fronts as a diagnostic and therapeutic tool. Molecular imaging using multimodal probes offers great potential

for early and accurate diagnosis, real time monitoring of in vivo pharmacokinetics as well as detailed information of pathologies. Versatility in liposomal surface functionalization to attach different molecular probes enables multimodal imaging that can be exploited to derive accurate and precise assessment of hallmarks of various diseases. The purpose of this review is to focus mainly on the clinical application of liposomes and their potential use as imaging agents as well as in image guided drug delivery systems.

2. Clinical Applications of Liposomes

Clinically, liposomal formulations are used as carriers for biologically active molecules. Liposomes have been extensively studied in areas such as gene therapy [23] and drug delivery [24] due to their observed stability and favorable toxicity profile over traditional treatments. Liposomes can encapsulate biomolecules or drugs that are hydrophilic and increase their internalization and solubility through the lipid bilayers of the cells [25]. Research interest in liposomal formulations have increased significantly in the last decade and have been shown to be safer than viral vectors due to their low immunogenicity, more limited toxicity and their ability to carry larger cargo to the target sites [26,27]. Liposomal formulations have shown to accumulate in the target tissue—with enhanced bio-distribution [28]. Drug formulations with liposomes are approved for intravenous, intramuscular [29] and oral delivery [30] and the delivery is determined by the mechanism of drug loading, composition of the membrane, and the tumor microenvironment [31]. Clinically approved liposomal drugs—are pegylated variants to improve their time in circulation and protect the integrity of the drug from various degrading mechanisms active inside a tissue or cell.

Liposome-mediated drug delivery systems have been successfully translated into clinical settings [32]. These delivery systems are used in diverse medical fields, including anti-cancer, anti-fungal and anti-inflammatory drugs as well as therapeutic gene delivery. Many clinical products, e.g., Doxil™, AmBisome® and DepoDur [33] have been formulated using liposomes for clinical applications. Therapeutic use of various agents through alterations in their pharmacokinetics and pharmacodynamics were enhanced by encapsulation of drugs in liposomes. A number of liposome-based drug formulations are approved for human use and many additional products are currently being assessed in different clinical trials.

In 1995, Doxil™ was first introduced in U.S., to treat ovarian cancer and AIDS-related Kaposi's sarcoma [33]. Doxil™, liposomal doxorubicin, was developed exploiting active loading by pH gradient method [34,35]. Further, DaunoXome® was developed by NeXstar Pharmaceuticals (Boulder, CO, USA) for the delivery of daunorubicin, and was FDA approved in 1996 for the management of advanced HIV-associated Kaposi's sarcoma. Other products since available include Mepact® by Takeda Pharmaceutical (Deerfield, IL, USA), DepoCyt® by SkyPharma Inc. (Belgravina, London, UK), Marqibo® by Talon Therapeutics (San Francisco, CA, USA) and a fluorouracil, leucovorin combination with liposomes (Merrimack Pharmaceuticals Inc., Cambridge, MA, USA) therapy-based product for metastatic adenocarcinoma of the pancreas and Myocet® by Elan Pharmaceuticals (San Francisco, CA, USA). Apart from cancer treatments, liposomal products were also developed for other diseases such as fungal infections (Amphotec® and AmBisome®). Liposomes have become an important carrier systems for vaccine development leading to the development of vaccines such as Epaxal® and Inflexal V® for hepatitis and influenza, respectively.

2.1. Liposomal Formulations in Clinical Trials

Currently, there are a number of liposomal products undergoing clinical trials. In the past decade, extensive research on lipid carriers and liposomal formulations lead to the development of new liposome mediated drug delivery. Here, we highlighted some of the liposomal products in clinical trials (Table 3).

Table 1. Liposomes under different phases of clinical trials.

Drug/Name	Phase I			Phase II			Phase III			References
	Agent/Target	Drug/Name	Agent/Target	Drug/Name	Agent/Target	Drug/Name	Agent/Target	Agent/Target		
1 BP1001	Antisense protein/Grb-2	Atropatin	L-NDDP/Platinum	Arikace	Amikacin/Ribosomal inhibitor				[34–38]	
2 INX-0125	Sphingomyelin/cholesterol	LEP-ETU	Paclitaxel/microtubule	Lipoplatin	Cisplatin				[39–41]	
3 INX-0076	Topotecan Sphingosomes	OSI-211	Lurtotecan/antineoplastic	Liprostin	PGE-1/Prostaglandin Receptor				[32,42,43]	
4 LiPlaCis	Cisplatin/solid tumors	S-ANNA	Annamycin/TOPO II	Stimuvax	Tecemotide/Immunosuppressant				[44–46]	
5 LEM-ETU	Mitoxantrone/TOPO II inhibitor	S-CKD602	TOPO I inhibitor	TAN5	T4 endonuclease V				[29,47,48]	
6 SGT-53	p-53	SPI-077	Cisplatin/Retinoids/Skin disease	Thermodox	Doxorubicin/antimitotic				[49–51]	
7 LDF01	Cationic liposomes/Microvessels	Tretnoin	Retinoids/Skin disease	MiR-122	MicroRNA-122/HCV				[52–54]	
8 Atu027	siRNA/Solid tumors	Irinotecan SN-37	Camptothecin/DNA damage	Cyclophosphamide	Nitrogen mustard/antineoplastic				[55–57]	
9 Navelbine	alkaloid/Immunosuppressant	Taxol	Paclitaxel/microtubule	CPX-351	Cytarabine:daunorubicin/DNA polymerase inhibitor				[58–60]	

2.1.1. Phase I

Liposomal formulations in phase I clinical trials include Grb-2, LEM-ETU, INX 0125 and 0076. We briefly discuss these trials under this section. Grb-2 is used for the treatment of breast cancer and leukemia.

Grb-2 liposomes (BP-100-1.01) inhibit the production of the growth factor receptor-bound protein-2. Grb-2 is a DOPC-integrated antisense oligonucleotide [61]. Grb-2 inhibits tumor cell proliferation due to its anti-neoplastic activities and the presence of antisense oligo-deoxy-nucleotide [62]. In a Phase 1 trial, Grb-2 is being studied for the treatment of relapsed or refractory acute myeloid leukemia and its safety, maximum tolerated dose, optimal therapeutic dose and anticancer activity is also being explored.

LEM-ETU liposomes is used in the management of various treatments including, leukaemia, breast, stomach, liver and ovarian cancers and are composed of DOPC, cholesterol and cardiolipin [63,64]. Compared to other liposomes, the presence of cardiolipin helps in drug entrapment and higher drug loading capability. Further, "NeoPharm's NeoLipid liposome technology" developed these liposomes for the treatment of various cancers.

INX-0125 and INX-0076 are developed by Inex pharmaceuticals (Burnaby, British Columbia, Canada) and are undergoing a phase I clinical trial. Both of these liposomal formulations are composed of cholesterol and sphingomyelin (SM) and are developed for the treatment of advanced solid tumors [23]. Sphingosomal formulations enhance tumor targeting and also increase the duration of exposure for loaded anticancer agents without any increase in toxicity in preclinical trials [31]. INX-0125 has also been used in the treatment of Hodgkin's and non-Hodgkin's lymphoma. Based on phase I clinical trials, INX-0076 protects the drug from in vivo degradation and has been shown to accumulate at target sites thus increasing the efficacy of the drug [32].

2.1.2. Phase II

Aroplatin™ (L-NDDP) is a chemotherapeutic platinum analogue (*cis*-bisneodecanoato-*trans*-*R,R*-1,2-diaminocyclohexane platinum II) and the first liposomal platinum formulation to enter into clinical trials; the loaded analogue is structurally similar to Eloxatin (Oxaliplatin; Sanofi Aventis, Bridgewater, NJ, USA). These platinum analogues have cytotoxic properties where, they form inter- and intra-strand cross-links of DNA, thereby inhibiting DNA synthesis in tumor cells [21,37]. Aroplatin™ analogues have been studied in preclinical models and found to be effective in inhibiting the emergence of liver metastasis of reticulosarcoma. This formulation reduced toxicity and, improved activity and bioavailability [65]. An early phase Phase I/II trial of Aroplatin™ was completed in 2002 for advanced solid malignancies, however, a phase I dose escalation trial was carried out in 2005 where a maximum tolerated dose was reached, followed by termination of this trial in spite of the clinical results obtained due to the inaccurate chemical composition along with the instability of the drug in liposomes [66].

LEP Easy-to-Use (LEP-ETU) is a novel delivery system of paclitaxel developed by NeoPharm, Inc. (Blainville, QC, Canada). Paclitaxel (taxol) is an anti-micro-tubular network agent that has been studied in different malignancies. Preclinical studies of liposome-entrapped paclitaxel (LEP) have demonstrated that LEP was associated with reduced toxicity while maintaining efficacy [40]. To enhance the solubility with Paclitaxel, this drug is formulated with polyoxyethylated castor oil that led to infusion-related hypersensitivity reactions. NeoPharm improved the safety profile by formulating LEP-ETU with a mixture of synthetic phospholipids and cholesterol that is necessary for administering higher doses than would commonly or safely be used with taxol. The results from phase I clinical trials of NeoPharm, showed LEP-ETU is better tolerated than taxol, as indicated by a higher maximum-tolerated dose (MTD).

OSI-211 liposomes (OSI Pharmaceuticals, Melville, NY, USA), a liposomal formulation of lurtotecan (LRT), are composed of a HSPC and cholesterol (2:1). OSI-211 is a topoisomerase I inhibitor, and is currently in Phase II clinical trials [67]. In pre-clinical studies the product demonstrated

increased drug accumulation in tumor. Compared to topotecan, OSI-211 showed a similar toxicity profile in a randomized phase II clinical trial in relapsed ovarian cancer treatment [88]. Next-generation formulations OSI-211 and NX 211 were used in the treatment of ovarian and head & neck cancer.

Cisplatin is a highly effective chemotherapeutic agent against epithelial cancers [89]. To reduce the systemic toxicity of this agent, a liposomal pegylated formulation, Liposomal cisplatin (SPI-077), was developed. Phase I studies of SPI-77 began in 1995 at doses ranging from 40 to 420 mg/m² [90]. Results from a Phase I study demonstrated the ability to deliver ten-fold the amount of cisplatin per dose without encountering any toxicities beyond grade 1. Side-effects included mild gastrointestinal toxicity (nausea and vomiting), and mild anemia, muscle weakness (at doses of ≥ 320 mg/m²) and a case of infusion-related reaction [91].

2.1.3. Phase III

Cyclophosphamide (CYP) is an alkylating agent broadly used as an anticancer chemotherapeutic agent for numerous malignancies [72–74]. The active carbonium ion produced by CYP reacts with nucleic acids and proteins of tumor cells. Pre-clinical studies have demonstrated that CYP entrapped in liposomes reduces non-specific toxicities and enhances anticancer effects [75,76]. Pre-clinical studies showed that encapsulation of CYP increased its mutagenicity resulting in accumulation of drug inside the cell and eventually causing chromosomal damage [77]. In a phase III trial of liposomal doxorubicin (Myocet) and a stereoisomer of doxorubicin (epirubicin) combined with cyclophosphamide as first-line therapy for metastatic breast cancer, it was shown that Myocet has modest but significant increase in efficacy than epirubicin [56].

Stimuvax[®] (L-BLP-25 or tecemotide, Merck, Kenilworth, NJ, USA), is a therapeutic vaccine for cancers expressing Tumor-Specific Antigens (TSA) that integrates an antigenic lipo-peptide, i.e., tecemotide, in a liposomal delivery system. Mucin 1 (MUC1) is overexpressed in different cancer cells (breast, prostate, non-small cell lung cancer (NSCLC) and colorectal cancer) that are the target for tecemotide. Stimuvax, triggers a cellular immune reaction after targeting TSA, leading to immune rejection of tumors that have the MUC1 antigen [78]. Stimuvax[®] looked promising in a randomized Phase II trial that led to a subsequent Phase III trial where Stimuvax[®] was administered after chemotherapy and radiation therapy for locally advanced (stage III) NSCLC. In Phase II trials, Stimuvax[®] showed a significant increase in life expectancy from 13.3 to 30.6 months and showed a positive outcome in stage III and IV NSCLC patients. However, in Phase III trials, Stimuvax[®] did not meet its primary or secondary end-points, which led to the termination of the trial [46,79].

Liposomal formulation of cisplatin (CPT), Lipoplatin, is a FDA approved cytotoxic agent. Its mechanisms include DNA cross linking and inhibition of DNA synthesis. For pancreatic cancer the product used was Lipoplatin and for lung cancer was Nanoplatin [43]. Lipoplatin is composed of lipids including 1,2-dipalmitoyl-*sn*-glycero-3-phosphorylglycerol (DPPG), soy PC, monomethoxy-polyethylene-glycol-1,2-distearoyl-*sn*-glycero-3-phosphoethanolamine (MPEG-DSPE) lipid conjugate and cholesterol. The advantages of CPT incorporation in liposomes include increased cell permeability, longer half-life of the drug in circulation, and higher concentration of drugs in tumors [80]. Toxicities including renal and neuropathy were considerably reduced with lipoplatin compared to CPT given alone [81].

2.2. Liposomes and Image Guided Delivery

Imaging plays an integral part in modern precision and individualized medicine. Wide applications of imaging such as monitoring drug delivery, accurate diagnosis of diseases, determining response to therapy, and guiding minimally invasive procedures are some of the applications of imaging in clinic. However, traditional imaging modalities such as computed tomography (CT), positron emission tomography (PET), magnetic resonance imaging (MRI), and single photon emission computed tomography (SPECT) all suffer from target specificity, limiting their clinical utility. Nanoparticles with their versatility in surface functionalization provide opportunities to

enhance target specificity and label nanoparticles with various isotopes that enables them to act as contrast agents.

Radionuclide imaging offers unique strengths in cancer diagnosis. Use of radiolabel liposomes could act as a companion diagnostic. Pre-administration of radiolabeled liposomes and quantifying the uptake of liposomes in target sites can help in determining drug responders vs. non-responders. This will also help in determining an optimal dose to predict a potential therapeutic response. Hence, insufficient accumulation may represent lack of therapeutic response. In such scenarios, the liposomes can be altered to better manage patients [82]. The majority of radionuclide imaging is carried out using PET and SPECT. Multimodality imaging such as MRI and CT provides detail anatomical information, however they are not capable of providing disease states. On the other hand, PET and SPECT can measure chemical changes pre- and post-treatment intervention [83]. The potential of functionalization of liposomes offers an advantage of engineering liposomes to target cancer cells for the use in radionuclide imaging of malignant lesions. For this purpose, the radionuclide can be directly conjugated on the surface of the liposomes or can be encapsulated in the aqueous core (Figure 1). Radiolabeling of liposomes can be achieved using various labeling procedures. Passive encapsulation of radionuclide, labeling the liposomal membrane or labeling the preformed liposomes by loading the radionuclide using an ionophore or chelator are different labeling ways. Application of radiolabeled liposomes for clinical settings require high incorporation efficiency and good retention of radiolabel agents. Remote afterloading of liposomal formulations had shown most efficient labeling and best radiolabel retention [82]. Various PET and SPECT radioisotopes have been utilized to conjugate with liposomes to evaluate their clinical utility in multimodal imaging. Quantitation of liposomes generated by SPECT or PET images also enables non-invasive data analysis over time [84,85].

2.3. PET Imaging

Quantitative imaging with nanoparticle provides accurate and precise assessment of pathologies in cancer care and opens up the pathway for personalized precision medicine. PET imaging is an outstanding tool to derive a quantitative measure and real time monitoring of the biomarker uptake in vivo. Various researchers have studied the feasibility of PET imaging by conjugating PET isotopes in long circulating liposomes [83,86–91]. Wong et al. [92] evaluated the clinical utility of ^{64}Cu ($T_{1/2} = 12.7$ h) labeled liposomes as diagnostic and therapeutic tools to measure tumor volume, as a contrast agent, and compared the biodistribution of ^{64}Cu -labeled liposomes to the clinical tracer ^{18}F -FDG. In this study, Wong et al. reported that the estimates of tumor diameter were comparable between ^{64}Cu -liposomes and ^{18}F -FDG and heterogeneity of uptake with both tracers. The feasibility of image contrast with both tracers was also reported. Another study by Seo et al. [93] studied two ^{64}Cu -radiolabeled lipids of different acyl chains (1 mol % DSPE vs. 1 mol % DPPE) in long circulating liposomes and presented the differences of stability of these lipids using PET imaging. Remote loading method of ^{64}Cu into liposomes using 2-hydroxyquinoline to transport ^{64}Cu through the membrane to the copper chelator was studied by Petersen et al. [89]. Seo et al. [84] also looked into the pharmacokinetics of ^{89}Zr ($T_{1/2} = 78.4$ h) labeled liposomes over the extended period of time in a murine model. Zirconium (Zr) with a relatively longer decay has been exploited as a potential isotope for PET imaging to study the pharmacokinetics for an extended period. In this study, Seo et al. reported that the location of ^{89}Zr label altered the clearance rate of intracellularly trapped radioactivity and suggested optimization of chelator and attachment strategies for future studies to use ^{89}Zr for image based pharmacokinetics. Perez-Medina et al. [94] also reported on ^{89}Zr labeling of liposomes using two different approaches for pharmacokinetic and biodistribution. They studied two different approaches of ^{89}Zr labeling using click labeling and surface chelation and observed that surface chelation is superior in terms of stability and in vivo performance. Marik et al. [95] synthesized ^{18}F ($T_{1/2} = 110$ min) radiolabeled diglyceride, 3- ^{18}F -fluoro-1,2-dipalmitoylglycerol [^{18}F] fluorodipalmitin ([^{18}F] FDP) and its conjugation to synthesize ^{18}F labeled liposomes. Marik et al. [95] reported the feasibility of PET imaging using both the radiolabeled [^{18}F] FDP and liposome-incorporated [^{18}F] FDP. Freely injected

[¹⁸F] FDP had the highest uptake in the liver, spleen and lungs. Liposomal [¹⁸F] FDP remained in blood circulation at near-constant levels for at least 90 min, with a peak concentration near 2.5% ID/cc. Hansen et al. studied the EPR effect in 11 canine cancer patients with spontaneous solid tumors using ⁶⁴Cu-loaded liposomes by PET/CT imaging. In this study, Hansen et al. included different tumor types and showed tumor dependent differences in accumulation and heterogeneity of uptake of the radiotracers. The study showed that the squamous cell carcinomas had the highest EPR effect as compared to other type of tumors [96]. Luo et al. studied the effects of porphyrin-phospholipid inclusion in ⁶⁴Cu-radiolabeled doxorubicin containing stealth liposomes (Dox-PoP). Luo et al. showed that Dox-PoP liposomes accumulated passively into tumor using both PET and fluorescence imaging. Luo et al. also demonstrated strong primary tumor growth inhibition with a single treatment of chemophototherapy using 665 nm light (200 J/cm²) [97].

Recent work on PET labeling has also focused on the optimization procedures using longer lived isotope such as ⁵²Mn (T_{1/2} = 5.6 days). A study by Jensen et al. [98] evaluated the optimal protocols on ⁵²Mn labeling through both remote-loading and surface labeling. In this study, Jensen et al. reported that the labeling efficiencies of ⁵²Mn with both labeling procedures were similar; however, the plasma half-life of surface conjugated ⁵²Mn liposomes were shorter than remote loading. The popularity of PET in routine clinical practice due to its ability to diagnose diseases, more accurately stage malignancies, evaluate treatment response, detect CT-occult metastatic lesions and various other characteristics have established this imaging modality as a workhorse of nuclear medicine procedures. Tremendous efforts on developing image drug delivery systems are still ongoing with the intent of obtaining better diagnosis and therapy of different diseases. PET labeling of liposomes is an effort at circumventing some of these challenges which requires precise formulation, surface architecture and functionalization, and accurate design of drug loading procedures.

2.4. SPECT Imaging

SPECT is another commonly used imaging modality in nuclear medicine procedures. Like PET, SPECT imaging also requires an injection of molecular probes that are labeled with radionuclides. ¹¹¹In (T_{1/2} = 2.81 days), ^{99m}Tc (T_{1/2} = 6 h) and ⁶⁷Ga (T_{1/2} = 78.26 h) represent some of the SPECT isotopes that are used to label liposome to enable SPECT signal. Espinola et al. [99] studied the organ distribution of ^{99m}Tc and ¹¹¹In oxine labeled multilamellar lipid vesicles in 1978. In that study, Espinola et al. reported that constant distribution of ¹¹¹In-oxine labeled vesicles was observed throughout 72 h as compared to ^{99m}Tc labeled vesicles that showed continuous leakage of radioactivity from the involved organs. Ogihara et al. [100–103] studied the differential uptake of ⁶⁷Ga and ⁶⁷Ga labeled liposomes in tumors and inflammatory regions in rats. In that study, Ogihara et al. reported that positively charged liposomes preferentially delivered ⁶⁷Ga to the tumor compared with granulation tissue, suggesting that ⁶⁷Ga labeled liposomes are able to discriminate tumor and inflammatory lesions. Proffitt et al. [104] successfully imaged EMT6 tumors in BALB/c mice using In-111 nitrilotriacetic acid loaded liposomes. Biodistribution studies performed using three different liposomes with different charges showed the highest uptake with neutral ¹¹¹In nitrilotriacetic acid loaded liposomes. Turner et al. [105] developed ¹¹¹In-labeled liposomes and studied dosimetric effects of these liposomes in 24 patients. Tumor was observed in 22 out of 24 patients in the scans. However, Turner et al. reported homogenous uptake of these liposomes in the liver and spleen with scans obtained 24 and 48 h post injection which is typical of nanoparticles. In clinical studies, Kubo et al. reported tumor imaging of seven patients using ¹¹¹In-labeled V-liposomes. Results from that study revealed increased activity in the tumors of four patients [106]. Furthermore, rapid blood clearance of liposomes with homogenous uptake in the liver and spleen was observed. One of the challenges in nuclear medicine is the localization of infectious and inflammatory lesions. In order to evaluate the potential of liposome to visualize foci of infection and inflammation, Boerman et al. [107] investigated ¹¹¹In-labeled pegylated liposomes in *S. aureus* infection induced in rats using gamma imaging. As a control, ¹¹¹In-IgG images were used as a comparison to ¹¹¹In-liposomes. Abscesses were visualized within an hour of

¹¹¹In-liposome post injection. Contrast between the infectious focus and the background increased with time. The ratio of abscess to background was significantly higher ($p < 0.04$) with ¹¹¹In-liposomes as compared to ¹¹¹In-IgG [108]. ^{99m}Tc labeled liposomes were also investigated from the same group to evaluate their feasibility to detect infection and inflammation. The authors reported that ^{99m}Tc liposomes preferentially accumulated in abscesses [107]. Another clinical study by Harrington et al. investigated the effective targeting of solid tumors in 17 patients with locally advanced cancers using ¹¹¹In-labeled PEGylated liposomes with tumor seen in 15 of these patients. In 12 of the 17 patients, the tumor was clearly visible in the whole body scan; in an additional 3 patients that included 2 gliomas and 1 cervical cancer, SPECT scans of the regions of interest were required to identify the tumors [109]. As a representation of the study, Harrington et al. presented gamma camera images of three patients with three different cancers at 72 h post ¹¹¹In-DTPA labeled pegylated liposomes that showed clear depiction of tumors in all three images [109]. Molecular imaging using SPECT enabling liposomes are increasingly being investigated to diagnose various diseases including inflammation, plaques, cancers and many more [110–115]. Molecular imaging using radiolabeled nanoparticles is also aimed at facilitating better delivery, in vivo pharmacokinetics monitoring, as well controlled release. In lieu of this, there has been limited research into radiolabeling liposomes with dual isotopes as a hybrid model [116,117]. A recent study by Lamichhane et al. also looked into ¹¹¹In-labeled liposomes as a drug delivery vehicle for a ¹⁸F-labeled carboplatin derivative. This hybrid liposome construct was used to acquire dual modality imaging of a liposome vehicle using SPECT and drug using PET. This allowed for determining the pharmacokinetics and in vivo behavior of drug and vehicle distinctively using two different imaging modalities [118].

2.5. MRI Imaging

MRI is the most powerful non-invasive imaging modality that offers high soft tissue contrast, spatial resolution, and penetration depth [119]. Despite the relatively high soft tissues contrast with MRI images, in some cases it does not allow for enough image contrast to diagnose the pathology of interest. Such cases require the use of contrast agents to improve the contrast-to-noise ratio by shortening the spin-lattice T_1 and/or spin-spin T_2 relaxation times of the water protons within the region of interest [120–122]. There is an increased interest in using liposomes as contrast agents for MRI due to their tunable properties and lower toxicities as compared to the currently used contrast agents such as gadolinium. Liposomes have long been proposed as a vehicle to deliver paramagnetic ions by entrapping them inside them to reduce the systemic toxicity and potential to increase the contrast to noise ratio [123]. Multimodality imaging offers an additional advantage of retrieving information based on different modalities. Researches have also assessed bimodal detection of tumor using optical/MRI tagged liposomes. Ding et al. studied the effectiveness of targeting by evaluating folate receptor targeted fluorescent paramagnetic liposomes for tumor imaging. In their study, folate targeting was verified by measuring the uptake of folate conjugated liposomes using confocal microscopy and comparing the uptake to the untargeted liposomes. The MR image of HeLa cells incubated with folate conjugated Gd containing liposomes was also brighter than that of HeLa cells incubated with only Gd-DTPA [124]. Local delivery of drug to the tumor region increases the therapeutic ratio of chemotherapeutic agents. Releasing the payload encapsulated inside liposomes and quantifying the amount of release provides feedback on optimizing liposomes for specific purposes. Encapsulating chemotherapeutic agents with gadolinium and releasing these agent in tumor using high intensity focused ultrasound offers promise in local delivery and MRI guided therapy [112,125,126]. A similar approach of encapsulating non-Gd-containing T_1 -MR contrast agents based on Fe-succinyl deferoxamine (Fe-SDFO) has been studied as a safe alternative [127]. In this study, Kneepkens et al. reported that the amount of doxorubicin delivered to the tumor correlated with the rate of relaxation change. Another challenge in drug delivery is the blood brain barrier. Convection enhanced delivery (CED) of drugs enables higher concentration of drugs insitu as compared to systemic administration. Nordling-David et al. studied the delivery of temozolomide (TMZ) encapsulated liposomes in

conjunction with GD-DTPA liposomes using CED to treat glioblastoma multiforme (GBM). This study reported that the co-infusion of pegylated Gd-DTPA liposomes and TMZ-liposomes by CED in GBM bearing rats, resulted in enhanced tumor detection with longer residence time than free Gd-DTPA. Treatment of GBM-bearing rats with either TMZ solution or TMZ-liposomes resulted in greater tumor inhibition and significantly higher survival; with no significant difference in survival with liposome formulation as compared to TMZ alone [128]. Shao et al. studied the difference of MR contrast using porphyrin-phospholipid and amino functionalized porphyrin phospholipid in BALB/c mouse. In this study Shao et al. synthesized manganese conjugated liposomes using 2-[1-hexyloxyethyl]-2-devinyl pyropheophorbide-a (HPPH), a porphyrin derivative. This derivative was amine modified to derive N-HPPH-lipid which was also used to synthesize manganese conjugated liposomes. With the amino modification, Shao et al. observed 150% higher T_1 relaxivity (mms^{-1}), increase to 2.46 for Mn-N-HPPH liposomes from 0.98 for Mn-HPPH liposomes [129].

3. Conclusions

Liposomes have been explored for various diseases ranging from cancer treatment to pain management. Advantages of using liposomal formulations include: (1) the properties of these liposomes like pharmacokinetics and pharmacodynamics are easily maneuverable, (2) improved bioavailability and (3) reduced toxicity. Different liposomal formulations are made for various applications such as temperature sensitive liposomes, cationic liposomes and liposomal vaccines. Collectively, these liposomal formulations have the ability to enhance or to overcome the limitations of conventional therapies. Furthermore, liposomes have shown great promise in their design to label them with molecular probes for imaging. Exploitation of liposomal characteristics to improve the target specificity and encapsulation can achieve significant therapeutic efficacy. Many liposomal formulations have successfully translated to clinical applications after extensive research on their efficacy and preclinical trials have demonstrated a greater impact on patients with various ailments, thereby improving the quality of life. Designing such liposomes with imaging probes can further enable real time delivery, monitoring and assessment of biological signatures that can ultimately lead to effective and personalized treatment.

Conflicts of Interest: The authors declare no conflict of interest.

References

1. Nagathihalli, N.S.; Castellanos, J.A.; Shi, C.; Beesetty, Y.; Reyzer, M.L.; Caprioli, R.; Chen, X.; Walsh, A.J.; Skala, M.C.; Moses, H.L.; et al. Signal transducer and activator of transcription 3, mediated remodeling of the tumor microenvironment results in enhanced tumor drug delivery in a mouse model of pancreatic cancer. *Gastroenterology* **2015**, *149*, 1932–1943. [[CrossRef](#)] [[PubMed](#)]
2. Sriraman, S.K.; Aryasomayajula, B.; Torchilin, V.P. Barriers to drug delivery in solid tumors. *Tissue Barriers* **2014**, *2*, e29528. [[CrossRef](#)] [[PubMed](#)]
3. Akhdar, H.; Legendre, C.; Aninat, C.; More, F. Anticancer drug metabolism: Chemotherapy resistance and new therapeutic approaches. In *Topics on Drug Metabolism*; Paxton, J., Ed.; InTech: Rijeka, Croatia, 2012; p. 6.
4. Ernsting, M.J.; Murakami, M.; Roy, A.; Li, S.D. Factors controlling the pharmacokinetics, biodistribution and intratumoral penetration of nanoparticles. *J. Control. Release* **2013**, *172*, 782–794. [[CrossRef](#)] [[PubMed](#)]
5. Phillips, W.T.; Bao, A.; Brenner, A.J.; Goins, B.A. Image-guided interventional therapy for cancer with radiotherapeutic nanoparticles. *Adv. Drug Deliv. Rev.* **2014**, *76*, 39–59. [[CrossRef](#)] [[PubMed](#)]
6. Lembo, D.; Cavalli, R. Nanoparticulate delivery systems for antiviral drugs. *Antivir. Chem. Chemother.* **2010**, *21*, 53–70. [[CrossRef](#)] [[PubMed](#)]
7. Massoud, T.F.; Gambhir, S.S. Molecular imaging in living subjects: Seeing fundamental biological processes in a new light. *Genes Dev.* **2003**, *17*, 545–580. [[CrossRef](#)] [[PubMed](#)]
8. Ostro, M.J.; Cullis, P.R. Use of liposomes as injectable-drug delivery systems. *Am. J. Hosp. Pharm.* **1989**, *46*, 1576–1587. [[PubMed](#)]

9. Caminade, A.M. Phosphorus dendrimers for nanomedicine. *Chem. Commun. (Camb.)* **2017**, *53*, 9830–9838. [[CrossRef](#)] [[PubMed](#)]
10. Elbayoumi, T.A.; Torchilin, V.P. Current trends in liposome research. *Methods Mol. Biol.* **2010**, *605*, 1–27. [[PubMed](#)]
11. Akbarzadeh, A.; Rezaei-Sadabady, R.; Davaran, S.; Joo, S.W.; Zarghami, N.; Hanifehpour, Y.; Samiei, M.; Kouhi, M.; Nejati-Koshki, K. Liposome: Classification, preparation, and applications. *Nanoscale Res. Lett.* **2013**, *8*, 102. [[CrossRef](#)] [[PubMed](#)]
12. Malam, Y.; Loizidou, M.; Seifalian, A.M. Liposomes and nanoparticles: Nanosized vehicles for drug delivery in cancer. *Trends Pharmacol. Sci.* **2009**, *30*, 592–599. [[CrossRef](#)] [[PubMed](#)]
13. Sercombe, L.; Veerati, T.; Moheimani, F.; Wu, S.Y.; Sood, A.K.; Hua, S. Advances and challenges of liposome assisted drug delivery. *Front. Pharmacol.* **2015**, *6*, 286. [[CrossRef](#)] [[PubMed](#)]
14. Medina, O.; Zhu, Y.; Kairemo, K. Targeted liposomal drug delivery in cancer. *Curr. Pharm. Des.* **2004**, *10*, 2981–2989. [[CrossRef](#)] [[PubMed](#)]
15. Torchilin, V. Recent advances with liposomes as pharmaceutical carriers. *Nat. Rev. Drug Discov.* **2005**, *4*, 145–160. [[CrossRef](#)] [[PubMed](#)]
16. Harrington, K.J.; Rowlinson Busza, G.; Syrigos, K.N.; Uster, P.S.; Abra, R.M.; Stewart, J.S. Biodistribution and pharmacokinetics of ¹¹¹In-DTPA-labelled pegylated liposomes in a human tumour xenograft model: Implications for novel targeting strategies. *Br. J. Cancer* **2000**, *83*, 232–238. [[CrossRef](#)] [[PubMed](#)]
17. Yang, T.; Choi, M.-K.; Cui, F.-D.; Kim, J.; Chung, S.-J.; Shim, C.-K.; Kim, D.-D. Preparation and evaluation of paclitaxel-loaded pegylated immunoliposome. *J. Control. Release* **2007**, *120*, 169–177. [[CrossRef](#)] [[PubMed](#)]
18. Klibanov, A.L.; Maruyama, K.; Torchilin, V.P.; Huang, L. Amphipathic polyethyleneglycols effectively prolong the circulation time of liposomes. *FEBS Lett.* **1990**, *268*, 235–237. [[CrossRef](#)]
19. Klibanov, A.L.; Maruyama, K.; Beckerleg, A.M.; Torchilin, V.P.; Huang, L. Activity of amphipathic poly(ethylene glycol) 5000 to prolong the circulation time of liposomes depends on the liposome size and is unfavorable for immunoliposome binding to target. *Biochim. Biophys. Acta* **1991**, *1062*, 142–148. [[CrossRef](#)]
20. Chow, T.-H.; Lin, Y.-Y.; Hwang, J.-J.; Wang, H.-E.; Tseng, Y.-L.; Pang, V.; Liu, R.-S.; Lin, W.-J.; Yang, C.-S.; Ting, G. Therapeutic efficacy evaluation of ¹¹¹In-labeled pegylated liposomal vinorelbine in murine colon carcinoma with multimodalities of molecular imaging. *J. Nucl. Med.* **2009**, *50*, 2073–2081. [[CrossRef](#)] [[PubMed](#)]
21. Immordino, M.L.; Dosio, F.; Cattel, L. Stealth liposomes: Review of the basic science, rationale, and clinical applications, existing and potential. *Int. J. Nanomed.* **2006**, *1*, 297–315.
22. Soundararajan, A.; Dodd, G.; Bao, A.; Phillips, W.; McManus, L.; Prihoda, T.; Goins, B. Chemoradiation therapy with ¹⁸⁶Re-labeled liposomal doxorubicin in combination with radiofrequency ablation for effective treatment of head and neck cancer in a nude rat tumor xenograft model. *Radiology* **2011**, *261*, 813–823. [[CrossRef](#)] [[PubMed](#)]
23. Tseng, W.-C.; Huang, L. Liposome-based gene therapy. *Pharm. Sci. Technol. Today* **1998**, *1*, 206–213. [[CrossRef](#)]
24. Allen, T.M.; Cullis, P.R. Liposomal drug delivery systems: From concept to clinical applications. *Adv. Drug Deliv. Rev.* **2013**, *65*, 36–48. [[CrossRef](#)] [[PubMed](#)]
25. Fahr, A.; van Hoogevest, P.; May, S.; Bergstrand, N.; ML, S.L. Transfer of lipophilic drugs between liposomal membranes and biological interfaces: Consequences for drug delivery. *Eur. J. Pharm. Sci.* **2005**, *26*, 251–265. [[CrossRef](#)] [[PubMed](#)]
26. Samad, A.; Sultana, Y.; Aqil, M. Liposomal drug delivery systems: An update review. *Curr. Drug Deliv.* **2007**, *4*, 297–305. [[CrossRef](#)] [[PubMed](#)]
27. Madeira, C.; Mendes, R.D.; Ribeiro, S.C.; Boura, J.S.; Aires-Barros, M.R.; da Silva, C.L.; Cabral, J.M. Nonviral gene delivery to mesenchymal stem cells using cationic liposomes for gene and cell therapy. *J. Biomed. Biotechnol.* **2010**, *2010*, 735349. [[CrossRef](#)] [[PubMed](#)]
28. Park, J.W. Liposome-based drug delivery in breast cancer treatment. *Breast Cancer Res.* **2002**, *4*, 95–99. [[CrossRef](#)] [[PubMed](#)]
29. Koshkina, N.V.; Gilbert, B.E.; Waldrep, J.C.; Seryshev, A.; Knight, V. Distribution of camptothecin after delivery as a liposome aerosol or following intramuscular injection in mice. *Cancer Chemother. Pharmacol.* **1999**, *44*, 187–192. [[CrossRef](#)] [[PubMed](#)]

30. Rogers, J.A.; Anderson, K.E. The potential of liposomes in oral drug delivery. *Crit. Rev. Ther. Drug Carrier Syst.* **1998**, *15*, 421–480. [CrossRef] [PubMed]
31. Torchilin, V.P. Multifunctional, stimuli-sensitive nanoparticulate systems for drug delivery. *Nat. Rev. Drug Discov.* **2014**, *13*, 813–827. [CrossRef] [PubMed]
32. Bulbake, U.; Doppalapudi, S.; Kommineni, N.; Khan, W. Liposomal formulations in clinical use: An updated review. *Pharmaceutics* **2017**, *9*, 12. [CrossRef] [PubMed]
33. Barenholz, Y. Doxil[®]—The first fda-approved nano-drug: Lessons learned. *J. Control. Release* **2012**, *160*, 117–134. [CrossRef] [PubMed]
34. Lasic, D.D.; Frederik, P.M.; Stuart, M.C.; Barenholz, Y.; McIntosh, T.J. Gelation of liposome interior. A novel method for drug encapsulation. *FEBS Lett.* **1992**, *312*, 255–258. [CrossRef]
35. Haran, G.; Cohen, R.; Bar, L.K.; Barenholz, Y. Transmembrane ammonium sulfate gradients in liposomes produce efficient and stable entrapment of amphipathic weak bases. *Biochim. Biophys. Acta* **1993**, *1151*, 201–215. [CrossRef]
36. Ohanian, M.; Kantarjian, H.M.; Ravandi, F.; Borthakur, G.; Garcia-Manero, G.; Andreeff, M.; Jabbour, E.; Konopleva, M.; Lim, M.; Pierce, S.; et al. Safety, pharmacokinetics, and efficacy of BP-100-1.01 (liposomal Grb-2 antisense oligonucleotide) in patients with refractory or relapsed acute myeloid leukemia (AML), philadelphia chromosome positive chronic myelogenous leukemia (CML), acute lymphoblastic leukemia (ALL), and myelodysplastic syndrome (MDS). *Blood* **2015**, *126*, 3801.
37. Harper, B.W.; Krause-Heuer, A.M.; Grant, M.P.; Manohar, M.; Garbutcheon-Singh, K.B.; Aldrich-Wright, J.R. Advances in platinum chemotherapeutics. *Chemistry* **2010**, *16*, 7064–7077. [CrossRef] [PubMed]
38. Clancy, J.P.; Dupont, L.; Konstan, M.W.; Billings, J.; Fustik, S.; Goss, C.H.; Lymp, J.; Minic, P.; Quittner, A.L.; Rubenstein, R.C.; et al. Phase II studies of nebulised arikace in cf patients with pseudomonas aeruginosa infection. *Thorax* **2013**, *68*, 818–825. [CrossRef] [PubMed]
39. Semple, S.C.; Leone, R.; Wang, J.; Leng, E.C.; Klimuk, S.K.; Eisenhardt, M.L.; Yuan, Z.N.; Edwards, K.; Maurer, N.; Hope, M.J.; et al. Optimization and characterization of a sphingomyelin/cholesterol liposome formulation of vinorelbine with promising antitumor activity. *J. Pharm. Sci.* **2005**, *94*, 1024–1038. [CrossRef] [PubMed]
40. Slingerland, M.; Guchelaar, H.J.; Rosing, H.; Scheulen, M.E.; van Warmerdam, L.J.; Beijnen, J.H.; Gelderblom, H. Bioequivalence of liposome-entrapped paclitaxel easy-to-use (LEP-ETU) formulation and paclitaxel in polyethoxylated castor oil: A randomized, two-period crossover study in patients with advanced cancer. *Clin. Ther.* **2013**, *35*, 1946–1954. [CrossRef] [PubMed]
41. Boulikas, T. Clinical overview on lipoplatin: A successful liposomal formulation of cisplatin. *Expert Opin. Investig. Drugs* **2009**, *18*, 1197–1218. [CrossRef] [PubMed]
42. Seiden, M.V.; Muggia, F.; Astrow, A.; Matulonis, U.; Campos, S.; Roche, M.; Sivret, J.; Rusk, J.; Barrett, E. A Phase II study of liposomal lurtotecan (OSI-211) in patients with topotecan resistant ovarian cancer. *Gynecol. Oncol.* **2004**, *93*, 229–232. [CrossRef] [PubMed]
43. Prostaglandin E1 (liprostin) Treatment with Lower Limb Angioplasty for Peripheral Arterial Occlusive disease. Available online: <https://clinicaltrials.gov/ct2/show/NCT00053716> (accessed on 2 October 2017).
44. De Jonge, M.J.; Slingerland, M.; Loos, W.J.; Wiemer, E.A.; Burger, H.; Mathijssen, R.H.; Kroep, J.R.; den Hollander, M.A.; van der Biessen, D.; Lam, M.H.; et al. Early cessation of the clinical development of lipplacis, a liposomal cisplatin formulation. *Eur. J. Cancer* **2010**, *46*, 3016–3021. [CrossRef] [PubMed]
45. Wetzler, M.; Thomas, D.A.; Wang, E.S.; Shepard, R.; Ford, L.A.; Heffner, T.L.; Parekh, S.; Andreeff, M.; O'Brien, S.; Kantarjian, H.M. Phase I/II trial of nanomolecular liposomal annamycin in adult patients with relapsed/refractory acute lymphoblastic leukemia. *Clin. Lymphoma Myeloma Leuk.* **2013**, *13*, 430–434. [CrossRef] [PubMed]
46. Kroemer, G.; Zitvogel, L.; Galluzzi, L. Victories and deceptions in tumor immunology: Stimuvax[®]. *Oncoimmunology* **2013**, *2*, e23687. [CrossRef] [PubMed]
47. Wu, H.; Ramanathan, R.K.; Zamboni, B.A.; Strychor, S.; Ramalingam, S.; Edwards, R.P.; Friedland, D.M.; Stoller, R.G.; Belani, C.P.; Maruca, L.J.; et al. Population pharmacokinetics of pegylated liposomal CKD-602 (S-CKD602) in patients with advanced malignancies. *J. Clin. Pharmacol.* **2012**, *52*, 180–194. [CrossRef] [PubMed]

48. Wolf, P.; Müllegger, R.R.; Peter Soyer, H.; Hofer, A.; Smolle, J.; Horn, M.; Cerroni, L.; Hofmann-Wellenhof, R.; Kerl, H.; Maier, H.; et al. Topical treatment with liposomes containing T4 endonuclease V protects human skin in vivo from ultraviolet-induced upregulation of interleukin-10 and tumor necrosis factor- α . *J. Investig. Dermatol.* **2000**, *114*, 149–156. [CrossRef] [PubMed]
49. Rose, P.G.; Smrekar, M.; Haba, P.; Fusco, N.; Rodriguez, M. A phase I study of oral topotecan and pegylated liposomal doxorubicin (Doxil) in platinum-resistant ovarian and peritoneal cancer. *Am. J. Clin. Oncol.* **2008**, *31*, 476–480. [CrossRef] [PubMed]
50. Harrington, K.J.; Lewanski, C.R.; Northcote, A.D.; Whittaker, J.; Wellbank, H.; Vile, R.G.; Peters, A.M.; Stewart, J.S. Phase I-II study of pegylated liposomal cisplatin (SPI-077) in patients with inoperable head and neck cancer. *Ann. Oncol.* **2001**, *12*, 493–496. [CrossRef] [PubMed]
51. Phase 3 Study of Thermodox with Radiofrequency Ablation (RFA) in Treatment of Hepatocellular Carcinoma (HCC). Available online: <https://clinicaltrials.gov/ct2/show/NCT00617981> (accessed on 2 October 2017).
52. Wang, R.; Billone, P.S.; Mullett, W.M. Nanomedicine in action: An overview of cancer nanomedicine on the market and in clinical trials. *J. Nanomater.* **2013**, *2013*, 12. [CrossRef]
53. Strieth, S.; Dunau, C.; Kolbow, K.; Knuechel, R.; Michaelis, U.; Ledderose, H.; Eichhorn, M.E.; Strelczyk, D.; Tschiesner, U.; Wollenberg, B.; et al. Phase I clinical study of vascular targeting fluorescent cationic liposomes in head and neck cancer. *Eur. Arch. Otorhinolaryngol.* **2013**, *270*, 1481–1487. [CrossRef] [PubMed]
54. Mukherjee, S.; Date, A.; Patravale, V.; Korting, H.C.; Roeder, A.; Weindl, G. Retinoids in the treatment of skin aging: An overview of clinical efficacy and safety. *Clin. Interv. Aging* **2006**, *1*, 327–348. [CrossRef] [PubMed]
55. Kanasty, R.; Dorkin, J.R.; Vegas, A.; Anderson, D. Delivery materials for siRNA therapeutics. *Nat. Mater.* **2013**, *12*, 967–977. [CrossRef] [PubMed]
56. Chan, S.; Davidson, N.; Juozaityte, E.; Erdkamp, F.; Pluzanska, A.; Azarnia, N.; Lee, L.W. Phase III trial of liposomal doxorubicin and cyclophosphamide compared with epirubicin and cyclophosphamide as first-line therapy for metastatic breast cancer. *Ann. Oncol.* **2004**, *15*, 1527–1534. [CrossRef] [PubMed]
57. Ma, M.K.; Zamboni, W.C.; Radomski, K.M.; Furman, W.L.; Santana, V.M.; Houghton, P.J.; Hanna, S.K.; Smith, A.K.; Stewart, C.F. Pharmacokinetics of irinotecan and its metabolites SN-38 and APC in children with recurrent solid tumors after protracted low-dose irinotecan. *Clin. Cancer Res.* **2000**, *6*, 813–819. [PubMed]
58. Eichhorn, M.E.; Ischenko, I.; Luedemann, S.; Strieth, S.; Papyan, A.; Werner, A.; Bohnenkamp, H.; Guenzi, E.; Preissler, G.; Michaelis, U.; et al. Vascular targeting by endotag-1 enhances therapeutic efficacy of conventional chemotherapy in lung and pancreatic cancer. *Int. J. Cancer* **2010**, *126*, 1235–1245. [CrossRef] [PubMed]
59. Zhigaltsev, I.V.; Maurer, N.; Akhong, Q.F.; Leone, R.; Leng, E.; Wang, J.; Semple, S.C.; Cullis, P.R. Liposome-encapsulated vincristine, vinblastine and vinorelbine: A comparative study of drug loading and retention. *J. Control. Release* **2005**, *104*, 103–111. [CrossRef] [PubMed]
60. Absalon, M.; O'Brien, M.M.; Phillips, C.L.; Burns, K.C.; Mangino, J.; Mizukawa, B.; Breese, E.H.; Shah, R.; Perentesis, J.P. A Phase I/pilot study of CPX-351 for children, adolescents and young adults with recurrent or refractory hematologic malignancies. *J. Clin. Oncol.* **2016**, *34*, 10541.
61. Ashizawa, A.T.; Cortes, J. Liposomal delivery of nucleic acid-based anticancer therapeutics: BP-100-1.01. *Expert Opin. Drug Deliv.* **2015**, *12*, 1107–1120. [CrossRef] [PubMed]
62. Tari, A.M.; Gutierrez-Puente, Y.; Monaco, G.; Stephens, C.; Sun, T.; Rosenblum, M.; Belmont, J.; Arlinghaus, R.; Lopez-Berestein, G. Liposome-incorporated Grb2 antisense oligodeoxynucleotide increases the survival of mice bearing bcr-abl-positive leukemia xenografts. *Int. J. Oncol.* **2007**, *31*, 1243–1250. [PubMed]
63. Wicki, A.; Witzigmann, D.; Balasubramanian, V.; Huwyler, J. Nanomedicine in cancer therapy: Challenges, opportunities, and clinical applications. *J. Control. Release* **2015**, *200*, 138–157. [CrossRef] [PubMed]
64. Ahmad, A.; Wang, Y.F.; Ahmad, I. Separation of liposome-entrapped mitoxantrone from nonliposomal mitoxantrone in plasma: Pharmacokinetics in mice. *Methods Enzymol.* **2005**, *391*, 176–185. [PubMed]
65. Farrell, N.P. Platinum formulations as anticancer drugs clinical and pre-clinical studies. *Curr. Top. Med. Chem.* **2011**, *11*, 2623–2631. [CrossRef]
66. Jakupec, M.A.; Galanski, M.; Keppler, B.K. Tumour-inhibiting platinum complexes—State of the art and future perspectives. *Rev. Physiol. Biochem. Pharmacol.* **2003**, *146*, 1–54. [PubMed]
67. Chang, H.I.; Yeh, M.K. Clinical development of liposome-based drugs: Formulation, characterization, and therapeutic efficacy. *Int. J. Nanomed.* **2012**, *7*, 49–60.

68. Tomkinson, B.; Bendele, R.; Giles, F.J.; Brown, E.; Gray, A.; Hart, K.; LeRay, J.D.; Meyer, D.; Pelanne, M.; Emerson, D.L. OSI-211, a novel liposomal topoisomerase I inhibitor, is active in scid mouse models of human aml and all. *Leuk. Res.* **2003**, *27*, 1039–1050. [CrossRef]
69. Seetharamu, N.; Kim, E.; Hochster, H.; Martin, F.; Muggia, F. Phase II study of liposomal cisplatin (SPI-77) in platinum-sensitive recurrences of ovarian cancer. *Anticancer Res.* **2010**, *30*, 541–545. [PubMed]
70. Meerum Terwogt, J.M.; Groenewegen, G.; Pluim, D.; Maliepaard, M.; Tibben, M.M.; Huisman, A.; ten Bokkel Huinink, W.W.; Schot, M.; Welbank, H.; Voest, E.E.; et al. Phase I and pharmacokinetic study of spi-77, a liposomal encapsulated dosage form of cisplatin. *Cancer Chemother. Pharmacol.* **2002**, *49*, 201–210. [CrossRef] [PubMed]
71. Kim, E.S.; Lu, C.; Khuri, F.R.; Tonda, M.; Glisson, B.S.; Liu, D.; Jung, M.; Hong, W.K.; Herbst, R.S. A phase II study of stealth cisplatin (SPI-77) in patients with advanced non-small cell lung cancer. *Lung Cancer* **2001**, *34*, 427–432. [CrossRef]
72. Colvin, O.M. An overview of cyclophosphamide development and clinical applications. *Curr. Pharm. Des.* **1999**, *5*, 555–560. [PubMed]
73. Thomson, A.B.; Critchley, H.O.; Kelnar, C.J.; Wallace, W.H. Late reproductive sequelae following treatment of childhood cancer and options for fertility preservation. *Best Pract. Res. Clin. Endocrinol. Metab.* **2002**, *16*, 311–334. [CrossRef] [PubMed]
74. Tripathi, D.N.; Jena, G.B. Astaxanthin inhibits cytotoxic and genotoxic effects of cyclophosphamide in mice germ cells. *Toxicology* **2008**, *248*, 96–103. [CrossRef] [PubMed]
75. Papagiannaros, A.; Hatziantoniou, S.; Lelong-Rebel, I.H.; Papaioannou, G.T.; Dimas, K.; Demetzos, C. Antitumor activity of doxorubicin encapsulated in hexadecylphosphocholine (HePC) liposomes against human xenografts on scid mice. *In Vivo* **2006**, *20*, 129–135. [PubMed]
76. Arif, K.; Ejaj, A.; Maroof, A.; Azmat, A.K.; Arun, C.; Fatima, N.; Gattoo, M.A.; Owais, M. Protective effect of liposomal formulation of tuftsin (a naturally occurring tetrapeptide) against cyclophosphamide-induced genotoxicity and oxidative stress in mice. *Indian J. Biochem. Biophys.* **2009**, *46*, 45–52. [PubMed]
77. Abdella, E.M. Short-term comparative study of the cyclophosphamide genotoxicity administered free and liposome-encapsulated in mice. *Iran. J. Cancer Prev.* **2012**, *5*, 51–60. [PubMed]
78. Wurz, G.T.; Kao, C.J.; Wolf, M.; DeGregorio, M.W. Tecemotide: An antigen-specific cancer immunotherapy. *Hum. Vaccines Immunother.* **2014**, *10*, 3383–3393. [CrossRef] [PubMed]
79. Bradbury, P.A.; Shepherd, F.A. Immunotherapy for lung cancer. *J. Thorac. Oncol.* **2008**, *3*, S164–S170. [CrossRef] [PubMed]
80. Stathopoulos, G.P.; Boulikas, T.; Vougiouka, M.; Deliconstantinos, G.; Rigatos, S.; Darli, E.; Viliotou, V.; Stathopoulos, J.G. Pharmacokinetics and adverse reactions of a new liposomal cisplatin (Lipoplatin): Phase I study. *Oncol. Rep.* **2005**, *13*, 589–595. [CrossRef] [PubMed]
81. Boulikas, T.; Stathopoulos, G.P.; Volakakis, N.; Vougiouka, M. Systemic lipoplatin infusion results in preferential tumor uptake in human studies. *Anticancer Res.* **2005**, *25*, 3031–3039. [PubMed]
82. Van der Geest, T.; Laverman, P.; Metselaar, J.M.; Storm, G.; Boerman, O.C. Radionuclide imaging of liposomal drug delivery. *Expert Opin. Drug Deliv.* **2016**, *13*, 1231–1242. [CrossRef] [PubMed]
83. Xing, Y.; Zhao, J.; Conti, P.S.; Chen, K. Radiolabeled nanoparticles for multimodality tumor imaging. *Theranostics* **2014**, *4*, 290–306. [CrossRef] [PubMed]
84. Seo, J.W.; Mahakian, L.M.; Tam, S.; Qin, S.; Ingham, E.S.; Meares, C.F.; Ferrara, K.W. The pharmacokinetics of Zr-89 labeled liposomes over extended periods in a murine tumor model. *Nucl. Med. Biol.* **2015**, *42*, 155–163. [CrossRef] [PubMed]
85. Mitra, A.; Nan, A.; Line, B.R.; Ghandehari, H. Nanocarriers for nuclear imaging and radiotherapy of cancer. *Curr. Pharm. Des.* **2006**, *12*, 4729–4749. [CrossRef] [PubMed]
86. Lee, H.; Zheng, J.; Gaddy, D.; Orcutt, K.D.; Leonard, S.; Geretti, E.; Hesterman, J.; Harwell, C.; Hoppin, J.; Jaffray, D.A.; et al. A gradient-loadable (64)Cu-chelator for quantifying tumor deposition kinetics of nanoliposomal therapeutics by positron emission tomography. *Nanomedicine* **2015**, *11*, 155–165. [CrossRef] [PubMed]
87. Oku, N.; Yamashita, M.; Katayama, Y.; Urakami, T.; Hatanaka, K.; Shimizu, K.; Asai, T.; Tsukada, H.; Akai, S.; Kanazawa, H. Pet imaging of brain cancer with positron emitter-labeled liposomes. *Int. J. Pharm.* **2011**, *403*, 170–177. [CrossRef] [PubMed]

88. Petersen, A.L.; Binderup, T.; Rasmussen, P.; Henriksen, J.R.; Elema, D.R.; Kjaer, A.; Andresen, T.L. ^{64}Cu loaded liposomes as positron emission tomography imaging agents. *Biomaterials* **2011**, *32*, 2334–2341. [[CrossRef](#)] [[PubMed](#)]
89. Zalutsky, M.R.; Noska, M.A.; Seltzer, S.E. Characterization of liposomes containing iodine-125-labeled radiographic contrast agents. *Investig. Radiol.* **1987**, *22*, 141–147. [[CrossRef](#)]
90. Li, N.; Yu, Z.; Pham, T.T.; Blower, P.J.; Yan, R. A generic ^{89}Zr labeling method to quantify the in vivo pharmacokinetics of liposomal nanoparticles with positron emission tomography. *Int. J. Nanomed.* **2017**, *12*, 3281–3294. [[CrossRef](#)] [[PubMed](#)]
91. Silindir, M.; Ozer, A.Y.; Erdogan, S. The use and importance of liposomes in positron emission tomography. *Drug Deliv.* **2012**, *19*, 68–80. [[CrossRef](#)] [[PubMed](#)]
92. Wong, A.W.; Ormsby, E.; Zhang, H.; Seo, J.W.; Mahakian, L.M.; Caskey, C.F.; Ferrara, K.W. A comparison of image contrast with (^{64}Cu)-labeled long circulating liposomes and (^{18}F)-FDG in a murine model of mammary carcinoma. *Am. J. Nucl. Med. Mol. Imaging* **2013**, *3*, 32–43. [[PubMed](#)]
93. Seo, J.W.; Qin, S.; Mahakian, L.M.; Watson, K.D.; Kheirloomoom, A.; Ferrara, K.W. Positron emission tomography imaging of the stability of Cu-^{64} labeled dipalmitoyl and distearoyl lipids in liposomes. *J. Control. Release* **2011**, *151*, 28–34. [[CrossRef](#)] [[PubMed](#)]
94. Perez-Medina, C.; Abdel-Atti, D.; Zhang, Y.; Longo, V.A.; Irwin, C.P.; Binderup, T.; Ruiz-Cabello, J.; Fayad, Z.A.; Lewis, J.S.; Mulder, W.J.; et al. A modular labeling strategy for in vivo pet and near-infrared fluorescence imaging of nanoparticle tumor targeting. *J. Nucl. Med.* **2014**, *55*, 1706–1711. [[CrossRef](#)] [[PubMed](#)]
95. Marik, J.; Tartis, M.S.; Zhang, H.; Fung, J.Y.; Kheirloomoom, A.; Sutcliffe, J.L.; Ferrara, K.W. Long-circulating liposomes radiolabeled with [^{18}F]fluorodipalmitin ([^{18}F]FDP). *Nucl. Med. Biol.* **2007**, *34*, 165–171. [[CrossRef](#)] [[PubMed](#)]
96. Hansen, A.E.; Petersen, A.L.; Henriksen, J.R.; Boerresen, B.; Rasmussen, P.; Elema, D.R.; af Rosenschold, P.M.; Kristensen, A.T.; Kjaer, A.; Andresen, T.L. Positron emission tomography based elucidation of the enhanced permeability and retention effect in dogs with cancer using copper-64 liposomes. *ACS Nano* **2015**, *9*, 6985–6995. [[CrossRef](#)] [[PubMed](#)]
97. Luo, D.; Goel, S.; Liu, H.J.; Carter, K.A.; Jiang, D.; Geng, J.; Kuttyreff, C.J.; Engle, J.W.; Huang, W.C.; Shao, S.; et al. Intrabilayer (^{64}Cu) labeling of photoactivatable, doxorubicin-loaded stealth liposomes. *ACS Nano* **2017**, *11*, 12482–12491. [[CrossRef](#)] [[PubMed](#)]
98. Jensen, A.I.; Severin, G.W.; Hansen, A.E.; Fliedner, F.P.; Eliassen, R.; Parhamifar, L.; Kjaer, A.; Andresen, T.L.; Henriksen, J.R. Remote-loading of liposomes with manganese-52 and in vivo evaluation of the stabilities of ^{52}Mn -DOTA and ^{64}Cu -DOTA using radiolabelled liposomes and pet imaging. *J. Control. Release* **2017**, *269*, 100–109. [[CrossRef](#)] [[PubMed](#)]
99. Espinola, L.G.; Beaucaire, J.; Gottschalk, A.; Caride, V.J. Radiolabeled liposomes as metabolic and scanning tracers in mice. II. In-111 oxine compared with Tc-99m DTPA, entrapped in multilamellar lipid vesicles. *J. Nucl. Med.* **1979**, *20*, 434–440. [[PubMed](#)]
100. Ogihara, I.; Kojima, S.; Jay, M. Differential uptake of gallium-67-labeled liposomes between tumors and inflammatory lesions in rats. *J. Nucl. Med.* **1986**, *27*, 1300–1307. [[PubMed](#)]
101. Ogihara-Umeda, I.; Kojima, S. Increased delivery of gallium-67 to tumors using serum-stable liposomes. *J. Nucl. Med.* **1988**, *29*, 516–523. [[PubMed](#)]
102. Ogihara-Umeda, I.; Kojima, S. Cholesterol enhances the delivery of liposome-encapsulated gallium-67 to tumors. *Eur. J. Nucl. Med.* **1989**, *15*, 612–617. [[CrossRef](#)] [[PubMed](#)]
103. Ogihara-Umeda, I.; Sasaki, T.; Kojima, S.; Nishigori, H. Optimal radiolabeled liposomes for tumor imaging. *J. Nucl. Med.* **1996**, *37*, 326–332. [[PubMed](#)]
104. Proffitt, R.T.; Williams, L.E.; Presant, C.A.; Tin, G.W.; Uliana, J.A.; Gamble, R.C.; Baldeschwieler, J.D. Tumor-imaging potential of liposomes loaded with In-111-NTA: Biodistribution in mice. *J. Nucl. Med.* **1983**, *24*, 45–51. [[PubMed](#)]
105. Turner, A.F.; Presant, C.A.; Proffitt, R.T.; Williams, L.E.; Winsor, D.W.; Werner, J.L. In-111-labeled liposomes: Dosimetry and tumor depiction. *Radiology* **1988**, *166*, 761–765. [[CrossRef](#)] [[PubMed](#)]
106. Kubo, A.; Nakamura, K.; Sammiya, T.; Katayama, M.; Hashimoto, T.; Hashimoto, S.; Kobayashi, H.; Teramoto, T. Indium-111-labelled liposomes: Dosimetry and tumour detection in patients with cancer. *Eur. J. Nucl. Med.* **1993**, *20*, 107–113. [[CrossRef](#)] [[PubMed](#)]

107. Oyen, W.J.; Boerman, O.C.; Storm, G.; van Bloois, L.; Koenders, E.B.; Claessens, R.A.; Perenboom, R.M.; Crommelin, D.J.; van der Meer, J.W.; Corstens, F.H. Detecting infection and inflammation with technetium-99m-labeled stealth liposomes. *J. Nucl. Med.* **1996**, *37*, 1392–1397. [[PubMed](#)]
108. Boerman, O.C.; Storm, G.; Oyen, W.J.; van Bloois, L.; van der Meer, J.W.; Claessens, R.A.; Crommelin, D.J.; Corstens, F.H. Sterically stabilized liposomes labeled with indium-111 to image focal infection. *J. Nucl. Med.* **1995**, *36*, 1639–1644. [[PubMed](#)]
109. Harrington, K.J.; Mohammadtaghi, S.; Uster, P.S.; Glass, D.; Peters, A.M.; Vile, R.G.; Stewart, J.S. Effective targeting of solid tumors in patients with locally advanced cancers by radiolabeled pegylated liposomes. *Clin. Cancer Res.* **2001**, *7*, 243–254. [[PubMed](#)]
110. Basu, S.; Zhuang, H.; Torigian, D.A.; Rosenbaum, J.; Chen, W.; Alavi, A. Functional imaging of inflammatory diseases using nuclear medicine techniques. *Semin. Nucl. Med.* **2009**, *39*, 124–145. [[CrossRef](#)] [[PubMed](#)]
111. Huang, F.Y.; Lee, T.W.; Kao, C.H.; Chang, C.H.; Zhang, X.; Lee, W.Y.; Chen, W.J.; Wang, S.C.; Lo, J.M. Imaging, autoradiography, and biodistribution of (188)Re-labeled pegylated nanoliposome in orthotopic glioma bearing rat model. *Cancer Biother. Radiopharm.* **2011**, *26*, 717–725. [[CrossRef](#)] [[PubMed](#)]
112. De Vries, A.; Kok, M.B.; Sanders, H.M.; Nicolay, K.; Strijkers, G.J.; Grull, H. Multimodal liposomes for spect/mr imaging as a tool for in situ relaxivity measurements. *Contrast Media Mol. Imaging* **2012**, *7*, 68–75. [[CrossRef](#)] [[PubMed](#)]
113. Ogawa, M.; Umeda, I.O.; Kosugi, M.; Kawai, A.; Hamaya, Y.; Takashima, M.; Yin, H.; Kudoh, T.; Seno, M.; Magata, Y. Development of 111in-labeled liposomes for vulnerable atherosclerotic plaque imaging. *J. Nucl. Med.* **2014**, *55*, 115–120. [[CrossRef](#)] [[PubMed](#)]
114. Ito, K.; Hamamichi, S.; Asano, M.; Hori, Y.; Matsui, J.; Iwata, M.; Funahashi, Y.; Umeda, I.O.; Fujii, H. Radiolabeled liposome imaging determines an indication for liposomal anticancer agent in ovarian cancer mouse xenograft models. *Cancer Sci.* **2016**, *107*, 60–67. [[CrossRef](#)] [[PubMed](#)]
115. Varga, Z.; Szigyarto, I.C.; Gyurko, I.; Doczi, R.; Horvath, I.; Mathe, D.; Szigeti, K. Radiolabeling and quantitative in vivo SPECT/CT imaging study of liposomes using the novel iminothiolane-^{99m}Tc-tricarboxyl complex. *Contrast Media Mol. Imaging* **2017**, *2017*, 4693417. [[CrossRef](#)] [[PubMed](#)]
116. Awasthi, V.D.; Goins, B.; Klipper, R.; Phillips, W.T. Dual radiolabeled liposomes: Biodistribution studies and localization of focal sites of infection in rats. *Nucl. Med. Biol.* **1998**, *25*, 155–160. [[CrossRef](#)]
117. Mougin-Degraef, M.; Bourdeau, C.; Jestin, E.; Sai-Maurel, C.; Bourgeois, M.; Saec, P.R.; Thedrez, P.; Gestin, J.F.; Barbet, J.; Faivre-Chauvet, A. Doubly radiolabeled liposomes for pretargeted radioimmunotherapy. *Int. J. Pharm.* **2007**, *344*, 110–117. [[CrossRef](#)] [[PubMed](#)]
118. Lamichhane, N.; Dewkar, G.K.; Sundaresan, G.; Mahon, R.N.; Zweit, J. [¹⁸F]-fluorinated carboplatin and [¹¹¹In]-liposome for image-guided drug delivery. *Int. J. Mol. Sci.* **2017**, *18*, 1079. [[CrossRef](#)] [[PubMed](#)]
119. Nakada, T. Clinical application of high and ultra high-field MRI. *Brain Dev.* **2007**, *29*, 325–335. [[CrossRef](#)] [[PubMed](#)]
120. Langereis, S.; Geelen, T.; Grull, H.; Strijkers, G.J.; Nicolay, K. Paramagnetic liposomes for molecular MRI and MRI-guided drug delivery. *NMR Biomed.* **2013**, *26*, 728–744. [[CrossRef](#)] [[PubMed](#)]
121. Ren, L.; Chen, S.; Li, H.; Zhang, Z.; Ye, C.; Liu, M.; Zhou, X. MRI-visible liposome nanovehicles for potential tumor-targeted delivery of multimodal therapies. *Nanoscale* **2015**, *7*, 12843–12850. [[CrossRef](#)] [[PubMed](#)]
122. Martinez-Gonzalez, R.; Estelrich, J.; Busquets, M.A. Liposomes loaded with hydrophobic iron oxide nanoparticles: Suitable T₂ contrast agents for MRI. *Int. J. Mol. Sci.* **2016**, *17*, 1209. [[CrossRef](#)] [[PubMed](#)]
123. Navon, G.; Panigel, R.; Valensin, G. Liposomes containing paramagnetic macromolecules as mri contrast agents. *Magn. Reson. Med.* **1986**, *3*, 876–880. [[CrossRef](#)] [[PubMed](#)]
124. Ding, N.; Lu, Y.; Lee, R.J.; Yang, C.; Huang, L.; Liu, J.; Xiang, G. Folate receptor-targeted fluorescent paramagnetic bimodal liposomes for tumor imaging. *Int. J. Nanomed.* **2011**, *6*, 2513–2520. [[CrossRef](#)] [[PubMed](#)]
125. De Smet, M.; Langereis, S.; van den Bosch, S.; Bitter, K.; Hijnen, N.M.; Heijman, E.; Grull, H. SPECT/CT imaging of temperature-sensitive liposomes for MR-image guided drug delivery with high intensity focused ultrasound. *J. Control. Release* **2013**, *169*, 82–90. [[CrossRef](#)] [[PubMed](#)]
126. Kim, H.R.; You, D.G.; Park, S.J.; Choi, K.S.; Um, W.; Kim, J.H.; Park, J.H.; Kim, Y.S. Mri monitoring of tumor-selective anticancer drug delivery with stable thermosensitive liposomes triggered by high-intensity focused ultrasound. *Mol. Pharm.* **2016**, *13*, 1528–1539. [[CrossRef](#)] [[PubMed](#)]

127. Kneepkens, E.; Fernandes, A.; Nicolay, K.; Grull, H. Iron(III)-based magnetic resonance-imageable liposomal T1 contrast agent for monitoring temperature-induced image-guided drug delivery. *Investig. Radiol.* **2016**, *51*, 735–745. [[CrossRef](#)] [[PubMed](#)]
128. Nordling-David, M.M.; Yaffe, R.; Guez, D.; Meirou, H.; Last, D.; Grad, E.; Salomon, S.; Sharabi, S.; Levi-Kalisman, Y.; Golomb, G.; et al. Liposomal temozolomide drug delivery using convection enhanced delivery. *J. Control. Release* **2017**, *261*, 138–146. [[CrossRef](#)] [[PubMed](#)]
129. Shao, S.; Do, T.N.; Razi, A.; Chitgupi, U.; Geng, J.; Alsop, R.J.; Dzikovski, B.G.; Rheinstadter, M.C.; Ortega, J.; Karttunen, M.; et al. Design of hydrated porphyrin-phospholipid bilayers with enhanced magnetic resonance contrast. *Small* **2017**, *13*. [[CrossRef](#)] [[PubMed](#)]

Sample Availability: None.



© 2018 by the authors. Licensee MDPI, Basel, Switzerland. This article is an open access article distributed under the terms and conditions of the Creative Commons Attribution (CC BY) license (<http://creativecommons.org/licenses/by/4.0/>).

Influence of liposomal irinotecan (nal-IRI) and non-liposomal irinotecan, alone and in combination, on tumor growth and angiogenesis in colorectal cancer (CRC) models

Annette K. Larsen^{1,4}, Anaïs Bouygues^{1,3}, Cristiano Trindade^{1,3}, Lila Louadj^{1,3}, Sandrine Thouroude^{1,3}, Stephan Klinz⁵, Ashish Kalra⁵, João AP Henriques⁶, Alexandre E Escargueil^{1,3}, Benoist Chibaudel⁷, Aimery de Gramont⁷, Paul Mésange^{1,3}

¹Cancer Biology and Therapeutics, Centre de Recherche Saint-Antoine (CRSA), Paris 75012, France, ²Institut National de la Santé et de la Recherche Médicale (INSERM) U938, Paris 75012, France, ³Institut Universitaire de Cancérologie (IUC), Faculté de Médecine, Sorbonne Université, Paris 75005, France, ⁴Centre National de la Recherche Scientifique (CNRS), Paris 75016, France, ⁵Biomarkers & Oncology, Ipsen Bioscience Inc., Cambridge MA 02142, USA, ⁶Departamento de Biofísica/Centro de Biotecnologia, Universidade Federal do Rio Grande do Sul, UFRGS Porto Alegre, RS, Brazil, ⁷Department of Medical Oncology, Institut Hospitalier Franco-Britannique, 92300 Levallois-Perret, France

INTRODUCTION

The long circulating liposomal irinotecan nal-IRI (MM-398/PEP02, Onivyde[®]) is approved for treatment of metastatic pancreatic cancer after disease progression with gemcitabine-based therapy. Besides their direct cytotoxic activity, camptothecins are thought to inhibit tumor angiogenesis via downregulation of hypoxia-inducible factors 1 and 2 leading to attenuation of VEGF expression. Due to different deposition kinetics, irinotecan HCl and nal-IRI are likely to show different activities *in vivo* suggesting that a combination of the two agents may optimize intratumoral exposure and improve treatment efficacy.

RESULTS

The *in vitro* activity of SN-38, the active metabolite of irinotecan, was determined by the MTT viability assay. The cell lines included **HT-29** (*RAS* wt, LOH, naturally resistance to irinotecan and to bevacizumab), **HCT-116** (*RAS* mut, MSI, naturally sensitive to irinotecan) and **HCT-116/SN-38** (derived from HCT-116 by prolonged exposure to SN-38).

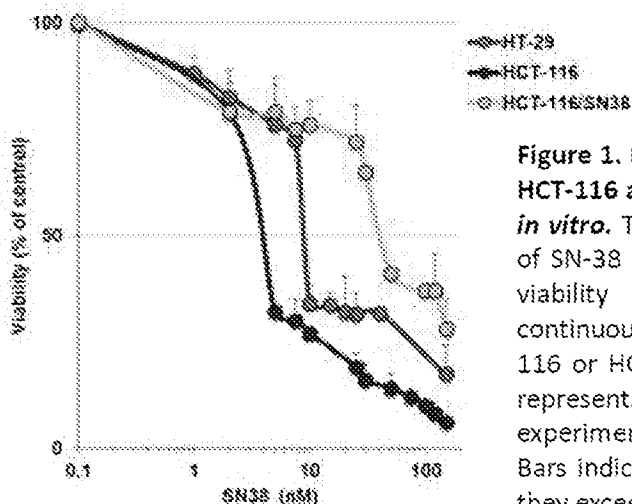


Figure 1. Influence of SN-38 on HT-29, HCT-116 and HCT-116/SN-38 CRC cells *in vitro*. The growth inhibitory activity of SN-38 was determined by the MTT viability assay after 120 hours continuous exposure of HT-29, HCT-116 or HCT-116/SN-38 cells. The data represents three independent experiments each done in duplicate. Bars indicate SD and are shown when they exceed symbol size.

Human CRC xenografts were established and the treatment started when the median tumor size was ~ 100 mm³. Irinotecan was given at 25 mg/kg *i.v.* on days 1 and 2 every week for 4 weeks while onivyde (nal-IRI) was given at 5 mg/kg *i.v.* once weekly for 4 weeks. Tumor size was determined 3 times weekly.

The results show that the addition of onivyde to irinotecan was significantly better than irinotecan alone for all three xenograft models although onivyde provided only 10% additional irinotecan. The activity of onivyde and irinotecan was comparable for the two more resistant xenograft models, HT-29 and HCT-116/SN-38, whereas irinotecan was more active than onivyde in the sensitive HCT-116 xenograft model.

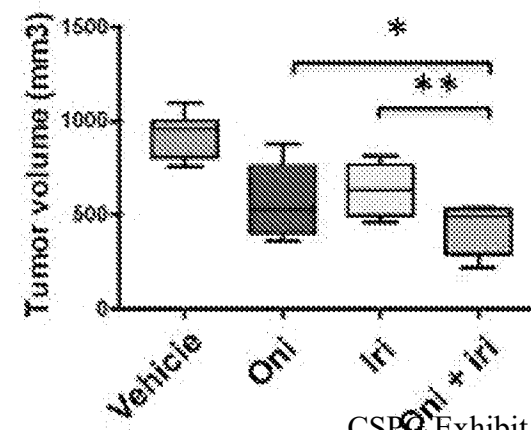
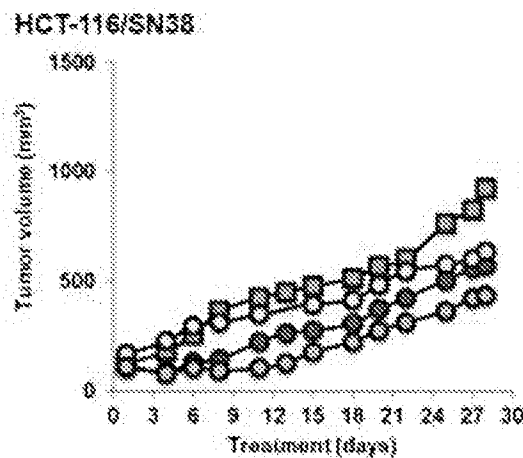
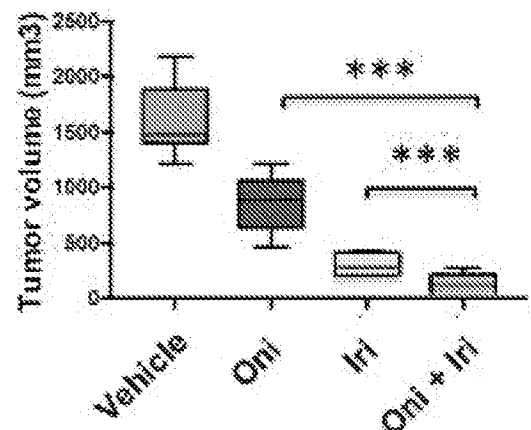
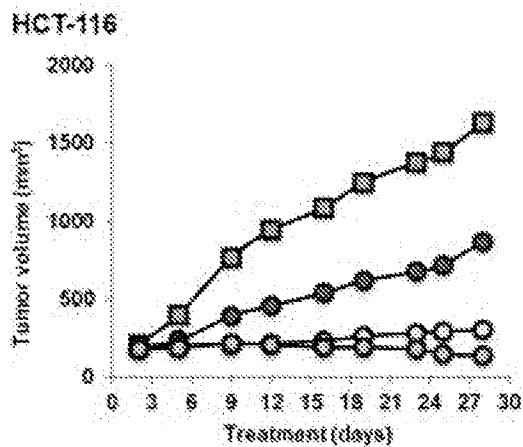
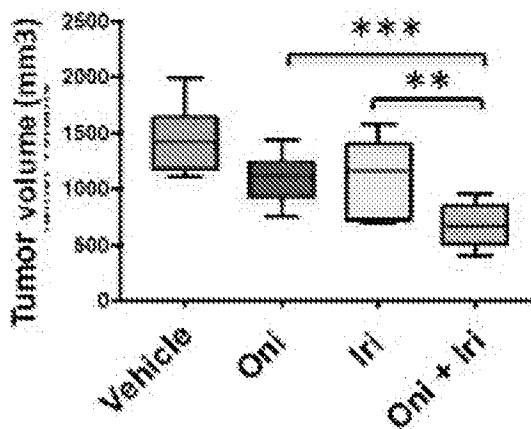
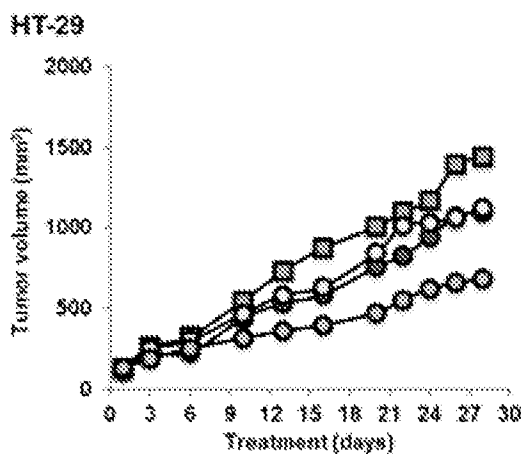
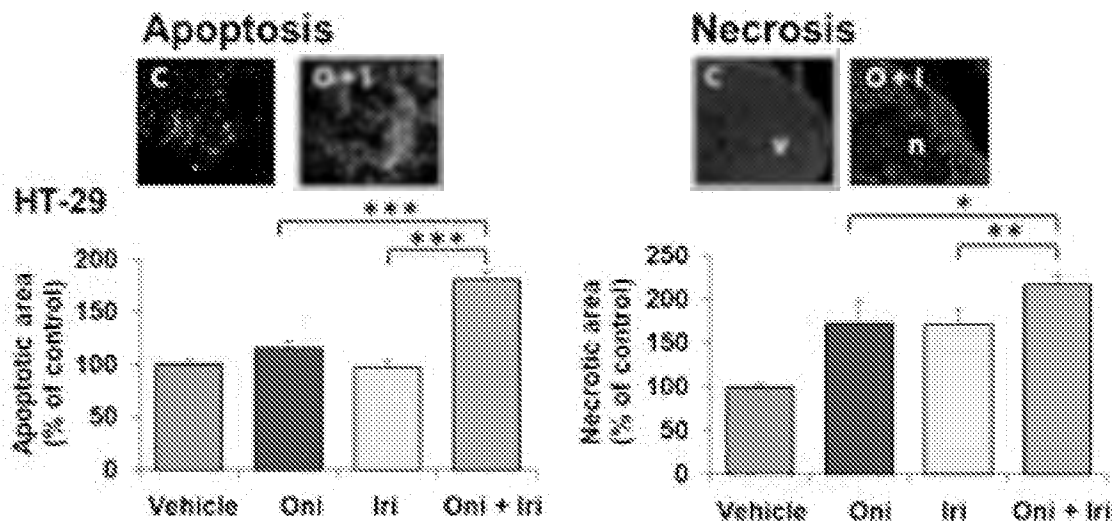


Figure 2. Tumor growth inhibitory activity of onivyde, irinotecan and their combination toward CRC xenografts. Mice with HT-29 (upper panels), HCT-116 (middle panels) or HCT-116/SN-38 (lower panels) human CRC xenografts were dosed for four weeks with vehicle (Vehicle, green), onivyde at 5 mg/kg *i.v.* once weekly (Oni, red), irinotecan at 25 mg/kg *i.v.* twice weekly (Iri, yellow) or their combination (Oni + Iri, orange). Each treatment group corresponds to at least seven animals. Left, tumor growth curves. Right, box and whisker plot of the tumor volumes of HT-29, HCT-116 and HCT-116/SN-38 xenografts after 4 weeks treatment with onivyde, irinotecan or their combination. Lines, medians; boxes, 25th to 75th percentile interquartile ranges; whiskers, the highest and lowest values for a given treatment.

The expressions of biomarkers associated with the hypoxia-stress response are strongly tumor-size dependent. Therefore, for biomarker analysis, the following protocol was used: tumor xenografts were grown to 700-800 mm³ and treated with vehicle, onivyde, irinotecan or their combination. Tumors were collected 5 days after treatment and subjected to fluorescence immunohistochemistry followed by quantitative image analysis.

The results show that treatment with onivyde, irinotecan or their combination was associated with increased apoptosis and necrosis. Tumor cell death was most pronounced for the combination of onivyde and irinotecan in agreement with the more pronounced tumor growth inhibitory activity of the combination.



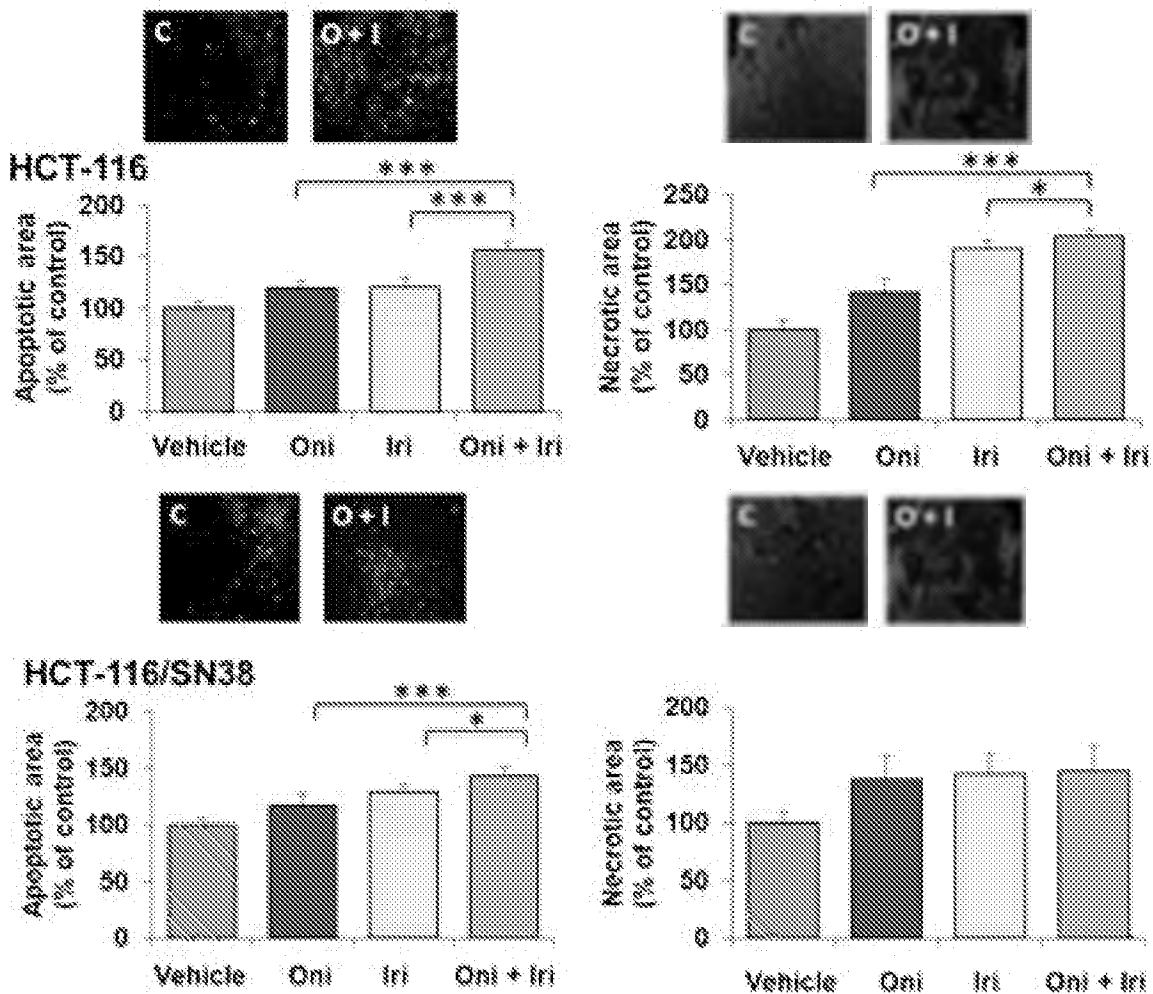


Figure 3: Cytotoxic activity of onivyde, irinotecan and their combination toward CRC xenografts. HT-29, HCT-116 and HCT-116/5-SN-38 xenografts were treated as described above and the levels of apoptosis (left) and necrosis (right) were determined. The photos illustrate typical staining patterns for the vehicle controls (C) and for the onivyde + irinotecan combination (O + I). v, viable tissue; n, necrotic tissue. Apoptosis is expressed as the area of TUNEL-positive cells, in % of the total area of viable cells, and is the average of 6 fields/tumor for at least 3 different tumors. For necrosis, the data indicates the surface of necrotic cells as % of the total surface and is the average of 6 fields/ tumor for at least 3 different tumors. The statistical analysis of experimental data was performed using a Student's paired *t*-test comparing the treatment group with the vehicle control. Bars, SD; * *p* < 0.05; ** *p* < 0.01; *** *p* < 0.001.

The influence of onivyde, irinotecan or their combination on the tumor microvascular density was determined using an antiCD31/PECAM1-directed antibody.

The results show that all treatment arms were associated with a significant decrease in tumor-associated blood vessels, even for the HT-29 model that is naturally bevacizumab resistant. The effect was most pronounced for the combination, where the microvascular density was reduced to 14-38% of the corresponding vehicle control.

CD31

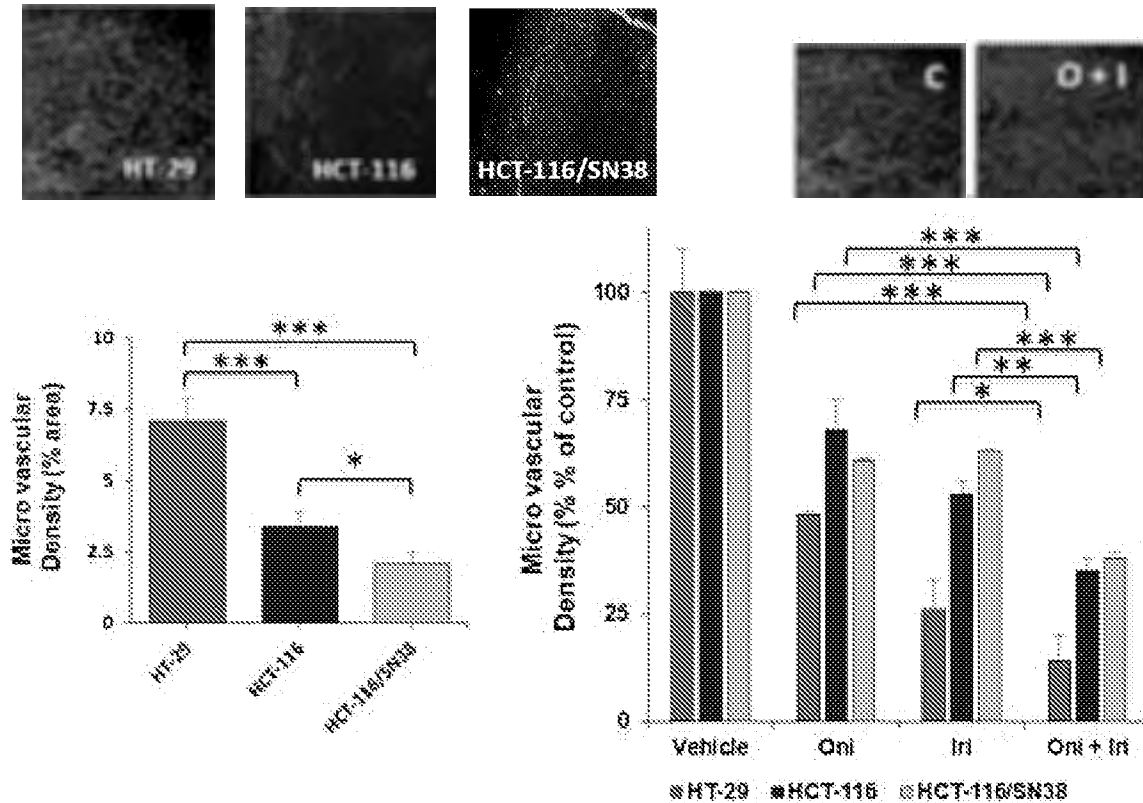
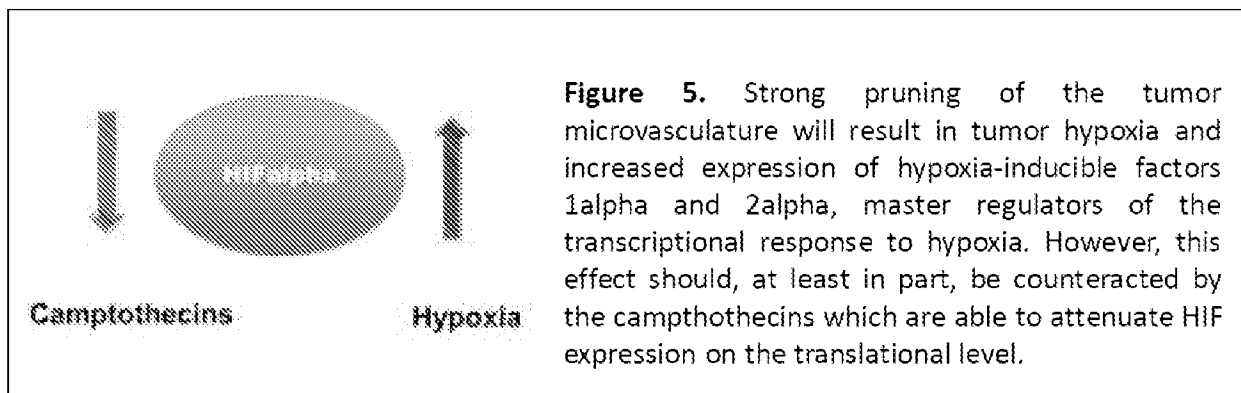


Figure 4. Onivyde, irinotecan and their combination reduce the microvascular density in CRC xenografts. HT-29, HCT-116 and HCT-116/5-SN-38 xenografts were collected and the microvascular density was determined using a CD31/PECAM1-directed antibody. *Left*, the basal levels of tumor microvessels in HT-29, HCT-116 and HCT-116/SN-38 xenografts as expressed as % CD31 positive-area. The photos illustrate typical staining patterns. CD31-positive blood vessels are outlined in red whereas the nuclei appear in blue. *Right*, the influence of onivyde, irinotecan and their combination on the microvascular density in HT-29, HCT-116 and HCT-116/5-SN-38 CRC xenografts. The photos illustrate typical staining patterns in tumors from the vehicle control (C) or after treatment with the onivyde + irinotecan combination (O + I). CD31-positive blood vessels are outlined in red whereas the nuclei appear in blue. The data show the CD31-positive area, in % of total, and represent the average of at least 6 fields/tumor for at least 3 different tumors. The statistical analysis of experimental data was performed using a Student's paired *t*-test comparing the treatment group with the vehicle control. Bars, SD; * *p* < 0.05; ** *p* < 0.01; *** *p* < 0.001.



In agreement with the model depicted in Figure 5, treatment with onivyde, irinotecan or their combination was associated with only a modest increase in the expression of HIF-1alpha (115-130%) suggesting that these compounds were able to counteract the hypoxia-mediated increase in HIF-1alpha in the CRC tumors. The influence on HIF-2alpha was less marked (130-180% compared with the corresponding vehicle control).

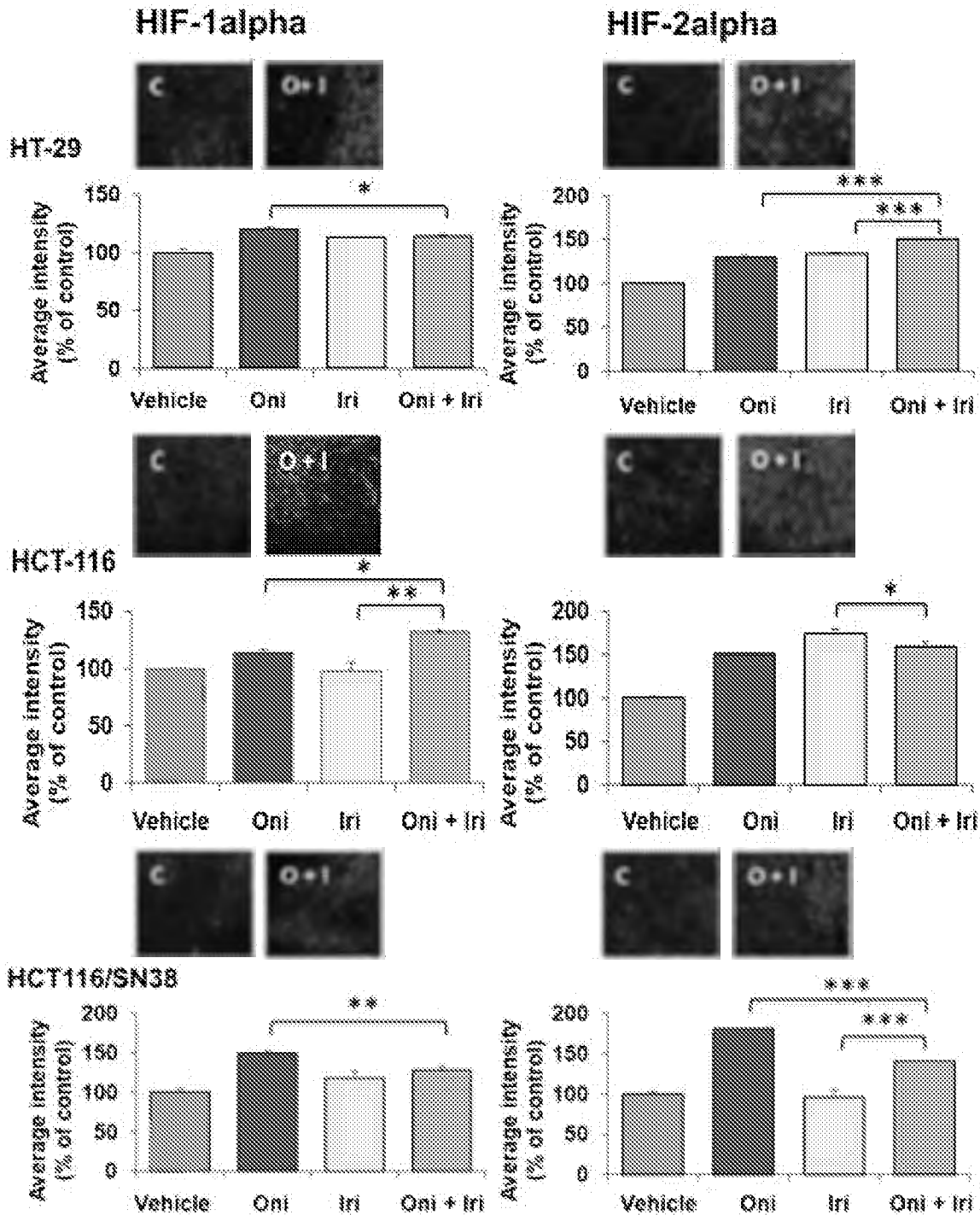


Figure 6. Influence of onivyde, irinotecan and their combination on the expression of hypoxia-induced factors. The expression of HIF-1alpha and HIF-2alpha was determined by immunohistochemistry followed by quantitative image analysis. The photos illustrate the typical staining patterns for tumors derived from animals treated with vehicle (V) or the onivyde + irinotecan combination (O+I) For the quantitative analysis of the signal intensity, the data represent the average fluorescence intensity of treated tumors compared to the treatment intensity of control tumors and are the average of 6 fields/tumor for at least 3 different tumors. The statistical analysis of experimental data was performed using a Student's paired t-test comparing the treatment group with the vehicle control. Bars, SD; * $p < 0.05$; ** $p < 0.01$; *** $p < 0.001$.

Carbonic anhydrase IX (CA9) and vascular endothelial cell factor A (VEGF-A) are major downstream targets of the HIFs. The results show that treatment with onivyde, irinotecan or their combination was associated with only modest modifications of VEGF levels (85-126%) suggesting that these compounds were able to counteract the hypoxia-mediated increase in VEGF. In comparison, CA9 levels were generally increased (133-168%) in HT-29 and HCT-116 xenografts whereas the changes were limited for the HCT-116/SN-38 model (94-128%)

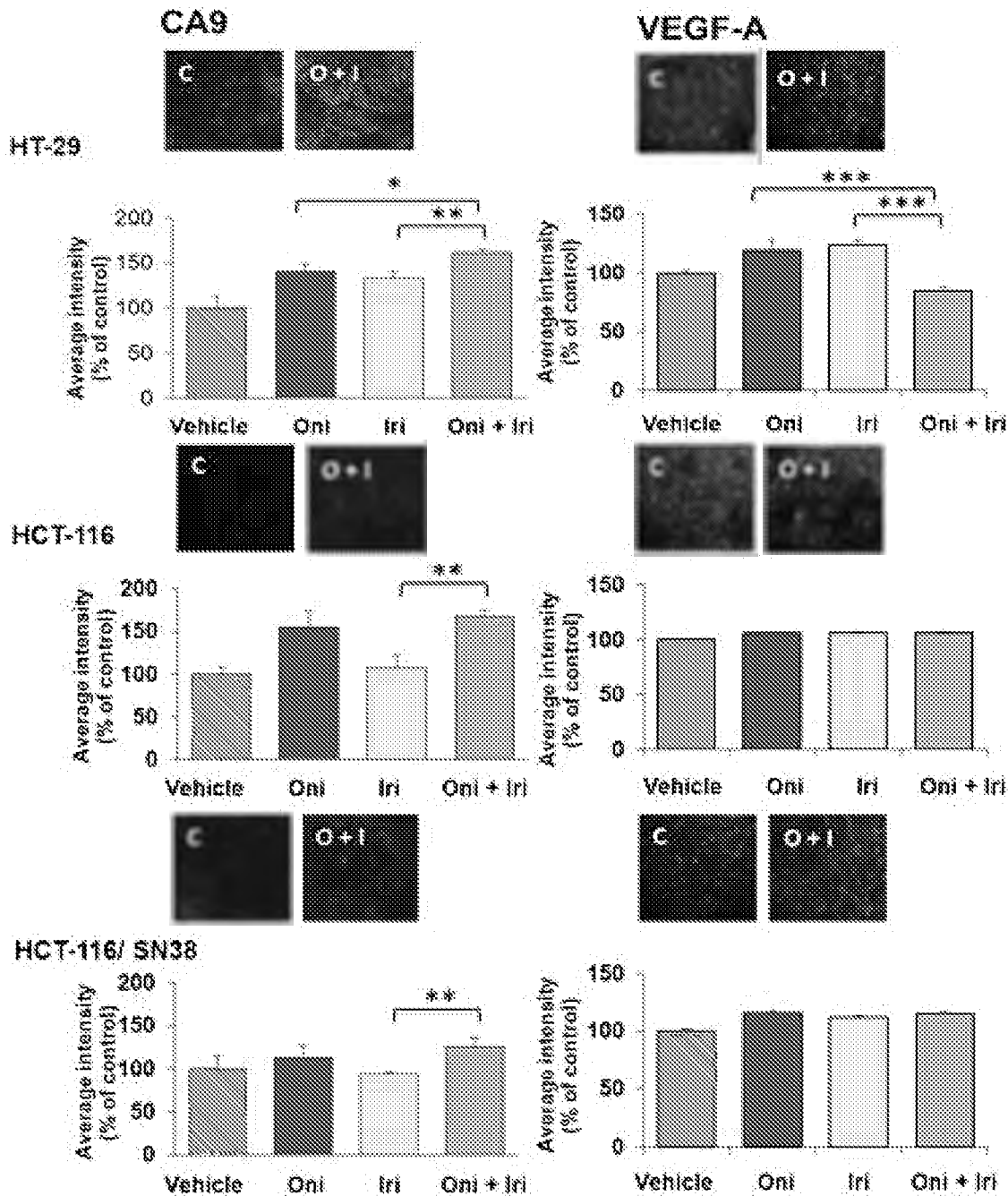


Figure 7. Influence of onivyde, irinotecan and their combination on the expression of carbonic anhydrase IX (CA9) and vascular endothelial cell factor A (VEGF-A). The expression of HIF-1alpha and HIF-2alpha was determined by immunohistochemistry followed by quantitative image analysis. The photos illustrate the typical staining patterns for tumors derived from animals treated with vehicle (V) or the onivyde + irinotecan combination (O+I) For the quantitative analysis of the signal intensity, the data represent the average fluorescence intensity of treated tumors compared to the treatment intensity of control tumors and are the average of 6 fields/tumor for at least 3 different tumors. The statistical analysis of experimental data was performed using a Student's paired *t*-test comparing the treatment group with the vehicle control. Bars, SD; * *p* < 0.05; ** *p* < 0.01; *** *p* < 0.001.

CONCLUSIONS

- The addition of liposomal irinotecan (nal-IRI/onivyde) to non-liposomal irinotecan was significant better than irinotecan alone for all three xenograft models although onivyde provided only 10% additional irinotecan.
- Compared with irinotecan, onivyde was relatively more active in tumor models with natural or acquired irinotecan resistance compared with irinotecan-sensitive tumors.
- The antitumor activity of onivyde and its combination was associated with tumor cell death as well as with decreased tumor vessel density.
- A combination of irinotecan HCl and nal-IRI/onivyde merits further clinical investigation.



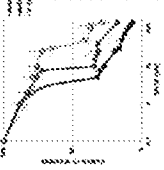
¹INSERM U1138, Centre de Recherche en Cancérologie de Montpellier, Montpellier, France; ²INSERM U1138, Centre de Recherche en Cancérologie de Montpellier, Montpellier, France; ³INSERM U1138, Centre de Recherche en Cancérologie de Montpellier, Montpellier, France; ⁴INSERM U1138, Centre de Recherche en Cancérologie de Montpellier, Montpellier, France; ⁵INSERM U1138, Centre de Recherche en Cancérologie de Montpellier, Montpellier, France

CONCLUSIONS

The long circulating liposomal irinotecan (nal-IRI) (NALIRI/IRI/PLGA) (Doxil[®]) is approved for treatment of metastatic colorectal cancer. Our data demonstrate that non-liposomal irinotecan (free IRI) and liposomal irinotecan (liposomal IRI) have similar effects on tumor growth and angiogenesis in subcutaneous and orthotopic CRC models. Furthermore, the combination of nal-IRI with anti-angiogenic agents (anti-VEGF or anti-angiogenic antibodies) significantly improved the survival of mice. These results suggest that the combination of nal-IRI with anti-angiogenic agents may be a promising therapeutic strategy for the treatment of CRC.

RESULTS

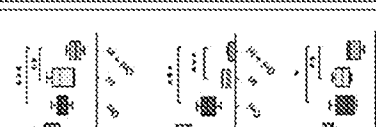
The in vivo activity of both the active ingredients of irinotecan, free IRI and liposomal IRI, was evaluated in subcutaneous and orthotopic CRC models. The results showed that both formulations had similar effects on tumor growth and angiogenesis. Furthermore, the combination of nal-IRI with anti-angiogenic agents (anti-VEGF or anti-angiogenic antibodies) significantly improved the survival of mice. These results suggest that the combination of nal-IRI with anti-angiogenic agents may be a promising therapeutic strategy for the treatment of CRC.



The effect of combination treatment with nal-IRI and anti-angiogenic agents on tumor growth and angiogenesis was evaluated. The results showed that the combination of nal-IRI with anti-angiogenic agents significantly improved the survival of mice. These results suggest that the combination of nal-IRI with anti-angiogenic agents may be a promising therapeutic strategy for the treatment of CRC.

INTRODUCTION

Irinotecan is a topoisomerase I inhibitor used in the treatment of colorectal cancer. However, its low water solubility and short half-life limit its clinical use. Liposomal formulations have been developed to improve its pharmacokinetics and reduce toxicity.



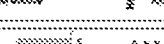
The in vitro activity of free IRI and liposomal IRI was evaluated. The results showed that liposomal IRI has a higher and more sustained cytotoxic effect compared to free IRI. These results suggest that liposomal formulations may improve the efficacy of irinotecan.

CONCLUSIONS

The addition of liposomal irinotecan (nal-IRI) to anti-angiogenic agents significantly improved the survival of mice. These results suggest that the combination of nal-IRI with anti-angiogenic agents may be a promising therapeutic strategy for the treatment of CRC.

RESULTS

The in vivo activity of both the active ingredients of irinotecan, free IRI and liposomal IRI, was evaluated in subcutaneous and orthotopic CRC models. The results showed that both formulations had similar effects on tumor growth and angiogenesis. Furthermore, the combination of nal-IRI with anti-angiogenic agents (anti-VEGF or anti-angiogenic antibodies) significantly improved the survival of mice.



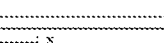
The in vivo activity of both the active ingredients of irinotecan, free IRI and liposomal IRI, was evaluated in subcutaneous and orthotopic CRC models. The results showed that both formulations had similar effects on tumor growth and angiogenesis. Furthermore, the combination of nal-IRI with anti-angiogenic agents (anti-VEGF or anti-angiogenic antibodies) significantly improved the survival of mice.

CONCLUSIONS

The addition of liposomal irinotecan (nal-IRI) to anti-angiogenic agents significantly improved the survival of mice. These results suggest that the combination of nal-IRI with anti-angiogenic agents may be a promising therapeutic strategy for the treatment of CRC.

RESULTS

The in vivo activity of both the active ingredients of irinotecan, free IRI and liposomal IRI, was evaluated in subcutaneous and orthotopic CRC models. The results showed that both formulations had similar effects on tumor growth and angiogenesis. Furthermore, the combination of nal-IRI with anti-angiogenic agents (anti-VEGF or anti-angiogenic antibodies) significantly improved the survival of mice.



The in vivo activity of both the active ingredients of irinotecan, free IRI and liposomal IRI, was evaluated in subcutaneous and orthotopic CRC models. The results showed that both formulations had similar effects on tumor growth and angiogenesis. Furthermore, the combination of nal-IRI with anti-angiogenic agents (anti-VEGF or anti-angiogenic antibodies) significantly improved the survival of mice.

CONCLUSIONS

The addition of liposomal irinotecan (nal-IRI) to anti-angiogenic agents significantly improved the survival of mice. These results suggest that the combination of nal-IRI with anti-angiogenic agents may be a promising therapeutic strategy for the treatment of CRC.

RESULTS

The in vivo activity of both the active ingredients of irinotecan, free IRI and liposomal IRI, was evaluated in subcutaneous and orthotopic CRC models. The results showed that both formulations had similar effects on tumor growth and angiogenesis. Furthermore, the combination of nal-IRI with anti-angiogenic agents (anti-VEGF or anti-angiogenic antibodies) significantly improved the survival of mice.



The in vivo activity of both the active ingredients of irinotecan, free IRI and liposomal IRI, was evaluated in subcutaneous and orthotopic CRC models. The results showed that both formulations had similar effects on tumor growth and angiogenesis. Furthermore, the combination of nal-IRI with anti-angiogenic agents (anti-VEGF or anti-angiogenic antibodies) significantly improved the survival of mice.

CANCERS OF THE COLON, RECTUM, AND ANUS

Influence of liposomal irinotecan (nal-IRI) and non-liposomal irinotecan, alone and in combination, on tumor growth and angiogenesis in colorectal cancer (CRC) models.

 Check for updates

[Annette K Larsen](#), [Cristiano Trindade](#), [Anaïs Bouygues](#), [Lila K Louadi](#), [Sandrine K Thouroude](#), [Stephan G Klinz](#), [Ashish Kalra](#), [João Henriques](#), [Benoist Chibaudel](#), [Aimery De Gramont](#), [Alexandre E Escarreau](#), [Paul Mesange](#)

Inserm/ Sorbonne Universités/ Saint Antoine Hospital, Paris, France; Cancer Biology and Therapeutics and Université Pierre et Marie Curie, Paris, France; Ipsen Bioscience, Inc., Cambridge, MA; Scholar Rock, Inc., Cambridge, MA; Centro de Biotecnologia-UFRGS, Porto Alegre, Brazil; Franco-British Institute, Levallois-Perret, France;

[Show Less](#)

[Abstract Disclosures](#)

Abstract

711

Background: The long circulating liposomal irinotecan nal-IRI (MM-398/PEP02, Onivyde) is approved for treatment of metastatic pancreatic cancer after disease progression with gemcitabine-based therapy. Besides their direct cytotoxic activity, camptothecins are thought to inhibit tumor angiogenesis via downregulating hypoxia-inducible factor 1 leading to attenuation of VEGF expression. Due to different deposition kinetics, irinotecan HCl and nal-IRI are likely to show different activities *in vivo* suggesting that a combination of the two agents may optimize intratumoral exposure and improve treatment efficacy. **Methods:** The activities of nal-IRI, irinotecan and their combination were compared in three human CRC xenograft models with different sensitivity to SN-38, the active metabolite of irinotecan, *in vitro*. Nal-IRI was dosed at 5 mg/kg q7d, while irinotecan HCl was dosed at 25 mg/kg at days 1 and 2 q7d. The activity of different regimens on tumor cell viability, hypoxia markers and the microvascular density was determined by quantitative biomarker analysis. **Results:** The relative antitumor activity of nal-IRI was most pronounced in tumor models with natural or acquired irinotecan resistance. Combinations of nal-IRI with irinotecan HCl was significantly better than irinotecan HCl alone in all tumor models although nal-IRI only provided 10% additional irinotecan. The antitumor activity of

nal-IRI and Irinotecan HCl in combination was accompanied by up to two times more tumor cell death and a marked 3-7 fold reduction of the microvessel density. Despite the strong antiangiogenic effect resulting in tumor hypoxia, the increase in HIF1 α and, to lesser degree, HIF2 α , was relatively modest and VEGF signal intensity remained at 85-115% of control values. **Conclusions:** Our results suggest that both irinotecan HCl and nal-IRI can counteract the hypoxia-mediated increase of HIF1 α *in vivo* as previously reported *in vitro*. Furthermore, the combination of the two formulations demonstrated significant efficacy benefits. A combination of irinotecan HCl and nal-IRI merits further clinical investigation.

© 2018 by American Society of Clinical Oncology

Leucovorin Calcium for Injection

Package Insert

Rx only

DESCRIPTION

Leucovorin is one of several active, chemically reduced derivatives of folic acid. It is useful as an antidote to drugs which act as folic acid antagonists.

Also known as folinic acid, Citrovorum factor, or 5-formyl-5,6,7,8-tetrahydrofolic acid, this compound has the chemical designation of L-Glutamic acid, N-[4-[[[(2-amino-5-formyl-1,4,5,6,7,8-hexahydro-4-oxo-6-geridyl)methyl]amino]benzoyl]-, calcium salt (1:1). The formula weight is 511.51 and the structural formula of leucovorin calcium is:



Leucovorin Calcium For Injection

Leucovorin calcium for injection is indicated for intravenous or intramuscular administration and is supplied as a sterile lyophilized powder. The 100 and 350 mg vials are preservative free. The inactive ingredient is sodium chloride 80 mg/vial for the 100 mg vial, and 140 mg/vial for the 350 mg vial. Sodium hydroxide and/or hydrochloric acid are used to adjust the pH during manufacture to approximately 6.9 for the 100 mg vial, and approximately 8.1 for the 350 mg vial. In each dosage form, one milligram of leucovorin calcium contains 0.002 mmol of leucovorin and 0.002 mmol of calcium.

CLINICAL PHARMACOLOGY

Leucovorin is a mixture of the diastereoisomers of the 5-formyl derivative of tetrahydrofolic acid (THF). The biologically active compound of the mixture is the (-)-isomer, known as Citrovorum factor or (-) folinic acid. Leucovorin does not require reduction by the enzyme dihydrofolate reductase in order to participate in reactions utilizing folates as a source of "one-carbon" moieties. L-Leucovorin (L-5-formyltetrahydrofolate) is rapidly metabolized (via 5,10-methylenetetrahydrofolate then 5,10-methylenetetrahydrofolate) to L-5-methyltetrahydrofolate. L-5-Methyltetrahydrofolate can in turn be metabolized via other pathways back to 5,10-methylenetetrahydrofolate, which is converted to 5-methyltetrahydrofolate by an irreversible, enzyme catalyzed reduction using the cofactors FAOHD and NADPH.

Administration of leucovorin can counteract the therapeutic and toxic effects of folic acid antagonists such as methotrexate, which act by inhibiting dihydrofolate reductase.

In contrast, leucovorin can enhance the therapeutic and toxic effects of fluoropyrimidines used in cancer therapy, such as 5-fluorouracil. Concurrent administration of leucovorin does not appear to alter the plasma pharmacokinetics of 5-fluorouracil. 5-Fluorouracil is metabolized to fluorodeoxyuridylic acid, which binds to and inhibits the enzyme thymidylate synthase (an enzyme important in DNA repair and replication).

Leucovorin is readily converted to another reduced folate, 5,10-methylenetetrahydrofolate, which acts to stabilize the binding of fluorodeoxyuridylic acid to thymidylate synthase and thereby enhances the inhibition of this enzyme.

The pharmacokinetics after intravenous, intramuscular, and oral administration of a 25 mg dose of leucovorin were studied in male volunteers. After intravenous administration, serum total reduced folates (as measured by *Lactobacillus casei* assay) reached a mean peak of 1259 ng/mL (range 897-1625). The mean time to peak was 10 minutes. This initial rise in total reduced folates was primarily due to the parent compound 5-formyl-THF (measured by *Streptococcus faecalis* assay) which rose to 1206 ng/mL at 10 minutes. A sharp drop in parent compound followed and coincided with the appearance of the active metabolite 5-methyl-THF which became the predominant circulating form of the drug.

The mean peak of 5-methyl-THF was 258 ng/mL and occurred at 1.3 hours. The terminal half-life for total reduced folates was 6.2 hours. The area under the concentration versus time curves (AUCs) for L-leucovorin, D-leucovorin and 5-methyltetrahydrofolate were 28.4 ± 3.5, 956 ± 97 and 129 ± 12 (mg/mL × h ± S.E.). When a higher dose of D-leucovorin (200 mg/mL) was used, similar results were obtained. The D-isomer persisted in plasma at concentrations greatly exceeding those of the L-isomer.

After intramuscular injection, the mean peak of serum total reduced folates was 436 ng/mL (range 281-725) and occurred at 52 minutes. Similar to IV administration, the initial sharp rise was due to the parent compound. The mean peak of 5-formyl-THF was 360 ng/mL and occurred at 28 minutes. The level of the metabolite 5-methyl-THF increased subsequently over time until at 1.5 hours it represented 30% of the circulating total folates. The mean peak of 5-methyl-THF was 226 ng/mL at 2.8 hours. The terminal half-life of total reduced folates was 6.2 hours. There was no difference of statistical significance between IM and IV administration in the AUC for total reduced folates, 5-formyl-THF, or 5-methyl-THF.

After oral administration of leucovorin reconstituted with amaranth elixir, the mean peak concentration of serum total reduced folates was 303 ng/mL (range 160-550). The mean time to peak was 2.3 hours and the terminal half-life was 5.7 hours. The major component was the metabolite 5-methyltetrahydrofolate to which leucovorin is primarily converted in the intestinal mucosa. The mean peak of 5-methyl-THF was 367 ng/mL at 2.4 hours. The peak level of the parent compound was 51 ng/mL at 1.2 hours. The AUC of total reduced folates after oral administration of the 25 mg dose was 92% of the AUC after intravenous administration.

Following oral administration, leucovorin is rapidly absorbed and expands the serum pool of reduced folates. At a dose of 25 mg, almost 100% of the L-isomer but only 20% of the D-isomer is absorbed. Oral absorption of leucovorin is saturable at doses above 25 mg. The apparent bioavailability of leucovorin was 97% for 25 mg, 75% for 50 mg, and 37% for 100 mg.

In a randomized clinical study conducted by the Mayo Clinic and the North Central Cancer Treatment Group (Mayo/NCCCTG) in patients with advanced metastatic colorectal cancer three treatment regimens were compared: leucovorin (LV) 200 mg/m² and 5-fluorouracil (5-FU) 370 mg/m² versus LV 20 mg/m² and 5-FU 425 mg/m² versus 5-FU 500 mg/m². All drugs were administered by slow intravenous infusion daily for 5 days repeated every 28-35 days. Response rates were 26% (p = 0.04 versus 5-FU alone), 42% (p = 0.001 versus 5-FU alone) and 10% for the high dose leucovorin, low dose leucovorin and 5-FU alone groups respectively. Respective median survival times were 12.2 months (p = 0.037), 12 months (p = 0.050), and 7.7 months. The low dose LV regimen gave a statistically significant improvement in weight gain of more than 5%, relief of symptoms, and improvement in performance status. The high dose LV regimen gave a statistically significant improvement in performance status and trended toward improvement in weight gain and in relief of symptoms but these were not statistically significant.

In a second Mayo/NCCCTG randomized clinical study, the 5-FU alone arm was replaced by a regimen of sequentially administered methotrexate (MTX), 5-FU, and LV. Response rates with LV 200 mg/m² and 5-FU 370 mg/m² versus LV 20 mg/m² and 5-FU 425 mg/m² versus sequential MTX and 5-FU and LV were respectively 31% (p < .01), 42% (p < .01), and 14%. Respective median survival times were 12.7 months (p < .04), 12.7 months (p < .01), and 8.4 months. No statistically significant difference in weight gain of more than 5% or in improvement in performance status was seen between the treatment arms.

INDICATIONS AND USAGE

Leucovorin calcium rescue is indicated after high-dose methotrexate therapy in osteosarcoma. Leucovorin calcium is also indicated to diminish the toxicity and counteract the effects of impaired methotrexate elimination and of inadvertent overdosages of folic acid antagonists.

Leucovorin calcium is indicated in the treatment of megaloblastic anemias due to folic acid deficiency when oral therapy is not feasible.

Leucovorin is also indicated for use in combination with 5-fluorouracil to prolong survival in the palliative treatment of patients with advanced colorectal cancer. Leucovorin should not be mixed in the same infusion as 5-fluorouracil because a precipitate may form.

CONTRAINDICATIONS

Leucovorin is improper therapy for pernicious anemia and other megaloblastic anemias secondary to the lack of vitamin B12. A hematologic remission may occur while neurologic manifestations continue to progress.

WARNINGS

In the treatment of accidental overdosages of folic acid antagonists, intravenous leucovorin should be administered as promptly as possible. As the time interval between antifolate administration [eg, methotrexate (MTX)] and leucovorin rescue increases, leucovorin's effectiveness in counteracting toxicity decreases. In the treatment of accidental overdosages of intrathecally administered folic acid antagonists, do not administer leucovorin intrathecally. LEUCOVORIN MAY BE HARMFUL OR FATAL IF GIVEN INTRATHECALLY.

Monitoring of the serum MTX concentration is essential in determining the optimal dose and duration of treatment with leucovorin.

Delayed MTX excretion may be caused by a third space fluid accumulation (ie, ascites, pleural effusion), renal insufficiency, or inadequate hydration. Under such circumstances, higher doses of leucovorin or prolonged administration may be indicated. Doses higher than those recommended for oral use must be given intravenously.

Because of the benzyl alcohol contained in certain diluents used for leucovorin calcium for injection, when doses greater than 10 mg/m² are administered, leucovorin calcium for injection should be reconstituted with sterile water for injection, USP, and used immediately. (See **CONTRAINDICATIONS AND ADMINISTRATION**.)

Because of the calcium content of the leucovorin solution, no more than 160 mg of leucovorin should be injected intravenously per minute (16 mL of a 10 mg/mL, or 8 mL of a 20 mg/mL, solution per minute).

Leucovorin enhances the toxicity of 5-fluorouracil. When these drugs are administered concurrently in the palliative therapy of advanced colorectal cancer, the dosage of 5-fluorouracil must be lower than usually administered. Although the toxicities observed in patients treated with the combination of leucovorin plus 5-fluorouracil are qualitatively similar to those observed in patients treated with 5-fluorouracil alone, gastrointestinal toxicities (particularly stomatitis and diarrhea) are observed more commonly and may be more severe and of prolonged duration in patients treated with the combination.

In the first Mayo/NCCCTG controlled trial, toxicity, primarily gastrointestinal, resulted in 7% of patients requiring hospitalization when treated with 5-fluorouracil alone or 5-fluorouracil in combination with 200 mg/m² of leucovorin and 30% when treated with 5-fluorouracil in combination with 20 mg/m² of leucovorin. In the second Mayo/NCCCTG trial, hospitalizations related to treatment toxicity also appeared to occur more often in patients treated with the low dose leucovorin/5-fluorouracil combination than in patients treated with the high dose combination—11% versus 3%. Therapy with leucovorin/5-fluorouracil must not be initiated or continued in patients who have symptoms of gastrointestinal toxicity of any severity, until those symptoms have completely resolved. Patients with diarrhea must be monitored with particular care until the diarrhea has resolved, as rapid clinical deterioration leading to death can occur. In an additional study utilizing higher weekly doses of 5-FU and leucovorin, elderly and/or debilitated patients were found to be at greater risk for severe gastrointestinal toxicity.

Seizures and/or syncope have been reported rarely in cancer patients receiving leucovorin, usually in association with fluoropyrimidine administration, and most commonly in those with CNS metastases or other predisposing factors; however, a causal relationship has not been established.

The concomitant use of leucovorin with trimethoprim-sulfamethoxazole for the acute treatment of *Pneumocystis carinii* pneumonia in patients with HIV infection was associated with increased rates of treatment failure and mortality in a placebo-controlled study.

PRECAUTIONS

General

Parenteral administration is preferable to oral dosing if there is a possibility that the patient may vomit or not absorb the leucovorin. Leucovorin has no effect on non-hematologic toxicities of MTX such as the nephrotoxicity resulting from drug and/or metabolite precipitation in the kidney.

Since leucovorin enhances the toxicity of fluorouracil, leucovorin/5-fluorouracil combination therapy for advanced colorectal cancer should be administered under the supervision of a physician experienced in the use of antimetabolite cancer chemotherapy. Particular care should be taken in the treatment of elderly or debilitated colorectal cancer patients, as these patients may be at increased risk of severe toxicity.

Laboratory Tests

Patients being treated with the leucovorin/5-fluorouracil combination should have a CBC with differential and platelets prior to each treatment. During the first two courses a CBC with differential and platelets has to be repeated weekly and thereafter once each cycle at the time of anticipated WBC nadir. Electrolytes and liver function tests should be performed prior to each treatment for the first three cycles then prior to every other cycle. Dosage modifications of fluorouracil should be instituted as follows, based on the most severe toxicities:

Diarrhea and/or Stomatitis	WBC/mm ³ Nadir	Platelets/mm ³ Nadir	5-FU Dose
Moderate	1,000-1,900	25-75,000	decrease 20%
Severe	<1,000	<25,000	decrease 30%

If no toxicity occurs, the 5-fluorouracil dose may increase 10%.

Treatment should be deferred until WBC's are 4,000/mm³ and platelets 130,000/mm³. If blood counts do not reach these levels within two weeks, treatment should be discontinued. Patients should be followed up with physical examination prior to each treatment course and appropriate radiological examination as needed. Treatment should be discontinued when there is clear evidence of tumor progression.

Drug Interactions

Folic acid in large amounts may counteract the antiepileptic effect of phenobarbital, phenytoin and primidone, and increase the frequency of seizures in susceptible pediatric patients.

Preliminary animal and human studies have shown that small quantities of systemically administered leucovorin enter the CSF primarily as 5-methyltetrahydrofolate and, in humans, remain 1-3 orders of magnitude lower than the usual methotrexate concentrations following intrathecal administration. However, high doses of leucovorin may reduce the efficacy of intrathecally administered methotrexate.

Leucovorin may enhance the toxicity of 5-fluorouracil. (See **WARNINGS**.)

Pregnancy

Teratogenic Effects

Pregnancy Category C

Animal reproduction studies have not been conducted with leucovorin. It is also not known whether leucovorin can cause fetal harm when administered to a pregnant woman or can affect reproduction capacity. Leucovorin should be given to a pregnant woman only if clearly needed.

Nursing Mothers

It is not known whether this drug is excreted in human milk. Because many drugs are excreted in human milk, caution should be exercised when leucovorin is administered to a nursing mother.

Pediatric Use

See **Drug Interactions**.

ADVERSE REACTIONS

Allergic sensitization, including anaphylactoid reactions and urticaria, has been reported following administration of both oral and parenteral leucovorin. No other adverse reactions have been attributed to the use of leucovorin per se.

The following table summarizes significant adverse events occurring in 316 patients treated with the leucovorin/5-fluorouracil combinations compared against 70 patients treated with 5-fluorouracil alone for advanced colorectal carcinoma. These data are taken from the Mayo/NCCCTG large multicenter prospective trial evaluating the efficacy and safety of the combination regimen.

PERCENTAGE OF PATIENTS TREATED WITH LEUCOVORIN/FLUOROURACIL FOR ADVANCED COLORECTAL CARCINOMA REPORTING ADVERSE EXPERIENCES OR HOSPITALIZED FOR TOXICITY

	(High LV)/5-FU (N=155)		(Low LV)/5-FU (N=161)		5-FU Alone (N=70)	
	Any (%)	Grade 3+	Any (%)	Grade 3+	Any (%)	Grade 3+
Leukopenia	69	14	83	23	93	48

High LV = Leucovorin 200 mg/m²

Low LV = Leucovorin 20 mg/m²

Any = percentage of patients reporting toxicity of any severity

Grade 3+ = percentage of patients reporting toxicity of grade 3 or higher

	(High LY)/5-FU (N=155)		(Low LY)/5-FU (N=161)		5-FU Alone (N=70)	
	Any (%)	Grade 3+ (%)	Any (%)	Grade 3+ (%)	Any (%)	Grade 3+ (%)
Thrombocytopenia	8	2	8	1	18	3
Infections	8	1	3	1	7	2
Nausea	74	10	80	9	60	6
Vomiting	46	8	44	9	40	7
Diarrhea	66	18	67	14	43	11
Stomatitis	75	27	84	29	58	16
Constipation	3	0	4	0	1	---
Lethargy/Malaise/ Fatigue	13	3	12	2	6	3
Alopecia	42	5	41	6	37	7
Dermatitis	21	2	25	1	13	---
Anorexia	14	1	22	4	14	---

Hospitalization for Toxicity: 2%, 15%, 7%

High LY = Leucovorin 200 mg/m²
Low LY = Leucovorin 20 mg/m²

Any = percentage of patients reporting toxicity of any severity
Grade 3+ = percentage of patients reporting toxicity of grade 3 or higher

OVERDOSAGE

Excessive amounts of leucovorin may nullify the chemotherapeutic effect of folic acid antagonists.

DOSAGE AND ADMINISTRATION

Advanced Colorectal Cancer

Either of the following two regimens is recommended:

1. Leucovorin is administered at 200 mg/m² by slow intravenous injection over a minimum of 3 minutes, followed by 5-fluorouracil at 370 mg/m² by intravenous injection.
2. Leucovorin is administered at 20 mg/m² by intravenous injection followed by 5-fluorouracil at 425 mg/m² by intravenous injection.

5-Fluorouracil and leucovorin should be administered separately to avoid the formation of a precipitate.

Treatment is repeated daily for five days. This five-day treatment course may be repeated at 4 week (28-day) intervals, for 2 courses and then repeated at 4-5 week (28-35 day) intervals provided that the patient has completely recovered from the toxic effects of the prior treatment course.

In subsequent treatment courses, the dosage of 5-fluorouracil should be adjusted based on patient tolerance of the prior treatment course. The daily dosage of 5-fluorouracil should be reduced by 20% for patients who experienced moderate hematologic or gastrointestinal toxicity in the prior treatment course, and by 30% for patients who experienced severe toxicity. (See PRECAUTIONS: Laboratory Tests.) For patients who experienced no toxicity in the prior treatment course, 5-fluorouracil dosage may be increased by 10%. Leucovorin dosages are not adjusted for toxicity.

Several other doses and schedules of leucovorin/5-fluorouracil therapy have also been evaluated in patients with advanced colorectal cancer; some of these alternative regimens may also have efficacy in the treatment of this disease. However, further clinical research will be required to confirm the safety and effectiveness of these alternative leucovorin/5-fluorouracil treatment regimens.

Leucovorin Rescue After High-Dose Methotrexate Therapy

The recommendations for leucovorin rescue are based on a methotrexate dose of 12-15 grams/m² administered by intravenous infusion over 4 hours. (See methotrexate package insert for full prescribing information.)

Leucovorin rescue at a dose of 15 mg (approximately 10 mg/m²) every 6 hours for 10 doses starts 24 hours after the beginning of the methotrexate infusion. In the presence of gastrointestinal toxicity, nausea or vomiting, leucovorin should be administered parenterally. Do not administer leucovorin intrathecally.

Serum creatinine and methotrexate levels should be determined at least once daily. Leucovorin administration, hydration, and urinary alkalinization (pH of 7.0 or greater) should be continued until the methotrexate level is below 5 × 10⁻⁸ M (0.05 micromolar). The leucovorin dose should be adjusted or leucovorin rescue extended based on the guidelines below.

GUIDELINES FOR LEUCOVORIN DOSAGE AND ADMINISTRATION DO NOT ADMINISTER LEUCOVORIN INTRATHECALLY

Clinical Situation	Laboratory Findings	Leucovorin Dosage And Duration
Normal Methotrexate Elimination	Serum methotrexate level approximately 19 micromolar at 24 hours after administration.	15 mg PO, IM, or IV q 6 hours for 60 hours (10 doses starting at 24 hours after start of methotrexate at infusion).
	1 micromolar at 48 hours, and less than 0.2 micromolar at 72 hours.	
Delayed Late Methotrexate Elimination	Serum methotrexate level remaining above 0.2 micromolar at 72 hours, and more than 0.05 micromolar at 96 hours after administration.	Continue 15 mg PO, IM, or IV q 6 hours, until methotrexate level is less than 0.05 micromolar.
	Serum methotrexate level of 50 micromolar or more at 24 hours, or 5 micromolar or more at 48 hours after administration. OR: a 100% or greater increase in serum creatinine level at 24 hours after methotrexate administration (eg, an increase from 0.5 mg/dL to a level of 1 mg/dL or more).	150 mg IV q 3 hours, until methotrexate level is less than 1 micromolar, then 15 mg IV q 3 hours until methotrexate level is less than 0.05 micromolar.

Patients who experience delayed early methotrexate elimination are likely to develop reversible renal failure. In addition to appropriate leucovorin therapy, these patients require continuous hydration and urinary alkalinization, and close monitoring of fluid and electrolyte status, until the serum methotrexate level has fallen to below 0.05 micromolar and the renal failure has resolved.

Some patients will have abnormalities in methotrexate elimination or renal function following methotrexate administration, which are significant but less severe than the abnormalities described in the table above. These abnormalities may or may not be associated with significant clinical toxicity. If significant clinical toxicity is observed, leucovorin rescue should be extended for an additional 24 hours (total of 14 doses over 84 hours) in subsequent courses of therapy. The possibility that the patient is taking other medications which interact with methotrexate (eg, medications which may interfere with methotrexate elimination or binding to serum albumin) should always be reconsidered when laboratory abnormalities or clinical toxicities are observed.

Impaired Methotrexate Elimination or Inadvertent Overdosage

Leucovorin rescue should begin as soon as possible after an inadvertent overdosage and within 24 hours of methotrexate administration when there is delayed excretion. (See **WARNINGS**.) Leucovorin 10 mg/m² should be administered IV, IM, or PO every 6 hours until the serum methotrexate level is less than 10-8 M. In the presence of gastrointestinal toxicity, nausea, or vomiting, leucovorin should be administered parenterally. Do not administer leucovorin intrathecally.

Serum creatinine and methotrexate levels should be determined at 24 hour intervals. If the 24 hour serum creatinine has increased 50% over baseline or if the 24 hour methotrexate level is greater than 5 × 10⁻⁶ M or the 48 hour level is greater than 9 × 10⁻⁷ M, the dose of leucovorin should be increased to 100 mg/m² IV every 3 hours until the methotrexate level is less than 10⁻⁸ M.

Hydration (3 L/d) and urinary alkalization with sodium bicarbonate solution should be employed concomitantly. The bicarbonate dose should be adjusted to maintain the urine pH at 7.0 or greater.

Megaloblastic Anemia Due to Folic Acid Deficiency

Up to 1 mg daily. There is no evidence that doses greater than 1 mg/day have greater efficacy than those of 1 mg; additionally, loss of folate in urine becomes roughly logarithmic as the amount administered exceeds 1 mg.

Each 100 mg vial of leucovorin calcium for injection when reconstituted with 10 mL of sterile diluent yields a leucovorin concentration of 10 mg per mL. Each 350 mg vial of leucovorin calcium for injection when reconstituted with 17 mL of sterile diluent yields a leucovorin concentration of 20 mg leucovorin per mL. Leucovorin calcium for injection contains no preservative. Reconstitute with bacteriostatic water for injection, USP, which contains benzyl alcohol, or with sterile water for injection, USP. When reconstituted with bacteriostatic water for injection, USP, the resulting solution must be used within 7 days. If the product is reconstituted with sterile water for injection, USP, it must be used immediately.

Because of the benzyl alcohol contained in bacteriostatic water for injection, USP, when doses greater than 10 mg/m² are administered, leucovorin calcium for injection should be reconstituted with sterile water for injection, USP, and used immediately. (See **WARNINGS**.) Because of the calcium content of the leucovorin solution, no more than 160 mg of leucovorin should be injected intravenously per minute (16 mL of a 10 mg/mL, or 8 mL of a 20 mg/mL solution per minute).

Parenteral drug products should be inspected visually for particulate matter and discoloration prior to administration, whenever solution and container permit. Leucovorin should not be mixed in the same infusion as 5-fluorouracil, since this may lead to the formation of a precipitate.

HOW SUPPLIED

Leucovorin Calcium for Injection is supplied in sterile, single-use vials.

NDC Number

0703-5140-01
0703-5145-01

Strength

100 mg vial packaged individually
350 mg vial packaged individually

STORE AT ROOM TEMPERATURE, 15°–30°C (59°–86°F).

PROTECT FROM LIGHT.

Manufactured by:
Teva Parenteral Medicines, Inc.
Irvine, CA 92618

Issued: September 2007

PRINCIPAL DISPLAY PANEL - 100 mg Vial Label

NDC 0703-5140-01

Rx only

Leucovorin
Calcium for Injection
equivalent to leucovorin

100 mg/vial

For IM or IV Use

STERILE

NDC 0703-5140-01 Rx only

Leucovorin
Calcium for Injection

100 mg/vial

When reconstituted with 10 mL of sterile diluent, the resulting solution will contain: leucovorin calcium equivalent to 10 mg leucovorin per mL; sodium chloride 8 mg/mL; sodium hydroxide and/or hydrochloric acid to adjust pH. pH between 6.5-8.5.

Contains no preservative. Reconstitute with 10 mL bacteriostatic water for injection, USP and use within 7 days or with sterile water for injection, USP and use immediately.

Usual Dosage: See Package insert. Do not use preservative containing solution for doses greater than 10 mg/m². (See **WARNINGS**.)

Store dry product and reconstituted solution at controlled room temperature 15°–30°C (59°–86°F).

Protect from light. Store in carton until contents are used. Do not use reconstituted product after.

For IM or IV Use
STERILE

Teva Parenteral Medicines, Inc., Irvine, CA 92618

00703514001

PRINCIPAL DISPLAY PANEL - 350 mg Vial Label

NDC 0703-5145-01

Rx only
 Leucovorin
 Calcium for Injection
 equivalent to leucovorin
 350 mg/vial
 For IM or IV Use
 STERILE

NDC 0703-5145-01

Rx only

Leucovorin Calcium for Injection

equivalent to leucovorin
 350 mg/vial

When reconstituted with 17 mL of sterile diluent, the resulting solution will contain: leucovorin calcium equivalent to 20 mg leucovorin per mL; sodium chloride 8.2 mg/mL; sodium hydroxide and/or hydrochloric acid to adjust pH, pH between 6.5-8.5.

Contains no preservative. Reconstitute with 17 mL bacteriostatic water for injection, USP and use within 7 days or with sterile water for injection, USP and use immediately.

Usual Dosage: See Package insert. Do not use preservative containing solution for doses greater than 10 mg/m². (See **WARNINGS**.)

Store dry product and reconstituted solution at controlled room temperature 15°-30°C (59°-86°F).

Protect from light. Store in carton until contents are used.

Do not use reconstituted product after:

For IM or IV Use

STERILE

Teva Parenteral Medicines, Inc., Irvine, CA 92618

1000000
 Y10099

LEUCOVORIN CALCIUM

leucovorin calcium injection, powder, lyophilized, for solution

Product Information

Product Type HUMAN PRESCRIPTION DRUG NDC Product Code (Source) 0703-5140
 Route of Administration INTRAVENOUS, INTRAMUSCULAR DEA Schedule

Active Ingredient/Active Moiety

Ingredient Name Basis of Strength Strength
 Leucovorin Calcium (Leucovorin) Leucovorin Calcium 100 mg in 10 mL

Inactive Ingredients

Ingredient Name Strength
 sodium chloride
 Sodium hydroxide
 hydrochloric acid

Product Characteristics

Color Score
 Shape Size
 Flavor Imprint Code
 Contains

Packaging

# NDC	Package Description	Multilevel Packaging
1 0703-5140-01	1 VIAL in 1 CARTON	contains a VIAL.
1	10 mL in 1 VIAL	This package is contained within the CARTON (0703-5140-01)

Marketing Information

Marketing Category Application Number or Monograph Citation Marketing Start Date Marketing End Date
 ANDA ANDA0061277 09/28/1993

LEUCOVORIN CALCIUM

leucovorin calcium injection, powder, lyophilized, for solution

Product Information

Product Type HUMAN PRESCRIPTION DRUG NDC Product Code (Source) 0703-5145
 Route of Administration INTRAVENOUS, INTRAMUSCULAR DEA Schedule

Active Ingredient/Active Moiety

Ingredient Name Basis of Strength Strength
 Leucovorin Calcium (Leucovorin) Leucovorin Calcium 350 mg in 17 mL

Inactive Ingredients

Ingredient Name Strength
 sodium chloride
 Sodium hydroxide
 hydrochloric acid

Product Characteristics

Color Score

Shape		Size
Flavor		Imprint Code
Contains		
Packaging		
# NDC	Package Description	Multilevel Packaging
1 0793-5145-01	1 VIAL in 1 CARTON	contains a VIAL
1	17 ml. in 1 VIAL	This package is contained within the CARTON (0793-5145-01)

Marketing Information

Marketing Category	Application Number or Monograph Citation	Marketing Start Date	Marketing End Date
ANDA	ANDA048174	06/12/1997	

Labeler - Teva Parenteral Medicines, Inc (794362533)

Establishment

Name	Address	ID/FEI	Operations
Teva Parenteral Medicines, Inc		794362533	MANUFACTURE
Revised: 10/2009/Teva Parenteral Medicines, Inc			

⁶⁴Cu-MM-302 Positron Emission Tomography Quantifies Variability of Enhanced Permeability and Retention of Nanoparticles in Relation to Treatment Response in Patients with Metastatic Breast Cancer

Heleen Lee¹, Anthony F. Shields², Barry A. Siegel³, Kathy D. Miller⁴, Ian Krop⁵, Cynthia X. Ma³, Patricia M. LoRusso⁶, Pamela N. Munster⁷, Karen Campbell¹, Daniel F. Gaddy¹, Shannon C. Leonard¹, Elena Geretti¹, Stephanie J. Blocker², Dmitri B. Kirpotin¹, Victor Moyo¹, Thomas J. Wickham¹, and Bart S. Hendriks¹

Abstract

Purpose: Therapeutic nanoparticles are designed to deliver their drug payloads through enhanced permeability and retention (EPR) in solid tumors. The extent of EPR and its variability in human tumors is highly debated and has been proposed as an explanation for variable responses to therapeutic nanoparticles in clinical studies.

Experimental Design: We assessed the EPR effect in patients using a ⁶⁴Cu-labeled nanoparticle, ⁶⁴Cu-MM-302 (⁶⁴Cu-labeled HER2-targeted PEGylated liposomal doxorubicin), and imaging by PET/CT. Nineteen patients with HER2-positive metastatic breast cancer underwent 2 to 3 PET/CT scans postadministration of ⁶⁴Cu-MM-302 as part of a clinical trial of MM-302 plus trastuzumab with and without cyclophosphamide (NCT01304797).

Results: Significant background uptake of ⁶⁴Cu-MM-302 was observed in liver and spleen. Tumor accumulation of ⁶⁴Cu-MM-302 at 24 to 48 hours varied 35-fold (0.52–18.5 %ID/kg),

including deposition in bone and brain lesions, and was independent of systemic plasma exposure. Computational analysis quantified rates of deposition and washout, indicating peak liposomal deposition at 24 to 48 hours. Patients were classified on the basis of ⁶⁴Cu-MM-302 lesion deposition using a cut-off point that is comparable with a response threshold in preclinical studies. In a retrospective exploratory analysis of patient outcomes relating to drug levels in tumor lesions, high ⁶⁴Cu-MM-302 deposition was associated with more favorable treatment outcomes (HR = 0.42).

Conclusions: These findings provide important evidence and quantification of the EPR effect in human metastatic tumors and support imaging nanoparticle deposition in tumors as a potential means to identify patients well suited for treatment with therapeutic nanoparticles. *Clin Cancer Res*. 23(15): 4190–202. ©2017 AACR.

Introduction

Nanoparticle drug delivery systems provide a means to alter the biodistribution and pharmacokinetics of small-molecule drugs. Such systems are of particular importance in oncology, where there

is a need to improve the toxicity profiles and therapeutic windows for small-molecule chemotherapies. Therapeutic nanoparticles can enable long-circulating pharmacokinetics and tunable sustained release and improved deposition in solid tumors through leaky vasculature. This phenomenon is referred to as the enhanced permeability and retention (EPR) effect and is well characterized in animal models (1–3). The extent to which the EPR effect is present in human tumor lesions remains controversial but has been proposed as an explanation for variable responses to nanotherapeutics and has important implications for the development and design of future nanomedicines (3, 4).

Liposomes are a class of nanomedicines that have been proven to be clinically useful drug delivery vehicles, with several approved agents for cancer treatment (Doxil/Caebyx, Myocet, DaunoXome, Marqibo, and ONIVYDE). The large size of liposomes, typically about 100 nm in diameter, prevents extravasation from normal vasculature and results in deposition and retention in areas of functionally porous vasculature, such as the liver and spleen, or leaky vasculature in some tumor lesions and areas of inflammation (5–7). Deposition of liposomes via the EPR effect is a nonspecific phenomenon governed primarily by their size and surface characteristics (8, 9).

¹Merrimack Pharmaceuticals, Inc, Cambridge, Massachusetts; ²Karmanos Cancer Institute, Detroit, Michigan; ³Siteman Cancer Center, Washington University, St. Louis, Missouri; ⁴Indiana University Melvin and Bren Simon Cancer Center, Indianapolis, Indiana; ⁵Dana-Farber Cancer Institute, Boston, Massachusetts; ⁶Yale Cancer Center, New Haven, Connecticut; ⁷Helen Diller Family Comprehensive Cancer Center, San Francisco, California.

Note: Supplementary data for this article are available at Clinical Cancer Research Online (<http://clincancerres.aacrjournals.org/>).

Current address for E. Geretti: Torque Therapeutics, Cambridge, Massachusetts; current address for V. Moyo: LEAF Pharmaceuticals, Padua, Pennsylvania; and current address for T.J. Wickham: Rubius Therapeutics, Cambridge, Massachusetts.

Corresponding Author: Heleen Lee, Merrimack Pharmaceuticals, Inc., One Kendall Square, B7201, Cambridge, MA, 02139. Phone: 617-441-7410; Fax: 617-812-8122; E-mail: hlee@merrimack.com

doi: 10.1158/1078-0432.CCR-16-3193

©2017 American Association for Cancer Research.

Translational Relevance

The field of nanomedicine has highly debated the presence and extent of the enhanced permeability and retention (EPR) effect in human tumors, a key mechanistic hallmark for nanomedicine to achieve effective drug delivery and subsequent therapeutic benefits. In this translational study, ⁶⁴Cu-labeled HER2-targeted liposomal doxorubicin was quantified by PET and found to accumulate in human tumors. On the basis of ⁶⁴Cu-PET quantification, the range of tumor drug concentrations is predicted to result in variable antitumor activity. High tumor deposition was stratified on the basis of a cutoff that is consistent with preclinical studies and was associated with more favorable treatment outcome. This suggests that a nanoparticle imaging approach may be applicable as a biomarker strategy for personalizing nanomedicines.

MM-302 (HER2-targeted PEGylated liposomal doxorubicin) is a nanoparticle in clinical development for patients with HER2-positive metastatic breast cancer (NCT01304797, NCT02213744). Targeting of liposomes to tumor antigens, such as HER2, serves as a means to alter the microdistribution of liposomes within tumor lesions and to direct deposited liposomes into tumor cells rather than macrophages (10). MM-302 was specifically designed to maximize doxorubicin uptake into tumor cells while minimizing uptake into nontarget cells and tissues (11) and to enable combination with trastuzumab (12). Although many have reported that antigen-targeted nanoparticles can lead to increased tumor uptake, the extent to which targeted nanoparticles can enhance tumor uptake is determined by many factors, such as choice of targeting ligand and particle size (13–15). For some nanoparticles, tumor accumulation is independent of targeting ligand and, therefore, may be dictated primarily by the EPR effect. Previous work in preclinical models has demonstrated that the HER2 targeting did not alter overall deposition of MM-302 into tumors (Supplementary Fig. S1), but only altered the cellular fate within the tumors (10).

Effective drug delivery is a necessary step for antitumor activity, and poor penetration of anticancer drugs is believed to limit the effectiveness of chemotherapy in solid tumors (16–18). As molecular size of a therapeutic agent increases, effective delivery becomes increasingly important (19). In preclinical models, effective tumor deposition of nanoparticles has also been shown to be a potentially rate-limiting step for effective drug delivery to tumor cells and the resulting antitumor activity (20–23).

The goal of this study was to understand the biodistribution and evaluate the potential role of the EPR effect on a nanotherapeutic in patients with metastatic breast cancer to determine whether tumor lesion delivery could ultimately be used to predict therapeutic efficacy. We transformed an HER2-targeted liposomal doxorubicin (MM-302) into a tracer for PET through labeling with ⁶⁴Cu to enable quantitative characterization of tumor delivery kinetics. ⁶⁴Cu is a positron-emitting radionuclide with a 12.7-hour half-life, well matched to the pharmacokinetics of MM-302. We demonstrated the clinical feasibility and safety of ⁶⁴Cu-liposome PET in patients. ⁶⁴Cu retention within liposomes was shown to be stable in patients within the image acquisition time frame. Computational modeling enab-

led detailed elucidation of the EPR kinetics, establishing both the deposition and washout components of tumor delivery. Variability of the EPR effect was established across lesions within a patient and across patients, as well as in nontarget tissues including the liver, spleen, and bone marrow. Despite heterogeneity at the individual lesion level, we described a method of patient classification based on minimum lesion deposition and demonstrated association of tumor deposition with response to treatment.

Materials and Methods

Clinical study overview

Patients imaged with ⁶⁴Cu-MM-302 PET were part of a multi-site phase I MM-302 study (NCT01304797). A companion imaging protocol was included after the dose escalation phase in which all patients who consented underwent ⁶⁴Cu-MM-302 PET. The primary objectives of the ⁶⁴Cu-MM-302 PET study were to determine the radiation dosimetry and biodistribution of ⁶⁴Cu-MM-302. The study was conducted following International Conference on Harmonization guidelines in accordance with Good Clinical Practice and the ethical principles based on the Declaration of Helsinki. The study was reviewed and approved by the local Institutional Review Board at each center prior to the start of the study, and each subject gave written informed consent.

Patients

Patients enrolled in this study were ≥18 years of age and had advanced HER2-positive (i.e., HER2 3+ by IHC, or HER2 2+ by IHC and FISH or CISH-positive disease) breast cancer, measurable disease by RECIST v1.1, an Eastern Cooperative Oncology Group performance status of 0 to 1, adequate bone marrow reserves (absolute neutrophil count ≥ 1,500/μL, platelet count ≥ 100,000/μL, hemoglobin ≥ 9 g/dL), adequate hepatic function [serum total bilirubin within normal limits, aspartate aminotransferase, alanine aminotransferase up to 2 × upper limit of normal (ULN)], adequate renal function (serum creatinine ≤ 1.5 × ULN), and adequate cardiac function (left ventricular ejection fraction of ≥50% by echocardiography or radionuclide ventriculography). The main exclusion criteria were total cumulative doxorubicin >300 mg/m², active infection or unexplained fever, symptomatic brain metastases, congestive heart failure, coronary artery disease, history of myocardial infarction, hypertension, angina pectoris, valvular heart disease, severe and/or uncontrolled ventricular arrhythmia, prolonged QTc interval, history of allogeneic transplant, and infection of HIV, hepatitis B or C.

MM-302, trastuzumab, and cyclophosphamide dose

Patients imaged with ⁶⁴Cu-MM-302 PET were in Arms 3 and 4 of the phase I study (NCT01304797) and received the following treatment: trastuzumab at 6 mg/kg (with an 8 mg/kg loading dose on cycle 1) administered as a 90-minute intravenous infusion, MM-302 at 30 mg/m² administered as a 60-minute intravenous infusion, as well as a tracer dose of ⁶⁴Cu-MM-302 as described below. The first 3 patients of Arm 3 received trastuzumab starting on cycle 2 to enable initial safety assessment of ⁶⁴Cu-MM-302. Patients in Arm 4 also received cyclophosphamide at 450 mg/m² 5 days prior to ⁶⁴Cu-MM-302 based on a preclinical study showing that tumor priming with cyclophosphamide enhanced tumor delivery of MM-302 in xenografts (24). All patients received prophylactic premedication with diphenhydramine or equivalent prior to dosing of MM-302.

⁶⁴Cu-MM-302 dose

⁶⁴Cu-MM-302 was prepared by a commercial radiopharmacy using ⁶⁴CuCl₂ obtained from Washington University (St. Louis, MO), a chelating/loading agent (diacetyl 4,4'-bis(3-(N,N-diethylamino)propyl)thiosemicarbazone, or 4-DEAP-ATSC), and MM-302. 2.5 mL of 0.06 mg/mL 4-DEAP-ATSC was added to ⁶⁴CuCl₂ and incubated for 1 minute at room temperature. The chelated ⁶⁴Cu mixture was passed through a 0.2-μm filter into a vial containing 5 mL of 2 mg/mL MM-302. The mixture was heated to 65°C for 10 minutes and then cooled to room temperature. The efficiency of loading was measured by size exclusion chromatography as described previously (25).

Quality control testing for ⁶⁴Cu-MM-302 consisted of total activity (400 MBq ± 10%), radiochemical purity (⁶⁴Cu loading efficiency ≥ 85%), appearance (red opalescent solution), endotoxin (≤35 EU/mL), and sterility. The effect of ⁶⁴Cu labeling on MM-302 was found to have negligible effects on key MM-302 characteristics (HER2-binding, doxorubicin content, phospholipid concentration) and maintain an acceptable pH for administration. Preclinical characterization and stability of ⁶⁴Cu-MM-302 was reported elsewhere (25).

For all patient doses, radiochemical purity was observed in the range of 95% to 99%. Within 3 hours after administration of 30 mg/m² MM-302 (doxorubicin equivalent), approximately 400 MBq of ⁶⁴Cu-MM-302 (~3–5 mg/m² doxorubicin) in 3 to 7 mL (depending on the ⁶⁴Cu-labeling-specific activity at the time of administration) was administered as an intravenous infusion over 10 minutes using an infusion pump, followed by a saline flush.

PET image acquisition and quantification

Each patient underwent PET/CT 0 to 3 hours after administration of ⁶⁴Cu-MM-302 on day 1 and additional scan(s) on day 2 and/or day 3 depending on scan group assignment upon enrollment. Five of the 19 patients consented to all three scan times. Image acquisition times on days 1, 2, and 3 were 3 to 5, 7 to 9, and 12 to 15 minutes per bed position, respectively. Approximately 6 bed positions were obtained for each patient, spanning from mid-brain to mid-thigh axially.

Quantification of images was performed using MIM software (MIM Software Inc., Version 6.2 or higher). Rather than maximum standardized uptake value (SUV_{max}), tracer concentration was reported as the percent injected dose per kg of tissue (%ID/kg) within a region of interest (ROI), derived from SUV_{median} normalized to body weight (BW). %ID/kg is related to SUV in the following manner: %ID/kg tissue = SUV/BW × 100%. This measure provides a quantitative measure of drug concentration in the ROI. It is hypothesized that drug activity will be closely related to absolute drug concentration, and for this reason, SUV_{max}, which is conventionally used to correlate with tumor metabolic activity [in the context of ¹⁸F-fluorodeoxyglucose (FDG)], is not appropriate. The median tissue uptake was determined by creating a 3D ROI in metastatic lesions and in normal tissues (heart, lung, liver, spleen, kidneys). Tumor lesion ROIs were selected by an independent radiologist board-certified in nuclear medicine. The median radioactivity for all tumor lesions and tissues was exported from the MIM software into an electronic case report form (eCRF) for further analysis. As an exploratory analysis, bone marrow uptake was quantified using an 8-mm spherical ROI in the lumbar vertebrae (average of L1-L5). Vertebrae with bone

metastases or sclerotic lesions based on CT were excluded from normal bone marrow analyses.

Safety monitoring

Safety of the underlying chemotherapy regimen is reported elsewhere (26, 27). Briefly, vital signs were monitored at multiple time points, both before and after the MM-302 and ⁶⁴Cu-MM-302 administrations. Hematology, liver, and kidney functions were assessed throughout the study. Continual follow-up assessment for adverse events at each study visit was in place to monitor for any possible sequelae of the radiopharmaceutical imaging study. Safety of ⁶⁴Cu-MM-302 as a PET tracer was established through radiation dosimetry as described below.

Radiation dosimetry

Data were presented as PET image files to an independent medical physicist with expertise in radiopharmaceutical dosimetry. Counts in tissues were extracted from the images using the MIPAV software (28). Activity in each visualized organ and the total body were expressed as fractions of injected activity, normalizing the activity in the whole body at the earliest time point to be 100% of the administered activity. Resultant values of percent of injected activity per organ were fit using the SAAM II software (29). Time integrals of activity (30) were entered into the OLINDA/EXM software (31), using the adult male model. The number of disintegrations in the "remainder of body" was assumed to be that in total body within the field of view minus the values in other organs of uptake.

Tracer kinetic modeling

The tracer kinetic model used follows a general form previously presented for describing liposome transport into and out of tumors (20, 32). The pharmacokinetics of ⁶⁴Cu-MM-302 was represented with a single blood compartment with volume V_c and clearance characterized by elimination rate constant k_{el}. The tumor (volume = V_t, assuming tissue density ρ = 1 kg/L) was described in a semiphysiologic manner with a vascular portion and tissue portion consisting of cellular and interstitial space. The fractional volume of the tumor occupied by vasculature was described by a vascular volume fraction (VVF). Blood flow rate into and out of the tumor (Q) was assumed constant at 0.0282 L/kg/minute (33). Washout of particles from the tumor, either back into the blood or via lymphatic drainage, is lumped into a single process for simplicity. Deposition and washout of ⁶⁴Cu-MM-302 into and out of the tumor tissue space were assumed to follow first-order kinetics and were characterized by rate constants k₁ and k₋₁, respectively.

Equations are listed below:

$$\begin{aligned} \frac{dC_b}{dt} &= \frac{1}{V_c} (-k_{el} \cdot C_b \cdot V_c - Q \cdot V_t \cdot \rho \cdot C_b + Q \cdot V_t \cdot \rho \cdot C_w) \\ \frac{dC_w}{dt} &= \frac{V_t \cdot \rho}{V_c \cdot VVF} (Q \cdot C_b - Q \cdot C_w - k_1 \cdot C_w + k_{-1} \cdot C_t) \\ \frac{dC_t}{dt} &= \frac{V_t \cdot \rho}{(1 - VVF)} (k_1 \cdot C_w - k_{-1} \cdot C_t) \\ C_{t,total} &= C_w \cdot VVF + C_t \cdot (1 - VVF) \end{aligned}$$

where C_b, C_w, C_t, and C_{t,total} are the concentrations of ⁶⁴Cu-MM-302 in the blood, tumor vasculature, tumor tissue, and total tumor, respectively. The following parameters were estimated directly from the kinetic data: k_{el}, VVF, k₁, k₋₁ using median

values extracted from ROI analysis from the images and associated tumor volume measurements. Additional information on the model parameters are provided in Supplementary Table S1. The model was implemented in MATLAB (The Mathworks).

Statistical analysis

Treatment outcome was not assessed on the companion imaging protocol, but was documented under the parent protocol per RECIST v1.1 criteria. Image-based ROI analysis data were captured using an eCRF developed in compliance with 21 CFR Part 11, with the exception of the bone marrow uptake data that were obtained for additional exploratory analysis. Uptake data were then exported for further computational analyses. Statistical and pharmacokinetic analyses were performed using MATLAB (The Mathworks) or GraphPad Prism version 6.0 (GraphPad Software). Only nonparametric statistical tests were utilized, including Mann-Whitney, Kruskal-Wallis, or Spearman correlation, wherever applicable. Data are shown as median (interquartile range) unless otherwise indicated.

Results

It is well established that there is a dose-activity relationship for liposomal anticancer agents in preclinical tumor models (34). We therefore sought to identify the minimum tumor delivery of MM-302 required for antitumor activity in preclinical models (details described in Supplementary Material). As expected, increased tumor delivery was observed with increasing dose (Supplementary Fig. S2A; range: 1–13 µg doxorubicin per gram of tumor tissue, or µg doxorubicin/g). The 3 mg/kg dose level, roughly corresponding to the dose level at which MM-302 can effectively inhibit tumor growth (Supplementary Fig. S2B), resulted in a minimum tumor concentration of 2.3 µg doxorubicin/g. On the basis of these findings, we sought to determine the concentrations of liposomal drug achieved in tumor lesions in patients and hypothesized that a minimum effective dose would be necessary for effective treatment with liposomal therapies such as MM-302.

PET/CT of ⁶⁴Cu-MM-302 in patients

Between July 2013 and July 2014, 25 patients were dosed with MM-302 as part of a phase I study (NCT01304797); 19 of the patients underwent ⁶⁴Cu-MM-302 PET. Patient demographics are shown in Supplementary Table S2. All 19 patients were imaged on day 1 between 0.2 and 2 hours (median 0.7 hour) postadministration of ⁶⁴Cu-MM-302; 16 and 8 patients also underwent scans on day 2 (median of 21.2 hours) and day 3 (median of 44.6 hours), respectively. A total of 5 patients had three PET scans on days 1, 2, and 3 postadministration. The median age of imaged patients was 54 (range, 41–71) and the median body weight was 71.7 kg (range, 56.5–97.3 kg). Patients were enrolled into two different arms where Arms 3 and 4 include treatment with trastuzumab + MM-302 and cyclophosphamide + trastuzumab + MM-302, respectively.

The mean activity of ⁶⁴Cu-MM-302 administered was 389 MBq (range, 337–432 MBq). The administration of ⁶⁴Cu-MM-302 was well tolerated by all subjects. Any study drug-related adverse events recorded could not be uniquely attributed to ⁶⁴Cu-MM-302 because ⁶⁴Cu-MM-302 is administered within a few hours of MM-302, and the exposures to the two molecules overlap during the period of treatment-emergent adverse event reporting.

Pharmacokinetics and biodistribution of ⁶⁴Cu-MM-302

Whole-body distribution of ⁶⁴Cu-MM-302 is shown for 2 patients on days 1 to 3 postadministration in Fig. 1. Immediately following administration, ⁶⁴Cu-MM-302 is almost exclusively localized in the blood pool, as expected for a PEGylated liposome. On days 2 to 3 (19–47 hours), deposition of ⁶⁴Cu-MM-302 was seen in the liver and spleen, but there was relatively slow clearance from the blood. Images were consistent with hepatic clearance of MM-302, and no significant uptake of the tracer was seen in the kidneys or bladder of any patients.

Decay-corrected time-activity plots for ⁶⁴Cu-MM-302 in selected normal tissues are shown in Fig. 2 for all patients. Because of the relatively long circulation time of ⁶⁴Cu-MM-302, the presence of large blood vessels in any ROI has the potential to skew the average values within an ROI. For this reason, median activity within each ROI was used to provide a more robust measure of tissue uptake. There was very little uptake in normal muscle and normal lung tissue (<6 %ID/kg). Median normal liver uptake was approximately 6.5 (5.2–7.3) %ID/kg postadministration and increased with time to 15.7 (12.4–21.8) %ID/kg on day 3 (decay-corrected). Uptake into normal spleen appeared to be the most variable with 10.5 (8.6–13.3) %ID/kg postadministration, with a mild increase to 17.0 (13.5–18.3) and 13.2 (7.8–19.6) %ID/kg on days 2 and 3, respectively. ⁶⁴Cu-MM-302 uptake was also observed in the bone marrow, peaking between days 2 and 3 at 4.2 (3.6–4.7) and 3.6 (2.0–4.0) %ID/kg, with similar uptake kinetics as normal spleen; this is consistent with the expected uptake of nanoparticles by the reticuloendothelial system (35). Although the level of uptake in bone marrow seems to be on par with that of lung tissue, the kinetics of bone marrow uptake resemble that seen in the liver/spleen instead of the constant decrease observed for muscle and lung (i.e., blood clearance).

The behavior of ⁶⁴Cu-MM-302 in the blood pool was assessed from PET/CT images using an ROI in the aorta and is shown in Fig. 2F and G. The clearance of ⁶⁴Cu-MM-302 was highly reproducible and consistent with monoexponential clearance kinetics previously reported for MM-302 based on doxorubicin content (26, 27). Monoexponential clearance kinetics made it possible to determine estimates of the pharmacokinetic parameters from the 2 to 3 images obtained per patient. Estimation of pharmacokinetic parameters (compartment model) from the imaging data (mean $t_{1/2} = 33$ hours) compared well with the 39-hour (95% confidence interval, 29–53 hours; $n = 10$) half-life reported for MM-302 at the 30 mg/m² dose level (26). One patient had significantly faster blood clearance ($t_{1/2} = 9.53$ hours) with significant sequestration of ⁶⁴Cu-MM-302 at 0.5 hour in the liver and spleen (Supplementary Fig. S3). This patient was in Arm 4 (with cyclophosphamide treatment), but rapid clearance does not seem to be attributed to cyclophosphamide, as the blood $t_{1/2}$ was not significantly different in Arm 3 without cyclophosphamide [median $t_{1/2} = 36.5$ (23.6–44.3 hours)] compared with Arm 4 [median $t_{1/2} = 35.4$ (25.2–40.9) hours; $P = 0.97$]. Most normal tissue uptake between the two groups were also comparable, with the exception of muscle on day 1 [Arm 3 = 1.9 (0.6–1.3) %ID/kg vs. Arm 4 = 0.6 (0.3–0.8) %ID/kg; $P = 0.027$] and bone marrow on day 2 [Arm 3 = 4.3 (4.1–5.4) %ID/kg vs. Arm 4 = 3.9 (2.9–4.4) %ID/kg; $P = 0.042$] where Arm 3 patients have higher uptake.

The stability of ⁶⁴Cu labeling of MM-302 was assessed in 3 patients. Free ⁶⁴Cu was not detectable above background any time

Lee et al.

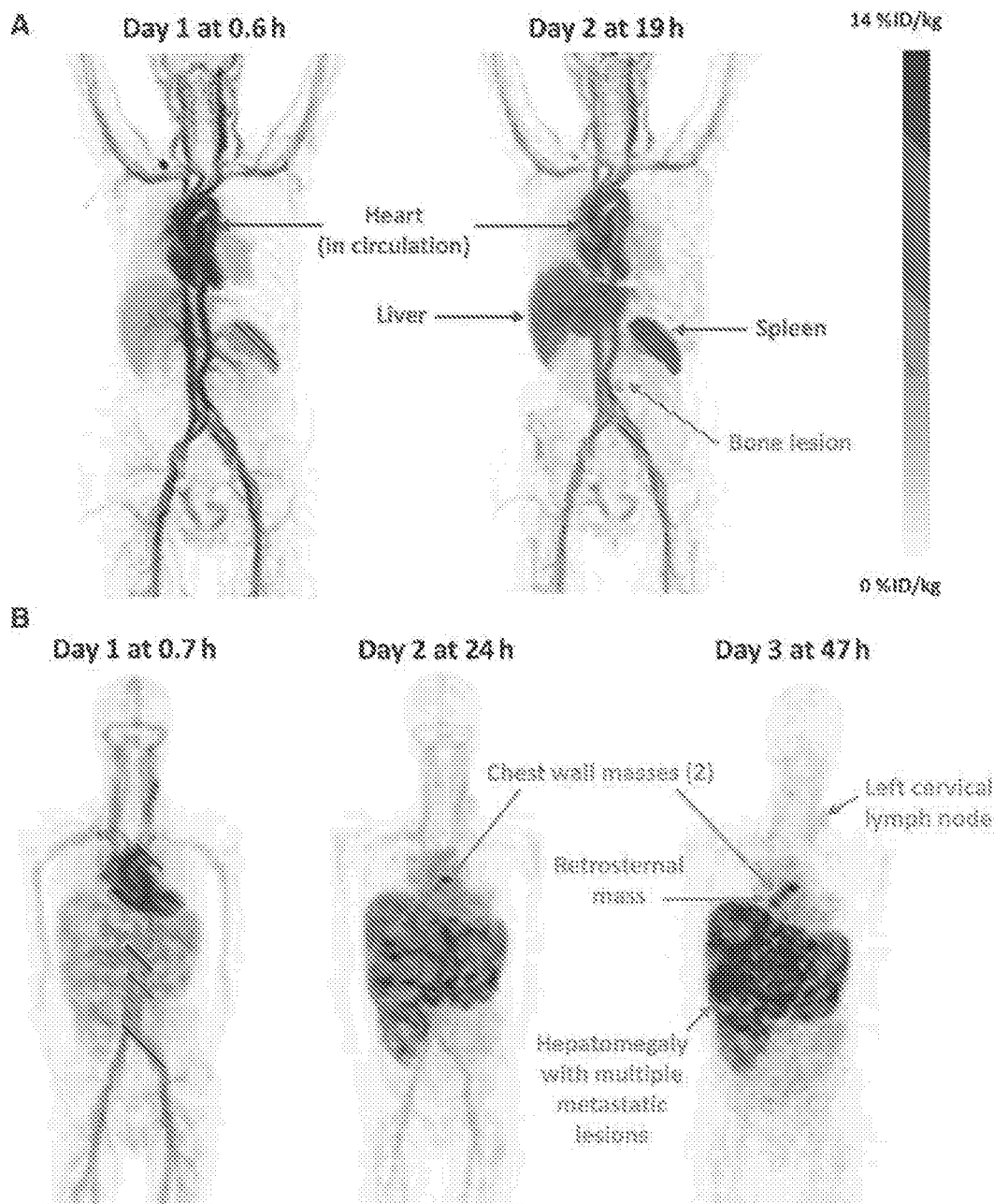


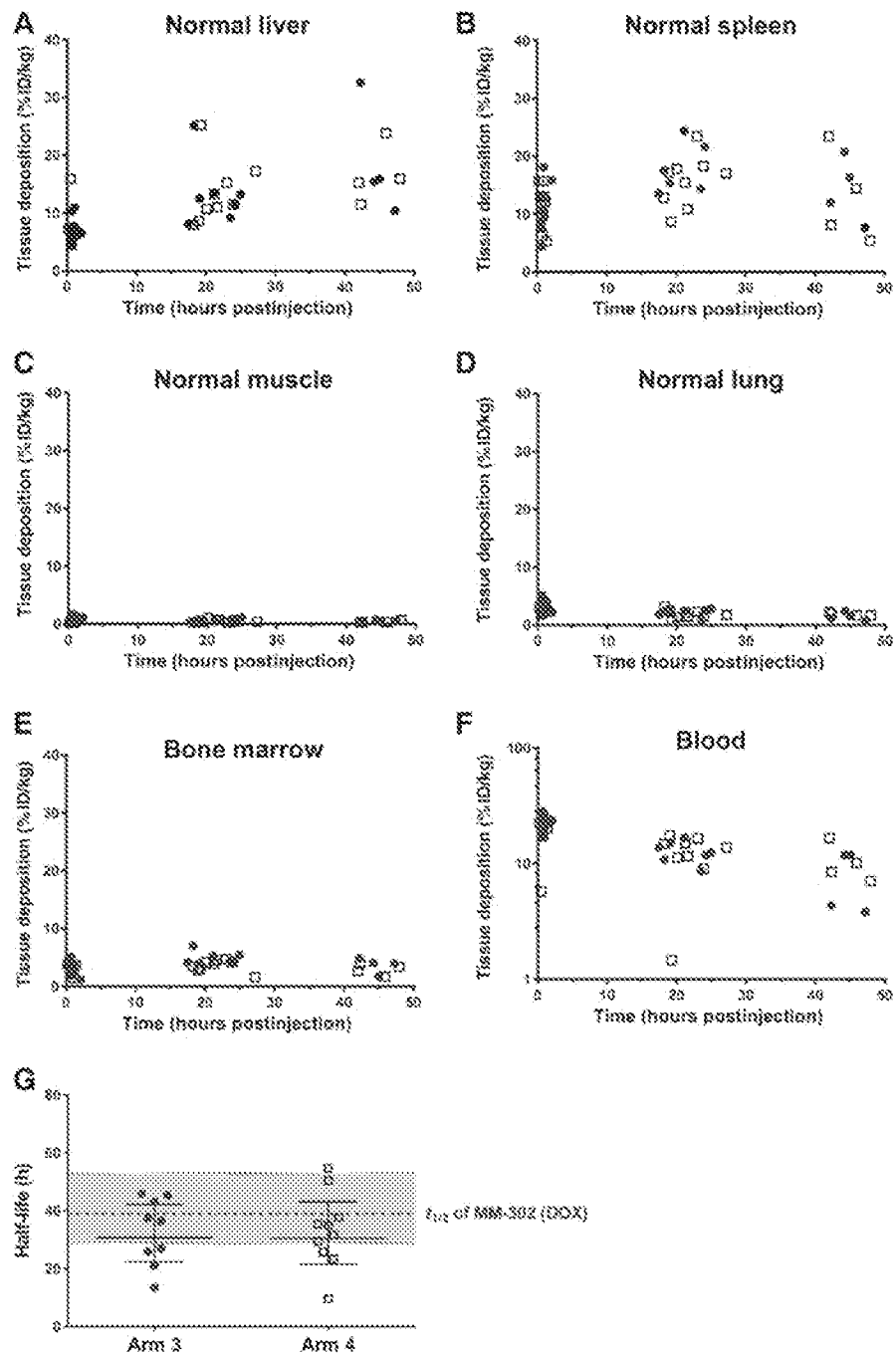
Figure 1.

Biodistribution of ^{64}Cu -MM-302 in patients. Maximum intensity projection PET images of 2 patients with HER2-positive breast cancer injected with 20 mg/m^2 of MM-302 and a tracer dose of ^{64}Cu -MM-302 (400 MBq). PET/CT images were acquired at 0.6 and 19 hours postinjection in patient 02 (A), and 0.7, 24, and 47 hours postinjection in patient 06 (B). Immediately after administration, ^{64}Cu -MM-302 activity was primarily confined in the blood pool because of the extended circulation property of liposomes. On days 2 and 3, ^{64}Cu -MM-302 uptake was evident in normal spleen and liver, as well as in various tumor lesions.

point (Supplementary Fig. S4), indicating highly stable labeling of MM-302 with ^{64}Cu . In addition, almost all the ^{64}Cu activity remained in the serum component, with <4% ^{64}Cu detected in blood cells. These results were consistent with preclinical development of the ^{64}Cu -MM-302 labeling method (25).

Radiation dosimetry

Internal radiation dosimetry was evaluated in a subset of patients ($n = 11$). The target radioactivity was 400 MBq, and the median radioactivity administered to the 11 patients for radiation dosimetry analysis was 389 (range, 337–432)



MBq. The mean estimated radiation absorbed dose for each organ, effective dose, and total body dose are shown in Supplementary Table S3. The highest absorbed radiation dose was in the heart wall, followed by the spleen, and liver receiving 0.25 (0.20–0.31), 0.12 (0.09–0.21), and 0.09 (0.09–0.12) mGy/MBq, respectively. The median effective dose was 0.028 mSv/MBq.

Tumor lesions uptake of ⁶⁴Cu-MM-302

Tumor lesions could be visualized on days 2 and 3 of ⁶⁴Cu-MM-302 PET scans (Fig. 3). Similar to normal tissue uptake, there was no significant difference in lesion uptake for patients treated versus not treated with cyclophosphamide (Arm 3 vs. 4, $P \geq 0.67$ for all 3 scans; Fig. 4A). On the basis of these findings, subsequent analyses were performed by combining data from

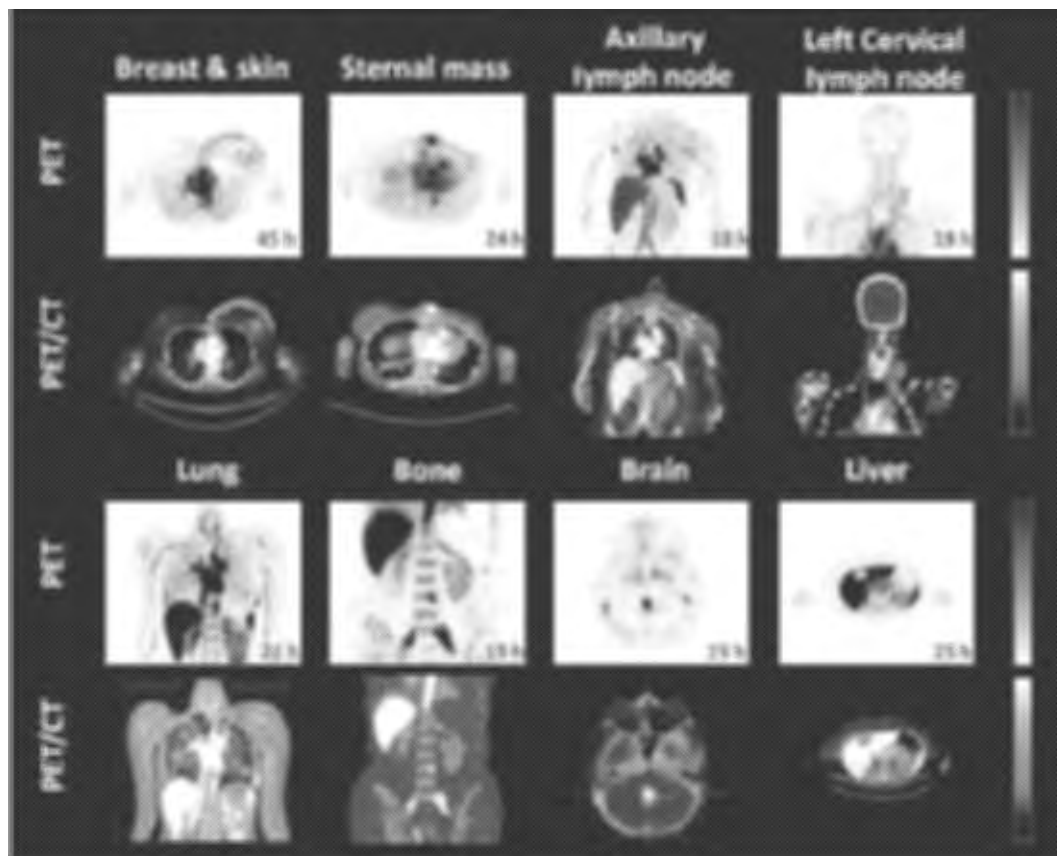


Figure 3. Visualization of ^{64}Cu -MM-302 lesion deposition. Representative PET and fused PET/CT images of ^{64}Cu -MM-302 in lesions at different anatomic locations. Intensity scale bars represent deposition from 0 to 10 %ID/kg (derived from $\text{SUV}_{\text{median}}$). The regions of interest used to measure tumor deposition of ^{64}Cu -MM-302 are shown in blue or turquoise outlines. ^{64}Cu -MM-302 uptake was detected at above muscle background level in lesions of various anatomic locations that are common for HER2-positive metastatic diseases.

the two treatment arms. Increasing activity in tumor lesions was noted from the initial scan on day 1 to days 2 to 3 scans at varying degrees (Fig. 4B), while the activity in the blood decreased over this time frame (Fig. 2F). In the initial scan, median ^{64}Cu -MM-302 signal in lesions was 2.3 %ID/kg (range, 0.24–7.1 %ID/kg, $n = 68$ lesions), reflecting predominantly tumor blood pool. Comparison with blood measurements yield a ratio of 0.13, which is consistent with the expected tumor vascular volume fraction determined by other methods (36–38). The median tumor-to-blood ratios were 0.080 (0.045–0.120), 0.208 (0.082–0.188), and 0.468 (0.111–0.451) on days 1, 2, and 3, respectively. There were a few lesions that showed either no change or a decrease in signal over time, but did not decrease as rapidly as the blood pool signal, still suggesting a small degree of ^{64}Cu -MM-302 deposition. Median ^{64}Cu -MM-302 depositions on days 2 and 3 were 3.7 (2.3–7.5) and 4.0 (2.3–10.6) %ID/kg, indicating no significant differences in lesion uptake between day 2 and day 3.

On the basis of the known ^{64}Cu -doxorubicin ratio, it is estimated that the tumor deposition of MM-302 on days 2 to 3 ranges from 0.22 to 11 μg doxorubicin/g. Ninety percent of the

patient lesions had deposition that are consistent with the range of MM-302 tumor uptake in preclinical xenograft models (Supplementary Fig. S2A, range, 1–13 μg doxorubicin/g). ^{64}Cu -MM-302 uptake was heterogeneous within each patient among multiple lesions (Fig. 4C). The extent to which ^{64}Cu -MM-302 accumulates in individual lesions is therefore unique to the lesion characteristics rather than the pharmacokinetics of ^{64}Cu -MM-302, as lesion uptake on days 2 or 3 was not correlated with exposure ($P > 0.08$, Pearson correlation with blood $\text{AUC}_{0-\infty}$; Fig. 4D). There was also no significant correlation between lesion signal and lesion volume ($P > 0.27$) for scan 2 or 3 (Fig. 4E).

Uptake was observed in lesions of various anatomic locations, including the lung, brain, lymph nodes, and bone, as shown in Fig. 3 with deposition quantification presented in Fig. 4F. Hepatic lesions primarily appeared as hypoactive regions, because of the high background activity of the liver, but showed evidence of signal enhancement over time. There were also several instances where hepatic lesions had uptake similar to that of normal liver tissue, requiring reference to contrast-enhanced diagnostic CT to guide ROI selection (Supplementary Fig. S5). In all three scan time points, hepatic lesions were consistently higher than other

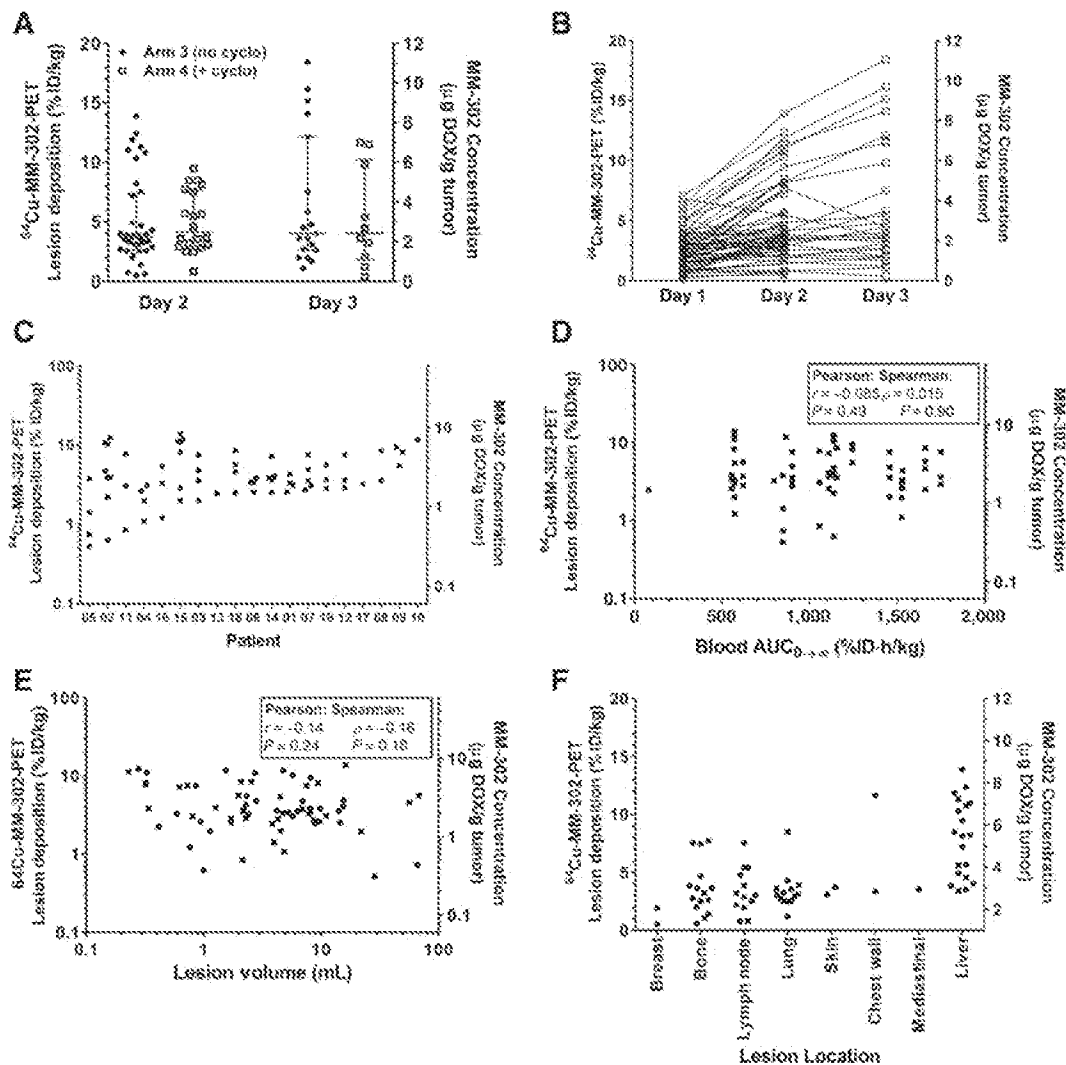


Figure 4.

Quantification of ⁶⁴Cu-MM-302 uptake in tumor lesions. **A**, Lesion uptake of ⁶⁴Cu-MM-302 in patients on days 2 and 3 in patients treated with (open square) and without (closed circle) cyclophosphamide (cyclo). No significant difference in lesion deposition was observed between the two treatment groups ($P \geq 0.67$, Mann-Whitney test). **B**, ⁶⁴Cu-MM-302 deposition kinetics in all patient lesions illustrating accumulation of MM-302 in lesions from day 1 to 3. Statistical difference in lesion uptake was only detectable from day 1 ($P < 0.0001$, ANOVA), but not between days 2 and 3 ($P > 0.67$). **C**, Tumor deposition of ⁶⁴Cu-MM-302 in individual patients was shown to be highly variable. No correlation of tumor deposition was detected with blood exposure (**D**) or tumor size (**E**). **F**, ⁶⁴Cu-MM-302 deposition in lesions of different anatomic locations. **C-F**, Data obtained on day 2, or day 3 if patient did not undergo PET scan on day 2.

anatomic locations (Fig. 4F; $P < 0.0001$ on days 2 and 3; only anatomic locations with more than three data points were included in statistical analyses).

Kinetics of ⁶⁴Cu-MM-302 tumor deposition

In patients who consented to undergo three scans, a detailed kinetic analysis of ⁶⁴Cu-MM-302 in tumor lesions was possible. Figure 5 shows the ⁶⁴Cu-MM-302 lesion deposition kinetic profiles of a patient, who had 4 tumor lesions that were selected for analysis by the independent reviewer. Quantification of ⁶⁴Cu-MM-302 uptake for the individual lesions is shown in Fig. 5A. A chest wall

lesion showed comparatively high uptake on day 3, whereas the two hepatic lesions and one neck lesion had comparatively lower uptake. Images corresponding to comparatively high (ROI 3) versus low (ROI 4) uptake lesions are shown in Fig. 5B.

Three imaging data points and a basic set of assumptions regarding ⁶⁴Cu-MM-302 transport (see Materials and Methods) enabled elucidation of the full kinetics of ⁶⁴Cu-MM-302 deposition into and out of the tumor lesions, including determination of the contribution of blood versus tissue-deposited ⁶⁴Cu-MM-302. A schematic of the tracer kinetic model used is shown in Fig. 5C. The model assumes first-order clearance of

Lee et al.

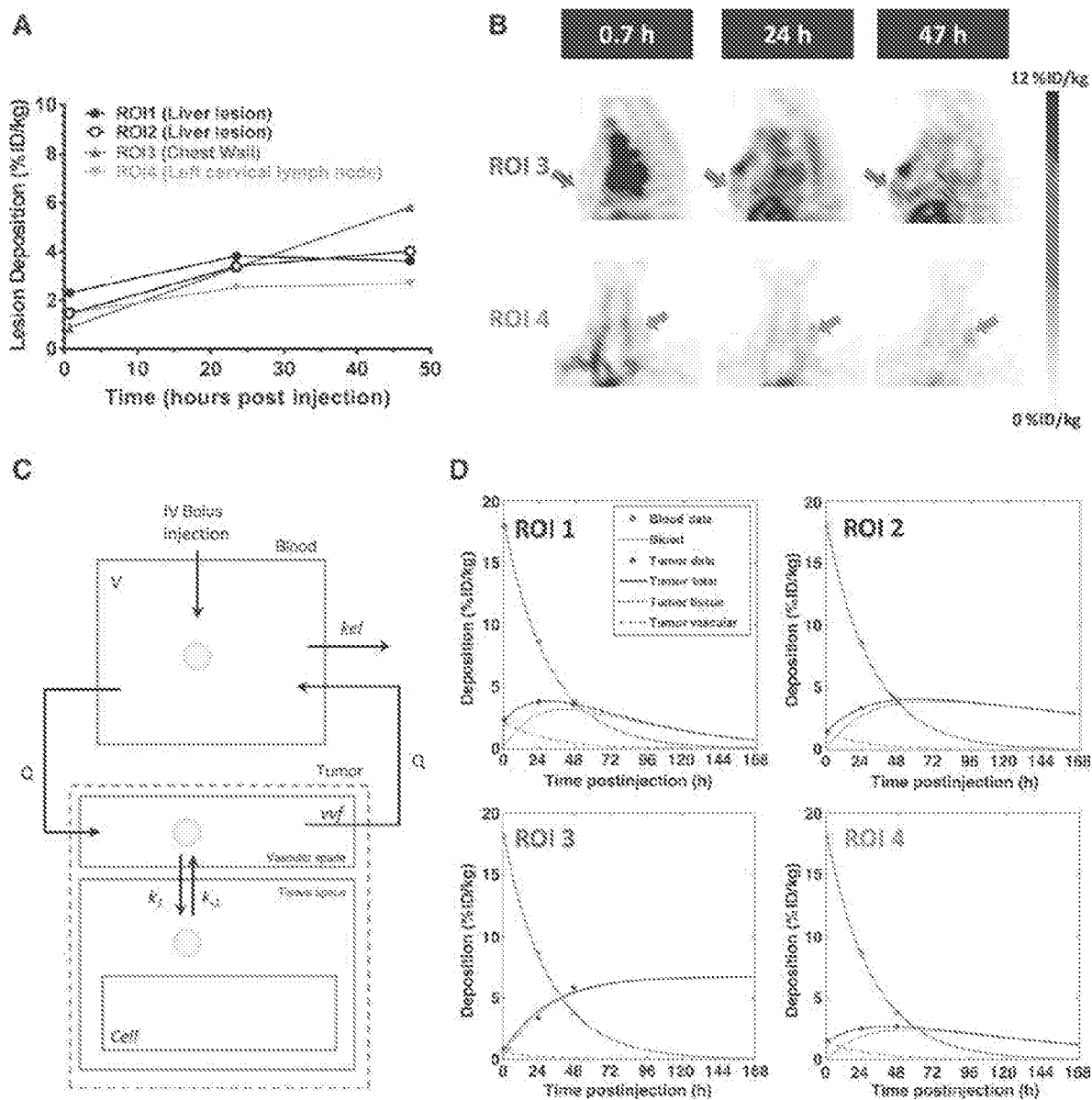


Figure 5.

Kinetics of ^{64}Cu -MM-302 deposition in tumor lesions. Lesion deposition kinetics of ^{64}Cu -MM-302 in an HER2-positive breast cancer patient who received three PET/CT scans at 0.7, 24, and 47 hours postinjection (patient 06). **A**, Lesion deposition for each ROI is expressed as %ID/kg derived from $\text{SUV}_{\text{lesion}}^{\text{decay-corrected}}$. **B**, Sagittal and coronal view of PET images illustrating deposition in ROI3 (chest wall mass) and ROI4 (left cervical lymph node), respectively. **C**, Schematic diagram of pharmacokinetics model describing ^{64}Cu -MM-302 transport kinetics postinjection. **D**, Blood and lesion deposition data fit to the model described in **C**, illustrating ^{64}Cu signal contribution kinetics from tumor vascular versus tumor tissue compartments at 0 to 168 hours postinjection.

^{64}Cu -MM-302 from the central blood pool and a fixed rate of convective transport (blood flow) from the central compartment into the vascular compartment of the tumor. The tumor is characterized by a vascular volume fraction and ^{64}Cu -MM-302 transport from the vascular compartment into the tissue, through a combination of convective and diffusive transport, is characterized by a first-order rate constant. Washout of ^{64}Cu -MM-302 is also assumed to follow first-order kinetics. Cellular

uptake and processing of ^{64}Cu -MM-302 is also assumed to be minimal over the 3-day time scale of imaging. Shown in Fig 5D, the kinetic model was fit to the blood and tumor data, demonstrating that this model framework was able to quantify the interlesion heterogeneity of uptake through variations in rates of deposition, washout, and vascular volume fraction (Supplementary Fig. S6). The model results indicate peak deposition of MM-302 in human tumors occurs on

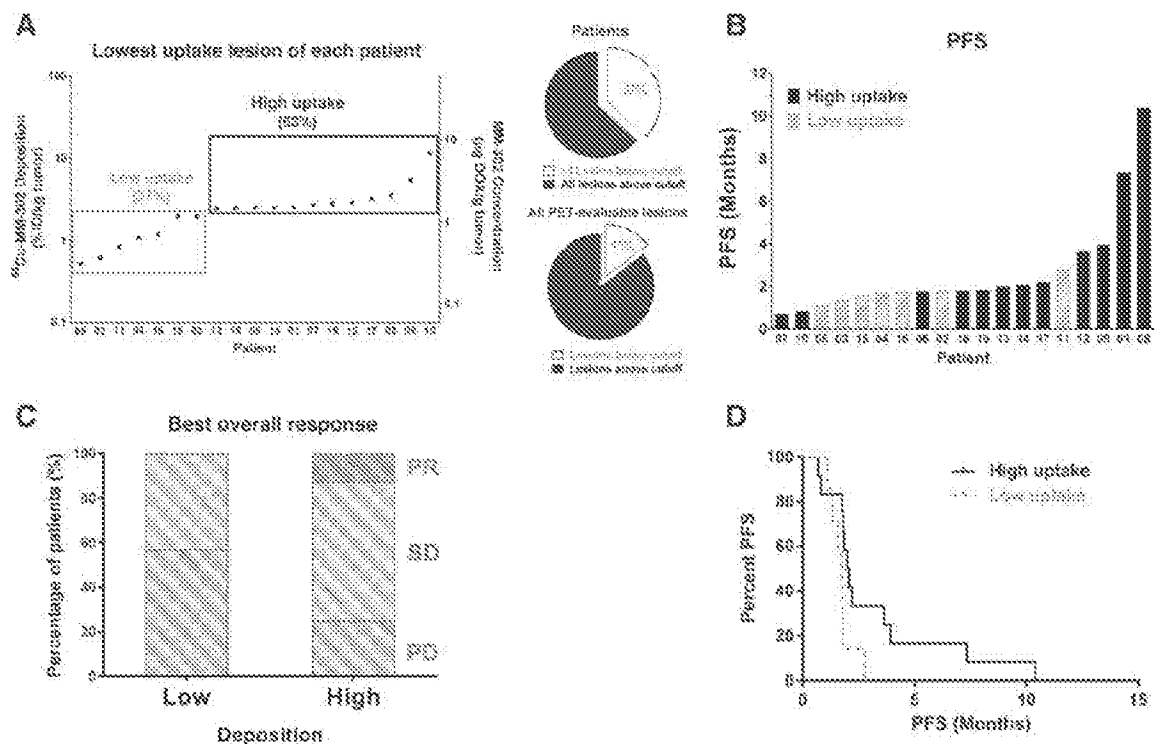


Figure 6.

Patient treatment outcome stratified by deposition of lowest uptake lesion. **A**, ⁶⁴Cu-MM-302 lesion deposition of the lowest uptake lesion within each patient from days 2 or 3 are shown and aligned in ascending order. A deposition threshold was selected on the basis of the inflection point of the deposition graph and confirmed by ROC analysis, where patients to the left of the inflection point were designated as "low uptake" group. The inset figures illustrate the percentage of patients with >1 lesion that are below or above the cutoff (top inset), and percentage of lesions that are below or above the cutoff (bottom inset). PFS of the imaged patients is shown in **B**, where "low uptake" patients are depicted with orange striped bars, and "high uptake" patients are depicted with black solid bars. The best overall response per RECIST v1.1 criteria was captured in **C** stratified into the "low uptake" and "high uptake" groups, where PR, SD, and PD represent partial response, stable disease, and progressive disease, respectively. **D**, Patient PFS of the high versus low uptake patients is shown in a Kaplan-Meier curve.

approximately days 2 to 3 and supports the selected imaging times used. The fraction of tumor ⁶⁴Cu-MM-302 signal on days 2 to 3 arising from the vascular versus deposited ⁶⁴Cu-MM-302 was minimal compared with the tumor tissue signal, suggesting that most ⁶⁴Cu tumor signal after day 1 is attributed to deposition of ⁶⁴Cu-MM-302 in the tumor tissue.

Patient classification and association with treatment outcome

Inadequate drug delivery to a single tumor lesion within a patient may be sufficient to result in progressive disease when patients are evaluated on the basis of RECIST v1.1. For this reason, we classified patients into two groups based on their lowest uptake lesion. At approximately 2 %ID/kg, a plateau was observed based upon the distribution of lowest uptake lesion deposition of each patient (Fig. 6A). Tracer deposition of 2 %ID/kg corresponds to approximately 1.2 µg doxorubicin/g, which is comparable with the preclinical effective threshold established previously (2.3 µg doxorubicin/g; Supplementary Fig. S2).

Although not a formal objective of the study, a preliminary retrospective analysis was attempted to correlate ⁶⁴Cu-MM-302 lesion uptake and patient response to treatment. The best overall responses per RECIST v1.1 for the two groups classified on the

basis of imaging data are shown in Fig. 6B-D. Seventy-five percent of subjects experienced a partial response (PR) and/or stable disease (SD) in the high deposition group, whereas 43% of patients experienced SD with no PR in the low deposition group. The patients in groups with the low and high ⁶⁴Cu-liposome deposition lesions had median progression-free survival (PFS) of 1.7 and 2.0 months, respectively, with an HR of 0.42 (log-rank method). ROC analysis of the minimum lesion uptake against PFS yielded a deposition threshold of 2.4 %ID/kg, which resulted in the same patient stratification. The limited number of imaged patients on each treatment arm with analyzable RECIST data ($n = 9$ and 10 for Arms 3 and 4, respectively) precluded a meaningful statistical comparison.

Discussion

The extent of therapeutic nanoparticle deposition in solid tumors is a vital component of establishing local drug concentrations and the overall therapeutic window. Understanding the extent and variability of the EPR effect in patient tumors is at the core of understanding whether local drug levels are limiting in patient responses to therapeutic nanoparticles (3). Although preclinical examples exist, this simple pharmacologic

concept has been difficult to translate into the clinical setting (39).

In this study, we utilized preclinical models to identify a minimum critical concentration threshold of MM-302 tumor delivery required to control tumor growth and translated this concept into a clinical study. We hypothesized that tumor lesion delivery of therapeutic nanoparticles, such as MM-302, is highly variable, and locally achievable drug concentrations span critical thresholds that determine sensitivity versus lack of response. To test this hypothesis, we transformed MM-302 into a PET tracer through ^{64}Cu -labeling and incorporated imaging with ^{64}Cu -MM-302 PET/CT into a clinical trial of MM-302 plus trastuzumab with or without cyclophosphamide. Patient tumor concentrations of MM-302, as determined with ^{64}Cu -MM-302, were remarkably consistent with those determined from preclinical data and span a range of concentrations that potentially impact therapeutic responses. Our results have important implications for clinical development of therapeutic nanoparticles.

To date, patients with cancer have been imaged in several clinical studies with ^{111}In -liposomes or $^{99\text{m}}\text{Tc}$ -liposomes via planar scintigraphy or single-photon emission CT (SPECT) to assess tumor uptake of the liposomes (40–43). However, these clinical studies were limited to visualization or semiquantitative analysis of liposome behavior because of the limitations of the imaging methods and/or the short half-life of the radionuclide tracer. Relative to SPECT, PET has the advantage of increased sensitivity and spatial resolution while allowing for straightforward data quantification and whole-body 3D imaging.

The kinetic nature of our studies with ^{64}Cu -MM-302, coupled with the accuracy afforded by PET/CT, clearly establish that the EPR effect is present in human metastatic tumors. The accumulation of ^{64}Cu -MM-302 in tumor lesions over time was not observed in normal tissues, such as muscle, and is consistent with the EPR effect of nanoparticles as reported in the literature (44, 45). The data indicate the variable nature of this process, not only in terms of deposition rates but washout rates as well. Rates of deposition and washout determined from human tumors compared well with rates estimated from mouse xenograft models (20). Furthermore, kinetic modeling indicated that at later times, the ^{64}Cu signal was predominantly the result of tissue-deposited liposomes. In contrast, early imaging times, as used in $^{99\text{m}}\text{Tc}$ -liposomes studies, are largely a measurement of tumor lesion vascular volume fraction (41–43).

This study also highlights the interplay between normal liver and hepatic tumor lesions for therapeutic nanoparticles. As expected, the liver was a site of high background signal because of its role in metabolizing and clearing liposomes. In contrast, little to no signal was observed in the kidney or bladder, supporting the stability of the ^{64}Cu -MM-302 tracer, as well as the liver being the primary route of clearance. The liver is also a common site of metastatic disease in breast and other cancers. Hepatic lesions were able to be visualized in most cases, as they tend to appear as hypoactive regions relative to the high normal tissue uptake background. In some cases, where hepatic lesion uptake was similar to normal liver tissue, diagnostic CT was required to help delineate the liver-lesion boundary. The spatial resolution of PET and partial volume effects make accurate quantification of these lesions difficult. This may be particularly true for lesions with an actively growing rim and/or necrotic core. Similarly, lesions with significant fibrosis or scar tissue may also be difficult to resolve from actively growing lesions by

CT. For these reasons, comparison of ^{64}Cu -MM-302 PET with $^{18\text{F}}$ -FDG PET would be an interesting future direction for identifying metabolically active lesions to further the understanding of liposome tumor deposition.

The data presented herein provide evidence supporting a mechanism by which ^{64}Cu -MM-302 liposomes deposit and accumulate in human tumors. An interesting and serendipitous finding of this study was the accumulation of ^{64}Cu -MM-302 in brain lesions. The delivery of large molecules to brain lesions has been previously shown by imaging with liposomes (41) and ^{64}Cu -/ ^{89}Zr -labeled trastuzumab (46, 47). Similarly, Siegal and colleagues had reported a 14-fold increase in liposomal doxorubicin delivery to brain tumor in a mouse model compared with adjacent normal brain tissue (48). This almost certainly reflects disruption of the blood-tumor barrier in metastatic lesions, rather than large liposomes traversing the blood-brain barrier directly. Greater disruption would be predicted to lead to increased delivery and might determine the extent of response to therapy (49, 50).

Variable ^{64}Cu -MM-302 uptake occurred both across lesions within a patient and across patients. In general, in patients with multiple lesions, not all of the lesions had the same level of uptake. This suggests that patient classification based on nanoparticle delivery is potentially complex and cannot be solely determined by systemic exposure. However, patient lesion data can be classified into two groups: (i) variable uptake including low-uptake lesions, and (ii) variable uptake with only high-uptake lesions, based on the rationale that poor delivery to a single lesion could be sufficient to presage disease progression. Classification based on imaging data selected about one third of patients as "low uptake" and enabled a subsequent exploratory analysis of patient outcomes. Although our retrospective analysis illustrates that patient level classification based on lesion delivery is possible and was consistent with our delivery-based hypothesis, these results are limited by the small sample size of this phase I study among other factors, including the inherent chemosensitivity. For instance, patient classification was performed on the basis of the imaging data only; however, some patients received cyclophosphamide and others did not. Nonetheless, we did not find a systematic difference in lesion uptake between lesions that were treated with cyclophosphamide versus those that were not, suggesting this was not a primary factor in dictating outcome.

The significance of this work also extends to an improved understanding of safety. EPR effect also occurs in bone marrow and explains well-known hematologic toxicities of therapeutic nanoparticles, such as liposomal doxorubicin. Interestingly, less variability in uptake was observed in bone marrow than in tumor lesions, in general. This implies that the primary opportunity for patient selection lies in identifying patients based on uptake in tumor lesions rather than safety.

Together, these data suggest that it may be possible to use pretreatment imaging of nanoparticle deposition in tumors as a potential means to identify patients most likely to benefit from treatment with therapeutic nanoparticles. Future directions include development of potential diagnostic imaging agents specifically designed to assess tumor delivery of therapeutic nanoparticles. These agents would enable a comprehensive understanding of the delivery of nanomedicines to tumor lesions as a function of indication and anatomic location. Identification of patient characteristics correlating with effective nanoparticle delivery has potential to greatly benefit patients and dramatically

influence clinical development decisions. Prospectively defined clinical trials will be needed to formally establish the relationships between therapeutic nanoparticle tumor delivery and treatment outcome.

Disclosure of Potential Conflicts of Interest

B.A. Siegel reports receiving commercial research grants from and is a consultant/advisory board member for Merrimack Pharmaceuticals. I. Krop reports receiving other commercial research support and speakers bureau honoraria from Genentech. K. Campbell and T.J. Wickham hold ownership interest (including patents) in Merrimack Pharmaceuticals. D.B. Kirpotin reports receiving other commercial research support from and holds ownership interest (including patents) in Merrimack Pharmaceuticals. V. Moyo is an employee of and holds ownership interest (including patents) in I.E.A.F. Pharmaceuticals. No potential conflicts of interest were disclosed by the other authors.

Authors' Contributions

Conception and design: H. Lee, A.F. Shields, B.A. Siegel, K.D. Miller, P.M. LoRusso, P.N. Munster, D.B. Kirpotin, V. Moyo, T.J. Wickham, B.S. Hendriks
Development of methodology: H. Lee, A.F. Shields, B.A. Siegel, P.N. Munster, E. Geretti, D.B. Kirpotin, T.J. Wickham, B.S. Hendriks
Acquisition of data (provided animals, acquired and managed patients, provided facilities, etc.): H. Lee, A.F. Shields, B.A. Siegel, K.D. Miller, I. Krop, C.X. Ma, P.M. LoRusso, P.N. Munster, S.C. Leonard, E. Geretti, S.J. Blecker
Analysis and interpretation of data (e.g., statistical analysis, biostatistics, computational analysis): H. Lee, A.F. Shields, B.A. Siegel, K.D. Miller, C.X. Ma, P.N. Munster, S.C. Leonard, T.J. Wickham, B.S. Hendriks

Writing, review, and/or revision of the manuscript: H. Lee, A.F. Shields, B.A. Siegel, K.D. Miller, I. Krop, C.X. Ma, P.M. LoRusso, D.F. Gaddy, E. Geretti, D.B. Kirpotin, V. Moyo, T.J. Wickham, B.S. Hendriks
Administrative, technical, or material support (i.e., reporting or organizing data, constructing databases): H. Lee, D.F. Gaddy
Study supervision: H. Lee, A.F. Shields, K.D. Miller, P.N. Munster, K. Campbell, E. Geretti, V. Moyo, T.J. Wickham

Acknowledgments

We thank the patients and the clinical staff for their participation and support of the study. We also thank Shari Rabenstein and Paul Galante from ICON Medical Imaging for their excellent study support, image interpretation, and fruitful discussions. Tom Volter from Washington University has been tremendously helpful in coordinating logistics and supply of ⁶⁴Cu for the clinical study. We would like to acknowledge Cardinal Health for their role in preparation and distribution of ⁶⁴Cu-MN-302 to clinical sites. We also appreciate Dr. Michael Stabin's participation in the radiation dosimetry analysis. Lastly, we would like to thank Jonathan Fitzgerald, Istvan Molnar, Ty McClure, and Ulrik Nielsen from Merrimack Pharmaceuticals for their helpful input.

Grant Support

This study was solely funded by Merrimack Pharmaceuticals. The costs of publication of this article were defrayed in part by the payment of page charges. This article must therefore be hereby marked *advertisement* in accordance with 18 U.S.C. Section 1734 solely to indicate this fact.

Received December 19, 2016; revised January 24, 2017; accepted March 8, 2017; published OnlineFirst March 15, 2017.

References

- Maizumi Y, Maeda H. A new concept for macromolecular therapeutics in cancer chemotherapy: mechanism of tumortropic accumulation of proteins and the antitumor agent smeanes. *Cancer Res* 1986;46:6387-92.
- Zheng J, Jaffray D, Allen C. Quantitative CT imaging of the spatial and temporal distribution of liposomes in a rabbit tumor model. *Mol Pharm* 2009;6:571-80.
- Prabhalat U, Blakey DC, Maeda H, Jain RK, Seville-Muroca EM, Zamboni WC, et al. Challenges and key considerations of the enhanced permeability and retention effect (EPR) for nanomedicine drug delivery in oncology. *Cancer Res* 2013;73:2412-7.
- Maeda H. Toward a full understanding of the EPR effect in primary and metastatic tumors as well as issues related to its heterogeneity. *Adv Drug Deliv Rev* 2015;91:3-6.
- Hansen AL, Petersen AL, Henriksen JR, Boerresen B, Rasmussen P, Elmsa DR, et al. Positron emission tomography based elucidation of the enhanced permeability and retention effect in dogs with cancer using copper-64 liposomes. *ACS Nano* 2015;9:6985-95.
- Greish K. Enhanced permeability and retention of macromolecular drugs in solid tumors: a royal gate for targeted anticancer nanomedicines. *J Drug Target* 2007;15:457-64.
- Nehoff H, Parayath NN, Domanovitch L, Tautin S, Greish K. Nanomedicine for drug targeting: strategies beyond the enhanced permeability and retention effect. *Int J Nanomedicine* 2014;9:2539-55.
- Drummond DC, Meyer O, Hong R, Kirpotin DB, Papahadjopoulos D. Optimizing liposomes for delivery of chemotherapeutic agents to solid tumors. *Pharmacol Rev* 1999;51:691-743.
- Beutand N, Wu J, Xu X, Kamaly N, Farokhzad OC. Cancer nanotechnology: the impact of passive and active targeting in the era of modern cancer biology. *Adv Drug Deliv Rev* 2013;66:2-25.
- Kirpotin DB, Drummond DC, Shao Y, Shalaby MR, Hong R, Nielsen DB, et al. Antibody targeting of long-circulating lipidic nanoparticles does not increase tumor localization but does increase internalization in animal models. *Cancer Res* 2006;66:6732-40.
- Reynolds JG, Geretti E, Hendriks BS, Lee H, Leonard SC, Klinz SG, et al. HER2-targeted liposomal doxorubicin displays enhanced anti-tumorigenic effects without associated cardiotoxicity. *Toxicol Appl Pharmacol* 2012;262:1-10.
- Espelin CW, Leonard SC, Geretti E, Wickham TJ, Hendriks BS. Dual HER2 targeting with trastuzumab and liposomal-encapsulated doxorubicin (MM-302) demonstrates synergistic antitumor activity in breast and gastric cancer. *Cancer Res* 2016;76:1517-27.
- Fiorillo KE, Chang EH. Does a targeting ligand influence nanoparticle tumor localization or uptake? *Trends Biotechnol* 2008;26:552-8.
- Hong M, Zhu S, Jiang Y, Tang C, Fei Y. Efficient tumor targeting of hydroxycamptothecin loaded PEGylated liposomes modified with transferrin. *J Control Release* 2009;133:96-102.
- Duskey JT, Rice EG. Nanoparticle ligand presentation for targeting solid tumors. *AAPS PharmSciTech* 2014;15:1345-54.
- Tunggal JK, Cowan DS, Shaikh H, Yarnock H. Penetration of anticancer drugs through solid tissue: a factor that limits the effectiveness of chemotherapy for solid tumors. *Clin Cancer Res* 1999;5:1583-6.
- Hsueh W-A, Kesner AL, Gangloff A, Pegram MD, Beryt M, Czernin J, et al. Predicting chemotherapy response to paclitaxel with 18F-fluoropavidaxel and PET. *J Nucl Med* 2006;47:1995-9.
- Kesner AL, Hsueh W-A, Htet NL, Pio BS, Czernin J, Pegram MD, et al. Biodistribution and predictive value of 18F-fluorocyclophosphamide in mice bearing human breast cancer xenografts. *J Nucl Med* 2007;48:2021-7.
- Schmidt MM, Wittup KD. A modeling analysis of the effects of molecular size and binding affinity on tumor targeting. *Mol Cancer Ther* 2009;8:2861-71.
- Hendriks BS, Reynolds JG, Klinz SG, Geretti E, Lee H, Leonard SC, et al. Multiscale kinetic modeling of liposomal Doxorubicin delivery quantifies the role of tumor and drug-specific parameters in local delivery to tumors. *CPT Pharmacometrics Syst Pharmacol* 2012;1:e15.
- Karathanasis E, Suryanarayanan S, Balusu SK, McNeelley K, Sechopoulos I, Karellas A, et al. Imaging nanoprobe for prediction of outcome of nanoparticle chemotherapy by using mammography. *Radiology* 2009;250:338-406.

22. Pérez-Medina C, Abdel-Ati D, Tang J, Zhao Y, Fayad ZA, Lewis IS, et al. Nanoreporter PET predicts the efficacy of anti-cancer nanotherapy. *Nat Commun* 2016;7:11838.
23. Miller MA, Gadge S, Pfirschke C, Engblom C, Sprachman MM, Kohler RH, et al. Predicting therapeutic nanomedicine efficacy using a companion magnetic resonance imaging nanoparticle. *Sci Transl Med* 2015;7:1-13.
24. Geretti E, Leonard SC, Dumont N, Lee H, Zheng L, De Souza R, et al. Cyclophosphamide-mediated tumor priming for enhanced delivery and antitumor activity of HER2-targeted liposomal doxorubicin (MM-302). *Mol Cancer Ther* 2015;14:2060-71.
25. Lee H, Zheng L, Caddy D, Orcutt KD, Leonard S, Geretti E, et al. A gradient-loadable ^{64}Cu -chelator for quantifying tumor deposition kinetics of nanopiposomal therapeutics by positron emission tomography. *Nanomedicine* 2014;11:155-65.
26. Lorusso P, Krop IE, Miller K, Ma C, Siegel BA, Shields AF, et al. A phase 1 study of MM-302, a HER2-targeted PEGylated liposomal doxorubicin, in patients with HER2-positive metastatic breast cancer (MBC). 2015. Available from: <http://www.merimack.com/sites/default/files/posters/MM-302%20-%20AACR%20presentation%20-%20FINAL%20-%2020APR2015.pdf>.
27. Munster P, Miller K, Krop IE, Dhindsa N, Niyikozo C, Oduyeungbo A, et al. A phase 1 study of MM-302, a HER2-targeted liposomal doxorubicin, in patients with advanced HER2-positive (HER2+) breast cancer. 2012. Available from: <http://www.merimack.com/sites/default/files/posters/MM-302%20Phase%20I%20SABC%202012%20FINAL.pdf>.
28. McAuliffe MJ, Lalonde FM, McGarry D, Gandler W, Csaky K, Tms BL. Medical Image Processing, Analysis and Visualization in clinical research. In: Proceedings of the 14th IEEE Symposium on Computer-Based Medical Systems; 2001 Jul 26-27; Bethesda, MD. New York, NY: IEEE; 2001. p 381-6.
29. Foster DM. Developing and testing integrated multicompartiment models to describe a single-input multiple-output study using the SAAMII software system. *Adv Exp Med Biol* 1998;445:59-78.
30. Stabin MG, Siegel JA. Physical models and dose factors for use in internal dose assessment. *Health Phys* 2003;85:294-310.
31. Stabin MG, Sparks RB, Crowe E. OLINDA/EXM: the second-generation personal computer software for internal dose assessment in nuclear medicine. *J Nucl Med* 2005;46:1023-7.
32. Caddy DE, Lee H, Zheng L, Jaffray DA, Wichham TJ, Hendriks BE. Whole-body organ-level and kidney micro-dosimetric evaluations of ^{64}Cu -loaded HER2/ErbB2-targeted liposomal doxorubicin ^{64}Cu -MM-302 in rodents and primates. *ENMME Res* 2015;5:24.
33. Baxter LJ, Zhu H, Mackensen DG, Butler WF, Jain RK. Biodistribution of monoclonal antibodies: scale-up from mouse to human using a physiologically based pharmacokinetic model. *Cancer Res* 1995;55:4611-22.
34. Gabizon AA, Tzemach D, Mak E, Bronslein M, Horowitz AT. Dose dependency of pharmacokinetics and therapeutic efficacy of pegylated liposomal doxorubicin (DOKIL) in murine models. *J Drug Target* 2002;10:539-48.
35. Jokersi JV, Lobovkina T, Zare RM, Gambhir SS. Nanoparticle PEGylation for imaging and therapy. *Nanomedicine (Lond)* 2011;6:715-28.
36. Detille J-P, Stanez P, Yeh ED, Kopans DB, Garrido L. Breast cancer: regional blood flow and blood volume measured with magnetic susceptibility-based MR imaging—initial results. *Radiology* 2002;223:558-65.
37. Jain RK. Determinants of tumor blood flow: a review. *Cancer Res* 1988;48:2641-58.
38. Bruz C, Bahner ML, Hoffmann U, Horvath A, Schreiber W. Regional blood flow, capillary permeability, and compartmental volumes: measurement with dynamic CT—initial experience. *Radiology* 1999;210:269-76.
39. Maeda H. Macromolecular therapeutics in cancer treatment: the EPR effect and beyond. *J Control Release* 2012;164:138-44.
40. Koukourakis MI, Koukouraki S, Giattomanolaki A, Katsolyris S, Georgoulas V, Velidakis A, et al. High intratumoral accumulation of stealth liposomal doxorubicin in sarcomas—rationale for combination with radiotherapy. *Acta Oncol* 2000;39:207-11.
41. Koukourakis MI, Koukouraki S, Fezoulidis I, Kelekis N, Kyrias G, Archimandritis S, et al. High intratumoral accumulation of stealth liposomal doxorubicin (Caelyx) in glioblastomas and in metastatic brain tumours. *Br J Cancer* 2000;83:1281-6.
42. Arrieta O, Medina LA, Estrada-Lobato E, Hernández-Pedro N, Villanueva-Rodríguez G, Martínez-Barrera L, et al. First-line chemotherapy with liposomal doxorubicin plus cisplatin for patients with advanced malignant pleural mesothelioma: phase II trial. *Br J Cancer* 2012;106:1027-32.
43. Arrieta O, Medina LA, Estrada-Lobato E, Ramírez-Urdo L-A, Mendoza-García V-O, de la Gata-Salazar J. High liposomal doxorubicin tumour tissue distribution, as determined by radiopharmaceutical labelling with ^{99m}Tc -D, is associated with the response and survival of patients with unresectable pleural mesothelioma treated with a combination of liposomal. *Cancer Chemother Pharmacol* 2014;74:211-5.
44. Bae YH, Park K. Targeted drug delivery to tumors: myths, reality and possibility. *J Control Release* 2011;153:198-205.
45. Nichols JW, Bae YH. Odyssey of a cancer nanoparticle: from injection site to site of action. *Nano Today* 2012;7:606-10.
46. Tamura K, Kurihata H, Yonemoto K, Tsuda H, Suzuki I, Kono Y, et al. ^{64}Cu -DOTA-trastuzumab PET imaging in patients with HER2-positive breast cancer. *J Nucl Med* 2013;54:1869-75.
47. Dijkers EC, Oude Munnink TH, Kosterink JG, Brouwers AH, Jager PL, de Jong JR, et al. Biodistribution of ^{89}Zr -trastuzumab and PET imaging of HER2-positive lesions in patients with metastatic breast cancer. *Clin Pharmacol Ther* 2010;87:586-92.
48. Siegel T, Horowitz A, Gabizon AA. Doxorubicin encapsulated in sterically stabilized liposomes for the treatment of a brain tumor model: biodistribution and therapeutic efficacy. *J Neurosurg* 1995;83:1029-37.
49. Lockman PK, Mittapalli RK, Taskat KS, Rudraraju V, Gill B, Bohn KA, et al. Heterogeneous blood-tumor barrier permeability determines drug efficacy in experimental brain metastases of breast cancer. *Clin Cancer Res* 2010;16:5664-78.
50. Sharma GS, Sharma A, Chau B, Straubinger RM. Liposome-mediated therapy of intracranial brain tumors in a rat model. *Pharm Res* 1997;14:922-8.

Clinical Cancer Research

⁶⁴Cu-MM-302 Positron Emission Tomography Quantifies Variability of Enhanced Permeability and Retention of Nanoparticles in Relation to Treatment Response in Patients with Metastatic Breast Cancer

Helen Lee, Anthony F. Shields, Barry A. Siegel, et al.

Clin Cancer Res 2017;23:4190-4202. Published OnlineFirst March 15, 2017.

Updated version	Access the most recent version of this article at: doi:10.1158/1078-0432.CCR-16-3193
Supplementary Material	Access the most recent supplemental material at: http://clincancerres.aacrjournals.org/content/suppl/2017/03/14/1078-0432.CCR-16-3193.DC1

Cited articles	This article cites 47 articles, 15 of which you can access for free at: http://clincancerres.aacrjournals.org/content/23/15/4190.full#ref-list-1
-----------------------	--

E-mail alerts	Sign up to receive free email-alerts related to this article or journal.
Reprints and Subscriptions	To order reprints of this article or to subscribe to the journal, contact the AACR Publications Department at pubs@aacr.org .
Permissions	To request permission to re-use all or part of this article, use this link http://clincancerres.aacrjournals.org/content/23/15/4190 . Click on "Request Permissions" which will take you to the Copyright Clearance Center's (CCC) Rightslink site.



A gradient-loadable ^{64}Cu -chelator for quantifying tumor deposition kinetics of nanoliposomal therapeutics by positron emission tomography

Helen Lee, PhD^{a,*}, Jinzi Zheng, PhD^b, Daniel Gaddy, PhD^a, Kelly D. Orcutt, PhD^c, Shannon Leonard, BS^a, Elena Geretti, PhD^a, Jacob Hesterman, PhD^c, Catey Harwell, SB^c, Jack Hoppin, PhD^c, David A. Jaffray, PhD^b, Thomas Wickham, PhD^a, Bart S. Hendriks, PhD^a, Dmitri Kirpotin, PhD^a

^aMerrimack Pharmaceuticals, Cambridge, MA, USA

^bSTARR Innovation Centre, Radiation Medicine Program, Princess Margaret Hospital, University Health Network, Toronto, ON, Canada

^cinvicRO, LLC, Boston, MA, USA

Received 13 June 2014; accepted 28 August 2014

Abstract

Effective drug delivery to tumors is a barrier to treatment with nanomedicines. Non-invasively tracking liposome biodistribution and tumor deposition in patients may provide insight into identifying patients that are well-suited for liposomal therapies. We describe a novel gradient-loadable chelator, 4-DEAP-ATSC, for incorporating ^{64}Cu into liposomal therapeutics for positron emission tomographic (PET). ^{64}Cu chelated to 4-DEAP-ATSC (>94%) was loaded into PEGylated liposomal doxorubicin (PLD) and HER2-targeted PLD (MM-302) with efficiencies >90%. ^{64}Cu -MM-302 was stable in human plasma for at least 48 h. PET/CT imaging of xenografts injected with ^{64}Cu -MM-302 revealed biodistribution profiles that were quantitatively consistent with tissue-based analysis, and tumor ^{64}Cu positively correlated with liposomal drug deposition. This loading technique transforms liposomal therapeutics into theranostics and is currently being applied in a clinical trial (NCT01304797) to non-invasively quantify MM-302 tumor deposition, and evaluate its potential as a prognostic tool for predicting treatment outcome of nanomedicines.

From the Clinical Editor: This study describes a PET-based detection method utilizing in vivo localization of ^{64}Cu -labeled liposomes. In addition to the presented rodent model, a clinical trial is already underway to investigate the clinical utility of this technique.

© 2015 Elsevier Inc. All rights reserved.

Key words: Liposome; ^{64}Cu ; PET imaging; Tumor deposition; Drug delivery

Effective drug delivery is a necessary condition for therapeutic success. Successful drug delivery to solid tumors is a particular challenge for anti-cancer agents and this barrier increases with increased molecular size from small molecules to

antibodies to nanotherapeutics.¹ For many clinical trials it is never determined whether the drug reaches the intended site of action in sufficient amounts. Preclinical data suggest that poor drug delivery may be a contributing factor in the lack of therapeutic response.^{2,3} With an increasing number of nanotherapeutic agents in clinical development, it is increasingly important to understand their biodistribution. In the clinical setting, non-invasive imaging of radiolabeled drug is the only viable means to study biodistribution.

Tumor deposition of liposomes is dictated by plasma exposure and tumor permeability via the enhanced permeability and retention (EPR) effect.⁴ Tumor permeability to liposomes is largely a function of particle size and surface characteristics. The conjugation of targeting moieties to the liposome generally has little effect on tumor deposition provided that the target is not expressed in the vascular endothelial cells⁵ or ubiquitously

This work was fully funded by Merrimack Pharmaceuticals. Authors affiliated with Merrimack Pharmaceuticals are employees and stock/stock option holders of Merrimack Pharmaceuticals. Jinzi Zheng and David A. Jaffray are collaborators of Merrimack Pharmaceuticals; a portion of the manuscript data was generated under a sponsored research agreement. Authors affiliated with invicRO are involved with Merrimack Pharmaceuticals as a contract research organization; however, data included in this study were generated in a collaborative nature with no compensation.

*Corresponding author at: Merrimack Pharmaceuticals, Inc., Cambridge, MA, USA.

E-mail address: hlee@merrimackpharma.com (H. Lee).

<http://dx.doi.org/10.1016/j.nano.2014.08.011>

1549-9634/© 2015 Elsevier Inc. All rights reserved.

expressed in non-target tissues, and the liposomal surface property is not significantly altered.⁶ The degree to which liposomes can deposit into tumors can also be attributed to the inherent tumor physiology, leading to highly variable deposition. In a clinical study of ¹¹¹In-labeled PEGylated liposomes, Harrington et al used single photon emission computer tomography (SPECT) to quantify liposome deposition in a variety of tumor types. They demonstrated that deposition was highly variable across tumor types and among patients with the same tumor type.⁷

Variability in therapeutic outcome can potentially arise from variable liposome deposition in tumors. This concept is supported by computational modeling, which indicates that liposomal deposition in tumors is a rate-limiting step for drug delivery to cells.⁸ Furthermore, Karathanasis et al have shown in a rat xenograft model that tumor deposition of a liposomal computed tomography (CT) contrast agent correlated with treatment outcome to a liposomal drug.⁹

Radiolabeled liposomes allow for direct quantification of tumor deposition and distribution to other tissues *in vivo* using nuclear imaging modalities such as positron emission tomography (PET) or SPECT. There have been multiple clinical studies using ^{99m}Tc- or ¹¹¹In-labeled liposomes in cancer patients for SPECT or gamma-camera imaging,^{7,10} mostly focused on lesion detection in oncology or inflammation. In the clinical setting, PET imaging of liposomes can offer improved sensitivity relative to SPECT, as well as increased quantification and anatomical accuracy, when combined with CT.

A variety of methods have been employed for labeling liposomes with longer-lived positron emitting isotopes such as ⁸⁹Zr ($t_{1/2} = 78.4$ h)¹¹ or ⁶⁴Cu ($t_{1/2} = 12.7$ h).^{12,13} Conjugating chelators such as DOTA or TETA to the liposome surface allows rapid radiolabeling of pre-formed liposomes.^{14,15} However, such systems are prone to instability *in vivo* due to potential transchelation of radioisotopes to plasma proteins. Petersen et al reported a DOTA-loaded liposome system with ⁶⁴Cu incorporated within the liposomal core via remote loading to enhance *in vivo* stability. 2-hydroxyquinoline was used to shuttle ⁶⁴Cu across the liposomal membrane, and the ⁶⁴Cu was then transchelated to pre-encapsulated DOTA.¹³ This remotely-loaded ⁶⁴Cu-DOTA-liposome system provides a stable means to radiolabel liposomes; however, it does not have the flexibility of labeling existing liposomal therapeutics as passive encapsulation of DOTA is required. While liposomes have also been labeled with ¹⁸F,¹⁶ the short half-life of ¹⁸F ($t_{1/2} = 110$ min) is poorly suited for the comparatively long time scale required for imaging tumor deposition of liposomes.

It is highly desirable to have a method suitable for labeling existing therapeutics for PET imaging rather than require *de novo* synthesis of the radiolabeled drug for imaging. Herein we describe such a method for stably labeling liposomal therapeutics with ⁶⁴Cu for PET. A novel chelator compound, 4-DEAP-ATSC, was synthesized to serve as the ⁶⁴Cu loading and entrapment agent. We demonstrate that ⁶⁴Cu:4-DEAP-ATSC was loaded into PEGylated liposomal doxorubicin (PLD, or Doxil®) and MM-302 (HER2-targeted PLD,¹⁷ currently in Phase I clinical development, NCT01304797). We have characterized the above ⁶⁴Cu-liposomes and showed that this

⁶⁴Cu-labeling method readily converts these liposomal therapeutics into PET agents for clinical use. This ⁶⁴Cu-labeling technique enables better understanding of the deposition kinetics of liposomal therapeutics in human tumors, providing valuable insights for nanomedicine development.

Methods

Materials

⁶⁴CuCl₂ was obtained from Mallinckrodt Institute of Radiology (Washington University; St. Louis, MO). Acetic acid, methanol, and acetonitrile were from EMD Chemicals Inc. (Gibbstown, NJ). PLD (Doxil®; Janssen Products; Titusville, NJ) was obtained from a pharmacy. HEPES was purchased from EMD (Philadelphia, PA). All other materials were obtained from Sigma (St. Louis, MO) unless otherwise noted.

Synthesis of 4-DEAP-ATSC

Diacetyl 4,4'-bis(3-(N,N-diethylamino)propyl)thiosemicarbazone (4-DEAP-ATSC) was synthesized in two steps from 2,3-butanedione (diacetyl), hydrazine hydrate, and 3-(N,N-diethylaminopropyl)isothiocyanate as shown in Figure 1. The identity of the product was confirmed by ¹H-NMR, mass spectrometry, and elemental analysis. The detailed synthetic protocol and analytical data are given in Supplemental Material.

Characterization of 4-DEAP-ATSC copper complex

The stoichiometry and binding constant of Cu²⁺:4-DEAP-ATSC complex were determined by spectrophotometry according to the method of Job.¹⁸ The formation constant of Cu²⁺:4-DEAP-ATSC was determined using the DTPA displacement method (Supplemental Figure S3). The data were plotted using the following equation:

$$\frac{(M_0 - ML)(L_0 - ML)}{ML} = \frac{1}{K_L} + \frac{K_Y Y_0}{K_L} \quad (1)$$

where M₀ and L₀ are overall concentrations of Cu²⁺ and 4-DEAP-ATSC, respectively; ML is the concentration of the Cu:4-DEAP-ATSC complex; Y₀ is the DTPA concentration in excess to both M₀ and L₀. K_Y and K_L are apparent formation constants of the Cu:DTPA and Cu:DEAP-ATSC complexes, respectively, under the experimental conditions. The value of K_Y for Cu:DTPA (log K_Y = 18.09) was calculated from published report.¹⁹ The value of K_L was calculated from K_Y and the slope of the linear plot above.

Liposome preparation

MM-302, was prepared as previously described.^{6,17} MM-302 is composed of HSPC:cholesterol:PEG-DSPE (3:2:0.3 mol ratio) with ammonium sulfate as the gradient-forming agent for loading doxorubicin. The anti-HER2 scFv F5-PEG-DSPE immunoconjugate was subsequently inserted into the doxorubicin-loaded liposomes. Details on the production of anti-HER2 scFv F5-PEG-DSPE immunoconjugate and insertion into liposomes were described elsewhere.^{20,21}

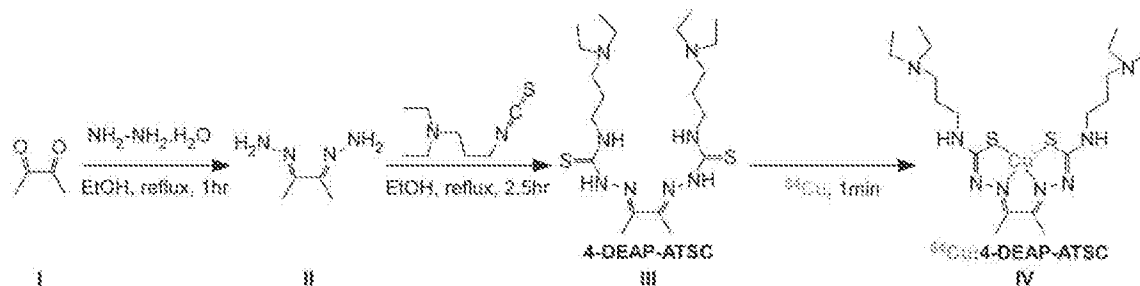


Figure 1. Synthesis of 4-DEAP-ATSC and formation of ^{64}Cu :4-DEAP-ATSC complex.

Chelation of ^{64}Cu to 4-DEAP-ATSC and loading into liposomes

4-DEAP-ATSC was dissolved in 0.05 M citric acid at 10 mg/mL and was subsequently diluted in 0.1 M citrate buffer (pH 6). ^{64}Cu was added to the 4-DEAP-ATSC solution and incubated for 1 min; chelation efficiency was then determined using instant thin layer chromatography developed in 0.1 M citrate buffer (pH 6). ^{64}Cu travels with the solvent front, while the ^{64}Cu :4-DEAP-ATSC complex remains at the sample origin. Chelation efficiency was calculated as follows:

$$\text{Chelation Efficiency} = \frac{\text{Radioactivity}_{\text{TopFraction}}}{\text{Radioactivity}_{\text{TopFraction}} + \text{Radioactivity}_{\text{BottomFraction}}} \times 100\% \quad (2)$$

For loading into liposomes, ^{64}Cu :4-DEAP-ATSC was mixed with the liposome solution, heated for 10 min at 65 °C, followed by cooling in an ice water bath.

^{64}Cu loading efficiency was determined by size exclusion chromatography (SEC) on an Illustra NICK column (GE Healthcare, Pittsburgh, PA) equilibrated with HBS (pH 6.5). The liposome fraction was eluted with 1 mL of HBS, while unloaded ^{64}Cu and ^{64}Cu :4-DEAP-ATSC remained in the column. Loading efficiency was calculated as follows:

$$\text{Loading Efficiency} = \frac{\text{Radioactivity}_{\text{elutedLiposomeFraction}}}{\text{Radioactivity}_{\text{elutedLiposomeFraction}} + \text{Radioactivity}_{\text{Column}}} \times 100\% \quad (3)$$

Separation of liposomal-bound, protein-bound, or released ^{64}Cu

SEC (Sephacose CL-4B resin) was used to separate liposomal ^{64}Cu from free ^{64}Cu and ^{64}Cu :4-DEAP-ATSC. Liposome and protein elution profiles were pre-determined by spectrophotometry. For evaluation of *in vitro* stability, ^{64}Cu -MM-302 liposomes were mixed with human plasma and incubated at 37 °C. At designated times, 50 μL aliquots were loaded onto the Sephacose CL-4B column and fractions were collected for radioactivity quantification. *In vivo* stability was evaluated in CD-1 mice following tail vein injection of ^{64}Cu -MM-302; blood samples were collected at designated times and 100 μL of serum was applied to the columns.

Animal studies

Pharmacokinetics and *in vivo* stability studies were performed in immunocompetent CD-1 mice (Charles River; Wilmington, MA).

Tumor studies were performed in BT474-M3 (HER2-overexpressing breast carcinoma) xenografts. BT474-M3 cells were cultured in RPMI1640 media supplemented with 10% FBS and 1% penicillin/streptomycin maintained at 37 °C in 5% CO_2 . Two days prior to tumor inoculation, estrogen pellets (0.72 mg at 60-day release rate, Innovative Research of America; Sarasota, FL) were implanted subcutaneously. BT474-M3 (15×10^6) cells were inoculated into the right mammary fat pad. Studies were initiated when tumors reached an average volume of approximately 250 mm^3 . All animal work followed guidelines approved by the University Health Network's Animal Care Committee, the Animal Welfare Act (AWA), and Animal Welfare Regulations (AWR).

Pharmacokinetics and biodistribution studies

^{64}Cu -compounds were administered intravenously in the tail vein (4.5 MBq/mouse, 20 μmol phospholipid/kg). Blood samples were collected via saphenous vein puncture at designated time points. Plasma ^{64}Cu was quantified via gamma-counting. Doxorubicin (liposome drug) was extracted from ^{64}Cu -MM-302 plasma samples for HPLC analysis as previously described.¹⁷ Pharmacokinetic parameters were computed using non-compartmental analysis.

For biodistribution studies, mice were perfused with PBS prior to organ excision, except for those used for studying correlation with PET/CT regions of interest (ROI) analysis. Organs were collected at 24 h post-injection, and radioactivity in each organ was measured via gamma-counting.

PET/CT imaging

Mice were injected with ^{64}Cu -compounds intravenously in the tail vein (10–13 MBq/mouse, 20 μmol lipid/kg). For image acquisition, mice were anesthetized using 2% inhaled isoflurane. PET images were acquired on a Focus 220 microPET (Siemens; Malvern, PA). At the center field of view, the nominal acquisition resolution was 1.4 mm. PET acquisition times for 5 min, 1, 5, and 20 h post-injection were 10, 15, 20, and 45 min, respectively. Data were reconstructed using a maximum a posteriori algorithm with voxel size of $0.146 \times 0.146 \times 0.796 \text{ mm}^3$. Anatomical CT scans were obtained on a Locus Ultra microCT scanner (GE Healthcare; Pittsburgh, PA) operated at 80 kVp and 50 mA. The CT images were reconstructed with an isotropic voxel size of 0.154 mm.

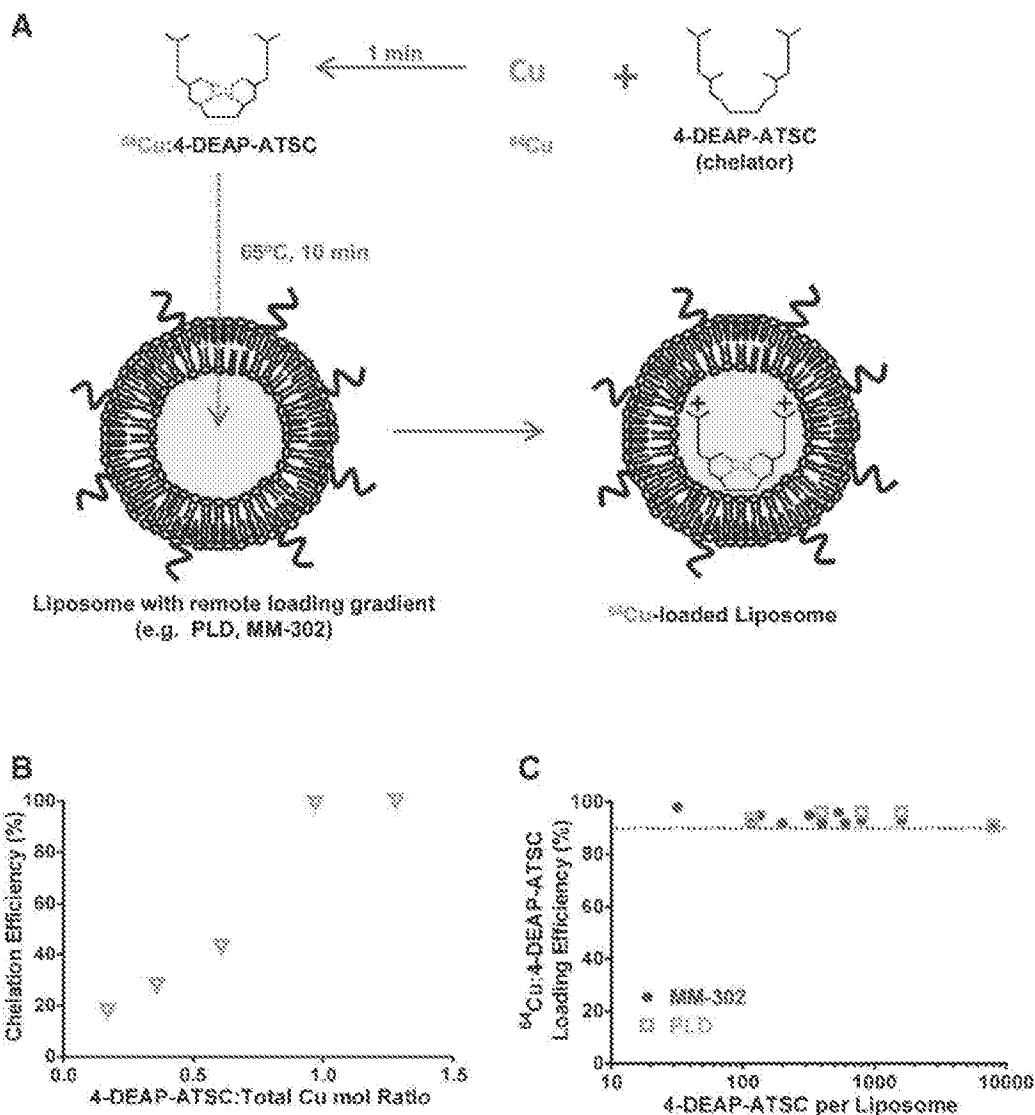


Figure 2. ^{64}Cu :4-DEAP-ATSC chelation and loading into liposomes. (A) Schematic depicting remote loading of ^{64}Cu into liposomes using the novel gradient-loadable chelator 4-DEAP-ATSC. (B) Chelation efficiency of ^{64}Cu :4-DEAP-ATSC at various chelator-to-total copper ratios by titrating increasing amount of cold CuCl_2 . (C) Loading efficiencies of ^{64}Cu :4-DEAP-ATSC complexes into MM-302 and PLD (Doxil[®]) at various chelator:liposome ratios.

PET/CT image registration and analysis

PET/CT images were registered using the Inveon Research Workplace software (Siemens; Malvern, PA). ROIs were drawn manually on PET/CT slices in each tissue of interest. A linear interpolation algorithm was applied to connect the ROIs to generate tissue volumes for quantification. The CT dataset was used to generate contours in regions with low PET signal and where known partial volume effect exists.

Tracer kinetic modeling using PET/CT data

The time course of ^{64}Cu signal in the tumor tissue was described with a physiologically-based model, with details provided in the Supplemental Material. The rate of ^{64}Cu transport between the tumor vascular and tissue space is described by deposition (k_1) and washout (k_{-1}) rates. Both

parameters implicitly incorporate the permeability-surface area products and reflect the net transport rates.

The ^{64}Cu tracer kinetic model equations are below:

$$\frac{dC_{\text{blood}}}{dt} = -k_0 C_{\text{blood}} \quad (4)$$

$$\frac{dC_{\text{cap}}}{dt} = Q C_{\text{blood}} - k_1 C_{\text{cap}} + k_{-1} C_{\text{int}} - \frac{Q}{VVF} C_{\text{cap}} \quad (5)$$

$$\frac{dC_{\text{int}}}{dt} = k_1 C_{\text{cap}} - k_{-1} C_{\text{int}} \quad (6)$$

where C_{blood} , C_{cap} and C_{int} are ^{64}Cu concentrations in the arterial blood, tumor capillary, and tumor interstitial compartments. C_{cap} and C_{int} are defined on a per tumor volume basis. Q is the blood flow rate through tumor tissue, and VVF is the tumor vascular

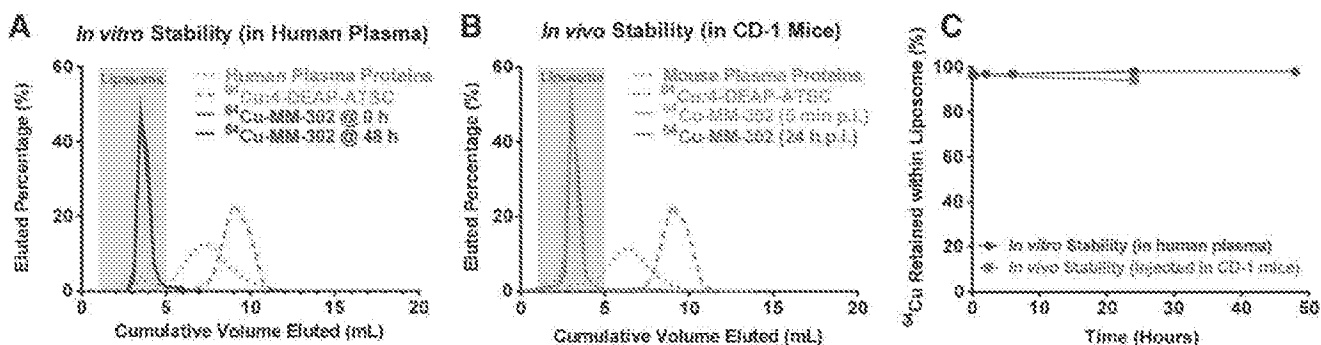


Figure 3. *In vitro* and *in vivo* stability of ⁶⁴Cu-MM-302. Size exclusion chromatography (Sephacrose CL4B) was used to separate liposomal ⁶⁴Cu, protein-bound ⁶⁴Cu (elute with plasma/serum protein), or ⁶⁴Cu:4-DEAP-ATSC complex. Elution profiles of ⁶⁴Cu-MM-302 in (A) human plasma following incubation at 37 °C, and (B) serum from mice injected intravenously with ⁶⁴Cu-MM-302; ⁶⁴Cu-MM-302 elution profiles were overlaid onto elution profiles of human plasma proteins and ⁶⁴Cu:4-DEAP-ATSC complex. (C) Percentage of ⁶⁴Cu remaining in the liposomes at designated stability time points. All data are decay corrected.

volume fraction (tumor-to-blood ratio) calculated assuming all activity in the tumor at 5 min is in the tumor capillaries.

Results

Synthesis and characterization of 4-DEAP-ATSC and its Cu(II) complex

The liposome-loadable Cu chelator 4-DEAP-ATSC was obtained by the reaction of diacetyl-bis-hydrazone with N,N-diethylaminopropyl isothiocyanate (DEAPITC) as suggested by Hoechst et al,²² except that in order to obtain a symmetric, bi-substituted product, two equivalents of DEAPITC were used. The structure of the product was confirmed by ¹H-NMR, mass spectrometry, and elemental analysis (Supplemental Material), and additionally with ¹³C-NMR and FTIR (data not shown). Upon addition of a copper(II) salt to a colorless solution of DEAP-ATSC, a yellow-brown solution was formed. Unlike copper(II) complexes of ATSM and quinoline-based chelators, Cu:4-DEAP-ATSC complex remained in solution even at relatively high concentrations (several mM). Spectrophotometric titration of 4-DEAP-ATSC with CuSO₄ showed a peak of the chelator at 327 nm, and an emerging peak of the complex at 455 nm ($\epsilon = 7.7 \times 10^3 \text{ M}^{-1} \text{ cm}^{-1}$), with an isosbestic point at 355 nm (Supplemental Figure S1). The binding stoichiometry of the Cu:4-DEAP-ATSC complex was found to be 1:1 (Supplemental Figure S2). The effective pK for association of Cu(II) with 4-DEAP-ATSC at pH 6.5 determined by competition with a known Cu(II) chelator DTPA was 21.1 (Supplemental Figure S3), which is higher than that for polyaminopolycarboxylic acid chelators under the same conditions. Bivalent metals other than Cu(II), such as cobalt, nickel, zinc, iron(II), as well as trivalent In(III) and monovalent Ag(I), also formed complexes with 4-DEAP-ATSC, as detected by the change of color and the shift in visible light absorbance spectra upon mixing of 4-DEAP-ATSC solution with the salts of these cations in HEPES-buffered physiological saline (data not shown). Thus, 4-DEAP-ATSC may be useful for complexation and liposome loading of metals other than Cu(II).

Loading of ⁶⁴Cu:4-DEAP-ATSC into drug-loaded liposomes

Figure 2, A schematically illustrates the process of chelating ⁶⁴Cu to 4-DEAP-ATSC and loading into liposomes. Formation of the ⁶⁴Cu:4-DEAP-ATSC complex was accomplished upon mixing at room temperature. Chelation efficiency of 94–98% was achieved at a specific activity of 2.5–15 MBq/μmol of 4-DEAP-ATSC. Chelation efficiency of >90% was achieved at a 4-DEAP-ATSC-to-Cu_{total} molar ratio of >1.03 (Figure 2, B), which agrees with the aforementioned binding stoichiometry results.

Loading of ⁶⁴Cu:4-DEAP-ATSC was tested in two liposomes with drugs pre-loaded by a transmembrane gradient: PLD and MM-302. Heating liposomes above the lipid bilayer phase transition temperature facilitates transmembrane transport of unprotonated 4-DEAP-ATSC, which becomes protonated within the liposome and remains entrapped (Figure 2, A). Loading efficiencies greater than 90%, reflecting up to 10,000 chelator molecules per liposome, were achieved with each liposomal therapeutic tested (Figure 2, C). The amount of doxorubicin that leaked from the liposomes following ⁶⁴Cu:4-DEAP-ATSC loading was 2% ± 4% and 1% ± 6% for PLD and MM-302, respectively. Extensive characterization (e.g. particle size, drug purity, phospholipid concentration, etc.) was also performed with ⁶⁴Cu-MM-302 to demonstrate that ⁶⁴Cu:4-DEAP-ATSC loading did not alter the physico-chemical properties of MM-302 (Supplemental Table S1).

In vitro and *in vivo* stability of ⁶⁴Cu-MM-302

Figure 3, A and B shows the representative SEC elution profiles of ⁶⁴Cu-MM-302 after incubation in human plasma at 37 °C and injection into CD-1 immunocompetent mice, respectively. Sepharose SEC was used to detect released ⁶⁴Cu or ⁶⁴Cu:4-DEAP-ATSC in human plasma or in circulation *in vivo* (expected elution from column after liposomal fraction). The MM-302 liposomes retained >99% and >94% of ⁶⁴Cu under physiologically relevant *in vitro* conditions (up to 48 h at 37 °C) and up to 24 h *in vivo*, respectively, with minimal binding or transchelation to protein components in plasma/serum (Figure 3, C).

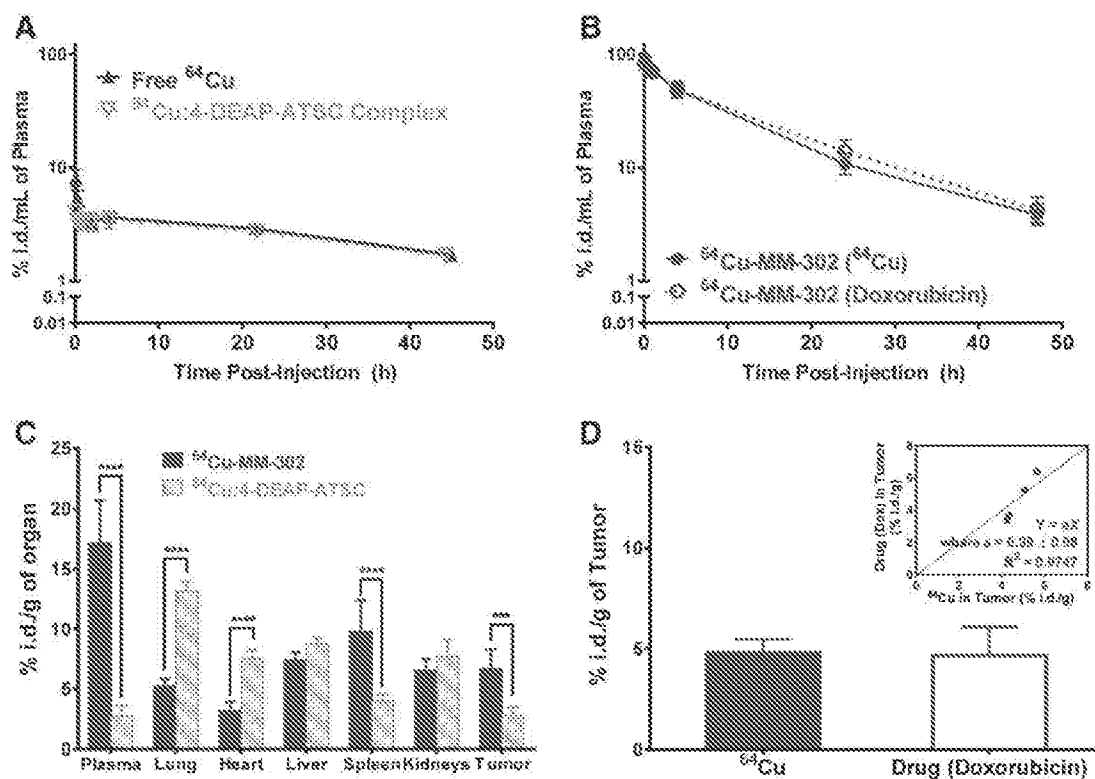


Figure 4. *In vivo* pharmacokinetics and biodistribution. Plasma levels of (A) free ^{64}Cu and ^{64}Cu :4-DEAP-ATSC, and (B) ^{64}Cu -MM-302 (drug and ^{64}Cu components) in CD-1 immunocompetent mice following intravenous injection. (C) Biodistribution (24 h post-injection) of ^{64}Cu -MM-302 and ^{64}Cu :4-DEAP-ATSC in BT474-M3 mammary carcinoma xenografts. (D) BT474-M3 tumor deposition of ^{64}Cu and the liposomal drug (doxorubicin). Inset illustrates correlation of ^{64}Cu and liposomal drug levels in individual tumors. All data are decay corrected.

Pharmacokinetics, biodistribution, and tumor deposition of ^{64}Cu -MM-302 and ^{64}Cu :4-DEAP-ATSC

In vivo stability was also evaluated in mice by comparing the pharmacokinetic profiles of free ^{64}Cu and ^{64}Cu :4-DEAP-ATSC complex (Figure 4, A, Table 1), ^{64}Cu -MM-302 and its drug contents (doxorubicin; Figure 4, B). The use of doxorubicin as a surrogate for liposomal doxorubicin is well-accepted as doxorubicin release from liposome is minimal *in vivo*.²³ Free ^{64}Cu and ^{64}Cu :4-DEAP-ATSC were cleared quickly from the bloodstream and distributed extensively into other tissues with prolonged elimination phases. In contrast, ^{64}Cu -MM-302 remained in circulation for a prolonged period, with a pharmacokinetic profile typical of other PEGylated liposomes. The ^{64}Cu and doxorubicin components of ^{64}Cu -MM-302 yielded comparable pharmacokinetic parameters (Table 1). The ^{64}Cu -to-doxorubicin ratios in plasma remained close to 1, indicating that ^{64}Cu was stably retained within MM-302 for at least 48 h *in vivo*.

Biodistribution of ^{64}Cu :4-DEAP-ATSC and ^{64}Cu -MM-302 (Figure 4, C) was investigated in BT474-M3 mammary tumor-bearing mice. Liver and spleen were the major uptake organs for ^{64}Cu -MM-302 at 24 h post-injection, consistent with tissue-based analyses of their drug contents.^{24,25} ^{64}Cu :4-DEAP-ATSC showed similar liver and kidney uptake as ^{64}Cu -MM-302, with distinct uptake profiles in other organs investigated. The tumor uptake (Figure 4, D) of ^{64}Cu and doxorubicin was comparable

(4.8 ± 0.7 %i.d./g and 4.7 ± 1 %i.d./g, $P = 0.86$). The deposition of ^{64}Cu also correlated with doxorubicin in individual tumors (Figure 4, D inset; $R^2 = 0.9747$, Pearson correlation).

PET/CT imaging of ^{64}Cu -loaded liposomes and ^{64}Cu :4-DEAP-ATSC in xenografts

Figure 5, A and B shows the PET/CT images of BT474-M3 tumor-bearing mice injected with ^{64}Cu -MM-302 or ^{64}Cu :4-DEAP-ATSC, respectively. At 5 min post-injection, the PET signal was almost exclusively confined in the blood pool for ^{64}Cu -MM-302. At later time points, ^{64}Cu -MM-302 was observed in the tumor, liver and spleen. The ^{64}Cu :4-DEAP-ATSC complex primarily accumulated in the liver, while splenic uptake was not significant. Moreover, the complex was rapidly cleared from circulation and tumor deposition was minimal. The presence of ^{64}Cu signal in the kidneys within 1 h of injection suggests renal clearance. The tumor-to-muscle ratios (Figure 5, C) for ^{64}Cu -MM-302 were 6.3 ± 2 and 7.1 ± 3 at 5 and 20 h post-injection, respectively, compared to 2.8 ± 1 and 2.3 ± 0.3 for ^{64}Cu :4-DEAP-ATSC ($P = 0.0018$ for 5 h, and $P = 0.0009$ for 20 h). Figure 5, D demonstrates the correlation between tumor uptake of ^{64}Cu -agents measured via PET/CT image-based and tissue-based analyses. Linear regression of PET versus gamma-counting indicated a slope of 0.96 ± 0.05 ($R^2 = 0.9854$), suggesting that the PET quantification correlates well with *ex vivo* quantification of tumor ^{64}Cu content.

Table 1
Pharmacokinetic parameters of ^{64}Cu , ^{64}Cu :4-DEAP-ATSC, and ^{64}Cu :MM-302 obtained by non-compartmental analysis.

Compound	Pharmacokinetic parameters			
	$t_{1/2, \text{terminal}}$ (h)	AUC (%L.D. · h/mL)	CL (mL/h)	V_{00} (mL)
Free ^{64}Cu	37 ± 5	220 ± 30	0.47 ± 0.05	25 ± 2
^{64}Cu :4-DEAP-ATSC	41 ± 8	219 ± 3	0.46 ± 0.01	27 ± 5
^{64}Cu :MM-302(^{64}Cu)	11.3 ± 0.8	1000 ± 200	0.10 ± 0.02	1.7 ± 0.2
^{64}Cu :MM-302(Dox)	12.2 ± 0.8	1000 ± 200	0.10 ± 0.02	1.6 ± 0.2

Kinetic modeling of tumor deposition

The ^{64}Cu signal visualized in the PET images is composed of ^{64}Cu deposited in the tissue and circulating in the vasculature. Since we hypothesize that only the tissue-deposited liposomes are likely to have anti-tumor activity, it is important to understand the fraction of the PET signal reflecting extravasated liposomes. The average VVF for the BT474-M3 tumors was $5.25 \pm 1.41\%$ as determined from the PET images. This value was consistent with histological analysis of the BT474-M3 tumors (CD-31 staining) in which the average blood vessel area/tumor area was 4–6% (data not shown). PET/CT imaging data obtained from mice injected with ^{64}Cu :MM-302 were fit to a kinetic model shown in Figure 6, A, and used to estimate the tumor interstitial and vascular components on a voxel-by-voxel basis (Figure 6, B). At 5 h post-injection, there was a significant contribution of vascular ^{64}Cu signal to the overall tumor signal (tissue signal = 19%). By 20 h post-injection, the tumor ^{64}Cu signal was almost exclusively from deposited liposomes (94%).

Table 2 summarizes the liposome transport kinetics parameters obtained from fitting PET/CT imaging data to the kinetic model. The $t_{1/2, \text{terminal}}$ and V_0 (whole blood) for ^{64}Cu :MM-302 obtained from the PET/CT images were 10.7 ± 0.7 h and 1.9 ± 0.3 mL (corrected for 60% hematocrit), respectively. These numbers were comparable to those obtained via plasma collection (Table 1), with no statistically significant difference ($P = 0.16$ and $P = 0.27$ for $t_{1/2, \text{terminal}}$ and V_0 , respectively). The ^{64}Cu :MM-302 voxel-by-voxel deposition (k_1) and washout (k_{-1}) parameter values were mapped spatially onto the tumors, shown in Figure 6, C.

Discussion

The potential importance of tumor deposition as a prognostic/treatment-planning factor for nanomedicines prompted us to develop a diagnostic imaging approach that would accurately, quantitatively, and non-invasively predict the accumulation of nanotherapeutics in patient tumors. In this work, we report a novel ^{64}Cu -liposome labeling method and the characterization of its ability to label clinically available liposomal anti-cancer therapies for PET/CT imaging. The optimized protocol described herein is fast (<2 h), simple, and can be translated to clinical studies with commercially available liposomal drugs (e.g. Doxil®). Importantly, the process was demonstrated to be efficient (>90%), obviating the need for any post-labeling purification.

Radiolabeling can be affected by the quality of radioisotope production (e.g. radionuclidic purity, specific activity of ^{64}Cu).

The 4-DEAP-ATSC labeling method is designed to accommodate the batch-to-batch variability of ^{64}Cu specific activities by incorporating an excess amount of chelator. For preclinical experiments, approximately an 8-fold excess of chelator was used. The ^{64}Cu -labeling method using 4-DEAP-ATSC presents the opportunity to utilize liposomal therapeutics as translational tools for studying *in vivo* distribution and transport kinetics, without the need for a complete *de novo* radio-synthesis of the encapsulated drug molecules.

The mechanism of 4-DEAP-ATSC loading into the liposome is believed to be conceptually similar to the doxorubicin loading process for PLD production.^{23,26} During the ^{64}Cu loading process, the tertiary amine groups of the ^{64}Cu :4-DEAP-ATSC complex become protonated after crossing the liposomal membrane and remain stably entrapped within the liposome. We have demonstrated that 4-DEAP-ATSC can be loaded into liposomes that are pre-loaded with drug molecules (PLD and MM-302), potentially utilizing the residual electrochemical gradients to form the stable ^{64}Cu -liposome imaging agents. This versatile radiolabeling approach is distinct from previously reported radiolabeled liposomes that involve pre-encapsulation of trans-chelating agents via passive loading, combined with the use of a shuttling agent such as 2-hydroxyquinoline.^{13,27} It is also distinct from the methods that involve modification of the liposome surface with copper-binding chelators,²⁸ which may influence the liposome uptake by tumor and other tissues. In addition, compared to the N,N-bis(2-mercaptoethyl)-N',N'-diethylethylenediamine system for loading $^{99\text{m}}\text{Tc}$ into PLD,²⁹ the 4-DEAP-ATSC ^{64}Cu -loading system has superior radioisotope loading efficiency and *in vivo* stability. Using the 4-DEAP-ATSC loading method, ^{64}Cu was shown to be stably encapsulated in MM-302, with the ^{64}Cu signal closely resembling the *in vivo* distribution of its encapsulated doxorubicin (Figure 4).

Due to the physical half-life of ^{64}Cu , clinical PET imaging of ^{64}Cu -agents is feasible up to 48 h post-injection while maintaining acceptable image quality and radiation dosimetry. Preclinically, tumor deposition of ^{64}Cu :MM-302 in xenografts was measured up to 20 h post-injection via PET imaging. One would expect minimal contribution from the vascular ^{64}Cu signal as the circulation half-life of ^{64}Cu :MM-302 is shorter than 12 h in mice. In humans, the half-life of PEGylated liposomes such as PLD and MM-302 is significantly longer (35–80 h).³⁰ Consequently, PET imaging of ^{64}Cu -labeled liposomes in humans up to 48 h post-injection may reveal tumor images that consist of more significant contribution from vascular signals. Here, we demonstrated the estimation of interstitial and vascular

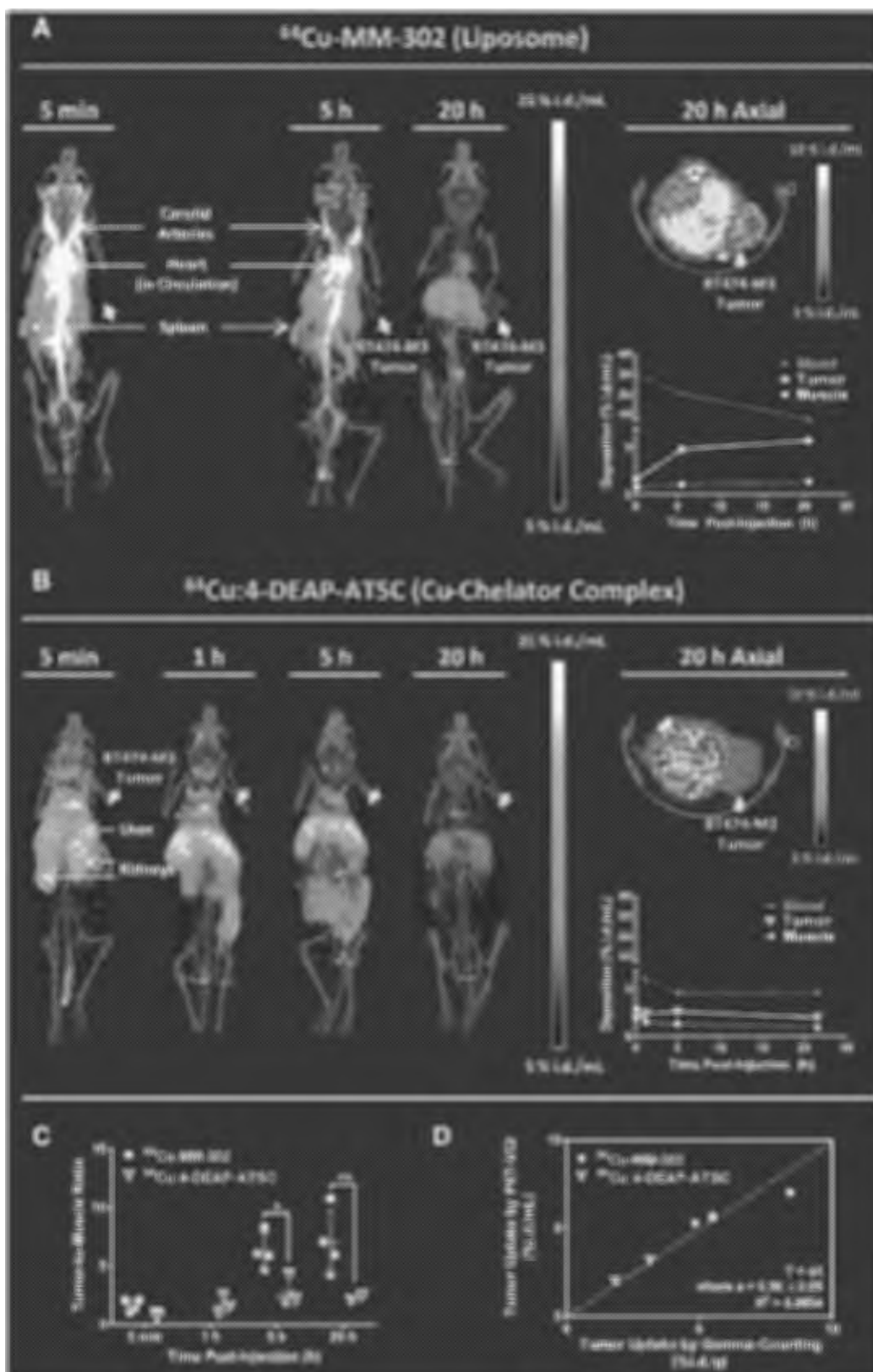


Figure 5. Maximum intensity projection (MIP) PET/CT or axial images of mice bearing BT474-M3 mammary tumors injected with (A) ⁶⁴Cu-MM-302, or (B) ⁶⁴Cu-4-DEAP-ATSC complex. The tumors are indicated with blue or brown arrows. Tumor uptake kinetics of the ⁶⁴Cu-labeled agents obtained via image-based analysis is shown on the right panel beside the corresponding images. (C) Tumor-to-muscle ratios of ⁶⁴Cu-4-DEAP-ATSC and ⁶⁴Cu-MM-302 in BT474-M3 tumors at different imaging time. At the end of image acquisition, organs were excised for quantification of ⁶⁴Cu accumulation using a gamma-counter. (D) Correlation of tumor uptake analyzed by PET/CT imaging and *ex vivo* tissue gamma-counting. All data and images are decay corrected.

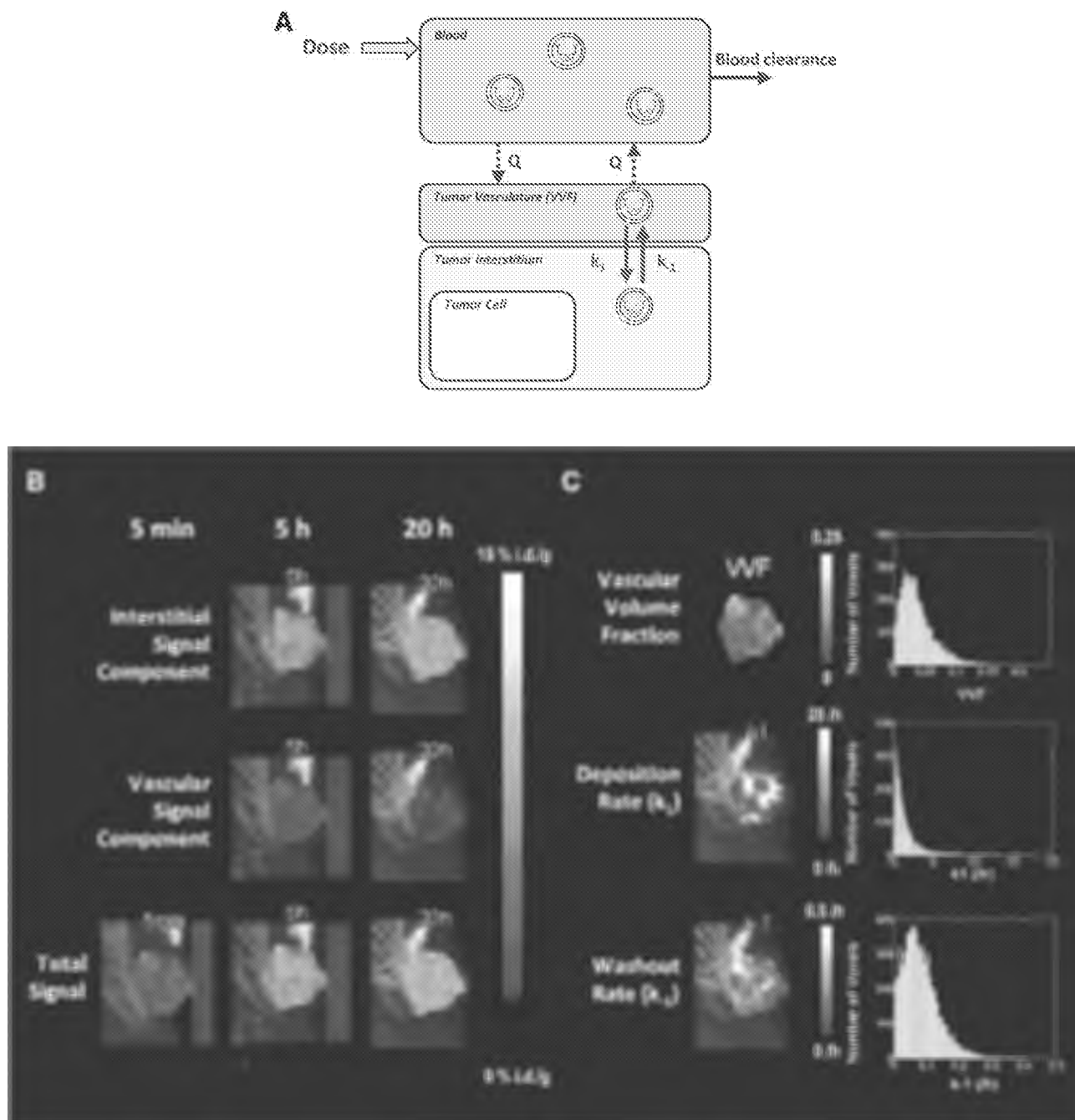


Figure 6. Tumor PK model analysis from images shown in Figure 5, A. (A) Schematic diagram of PK model. The liposomes are injected intravenously into the blood compartment and undergo blood clearance, blood flow (Q), tumor deposition (k_1), and washout (k_{-1}). (B) 3D maps of tumors interstitial and vascular components, and total ^{64}Cu signal displayed to a maximum voxel value of 15 % i.d./g. The CT images are displayed in grayscale. (C) PET data were fit voxel-wise to the model. 3D maps (MIPs) and histograms of voxel-by-voxel VVF, k_1 , and k_{-1} , scaled to a maximum voxel value of 0.25, 20 h^{-1} , and 0.5 h^{-1} , respectively. Voxels where the model did not successfully fit the data (i.e. one or more parameters hit the upper or lower bound) were excluded in the histograms.

signals in tumors, on a voxel-by-voxel basis (Figure 6, B). Estimation of interstitial ^{64}Cu -liposome signal from PET images may provide a more accurate means to assess tumor drug delivery. Using a tracer kinetic model, differential rates of liposome deposition and washout within or across lesions provide additional means to functionally characterize tumor properties. The ^{64}Cu -MM-302 deposition rates for the tumor voxels (median of $\text{VVF} \cdot k_1 = 0.0248/\text{h}$, Figure 6, C) are comparable to the

previously reported PLD k_1 values (defined on a per compartment basis, physiologically relevant range of 0.005–0.033/h in xenografts),⁸ suggesting that PET imaging of ^{64}Cu -liposomes may serve as a reliable non-invasive tool for studying transport kinetics of liposomal drugs, providing that the encapsulated drugs and ^{64}Cu have similar release rates *in vivo*.

Similar modeling techniques have been used with dynamic contrast enhanced magnetic resonance imaging for estimating

Table 2

Blood pharmacokinetic parameters and tumor-averaged VVF estimated from PET/CT images of mice injected with ^{64}Cu -MM-302.

Subject	Pharmacokinetic parameters			
	k_0 (h)	$t_{1/2, \text{terminal}}$ (h)	V_0 (mL)	VVF _{tumor}
MOU#1 (Figure 5, A)	0.071	9.9	3.0	4.0%
MOU#2	0.058	11.9	3.3	5.8%
MOU#3	0.065	10.7	3.6	7.9%
MOU#4	0.067	10.3	2.6	4.2%

tumor vascular permeability for small molecules and macromolecules. Nonetheless, the modeling approach has some limitations. This simplified model assumes that ^{64}Cu release from the liposomes is negligible over the imaging time scale. Release of ^{64}Cu from the liposomes in the tumor interstitium and tumor cells may occur and affect the *in vivo* tracking of ^{64}Cu -liposomes, which were not considered in this model. This assumption is considered valid in the case of ^{64}Cu -MM-302 as substantiated by its *in vivo* stability as shown in Figure 3. The voxel-by-voxel analysis is sensitive to the ability to accurately register images across time points and assumes that there is no significant change in tumor shape over the timescale of imaging. In addition, k_1 and k_{-1} mapping is more prone to errors at the tissue-air interface as a result of image-registration errors, although we have attempted to minimize such errors by eroding two-voxel layers at the outer boundaries of the tumor ROIs. Lastly, the model also assumes that blood flow rate is not limiting to each tumor voxel. This is supported by previous work suggesting that typical time scales for liposome deposition are longer than typical blood flow rates.⁸ It is possible, however, that local regions may be limited by blood flow rather than permeability and the current model is not able to make this distinction.

PET/CT images of ^{64}Cu -MM-302 show heterogeneous distribution within tumors, consistent with previously published studies.³¹ Further, kinetic modeling also identified heterogeneous rates of liposome deposition and washout within tumors as well. It may be valuable to evaluate the role that intratumoral distribution patterns and transport heterogeneity play in predicting response to liposomal therapeutics.

We have presented a novel gradient-based method for ^{64}Cu -labeling of existing liposomal therapeutics for PET/CT imaging. The labeling process was shown to be robust and efficient, producing images that accurately reflect liposome deposition in tumors. This method is currently being utilized as part of an ongoing clinical study with ^{64}Cu -MM-302 (NCT01304797).³² This may provide new insights into the biodistribution and tumor deposition kinetics of liposomes in human tumors including variability across patients and/or tumor types. Assessment of these parameters may aid in identifying cancer patients that are well-suited for treatment with liposomal therapies. Extending this concept, we are currently developing a drug-free ^{64}Cu -liposomal PET agent, which can be implemented as a companion diagnostic agent with the intent of prospectively selecting patients for liposomal therapies and potentially other nanomedicines.

Acknowledgments

The authors would like to acknowledge the contributions of Michael Dunne and Raquel de Souza for their technical support, Suresh Tipparaju for organic chemistry input, as well as Daryl Drummond, Ulrik Nielsen, and Richard Huang for helpful discussions.

Appendix A. Supplementary data

Supplementary data to this article can be found online at <http://dx.doi.org/10.1016/j.nano.2014.08.011>.

References

- Schmidt MM, Wittrup KD. A modeling analysis of the effects of molecular size and binding affinity on tumor targeting. *Mol Cancer Ther* 2009;8(10):2861–71.
- Kesner AL, Hsueh W-A, Htet NL, et al. Biodistribution and predictive value of 18F-fluorocyclophosphamide in mice bearing human breast cancer xenografts. *J Nucl Med* 2007;48(12):2021–7.
- Hsueh W-A, Kesner AL, Gangloff A, et al. Predicting chemotherapy response to paclitaxel with 18F-Fluoropaclitaxel and PET. *J Nucl Med* 2006;47(12):1995–9.
- Maeda H, Wu J, Sawa T, Maehara Y, Hori K. Tumor vascular permeability and the EPR effect in macromolecular therapeutics: a review. *J Control Release* 2000;65(1–2):271–34.
- Dunne M, Zheng J, Rosenblatt J, Jaffray DA, Allen C. APN/CD13-targeting as a strategy to alter the tumor accumulation of liposomes. *J Control Release* 2011;154(3):298–305.
- Kirpouti DB, Drummond DC, Shao Y, et al. Antibody targeting of long-circulating lipidic nanoparticles does not increase tumor localization but does increase internalization in animal models. *Cancer Res* 2006;66(13):6732–40.
- Harrington KJ, Mohammadzadeh S, Uster PS, et al. Effective targeting of solid tumors in patients with locally advanced cancers by radiolabeled pegylated liposomes. *Clin Cancer Res* 2001;7(2):243–54.
- Hendriks BS, Reynolds JG, Klinz SG, et al. Multiscale kinetic modeling of liposomal doxorubicin delivery quantifies the role of tumor and drug-specific parameters in local delivery to tumors. *CPT pharmacometrics Syst Pharmacol* 2012;1(1):e15.
- Karathanasis E, Suryanarayanan S, Balusu SR, et al. Imaging nanoprobe for prediction of outcome of nanoparticle chemotherapy by using mammography. *Radiology* 2009;250(2):398–406.
- Koukourakis MI, Koukouraki S, Fezoulidis I, et al. High intratumoral accumulation of stealth liposomal doxorubicin (Caelyx) in glioblastomas and in metastatic brain tumours. *Br J Cancer* 2000;83(10):1281–6.
- Abou DS, Thorek DLJ, Ramos NN, et al. (89)Zr-labeled paramagnetic octeotide-liposomes for PET-MR imaging of cancer. *Pharm Res* 2013;30(3):S78–88.
- Petersen AL, Binderup T, Islek RJ, et al. Positron emission tomography evaluation of somatostatin receptor targeted 64Cu-TATE-liposomes in a human neuroendocrine carcinoma mouse model. *J Control Release* 2012;160(2):254–63.
- Petersen AL, Binderup T, Rasmussen P, et al. 64Cu loaded liposomes as positron emission tomography imaging agents. *Biomaterials* 2011;32(9):2334–41.
- Ting G, Chang C-H, Wang H-E, Lee T-W. Nanotargeted radionuclides for cancer nuclear imaging and internal radiotherapy. *J Biomed Biotechnol* 2010 [2010].
- Li S, Goins B, Zhang L, Bao A. Novel multifunctional theranostic liposome drug delivery system: construction, characterization, and

- multimodality MR, near-infrared fluorescent, and nuclear imaging. *Bioconjug Chem* 2012;23(6):1322–32.
16. Urakami T, Akai S, Katayama Y, Harada N, Tsukada H, Oku N. Novel amphiphilic probes for [¹⁸F]-radiolabeling preformed liposomes and determination of liposomal trafficking by positron emission tomography. *J Med Chem* 2007;50(26):6454–7.
 17. Reynolds JG, Geretti E, Hendriks BS, et al. HER2-targeted liposomal doxorubicin displays enhanced anti-tumorigenic effects without associated cardiotoxicity. *Toxicol Appl Pharmacol* 2012;262(1):1–10.
 18. Huang CY. Determination of binding stoichiometry by the continuous variation method: the Job plot. *Methods Enzymol* 1982;87:509–25.
 19. Baranyai Z, Pálincás Z, Uggeri F, Brücher E. Equilibrium studies on the Gd³⁺, Cu²⁺ and Zn²⁺ complexes of BOPTA, DTPA and DTPA-BMA ligands: kinetics of metal-exchange reactions of [Gd(BOPTA)]²⁺. *Eur J Inorg Chem* 2010;2010(13):1948–56.
 20. Nellis DF, Ekstrom DL, Kirpotin DB, et al. Preclinical manufacture of an anti-HER2 scFv-PEG-DSPE, liposome-inserting conjugate. 1. Gram-scale production and purification. *Biotechnol Prog* 2005;21(1):205–20.
 21. Park JW, Kirpotin DB, Hong K, et al. Tumor targeting using anti-her2 immunoliposomes. *J Control Release* 2001;74(1–3):95–113.
 22. Hoechst F. Bis-Thiosemicarbazones. U.S. Patent 3,520,924. 1970.
 23. Barenholz Y. Doxil®—the first FDA-approved nano-drug: lessons learned. *J Control Release* 2012;160(2):117–34.
 24. Drummond, Meyer O, Hong K, Kirpotin DB, Papahadjopoulos D. Optimizing liposomes for delivery of chemotherapeutic agents to solid tumors. *Pharmacol Rev* 1999;51(4):691–743.
 25. Gabizon A, Goren D, Horowitz AT, Tzermach D, Lissos A, Siegal T. Long-circulating liposomes for drug delivery in cancer therapy. a review of biodistribution studies in tumor-bearing animals. *Adv Drug Deliv Rev* 1997;24(2–3):337–44.
 26. Haran G, Cohen R, Bar LK, Barenholz Y. Transmembrane ammonium sulfate gradients in liposomes produce efficient and stable entrapment of amphiphilic weak bases. *Biochim Biophys Acta* 1993;1151(2):201–15.
 27. Jensen GM, Bunch TR. Conventional liposome performance and evaluation. lessons from the development of Vescom. *J Liposome Res* 2007;17(3–4):121–37.
 28. Seo JW, Mahakian LM, Kheirulomoom A, et al. Liposomal Cu-64 labeling method using bifunctional chelators: poly(ethylene glycol) spacer and chelator effects. *Bioconjug Chem* 2010;21(7):1206–15.
 29. Bao A, Goins B, Klipper R, Negrete G, Phillips WT. Direct 99mTc labeling of pegylated liposomal doxorubicin (Doxil) for pharmacokinetic and non-invasive imaging studies. *J Pharmacol Exp Ther* 2004;308(2):419–25.
 30. Gabizon A, Shmeeda H, Barenholz Y. Pharmacokinetics of pegylated liposomal Doxorubicin: review of animal and human studies. *Clin Pharmacokinet* 2003;42(5):419–36.
 31. Zheng J, Jaffray D, Allen C. Quantitative CT imaging of the spatial and temporal distribution of liposomes in a rabbit tumor model. *Mol Pharm* 2009;6(2):571–80.
 32. U.S. National Institute of Health. *Safety and pharmacokinetic study of MM-302 in patients with advanced breast cancer*, 2014.

Mapping Tumor Epitope Space by Direct Selection of Single-Chain Fv Antibody Libraries on Prostate Cancer Cells

Bin Liu,^{1,2} Fraser Conrad,¹ Matthew R. Cooperberg,³ Dmitri B. Kirpotin,⁴ and James D. Marks^{1,2}

¹Departments of Anesthesia and Pharmaceutical Chemistry, ²Comprehensive Cancer Center, and ³Department of Urology, University of California at San Francisco, San Francisco General Hospital, and ⁴California Pacific Medical Center Research Institute, San Francisco, California

ABSTRACT

The identification of tumor-specific cell surface antigens is a critical step toward the development of targeted therapeutics for cancer. The epitope space at the tumor cell surface is highly complex, composed of proteins, carbohydrates, and other membrane-associated determinants including post-translational modification products, which are difficult to probe by approaches based on gene expression. This epitope space can be efficiently mapped by complementary monoclonal antibodies. By selecting human antibody gene diversity libraries directly on the surface of prostate cancer cells, we have taken a functional approach to identifying fully human, tumor-specific monoclonal antibodies without prior knowledge of their target antigens. Selection conditions have been optimized to favor tumor-specific antibody binding and internalization. To date, we have discovered >98 monoclonal antibodies that specifically bind and enter prostate cancer cells, with little or no binding to control cells. These antibodies are able to efficiently deliver intracellular payloads when attached to nanoparticles such as liposomes. In addition, a subset of the antibodies displayed intrinsic antiproliferative activity. These tumor-specific internalizing antibodies are likely to be useful for targeted therapeutics either alone or in combination with effector molecules. The antigens they bind constitute a tumor-specific internalizing epitope space that is likely to play a significant role in cancer cell homeostasis. Targeting components of this epitope space may facilitate development of immunotherapeutic and small molecule-based strategies as well as the use of other therapeutic agents that rely upon delivery to the interior of the tumor cell.

INTRODUCTION

Cancer cells differ from normal cells in a variety of ways, one of which is the molecular composition of the cell surface. These differences may be exploited in the development of targeted therapeutics. In principle, a variety of antineoplastic agents can be attached to affinity molecules, such as monoclonal antibodies (mAbs), which recognize tumor-specific cell surface molecules to achieve targeted killing (1). The epitope space⁵ at the tumor cell surface, however, is highly complex, including, in addition to proteins, carbohydrate determinants and other post-translational modification products that are difficult to probe by gene expression-based approaches (2, 3). For carcinoma of the prostate (CaP), there are few known specific cell surface markers and even fewer specific markers for hormone-refractory CaP (4-9). Moreover, despite recent advances in early diagnosis and treatment, prostate cancer remains the most common and second most lethal

tumor in American men (10), and no curative treatment currently exists for metastatic disease (11).

Tumor-specific epitope space may be efficiently mapped by complementary mAbs. Phage display of nonimmune, single-chain Fv (scFv) or Fab antibody repertoires has proven to be an important tool for generating highly specific antibody-combining sites that may be readily converted into mAbs (12-15), if needed. Nonimmune phage libraries are derived from naive human lymphocytes and thus recapitulate the primary immune response (12) and overcome difficulties with generating antibodies to evolutionarily conserved, or "self", antigens that may make up a large portion of tumor antigens (16, 17). This broader repertoire of specificities allows a less biased and more thorough mapping of epitope space (18). mAbs to tumor antigens have been isolated by directly selecting phage libraries on native and modified tumor antigens (19). The success of direct cell selections in generating tumor-targeting mAbs has been limited, however, by high nonspecific binding of phage to cell surfaces and by high representation of phage antibody binding to common cell surface molecules (19, 20).

Recently, we reported that phage antibody selections on cells could be significantly improved by selecting for mAbs that trigger receptor-mediated endocytosis, because endocytosed phage may be recovered from within the tumor cell after stripping nonspecific binders from the cell surface (21). Besides increasing selection efficiency, this approach generates mAbs that have desirable biological properties: receptor-mediated intracellular drug delivery, induction of apoptosis, or inhibition of proliferation (22-24). We applied this approach to breast tumor cells and generated mAbs to a number of known internalizing receptors, including epidermal growth factor receptor and ErbB2 (23, 24). To broaden applicability, libraries of phage displaying multiple copies of scFv were engineered (25-27), which unlike existing phage libraries can cross-link receptors, allowing more efficient phage endocytosis (21).

Here we report, for the first time, the application of this library to generate prostate cancer-targeting mAbs that bind to components of the tumor-specific internalizing epitope space. By using a library designed to trigger receptor endocytosis and by devising selections to eliminate cross-reactive mAbs, a panel of 93 CaP-specific mAbs were generated without prior knowledge of their target antigens. Over 70 of those mAbs recognize hormone-refractory prostate cancer cells. All mAbs examined were efficiently endocytosed by CaP cell lines and thus can be used for efficient delivery of antitumor drugs to the cytosol. In addition, a subset of the mAbs possesses intrinsic antiproliferative activity and may have therapeutic utility as "naked" mAbs.

MATERIALS AND METHODS

Phage Display Library Construction and Preparation. A multivalent fd phage display library consisting of 5×10^8 members was derived from a 7×10^9 -member phagemid library (16) by subcloning the *SfiI/NotI* scFv insert from pHEN1 into bacterial vector fd-*SfiI/NotI* (25-27). Phage were produced via growth in culture of *Escherichia coli* TG1, concentrated by precipitation with polyethylene glycol 8000, and purified by CsCl gradient centrifugation, as reported previously (25-27).

Received 8/29/03; revised 10/21/03; accepted 11/10/03.

Grant support: NIH Grant P50 CA 89520 (to J. D. M.) and a grant from the CaPCure research foundation (to B. L.).

The costs of publication of this article were defrayed in part by the payment of page charges. This article must therefore be hereby marked advertisement in accordance with 18 U.S.C. Section 1734 solely to indicate this fact.

Requests for reprints: Bin Liu or James D. Marks, Department of Anesthesia, 1001 Potrero Avenue, Room 3C-38, San Francisco, CA 94110. Phone: (415) 206-3253/3256; Fax: (415) 206-3253; E-mail: Lihb@anesthesia.ucsf.edu or Marksj@anesthesia.ucsf.edu.

⁵Epitope space is the complete set of antigenic determinants (epitopes) recognizable by an ideal, naive phage antibody library. Operationally, the size of this space is a function of experimental details, such as the size and quality of the library, selection methods, and the cell biology involved in handling cells of interest. Tumor epitope space is the complete set of tumor-specific or tumor-associated epitopes on a particular tumor specimen or tumor cell lines, recognizable by an ideal, naive phage antibody library. Operationally, the size of this space is a function of experimental details, such as the size and quality of the library, the success of preadsorption against a corresponding normal cell line, the selection methods, and the cell biology involved in handling tumor cells or cell lines of interest.

Selection for Prostate Cancer-specific Internalizing Antibody. Normal human fibroblasts and noncancerous epithelial lines RWPE-1, BPH-1, MCF10A, and human mammary epithelial cell (HMEC) were used to deplete the phage library of nonspecific binders by incubating 10^{12} phage particles with 10^8 cells for 4 h at 4°C. Supernatant containing the depleted phage library was then incubated with 10^6 prostate cancer cells for 1 h at 4°C. Cells were washed with cold PBS and incubated with prewarmed (37°C) medium/10% FCS at 37°C for 30 min to allow receptor-mediated internalization. Non-internalized phage were removed by washing cells with glycine buffer (50 mM glycine, 150 mM NaCl, 200 mM urea, and 2 mg/ml polyvinylpyrrolidone, pH 2.8) and by digesting cells with trypsin at 37°C for 10 min. Cells were collected by centrifugation and lysed with 1 ml of 100 mM triethylamine. Lysate was neutralized with 0.5 ml of 1 M Tris-HCl (pH 6.8) and was used to infect exponentially growing *E. coli* TGI as described previously (25–27). The number of unique phage antibodies was determined by patterns of *Bst*NI digestion of scFv genes amplified by PCR from phage-infected bacteria (28). When restriction digestion patterns were ambiguous, scFv genes were sequenced to determine uniqueness.

Analysis of Phage Antibody Binding by Flow Cytometry. Cells (10^6) were incubated with phage antibody (5×10^{11} colony-forming units/ml) for 1 h at 4°C. Bound phage were detected by using biotinylated anti-M13 antibody (Amersham Pharmacia) and streptavidin-R-phycoerythrin or streptavidin-FITC (Molecular Probes). Cells were analyzed using a FACSort (Becton Dickinson). Mean fluorescence intensity was calculated using CellQuest software (Becton Dickinson). For analysis of mixed cell populations by two-color flow cytometry, the relevant normal cell line was prelabeled with FITC labeling reagent, 6-(fluorescein-5-[and-6]-carboxamido)hexanoic acid, succinimidyl ester (Molecular Probes) according to the manufacturer's instructions. Labeled and unlabeled cells were mixed and incubated with phage antibody at 4°C for 1 h. Bound phage were detected by biotinylated anti-M13 polyclonal antibody (Sigma) and streptavidin-phycoerythrin. For cytometry, the prelabeled cell population was identified on the FL1 (FITC) channel, and the bound phage were detected on the FL2 (PE) channel, appropriately compensated. Experiments were performed with either cell population (normal versus prostate cancer) labeled with similar results.

Expression and Purification of Prostate Cancer-specific, Single-Chain Fv Antibody. The scFv gene was subcloned from the phage vector into the secretion vector pUC119mycHis, resulting in the addition of a c-myc epitope tag and hexahistidine tag at the COOH terminus of the scFv. To create the (scFv)₂ dimer (29) for immunohistochemistry, the c-myc epitope tag was genetically removed from pUC119mycHis, and a free cysteine was introduced at the COOH terminus of the scFv preceding the hexahistidine tag. scFv or (scFv)₂ dimer protein was harvested from the bacterial periplasm and purified by immobilized metal affinity chromatography and gel filtration (22). After purification of the (scFv)₂ dimer protein, ~50% of scFv was in dimeric form as determined by nonreducing SDS-PAGE.

Immunohistochemistry. Tissue sections from frozen and paraffin-embedded blocks were obtained from the Tissue Core of UCSF Comprehensive Cancer Center. For immunohistochemical analysis, tissue sections were incubated with purified dimeric scFv (50 µg/ml in 2% milk/PBS) at 4°C for 4 h, washed with PBS, incubated with a rabbit polyclonal anti-(His)₆ antibody diluted 1:400 (Santa Cruz Biotechnology), followed by biotinylated anti-rabbit antibody diluted 1:400 (Vector Lab) and horseradish peroxidase-conjugated streptavidin diluted 1:400 (Sigma). Binding was detected using diaminobenzidine as the substrate (Sigma).

Growth Inhibition and Internalization Assays. PC3 cells at 30% confluence were incubated with various concentrations of affinity-purified scFv at 37°C for 72 h in medium containing 1% FCS. Growth status was assessed using the tetrazolium salt 3-(4,5-dimethylthiazol-2-yl)-2,5-diphenyltetrazolium bromide assay (Promega), and the IC₅₀ was calculated using KaleidaGraph 3.5 (Synergy Software). For internalization assays, CaP-specific phage antibodies were biotinylated with sulfo-NHS-LC-biotin (Pierce), mixed with unlabeled helper phage M13K07 at the molar ratio of 1:100, and incubated with target cells at 37°C for various amounts of time. Cells were washed with 100 mM glycine buffer (pH 2.8), fixed with 2% formaldehyde, permeabilized with ice-cold 100% methanol, and incubated with streptavidin-FITC. The stained cells were first examined with an AxioPhot fluorescence microscope (Zeiss) and further studied with a Leica TCS NT confocal laser fluorescence microscope (Leica).

Immunoliposome Preparation and Assay of Intracellular Delivery. Liposomes were prepared from 1-palmitoyl-2-oleoyl-phosphatidylcholine, cholesterol, and methoxy-poly(ethylene glycol) (molecular weight 2000)-distearylphosphatidylethanolamine (3:2:0.5 molar ratio, Avanti Polar Lipids) by lipid film hydration in a solution containing the pH-sensitive fluorophore 1-hydroxypyrene-3,6,8-trisulfonic acid, pyrimine (HPITS), followed by extrusion through track-etched polycarbonate membranes with 100-nm pore size (22, 30). A lipophilic derivative of nitrilotriacetic acid-nickel (Avanti Polar Lipids) was further inserted into the liposome to create a surface capable of capturing (His)₆-tagged scFv. To assess intracellular liposome delivery, HPITS liposomes (0.2 mM phospholipid) were added to cells along with 1 µg/ml of purified (His)₆-tagged scFv, incubated at 37°C for 30 min, and washed three times with saline containing 1 mM EDTA to remove cell surface-bound liposomes that failed to internalize. Uptake of scFv-HPITS immunoliposomes was determined by microfluorimetry with a Gemini microfluorometer (Molecular Devices) and by an inverted fluorescence microscope (Nikon).

RESULTS

Subtractive Selection for CaP-specific Internalizing Phage Antibody. A nonimmune, multivalent phage display library that contains >100 million different antibody variable fragments was used for subtractive cell selection. The phage display library was pre-absorbed against a panel of normal cell lines, including a normal, immortalized prostate epithelium line (RWPE-1), epithelial cells derived from benign prostatic hyperplasia glands (BPH-1; Ref. 31), normal human fibroblasts, and normal breast epithelial lines (MCF10A and HMEC), to remove those antibodies that bind to common cell surface molecules. The depleted antibody library was incubated with either one of two hormone-refractory CaP lines (PC3 and DU-145) and one hormone-sensitive line (LNCaP) under conditions that allowed receptor-mediated endocytosis (Fig. 1A). Surface-bound phage that failed to internalize were removed by low-pH glycine buffer washes, and internalized phage were recovered by lysing the cells, followed by amplifications in *E. coli*.

After two rounds of subtractive selection, 22–43% of the phage output bound the selecting cell line (Table 1), as determined by cell ELISA (Fig. 1B). Using comparative cell ELISA and flow cytometry, it was determined that 90 of 1320 (6.8%) phage antibodies selected on CaP cell line PC3 bound PC3 cells but not normal cells, including BPH-1, RWPE-1, MCF10A, and HMEC (Fig. 1, B–D; and Table 1). These phage antibodies were designated as “highly” specific binders. By the same criteria, 30 of 360 (8.3%) and 25 of 270 (9.3%) phage antibodies were highly specific for DU-145 and LNCaP prostate tumor cell lines, respectively. The number of unique antibodies was determined by DNA fingerprinting and sequencing. Ninety unique antibodies were identified that were highly specific for CaP cell lines; 72 of these antibodies bound specifically to hormone-refractory metastatic cell lines PC3 and DU-145. Most of these antibodies (total, 70 of 72) bound to both the hormone-refractory cell lines (Fig. 1C). Fifty of 51 Du-145 binders cross-reacted with PC3 cells, whereas 20 of 21 PC3 binders cross-reacted with Du-145 cells. These results indicate that a large number of unique antibodies recognizing membrane antigens specific to prostate cancer cells were identified.

To further confirm antibody specificity, the ability of phage antibodies to identify tumor cells in mixed cell populations was assessed using two-color fluorescence-activated cell sorter. FITC-labeled normal cells were mixed with unlabeled prostate cancer cells and incubated with CaP-specific phage antibody. CaP-specific phage antibodies specifically stained prostate cancer cells but not normal cells in the mixed populations (Fig. 1D).

Selected Phage Antibodies Recognize Different Antigens Than Existing Antibodies. Cell profiling experiments were performed using flow cytometry with CaP-specific phage antibodies in comparison

Fig. 1. Subtractive selection of CaP-specific internalizing antibody. **A**, selection scheme. A naive human phage antibody library was depleted on normal cells and subsequently incubated with prostate cancer cells at 37°C to induce receptor-mediated endocytosis. **B**, comparative cell ELISA. Supernatants containing monoclonal phage antibody were incubated with PC3 and BPH-1 cells in parallel to reveal differential binding. **C**, binding specificity determined by flow cytometry. Phage antibody A12 was incubated with prostate cancer cells (PC3 and DU-145) and control cells, and bound phage were detected by FITC-conjugated anti-M13 antibodies. *Filled peak*, control, an irrelevant, heparin-binding phage mAb. *Unfilled peak*, CaP-specific phage mAb. **D**, binding specificity determined by two-color FACS analysis of mixed cell populations. RWPE-1 (control) cells were labeled with FITC, mixed with unlabeled PC3 cells, and incubated with phage antibodies that bind to prostate cancer (MDE4, M10A12, and M11G12). *Control*, helper phage only. *H3*, pan cell binding antibody. Binding of erbB2 phage antibody *E5* is shown as a reference.

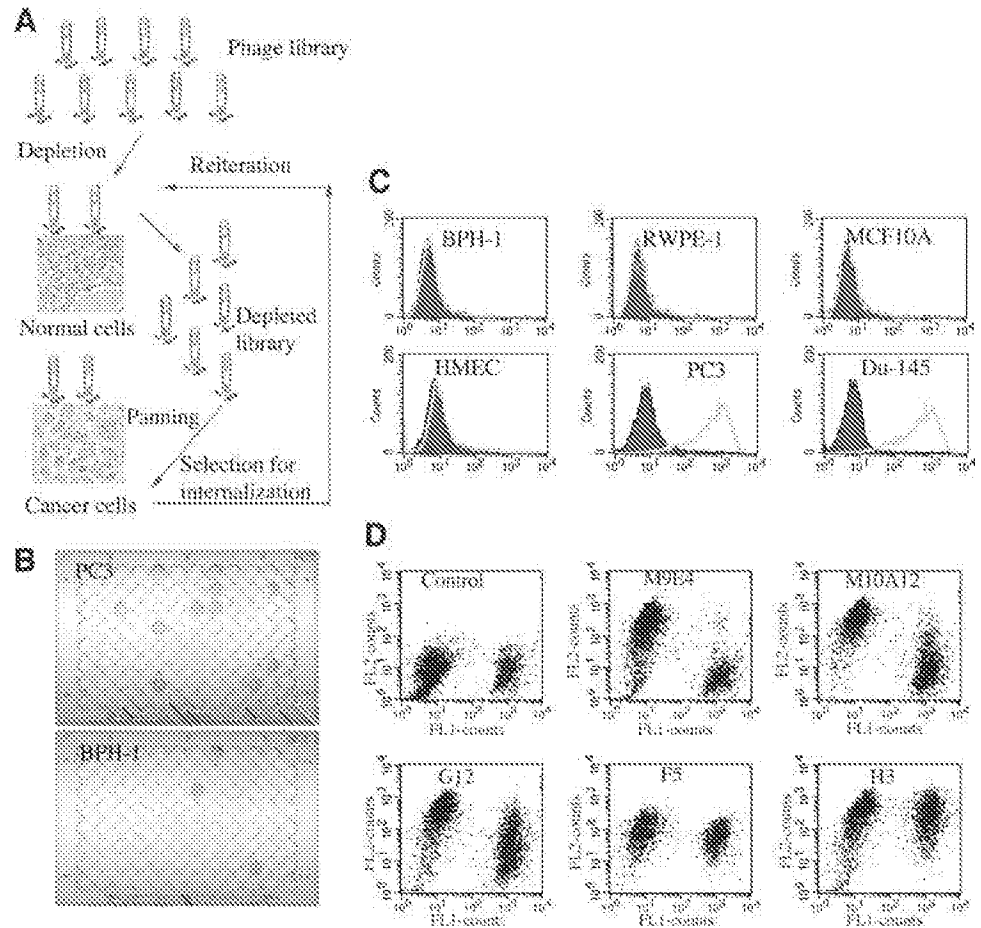


Table 1. Summary of selection results on PC3, DU-145 (hormone-refractory), and LNCaP (hormone-sensitive) prostate cancer cell lines.

Binding specificities were determined by whole-cell ELISA and flow cytometry. DNA fingerprinting and sequencing were used to identify the number of unique antibodies.

	PC3	DU-145	LNCaP
Total output (cfu ^a)	4 × 10 ⁹	3 × 10 ⁹	2 × 10 ⁹
Positive/clones screened	255/1320 = 19.3%	116/360 = 32.2%	95/270 = 35.2%
Nonspecific binder	67/1320 = 5.1%	35/360 = 9.7%	24/270 = 8.8%
Binding to overexpressed marker	137/1320 = 10.4%	60/360 = 16.7%	68/270 = 25.2%
Highly specific binder	90/1320 = 6.8%	30/360 = 8.3%	25/270 = 9.3%
Unique clones	51/1320 = 3.9%	21/360 = 5.8%	21/270 = 7.8%

^a cfu, colony-forming units

with known antibodies that have been described as prostate- or prostate cancer-specific in the literature. The results are summarized in Table 2. The binding patterns of the selected CaP-specific phage antibodies are very different from those of known CaP antibodies, including anti-prostate-specific membrane antigen (PSMA), anti-prostate stem cell antigen, anti-STEAP, and anti-hepsin, and therefore likely recognize novel antigens or epitopes on the prostate cancer cell surface (Table 2). Phage antibodies that exhibited the most specific binding patterns to both hormone-refractory lines (PC3 and DU-145) were selected for further analysis.

Selected Phage Antibodies Are Rapidly Internalized and Can Be Used to Construct a Targeted Drug Delivery Vehicle. Phage antibodies were isolated using a functional selection for triggering receptor endocytosis. To confirm that the selected antibodies possessed this phenotype and were endocytosed by CaP cells, the intracellular uptake of six unique phage antibodies was measured. All six phage antibodies were efficiently internalized by PC3 cells (Fig. 2A).

This property of tumor cell-specific internalization can be exploited to create a generic approach for efficient tumor-specific drug delivery. When attached to drug-encapsulated nanoparticles such as liposomes, CaP-specific scFv are expected to deliver the liposomes to the tumor cytosol. To determine the utility of the CaP antibodies for intracellular drug delivery, we determined the quantitative uptake of immunoliposomes. Liposomes with surface-bound CaP scFv were loaded with a pH-sensitive fluorophore, pyranine (HPTS; Ref. 22), and intracellular uptake was determined by measurement of the pH-dependent fluorescence of HPTS, allowing quantification of scFv-HPTS-liposome in

Table 2. Summary of flow cytometry profiling of selected phage antibodies and known antibodies to prostate tumor antigens.

Data were compiled from current studies and published data. Mean fluorescent intensity (MFI) per cell is indicated as: ++, strongly positive (sample/control > 100); +, positive (10 < sample/control < 100); +/-, weakly positive (5 < sample/control < 10); -/+, slightly positive (2 < sample/control < 5). PSMA, prostate specific membrane antigen; PSCA, prostate stem cell antigen; STEAP, six-transmembrane epithelial antigen of the prostate; PSGR, prostate-specific G protein coupled receptor.

	BPH-1	RWPE-1	LNCaP	PC3	DU-145	Ref.
PSMA	+	+/-	+	-	-	This study + Ref. 4
PSCA	ND ^a	ND	-	-	-	Ref. 9
STEAP	+	+	+/-	+	+	This study + Ref. 7
PSGR	-	-	+/-	-	-	Ref. 6
Hepsin	ND	ND	+/-	-	+/-	This study + Ref. 5
A33	-	-	-	++	++	This study
M10A12	-	-	-	++	++	# ^b
M9E4	-	-	++	++	++	#
OA12	-	-	-	++	++	#
M11G12	-	-/+	++	++	++	#
M11F12	-	-	++	-	++	#
C10	-	++	++	++	++	#

^a ND, not done.
^b #, this study.

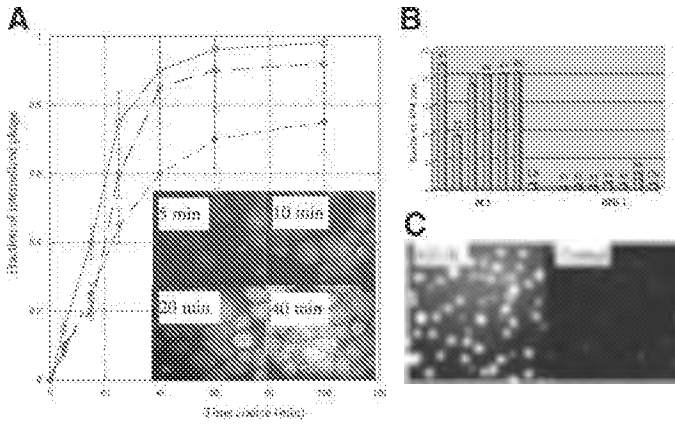


Fig. 2 *A*, time course of phage antibody internalization by PC3 cells. The percentage of internalized phage is calculated as a fraction of the total phage bound and plotted as a function of time. *Circle*, M9E4 phage antibody; *square*, A33 phage antibody; *diamond*, M10A12 phage antibody. *Insert*, internalized phage visualized by fluorescent microscopy. *Bars*, SD. *B*, ScFv-directed liposome endocytosis by prostate cancer cells. Fluorescent dye containing immunoliposomes (ILs) were constructed from six scFv that bound PC3 cells but not noncancerous BPH-1 cells. After removal of surface bound ILs, internalized liposomes were quantified by fluorescence at 404 nm. *Ch*, control, nitrilotriacetic acid-nickel liposome containing HPTS but without scFv coating. The ratio of sample reading over control was shown for comparison between PC3 and BPH-1 cells. *C*, direct observation of liposome HPTS uptake by PC3 cells using fluorescent microscopy. The result is shown for PC3 with A33 scFv (clone 1 in *A*). *Control*, liposome containing HPTS but without scFv coating.

acidic endosomal compartments. Such immunoliposomes prepared from six different CaP-specific scFv were efficiently endocytosed by PC3, with minimal uptake into BPH-1 cells (Fig. 2*B*). Without scFv, untargeted liposomes were not efficiently taken up by prostate cancer cells (Fig. 2*C*). These experiments demonstrate that scFv antibodies obtained via selection for internalization are capable of mediating targeted payload delivery. Those antibodies are candidates for the development of immunoliposome-based targeted prostate cancer therapeutics.

Intrinsic Antiproliferative Activity of CaP Binding scFv. It is likely that some of the surface molecules bound by internalizing CaP scFv are receptors, transporters, or adhesion molecules that mediate important physiological processes of tumor cells. We thus hypothesized that a subset of the scFv might have intrinsic antiproliferative activity. To test this hypothesis, the ability of CaP-specific internalizing scFv to inhibit CaP cell proliferation *in vitro* was assessed. PC3 and DU-145 cells were incubated with various concentrations of highly purified, soluble native A33 or M9E4 scFv, and cell proliferation was assessed by the tetrazolium salt 3-(4,5-dimethylthiazol-2-yl)-2,5-diphenyltetrazolium bromide assay. Both scFv showed dose-dependent growth inhibition, with IC_{50} s between 0.5 and 1.8 μ M, with a control scFv showing no inhibitory effect (Fig. 3). No inhibitory effect was observed on BPH-1 cells. These inhibitory scFv are candidates for the development of naked antibody-based therapeutics.

Immunohistochemistry. There is some controversy in the literature as to how well cell lines actually represent patient tumors, because cell lines may have undergone genetic and physiological changes during *in vitro* culture. To further address the relevance of the CaP-specific antibodies to human prostate cancer, immunohistochemical studies were performed on tissue sections from primary prostate tumor of high Gleason grades. Fig. 4 shows the staining results of the A33 (scFv)₂ dimer antibody on two different tissue specimens obtained from Gleason 3 + 4 patients (Fig. 4, *A* and *B*). There is intense staining of tumor epithelium, with minimal staining of normal adjacent prostate epithelium (Fig. 4*C*), normal breast epithelium (data not shown), or normal colon epithelium (Fig. 4*D*). A total of 20 high-grade prostate cancer patient samples have been examined, and pos-

itive A33 staining patterns were observed in 18 of 20 cases. A total of eight CaP-specific scFv antibodies have been subjected to immunohistochemistry studies on frozen tissue slides, six of which showed specific reactivity to prostate cancer epithelium. These experiments indicate that antibodies obtained from selection on tumor cell lines bind antigens that exist in patient samples and thus are clinically relevant to human prostate cancer. The corresponding antigens are overexpressed in prostate cancer and are likely targets for therapeutic intervention.

DISCUSSION

Mapping Tumor Cell Surface Epitope Space by a Direct, Antibody Library-based Approach. Tumor-specific cell surface markers are invaluable for the development of targeted oncologic therapeutics because of their relatively easy accessibility to targeting molecules. Differential gene expression-based approaches have been used widely for discovery and identification of these markers, but these approaches have significant limitations: (a) the level of mRNA transcript production does not always correlate with that of protein expression (32); and (b) neither cDNA microarray nor other gene expression-based approaches can profile neoplastic changes in glycosylation or other post-translational modifications. Such changes have been shown to play an important role in tumor metastasis (33) and may be critical determinants in modulating active antitumor immunity. Thus, to analyze the entire epitope space on the tumor cell surface, alternative methodologies must be explored and developed.

For this work, a functional approach was taken to tumor-cell epitope mapping; specifically, we sought to identify tumor-specific epitopes not readily predicted or identified from microarray or other gene expression-based analyses. A large nonimmune phage antibody library was constructed and selected directly on the tumor cell surface to generate CaP-specific antibodies. The nonimmune antibody library functions as an unbiased random shape repertoire potentially capable of recognizing any shape of antigen on the tumor cell surface. Unbiased repertoires should provide more complete coverage of the tumor

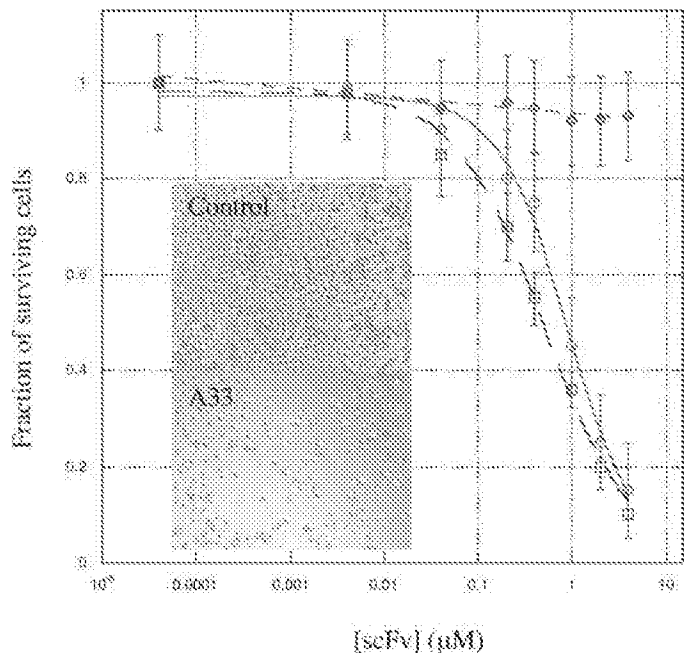


Fig. 3. Cell proliferation assay. Purified scFv were incubated with PC3 cells. *Circle*, M9E4 scFv; *square*, A33 scFv; *diamond*, irrelevant, anti-hapten scFv. *Insert*, PC3 treated with PBS (*Control*) and 1.8 μ M A33. *Bars*, SD.

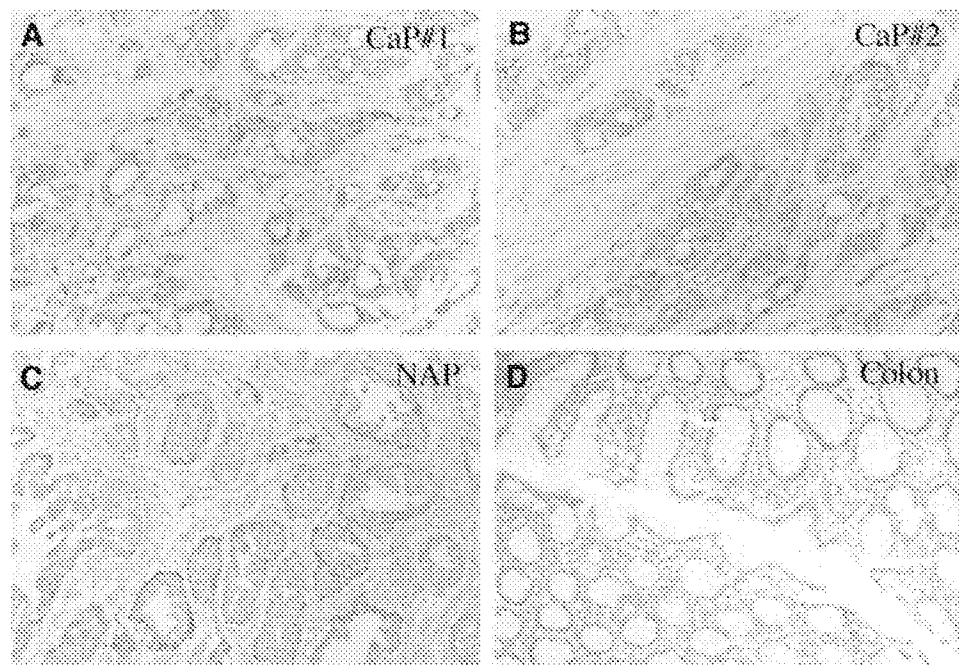


Fig. 4. Immunohistochemistry studies of scFv binding to prostate cancer tissue. Frozen tissue sections were stained with A33 (scFv)₂ using horseradish peroxidase-diaminobenzidine, and the tissues were counterstained with hematoxylin. *A* and *B*, staining on sections of prostate cancer, Gleason scale 4 + 3, from two different patients (CaP#1 and CaP#2). *C*, staining on NAP, normal prostate tissue adjacent to prostate cancer. *D*, staining on normal colon epithelium. Magnification, 12.5×10 .

epitope space, compared with immunization and hybridoma technology, which typically yield multiple antibodies against a few dominant epitopes.

Although phage libraries have been used previously to identify tumor-specific antigens, the number of specific mAbs isolated has typically been small (20, 23, 34, 35). Previously used antibody libraries were constructed in phagemid vectors that on average have only a single scFv molecule displayed on each phagemid particle. For this work, a multivalent antibody library was used where three to five identical scFv molecules are displayed per phage. Multivalent display increases both the efficiency of depletion of nonspecific antibodies and the positive selection of specific antibodies attributable to the increased binding from avidity effects of the multivalent phage antibody to the target cell surface (27, 28). Moreover, the selection methodology was devised to isolate antibodies that trigger receptor-mediated endocytosis (23) and are thereby delivered directly into the tumor cell. This not only selects for antibodies with desirable biological effects that can be exploited for intracellular drug delivery (22) but also leads to more efficient selection of phage libraries (21). Because many receptors require dimerization or cross-linking for efficient internalization, the use of a multivalent phage display library increases the efficiency of phage internalization through receptor cross-linking (21). This allows more efficient recovery of phage antibody binding to more epitopes on more receptors and probably accounts for the much larger number of antibodies generated in this study, compared with the same antibody repertoire displayed monovalently and selected on breast tumor cells (23).

A Panel of Novel CaP-specific Monoclonal mAbs. Direct cell selection yielded >90 phage antibodies that bind specifically to prostate cancer cells, including hormone-refractory ones. Profiling by flow cytometry on a panel of normal and tumor cell lines revealed that the majority of CaP-specific antibodies display binding patterns different from those of known tumor antibodies and therefore likely recognize novel cell surface antigens. Because only a few thousand clones were screened from the second-round output of 5×10^7 antibodies, it is likely that a much larger number of tumor-specific cell surface epitopes and antibodies remain to be identified. It is possible that a phage antibody that is unique in sequences may nevertheless

bind to the same epitope, effectively reducing the size of the tumor epitope space in our estimation. We have performed competition experiments with 15 unique phage antibodies by examining phage binding to target cells in the presence of soluble scFv of a different sequence. In all cases examined, there were no significant, dose-dependent competitions except when the phage antibody was coincubated with soluble scFv of the same sequence (data not shown). Although this type of analysis has not been performed on all 93 CaP-specific phage antibodies, we conclude, based on the available data, that the majority of those antibodies recognize different epitopes. We have therefore not grossly overestimated the size and complexity of the tumor-specific epitope space.

Our study points to a significant up-regulation of antigenic determinants on the surface of prostate cancer cells. This contrasts with previous studies using cDNA microarrays that suggest that a global transcriptional repression mediated by the polycomb gene *EZH2* is the principal force driving prostate cancer development (36). Our results indicate that functional, proteome-based approaches provide complementary information on the immunochemical features characteristic of cancer cells that may not be revealed by gene expression-based studies.

Phage Antibodies Are Efficiently Endocytosed. All phage antibodies studied possessed the phenotype that the selections were designed to capture, the ability to trigger receptor-mediated endocytosis. Purified native CaP-specific scFv were rapidly internalized into tumor cells and were capable of delivering nanoparticles (liposomes) specifically into prostate cancer cells. Drug-loaded immunoliposomes must be endocytosed for antitumor activity to provide both direct killing of tumor cells and bystander killing by diffusion of small-molecule drugs to neighboring tumor cells (37). Immunoliposomes can be constructed from scFv (22) and can be designed to have a long circulating half-life and to be nonimmunogenic (30). Other strategies can be designed to use internalizing antibody fragments for targeted tumor therapeutics. These applications include intracellular delivery of small molecule drugs via direct conjugation, cytotoxic gene fusions, immunotoxins, viral and nonviral gene delivery vehicles, and radionuclides (1).

Phage Antibodies Have Intrinsic Antitumor Activities. A subset of CaP-specific scFv had intrinsic antitumor activity, inhibiting proliferation of prostate cancer cells *in vitro* at submicromolar concentrations. This antitumor activity has not been typically observed with scFv isolated previously from cell selections of phage antibody libraries (19). This direct antitumor activity may have resulted from selecting for antibodies that trigger internalization and that are likely to bind to biologically active receptors, transporters, or adhesion molecules that may play significant roles in tumor physiology. Such antigens, in effect, may not be merely byproducts of tumor transformation but rather may play an integral role in this process. On the basis of this investigation, it appears that antibody endocytosis can be used as a surrogate marker for selection of antibodies with direct, intrinsic antitumor activity.

Clinical Relevance to Human Prostate Cancer. A panel of >90 internalizing antibodies was generated that can be used therapeutically, either for intracellular drug delivery or as naked antibodies with direct antiproliferative effects. These phage antibodies may also be useful diagnostically, and they may provide the means to identify novel tumor antigens that might be vaccine candidates or important new targets for the treatment of prostate cancer. Currently, few monoclonal antibodies exist that specifically recognize CaP cells, and fewer still are specific for hormone-refractory cells. These include antibodies to a number of cell surface molecules including PSMA (4), prostate stem cell antigen (PSCA, Ref. 9), PSGR (6), STEAP (7), and hepsin (5). PSMA was isolated via murine immunization with membrane preparations of LNCaP cells. The other markers were identified during various studies of differential mRNA expression. Although originally considered to be prostate or prostate cancer specific, follow-up studies have found that expression of these markers in many cases is actually less restricted (5, 9).

Phage selections were performed on established CaP cell lines. PC3 and DU-145 cells do not express PSA or androgen receptor and exhibit androgen-independent growth. LNCaP cells, on the other hand, retain PSA and androgen receptor expression and remain dependent on androgens. These diverse phenotypes were used because they may reflect distinct stages of prostate cancer development. It is possible that such cell lines cultured *in vitro* have undergone physiological and genetic changes and do not truly represent human prostate cancer *in vivo*. Tissue staining with CaP-specific single-chain antibodies on frozen tissue was performed to observe binding patterns *in situ* within tumors and identify those antibodies that are relevant to human prostate cancer. The results show that antibody obtained from cell line studies may be highly relevant clinically, consistent with previous observations (33).

Several challenges remain to be addressed for the development of these antibodies in therapeutic applications. Foremost is the identification of the antigen bound by the antibodies. Although we have been able to immunoprecipitate small amounts of antigen with some of the scFv, immunoprecipitation with high-avidity IgG based on these scFv is the method of choice. Toward this objective, full-length IgG are being constructed from the V genes of six of the scFv with the most specific staining patterns by immunohistochemistry. IgG will be used for immunoprecipitation, and the antigen bound can be readily identified by mass spectrometry. Construction of IgG will overcome two other scFv limitations: their use for *in vivo* studies of antitumor activity, which are precluded by the small size and rapid clearance of scFv, and their limited use in immunohistochemistry. In the future, we anticipate that use of the IgG will allow antigen identification, determination of its temporal and spatial pattern of expression, and determination of direct *in vivo* antitumor activity. Such data combined with *in vivo* studies of the drug delivery ability of the antibodies (22) should result in the identification of new antigens and targets for

metastatic prostate cancer and the development of therapeutically useful antibodies for improved clinical strategies.

ACKNOWLEDGMENTS

We thank Drs. Marc Shuman and Peter Carroll for help with clinical specimen acquisition; Karen Chew and the UCSF Cancer Center Tissue Core for tissue slides; Dr. Jeff Simko for advice on prostate cancer pathology; and Dr. E. Yu Zhou, Dr. Jianlong Lou, Adam Sassoon, Richard Tsai, Brittney Jung, Kelly Choi, and Connie Young for help with experiments.

REFERENCES

1. Carter, P. Improving the efficacy of antibody-based cancer therapies. *Nat. Rev. Cancer*, *7*: 118-129, 2001.
2. Theodorakis, A. Human colon adenocarcinoma is associated with specific post-translational modifications of versican and decorin. *Biochim. Biophys. Acta*, *1535*: 165-172, 2002.
3. Lee, K. J., Mao, S., Sun, C., Gao, C., Büxt, O., Armes, S., How, I. G., Kaufmann, G. P., Hoffman, T. Z., Coyle, A. R., Paulson, J., Felding-Habermann, B., and Janda, K. D. Phage-display selection of a human single-chain Fv antibody highly specific for melanoma and breast cancer cells using a chemoenzymatically synthesized G_{M2}-carbohydrate antigen. *J. Am. Chem. Soc.*, *124*: 12439-12446, 2002.
4. Fair, W. P., Israeli, P. S., and Heston, W. D. Prostate-specific membrane antigen. *Prostate*, *32*: 140-148, 1997.
5. Dhanasekaran, S. M., Barrette, T. R., Ghosh, D., Shah, R., Varambally, S., Kusch, K., Pienta, K. J., Rubin, M. A., and Clinchayan, A. M. Delineation of prognostic biomarkers in prostate cancer. *Nature (Lond)*, *412*: 822-826, 2001.
6. Xu, L. L., Stackhouse, B. G., Florence, K., Zhang, W., Shanmugam, N., Sesterhenn, I. A., Zou, Z., Srikantan, V., Augustus, M., Poschke, V., Carter, K., McLeod, D. G., Moul, J. W., Soppet, D., and Srivastava, S. PSGR, a novel prostate-specific gene with homology to a G protein-coupled receptor, is overexpressed in prostate cancer. *Cancer Res.*, *60*: 6568-6572, 2000.
7. Hubert, R. S., Vivianco, I., Chen, E., Rastegar, S., Leong, K., Mitchell, S. C., Madraswala, P., Zhou, Y., Luo, J., Raitano, A. B., Jakobovits, A., Saffran, D. C., and Alfari, D. E. STEAP: a prostate-specific cell-surface antigen highly expressed in human prostate tumors. *Proc. Natl. Acad. Sci. USA*, *96*: 14523-14528, 1999.
8. Saffran, D. C., Raitano, A. B., Hubert, R. S., Witte, O. N., Reiter, R. E., and Jakobovits, A. Anti-PSCA mAbs inhibit tumor growth and metastasis formation and prolong the survival of mice bearing human prostate cancer xenografts. *Proc. Natl. Acad. Sci. USA*, *98*: 2638-2663, 2001.
9. Reiter, R. E., Gu, Z., Watabe, T., Thomas, G., Szegedi, K., Davis, E., Waid, M., Naitani, S., Yamashiro, J., Le Beau, M. M., Loda, M., and Witte, O. N. Prostate stem cell antigen: a cell surface marker overexpressed in prostate cancer. *Proc. Natl. Acad. Sci. USA*, *95*: 1735-1740, 1998.
10. Jamal, A., Murray, T., Samuels, A., Ghafoor, A., Ward, E., and Thun, M. J. Cancer statistics, 2003. *CA Cancer J. Clin.*, *53*: 5-26, 2003.
11. Coleman, R. E. Future directions in the treatment and prevention of bone metastases. *Am. J. Clin. Oncol.*, *25*: S32-S38, 2002.
12. Marks, J. D., Hoogenboom, H., Bonnett, T., McCafferty, J., Griffiths, A., and Winter, G. By-passing immunization. Human antibodies from V-gene libraries displayed on phage. *J. Mol. Biol.*, *222*: 581-597, 1991.
13. de Haard, H. J., van Neer, N., Reurs, A., Huison, S. E., Roovers, R. C., Henderikx, P., de Bruijne, A. P., Arends, J. W., and Hoogenboom, H. R. A large non-immunized human Fab fragment phage library that permits rapid isolation and kinetic analysis of high affinity antibodies. *J. Biol. Chem.*, *274*: 18218-18230, 1999.
14. McCafferty, J., Griffiths, A., Winter, G., and Chiswell, D. Phage antibodies: filamentous phage displaying antibody variable domains. *Nature (Lond)*, *348*: 552-554, 1990.
15. Barbas, C. F., III, Kang, A. S., Lerner, R. A., and Benkovic, S. J. Assembly of combinatorial antibody libraries on phage surfaces: the gene III site. *Proc. Natl. Acad. Sci. USA*, *88*: 7978-7982, 1991.
16. Sheets, M., Amersdorffer, P., Fineman, R., Sargent, P., Lindqvist, E., Schier, R., Hemmingsen, G., Wong, C., Gerhart, J. C., and Marks, J. D. Efficient construction of a large nonimmune phage antibody library: the production of high-affinity human single-chain antibodies to protein antigens. *Proc. Natl. Acad. Sci. USA*, *95*: 6157-6162, 1998.
17. Griffiths, A. D., Malmqvist, M., Marks, J. D., Bye, J. M., Embleton, M. J., McCafferty, J., Baier, M., Holliger, K. P., Gorick, B. D., Hughes-Jones, N. C., et al. Human anti-self antibodies with high specificity from phage display libraries. *EMBO J.*, *12*: 725-734, 1993.
18. Amersdorffer, P., Wong, C., Smith, T., Chen, S., Deshpande, S., Sheridan, P., and Marks, J. D. Genetic and immunological comparison of anti-botulinum type A antibodies from immune and non-immune human phage libraries. *Vaccine*, *20*: 1640-1648, 2002.
19. Hoogenboom, H. R. Overview of antibody phage-display technology and its applications. *Methods Mol. Biol.*, *178*: 1-37, 2002.
20. Gao, C., Mao, S., Rouca, F., Zhuang, S., Quaranta, V., Wuschling, P., and Janda, K. D. *De novo* identification of tumor-specific internalizing human antibody-receptor pairs by phage-display methods. *J. Immunol. Methods*, *274*: 185-197, 2003.
21. Becerril, B., Poul, M. A., and Marks, J. D. Toward selection of internalizing antibodies from phage libraries. *Biochem. Biophys. Res. Commun.*, *255*: 386-393, 1999.

22. Nielsen, U. B., Kirpotin, D. B., Pickering, E. M., Hong, K., Park, J. W., Refaai Shalaby, M., Shao, Y., Benz, C. C., and Marks, J. D. Therapeutic efficacy of anti-ErbB2 immunoliposomes targeted by a phage antibody selected for cellular endocytosis. *Biochim. Biophys. Acta*, *1591*: 109-118, 2002.
23. Poul, M. A., Becerril, B., Nielsen, U. B., Morrison, P., and Marks, J. D. Selection of tumor-specific internalizing human antibodies from phage libraries. *J. Mol. Biol.*, *307*: 1149-1161, 2000.
24. Heitner, T., Moor, A., Garrison, J. L., Marks, C. C., Hasan, T., and Marks, J. D. Selection of cell binding and internalizing epidermal growth factor receptor antibodies from a phage display library. *J. Immunol. Methods*, *248*: 17-30, 2001.
25. O'Connell, D., Becerril, B., Roy-Burman, A., Daws, M., and Marks, J. D. Phage versus phagemid libraries for generation of human monoclonal antibodies. *J. Mol. Biol.*, *327*: 49-56, 2002.
26. Liu, B., and Marks, J. D. Applying phage antibodies to proteomics: selecting single chain Fv antibodies to antigens blotted on nitrocellulose. *Anal. Biochem.*, *286*: 119-128, 2000.
27. Huie, M. A., Cheung, M. C., Muench, M. O., Becerril, B., Kan, Y. W., and Marks, J. D. Antibodies to human fetal erythroid cells from a nonimmune phage antibody library. *Proc. Natl. Acad. Sci. USA*, *98*: 2682-2687, 2001.
28. Liu, B., Huang, L., Silthorn, C., Burlingame, A., and Marks, J. D. Towards proteome-wide production of monoclonal antibody by phage display. *J. Mol. Biol.*, *315*: 1063-1073, 2002.
29. Adams, G. P., McCarney, J. E., Tai, M. S., Oppermann, H., Huston, J. S., Stafford, W. F., III, Bookman, M. A., Fand, I., Houston, L. L., and Weiner, L. M. Highly specific *in vivo* tumor targeting by monovalent and divalent forms of 741F8 anti-erbB-2 single-chain Fv. *Cancer Res.*, *53*: 4926-4934, 1993.
30. Papahadjopoulos, D., Allen, T. M., Gabizon, A., Mayhew, E., Matthay, K., Huang, S. K., Lee, K. D., Woodle, M. C., Lasic, D. D., Redemann, C., *et al.* Sterically stabilized liposomes: improvements in pharmacokinetics and antitumor therapeutic efficacy. *Proc. Natl. Acad. Sci. USA*, *88*: 11460-11464, 1991.
31. Hayward, S. W., Dahiya, R., Cunha, G. R., Barick, J., Deshpande, N., and Narayan, P. Establishment and characterization of an immortalized but non-transformed human prostate epithelial cell line: EPH-1. *In Vitro Cell Dev. Biol. Anim.*, *31*: 14-24, 1995.
32. Watkins, S. J., and Norbury, C. J. Translation initiation and its deregulation during tumorigenesis. *Br. J. Cancer*, *86*: 1023-1027, 2002.
33. Skubitz, A. Adhesion molecules. *Cancer Treat. Res.*, *107*: 305-329, 2002.
34. Cai, X., and Garen, A. Anti-melanoma antibodies from melanoma patients immunized with genetically modified autologous tumor cells: selection of specific antibodies from single-chain Fv fusion phage libraries. *Proc. Natl. Acad. Sci. USA*, *92*: 6537-6541, 1995.
35. Li, J., Pereira, S., Van Belle, P., Tsui, P., Elder, D., Speicher, D., Deen, K., Linnesbach, A., Somasundaram, R., Swoboda, R., and Herlyn, D. Isolation of the melanoma-associated antigen p23 using antibody phage display. *J. Immunol.*, *166*: 432-438, 2001.
36. Varambally, S., Dhanasekaran, S. M., Zhou, M., Barrette, T. P., Kumar-Sinha, C., Sanda, M. G., Ghosh, D., Pienta, K. J., Sewalt, R. G., Otto, A. P., Rubin, M. A., and Chinnaiyan, A. M. The polycomb group protein EZH2 is involved in progression of prostate cancer. *Nature (Lond.)*, *419*: 624-629, 2002.
37. Park, J. W., Hong, K., Kirpotin, D. B., Colbern, G., Shalaby, R., Baseiga, J., Shao, Y., Nielsen, U. B., Marks, J. D., Moore, D., Papahadjopoulos, D., and Benz, C. C. Anti-HER2 immunoliposomes: enhanced efficacy attributable to targeted delivery. *Clin. Cancer Res.*, *8*: 1172-1181, 2002.
38. Cai, X., and Garen, A. A melanoma-specific VH antibody cloned from a fusion phage library of a vaccinated melanoma patient. *Proc. Natl. Acad. Sci. USA*, *93*: 6280-6285, 1996.

Cancer Research

The Journal of Cancer Research (1916-1930) | The American Journal of Cancer (1931-1940)

Mapping Tumor Epitope Space by Direct Selection of Single-Chain Fv Antibody Libraries on Prostate Cancer Cells

Bin Liu, Fraser Conrad, Matthew R. Cooperberg, et al.

Cancer Res 2004;64:704-710.

Updated version Access the most recent version of this article at:
<http://cancerres.aacrjournals.org/content/64/2/704>

Cited articles This article cites 38 articles, 14 of which you can access for free at:
<http://cancerres.aacrjournals.org/content/64/2/704.full#ref-list-1>

Citing articles This article has been cited by 13 HighWire-hosted articles. Access the articles at:
<http://cancerres.aacrjournals.org/content/64/2/704.full#related-urls>

E-mail alerts Sign up to receive free email-alerts related to this article or journal.

Reprints and Subscriptions To order reprints of this article or to subscribe to the journal, contact the AACR Publications Department at pubs@aacr.org.

Permissions To request permission to re-use all or part of this article, contact the AACR Publications Department at permissions@aacr.org.

Recombinant full-length human IgG1s targeting hormone-refractory prostate cancer

Bin Liu · Fraser Conrad · Audrey Roth ·
Daryl C. Drummond · Jeff P. Simko · James D. Marks

Received: 25 January 2007 / Revised: 2 March 2007 / Accepted: 13 March 2007 / Published online: 7 June 2007
© Springer-Verlag 2007

Abstract We have used a naive human single-chain fragment variable (scFv) library as a source of random shape repertoire to directly probe the altered surface chemistry of tumor cells. We reported previously the identification of more than 90 internalizing phage monoclonal antibodies targeting prostate cancer cells, including those that are hormone refractory. In this report, we describe the conversion of a panel of those scFvs into full-length human immunoglobulins (IgGs) and show that tumor specificity is retained. We have further shown that antibodies isolated from a naive phage display library can nevertheless be of high affinity towards target tumor cells.

Bin Liu received his Ph.D. in Biochemistry and Biophysics from University of California at San Francisco. He is currently an assistant professor and a program member of the UCSF Comprehensive Cancer Center. Dr. Liu's laboratory focuses on identifying cell surface molecules associated with tumor stem cells and human embryonic stem cells.

JAMES D. MARKS received his M.D. from University of California at San Francisco and Ph.D. from MRC Laboratory of Molecular Biology, Cambridge, England. He is currently a professor and Chief of Anesthesia and a program member of the UCSF Comprehensive Cancer Center. Dr. Marks's laboratory focuses on developing monoclonal antibody-based therapies against botulinum toxin and cancer.

Electronic supplementary material The online version of this article (doi:10.1007/s00109-007-0208-z) contains supplementary material, which is available to authorized users.

B. Liu · F. Conrad · A. Roth · J. D. Marks
Department of Anesthesia,
University of California at San Francisco,
1001 Potrero Avenue, 3C-38,
San Francisco, CA 94110, USA

B. Liu (✉) · J. P. Simko · J. D. Marks (✉)
UCSF Comprehensive Cancer Center,
University of California at San Francisco,
1001 Potrero Avenue, 3C-38,
San Francisco, CA 94110, USA
e-mail: liub@anesthesia.ucsf.edu
e-mail: marksj@anesthesia.ucsf.edu

D. C. Drummond
Hermes Biosciences, Inc.,
South San Francisco, CA 94115, USA

J. P. Simko
Department of Anatomical Pathology,
University of California at San Francisco,
San Francisco, CA 94143, USA

In addition, full-length IgGs retain the functionality of parental scFvs including the ability to rapidly enter target cells through receptor-mediated endocytosis and thereby to mediate efficient and specific intracellular payload delivery to tumor cells. We have used recombinant IgGs to immunoprecipitate target antigens and analyzed their molecular composition by mass spectrometry. We have identified one target antigen as activated leukocyte cell adhesion molecule (ALCAM)/MEMD/CD166 and have further studied tissue specificity of this internalizing ALCAM epitope by immunohistochemistry. Our study shows that cell type-specific internalizing human antibody can be readily identified from a naive phage antibody display library, characterized with regards to sequence, affinity, tissue specificity, and antigen identity, and modified genetically and chemically to generate various forms of targeted therapeutics.

Keywords Internalizing phage antibody · Recombinant human IgG1 · Hormone-refractory prostate cancer · Immunoliposomes · ALCAM/MEMD/CD166

Abbreviations

MAB	Monoclonal antibody
ScFv	Single-chain variable domain fragment
CaP	carcinoma of the prostate
AR	androgen receptor
ILs	immunoliposomes
MTX	methotrexate
K_D	dissociation equilibrium constant
LC-MS/MS	liquid chromatography–tandem mass spectrometry
IHC	immunohistochemistry
ALCAM	activated leukocyte cell adhesion molecule

Introduction

Carcinoma of the prostate (CaP) remains the most common and second most lethal cancer in American men [1]. Androgen deprivation and androgen receptor blockade have been commonly employed in the treatment of prostate cancer [2]. Although initially effective, hormone therapy fails for the majority of initial responders, as subpopulations of tumor cells undergo mutations and gain the capacity to proliferate in an androgen-deprived environment [3]. Identification of new target molecules and treatment strategies remains a critical goal of prostate cancer research, especially for the hormone-resistant form of this disease.

Due to their relatively easy accessibility to extracellularly administered targeting molecules, tumor-associated cell surface markers are invaluable for the development of targeted therapeutics. Targeted therapeutics are modular in nature: The tumor recognition may be provided by monoclonal antibodies (mAbs) to tumor antigens, and the tumor killing function may be provided by effectors, including but not limited to small molecule drugs, toxins, radionuclides, and immune effector cells. Therapeutic agents may be linked directly to the targeting ligand [4], linked covalently through a scaffold such as a polymer [5], or encapsulated in nanoparticle drug carriers such as immunoliposomes [6].

Despite the identification of a few markers associated with prostate cancer, the number of validated CaP cell surface receptors is limited, especially for the hormone-refractory form of this disease [7–15]. The quest continues for additional cell surface markers with more restricted patterns of tissue distribution and more specific associations with hormone-refractory CaP.

We have previously employed a functional approach to address the problem of identifying tumor-associated cell surface molecules [15]. Specifically, we sought to identify tumor epitopes not readily predicted or identified from microarray or other gene expression-based analyses. Using a naive human antibody library as a source of random shape

repertoire, we have performed selections on live tumor cells and identified a panel of phage antibodies that specifically target the surface of prostate cancer cells [15]. We have further devised the selection scheme to isolate antibodies that trigger receptor-mediated endocytosis [15–17]. Those antibody fragments are potential building blocks for various forms of targeted cancer therapeutics.

There are several issues that limit the use of naked single-chain fragment variables (scFvs) as therapeutics. The size of the scFv is below the renal threshold, leading to rapid clearance *in vivo* through the kidney [18]. In addition, the lack of an Fc component prevents engagement of effector cells, further limiting therapeutic effects of unmodified scFvs [19].

Given that the gene encoding the variable region of human antibodies can be readily sequenced, it is possible to create human immunoglobulins (IgGs) based on the genetic blueprint of corresponding scFvs. The Fc portion imparts the mAb with a circulating half-life of up to 4 weeks and the ability to interact with effector cells and complement molecules to achieve significant therapeutic benefit. We have, therefore, sought to convert scFvs into full-length IgGs, which are expected to display longer half-lives, higher thermal stability, higher functional affinity, and enhanced ability to engage effector cells [19].

The few published studies on IgG conversions have been performed mainly on scFvs selected against purified, recombinant antigens [20–27] or partially purified single antigen [28]. Our scFvs, however, have been selected against the complex antigen space on the surface of living cells. Thus, it is uncertain whether the conversion of these scFvs to IgGs would result in alterations to targeting specificity and in functionality such as internalization and tumor-specific payload delivery.

In this report, we describe the conversion of a panel of CaP-targeting internalizing scFvs to full-length human IgG1s. The recombinant IgG1 molecules have been subsequently characterized with regards to binding specificity, affinity, and the ability to target liposomes to hormone-refractory prostate cancer cells. Recombinant IgG1s have also been used to identify corresponding tumor antigens by immunoprecipitation and mass spectrometry analysis. We have identified activated leukocyte cell adhesion molecule (ALCAM)/MEMD/CD166 as the target antigen for one of our internalizing antibodies and have examined the expression pattern of this internalizing epitope on a panel of prostate cancer and normal human tissues.

Materials and methods

Materials Reagents for Chinese hamster ovary (CHO) cell transformation and propagation included G418 (Genetecin;

Life Technologies, Gaithersburg, MD), methotrexate (MTX), and hypoxanthine and thymidine (HT; Invitrogen, Carlsbad, CA). Reagents for IgG purification and characterization included protein G (Pharmacia-Pfizer, New York, NY); streptavidin-PE (Invitrogen/BioSource, Camarillo, CA); 5(6)-SFX (Invitrogen/Molecular Probes, Eugene, OR); 2,2'-azinobis(3-ethylbenzothiazoline-6-sulfonate) (ABTS), diaminobenzedime tetrahydrochloride (DAB), and protein A Sepharose (Sigma-Aldrich, St. Louis, MO); biotinylated monoclonal anti-CD166 antibody (Research Diagnostics, Flanders, NJ); hematoxylin (VectorLab, Burlingame, CA). Reagents for liposome preparation included DiI18(3)-DS (Invitrogen/Molecular Probes), 1-2-distearoyl-3-*sn*-glycerophosphocholine (DSPC) and methoxy poly(ethylene glycol)-distearoyl phosphatidylethanolamine (mPEG-DSPE; Avanti Polar Lipids, Alabaster, AL), cholesterol (Chol; Calbiochem, San Diego, CA) and Mal-PEG-DSPE (Shearwater Polymers, Huntsville, AL).

Cell lines PC3 and Du-145 prostate cancer cell lines were obtained from the American Type Culture Collection (ATCC, Rockville, MD). BPH-1 line was a kind gift from Dr. Jerry Cunha at UCSF. Cell lines were maintained in RPMI-1640 medium supplemented with 10% bovine calf serum, 100 IU/ml penicillin, and 100 µg/ml streptomycin in a humidified atmosphere of 95% air and 5% CO₂ at 37°C. The CHO-DG44 cell line (dhfr⁻; Invitrogen) was cultured in CHO-S-SFM II with HT according to manufacturer's instructions.

IgG construction VH genes of scFv were amplified using polymerase chain reaction from the respective phage DNA using primer pairs with overhangs containing *Mlu*I and *Nhe*I sites. DNA was digested with *Mlu*I and *Nhe*I, ligated into NSL-SerG1Val-Lark (kindly provided by Dr. Mitch Reff), and clones containing the correct VH identified by DNA sequencing [20]. VL genes were amplified from the respective phage DNA with the primer pairs with overhangs containing *Dra*III and *Kpn*I and ligated into *Dra*III- and *Kpn*I-digested NSL-SerG1Val-Lark DNA containing the appropriate VH gene. Clones containing the correct VH and VL gene were identified by DNA sequencing, and vector DNA was used to transfect CHO-DG44 cells by electroporation as described previously [20]. Stable cell lines were established by selection using G418 and expanded into 1-l spinner flasks. Supernatant containing IgG1 was collected, concentrated by ultrafiltration, and purified on protein G columns.

Increasing IgG production Two strategies were used to enrich for high IgG producers. In one approach, MTX was used to select for clones that have undergone gene amplifications. Fourteen days after electroporation, trans-

formed CHO-DG44 cells were stepwise exposed to increasing concentrations of MTX (5, 10, 40, and 100 nM). Surviving cells at a given MTX concentration were expanded in T-75 flasks in media containing the next higher levels of MTX. Cells surviving the final MTX concentration (100 nM) were expanded in 1-l spinner flasks in CHO-S-SFM II containing G418 and 100 nM MTX. In another approach, flow cytometry sorting was used to directly select high producers. Stably transformed CHO cells were incubated with phycoerythrin (PE)-conjugated F(ab')₂ raised against human IgG1s at 4°C for 30 min to detect membrane-bound IgG1s in the process of being secreted as described [29]. CHO cells were analyzed first by forward and side scatter dot plot to reveal two populations that were separated by P1 and P2 gates. Cells in the P2 gate were highly autofluorescent and were excluded for further analysis. The P1 population was gated by width and height of side and forward scatter sequentially to remove doublets from analysis. The non-autofluorescent, single cell population was sorted according to PE levels in the histogram (the P5 gate) [29]. About 100,000 cells were sorted and grown in CHO-S-SFM II media containing G418.

Affinity measurement on target cells Prostate cancer cells (PC3 and Du-145) were grown to 90% confluence in RPMI-1640 media supplemented with 10% fetal calf serum. Cells were harvested by brief digestion with trypsin (0.2%) in 2 mM ethylenediaminetetraacetic acid/phosphate buffered saline (EDTA/PBS). Biotinylated IgG1s were incubated with 10⁵ cells for 1 h at varying concentrations. Cell binding was performed at 4°C in PBS containing 0.25% bovine serum albumin (BSA) in a total volume of 100 µl. After two washes in PBS/BSA, cells were incubated with saturating amounts of streptavidin-PE for 30 min to detect bound IgG1s. Cells were washed twice and resuspended in PBS containing 1% paraformaldehyde. Binding affinity was determined using a fluorescence activated cell sorting (FACS)-based method as previously described [30, 31] with data fitted using KaleidaGraph (Synergy Software, Reading, PA).

Labeling IgG1s with fluorescent molecules Fluorescein isothiocyanate (FITC)-labeling reagent, 5(6)-SFX, was dissolved in dimethyl sulfoxide (5–10 mg/ml) and added to IgG1s in 50 mM carbonate buffer, pH 8.5 at a volume/volume ratio of 1:20. The reaction was allowed to proceed for 20 min on ice and stopped by the addition of excess Tris-HCl. Free labeling reagent was separated from the labeled antibody by dialysis (molecular weight cutoff 10,000 Da).

Fab' preparation IgG1 was incubated with pepsin (weight ratio 1:20) in 0.1 M sodium acetate (pH 3.7) at 37°C for

3 h, followed by dialysis against 4-(2-hydroxyethyl)-1-piperazineethanesulfonic acid (HEPES)-buffered saline (pH 6.0). The resulting F(ab')₂ was reduced with 2-mercaptoethylamine (20 mM) under argon for 15 min at 37°C and then recovered by gel filtration using Sephadex G-25 eluted with HEPES buffered saline (pH 7.0). The efficiency of cysteine reduction was assayed assessed by gel electrophoresis with Coomassie blue staining and was typically greater than 90% as determined by integration of the various bands in the lane.

Liposome preparation Unilamellar liposomes composed of DSPC, Chol, DiIc18(3)-DS, and mPEG-DSPE (molar ratio 6:6:0.03:0.03) were hydrated in HEPES buffered saline (5 mM HEPES, 145 mM NaCl, pH 6.5) using a repeated freeze-thawing method [32]. Liposomes were subsequently extruded ten times through polycarbonate filters with defined pore sizes of 0.1 μm and yielded liposomes of 100- to 120-nm diameter as determined by dynamic light scattering. Liposome concentration was measured using a standard phosphate assay [33].

To construct immunoliposomes, Fab's were conjugated to Mal-PEG-DSPE as described [34, 35]. Conjugation efficiencies were evaluated by sodium dodecyl sulfate-polyacrylamide gel electrophoresis (SDS-PAGE), allowing comparison of free mAb fragment vs conjugate. Typically 50–70% of Fab' molecules were conjugated. For incorporation into preformed liposomes, Fab'-PEG-DSPE, which form micellar solutions, were incorporated into liposomes by co-incubation at 55°C for 45 min at the ratio of 30 μg Fab' per mol phospholipid. The immunoconjugates, thus, resided exclusively in the outer lipid monolayer of the liposomes anchored by hydrophobic DSPE lipid molecules. Unincorporated unconjugated antibody fragments were separated from the immunoliposomes (ILs) by Sepharose CL-4B gel filtration chromatography.

Internalization experiment For flow cytometric assay, cells were seeded in 24 well plates at 80% confluence, incubated with DiIc18(3)-DS labeled naked liposomes or ILs at 37°C for 2 h, washed three times with PBS, removed from the dish by brief trypsin digest, exposed to glycine pH 2.8 at RT for 5 min to remove any residue surface-bound liposomes, washed once with PBS, and analyzed using LSR II (BD Biosciences, San Jose, CA).

For fluorescence microscopy studies, 100,000 cells were incubated in 12 well plates with nontargeted liposomes or Fab'-targeted ILs labeled with DiIc18(3)-DS for 2 h at 37°C, washed twice with glycine pH 2.8 containing 150 mM NaCl₂ followed by one wash with PBS, and observed using an inverted fluorescence microscope (Nikon Eclipse TE300, Nikon, Japan) with excitation using a band pass filter at 540/25 nm and a long pass filter at 565 nm for emission.

Immunoprecipitation and mass spectrometry analysis Ten million PC3 cells were lysed in 1% NP40, 0.15 M NaCl, and 0.01 M sodium phosphate, pH 7.2, on ice for 2 h. Lysis were incubated with H3 IgG (10 μg/ml) at 4°C for 1 h, followed by incubation with protein A Sepharose at 4°C for 1 h. Captured proteins were analyzed by 8% SDS-PAGE. Protein bands were visualized by Coomassie blue stain, excised and digested with trypsin. Peptides were extracted and analyzed by liquid chromatography-tandem mass spectrometry (LC-MS/MS) as described previously [36]. For Western blot analysis, H3-immunoprecipitation products were run on SDS-PAGE, blotted onto nitrocellulose membrane, and probed with a biotinylated mAb against ALCAM.

Immunohistochemistry study H3 IgG and a control IgG (anti-botulinum toxin) were labeled with sulfo-NHS-LC-biotin according to manufacturer's instructions (Pierce, Rockford, IL) and dialyzed against PBS. Eighteen frozen prostate cancer specimen and a panel of normal human tissues were obtained from the UCSF Comprehensive Cancer Center GU Tissue Core with approval by Committee on Human Research and with informed consent from each subject, stained with biotinylated H3 and control IgGs (1 μg/ml) at RT for 1 h. Bound IgGs were detected by streptavidin-conjugated horseradish peroxidase (HRP) using DAB as substrate as described [37]. The slides were counterstained with hematoxylin, dried in 70, 95, and 100% ethanol, mounted and analyzed by one of us (JS, a board certified pathologist).

Results

Generation of recombinant full-length human IgG1s from a panel of CaP-targeting scFvs IgG1s were constructed from seven internalizing scFvs. Six of these scFvs bind to CaP cell lines specifically. The seventh scFv, H3, binds to a broad spectrum of cell lines cultured in vitro but recognizes prostate cancer cells in tissue slides in a specific manner. DNA fragments encoding these scFvs were excised from the phage genome and spliced into a mammalian expression vector containing dual VH and VL expression cassettes [20, 23]. In this vector, VH and VL were fused to CH and CL, respectively, in the same plasmid to allow co-expression of human heavy and light chains in CHO-DG44 cells [20]. Transformed CHO cells were arrayed in 96 well plates and screened for IgG1 production by dot blot and enzyme-linked immunosorbent assay (ELISA; Fig. 1a). IgG1s were purified from serum-free media on a protein G column. Analysis of purified IgG1s by reducing SDS-PAGE showed the heavy and light chains with expected molecular weights (Fig. 1b).

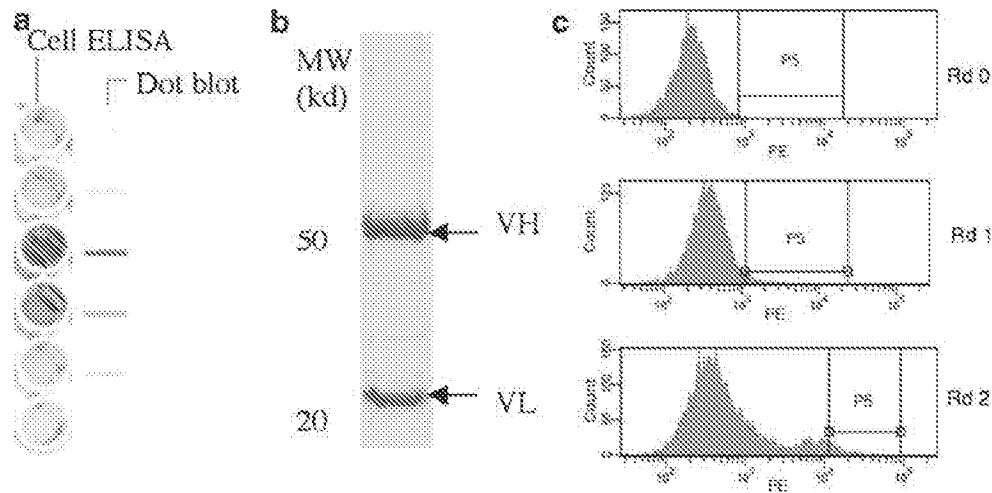


Fig. 1 Recombinant IgG1 production. **a** Screen for IgG1 producing CHO cells by dot blot and ELISA. **b** Analysis of purified IgG1 by reducing SDS-PAGE gel. Heavy and light chains are indicated. The purity is typically >97%. **c** Enriching high producers by flow sorting. Transfected CHO cells were incubated at 4°C for 30 min with PE-conjugated antihuman Fc F(ab')₂ to detect membrane-bound IgG1s. A

gate (P5) was set on histogram to sort cells with the top 5% of the fluorescence intensity of the sample population. The sorted cells were then expanded by culture under selective conditions, and the process was repeated two more times. *Rd0* Unselected population. *Rd1* Population after one round of selection. *Rd2* Population after two rounds of selection

Production levels varied between 1 and 25 mg/l. Two of the seven IgG1s produced at levels >20 mg/l, while the rest produced between 1 and 5 mg/l. Two strategies were used to improve yields of the moderate producers: One employed the MTX-induced gene amplification and the other direct FACS sorting of high producing cells [27]. The IgG1 expression vector contains the DHFR gene within the intron of the gene encoding the neomycin phosphotransferase. Stepwise exposure to increasing concentrations of MTX allows selection of clones with genomic amplification in regions containing the integrated IgG1 expression vector. We succeeded in using this method to improve production levels of two CHO–IgG1 clones. Alternatively, we have used the FACS method to directly enrich CHO cells that secrete high levels of IgG1s. Transformed CHO cells were stained with PE-conjugated antihuman Fc polyclonal antibody and sorted according to the amount of surface-bound IgG1s (Fig. 1c). After two rounds of sorting, selected cells were cultured in serum-free media containing G418, and secreted IgG1s were purified from the media. We achieved a three to fourfold improvement in production levels for the three IgG1s we applied this method to.

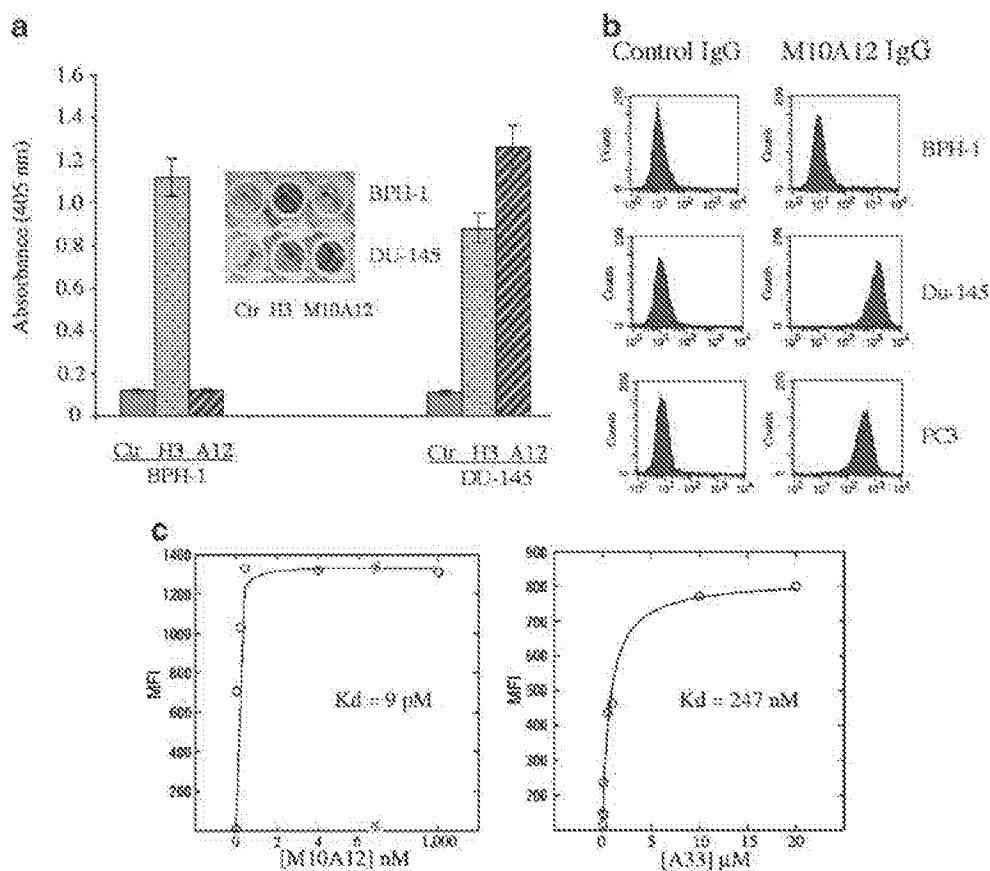
High-affinity binding of recombinant IgG1s to CaP cells We tested the binding activity of purified, recombinant IgG1s on CaP cells. Using cell ELISA assay, IgG1s were shown to be active in binding to target cells (Fig. 2a). FACS analysis confirmed this observation (Fig. 2b). To determine the range of affinities of these converted IgG1s,

we determined equilibrium binding constants (K_D) to CaP cells by FACS (Fig. 2c). Measured against Du-145 cells, four of the seven IgG1s showed affinity between 4 and 20 pM. On PC3 cells, the affinities were determined to be between 22 pM and 275 nM (Table 1). These results suggest that antibodies selected from a naive repertoire can nevertheless be of high affinity to target cells. The differences in apparent affinities towards PC3 and Du-145 cells are likely due to the cellular context of the target epitopes, including density on the cell surface and interaction with endogenous proteins competing with antibody binding.

Recombinant IgG1s retain binding specificity of parental scFvs Because differences in the fine specificity of antibodies can lead to differences in the panel of tumors recognized, we compared recombinant IgG1s with parental phage antibodies and scFvs, for their binding patterns to control and CaP cells. We observed by FACS that the binding patterns of IgG1s resemble that of parental phage antibodies (Fig. 3a). The patterns were also consistent with that of corresponding scFvs, although scFvs generated weaker signals than IgG1s and phage antibodies (Fig. 3b). These experiments demonstrate that recombinant full-length human IgG1s retain the binding specificity of parental phage antibodies and scFvs.

Internalization of IgG1s in CaP cells In addition to high-affinity binding to tumor cells, this panel of scFvs was originally selected for their ability to be internalized by CaP

Fig. 2 Evaluating binding specificity of recombinant IgG1s. **a** Cell ELISA. Recombinant M10A12 and H3 IgG1s were incubated with Du-145 and control BPH-1 cells. Bound IgG1s were detected by HRP-conjugated anti-human Fc. **b** FACS analysis. Binding of M10A12 IgG1 to CaP cell lines (PC3 and Du-145) and control BPH-1 cells. Control IgG1 is recombinant human IgG1 binding to botulinum toxin. **c** K_D measurement on Du-145 cells by FACS. Mean fluorescent intensity (MFI) data were plotted, and the K_D was determined by curve fit using KaleidaGraph



cells [37]. To examine if the recombinant IgG1s retain this property, we labeled IgG1s with FITC and examined their subcellular distribution by fluorescence microscopy. As shown in Fig. 4a, recombinant IgG1s were efficiently internalized by CaP cells. To quantify the ratio of surface bound vs internalized IgG1s, we measured fluorescent intensity of single cells by FACS and compared changes before and after glycine treatment that strips away surface-bound but not internalized IgG1s. As shown in Fig. 4b, glycine treatment caused a significant reduction (>90%) in fluorescence intensity for cells incubated with IgG1 at 4°C

but only a moderate reduction (40–60%) for cells incubated with IgG1 at 37°C (Fig. 4b). The percentage of internalized IgG1s was estimated from the ratios of fluorescence intensity before and after glycine treatment (Fig. 4b). Between 40 and 60% of the IgG1s were internalized by CaP cells.

Table 1 Binding affinities of recombinant IgG1s to CaP cells

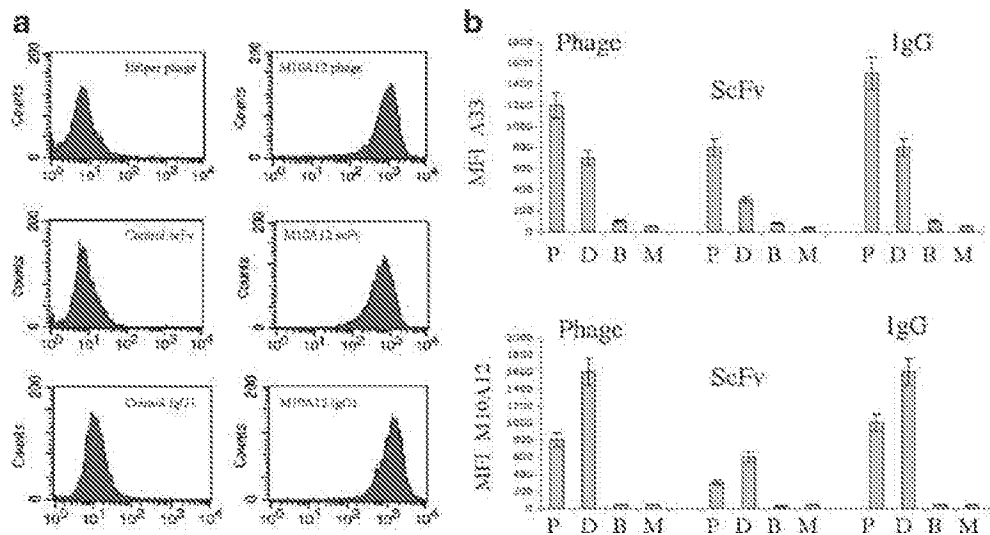
IgG1s	Affinity (K_D , in nM)	
	PC3	Du-145
A33	81	247
M10A12	0.040	0.009
C10	20	0.11
M9E4	ND	156
OA12	275	0.02
G12	0.022	0.009
H3	0.028	0.0044

K_D s were determined by FACS.

ND Not determined

Targeted payload delivery by Fab' immunoliposomes The internalizing activity of IgG1s suggests that they are capable of mediating intracellular payload delivery to CaP cells. We constructed targeted fluorescently labeled immunoliposomes and tested their uptake by CaP and control cells. We cleaved recombinant IgG1s with pepsin to generate $F(ab')_2$, which were reduced to generate Fab' with reactive sulfhydryl groups for conjugation with Mal-PEG-DSPE. The resulting Fab-PEGPE was inserted into liposomes labeled with fluorescent DiIC18(3)-DS. We tested these targeted DiIC18(3)-DS liposomes for specific internalization into CaP cells (Fig. 5). We found that A33-DiIC18(3)-DS-ILs were efficiently and specifically internalized into PC3 but not BPH-1 cells by direct fluorescence microscopic observation (Fig. 5a) and by quantitative analysis using FACS (Fig. 5b). Similar results were obtained with C10-DiIC18(3)-DS-ILs (Fig. 5b). By fluorescence microscopy, the liposomes appeared to accumulate in a

Fig. 3 Binding patterns of phage antibodies, scFvs, and IgG1s. **a** M10A12 phage antibody (10^{11} CFU/ml), scFv (50 μ g/ml), and recombinant IgG1 (5 μ g/ml) were tested for binding to Du-145 cells. Helper phage was used as a control. A scFv and a recombinant IgG1 against botulinum toxin were used as controls for scFv and IgG1 binding, respectively. **b** Quantification of binding to CaP and control cells by three forms (phage mAb, scFv, and IgG) of A33 and M10A12 antibodies. *P* PC3; *D* Du-145; *B* BPH-1 (control); *M* MCF10A (control)



punctuate perinuclear pattern, consistent with receptor-mediated endocytosis (Fig. 5a). These experiments show that Fab fragments of full IgG1s retain the highly specific internalizing functions of the parental scFvs and are capable of intracellular delivery of payloads to CaP cells.

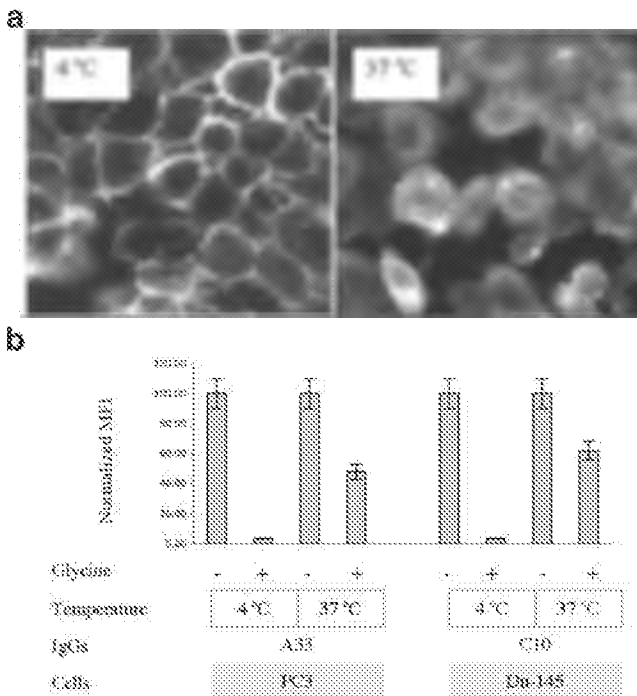
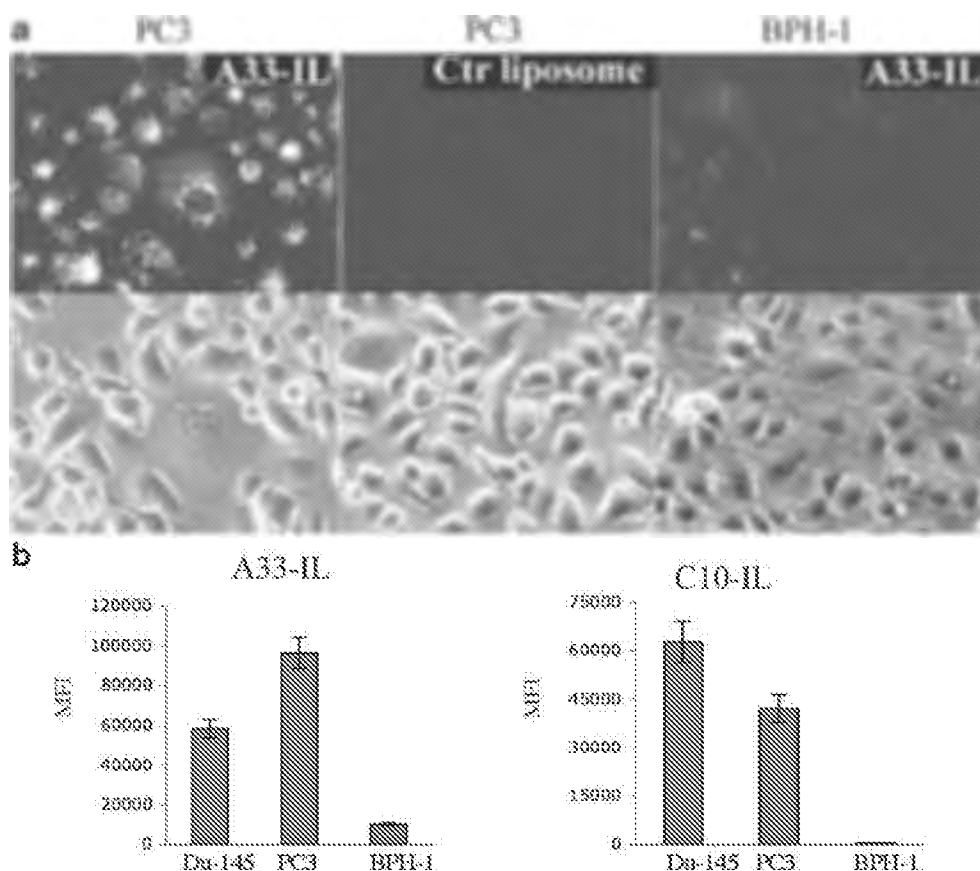


Fig. 4 Internalization of FITC-labeled IgG1s. **a** C10 IgG1 was incubated with Du-145 cells, and the reaction was allowed to proceed at either 4°C or 37°C for 2 h. Cellular distribution was examined by fluorescence microscopy. At 4°C, C10 IgG1 binds to cell membrane. Upon incubation at 37°C, C10 IgG1 is internalized by Du-145 cells. **b** Quantification of internalized fraction by FACS after surface stripping by glycine

Tumor antigen identification Recombinant IgGs have been routinely used in immunoprecipitation studies due to their ability to bind target antigens and protein A/G. We used our recombinant IgG1s to capture tumor antigens from prostate cancer cell lysates. We analyzed immunoprecipitation products of H3 IgG1 by LC-MS/MS and identified a set of peptides corresponding to ALCAM, also known as MEMD or CD166 (Fig. 6a). We further probed the captured tumor antigens with a commercial antibody raised against a unique ALCAM peptide. This antibody recognized immunoprecipitation products of H3 IgG but not two other IgGs (C10 and OA12; Fig. 6b), thus confirming the identity of H3 antigen as ALCAM.

Tumor association and tissue specificity To study tissue expression of the ALCAM epitope targeted by our H3 antibody, we performed IHC studies on a panel of frozen CaP (18 cases) and normal human tissues. H3 IgG1 showed intense tumor staining in all cases (18/18; Fig. 6c and Table 2 and Supplementary Fig. 1a, b). H3 IgG1 also stained some basal cells (6/18) and some normal adjacent epithelium (3/18; Table 2), often with reduced intensity (Supplementary Fig. 1b). H3 IgG1 also stained breast cancer tissues (5/5; Supplementary Fig. 1c) but not colon cancer specimens (4/4; Supplementary Fig. 1d). On normal tissues, H3 IgG did not stain brain, heart, liver, kidney, bladder, and oral tissues (Table 2). H3 IgG stained ganglion but not other cells in normal colon (Supplementary Fig. 2). In lung, H3 IgG did not stain alveoli cells but stained airway epithelial cells. In skin, H3 IgG stained only eccrine but not other skin structures. There was some weak salivary gland stain in one of four oral tissues studied (Supplementary Fig. 2). Pancreas tissues were not studied due to a lack of frozen specimens. Overall, the H3 epitope is strongly overexpressed in human prostate cancer, but is expressed at

Fig. 5 Internalization of immunoliposomes by CaP cells. **a** Fluorescence microscopic evaluation of uptake of DiI-labeled A33 immunoliposome (A33-IL) and nontargeted liposome (Ctr) in PC3 and BPH-1 cells. Corresponding phase contrast pictures are shown below. **b** Quantification of internalization of DiI-labeled immunoliposomes by CaP and control cells using FACS. A33-ILs and C10-ILs were shown. Errors <10%



undetectable or low levels on most of normal human tissues except airway epithelium, colon ganglion, and skin eccrine.

Discussion

We have generated recombinant full-length human IgG1s from a panel of prostate cancer targeting phage antibodies. We have found that (1) recombinant human IgG1s recapitulate binding specificity of their parental scFvs and phage antibodies; (2) recombinant IgG1s bind to target tumor cells with high affinity with K_{DS} in the range of 4 to 275 nM; (3) functionality of the parental phage antibody has been preserved, including the ability to enter tumor cells through receptor-mediated endocytosis and to mediate targeted intracellular payload delivery. Our studies thus demonstrate that (1) complex antigenic determinants such as the entire cell surface can be targets for selection of phage antibody library; (2) The resulting phage antibody can be routinely converted into various forms, including full-length IgG molecule, without losing desired, preselected specificity and functionality, thus providing a direct route to the development of mAb-based therapeutics.

Recombinant antibodies are an important class of drugs for treatment of diseases caused by infectious agents,

autoimmunity, and cancer [19]. Our panel of recombinant IgG1s are entirely human in sequence, avoiding human anti-mouse antibody reactions [38]. Compared to antibodies generated against peptides or recombinant antigens, our IgG1s recognize antigens in their native states and are more likely to retain reactivity during subsequent in vivo applications. In addition to prolonging the circulating half-life, the addition of Fc enables IgG1 to engage effector cells to achieve enhanced antitumor function. Our initial study on Du-145 xenografts using naked IgG1s has shown that in addition to growth inhibition in vitro, other factors such as antibody-dependent cell-mediated cytotoxicity and antibody-dependent complement cytotoxicity contribute significantly to IgG1 activities in vivo (data not shown), consistent with previous studies [39, 40].

In addition to IgG, recombinant antibody fragments (scFv and Fab) are themselves valuable agents for drug development [41–45], as certain therapeutic applications require the absence of the Fc region to minimize side effects. We have conjugated Fab' to the surface of liposomes and demonstrated their specific uptake by prostate cancer cells. Liposomes [46] and immunoliposomes [6, 47] are effective drug delivery strategies when constructed properly. We have previously demonstrated potent and specific antitumor efficacy with HER2-targeted ILs gener-

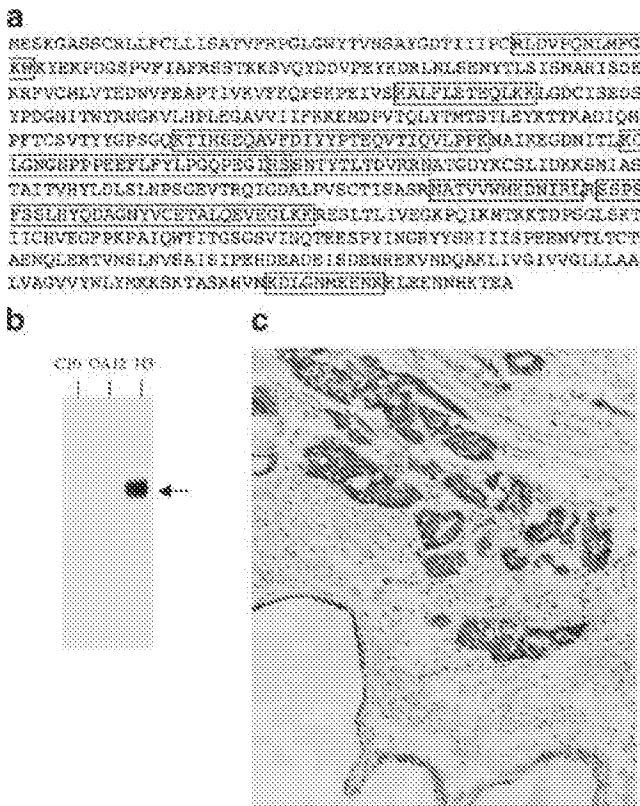


Fig. 6 Antigen identification and IHC study. **a** Antigen identification by LC-MS/MS. The H3 immunoprecipitation products were analyzed by LC-MS/MS, and the antigen was identified as *Homo sapiens* MEMD, with MW 64,972 Da, and pI 5.9. Peptides identified by LC-MS/MS are boxed. **b** Analysis of immunoprecipitation products by Western blot using a commercial monoclonal anti-ALCAM antibody. H3 IgG and two other control IgGs (C10 and OA12) were used in this study. Arrow indicates ALCAM. **c** IHC study on prostate cancer tissues using biotinylated H3 IgG1. Tumor epithelium is stained intensely

ated using either scFv or Fab' fragments [35, 48]. For the majority of antibodies studied (3/5), we have not found significant differences in internalizing activity between ILs constructed from either Fab' or scFv (data not shown). For the rest (2/5), Fab'-ILs showed more active internalizing activities than scFv-ILs. This is likely due to methods that we used to construct ILs, where pre-conjugated scFv- or Fab'-PEG-DSPE were inserted into liposomes during phase transition at 55°C. Fab' may be more stable than scFv under this condition. We are developing alternative construction methods that do not require insertion through lipid phase transition, which would be generally applicable to scFv and Fab'.

The availability of a panel of well-characterized recombinant human IgG1 allows identification of target antigens by immunoprecipitation and mass spectrometry. We have used one of our recombinant IgG1s, H3, to capture the target antigen from cell lysates and have analyzed the immunoprecipitation products by LC-MS/MS. We have identified ALCAM/MEMD/CD166 as the antigen bound by

Table 2 Summary of IHC studies

Tissue type	Staining results
CaP	Tumor (18/18) Tumor and basal cells (6/18) Tumor and basal cells and adjacent normal (3/18)
Normal	
Brain	No stain (7/7)
Heart	No stain (2/2)
Liver	No stain (3/4); some bile duct stain (1/4)
Kidney	No stain (4/4)
Lung	No stain of alveoli (5/5); stain bronchial epithelium (5/5)
Colon	No stain except ganglion cells (4/4)
Bladder	No stain (3/3)
Skin	No stain except eccrine (2/3)
Oral	No stain (3/4); some stain of salivary gland (1/4)

A panel of frozen high-grade (Gleason >3+3) primary prostate cancer tissues and normal tissues were stained with biotinylated H3 IgG. A biotinylated anti-botulinum toxin IgG was used as the negative control. The number of positively stained specimens is indicated along with total cases studied.

the H3 IgG1. ALCAM is a member of the immunoglobulin superfamily with five extracellular immunoglobulin-like domains. Its role in cancer development was reported initially in metastasizing human melanoma cells [49]. To determine tissue distribution, we performed IHC studies using labeled H3 IgG1 on a panel of frozen prostate cancer and normal human tissues. The internalizing ALCAM epitope targeted by our H3 IgG1 is strongly expressed on all prostate cancer tissues examined (18 cases with Gleason scores >3+3). The epitope is also expressed at a reduced level on prostate basal cells. Given that the prostate is not a vital organ, this expression pattern does not preclude the use of this ALCAM epitope for targeting. Except for airway epithelium, colon ganglion, and skin eccrine, this ALCAM epitope is not significantly expressed on normal human tissues that we have studied, including vital organs such as the brain, heart, kidney, and liver. Further studies are needed to determine if primary cells derived from normal human airway take up H3 antibody less efficiently than tumor cells and if they are, consequently, less sensitive to liposomal drugs targeted by the H3 antibody. While this work is in progress, independent studies by other investigators have identified ALCAM as a prognostic and diagnostic marker for prostate cancer [50] and a target for immunotoxin-based anticancer therapy [51], consistent with our results.

Our studies demonstrate that cell type-specific, fully human mAbs can be readily identified from phage antibody display libraries and modified genetically and chemically to produce various forms of targeted therapeutics. Studies are under way to evaluate the efficacy of naked IgG1s in prostate

cancer xenografts and to construct immunoliposomes containing small molecule drugs disrupting various pathways required by neoplastic cells for growth and survival.

Acknowledgement We thank the UCSF Biomolecular Resource Center and the National Mass Spectrometry Facility for analysis of protein samples, Dr. Jianlong Lou and Richard Tsai for help with mammalian cell transfection. This work is supported by grants from the National Cancer Institute Specialized Programs of Research Excellence (SPORE) in Prostate Cancer (P50 CA89520; JDM) and the National Institute of Health (R01 CA118919 and R21 DK066429; BL).

References

- Jamal A, Kulldorff M, Devesa SS, Hayes RB, Fraumeni JF Jr (2002) A geographic analysis of prostate cancer mortality in the United States, 1970–89. *Int J Cancer* 101:168–174
- Rini BI, Small EJ (2001) An update on prostate cancer. *Curr Opin Oncol* 13:204–211
- Cude KJ, Montgomery JS, Price DK, Dixon SC, Kincaid RL, Kovacs KF, Venzon DJ, Liewehr DJ, Johnson ME, Reed E, Figg WD (2002) The role of an androgen receptor polymorphism in the clinical outcome of patients with metastatic prostate cancer. *Urol Int* 68:16–23
- Tolcher AW, Sugarman S, Gelmon KA, Cohen R, Saleh M, Isaacs C, Young L, Healey D, Onetto N, Slichenmyer W (1999) Randomized phase II study of BR96-doxorubicin conjugate in patients with metastatic breast cancer. *J Clin Oncol* 17:478–484
- Kasuya Y, Lu ZR, Kopeckova P, Minko T, Tabibi SE, Kopecek J (2001) Synthesis and characterization of HPMA copolymer-aminopropylgeldanamycin conjugates. *J Control Release* 74:203–211
- Noble CO, Kirpotin DB, Hayes ME, Mamot C, Hong K, Park JW, Benz CC, Marks JD, Drummond DC (2004) Development of ligand-targeted liposomes for cancer therapy. *Expert Opin Ther Targets* 8:335–353
- Fair WR, Israeli RS, Heston WD (1997) Prostate-specific membrane antigen. *Prostate* 32:140–148
- Magee JA, Araki T, Patil S, Ehrig T, True L, Humphrey PA, Catalona WJ, Watson MA, Milbrandt J (2001) Expression profiling reveals hepsin overexpression in prostate cancer. *Cancer Res* 61:5692–5696
- Varambally S, Dhanasekaran SM, Zhou M, Barrette TR, Kumar-Sinha C, Sanda MG, Ghosh D, Pienta KJ, Sewalt RG, Otte AP, Rubin MA, Chinnaiyan AM (2002) The polycomb group protein EZH2 is involved in progression of prostate cancer. *Nature* 419:624–629
- Dhanasekaran SM, Barrette TR, Ghosh D, Shah R, Varambally S, Kurachi K, Pienta KJ, Rubin MA, Chinnaiyan AM (2001) Delineation of prognostic biomarkers in prostate cancer. *Nature* 412:822–826
- Hubert RS, Vivanco I, Chen E, Rastegar S, Leong K, Mitchell SC, Madraswala R, Zhou Y, Kuo J, Raitano AB, Jakobovits A, Saffran DC, Afar DE (1999) STEAP: a prostate-specific cell-surface antigen highly expressed in human prostate tumors. *Proc Natl Acad Sci USA* 96:14523–14528
- Yang D, Holt GE, Velders MP, Kwon ED, Kast WM (2001) Murine six-transmembrane epithelial antigen of the prostate, prostate stem cell antigen, and prostate-specific membrane antigen: prostate-specific cell-surface antigens highly expressed in prostate cancer of transgenic adenocarcinoma mouse prostate mice. *Cancer Res* 61:5857–5860
- Reiter RE, Gu Z, Watabe T, Thomas G, Szigeti K, Davis E, Wahl M, Nisifani S, Yamashiro J, Le Beau MM, Loda M, Witte ON (1998) Prostate stem cell antigen: a cell surface marker overexpressed in prostate cancer. *Proc Natl Acad Sci USA* 95:1735–1740
- Saffran DC, Raitano AB, Hubert RS, Witte ON, Reiter RE, Jakobovits A (2001) Anti-PSCA mAbs inhibit tumor growth and metastasis formation and prolong the survival of mice bearing human prostate cancer xenografts. *Proc Natl Acad Sci USA* 98:2658–2663
- Liu B, Conrad F, Cooperberg MR, Kirpotin DB, Marks JD (2004) Mapping tumor epitope space by direct selection of single-chain Fv antibody libraries on prostate cancer cells. *Cancer Res* 64:704–710
- Pouli MA, Becerril B, Nielsen UB, Moirsson P, Marks JD (2000) Selection of tumor-specific internalizing human antibodies from phage libraries. *J Mol Biol* 301:1149–1161
- Becerril B, Poul MA, Marks JD (1999) Toward selection of internalizing antibodies from phage libraries. *Biochem Biophys Res Commun* 255:386–393
- Lamarre A, Yu MW, Chagnon F, Talbot PJ (1997) A recombinant single chain antibody neutralizes coronavirus infectivity but only slightly delays lethal infection of mice. *Eur J Immunol* 27:3447–3455
- Carter P (2001) Improving the efficacy of antibody-based cancer therapies. *Nat Rev Cancer* 1:118–129
- Nowakowski A, Wang C, Powers DB, Anisendorfer P, Smith TJ, Montgomery VA, Sheridan R, Blake R, Smith LA, Marks JD (2002) Potent neutralization of botulinum neurotoxin by recombinant oligoclonal antibody. *Proc Natl Acad Sci USA* 99:11346–11350
- Ames RS, Tornetta MA, Deen K, Jones CS, Swift AM, Ganguly S (1995) Conversion of murine Fabs isolated from a combinatorial phage display library to full length immunoglobulins. *J Immunol Methods* 184:177–186
- Thompson JE, Vaughan TJ, Williams AJ, Wilton J, Johnson KS, Bacon L, Green JA, Field R, Ruddock S, Martins M, Pope AR, Tempest PR, Jackson RH (1999) A fully human antibody neutralising biologically active human TGFbeta2 for use in therapy. *J Immunol Methods* 227:17–29
- Miescher S, Zahn-Zabal M, De Jesus M, Moudry R, Fisch I, Vogel M, Kohn M, Imboden MA, Kragten E, Biehler J, Mermod N, Stadler BM, Amstutz H, Wurm F (2000) CHO expression of a novel human recombinant IgG1 anti-RhD antibody isolated by phage display. *Br J Haematol* 111:157–166
- Simmons LC, Reilly D, Klimowski L, Raju TS, Meng G, Sims P, Hong K, Shields RL, Damico LA, Rancatore P, Yansura DG (2002) Expression of full-length immunoglobulins in *Escherichia coli*: rapid and efficient production of glycosylated antibodies. *J Immunol Methods* 263:133–147
- Chen L, Liebman MA, Teodorescu-Frumosu S, Schnitzler AC, Sharon J (2003) Expression of a prototypic anti-colorectal cancer polyclonal antibody library in mammalian cells. *Immunol Lett* 88:135–140
- Huis GA, Hojnen IA, Cuomo ME, Koningsberger JC, Wiegman L, Boel E, van der Vuurst de Vries AR, Loyson SA, Helfrich W, van Berge Henegouwen GR, van Meijer M, de Kruif J, Logtenberg T (1999) A recombinant, fully human monoclonal antibody with antitumor activity constructed from phage-displayed antibody fragments. *Nat Biotechnol* 17:276–281
- Borrebaeck CA, Malmberg AC, Furebring C, Michaelsson A, Ward S, Danielsson L, Ohlin M (1992) Kinetic analysis of recombinant antibody-antigen interactions: relation between structural domains and antigen binding. *Biotechnology (N Y)* 10:697–698
- Geuijen CA, Clijsters-van der Horst M, Cox F, Rood PM, Throsby M, Jongeneelen MA, Backus HH, van Deventer E, Kruisbeek AM, Goudsmit J, de Kruif J (2005) Affinity ranking of antibodies using flow cytometry: application in antibody phage display-based target discovery. *J Immunol Methods* 302:68–77

29. Brezinsky SC, Chiang GG, Szilvasi A, Mohan S, Shapiro RI, MacLean A, Sisk W, Thill G (2003) A simple method for enriching populations of transfected CHO cells for cells of higher specific productivity. *J Immunol Methods* 277:141–155
30. Henderikx P, Coolen-van Neer N, Jacobs A, van der Linden E, Arends JW, Mullberg J, Hoogenboom HR (2002) A human immunoglobulin G1 antibody originating from an in vitro-selected Fab phage antibody binds avidly to tumor-associated MUC1 and is efficiently internalized. *Am J Pathol* 160:1597–1608
31. Benedict CA, MacKrell AJ, Anderson WF (1997) Determination of the binding affinity of an anti-CD34 single-chain antibody using a novel, flow cytometry based assay. *J Immunol Methods* 201:223–231
32. Szoka F Jr, Papahadjopoulos D (1980) Comparative properties and methods of preparation of lipid vesicles (liposomes). *Annu Rev Biophys Bioeng* 9:467–508
33. Bartlett GR (1959) Phosphorus assay in column chromatography. *J Biol Chem* 234:466–468
34. Kirpotin D, Park JW, Hong K, Zalipsky S, Li WL, Carter P, Benz CC, Papahadjopoulos D (1997) Sterically stabilized anti-HER2 immunoliposomes: design and targeting to human breast cancer cells in vitro. *Biochemistry* 36:66–75
35. Park JW, Hong K, Kirpotin DB, Colbern G, Shalaby R, Baseiga J, Shao Y, Nielsen UB, Marks JD, Moore D, Papahadjopoulos D, Benz CC (2002) Anti-HER2 immunoliposomes: enhanced efficacy attributable to targeted delivery. *Clin Cancer Res* 8:1172–1181
36. Liu B, Huang L, Silibom C, Burlingame A, Marks JD (2002) Towards proteome-wide production of monoclonal antibody by phage display. *J Mol Biol* 315:1063–1073
37. Liu G, Dou S, He J, Vanderheyden JL, Ruszkowski M, Hnatowich DJ (2004) Preparation and properties of $^{99m}\text{Tc}(\text{CO})_3^+$ -labeled *N,N*-bis(2-pyridylmethyl)-4-aminobutyric acid. *Bioconjug Chem* 15:1441–1446
38. Bradbury A (2000) Evolution of the display technologies. *Trends Biotechnol* 18:183–184
39. Clynes RA, Towers TL, Presta LG, Ravetch JV (2000) Inhibitory Fc receptors modulate in vivo cytotoxicity against tumor targets. *Nat Med* 6:443–446
40. Spiridon CL, Guinn S, Vitetta ES (2004) A comparison of the in vitro and in vivo activities of IgG and F(ab')₂ fragments of a mixture of three monoclonal anti-Her-2 antibodies. *Clin Cancer Res* 10:3542–3551
41. Hoogenboom HR, Henderikx P, de Haard H (1998) Creating and engineering human antibodies for immunotherapy. *Adv Drug Deliv Rev* 31:5–31
42. Hoogenboom HR, de Bruijn AP, Hufton SE, Hoet RM, Arends JW, Roovers RC (1998) Antibody phage display technology and its applications. *Immunotechnology* 4:1–20
43. Adams GP, Shaller CC, Dadachova E, Simmons HH, Horak EM, Tesfaye A, Klein-Szanto AJ, Marks JD, Brechbiel MW, Weiner LM (2004) A single treatment of yttrium-90-labeled CHX-A[®]-C6.5 diabody inhibits the growth of established human tumor xenografts in immunodeficient mice. *Cancer Res* 64: 6200–6206
44. Horak E, Helmer T, Robinson MK, Simmons HH, Garrison J, Russeva M, Furmanova P, Lou J, Zhou Y, Yuan QA, Weiner LM, Adams GP, Marks JD (2005) Isolation of scFvs to in vitro produced extracellular domains of EGFR family members. *Cancer Biother Radiopharm* 20:603–613
45. Robinson MK, Doss M, Shaller C, Narayanan D, Marks JD, Adler LP, Gonzalez Trotter DE, Adams GP (2005) Quantitative immuno-positron emission tomography imaging of HER2-positive tumor xenografts with an iodine-124 labeled anti-HER2 diabody. *Cancer Res* 65:1471–1478
46. Drummond DC, Meyer O, Hong K, Kirpotin DB, Papahadjopoulos D (1999) Optimizing liposomes for delivery of chemotherapeutic agents to solid tumors. *Pharmacol Rev* 51:691–743
47. Sapsa P, Allen TM (2003) Ligand-targeted liposomal anticancer drugs. *Prog Lipid Res* 42:439–462
48. Nielsen UB, Kirpotin DB, Pickering EM, Hong K, Park JW, Refaat Shalaby M, Shao Y, Benz CC, Marks JD (2002) Therapeutic efficacy of anti-ErbB2 immunoliposomes targeted by a phage antibody selected for cellular endocytosis. *Biochim Biophys Acta* 1591:109–118
49. Degen WG, van Kempen LC, Gijzen EG, van Groningen JJ, van Kooyk Y, Bloemers HP, Swart GW (1998) MEMD, a new cell adhesion molecule in metastasizing human melanoma cell lines, is identical to ALCAM (activated leukocyte cell adhesion molecule). *Am J Pathol* 152:805–813
50. Kristiansen G, Pilarsky C, Wissmann C, Kaiser S, Bruemendorf T, Roepcke S, Dahl E, Hinzmann B, Specht T, Pervan J, Stephan C, Loening S, Dietel M, Rosenthal A (2005) Expression profiling of microdissected matched prostate cancer samples reveals CD166/MEMD and CD24 as new prognostic markers for patient survival. *J Pathol* 205:359–376
51. Piazza T, Cha E, Bongarzone I, Canevari S, Bolognesi A, Polito L, Bargellesi A, Sassi F, Ferrini S, Fabbri M (2005) Internalization and recycling of ALCAM/CD166 detected by a fully human single-chain recombinant antibody. *J Cell Sci* 118:1515–1525

Report

Simple and efficient liposomal encapsulation of topotecan by ammonium sulfate gradient: stability, pharmacokinetic and therapeutic evaluation

Jun-Jen Liu,¹ Ruey-Long Hong,² Wen-Fang Cheng,³ Keelung Hong,⁴ Fu-Hsiung Chang¹ and Yun-Long Tseng²

¹Graduate Institute of Biochemistry and Molecular Biology, and Departments of ²Oncology and ³Gynecology, National Taiwan University Hospital, Taipei 10016, Taiwan, ROC. ⁴California Pacific Medical Center, Research Institute, San Francisco, CA 94115, USA

Topotecan (TPT), a topoisomerase I inhibitor, is presently undergoing clinical evaluation worldwide. Previous studies have shown that entrapping TPT within multi-lamellar vesicle liposome can stabilize the lactone moiety, which is structurally important for biological activity. However, low drug:lipid ratios due to the amphipathic character and small entrapment volume in the unilamellar vesicle limits the development of pharmaceutically acceptable liposomal formulation. With an aim to improve on this drawback, we herein describe a method that utilizes the ammonium sulfate gradient to entrap TPT into liposomes. By this method, the encapsulation efficiency was over 96% and a drug:lipid molar ratio as high as 1:5.4 was reached. In comparison with free drug, liposome-encapsulated TPT is more stable in physiological conditions and shows higher *in vitro* cytotoxicity. Because of increased blood circulation time, the initial plasma concentration and area under the plasma concentration of liposomal drugs were 14 and 40 times, respectively, of those of free drug. Furthermore, liposome encapsulation enhanced the antitumor activity of TPT in syngeneic murine C-26 and human HTB-9 xenograft models *in vivo*. At a dose of 5 mg/kg, the tumor growth delay of liposomal formulation was significantly than that of free TPT. Based on these results, we believe that this liposomal TPT formulation is worthy of further clinical study. [© 2002 Lippincott Williams & Wilkins.]

Key words: Ammonium sulfate gradient, drug delivery system, liposome, topotecan.

Introduction

Topotecan (TPT, 9-dimethylaminomethyl-10-hydroxy-camptothecin), a semisynthetic analog of camp-

tothecin (CPT), has enhanced aqueous solubility and reduced protein binding relative to CPT. Its anti-tumor activity has been demonstrated in preclinical tumor models,¹ and in phase II clinical trials of ovarian cancer,² non-small cell lung cancer³ and colorectal cancer.⁴ Similar to CPT and other derivatives, TPT is a cell cycle-specific drug and acts as stabilizer of complex of DNA and topoisomerase I. This results in single-strand break of DNA, which leads to severe DNA damage during subsequent replication followed by cell death.^{1,5,6} Therefore, it is advantageous to expose tumor cells to the drug for a prolonged period. This point is supported by clinical observations that patients refractory to TPT exhibited increased response rates when the drug was administered as a low-dose infusion.⁷ Unfortunately, TPT is extremely unstable in physiological conditions.^{5,8} Conversion of the lactone form into the carboxylate form occurs rapidly at physiological pH.⁹ Although the cellular basis of its antitumor activity is still incompletely understood, available data indicates that an intact α -hydroxylactone ring is important both for passive diffusion of the drug into cells as well as for inhibition of topoisomerase I.^{5,10,11} Accordingly, efforts have been made to explore factors affecting its structure stability in order to improve the cytotoxic activity.¹²⁻¹⁴

Liposomes have been used for drug delivery in the past three decades. Several studies have shown that liposome encapsulation of anticancer agents can alter tissue disposition,^{15,16} reduce blood clearance rate,¹⁷ decrease toxicity and enhance antitumor activity.^{18,19} In addition to these advantages, the properties of TPT, i.e. S phase-specific cytotoxicity and fast inactivation at physiological pH, make it worthwhile to develop liposomal TPT. Previous work

This work was supported in part by a Grant from the National Science Council, Taiwan.

Correspondence to Y-L Tseng, Department of Oncology, National Taiwan University Hospital, National Taiwan University, 7 Chung-Shan South Road, Taipei 10016, Taiwan. Tel: (+886) 2 23123456; Fax: (+886) 2 23711174; E-mail: d4442008@nmsun.mc.ntu.edu.tw

has shown that complex of CPTs with lipid vesicles, composed of DMPC or DMPG, can stabilize its lactone moiety and thereby prevent drug inactivation.²⁰ However, low drug:lipid ratios due to the amphipathic character and small entrapment volume in the unilamellar vesicle limited the development of pharmaceutically acceptable liposomal formulations.^{21,22} To improve trapping efficiency, a strategy that uses a transmembrane ionic gradient to pack drugs within the liposome would be useful. In the present work, therefore, the ammonium sulfate remote-loading method was selected for developing an acceptable liposomal TPT formulation. With this method, higher TPT loading could be achieved. In addition, the low pH environment spontaneously generated after removal of ammonium ions²³ could maintain TPT in its active lactone form. The pharmacokinetic properties and antitumor activity of both free and liposomal TPT were compared in the present work.

Materials and methods

Materials

TPT (SmithKline Beecham, King of Prussia, PA) was obtained as a commercially available product. Distearoyl phosphatidylcholine (DSPC) and cholesterol (Chol) were purchased from Avanti Polar Lipids (Alabaster, AL). The lipids were dissolved in chloroform, sealed in ampoules under argon and stored at -20°C before use. HPLC-grade acetonitrile and glacial acetic acid were purchased from JT Baker (Mallinckrodt Baker, Phillipsburg, NJ). Cell culture materials were obtained from Gibco/BRL (Grand Island, NY). All other chemicals were purchased from Sigma (St Louis, MO).

Cells and cell culture

Cells of HTB-9 (human bladder carcinoma) and C-26 (murine colon carcinoma) were cultured as exponentially growing subconfluent monolayers on 100-mm plates (Corning, Corning, NY) or 75-cm² tissue culture flask (TPP, Zollstrasse, Switzerland) in RPMI 1640 medium supplemented with 10% (v/v) fetal calf serum and 2 mM glutamine at $37^{\circ}\text{C}/5\% \text{CO}_2$ in a humidified incubator.

Preparation of liposomes

Small unilamellar vesicles (SUV, size less than 100 nm) were prepared by a combination of the

standard thin-film hydration method and repeated extrusion in the following way.²⁴ DSPC:Chol (molar ratio 3:2) were dissolved in chloroform and placed in a round-bottomed flask. The solvent was removed by rotary evaporation under reduced pressure. The resulting dry lipid film was hydrated at 60°C in ammonium sulfate solution [250 mM $(\text{NH}_4)_2\text{SO}_4$, pH 5.0, 530 mOs] and dispersed by hand shaking at 60°C . The suspension was frozen and thawed 5 times,²⁵ and followed by repeated extrusion through polycarbonate membrane filters (Costar, Cambridge, MA) of 0.1- μm pore size 3 times and 0.05- μm pore size 7 times by using high-pressure extrusion equipment (Lipex Biomembranes, Vancouver, BC) at 60°C . After extrusion, the extra-liposomal salt was removed by a Sephadex G-50 column (Pharmacia Biotech, Uppsala, Sweden) equilibrated with 100 mM MES buffer solution containing 260 mM NaCl and 2 mM EDTA (pH 5.5, 580 mOs).

TPT encapsulation

TPT was encapsulated into liposome using an ammonium sulfate gradient.²⁶ After removing the extra-liposomal salt by a Sephadex G-50 column, TPT in powder form was added immediately into the solution at a concentration of 1 mg TPT/10 μmol phospholipid. The mixture of liposome and TPT was incubated in 60°C water bath for 30 min with agitation (100 r.p.m.). After loading, untrapped TPT was removed by Sephadex G-50 gel filtration in 0.9% NaCl solution at pH 6.0 and osmolarity of 286 mOs. For the passive loading method, thin lipid film was hydrated at 60°C in ammonium sulfate solution with 2 mg/ml of TPT. The mixture was then extruded and separated from free drug by Sephadex G-50 gel filtration in 0.9% NaCl solution.

The extent of encapsulation was determined by measuring lipid and TPT concentration. In brief, the final concentration of liposomes was estimated by phosphate assay.²⁷ The amount of TPT trapped inside the liposomes was determined with a spectrofluorometer (Hitachi F-4500; Hitachi, Tokyo, Japan), after adding 0.8 ml acidic ethanol (0.6 N HCl in ethanol) to 0.2 ml diluted drug-loaded liposomes, using 381 nm as the excitation wavelength and 525 nm as the emission wavelength. Vesicle sizes were measured by dynamic laser scattering with a submicron particle analyzer (model N4+; Coulter, Hialeah, FL). In our preparations, TPT-loaded liposomes contained 90–100 μg TPT/ μmol phospholipid.

The particle size of our liposome preparations ranged from 65 to 75 nm in diameter (Table 1).

Release of TPT from liposomes

An aliquot of 100 μ l of liposome suspension (0.5 mg/ml), was incubated with 900 μ l of PBS (pH 7.4) and human blood plasma (HBP) at 37°C. At time points of 0.083 (5 min), 1, 2, 6, 12, 24 and 48 h, aliquots of 100 μ l were withdrawn and the free TPT was removed by Sepharose CL-4B gel filtration. A small aliquot of liposomal TPT was diluted (as necessary) with unbuffered saline. Phospholipid and TPT concentrations were determined by phosphorus analysis and spectrofluorometry (Hitachi F-4500) as described.

Kinetic evaluation of lactone ring opening

The lactone ring opening rates for TPT as a result of hydrolysis were determined by reverse-phase HPLC assays. A drug concentration of 1 mM was prepared in PBS (pH 7.4) at 37°C. At time points of 0.083 (5 min), 0.5, 1, 2, 6, 24, 48 and 72 h, 200 μ l of aliquots were withdrawn and mixed with 0.8 ml of methanol. The mixture (20 μ l) was injected into HPLC directly for analysis. HPLC analysis of TPT was based on the method described by Warner.²⁸ The mobile phase consisted of TEAA buffer [2% triethylamine in water (v/v), adjusted to pH 5.5 with glacial acetic acid] and acetonitrile. The ratio of acetonitrile:TEAA buffer (v/v) was adjusted to 12:88. All mobile phases were filtered and degassed using sonication prior to use. For analysis of TPT, the isocratic HPLC system utilized a Shimadzu LC-9A pump, a Waters 717 autosampler and a Shimadzu RF-551 spectrofluorometric detector (excitation wavelength 381 nm, emission wavelength 525 nm). Separation was carried out at ambient temperature using a Waters NovaPak-C18 reverse-phase column (4 μ m particle size; 150 \times 3.9 mm i.d.). In all instances, a flow rate of 1.0 ml/min was employed.

In vitro antiproliferative effect of liposomal TPT

The antiproliferative effect of TPT-loaded liposomes was determined by MTT assay.²⁹ Briefly, 5×10^3 tumor cells were seeded into each well of 96-well microtiter plates in appropriate medium. The C-26 and HTB-9 cells were either incubated with free TPT or liposomal TPT for 2 days before the MTT assay. The concentrations of test drugs ranged from 0.01 to 100 μ g/ml. As the control, same dose of empty liposome was added into culture medium.

Pharmacokinetics studies in BALB/c mice

Plasma clearance studies were performed with male BALB/c mice (five mice per group). Each mouse was treated with a drug dose of 5 mg/kg in a volume of 10 ml/kg via the lateral tail vein using a 26-gauge needle. Blood samples (0.05 ml) were collected at 0.083 (5 min), 0.5, 1, 2, 6, 12 and 24 h after the i.v. injection. Blood samples were then mixed immediately with 250 μ l of 0.5 mM EDTA/PBS followed by centrifuging at 200g for 5 min. The cell pellets were washed once with the same solution and the supernatants were combined. TPT was extracted with 2.5 ml of acidic ethanol (0.6 N HCl in ethanol) and incubated overnight at 4°C to precipitate protein before detection by spectrofluorometer (Hitachi F-4500).

Pharmacokinetic analysis was done by non-linear least-squares analysis using Pkanalyst software (MicroMath, Salt Lake City, UT). The plasma concentration-time data were fitted to a biexponential equation as:

$$C(t) = A_1 e^{-k_1 t} + A_2 e^{-k_2 t}$$

where $C(t)$ is the drug concentration (y -axis) at time t (x -axis), k_1 and k_2 are slopes or apparent first-order elimination rate constants, and A_1 and A_2 are the y -intercepts.

The area under the concentration-time curve (AUC) was calculated from the sums of the ratios A_1/k_1 and A_2/k_2 . Clearance (CL) was calculated by

Table 1. Characteristics of liposomal TPT preparations

	Drug: lipid (mol: mol)	Encapsulation efficiency (%)	Size (nm)
Active remote loading	1:5.4	93.1 \pm 0.8	68.3 \pm 16.2
Passive loading	1:146.0	5.23 \pm 0.2	73.1 \pm 11.8

All data calculated from experiments conducted in triplicate.

dividing dose over AUC. Volume of distribution at steady state (V_{ss}) was calculated using the equation:

$$V_{ss} = \text{Dose} \times \text{AUMC} / (\text{AUC}^2)$$

where AUMC was the area under the product of $C \times t$ plotted against t from time 0 to infinity.

Animal models for therapy study

BALB/c mice and SCID mice (6–8 weeks, weighing 17–20 g) were purchased from the Animal Center at the College of Medicine, National Taiwan University, Taipei, Taiwan. At day 0, BALB/c and SCID mice were injected s.c. with 2×10^5 of C-26 and HTB-9 tumor cells respectively. When the mean tumor diameter reached 5 mm, mice in groups of eight or 10 were randomly divided into four groups. The tumor-bearing mice were treated with free or liposomal TPT at a dose of 5 mg/kg through the tail vein weekly for 2 weeks. For the control groups, mice were treated with equal amounts of empty liposome or normal saline. Tumor size of each mice was measured by caliper and measure calculated by the formula: $a \times b^2 / 2$, where a =length and b =width (in mm). The study was repeated 3 times and the results were consistent.

Statistical analysis

Statistical comparison between free TPT and liposomal TPT were carried out using Student's t -test. A level of $p < 0.05$ was considered to be indicative of statistical significance.

Results

Improvement on drug encapsulation by active loading

Consistent with previous studies,²¹ due to the amphipathic character and small entrapment volume in the unilamellar vesicle, passive loading of TPT by directly hydrating the drug with dried lipid film resulted in low encapsulation efficiency (5%, Table 1). The molar ratio of TPT to phospholipids was merely 1:146. In contrast, when the ammonium sulfate remote loading method was used, the encapsulation efficiency was approximately 90%, which is 18-fold higher than that of the passive loading method. The molar ratio of drug to phospholipids was also increased 27-fold, up to 1:5.4.

Stability of liposomal TPT

Based on Haran's study,²³ the intraliposomal space could maintain at a low pH environment after ammonium sulfate remote loading. Therefore, the active lactone structure would be kept while TPT retain within liposome (Figure 1). For this reason, retention of TPT within liposome was studied. As shown in Figure 2(A), there was no significant change in TPT content of liposomal TPT after 48 h incubation with PBS at 37°C. However, in the presence of 90% HBP, encapsulated TPT leaked out of liposome gradually in a time-dependent manner. It is apparent that the leakage of liposomal TPT is markedly affected by HBP interaction.

Figure 2(B) depicts the changes of lactone percentage in physiological pH as a function of time. Hydrolysis of free TPT proceeded quickly with a short half-life ($t_{1/2}$ value) of about 19.7 min. In contrast, for

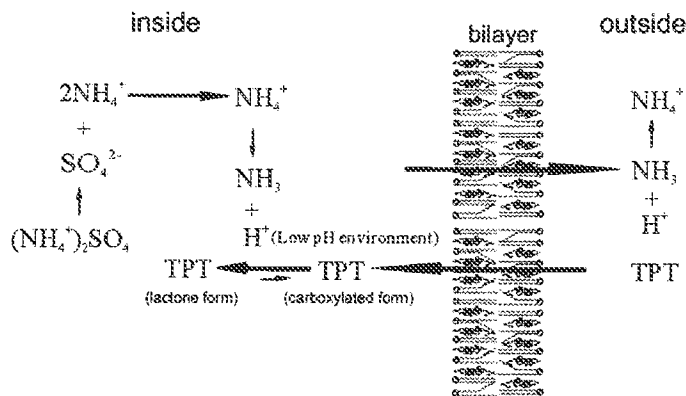


Figure 1. Scheme of liposomal TPT loaded by an ammonium sulfate gradient.

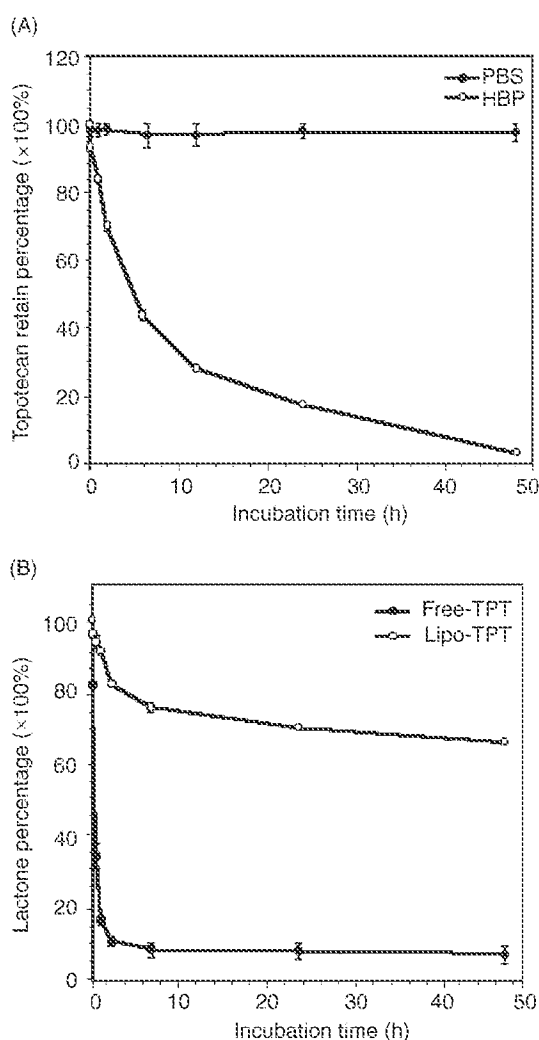


Figure 2. Characterization of liposomal TPT. (A) Release of TPT from liposomes in the presence of PBS or HBP. (B) Kinetic evaluation of the rate of lactone ring opening for free TPT and liposomal TPT in PBS. A drug concentration of 1 μ M was incubated in PBS (pH 7.4) at 37°C. At each time point, each sample was manipulated as described in Materials and methods. Each value represents the mean \pm SD of three independent experiments.

liposomal TPT, the stability of the lactone moiety was markedly enhanced by liposome encapsulation. Seventy percent of TPT remained in lactone form after 48h incubation with PBS (pH 7.4) at 37°C. Clearly, the lactone ring of TPT was notably preserved upon liposome encapsulation.

In vitro toxicity of free and liposomal TPT

Mouse C-26 cells were treated with varying doses of free or liposomal TPT. As shown in Figure 3(A),

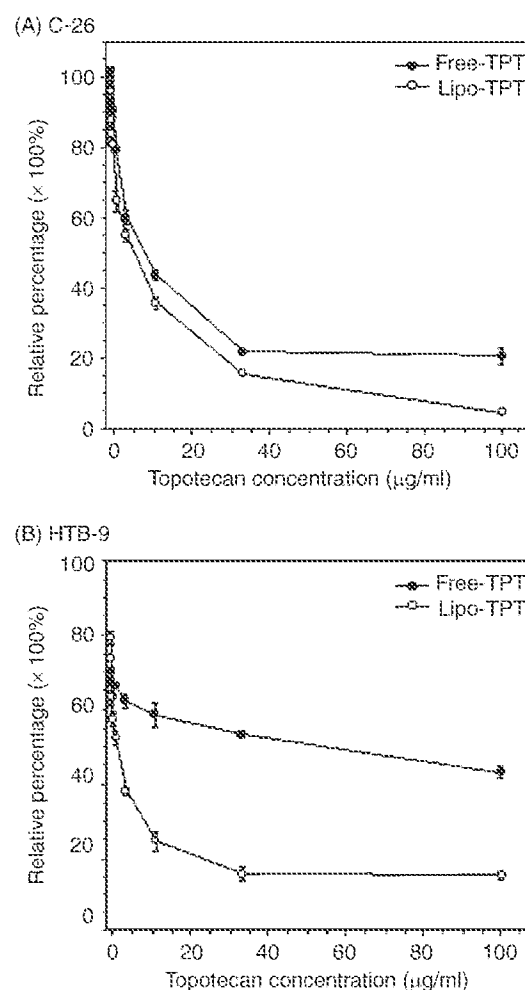


Figure 3. *In vitro* comparison of antiproliferative activities of free TPT and liposomal TPT against (A) C-26 and (B) HTB-9 cells. Cells in 96-well microtiter plates were treated with free TPT and liposomal TPT at doses indicated, and relative cell growth was determined by MTT assay as described in Materials and methods. Control empty liposomes were dosed according to phospholipid concentration. Each value represents the mean \pm SD of five determinations.

liposome encapsulation slightly enhance antiproliferation ability of TPT (IC_{50} = 4.9 ± 0.7 and $6.7 \pm 0.5 \mu$ g/ml for liposomal TPT and free TPT, respectively). However, the cytotoxic superiority of liposomal TPT was more pronounced in the HTB-9 tumor cell line (Figure 3B), for which IC_{50} s are 1.6 ± 0.4 and $41.7 \pm 6.3 \mu$ g/ml for liposomal TPT and free drug, respectively. As a control, empty liposome did not cause any inhibition of cell growth (data not shown).

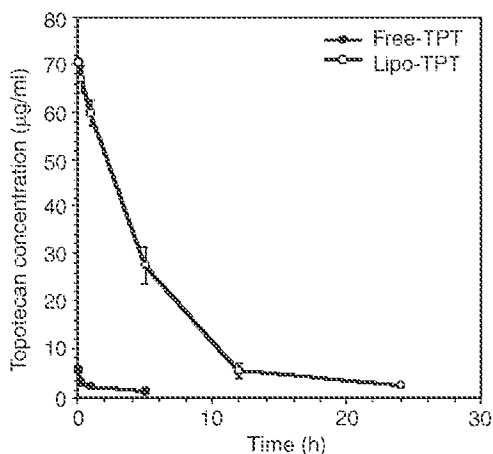


Figure 4. Plasma concentration–time relationship for free TPT and TPT encapsulated in liposomes. Male BALB/c mice were injected i.v. with a 5 mg/kg dose of free TPT or liposomal TPT. Plasma levels of TPT equivalents were determined as described in Materials and methods. Each point represents the mean \pm SD of five animals.

Pharmacokinetics of liposomal TPT

The plasma drug concentrations of free or liposome-encapsulated TPT are presented in Figure 4. Following injection of 5 mg/kg free TPT, at 5 min post-injection time, the plasma concentration (C_{max}) of free TPT achieved was 5 μ g/ml and it decreased rapidly within 15 min. On the other hand, at 5 min post-dose, the concentration of liposomal TPT achieved was 70.5 μ g/ml, which was 14 times higher than that of free TPT. The pharmacokinetic parameters of free and liposomal TPT are compared in Table 2. Liposomal drugs had a 40-fold higher area under the AUC in comparison to free drug. V_{ss} was substantially reduced with liposomes as compared with free drug. CL for liposomes was also decreased 38-fold than free TPT.

Effects of TPT on tumor growth in mice

Because of the improved pharmacokinetic profile of liposomal TPT, we next assessed its antitumor activity with syngeneic C-26 tumor in BALB/c mice and HTB-9 xenograft in SCID mice models.

In the C-26 tumor model, when mean tumor diameter reached 5 mm, TPT was given at a dose of 5 mg/kg i.v. injection weekly for 2 weeks (Figure 5A). The mean tumor size reached 3925 ± 545 and $3922 \pm 529 \text{ mm}^3$ in the saline and empty liposome-treated control respectively at day 32, whereas mice

Table 2. Pharmacokinetic parameters of free and liposomal TPT in BALB/c mice after a single i.v. dose of 5 mg/kg

	Liposomal TPT	Free TPT	Increase
C_0 (mg/l)	70.6	5.0	14 \times
$T_{1/2\alpha}$ (h)	2.1	0.1	
$T_{1/2\beta}$ (h)	2.9	2.6	
AUC (mg · h/ml)	358.4	9.4	40 \times
V_{ss} (l/kg)	0.06	1.88	
CL (l/kg/h)	0.01	0.53	

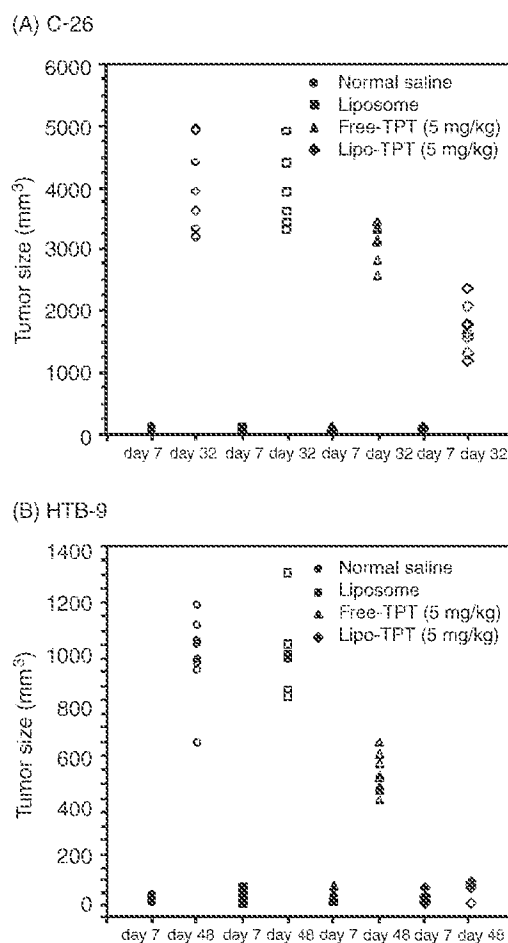


Figure 5. *In vivo* comparison of antitumor activity against (A) mouse C-26 colon carcinoma and (B) human HTB-9 xenograft. Mice were injected s.c. with 2×10^6 tumor cells in one flank on day 0 and randomly divided into four groups when mean tumor diameter reached 5 mm. Each group of mice was given a tail vein injection of different formulations at 5 mg/kg. Control groups received the same volume of normal saline and empty liposome. Tumor size was measured as described in Materials and methods.

receiving free TPT showed minimal growth delay (mean tumor size = $3094 \pm 303 \text{ mm}^3$). In contrast, a significant delay in tumor growth rate was observed

in the liposomal TPT group (mean tumor size = $1668 \pm 386 \text{ mm}^3$). This therapeutically superiority of liposomal TPT was also observed in HTB-9 tumor xenografts (Figure 5B). At day 48, the mean tumor sizes for saline and empty liposome were 969 ± 152 and $933 \pm 214 \text{ mm}^3$, respectively. The mean tumor size was slightly affected by free TPT treatment (mean tumor size = $561 \pm 171 \text{ mm}^3$). However, liposomal TPT caused tumor remission among half of mice treated. Thus, liposomal TPT exhibited better therapeutic efficacy versus free TPT and the control groups in the animal tumor models.

Discussion

Complexes of CPT with lipid can stabilize the lactone moiety and prevent its inactivation.²⁰ Correspondingly, entrapment of TPT within the liposome can prolong the half-life of the drug.²¹ However, the obstacle to the development of pharmaceutically acceptable liposome formulations is low CPT:phospholipid ratios, especially the TPT.²⁰ Although Tardi and his colleagues had used an ionophore-generated proton gradient to enhance the encapsulation of TPT into liposome,³⁰ the drug-loading procedure is slightly complicated. In this study, we adopted ammonium sulfate remote loading to achieve higher entrapment levels. This technique was applied for loading of amphiphathic weak bases such as doxorubicin for many years. It takes advantage of the large difference of ammonium sulfate gradient, $[(\text{NH}_4)_2\text{SO}_4]_{\text{lip}} > [(\text{NH}_4)_2\text{SO}_4]_{\text{med}}$, across the lipid bilayer to generate a high driving force to active loading drugs into the aqueous compartment of liposome efficiently.²³ Therefore, there is no need for buffer or pH titration during the procedure and drug encapsulation is easier. This was illustrated by the 18-fold encapsulation efficiency and a drug:lipid ratio in excess of 27-fold greater than that achieved by the direct hydration method.

In addition to the increased trapping efficiency, another important advantage provided by ammonium sulfate loading is the acidic intraliposomal environment formed spontaneously during drug encapsulation. Because CPT undergoes a pH-dependent reversible hydrolysis from active lactone form (at low pH) to inactive carboxylate form (at high pH),^{9,12} the drug molecules should be kept in a low pH environment so that their biological activity can be preserved. According to the study of Haran previously, the pH of internal liposomal aqueous space will drop below 5 after complete removal of

external ammonium sulfate as indicated by pH-sensitive fluorescence dye.²⁵ It implies that the intraliposomal environment created by ammonium sulfate loading is suitable for maintaining the lactone form (Figure 1). As showed in the TPT hydrolysis test, free TPT displayed a rapid hydrolysis kinetic with a short half-life of about 20 min and had 8.7% of the lactone form at equilibrium, whereas liposome-encapsulated TPT exhibited an enhanced stability with about 70% of lactone form at equilibrium (Figure 2B). It should be noted that up to 30% of liposome-encapsulated TPT exists in the carboxylate form when incubated in PBS, although there was no significant TPT loss in leakage tests (Figure 2A). Theoretically, because of the acidic environment, a higher proportion of TPT should exist in the lactone form if all the drug molecules have been entrapped inside the liposome. This suggested that a portion of TPT, although still associated with phospholipid, might contact with the external basic buffer and be subjected to hydrolysis.

Although the enzyme level may affect cellular sensitivity to topoisomerase I inhibitors,^{31,32} the effectiveness of CPT treatment also depends on the form of cells exposed. For the reason that the intact lactone moiety is structurally important for biological activity,^{5,11} liposomal TPT is much more effective than free drug to inhibit C-26 and HTB-9 cells growth (Figure 3). The enhanced antitumor activity of liposomal TPT can be accounted by its ability to maintain a higher portion of active lactone form, whereas free TPT is quickly hydrolyzed into its inactive carboxylate form.

Pharmacokinetic analysis indicated that liposomal-TPT had a smaller volume of distribution, which is close to total blood volume, but there was little difference in $t_{1/2\beta}$. This could be explained by the poor retention of TPT in the presence of serum. Although some reports argued that liposomes comprised of saturated neutral phospholipids and a high percentage of cholesterol can reduce protein interaction and drug leakage,³³⁻³⁵ nevertheless, TPT escaped from the DSPC/Chol-based liposome used in this study faster than other drugs, such as vincristine³⁶ or doxorubicin.³⁷ We do not have a good explanation for this phenomenon. One possibility is that TPT does not form a gel-like precipitate with ammonium sulfate as doxorubicin does.³⁸

Preclinical *in vitro* and *in vivo* studies indicated that prolonged exposure to low-dose topoisomerase I inhibitors is the most efficacious.³⁹⁻⁴¹ As the result of pharmacokinetic tests, the overall plasma AUC of liposomal TPT was around 35 times that of free drug. This altered distribution may reduce the toxicity to

normal tissues and the higher plasma AUC may facilitate drug distribution to tumor. The improvement in pharmacokinetic parameters was reflected in the therapeutic efficacy (Figure 5). In the C-26 model, the tumor size decreased from $3094 \pm 303 \text{ mm}^3$ of free TPT-treated mice to $1668 \pm 386 \text{ mm}^3$ of liposomal TPT treated. More significantly, in the HTB-9 xenograft model, the total tumor regressions were observed in half of liposomal TPT-treated mice. It might be argued the similar results would be achieved with a higher dose or several dose regimens of free drugs. However, in the initial animal study, the dose-dependent antitumor effects and various dose regimens of free and encapsulated TPT were been examined on C-26 tumor-implanted mice (data not show). According to the results in such experiments, we found that for 2 and 5 mg/kg free drug treatment the final tumor volumes were 1828 ± 462 and $1857 \pm 300 \text{ mm}^3$, respectively, at the end of the experiment. There are no significant difference between these two groups and the control group (final tumor volume $2009 \pm 257 \text{ mm}^3$). In contrast, after treatment with 2 and 5 mg/kg liposomal TPT, the tumor growth was markedly delayed and the final tumor volumes were 1298 ± 211 and $1001 \pm 210 \text{ mm}^3$, respectively. Even more, the therapeutic effects of liposomal TPT administrated once weekly for 2 weeks were superior to those mice administrated free TPT twice weekly for 2 weeks (final tumor volumes $1709 \pm 287 \text{ mm}^3$ for 2 mg/kg and $1529 \pm 387 \text{ mm}^3$ for 5 mg/kg). In addition, results of TPT hydrolysis and *in vitro* cytotoxicity tests suggested that the increased therapeutic activity achieved with liposomal TPT is not only due to a change of the pharmacokinetics, but also due to enhanced drug stability. Therefore, the improvement of therapeutic efficacy may not be achievable with multi-dose regimens or continuous i.v. infusion of free drug.

In summary, the use of active ammonium sulfate remote loading to encapsulate TPT has several advantages. The powerful ionic gradient driving force considerably increased encapsulation efficiency. Furthermore, acidification of liposomal internal space during the loading process tips the equilibrium to the biologically active lactone form. The low activity of free TPT against C-26 and HTB-9 tumors can be markedly enhanced after encapsulation in liposome. Although the retention of TPT within the DSPC/Chol-based liposome was shorter than that observed for doxorubicin, the improvement of pharmacological properties still significantly contributes to therapeutic efficacy. Further studies on the behavior of liposomal TPT in circulation will

be important to design formulations with better therapeutic activity.

Conclusion

The use of ammonium sulfate ionic gradient loading provides a simple and efficient method to formulate liposomal TPT for pharmaceutical use. In addition, the stability and antitumor activity of TPT can be markedly enhanced after liposome encapsulation.

References

1. Kingsbury WD, Boehm JC, Jakas DR, *et al.* Synthesis of water-soluble (aminoalkyl)-camptothecin analogues: inhibition of topoisomerase I and antitumor activity. *J Med Chem* 1991; 34: 98-107.
2. Kavanagh JJ, Kudelka AP. Systemic therapy for gynecologic cancer. *Curr Opin Oncol* 1993; 5: 891-9.
3. Lynch TJJ, Kalish L, Strauss G, *et al.* Phase II study of TPT in metastatic non-small-cell lung cancer. *J Clin Oncol* 1994; 12: 347-52.
4. Creemers GJ, Wanders J, Gamucci T, *et al.* Topotecan in colorectal cancer: a phase II study of the EORTC early clinical trials group. *Ann Oncol* 1995; 6: 844-6.
5. Hertzberg RP, Caranfa MJ, Holden KG, *et al.* Modification of the hydroxy lactone ring of camptothecin: inhibition of mammalian topoisomerase I and biological activity. *J Med Chem* 1989; 32: 715-20.
6. Caserini C, Pratesi G, Tortoreto M, *et al.* Apoptosis as a determinant of tumor sensitivity to TPT in human ovarian tumors: preclinical *in vitro/in vivo* studies. *Clin Cancer Res* 1997; 3: 955-61.
7. Hochster H, Liebes L, Speyer J, *et al.* Phase I trial of low-dose continuous TPT infusion in patients with cancer: an active and well-tolerated regimen. *J Clin Oncology* 1994; 12: 553-9.
8. Burke TG, Mi Z. Preferential binding of the carboxylate form of camptothecin by human serum albumin. *Anal Biochem* 1993; 212: 285-7.
9. Fassberg J, Stella VJ. A kinetic and mechanistic study of the hydrolysis of camptothecin and some analogues. *J Pharm Sci* 1992; 81: 676-84.
10. Hsiang YH, Liu LF, Wall ME, *et al.* DNA topoisomerase I-mediated DNA cleavage and cytotoxicity of camptothecin analogues. *Cancer Res* 1989; 49: 4385-9.
11. Jaxel C, Kohn KW, Wani MC, Wall ME, Pommier Y. Structure-activity study of the actions of camptothecin derivatives on mammalian topoisomerase I: evidence for a specific receptor site and a relation to antitumor activity. *Cancer Res* 1989; 49: 1465-9.
12. Burke TG, Mi Z. The structural basis of camptothecin interactions with human serum albumin: impact on drug stability. *J Med Chem* 1994; 37: 40-6.
13. Mi Z, Burke TG. Differential interactions of camptothecin lactone and carboxylate forms with

- human blood components. *Biochemistry* 1994; 33: 10325-36.
14. Mi Z, Malak H, Burke TG. Reduced albumin binding promotes the stability and activity of TPT in human blood. *Biochemistry* 1995; 34: 13722-8.
 15. Rahman A, Kessler A, More N, *et al.* Liposomal protection of adriamycin-induced cardiotoxicity in mice. *Cancer Res* 1980; 40: 1532-7.
 16. Gabizon A, Dagan A, Goren D, Barenholz Y, Fuks Z. Liposomes as *in vivo* carriers of adriamycin: reduced cardiac uptake and preserved antitumor activity in mice. *Cancer Res* 1982; 42: 4734-9.
 17. Hong RL, Huang CJ, Tseng YL, *et al.* Direct comparison of liposomal doxorubicin with or without polyethylene glycol coating in C-26 tumor-bearing mice: is surface coating with polyethylene glycol beneficial?. *Clin Cancer Res* 1999; 5: 3645-52.
 18. Hong RL, Tseng YL, Chang FH. Pegylated liposomal doxorubicin in treating a case of advanced hepatocellular carcinoma with severe hepatic dysfunction and pharmacokinetic study. *Ann Oncol* 2000; 11: 349-53.
 19. Forssen EA, Tokes ZA. Improved therapeutic benefits of doxorubicin by entrapment in anionic liposomes. *Cancer Res* 1983; 43: 546-50.
 20. Burke TG, Mishra AK, Wani MC, Wall ME. Lipid bilayer partitioning and stability of camptothecin drugs. *Biochemistry* 1993; 32: 5352-64.
 21. Burke TG, Gao X. Stabilization of TPT in low pH liposomes composed of distearoylphosphatidylcholine. *J Pharm Sci* 1994; 83: 967-9.
 22. Subramanian D, Muller MT. Liposomal encapsulation increases the activity of the topoisomerase I inhibitor TPT. *Oncol Res* 1995; 7: 461-9.
 23. Haran G, Cohen R, Bar LK, Barenholz Y. Transmembrane ammonium sulfate gradients in liposomes produce efficient and stable entrapment of amphipathic weak bases. *Biochim Biophys Acta* 1993; 1151: 201-15.
 24. Szoka F, Olson F, Heath T, Vail W, Mayhew E, Papahadjopoulos D. Preparation of unilamellar liposomes of intermediate size (0.1-0.2 μmol) by a combination of reverse phase evaporation and extrusion through polycarbonate membranes. *Biochim Biophys Acta* 1980; 601: 559-71.
 25. Mayer LD, Hope MJ, Cullis PR, Janoff AS. Solute distributions and trapping efficiencies observed in freeze-thawed multilamellar vesicles. *Biochim Biophys Acta* 1985; 817: 193-6.
 26. Tseng, Y L, Hong R L, Tao MH, Chang FH. Sterically stabilized anti-idiotype immunoliposomes improve the therapeutic efficacy of doxorubicin in a murine B-cell lymphoma model. *Int J Cancer* 1999; 80: 723-30.
 27. Bartlett GR. Phosphorus assay in column chromatography. *J Biol Chem* 1959; 234: 466-8.
 28. Warner DL, Burke TG. Simple and versatile high-performance liquid chromatographic method for the simultaneous quantitation of the lactone and carboxylate forms of camptothecin anticancer drugs. *J Chromatogr B* 1997; 691: 161-71.
 29. Alley MC, Scudiero DA, Monks A, *et al.* Feasibility of drug screening with panels of human tumor cell lines using a microculture tetrazolium assay. *Cancer Res* 1988; 48: 589-601.
 30. Tardi P, Choice E, Masin D, Redelmeier T, Bally MB, Madden TD. Liposomal encapsulation of TPT enhances anticancer efficacy in murine and human xenograft models. *Cancer Res* 2000; 60: 3389-93.
 31. Giovanello BC, Stehlin JS, Wall ME, *et al.* DNA topoisomerase I-targeted chemotherapy of human colon cancer in xenografts. *Science* 1989; 246: 1046-8.
 32. Kijima T, Kubota N, Nishio K. Establishment of a CPT-11-resistant human ovarian cancer cell line. *Anticancer Res* 1994; 14: 799-803.
 33. Semple SC, Chonn A, Cullis PR. Influence of cholesterol on the association of plasma proteins with liposomes. *Biochemistry* 1996; 35: 2521-5.
 34. Kirby C, Clarke J, Gregoriadis G. Effect of the cholesterol content of small unilamellar liposomes on their stability *in vivo* and *in vitro*. *Biochem J* 1980; 186: 591-8.
 35. Mayer LD, Tai LC, Ko DS, *et al.* Influence of vesicle size, lipid composition, and drug-to-lipid ratio on the biological activity of liposomal doxorubicin in mice. *Cancer Res* 1989; 49: 5922-30.
 36. Mayer LD, Bally MB, Loughbrey H, Masin D, Cullis PR. Liposomal vincristine preparations which exhibit decreased drug toxicity and increased activity against murine L1210 and P388 tumors. *Cancer Res* 1990; 50: 575-9.
 37. Bally MB, Nayar R, Masin D, Hope MJ, Cullis PR, Mayer LD. Liposomes with entrapped doxorubicin exhibit extended blood residence times. *Biochim Biophys Acta* 1990; 1023: 133-9.
 38. Lasic DD, Frederik PM, Stuart MC, Barenholz Y, McIntosh TJ. Gelation of liposome interior: a novel method for drug encapsulation. *FEBS Lett* 1992; 312: 255-8.
 39. Houghton PJ, Cheshire PJ, Hallman JD, *et al.* Efficacy of topoisomerase I inhibitors, TPT and irinotecan, administered at low dose levels in protracted schedules to mice bearing xenografts of human tumors. *Cancer Chemother Pharmacol* 1995; 36: 393-403.
 40. Burris HA, Hanauske AR, Johnson RK, *et al.* Activity of TPT, a new topoisomerase I inhibitor, against human tumor colony-forming units *in vitro*. *J Natl Cancer Inst* 1992; 23: 1816-20.
 41. Houghton PJ, Cheshire PJ, Myers L, *et al.* Evaluation of 9-dimethylaminomethyl-10-hydroxycamptothecin against xenografts derived from adult and childhood solid tumors. *Cancer Chemother Pharmacol* 1992; 31: 229-39.

(Received 15 April 2002; accepted 7 May 2002)



CANCER RESEARCH

Clinical Trials

Abstract CT325: Combination of the PARP inhibitor veliparib (ABT888) with irinotecan in patients with triple negative breast cancer: Preliminary activity and signature of response

Patricia M. LoRusso, Sara M. Tolaney, Shukmei Wong, Ralph E. Parchment, Robert J. Kinders, Lihua Wang, Jessica Aldrich, Alice Chen, Diane Durecki, Scott A. Boerner, Tina Guthrie, Adam Bowditch, Lance K. Heilbrun, Mary Jo Pilat, David Craig, Dongpo Cai, Tracy Bell, John Carpten, and Geoffrey Shapiro

DOI: 10.1158/1538-7445.AM2015-CT325 Published August 2015

Abstract

Info & Metrics

Proceedings: AACR 106th Annual Meeting 2015; April 18-22, 2015; Philadelphia, PA

Abstract

Background: The nuclear enzyme PARP is essential in recognition and repair of DNA damage. Preclinical evidence suggests that PARP inhibitors work as sensitizing agents for DNA-damaging agents such as irinotecan. Veliparib is an orally bioavailable PARP 1 and 2 inhibitor. This expansion to a phase I study, which demonstrated veliparib reduces PAR levels in tumor after irinotecan exposure, was conducted to assess the safety, tolerability and preliminary anti-tumor activity of the combination of veliparib and irinotecan in triple negative breast cancer (TNBC) patients (pts), as well as to apply next generation sequencing technologies to define a signature of response.

Methods: Pts were enrolled to two breast cancer cohorts: (1) TNBC, germline BRCA-mutant positive and (2) TNBC, non-BRCA mutated (wt). Eligibility included performance status 0-2; \geq age 18; adequate bone marrow, hepatic and renal function. Cycles were 21 days. Irinotecan was given i.v. 100 mg/m² over 90 min on Days 1 and 8. Twice daily (BID) oral dosing of 40 mg veliparib occurred Days 2-15 (Cycle 1) and Days 1-15 (subsequent cycles) followed by a 6-day rest. Tumor biopsies were collected at baseline, 4-6 hours after the first dose of irinotecan (day 1) and the combination (day 8) in cycle 1. Whole exome and transcriptome sequencing was performed using both normal and tumor tissue. Circulating tumor cells (CTC) were evaluated using the CellSearch platform.

Results: 24 TNBC pts were enrolled, with 20 pts treated and evaluable for response (8 germline BRCA-mutation positive, 10 non-BRCA mutated, 2 suspected deleterious). Median age was 51 (range 31-63). Median number of prior treatments was 4 (range 1-7). Most frequent drug-related toxicities included: leukopenia (60%), neutropenia (60%), nausea (55%), diarrhea (40%), fatigue (40%), anemia (30%), and vomiting (30%). Best responses were as follows: Germline BRCA-mutant positive 7/8 PR (88%; median number of days on study = 330; range 148-594 days), 1/8 PD (12%); suspected deleterious 2/2 PD (100%); non-BRCA mutated 7/10 SD (70%; median number of days on study = 70; range 42-98 days), 3/10 PD (30%). Exploratory molecular profiling has been performed in a subset of these pts and the results will be presented. EpCAM+ CTC numbers were evaluable in 11 of 22 enrolled pts, and nuclear γ H2Ax+, a pharmacodynamic biomarker of DNA damage, was identified in a fraction of CTCs from all 11 of these pts.

Conclusions: Veliparib in combination with irinotecan was safe and tolerable in TNBC pts. Although the cohort in this trial is small, the preliminary response rate of 88% in pts with germline BRCA mutation is encouraging and higher than that historically reported with PARP inhibitor monotherapy in this population. Deep molecular profiling among BRCA mutant carriers will be validated in a larger, independent cohort to define potential biomarkers of response. Support: NCI U01-CA062487, NCI U01-CA062490, Komen KG120001, NCI R21-CA135572, and HHSN261200800001E.

Citation Format: Patricia M. LoRusso, Sara M. Tolaney, Shukmei Wong, Ralph E. Parchment, Robert J. Kinders, Lihua Wang, Jessica Aldrich, Alice Chen, Diane Durecki, Scott A. Boerner, Tina Guthrie, Adam Bowditch, Lance K. Heilbrun, Mary Jo Pilat, David Craig, Dongpo Cai, Tracy Bell, John Carpten, Geoffrey Shapiro. Combination of the PARP inhibitor veliparib (ABT888) with irinotecan in patients with triple negative breast cancer: Preliminary activity and

CSPC Exhibit 1109

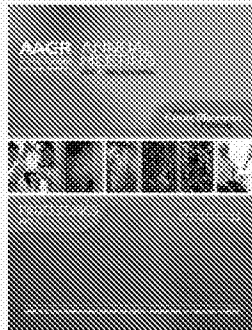
Page 337 of 339

signature of response. [abstract]. In: Proceedings of the 106th Annual Meeting of the American Association for Cancer Research; 2015 Apr 18-22; Philadelphia, PA. Philadelphia (PA): AACR; Cancer Res 2015;75(15 Suppl):Abstract nr CT325. doi:10.1158/1538-7445.AM2015-CT325

©2015 American Association for Cancer Research.

← Previous

▲ Back to top



August 2015
Volume 75, Issue 15 Supplement
Table of Contents

Search this issue



Sign up for alerts

© Request Permissions

! Article Alerts

✉ Email Article

🔗 Citation Tools

↪ Share

Twitter

Like 0

↪ Related Articles

No related articles found.

Google Scholar

▶ Cited By...

▶ More in this TOC Section

Home

Alerts

Feedback

Privacy Policy



Articles

Online First

Current Issue

Past Issues

Meeting Abstracts

Info for

- [Authors](#)
- [Subscribers](#)
- [Advertisers](#)
- [Librarians](#)
- [Reviewers](#)
- [About Cancer Research](#)**
- [About the Journal](#)
- [Editorial Board](#)
- [Permissions](#)
- [Submit a Manuscript](#)



Copyright © 2020 by the American Association for Cancer Research.

Cancer Research Online ISSN: 1538-7445
Cancer Research Print ISSN: 0008-5472
Journal of Cancer Research ISSN: 0099-7013
American Journal of Cancer ISSN: 0099-7374